9TH INTERNATIONAL PGM CONFERENCE

PGMs - Enabling a cleaner world

SAIMM
THE SOUTHERN AFRICAN INSTITUTE OF MINING AND METALLURGY



Proceedings Book

27-28 October 2025
Sun City, Rustenburg, South Africa

THE SOUTHERN AFRICAN INSTITUTE OF MINING AND METALLURGY
JOHANNESBURG 2025

9TH INTERNATIONAL PGM CONFERENCE

PGMs - Enabling a cleaner world

27-28 OCTOBER 2025
Sun City, Rustenburg, South Africa

SAIMM PUBLICATIONS

THE MONOGRAPH SERIES

Ml **Lognormal-De Wijsian Geostatistics for Ore Evaluation**
(2nd ed 1981) D.G. Krige

M2 **An Introduction to Geostatistical Methods of Mineral Evaluation**
(2nd ed 1981) J.-M.M. Rendu

M3 **Principles of Flotation**
(1982) (3rd imp. 1986) Edited by R.P. King

M4 **Increased Underground Extraction of Coal**
(1982) Edited by C.J. Fauconnier and R.W.O. Kersten

M5 **Rock Mechanics in Mining Practice**
(1983) (3rd imp. 1986) Edited by S. Budavari

M6 **Assay and Analytical Practice in the South African Mining Industry**
(1986) W.C. Lenahan and R. de L. Murray-Smith

M7 **The Extractive Metallurgy of Gold in South Africa,**
2 volumes (1987) Edited by G.G Stanley

M8 **Mineral and Metal Extraction — An Overview**
(1994) L.C. Woollacott and R.H. Eric

M9 **Rock Fracture and Rockbursts—an illustrative study**
(1997) Edited by W.D. Ortlepp

THE SPECIAL PUBLICATIONS SERIES

SPI **Proceedings, Underground Transport Symposium**
(1986) Edited by R.C.R. Edgar

SP2 **Backfill in South African Mines (1988)**

SP3 **Treatment and Re-use of Water in the Minerals Industry (1989)**

SP4 **COREX Symposium 1990**
(1990) Edited by H.M.W. Delport and P.J. Holaschke

SP5 **Measurement, Control, and Optimization in Mineral Processing**
(1994) Edited by H.W. Glen

SP6 **Handbook on Hard-rock Strata Control**
(1994) A.J.S. Spearing

SP7 **Rock Engineering for underground coal mining**
(2002) J. Nielen van der Merwe and Bernard J. Madden

SP8 **Second Edition: Rock Engineering for underground coal mining**
(2010) J. Nielen van der Merwe and Bernard J. Madden

SP9 **Theoretical Rock Mechanics for Professional Practice**
(2016) M. Handley

SP10 **Johannesburg and its Holey Mining Heritage 2021**
(2021) T.R. Stacey

SP11 **Mineral and Metal Extraction — An Overview**
(2021) L.C. Woollacott and R.H. Eric

SP12 **The Fall of a Giant: The story of the disintegration of the South African Mining Industry**
(2022/2023) Dr I. Robinsoin

SP13 **COMRO's Legacy: Research and Development of Stoping Mining Machinery and Technologies**
(2023) B. Protheroe

SUPPLEMENT TO THE SAIMM JOURNAL

The Metals and Minerals Industry in South Africa - Part 1 (1989)
Edited by H.W. Glen

THE SYMPOSIUM SERIES

S1 **Mathematical Statistics and Computer Applications in Ore Valuation (1966)**

S2 **Planning Open Pit Mines** (1970) (4th imp.)
Edited by P.W.J. van Rensburg

S3 **Application of Computer Methods in the Mineral Industry** (APCOM 1973) Edited by M.D.G. Salamon

S4 **Infacon 1974** Edited by H.W. Glen

S5 **Proceedings of the 12TH CMMI Congress** 2 volumes (1982)
Edited by H.W. Glen

S6 **Rockbursts and Seismicity in Mines** (1984)
Edited by N.C. Gay and E.H. Wainwright

S7 **The Planning and Operation of Open Pit and Strip Mines** (1986) Edited by J.P. Deetlefs

S8 **GOLD 100: Proceedings of the International Conference on Gold (1986)**
Volume 1: Gold Mining Technology
Edited by H. Wagner and R.P. King
Volume 2: Extractive Metallurgy of Gold
Edited by C.E. Fivaz and R.P. King
Volume 3: Industrial Uses of Gold
Edited by G. Gafner and R.P. King

S9 **APCOM 87: Proceedings of the Twentieth International Symposium on the Application of Computers and Mathematics in the Mineral Industries (1987)**
Volume 1: Mining
Edited by L. Wade, R.W.O. Kersten and J.R. Cutland
Volume 2: Metallurgy
Edited by R.P. King and I.J. Barker
Volume 3: Geostatistics
Edited by I.C. Lemmer, H. Schaum and F.A.G.M. Camisani-Calzolari

S10 **International Deep Mining Conference (1990)**
Volume 1: Innovations in Metallurgical Plant
Edited by G.A. Brown and P. Smith
Application of Materials Engineering in the Mining Industry Edited by B. Metcalfe
Volume 2: Technical Challenges in Deep Level Mining
Edited by D.A.J. Ross-Watt and P.D.K. Robinson

S11 **Infacon 6 (Incorporating Incsac) (1992)**
Edited by H.W. Glen

S12 **Massmin 92**
Edited by H.W. Glen (out of print)

S13 **Minefill 93**
Edited by H.W. Glen

S14 **XVTH CMMI Congress Publications (1994)**
Volume 1: Mining
Edited by H.W. Glen
Volume 2: Metals Technology and Extractive Metallurgy (1994) Edited by H.W. Glen

S15 **Surface Mining 1996**
Edited by H.W. Glen

S16 **Hidden Wealth (1996)**
Edited by H.W. Glen

S17 **Heavy Minerals 1997**
Edited by R.E. Robinson

S18 **The 8TH International Platinum Symposium (1998)**

S19 **Mining in Africa '98**

S20 **Extraction Metallurgy Africa '98**

S21 **Sixth International Symposium for Rock Fragmentation by Blasting (1999)**

S22 **Metallurgy Africa '99**

S23 **Heavy Minerals 1999**
Edited by R.G. Stimson

S24 **Tunnels under Pressure**
Technical Editor T.R. Stacey

S25 **Mine Hoisting 2000**

S26 **Coal–The Future (2000)**

S27 **The Fifth International Symposium on Rockburst and Seismicity in Mines (RaSim 5) (2001)**

S28 **6TH International Symposium on Mine Mechanization and Automation (2001)**

S29 **XIV International Coal Preparation Congress and Exhibition**

S30 **Surface Mining 2002—Modern Developments for the New Millennium**

S31 **IFSA 2002, Industrial Fluidization South Africa**

S31a **APCOM 2003—Application of Computers and Operations Research in the Minerals Industries**

S32 **ISSA/Chamber of Mines Conference—Mines and Quarries: Prevention of Occupational Injury and Disease**

S33 **ISRM—Technology Roadmap for Rock Mechanics**

S34 **Heavy Minerals Conference 2003**

S35 **Safety in Mines Research Institutes (2003)**

S36 **VII International Conference on Molten Slags, Fluxes & Salts (2004)**
Tenth International Ferroalloys Congress INFACONX 2004

S37 **Deep and high stress mining 2004**

S38 **'Platinum adding value' 2004**

S39 **Base Metals—Southern Africa's response to changing global base metals market dynamics 2005**

S40 **Strategic *versus* Tactical approaches in mining 2005**

S41 **Best practices in rock engineering SARES 2005**

S42 **IFSA 2005, Industrial Fluidization South Africa**

S43 **Southern African Pyrometallurgy 2006 International Conference**

S44 **Stability of rock slopes in open pit mining and civil engineering situations**

S45 **'Platinum Surges Ahead' 2006**

S46 **Hydraulic Transport of Solids - Hydrotransport 17 (2007)**

S47 **Fourth Southern African Base Metals Conference 'Africa's base metals resurgence'**

S48 **Heavy Minerals Conference, 2007**

S49 **Cave Mining Conference, 2007**

S50 **International Symposium on Lead and Zinc processing – Lead & Zinc 2008**

S51 **Surface Mining 2008**

S52 **Platinum in transformation 2008**

S53 **IFSA 2008, Industrial Fluidization South Africa**

S54 **Hydrometallurgy Conference 2009**

S55 **Shotcrete for Africa 2009**

S56 **Base Metals Conference 2009**

S57 **Heavy Minerals Conference, 2009**

S58 **Hard Rock Safe—Safety Conference 2009**

S59 **Sampling and Blending 2009**

S60 **World Gold 2009 Conference**

S61 **Physical Beneficiation Conference 2010**

S62 **Second Hardrock Safe—Safety Conference 2010**

S63 **Platinum in Transition 'Boom or Bust' 2010**

S64 **South African Pyrometallurgy 2011 International Conference**

S65 **Minefill 2011 (10TH International Symposium on Mining with Backfill)**

S66 **Base Metals Conference 2011**

S67 **MineSafe 2011 Conference**

S68 **Iron Ore and Manganese Ore Metallurgy 2011**

S69 **Percolation leaching: The status globally and in Southern Africa 2011**

S70 **IFSA 2011, Industrial Fluidization South Africa**

S71 **Southern Hemisphere International Rock Michanics Symposium 2012**

S72 **Platinum Conference 'A catalyst for change' 2012**

S73 **Ferrous 2012—Ferrous and Base Metals Development Network Conference**

S74 **Diamonds - Source to use 2013**

S75 **Sampling and analysis: Best-practice in African mining 2013**

S76 **Base Metals Conference 2013**

S77 **Precious Metals 2013 Conference—The Precious Metals Development Network (PMDN)**

S78 **Physical Beneficiation 2013 Conference**

S79 **21st Century challenges to the southern African coal sector 2014**

S80 **Furnace Tapping Conference 2014**

S81 **Platinum Conference 'Platinum—Metal for the Future' 2014**

S82 **IFSA 2014, Industrial Fluidization South Africa**

S83 **Copper Cobalt Africa 2015**

S84 **The Danie Krige Geostatistical Conference 2015 - Vol. 1**

The Danie Krige Geostatistical Conference 2015 - Vol. 2

S85 **World Gold Conference 2015**

S86 **Slope Stability 2015**

S87 **2nd Annual Young Professionals Conference 2015**

S88 **AMI–Nuclear Materials Development Network 2015**

S89 **MPES–23rd International Symposium on Mine Planning & Equipment Selection 2015**

S90 **Diamonds still Sparkling Conference 2016**

S91 **The SAMREC/SAMVAL Companion Volume Conference 2016**

S92 **New Technology and Innovation in the Minerals Industry Colloquium 2016**

S93 **Theoretical Rock Mechanics for Professional Practice** (Special Publications Series 9) by M. Handley - 2016

S94 **Hydrometallurgy Conference 2016**

S95 **10TH Heavy Minerals Conference 2016**

S96 **MineSafe Conference 2016**

S97 **AMI-Ferrous and Base Metals Development Conference 2016**

S98 **3rd Young Professionals Conference 2017**

S99 **Proximity Detection and Collosion Avoidance Systems in Mining Colloquium 2017**

S100 **6TH Sulphur and Sulphuric Acid Conference 2017**

S101 **Mine Planning Colloquium 2017**

S102 **Chrome Colloquium 2017**

S103 **4TH Mineral Project Valuation Colloquium 2017**

S104 **Water Conference 2017**

S105 **Rapid Underground Mine and Civil Access Engineering 2017**

S106 **MineSafe Conference 2017**

S107 **Uranium 2017 International Conference 2017**

S108 **IFSA 2017–Industrial Fluidization Conference 2017**

S109 **AfriRock 2017–ISRM International Symposium 2017**

S110 **AMI Precious Metals 2017–The Precious Metals Development Network (PMDN) Symposium**

S111 **7TH International Platinum Conference 2017**

S112 **Infacon XV: International Ferro-Alloys Conrgress 2018**

S113 **SOMP–Society of Mining Professors 6TH Regional Conference 2018**

S114 **Digitalization in Mining Conference 2018**

S115 **Diamonds – Source to Use 2018 Conference 2018**

S116 **The 9TH Southern African Base Metals Conference 2018**

S117 **Geometallurgy Conference 2018**

S118 **Mine Safe Technical Conference and Industry Day 2018**

S119 **ASM Conference 2018**

S120 **4TH Young Professionals Conference 2018**

S121 **Furnace Tapping 2018 Conference 2018**

S122 **7TH Sulphur and Sulphuric Acid Conference 2019**

S123 **Mine Planner's Colloquium 2019**

S124 **9TH International Conference on Deep & High Stress Mining 2019**

S125 **New Technology Conference and Trade Show 2019**

S126 **Smart Mining Smart Environment Smart Society Conference 2019**

S127 **The Eleventh International Heavy Minerals Conference 2019**

S128 **Surface Mining Masterclass 2019**

S129 **International Mine Health and Safety Conference 2019**

S130 **Tailings Storage Conference 2020**

S131 **IMPC2020 XXX International Mineral Processing Congress**

S132 **Johannesburg and its Holey Mining Heritage**
(Special Publications Series 10) by T.R. Stacey - 2021

S133 **Mineral and Metal Extraction — An Overview**
(Special Publications Series 11) by L.C. Woollacott and R.H. Eric - 2021

S134 **Diamonds - Source to Use - 2021 Online Conference 2021**

S135 **WorldGold Online Conference 2021**

S136 **APCOM 2021 Minerals Industry4.0-The next digital transformation in mining**

S137 **5TH Young Professionals Online Conference 2021**

S138 **Southern African Rare Earths International Online Conference 2021**

S139 **SAMCODES Conference 2021**

S140 **Global Tailings Standards and Opportunities`For the Mine of the Future Conference 2022**

S141 **The Fall of a Giant: The story of the disintegration of the South African Mining Industry**
(Special Publications Series 12) by I. Robinson - 2022/2023

S142 **Battery Materials Conference 2022**

S143 **32ND SOMP Annual Meeting and Conference 2022**

S144 **SDIMI (Sustainable Development in the Minerals Industry) 10TH International Conference 2022**

S145 **THANOS International Conference 2022**

S146 **Mine Impacted Water Online Conference 2022 (Abstract Book Only)**

S147 **8TH International PGM Conference 2022**

S148 **SANCOT Symposium 2022**

S149 **8TH Sulphur and Sulphuric Acid Conference 2023**

S150 **Southern African Hydrogen and Fuel Cell Conference 2023**

S151 **COMRO's Legacy: Research and Development of Stoping Mining Machinery and Technologies**
(Special Publications Series 13) by B. Protheroe - 2023

S152 **Copper Cobalt Africa in Association with The 10TH Southern African Base Metals Conferenc 2023**

S153 **Digital Transformation in Mining Conference 2023**

S154 **Diamonds Source to Use 2023 Online Conference**

S155 **12TH International Heavy Minerals Conference 2023**

S156 **Geometallurgy Conference 2023**

S157 **Next Generation Tailings Opportunitiy or Risk? Conference 2023**

S158 **6TH Young Professionals Conference 2023**

S159 **Southern African Pyrometallurgy 2024 International Conference**

S160 **The 11TH World Conference of Sampling and Blending 2024**

S161 **SANIRE Symposium 2024**
Technical Applications in Rock Engineering

S162 **2ND International Conference 2024 Southern African Rare Earths**

S163 **2ND Battery Materials Conference 2024**

S164 **Hydrometallurgy Conference 2024**

S165 **Environmental Social Governance Sustainability Conference 2024**

S166 **MineSafe Mine Health and Safety Conference 2024**

S167 **Mintek@90 Conference 2024**

S168 **Mine Closure Conference 2025**

S169 **2ND Southern African Hydrogen and Fuel Cell Conference 2025**

S170 **9TH Sulphur and Sulphuric Acid Conference 2025**

S171 **4TH Digital Transformation in Mining Conference 2025**

S172 **AfriRock 2025 Pioneering Progress Conference**

S173 **Thirteen International Heavy Minerals Conference 2025**

S174 **International Mineral Asset Valuation Conference 2025**

S175 **Geometallurgy Conference 2025**

Published by The Southern African Institute of Mining and Metallurgy
Minerals Council South Africa, 7th Floor, Rosebank Towers, 19 Biermann Avenue, Rosebank, 2196
Republic of South Africa

© The Southern African Institute of Mining and Metallurgy, 2025

ISBN 978-0-6398820-5-5

The papers in this volume have been for the most part prepared from Word documents supplied by the authors, with additional typesetting and formatting by The Southern African Institute of Mining and Metallurgy.

Organising Committee

B.S. Xakalashe, Conference Chairperson
M.A. Mello, Co-Chairperson

R.T. Jones
S.M. Rupprecht
M.A. Mello
E. Townshend
I.P. Dikgwatlhe
H. de Hoop
G.L. Smith
I.J. Geldenhuys
S. Louw
N. Patterson
A. Majavu
G.Mulder
G.R. Lane

The Organising Committee would like to thank the reviewers listed below for the efforts in the reviewing process

I. Barker
C. Bergmann
H. Bornman
A. Cherkaev
T. Chiya
P. den Hoed
H. de Hoop
M. Erwee
E. Ford
I.J. Geldenhuys
X.C. Goso
R.T. Jones
J. Kabangu
G. Kornelius
G.R. Lane
N. Lameck
S. Louw
A. Majavu
M. Malibongwe
L. Masikini
T. Masinga
M.A. Mello
T. Moodley
G. Mulder
S. Ngwenya
N. Patterson
S.M. Rupprecht
M. Safari
M. Saffy
W. Shipman
G.L. Smith
S. Swanepoel
C. Sweet
A. Tapfuma
L. Wentzel
M. Woodhall
B.S. Xakalashe

Desktop prepared by Camera Press, Johannesburg

FOREWORD

Building on the success of previous events since its inception in 2004, the Platinum Conference Series continues to address the challenges and opportunities facing the global platinum group metals (PGMs) industry. As the sector faces increasing demands, from technological innovation and decarbonisation to cost management and market volatility, the 9th International PGM Conference offers a critical platform for addressing these challenges head-on. The main theme for the conference is 'PGMs – Enabling a Cleaner World'; the conference seeks to drive competitiveness, relevance and self-determination of the PGM industry through strategic positioning. Guided by an expert Organising Committee and informed by insights from the industry, this year's conference will delve into various topics designed to spark meaningful dialogue to drive innovation at every level of the PGM value chain and maintain competitiveness in a rapidly changing global landscape. Attendees can expect high-quality technical papers and presentations, robust networking opportunities, and strategic insights that help shape the future of the industry. Now more than ever, the PGM industry needs fresh ideas, collaborative partnerships, and forward-thinking strategies to remain relevant. Whether you're an academic, industry professional, sponsor, or policy leader, your participation will contribute to a dynamic exchange of expertise and solutions that can safeguard the sector's long-term success. Join us as we explore cutting-edge developments, address the industry's most pressing issues, and shape a sustainable, competitive future for the PGM industry. Be part of this dynamic event and help shape the future of the platinum and PGM sector. We look forward to your participation to ensure that this conference continues to be the premier platform for exchanging knowledge, ideas, and best practices in the PGMs space.

B.S. Xakalashe
Chairperson: Organising Committee
M.A. Mello
Co-Chairperson: Organising Committee

Contents

Page No

Platinum's strategic positioning and economic importance in South Africa
A.A. Mkonde, I.P. Dikgwatlhe 1

The use of ultrasonic atomisation methods to produce PGM and alloy powder for 3D printing at Mintek
D. Mkhonto, K. Dyal Ukabhai, L. Mampuru, R. Diale, M.J. Phasha, S.J. Moema 13

Powder production of pre alloyed PGMs for jewellery applications
K.D. Ukabhai, D. Mkhonto, L. Mampuru, R. Diale, M.J. Phasha, S.J. Moema 27

Decarbonising the Platinum Group Metals value chain to lower the carbon footprint of energy transition technologies
D. van Wyk, S. Thakurdin 35

Implementation of high frequency power supplies and dual flue gas conditioning in particulate matter abatement in the PGM industry
B.P. Havenga, E. Eichler, H. Heller 49

Quantitative spectroscopic analysis of co-existing Platinum Group Metals (PGMs) and iron matrix
T. Ncedo, A. Mkhohlakali, R. Letsoalo, J. Sehata, H. Mabowa, N. Ntsasa, J. Tshilongo 61

Quantification and mineral association of rhodium in low concentration ores using inductively coupled plasma-optical emission spectrometry
R. Letsoalo, A. Mkhohlakali, J. Sehata, N. Ntsasa, J. Tshilongo 69

Comparison of dissolution methods for ICP-OES analysis of PGMs from printed circuit boards
A. Mkhohlakali, J. Sehata, N. Ntsasa, R. Letsoalo, M.H. Mabowa,J. Tshilongo 77

The Integrated mine of the future: How five global trends are driving integrated and intelligent mining operations
C. Bleazard, M. Dwyer 89

Improved control of an electric arc furnace in a PGM smelting operation
J. Siecker, J. van Rensburg, L Mathevula, N. Wanblad, N. Kotze, L. Mukengeshayi 97

Comparative study of the interaction of alumina-chrome refractories with PGM smelter slag
N. Fotoyi, Y. Thakurdin, X.C. Goso, D. Chetty 107

Factors influencing campaign life of PGM furnace hearths
M. Nagorski, M. v.d. Merwe, G. Mulder, M. DeGorter, T. Kingsley 127

Challenges in crucible- and pilot-scale refining of a PGM-bearing iron alloy
M.S. Moholwa, S.P. Tsebe, E. Matinde 139

Evaluation of an alternative furnace cooling medium for enhanced operational safety
K.C. Maluleke, H. Joubert, P. Jonker, G. Tawane, X.C. Goso 153

Optimising reverts addition in PGM smelting: Strategies for enhanced furnace stability and efficiency
C. Sikiotis, G. Mulder, J. Bezuidenhout, S. Matutu, T. Sisya 167

Reductive matte smelting of UG2 concentrate using Al, FeSi, and SiC reductants
S.B. Nkosi, X.C. Goso 179

Commissioning the Zimplats smelter expansion
M. Crafford, M. Monobe, G. Erasmus, S. Matuta 195

An overview of Mintek's pyrometallurgical research in PGM processing: From conceptualisation to demonstration
X.C. Goso, S.P. Tsebe, B.S Xakalashe, E. Matinde 209

The influence of impellor geometry on stirred media mill performance
C. Lekgoro, S. Nkwanyana, N. Lameck, I. Govender, T. Moodley, M. Ramakokovhu 225

Comminution behaviour of the middle group ores
P.C. Siwela, M.M. Ramakokovhu, M.L. Teffo 235

Improving PGM recovery through optimised solid liquid separation
M. Hove, N. Nhleko, T. Moretsele, S. Mhlongo, K. Tshenye, C. Mtileni 249

Investigating the impact of stirred milling to improve the fineness of the grind for PGM tailings reprocessing - IsaMill case study
K.I. Mohapi, M. Becker, K.C. Corin, D. Makhubele, T. Pienaar, A.N. Mainza 259

Blower system energy cost improvement in platinum group metalconcentrators
H. Janse van Vuuren, W.H. Sterrenberg, J. Siecker, J.H. Marais 271

Revisiting the role of pH modifer and process water ions in platreef Cu-Ni-PGM ore flotation: What's the matter with choosing a pH modifier?
M.S. Manono 285

Beyond recovery: Rethinking reagent strategies for sustainable middle group ore processing
P.C. Siwela, M.M. Ramakokovhu, M.L. Teffo 297

Automated statistical anomaly detection in an integrity- monitoring application for a furnace
T. Moodley, W. Smith, J. Yelland 309

Comparison of technical operating flexibility and operating cost performance at selected underground platinum mines for long-term operational viability
B.M. Grobbelaar, C. Musingwini, L.J. Mohloki, B. Mutandwa 323

Optimisation of proportional influence of mining and processing costs on the production of an open pit mine
R.G. Thage, F.K. Mulenga 335

The impact of data quality on budget development and reporting in mining operations
Z. Mqoqi, H.P.R. Joubert, J.H. Marais 349

Improving compressed air system efficiency using Life of Mine planning
Q.A. Bekeur, J.H. Marais, P. Burger 361

A method to reduce compressed air usage through half-level control and usage scheduling
W. Bekker, J.H. Marais, W.H. Sterrenberg 373

Energy savings achieved through compressed air control valve control
W. Biermann, J. van Rensburg, T. Deysel, I. Rudolph, L. Mukengeshayi 383

Evaluating water performance on platinum mine shafts using a benchmarking technique
J. Korkie, J.H. van Laar, A.G.S. Gous, C.S.L. Schutte 395

In stope water handling strategies to achieve a dry mine
L.N. Senda, J.F. van Rensburg, J.C. Vosloo, S.M. Sithole, K.P Petja, D.N. Morare, N. Bandi 409

Time, water and energy to clean a stope panel using water jetting
P.D. Fraser 423

Automating energy baseline development for energy-intensive mining systems in South Africa
N.T. Tshitenge, J.A. Swanepoel, J.H. Marais, H.P.R. Joubert 437

The organisers of the conference thanks the following sponsors for their support

CORPORATE PARTNER SPONSORS

SAIMM CORPORATE PARTERSHIPS

IMPLATS EXCELLENCE IN PGMs

Sibanye Stillwater we are one

Valterra PLATINUM

srk consulting

UKWAZI we do mining

SOUND MINING

SPONSORS

AECI MINING CHEMICALS

BLUE NICKEL Unique solutions in the processing industry

ENPROTEC

EX MENTE

HATCH

INTOCAST

LESEDI ENERGY ENGINEERING

METIX SMS group

MINTEK A global leader in mineral and metallurgical innovation

NWU

oculus an EGROUP company

Qotho Minerals Proficiency Testing - Reference Materials

RST A Siyanda Group Company

StoneThree The Future of Work. Now.™

SYLVANIA METALS (PTY) LTD

tenova PYROMET

UKWAZI we do mining

Valterra PLATINUM

Platinum's strategic positioning and economic importance in South Africa

A.A. Mkonde, I.P. Dikgwatlhe

University of South Africa, South Africa

South Africa's strategic importance in the global platinum market is further underscored by the government's declaration of platinum as a strategic mineral. This policy decision, coupled with the nation's significant share of the world's production and reserves, and its production of 70-80% of the world's platinum supply, solidifies its leading position in the industry.

Platinum's economic impact is profound, influencing industrialisation, investment, and the advancement of alternative technologies. Its use in various sectors, from jewellery, automotive to renewable energy, drives demand. However, factors such as political instability, price fluctuations, water, electricity, infrastructure and electric vehicles pose risks to its strategic status.

The paper aims to develop a model to position platinum and enhance its economic importance strategically. Analyses of data patterns, economic effects, mining output reserves and resources, operational efficiencies, policy framework effects, and SWOT and PESTEL were considered. Key findings include critical importance to high-tech industries, resource endowment, economic and energy security, international and national interests, socio- economic contribution to GDP, exports, employment, industrial and technological inputs, taxes and foreign investment, which lead to strategic importance and positioning.

The framework promotes and positions platinum as a strategic mineral in South Africa. Some parameters of the model are strategic and economic drivers, international collaboration, private partnerships, educational awareness, employee upskilling, research initiatives into new applications and utilisation of platinum. The model ensures that all stakeholders strategically position platinum and enhance its economic importance, including equal benefit- sharing in all sectors of the economy.

Keywords: Platinum, strategic mineral, economic importance, energy

INTRODUCTION

Platinum is one of the planet's rarest metals, and its extraction on Earth can be challenging and laborious for the mining industry. The platinum group metals (PGMs) include platinum, palladium, rhodium, iridium, ruthenium and osmium. Each year, less than 200 tons of these metals are mined (U.S. Geological Survey, 2022) using open-pit and underground operations to extract the PGMs. PGMs, ni*ckel, copper, and other metals are extracted from polymetallic sulfide ores in the mines. Following processing, refined PGMs and other by-products are extracted from these ores. Mining to refining is integrated, thus the majority of PGM miners maintain significant processing (Ndlovu, 2023).*

Table 1. Applications and uses of PGMs (After International Platinum Group Metals Association 2017)

PRODUCT	PGM	APPLICATIONS
Automobiles	Pt,Pd,Rh,Pt,Pd,Ir Pt, Pd, Ru	Pollution control catalyst Spark plugs Engine control sensors, airbag initiators Electronics for engine management systems
Electronic equipment	Pt, Pd, Ru, Ir	Connectors, printed circuits, and resistors capacitors, lasers
Computers	Pt, Ru	Thin layer in hard disks to increase memory storage capacity
Jewellery	Pt, Pd, Rh	Rings, chains, pendants, watch cases and straps
Glass and ceramics	Pt, Rh	Glass fibre, display glass, optical glass, ceramic glass, tableware decorative patterns and finishes
Medical and biomedical	Pt,Pd,Rh,Ru,Ir,Os	Antitumor drugs, implants, and treatments for heart disease Cancer screening
Chemical and petroleum	Pt, Pd, Rh, Ru, Ir	Plastics, polyester, pharmaceutical ingredients, high-octane gasoline fertilisers and explosives, silicones
Aircraft engines	Pt	Turbine blades, spark plugs
Dental restorations	Pt, Pd, Ru, Ir	Dental inlays, crowns, and bridges
Fuel cells	Pt, Ru	Electric vehicles, standby and auxiliary power domestic power and heating

As seen in Table 1, PGMs today are used in a wide range of industrial settings, such as catalytic converters, laboratory apparatus, electrical contacts and electrodes, the glass and chemical industries, medical equipment, industrial applications, hydrogen fuel cells and jewellery (International Platinum Group Association, 2017). As listed above, utilisation in various sectors increases the demand for PGMs. South Africa has made significant global contributions to PGMs, gold, diamonds, manganese, coal, iron ore, and chrome. It has most of the platinum and manganese resources in the world (Department of Mineral Resources and Energy, 2018).

The two large, well-known complexes in Southern Africa are the Great Dyke in Zimbabwe and the Bushveld Complex in South Africa. The largest and most economical is the Bushveld Igneous Complex (BIC), estimated at 66,000 km². Platinum in South Africa is found within the BIC, which hosts approximately 80% of platinum-bearing ore in the northern portion of South Africa. It is the world's most considerable layered intrusion. The intrusion is divided into four limbs, namely western, eastern, northern and southern limbs as indicated below in the platinum operations (Figure 1).

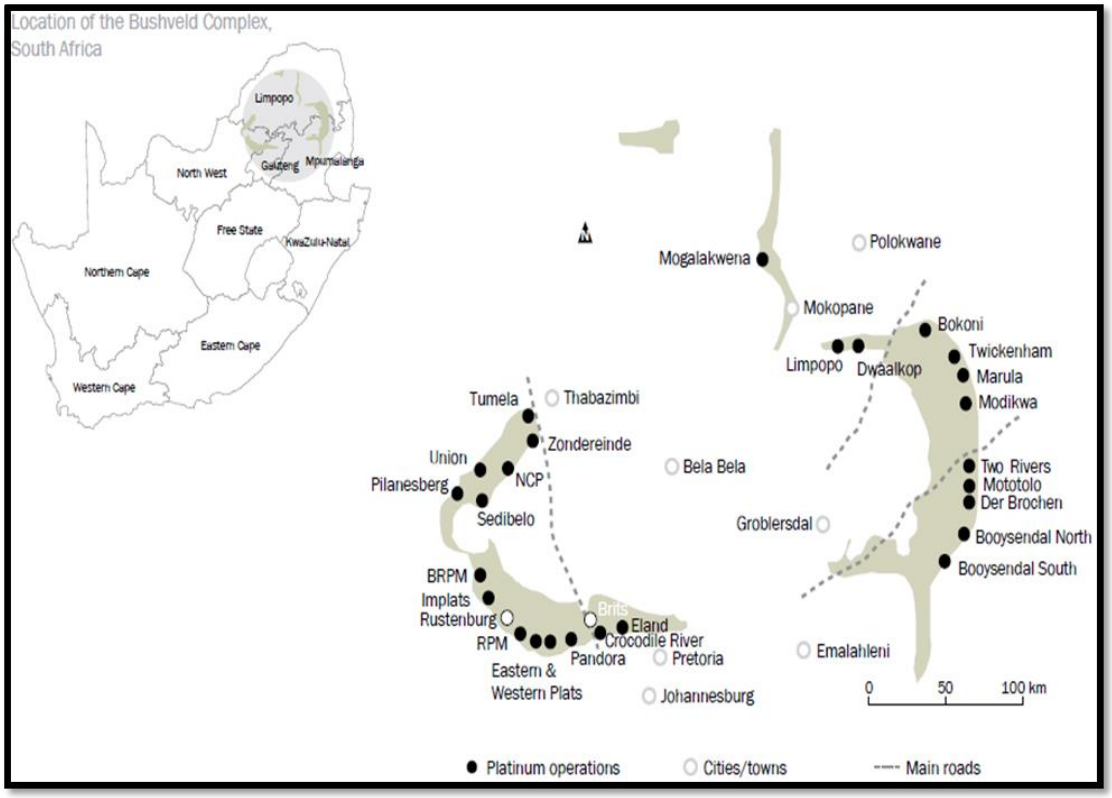


Figure 1: Bushveld Complex showing the limbs (after MCSA).

The paper takes a comprehensive approach to critically analysing Platinum's significance, strategic opportunities, risks, and economic importance in South Africa. A multi-layered, mixed-method quantitative metric was used to evaluate the strategic positioning of platinum. The review of platinum's strategic role and economic importance was conducted using both qualitative and quantitative analysis. The paper also considered data from statistical sources regarding platinum's economic and employment contribution in the country, as well as data patterns, economic effects, mining output reserves and resources, operational efficiencies, and the policy framework effects. SWOT and PESTEL analyses were applied to establish platinum as a strategic mineral. The paper also develops a framework for strategic positioning and economic importance with clear parameters and provides policy recommendations. Case studies and examples of challenges experienced in the different operations and communities in the platinum industry were assessed and evaluated towards positioning platinum as a strategic mineral in the country.

Strategic positioning of platinum

The status of a mineral and its dependency are affected by mineralised ore deposits, location, proximity to cheaper energy resources, distance to the market, low-cost labour, and industrial demand, as well as adverse effects of higher energy costs and environmental restrictions. The industry should be competitive, sustainable and environmentally responsible for platinum to remain strategic. South Africa hosts the majority of the global reserves of platinum. The major producer gives the country leverage and a good strategic position globally. The country dominates the market share of the PGMs and is the top exporter of platinum.

South African companies continue to review mining strategies to remain relevant and competitive and improve production quantities. This is noted in the unbundling and changes in different platinum mining companies, such as Anglo-America and the introduction of Valtera.

Most developed and developing countries listed platinum as a critical mineral and have developed strategies to source it from producing countries (USGS, 2025). This places South Africa strategically positioned for supply, partnerships and trade agreements.

Strategic opportunities and risks are critical for positioning platinum as a strategic mineral according to the issues identified in a SWOT analysis (Table 2). The government has listed platinum as a strategic mineral (Department of Minerals and Petroleum Resources, 2025) and promotes the development of the hydrogen economy. Government has endorsed initiatives from Hydrogen South Africa (HySA) (Moumakwa, 2013). The hydrogen economy presents an excellent opportunity for the country in the downstream value chain, such as beneficiation and industrialisation. It will counter the over-reliance on the export market and the high value of exported raw material. This will result in job creation to address the triple challenge of poverty, inequality, and unemployment experienced in the country.

Table 2: SWOT analysis of platinum

SWOT ANALYSIS - STRATEGIC FACTORS OF PLATINUM - SOUTH AFRICA	
STRATEGIC OPPORTUNITIES	
STRENGTHS	**OPPORTUNITIES**
Largest reserves in the world	Hydrogen economy
Leading producer in the world	Industrialisation and technology innovation
Leading exporter (global market share)	Downstream value chain development
Platinum is a critical mineral for green technologies	Demand for cleaner energy
Platinum is a strategic mineral for technology development	Job creation
Platinum is listed as a strategic mineral (including other countries)	Strategic partnerships
High economic and social contribution to the country	Global exporting opportunities
STRATEGIC RISKS	
WEAKNESS	**THREATS**
Infrastructural development	Energy crisis
Insecurity of energy supply	Labour strikes
Heavy reliance on the export market	Market shifts and price volatility
Inability to reach stable and lasting labour agreements	Rising community tensions
High production costs	Substitution and recycling
Deep-level mining	Geopolitical challenges

The demand for platinum for green energy, changing technology, and continued pressure of global environmental policy on climate change (emissions standards, etc.) are the key drivers towards positioning platinum as a strategic mineral in the country.

Several weaknesses and threats are facing the industry, which can negatively affect the strategic position of the platinum industry (Table 2). The challenges include ageing and underdeveloped infrastructure (poor rail infrastructure and logistics challenges), unstable and expensive energy supply, high production and labour costs, reliance on export market, deeper ore deposits and unpredictable labour force response during difficult economic times. Rising community tensions, labour strikes, price and market changes, possible substitution and recycling, trade wars, and geopolitical challenges threaten platinum's stability and strategic position in the global market. Mining is labour-intensive in the country and requires a sufficient energy supply. Any situation of an energy crisis will impact production and operational costs.

Furthermore, analysing political, economic, social, technological, environmental, and legal factors is crucial for platinum's strategic positioning and economic importance (Table 3). The geopolitical challenges experienced in the world, such as the Russia-Ukraine war, affect the stability of supply

and demand. The platinum industry requires a stable legal framework, which can be facilitated in the Mineral and Petroleum Resources Development Act (MPRDA, 2002). Legal protection for mining tenure and compliance with international laws ensure certainty in the regulatory environment. Government initiatives and incentives in the policy framework promote local beneficiation, industrialisation and employment.

The platinum industry is one of the major contributors to employment and investment. Global demand is presenting long-term growth opportunities for the industry. A growing demand for environmental, social, governance and sustainability (ESGS) compliance drives towards inclusive growth, favouring equitable economic distribution to communities and sustainable mining practices. In addition, a demand for cleaner technology is an opportunity for green technology innovation and improved expertise in deep-level mining, downstream value chains and digital technology.

Table 3: PESTEL analysis of the platinum

PESTEL ANALYSIS- STRATEGIC FACTORS OF PLATINUM	
POLITICAL	**ECONOMIC**
Stable legal framework	GDP and exports
Conducive policy environment	Foreign investment
Clear ownership rules from the government	Tax revenue
Promotion of beneficiation and industrialisation	Royalties
Labour strikes and community tensions	Diversification
Trade agreements	Price volatility
Geopolitical issues	Operational and labour costs
	Supply and demand factors
SOCIAL	**TECHNOLOGICAL**
Increased employment and improved livelihoods	Mining expertise and technology
Social benefits for the communities	Exploration, research and innovation
Impacts of automation and mechanisation	Industrialisation and beneficiation
Lack of training and skills development	Smart mining - automation and digitalisation
ESGS awareness and compliance	
ENVIRONMENTAL	**LEGAL**
High water and electricity usage	Legal and policy framework
Land use and degradation	Land claims and community rights
Pollution and emissions control	Labour laws
Sustainability compliance and reporting	Licensing and environmental compliance

Platinum is a crucial mineral for the energy transition and its socio-economic impact. Industrialisation, the investment market, and the advancement of alternative technologies are all significantly impacted by platinum. Considering the significant opportunities presented by local and global demands, mining constraints and challenges are not insurmountable.

Economic importance

Minerals are important in their application, use, and potential for mining production, demand, and supply. Consequences of the lack of supply and demand will result in a dire situation for the nation's economy and security, including the social well-being of the society. Market forces such as the demand and supply alone cannot provide control and optimal utilisation of strategic minerals. Some form of government action is required. The South African government has declared and classified platinum as a strategic mineral.

The mining sector's contribution is important to the country, totalling 6.0% of the Gross Domestic Product in 2024. Table 4 shows the contribution in 2024 according to the factors such as employment, employee earnings (wages and salaries), royalties, production and sales (Minerals Council, 2024).

Other contributions include foreign exchange, investment, foreign savings, corporate tax, operational and capital expenditures, Transnet's rail and port, electricity generation, electricity demand (consumption) and liquid fuels.

Table 4: Economic contribution of PGMs in 2024

ECONOMIC CONTRIBUTION OF PLATINUM GROUP METALS	
Contributing factor	**2024**
1. Direct Employees	173,424
2.Employee Earnings (R billion)	76.8
3. Royalties (R billion)	3.6
4. Production (Tonnes)	256.5
5. Total Sales (R billion)	173.1

Today, PGMs are used in various industrial settings, such as catalytic converters, laboratory apparatus, electrical contacts and electrodes, the glass and chemical industries, dental equipment, and jewellery (International Platinum Group Association, 2017) (Table 1). As listed above, utilisation in various sectors grows the demand for PGMs locally and globally.

Global metal consumption, including PGMs, is expected to soar in the near future to achieve net zero emissions by 2050 (Berahab 2022); (Hund *et al*., 2020); (Watari et al. 2020); (Watari *et al*., 2018); (International Energy Agency 2021); (World Bank 2021). The enormous potential demand for fuel cell and green hydrogen vehicles could cause the demand for platinum to increase 240 times globally by 20250 (Li *et al*., 2023). Meanwhile, the energy transition will have a more modest contribution to the growth in PGM demand (Boer *et al*., 2021).

Investment and price fluctuation

In the commodities and financial markets, PGM prices are important factors. Investors in the mining industry accept high levels of risk in the hope that businesses will be able to produce sizable capital gains and cash distribution during brief boom periods, as opposed to lower-risk investments in less volatile industrial or utility stocks, which are the primary focus of studies in company financialisation. According to De Los Reyes (2017) and Parker (2018), "rapid extraction of large volumes of resources becomes a primary driver of firm strategy" during such booms.

Since the early 2000s, precious metals like gold and platinum have seen a sharp price increase, but since 2012, there have also been fluctuations and a decline (Fig. 2). The financial viability of PGM companies has been under pressure since 2012 due to the fluctuation and decline in platinum prices brought on by a seismic shift in demand and businesses struggling with labour costs and protracted production-halting strikes (Baskaran, 2021). Furthermore, PGMs are susceptible to geopolitical risk (Das *et al*., 2019); (Cheng *et al*., 2022); (Smales *et al*., 2020), and if the price of PGMs fell below the cost of extraction, the high expense of the mining process could result in losses.



Figure 2. Gold and platinum prices from the World Bank Commodity Price Data (2021).

The capital intensity of production and lengthy lead times for new capacity, in addition to the highly cyclical demand for minerals, result in low price elasticity of supply in most mineral-commodity categories (Runge, 1998). This generates the possibility of price spikes due to undersupply and protracted price declines when a glut is produced by too-optimistic capital expenditure. The ability of mining corporations to expand and manage these variations is mediated by access to and control over reserves. In order to avoid overexploitation of current reserves, companies should ideally consolidate control while continuously pursuing access to new reserves (Bridge, 2008; Fine, 1994). The government and communities that already possess rights to lands and resources are unavoidably brought into contact with these mining companies through this 'search for access,' and they exert distributional pressure on these mines by requesting rents and royalties.

Challenges affecting the platinum industry: Case studies

The industry saw notable booms and slumps from 1932 until 1957. Between 1953 and 1957, advancements in oil production significantly decreased the amount of platinum required for catalytic converters. However, platinum experienced a period of consistent employment development until 1973 following the 1957 crisis. The increased demand for hard assets after the 1973 oil crisis contributed significantly to the global demand for platinum mining. These incidents are an early reminder that platinum is sensitive to outside pricing forces.

During the commodities boom of the 2000s and the ensuing period of volatility and slump from 2009 to 2016, the three largest PGM mining companies at the time financialised their management strategies (Erturk *et al.*, 2008; Fligstein and Shin, 2007; Froud *et al.*, 2006; Lazonick, 2010; Morgan, 2014). Pressure to maximise shareholder value during the boom years led to costly expansion, mergers, and acquisitions expenditures, balance sheet engineering, and big cash payments to investors. Thus, the 'super-cycle' of platinum led to a rise in risk-taking by significant institutional investors, stock market experts, and corporate management, increasing capacity and financial fragility, which have worsened the effects of the slump.

The 2012 Marikana massacre, in which the South African police force shot dead 34 striking Lonmin workers, was the worst single incident of state killing since the 1960 Sharpeville massacre. Continuing demands for a 'living wage' resulted in a five-month strike by mine workers in 2014,

the longest in South African history. Labour strikes and wage disputes affect the industry.

The mining industry is energy-intensive, so the insecurity of the electricity supply will be a significant challenge. Other factors affecting the industry are Transnet's logistics challenges and ageing infrastructure, deeper and decreased quality ore grades, climate change requirements, land rights, environmental degradation, water pollution, demand shifts from the market to electric vehicles, and substitution and recycling.

DISCUSSION

T

he strategic relevance and economic importance of platinum enhance its position locally and internationally. Some countries aim for mineral independence and craft strategies to source platinum from producing countries. These countries have classified platinum as their strategic mineral and have included it in their Critical Material or Metal List. There is an increase in the demand for platinum from 2014 to 2024 from the top five destination countries for export (Table 5). Considering its global status, South Africa has leverage in pricing, trade agreements and strategic partnerships.

Table 5: Top five destinations of platinum from South Africa

TOP 5 PGM IMPORTING COUNTRIES		
COUNTRY	QUANTITY(TONNES)	
	2024	2014
1. United States	71.1	40.6
2. Japan	67.5	57.0
3. United Kingdom	56.2	38.0
4. Germany	26.8	12.3
5. Hong Kong	25.8	23.4

The critical parameters in the position are strategic opportunities and risks, economic drivers and challenges, and enablers from private and public partnerships (Table 6). These are significant drivers in the model supported by regulatory and environmental compliance and reporting. Adherence to implementing environmental, governance, social and sustainability requirements solidifies the framework.

Table 6: Proposed framework for strategic positioning of platinum

STRATEGIC POSITIONING AND ECONOMIC IMPORTANCE OF PLATINUM IN SOUTH AFRICA		
	INPUTS	
STRATEGIC POSITION		**ECONOMIC IMPORTANCE**
Largest reserves	**ENABLERS**	Contribution to GDP
Leading producer	**Private & Public partnerships**	Contribution to export market
Major global supplier	**Strategic partnerships**	Foreign investment
Geopolitical significance	*Mining companies*	Tax revenues & taxes & royalties
Geopolitical leverage	*Communities*	Employment
	Employees	
Energy supply risk	*Government*	Price volatility
Mining constraints	*Investors*	Shifting demand patterns
Technology changes		Supply shortfall
Geopolitical instability		Retrenchments - job losses
Ownership & licensing		Demand substitution
REGULATORY AND ENVIRONMENTAL COMPLIANCE & REPORTING		
E - NVIRONMENT S - OCIAL G - GOVERNANCE S - USTAINABILITY		
	OUTPUTS	
BENEFIT-SHARING WITH ALL STAKEHOLDERS		
Resource endowment	Infrastructure development	Hydrogen economy
Global supply leadership	Beneficiation & industrialisation	Jewellery market
Cleaner energy demand	Expertise & skills & training	Automotive market
Industrial demand	Job creation	Labour market dynamics
Technology demand(PEM)	Community trusts & co-operatives	Infrastructure investment
Investment demand	Green technology	Employment
Export demand	Energy security	Supply & trade concentration
Regulatory environment	Investment (coins & ETFs & bars)	Circular economy
PLATINUM AS A STRATEGIC MINERAL		

The regulatory environment and policy implementation are critical to ensure value addition downstream for beneficiation and industrialisation. This can be achieved through local investment in manufacturing, the jewellery market, and the hydrogen economy, as well as support for creativity and innovation in Hydrogen South Africa (HySA) and infrastructure development as listed earlier from government publication. It is important to take advantage and reduce risks related to ESGS-compliance, job losses due to mechanisation and automation, and minimise too much dependence on the export market by growing alternative domestic market opportunities (e.g., jewellery, hydrogen economy, clean energy technologies, etc.)

Resource endowment, geopolitical leverage, strategic drivers and demand growth, market growth and opportunities, socio-economic and investment opportunities, value addition and stakeholders' collaboration and partnerships form the basis of the outputs in the framework. All these factors lead to a comprehensive benefit-sharing framework with all stakeholders, strengthening the position of platinum as a strategic mineral in South Africa.

CONCLUSION

South Africa is the leading producer and exporter, with the world's largest reserves critical for strategic positioning and economic importance. The strategic opportunities, such as energy transition, climate change and global demands for sustainable development, favour the country. Some challenges and constraints, such as infrastructure and energy supply can be addressed, especially considering government support by declaring platinum as a strategic mineral.

The multifaceted importance of platinum, considering its economic contributions, global market dynamics, policy formulation, economic planning and strategic positioning, results in comprehensive benefit-sharing with all stakeholders. Global trends in relation to emissions, carbon footprint, cleaner energy, green hydrogen incentives, and sustainability will influence the demand for platinum. This gives South Africa an excellent opportunity to develop a thriving economy through a clear strategic policy, beneficiation and industrialisation, effective governance and community development for global economic and strategic positioning.

REFERENCES

Baskaran, G. 2021. Firms' approach to mitigating risks in the platinum group metals sector. Mineral Economics 2021(34):385–398

Berahab, R. 2022. The energy transition amidst global uncertainties: A focus on critical minerals. Policy Brief - N° 37/22.

Department of Minerals and Petroleum Resources, South Africa (2025): Critical minerals and metals strategy South Africa.

Department of Mineral Resources, South Africa (2019): South Africa's Mineral Industry. https://www.dmr.gov.za

Chaskalson, R. 2016.The road to Marikana: Transformation in South Africa's Platinum industry, 1994-2012. *Journal of Southern African Studies*. 42. 5. 857 -873

Edward, A., and Silk, M.H. 1987. Platinum in South Africa: A concise account with an examination of the outlook for producers during the 1990s. Council for Mineral Technology, Johannesburg. 11 – 19

Hund, K., Porta, D.L,. Fabregas, T.P., Laing, T., and Drexhage, J. 2020. Minerals for Climate Action: The Mineral Intensity of the Clean Energy Transition. International Bank for Reconstruction and Development/The World Bank.

International Energy Agency, 2021. The role of critical minerals in clean energy transitions. World energy outlook special report. May 2021.

International Platinum Group Association, 2017. Safe Use of Platinum Group Metals in the Workplace. Workplace Guidance Document.

Li, P., Liu, Q., Zhou, P., and Li, Y. 2023. Mapping global platinum supply chain and assessing potential supply risks. Front Energy Res 11:1033220

Minerals Council of South Africa (2024). Annual Report.

Moumakwa, D. O,. 2013. Fuel cells and the future role of South Africa though its platinum resources. Department of Mineral Resources: Mineral Economics. Report R99

Ndlovu, J. 2023. Anglo American: Overview of PMG processing. Available from https://www.anglamericanplatinum.com Accessed 2025

U.S. Geological Survey (2022) Mineral commodity summaries 2022. U.S. Geological Survey, 202 p.

U.S. Geological Survey (2025) Mineral commodity summaries 2025. U.S. Geological Survey. Draft List of Critical Minerals List.

Watari, T., McLellan, B., Ogata S., and Tezuka, T .2018. Analysis of Potential for Critical Metal Resource Constraints in the International Energy Agency's Long- Term Low-Carbon Energy Scenarios. Minerals 2018(8):156.

Watari, T., Nansai, K., and Nakajima, K. 2020. Review of Critical Metal Dynamics to 2050 for 48 Elements. Resour Conserv Recycl 155:104669

World Bank, 2021. Commodity Markets Outlook: Urbanisation and Commodity Demand. International Bank for Reconstruction and Development / World Bank.



Amanda Akhona Mkonde

Junior Lecturer
University of South Africa

Ms Akhona Mkonde is a Geologist by profession with experience in academic and scientific research. She started her career as an intern for South African National Biodiversity Institution and moved to the University of South Africa as a Technical Officer working in the Mining Engineering Laboratory. She has upgraded and developed Mining Engineering Laboratory at UNISA from a classroom state to a laboratory. She has also been involved in several Water Research Commission and National Research Foundation funded projects.

The use of ultrasonic atomisation methods to produce PGM and alloy powder for 3D printing at Mintek

D. Mkhonto, K. Dyal Ukabhai, L. Mampuru, R. Diale, M.J. Phasha, S.J. Moema

Mintek, South Africa

Additive manufacturing is a growing industry and there is need for new methods to produce spherical powders with a specific particle size distribution suitable for 3D printing in South Africa. While platinum group metals (PGMs) are important minerals in various applications including jewellery, intricate designs from their alloys that may be malleable could be difficult to achieve. This is where additive manufacturing and metal 3D printing in particular become crucial. It is thus necessary that better and more efficient methods for atomisation are implemented in order to produce suitable powder that also add value to PGMs produced in the country. Powders used in 3D printing are mainly imported and there are a times limited alloys available, leading to in-situ 3D printing. In this paper, we present powder production results from an ultrasonic atomisation method using the Amazemet rePowder machine. Recycled Ti-Al powder, 304L stainless steel wire and pure platinum were successfully atomised into spherical and narrow particle size distribution (PSD) suitable for laser powder bed fusion (LPBF) 3D printers and for sintering technologies. More than 80% of produced powders were found to be spherical and the compositions resulted as expected for the alloy material in 304L steel wire. The methods produced Ti-Al powder with PSD of d50 = 45 µm, 304L steel wire powder with PSD of d50 = 50 µm and for pure platinum, d50 = 35 µm. The platinum powder was tested for 3D printing and found to be flowing and produced continuous single tracks without satellites and good density. The results show that used metal powders can be recycled into useful powder in additive manufacturing; pre-alloyed metals, in this case 304L steel wire, can be produced into alloyed spherical powder and PGM materials. In this paper pure platinum as an example can be atomised to spherical powder, and all the produced powders are within PSD that is suitable for LPBF printers and sintering technologies.

Keywords: Ultrasonic atomisation, metal 3D printing, particle size distribution, particle shape, platinum group metals, jewellery, powder metallurgy

INTRODUCTION

Additive manufacturing is a growing industry and there is a need for new methods to produce spherical powders with a specific particle size distribution suitable for 3D printing in South Africa. The additive manufacturing technology and metal 3D printing can produce high volumes of intricate components and improve on lead time to production of parts. Platinum group metals (PGMs) are important minerals in various applications including jewellery, catalysts, glass manufacturing and high temperature shape memory alloys as well as in aerospace. South Africa produces significant amount of PGMs; thus, it is important to value-add near source. Metal powder production for additive manufacturing is crucial technology; thus, it is essential that better and efficient methods for atomisation are implemented.

South Africa is the largest producer of PGMs in the world, accounting for over 80%, and the largest producer of gold, manganese and chromium. Notably South Africa ranks high in production and reserves of titanium and, vanadium and zirconium [USGS, 2024]. Value addition and beneficiation of these minerals is of utmost importance, with additive manufacturing a key manufacturing technology in current developments globally.

Powder metallurgy plays an important role in additive manufacturing in producing the most important feedstock. These powders have to be in a particular form or shape and should be within a specific particle size distribution (PSD). In metal 3D printing, usually using laser powder bed fusion (LPBF) [Yap, *et al.*, 2015] machines, powder should be spherical and mainly have PSD of d50 = 60 µm and within a range of 20 µm to 60 µm depending on specific materials. For example, Seungkyun *et al.*, demonstrated that trimodal PSD is more suitable for selective laser melting or powder bed fusion additive manufacturing, because of its enhanced powder bed density and homogeneity [Seungkyun Yim, *et al.*, 2025]. Spherical powder and PSD are not only important for 3D printing but also in sintering technologies where a good mix between relatively coarse and fine powder is important. This means that factors as mentioned: PSD, shape/sphericity, chemical composition and density affect powder quality with roughness also affecting the flowability and surface finish [Chua, *et al.*, 2017; Lyckefeldt, *et al.*, 2013]. A mix of powders with large diameter flows readily compared to fine particles. However, larger particles sinter poorly, whereas particles with diameter less than 20 µm lead to more efficient sintering and higher density and also, nonspherical particles exhibiting low packing density than spherical particles ([Marczyk, *et al.*, 2023]. Furthermore, powder with a single particle size result in poor flowability because it lacks mix between finer and coarse particles to fill in the gaps, resulting in cohesive or sticky powder [Brika, 2020]. In situ 3D printing, while it can produce good products, results in segregation. At the same time, alloys with a very small percentage of alloying element may not distribute well in an attempt to have a homogeneous mix. Pre-alloying material before atomisation results in good homogeneity of chemical composition and thus improves melting dynamics relating to applied laser and produces higher densities, less defects and better corrosion behaviour [Qin, *et al.*, 2021]. Recycling of failed prints, scrap metal and used powder is crucial in the cycle economy in that it minimises material loss and promotes reuse. However, there is a need for proper and advanced methods of powder recycling and handling techniques or methods to maintain resulting powder quality, [Alex Lanzutti, *et al*, 2024] as well as effective strategies of powder management [Wu, *et al.*, 2018].

Powders used in 3D printing are mainly imported in South Africa and there are limited alloys available leading to in situ 3D printing at times. Generally, powder alloys are made using water or gas atomisation which are not without drawbacks. These methods result in oxidation of powder and moisture, mainly from the water atomisers, while particles may not be very spherical. Gas atomisers while good, may also result in non-spherical particles due to nozzle design and atomisation parameters and not all materials are suitable for it [Balasz, *et al.*, 2023]. A recent development in technology has been ultrasonic atomisation, which uses ultrasonic frequencies to produce powder. This technology involves melting of material that is poured or dropped onto a vibrating surface (sonotrode) at high frequency, which then disperses it into fine particles. This system uses a highly controlled inert environment to produce powder from different feedstocks: rods, buttons and wire, and can also be used to make alloys from elemental input materials. Using the induction and arc melting techniques, alloy ingots and spheroidal metal powder can be produced from pure or alloyed materials with low melting temperatures (up to 1300˚C in the induction) and high melting temperatures (up to 3500˚C in the arc system). Alloying of material from elemental powder followed by atomisation to alloyed spherical powders has been done before using the Amazemet re-Powder machine, for example by Moller *et al.*, where Pt84-Al11-Cr3-Ru2 superalloy was successfully investigated [Möller, *et al.*, 2022].

In this study results from ultrasonic atomisation of different feedstocks of materials at Mintek are presented. Starting with used Ti-Al powder, that is formed into a metal rod as feed stock first and 304L steel wire as continuous feed, the spherical powder with particle size distribution suitable for metal 3D printing is produced. This technology is embedded withing the Amazemet RePowder machine that was used to carry out the experiments. For both feedstocks (rods and wire), the 40 kHz sonotrode on which

arc melted material was dropped, has been used in an inert environment filled with argon gas to prevent oxidisation. Because the drive is to use the system for PGM atomisation and thus beneficiation in different applications including jewellery, this method was further used to atomise pure platinum. Metallurgical analysis of produced powder was done to determine composition, particle shape or sphericity and particle size distribution.

EXPERIMENTAL PROCEDURE

Atomisation was done in the arc chamber of the Amazemet rePowder system [Żrodowski *et al.*, 2021]. The machine has two systems: First is the induction system which can melt material using an induction furnace and atomise any alloy up to 1300°C melting point. In this system, molten material is atomised by bottom pouring from the crucible through a narrow nozzle that pours on to a vibrating plate at 40 kHz. The vibration is due to the plate being connected onto a transducer via a sonotrode. The plate then disperses the molten steam into a fine spherical powder. Second is the arc system. This uses an electric arc to melt any alloy with the arc tip reaching temperature in excess of 3500°C. From this system, alloys can be formed into buttons or rods that are used as feedstock for atomisation. Under high inert environment, this system minimises any contamination and oxidation. When making alloys, rotating of the sample is enabled by a manipulator jaw. That is; the sample can be rotated multiple times without opening the chamber. Rods are made by placing material on a rod forming copper hearth and a titanium oxygen getter placed on a slot. The chamber is closed airtight, and purged at least three times. Purging is done by attaining a vacuum of 3×10^{-4} bar in the chamber, then filled with argon gas with the process repeated three times. The arc is then ignited and the titanium getter melted. The getter is allowed to cool and when clean, melting of material starts. When the getter is coloured due to oxygen presence in the chamber, purging continues, and the process repeated till the chamber is clean of oxygen. Atomisation of the rods is done by mounting the rods on a rod holder, the arc is used to melt and drop onto a sonotrode which is subjected to ultrasonic vibration using a 20 kHz or 40 kHz frequency transducer and forms powder by dispersing the molten material into fine spherical particles. System purging is also done in a similar way like when, melting the material into rods to be used as feed stock for the atomisation process. In the arc system atomisation of material can also be done using a wire as feedstock.. Using a wire feeder, equipped with a controller for feed rate, the wire is melted on to a vibrating sonotrode which then forms powder from the molten material. Depending on the melting temperature and density of the material, a low heat or high heat maybe be required when atomising. This heat intensity can be adjusted using the current values of the arc. For our study, a current between 190A and 200A was sufficient for titanium-aluminum (Ti-Al) and 304L steel while a current between 200A and 260A was enough for pure platinum. The setup for melting and atomisation is shown in Figure 1.

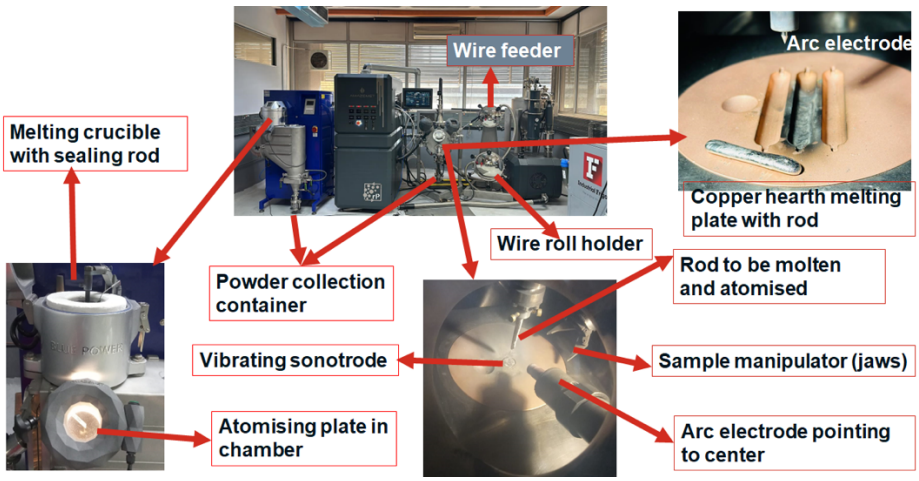


Figure 1. Images showing general setup of the Amazemet rePowder machine in which material is melted and atomised.

For this paper, the arc system was used to melt and atomise Ti-Al, 304L steel and platinum. Ti-Al rods were made from used Ti-Al powder (recycling of Ti-Al powder), and these were used as feedstock for atomisation. The compacted Ti-Al powder was placed into the chamber on the rod forming copper hearth (Figure 1) and formed into rods through the process shown in Figure 1. The rods were used as feedstock for atomisation by placing on a rod holder and molten using the arc electrode onto a vibrating sonotrode using a 20 kHz transducer. The 20 kHz transducer gives a bigger yield of finer particle size distribution than a 40 KHz. This means that using a 40 kHz transducer will result in a wider range of particle size distribution (PSD) with more concentration on the bigger size [Żrodowski *et al.*, 2021]. However, a fine PSD can be attained by re-atomisation of coarse particles which is done by following the same process of forming rods and atomising.

Pure platinum material from ingots was melted on the rod forming copper hearth to form rods that were used as feedstock for atomisation. This was done by mounting the platinum rods on the rod feeder and molten onto a sonotrode vibrating at 40 kHz to form spherical particles. And finally, Steel 304L steel wire was fed through the process described above and melted onto a sonotrode vibrating a 40 kHz to form spherical powder.

The formed powder was then sieved with 75 μm sieves and the powder analysed using a scanning electron microscope (SEM). That is, the powder was mounted on conductive tape and analysed using SEM to get secondary electron (SE) images and the composition determined using energy dispersive X-ray spectroscopy (EDS) detector. To determine the PSD and shape the powder was cold-mounted in clear resin and analysed using Tescan Integrated Mineral Analyser (TIMA) on the SEM.

RESULTS AND DISCUSSION

We present results following the process of melting and atomising different materials using the Amazemet rePowder machine at Mintek. The aim of this paper was to develop the process of atomising PGM minerals for production of spherical powder suitable for metal 3D printing in LPBF machines. These metal 3D printing machines require spherical powder and specific particle size distribution. The results of melting and atomising Ti-Al, 304L steel wire and pure platinum are presented.

Ti-Al Powder:
Figure 2A shows the image of the used Ti-Al powder to be recycled that was melted into rods (Figure 2B) and atomised into powder (Figure 2C). The particles of Ti-Al are spherical with minor irregular shapes. These irregular shapes are as a result of high temperature molten material that at times lead to particles landing uncooled and deformed. Often these irregular shapes within the specified particle size range would be due to knocking among other particles and fuse or knocking on the walls of the chamber and deform. The resulting powder has been washed with ethanol in an ultrasonic bath to get rid of soot. Soot and ash are formed from the material due to the high temperature of the arc tip (+3500°C) compared to materials being atomised. Depending on the intensity of the washing process, particles may result in minor black spots as seen in the high-resolution particles in Figure 2D. The spherical nature of the particles means these are suitable for use in LPBF metal 3D printing because they will flow and thus result in homogeneous layers with good density of the materials. The LPBF result in complete melt of metal powder and thus density and homogeneous metal part is attained [Olakanmi, E.O. 2015]. This is important because homogeneous laser melted layers, and high density will minimise residual stresses and internal defects such as porosity and thus result in solid samples that will be relatively easy to handle during post-processing. In jewellery where intricate parts are common, and sometimes with very thin structures, homogeneous printed layers are crucial for structural integrity and shape retention. The use of Amazemet re-Powder machine in recycling of metals from scrap has been done before, for example Vinzenz Müller *et al.*, showed that atomisation using this system produced better yield of powder from aluminium bronze chips compared to gas atomisation and that the produced powder was more spherical and printed good density products [Vinzenz Müller *et al.*, 2023].

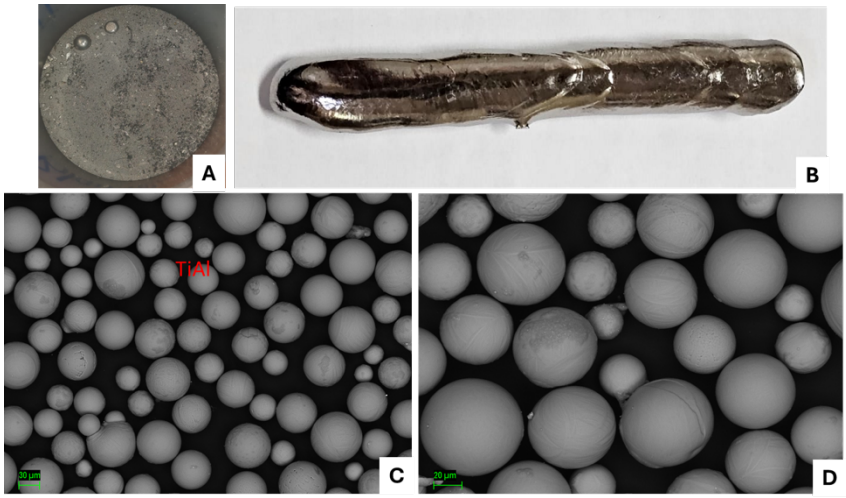


Figure 2. A. Used Ti-Al powder to be atomised, B. Rods made from melting the Ti-Al powder, C. SEM-SE images of atomised Ti-Al powder showing spherical particles with minor irregular shapes, D. Higher resolution of Ti-Al spherical particles.

Table I shows the EDS analysis of Ti-Al powder and is an overall composition over a bigger surface area. The material composition is 97.8 wt%Ti and 2.2 wt%Al. As explained above, atomisation takes place at a high temperature, with the arc tip at +3500°C and when atomised, the spherical particles fall and knock on the steel chamber that is continuously cooled with water at 17°C. And with EDS results showing this material composition, we shall not get into analysis of whether these are αTi or βTi because these powders are aimed at metal 3D printing that involves laser melting of 20 µm – 100 µm powder layers and cooled in the process. It is these printed objects that will require analysis of phases which is outside the scope of this paper. However, the EDS analysis shows that indeed Al was not lost/ evaporated during the high temperatures used in atomisation, and the Ti-Al alloy is retained in the atomised particles.

Table I. EDS compositional analysis for Ti-Al powder

	Ti (Wt.%)	**Al (Wt.%)**
Overall	97.80 ± 0.17	2.20 ± 0.17

Figure 3 shows grain shape analysis of the produced T-Al powder. This is determined using the ellipse ratio characteristics that denote the relationship between the minor axis of a grain relative to its major axis. The lowest ratio (closest to 0) denotes more linear/oval/thin strip shapes, and the highest (1) is more circular or spherical. It is evident from the plot that the majority of the particles are spherical with more than 93% of particles having an ellipse ratio greater than 0.6; more than 89% with ellipse ratio greater than 0.7, more than 83% with ellipse ratio greater than 0.8 and these are mainly grains that are between 40 µm and 75 µm in size.

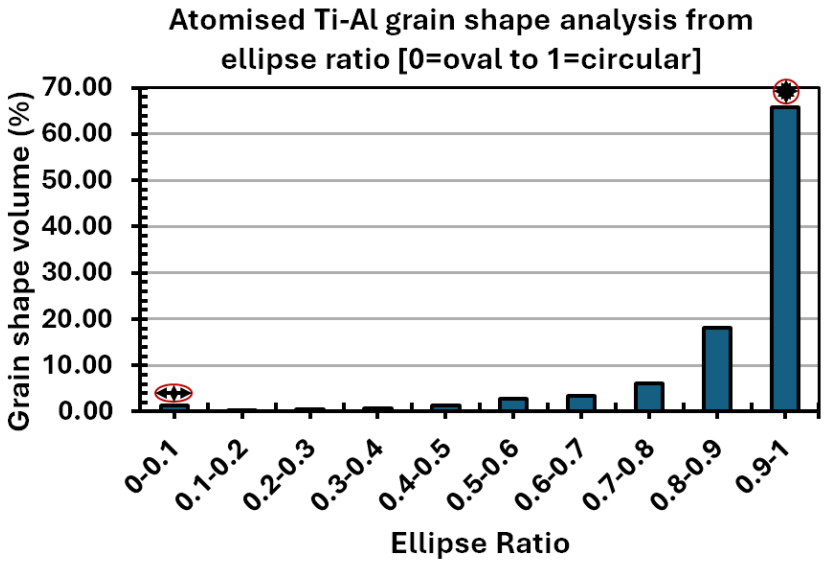


Figure 3. Grain shape analysis graph of Ti-Al powder obtained from ellipse ratio which gives the relationship between the minor axis of a grain relative to its major axis. The lowest ratio closest to 0 denotes more oval and the highest (1) is more spherical.

Figure 4 shows the plot of particle size distribution of the Ti-Al powder. From the plot, looking at the cumulative PSD volume density, we can see that d90 = 70 µm, d50 = 45 µm and d10 = 25 µm. This is good for metal 3D LPBF printers that require powder with 15 µm – 70 µm particle size. This is evidenced in a report by Muhan Xue *et al.*, (2023) where different particle sizes of Ti-6Al-4V were examined against density of printed objects where they show that different printing parameters have an effect, however particle distribution up to 60 µm yields better results. It is evident that though we used a 75 µm sieve, powder above 70 µm is a minority. Thus, the PSD range mixes well between the finer and coarse powders which can contribute well to surface finish and flowability.

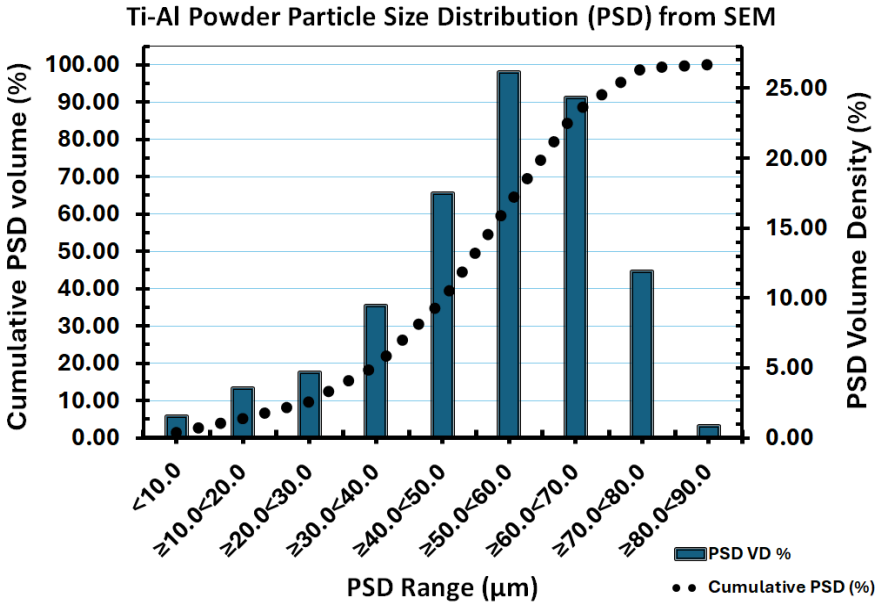


Figure 4. Graph showing the particle size distribution for Pt-Al powder.

304L stainless steel powder

Figure 5 shows the image of the roll feeder- (A) of 304L steel wire that was atomised in the Amazemet rePowder machine. Because the machine is equipped with a wire feeder (this replaces the manipulating jaws in Figure 1x), there is no need to form rods. The particles of 304L steel are spherical with minor irregular shapes. Unlike the Ti-Al powder, there is not much soot seen on the powder though soot always occurs and is washed with alcohol and an ultrasonic bath. It is however desirable to thoroughly wash the formed powder clean to avoid soot presence during 3D printing because this would affect the quality of the product. The shape of the particles is spherical as mentioned above and this shows the success in the atomisation process of 304L steel wire from the Amazemet rePowder machine to produce powder suitable for metal 3D printing in LPBF machines.

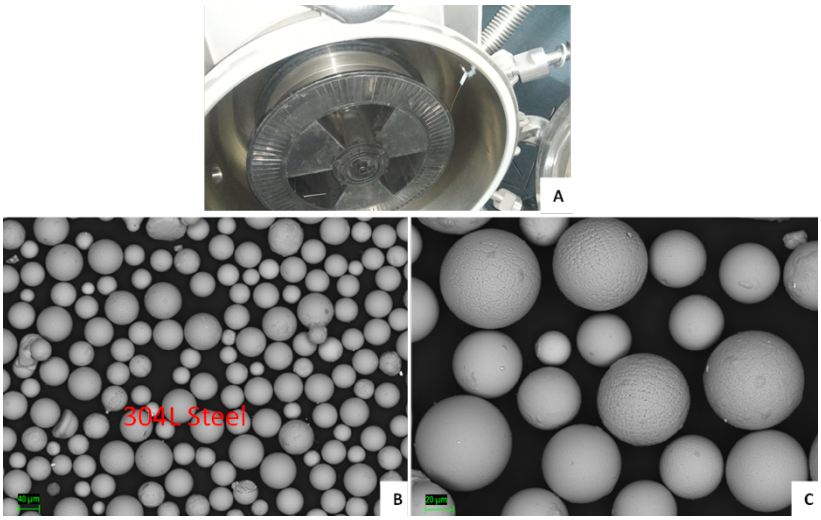


Figure 5. A. S304L steel wire on a roll inserted in the machine wire feeder compartment, B. SEM-SE images of 304L stell powder after atomisation and sieved with a 75 µm sieve, C. Higher resolution of 304L steel powder confirming uniform spherical shapes.

Table II shows the EDS analysis of 304L steel wire powder obtained from the Amazemet rePowder machine using a wire feeder. Showing results from the overall surface area of the powder mounted on a tape for the SEM analysis, the material composition is 10 wt%Nickel (Ni), 18.7 wt%Chromium (Cr) and 0.7 wt%Silicon (Si). This is a confirmation of 304L steel composition [Outokumpu, *et al.*, 2013, AlHazaa, *et al.*, 2020, Zhao, *et al.*, 2023] and shows that though atomisation of the material in the Amazemet rePowder machine happens at much higher temperature due to the arc tip at +3500°C; material composition is retained in the powder particles.

Table II. EDS compositional analysis for 304L steel powder from wire

	Fe	**Si (Wt.%)**	**Cr (Wt.%)**	**Ni (Wt.%)**
Overall	Balance	0.7 ± 0.03	18.7 ± 0.01	10.0 ± 0.10

Figure 6 shows grain shape analysis of the 304L steel powder produced. This was determined using the ellipse ratio as described previously. We can see from the plot that more than 90% of the powder has ellipse ratio above 0.7 which confirms that the majority of produced powder is spherical with the highest percentage in the region of 0.9-1.

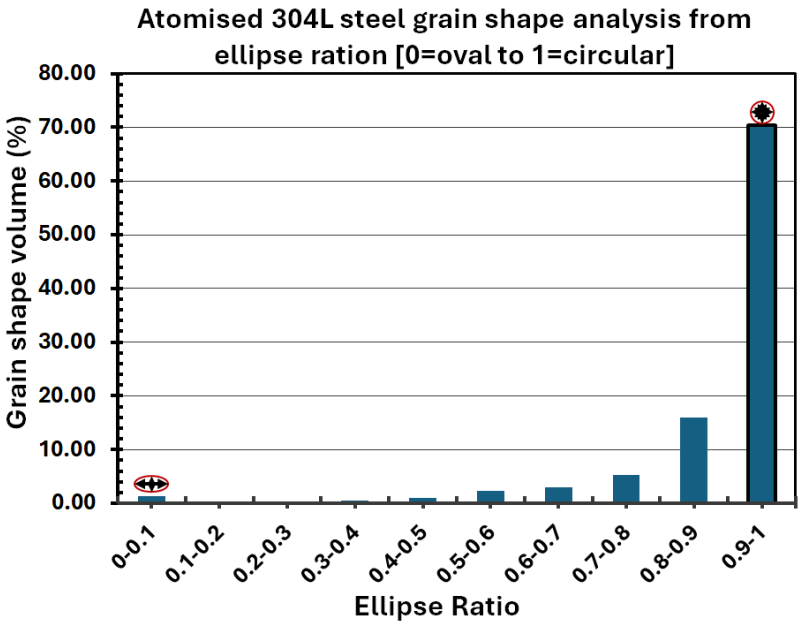


Figure 6. Grain shape analysis graph of 304L steel wire powder obtained from ellipse ratio which gives the relationship between the minor axis of a grain relative to its major axis. The lowest ratio closest to 0 denotes more oval and the highest (1) is more spherical.

Figure 7 shows the plot of particle size distribution of 304L steel wire powder. The cumulation plot shows that d90=65 µm, d50=50 µm. Most of the powder is between 30 µm and 65 µm in size and thus falls within a good range for LPBF metal 3D printer requirement for flowability and good density of printed products. Powders above 65 µm but less than 75 µm and those finer below 25 µm are mixed well with the rest and flowability should not be affected as well as density of prints.

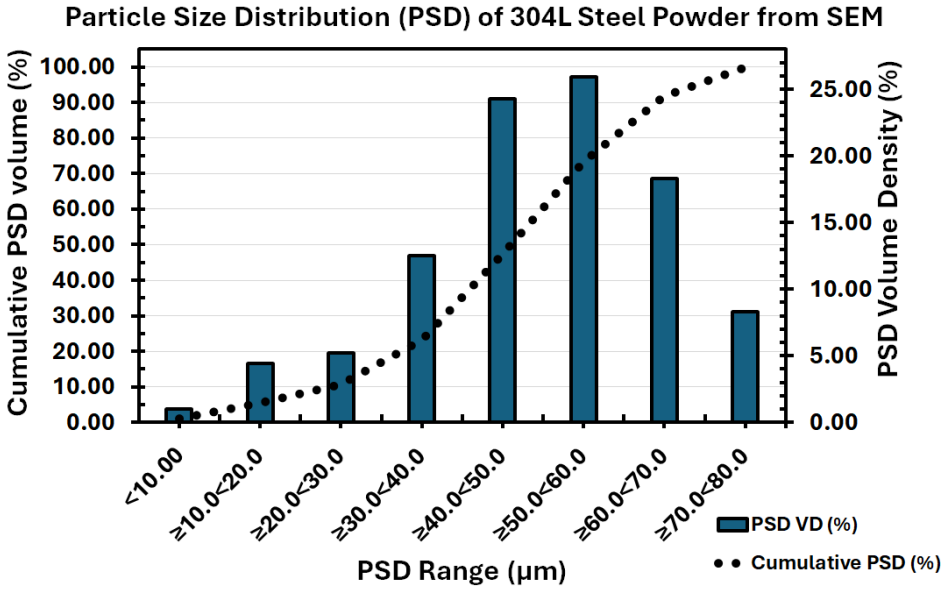


Figure 7. Graph showing the particle size distribution of 304L steel wire powder.

Platinum powder

Because the aim was to establish parameters and process that should be useful to make powder for all materials and in particular PGM metals and their alloys, the method used to make Ti-Al and 304L steel powders was then adapted to make pure platinum powder. Pt has a higher melting point and hence higher current (above 200A) was found to be suitable for atomisation compared to Ti-Al and 304L steel on which 200A was maximum. Figure 8 shows an ingot of platinum (A) on a rod making copper heart with an arc electrode above, a platinum rod made from the ingot (B) EDS_SE image of spherical platinum powder produced from the Amazemet rePowder machine and an image of powder that was cold mounted in a resin, polished and analysed using Tescan Integrated Mineral Analyser (TIMA) on the SEM. The particles are spherical with a narrow particle size distribution and EDS showed that we have pure Pt with no contamination on the powders. Because soot is inevitable, the platinum powder was also washed in alcohol using an ultrasonic bath.

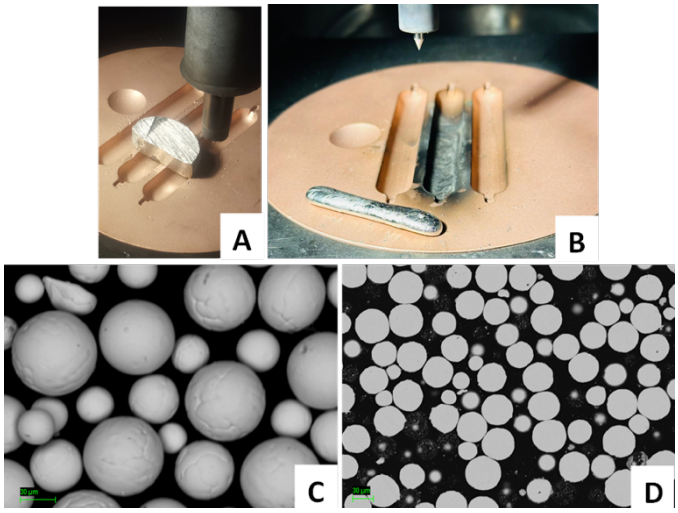


Figure 8. A. Platinum ingot to be melted with arc electrode above on a rod forming copper hearth in the Amazemet rePowder machine, B. Platinum rod formed from the ingot inside the Amazemet rePowder machine. C. Spherical platinum powder with different particle sizes formed from atomiser. D. SEM images of platinum powder on a cold mount, when polished and analysed using TIMA.

In Figure 9 we show results of pure Pt powder shape analysis from ellipse ratio. Overall, in the platinum (Pt) sample, grains are predominantly circular. Over 90% have ellipse ratio >0.5, more than 84% has ellipse ratio > 0.6 and more than 75% has ellipse ratio >0.7 and all these grains fall within the 20 µm and 50 µm size. Based on these results and the BSE images, the grains appear to be more circular or spherical and this shows that the ultrasonic atomisation process using the Amazemet rePowder machine works well to produce powder suitable for metal 3D printing and thus, this process can be used for production of other PGM powders and their alloys. The less spherical is due to higher temperature used, with molten particles landing on each other and knocking on the machine walls to deform. and the latter mainly happens on the lower or smaller particles below 25 µm. Furthermore, the particle size distribution is suitable for LPBF metal 3D printers. The particle size distribution analysis is shown in Figures 9.

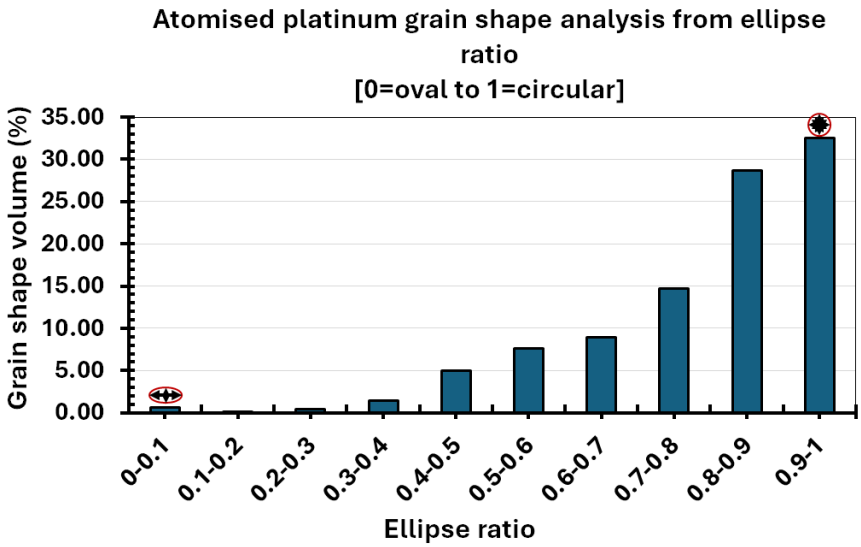


Figure 9. Grain shape analysis graph of pure platinum powder obtained from ellipse ratio which gives the relationship between the minor axis of a grain relative to its major axis. The lowest ratio closest to 0 denotes more oval and the highest (1) is more spherical.

Figure 10 shows the plot of particle size distribution of pure Pt powder formed. From the plot, looking at the cumulative PSD volume density, d10 = 20 µm, d50 = 35µm and d90 = 40 µm. The PSD is suitable for metal 3D LPBF printers that require powder with 15 – 70 µm particle size. The presented powder was sieved using a 75 µm sieve, thus from our results, we can see that all captured above 75 µm are coarse and big particles because the PSD plot for the produced sieved pure Pt is up to 60 µm. Furthermore, the PSD range mixes well between the finer and coarse powders which can be a good contribution to surface finish and flowability. Though printing of the powder is outside the scope of this work, which is to make powder, the produced platinum powder was tested on a LPBF metal 3D printer to see if the powder can flow and print. The powder could flow very well, and Figure 11 shows an SEM image which shows that the powder produced a continuous print of single tracks without satellites and thus the printed samples will have higher density and quality product.

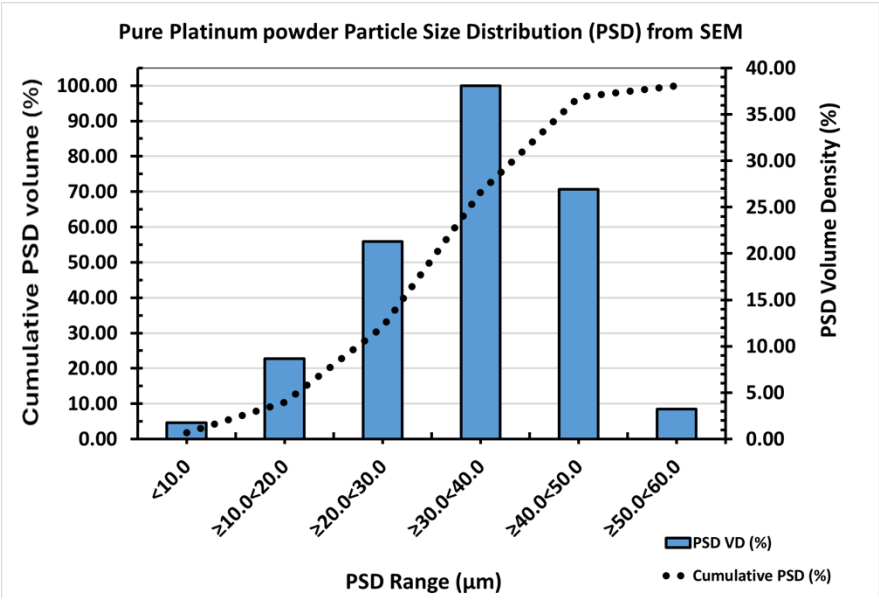


Figure 10. Graph showing the particle size distribution of pure platinum powder.

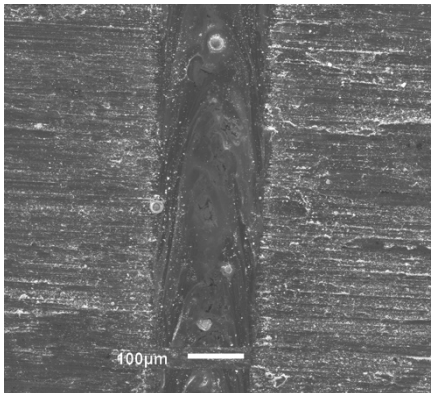


Figure 11. SEM image of a single layer print of platinum from the produced powder using an LPBF metal 3D printer.

CONCLUSION

Three different materials were melted and atomised using the Amazemet rePowder machine at Mintek. Because the machine uses arc to melt the material it was determined that the electric current required to melt and successfully atomise Ti-Al and 304L steel wire is between 190A and 200A. For pure platinum, a current of 200A – 260A was more suitable. With two options of ultrasonic vibrator (i.e., 20 kHz and 40 kHz actuators), a 40 kHz actuator and corresponding sonotrode was used. Produced powder was found to be spherical with PSD ranging mainly between 20 µm and 70 µm. The Amazemet rePowder machine when using 40 KHz actuator produced the majority of powder in the range of d50 between 45 µm – 60 µm [Żrodowski *et al.*, 2021]. The produced powder is suitable for LPBF and sintering technologies. The produced powder however does have soot and ash as a result of high temperature melting of the material due to tip of the arc at +3500°C. However, this is minimised by a technique avoiding prolonged exposure of the material to high heat. Soot remaining on the powder was successfully washed using alcohol and an ultrasonic bath. The few particles that are not spherical in all three materials are due to molten material knocking on each other and on the walls of the chamber before cooling off, and this is mainly in the particle size distribution range below 25 µm. It is worth noting that the 304L steel powder is more between 30 µm – 70 µm which have more spherical particles than the other two materials as seen from the ellipse ratio graph. The Ti-Al powder also has a similar particle size distribution, however slightly more particles that are less spherical than the 304L steel. Platinum powder has fairly distributed spherical particles from 0.1 to 1 of the ellipse ratios. However, the graph increases exponentially in favour of spherical particles. Particle size distribution of platinum powder is mainly between 20 µm – 60 µm. Among the three, platinum is the only material that produced powder within this range which, like all other materials, was sieved with a 75 µm sieve. The spherical nature of the particles means these are suitable for use in metal 3D printing because they will flow and thus result in homogeneous layers with good density of the materials. And this was further proven by 3D printing a single layer of the produced Pt powder using a LPBF printer which printed without satellites and showed high density. This is important because homogeneous laser melted layers, and high density will minimise residual stresses and internal defects such as porosity and thus result in solid samples that will be relatively easy to handle during post processing. In jewellery where intricate parts are common, and sometimes with very thin structures, homogeneous printed layers are crucial for structural integrity and shape retention.

The use of the Amazemet rePowder machine and ultrasonic atomisation technique in this paper has demonstrated the capability of atomisation that can be done from any feedstock material despite its initial shape. And therefore, recycling of failed printouts, castings and powders can be re-atomised to useful powders as feedstock for additive manufacturing; thus having added a crucial part of technology in powder metallurgy.

From this paper, we have demonstrated that used Ti-Al can be recycled to produce usable powder suitable for metal 3D printing. Also, that 304L wire can be atomised to produce usable powder in 3D printing. Most importantly, the process of powder production using this system has demonstrated that we can produce Pt powder suitable for 3D printing in LPBF metal 3D printers. This is important for further production of PGM metal powders and their alloys for value addition in South Africa.

ACKNOWLEDGEMENT
The Department of Science and Innovation)'s Precious Metals Development Network for funding support.

REFERENCES

Abdulaziz AlHazaa and Nils Haneklaus; Difusion Bonding and Transient Liquid Phase (TLP) Bonding of Type 304 and 316 Austenitic Stainless Steel—A Review of Similar and Dissimilar; Material Joints Metals 2020, 10, p. 613.

Bałasz, B., M. Bielecki, W. Gulbiński, Ł. Słoboda, Comparison of ultrasonic and other atomization methods in metal powder production, Journal of Achievements in Materials and Manufacturing Engineering, Volume 116, Issue 1, January 2023, p. 11.

Chen, Q.; Juste, E.; Lasgorceix, M.; Petit, F.; Leriche, A. Binder Jetting Process with Ceramic Powders: Influence of Powder Properties and Printing Parameters. *Open Ceram.* 2022, *9*, p. 100218.

Chua, C.K.; Wong, C.H.; Yeong, W.Y. Standards, Quality Control, and Measurement Sciences in 3D Printing and Additive Manufacturing; Academic Press: Cambridge, MA, USA, 2017. Available online:

Lanzutti Alex, and Elia Marin; The Challenges and Advances in Recycling/Re-Using Powder for Metal 3D Printing: A Comprehensive Review; Metals 2024, 14, p. 886.

Lyckfeldt, O. Powder Characterisation: Powder rheology of steel powders for additive manufacturing. In Proceedings of the European Congress and Exhibition on Powder Metallurgy, Gothenburg, Sweden, 15–18 September 2013; European PM Conference Proceedings; The European Powder Metallurgy Association: Chantilly, Frane, 2013; p. 1. Available online: Powder Characterisation: Powder rheology of steel - ProQuest

Marczyk Joanna and Marek Hebda; Effect of the Particle Size Distribution of Irregular Al Powder on Properties of Parts for Electronics Fabricated by Binder Jetting, Electronics 2023, 12(12), p. 2733.

Möller H., V. Motsweni, L. Zrodowski, and T. Choma, Powder characterisation of Pt84-Al11-Cr3-Ru2 superalloy manufactured by ultrasonic atomisation, 8th International PGM Conference Sun City, 2 – 3 November 2022, The Southern African Institute of Mining and Metallurgy, https://www.researchgate.net/publication/365616200.

Muller Vinzenz, Janek Maria Fasselt, Tobias Kruse, Christian Klötzer, Rafael Kleba-Ehrhardt, Tomasz Choma, Max Biegler, Michael Rethmeier, Using ultrasonic atomization to recycle aluminium bronze chips for additive laser directed energy deposition, IOP Conf. Series: Materials Science and Engineering 1296, 2023, 012036, doi:10.1088/1757-899X/1296/1/012036.

Olakanmi, E.O.; Cochrane, R.F.; Dalgarno, K.W. A review on selective laser sintering/melting (SLS/SLM) of aluminium alloy powders: Processing, microstructure, and properties. Prog. Mater. Sci. 2015, 74, p. 401–477.

Outokumpu Oyj; Handbook of Stainless Steel"; 2013. p. 12.

Qin P. , L.Y. Chen, C.H. Zhao, Y.J. Liu, C.D. Cao, H. Sun, L.C. Zhang, Corrosion behavior and mechanism of selective laser melted Ti35Nb alloy produced using pre-alloyed and mixed powder in Hank's solution, Corrosion Science, Volume 189, 15 August, 2021, p. 109609.

Salah Eddine Brika, Morgan Letenneur, Christopher Alex Dionb, Vladimir Brailovski, Influence of particle morphology and size distribution on the powder flowability and laser powder bed fusion manufacturability of Ti-6Al-4V alloy, Additive Manufacturing, Volume 31, January 2020, p. 100929.

Standards, Quality Control, and Measurement Sciences in 3D Printing and ... - Chee Kai Chua, Chee How Wong, Wai Yee Yeong - Google Books

USGS 2024: https:/pubs.usgs.gov/periodicals/mcs2024, Index of /pubs/periodicals/mcs2024.

Wu, H.C.; Chen, T.C.T. Quality control issues in 3D-printing manufacturing: A review. Rapid Prototyp. J. 2018, 24, 607–614.

Yap, C.Y.; Chua, C.K.; Dong, Z.L.; Liu, Z.H.; Zhang, D.Q.; Loh, L.E.; Sing, S.L. Review of selective laser melting: Materials and applications. Appl. Phys. Rev. 2015, 2, 041101.

Yim Seungkyun, Koki Minowa, Kenta Yamanaka, Akihiko Chiba, Influence of particle size distribution on the powder bed quality in the powder bed fusion additive manufacturing process, Journal of Materials Research and Technology 37, 2025, p. 2038–2050.

Zhao Xiaohui , Ziwei Li, Bin Yang, Xiaoyu Sun, Guorui Sun, Shupeng Wang; Microstructure and mechanical properties of 304 stainless steel produced by interpass milling hybrid direct energy deposition-arc; Journal of Materials Research and Technology Volume 27, November–December 2023, p. 3744-3756.

Żrodowski, L., Wróblewski, R., Choma, T., Morończyk, B., Ostrysz, M., Leonowicz, M., Łacisz, W., Błyskun, P., Wróbel, J.S., Cieślak, G., Wysocki, B., Żrodowski, C. and Pomian, K., Novel cold crucible ultrasonic atomization powder production method for 3D printing. *Materials,* 2021, 14, p. 2541.



Donald Mkhonto

Principal Scientist
Mintek

Donald Mkhonto is a principal scientist researcher at Mintek with over 25 years of experience in the field of materials science and physics. Having obtained his PhD in computational materials science more than 20 years ago, his previous work and contribution has been disseminated in many conference presentations over the years and published in several peer reviewed journal articles. Donald has worked for different institutions internationally like the Crystallography department at Birkbeck College University of London-UK and geology-geochemistry department at University of Wisconsin in the United States of America. Locally, prior to joining Mintek, Donald Mkhonto worked for institutions like the University of Limpopo (UL), Council for Scientific and Industrial Research (CSIR), Tshwane University of Technology (TuT), and the UK based Johnson Matthey PLC. His scientific contribution in the field was on atomistic simulation methods and interatomic potentials development mainly applied on oxide materials surfaces and surface interaction with organic adsorbents. This work is extensively demonstrated in several publications on biomaterials for implant applications as well as geological understanding of carbonate materials found in mars. He has also worked on classified work in catalysis and metal surface tarnishing at Johnson Matthey. In addition to his teaching experience at various academic institutions, Donald is currently heavily invested at Mintek Advanced materials division where he is responsible for research and development of materials aimed towards additive manufacturing technology development in the country. Leading a team in additive manufacturing and alloying of systems, he has contributed immensely to several publications of metal alloys and alloying procedures using state of the art systems under highly controlled inert environment at Mintek and has also worked on several metal powder production suitable for metal 3D printing, tested, and continues to do so.

Powder production of pre-alloyed Platinum alloys for jewellery applications

K.D. Ukabhai, D. Mkhonto, L. Mampuru, R. Diale, M.J. Phasha, S.J. Moema

Mintek, South Africa

The advancements in additive manufacturing have created a new interest in platinum (Pt) jewellery alloys. There is interest in Pt as it is difficult to cast intricate patterns, but these can be done by additive manufacturing. Platinum powder is imported and there are limited alloys available. It is produced by gas or water atomisation which has its drawbacks due to moisture content and particles not being spherical. Ultrasonic atomisation uses vibrations to create powder from molten metal. It is known to produce clean spherical powders that are ideal for laser powder bed fusion printing. For this paper a known jewellery alloy Pt-5Cu (wt%) and studied at Mintek; Pt-2.5Ag2.5Au (wt%) was used to make powder by ultrasonic atomisation on the Amazemet rePowder machine. The powder was analysed for suitability to use in 3D printing and characterised to determine if particles were alloyed. It was found that Pt-5Cu (wt%) alloyed well and had particles within the size range. The Pt-2.5Ag2.5Au (wt%) powder did alloy but did not have the correct composition and had some non-spherical particles, therefore process optimisation is needed for this alloy. The machine does produce spherical powder that is suitable for laser powder bed fusion printing.

Keywords: Ultrasonic atomisation, additive manufacturing, platinum group metals, jewellery, powder metallurgy

INTRODUCTION

There is rising global emphasis on the circular economy in materials as well as the need to beneficiate minerals at the source. In places with an abundance of platinum group metals (PGMs), this has led to a renewed interest in the platinum (Pt) jewellery industry and in general, PGM-bearing jewellery. The advancement in additive manufacturing has also sparked interest as new methods of powder production, machine technology and build techniques are available (Corti, 2022). Additive manufacturing allows intricate, unique and detailed pieces to be produced, which is difficult and, in many instances impossible with the known casting and forging techniques. The additive manufacturing of jewellery provides less production time, lower production cost, lower environmental impact and enables unique alloys with thermal and mechanical properties (that make them difficult to cast) to be used. (Klotz and König, 2023). A great deal of work has been done since the early 2000s on additive manufacturing of precious metals by Zito *et al*., (2012, 2013, 2014), however the focus was gold alloys (Klotz *et al*., 2017, 2019; Fletcher and Cooper, 2019). It was discovered that gold was difficult to work with due to its high thermal conductivity (318 W/mK)) (Zito *et al*., 2014) and porosity, hence there was a shift of interest to platinum (Klotz and König, 2023). Platinum is easier to work with due to its lower thermal conductivity (71.6 W/mK) (Zito *et al*., 2014) and the addition of alloying elements improved its surface quality and reduced porosity (Klotz and König, 2023).

The majority of the world's platinum is supplied by South Africa (Nhede, 2024); however most of it is exported with minimal beneficiation. PGMs are used in many industries and platinum has for many years been used in catalysts and secondly for jewellery (Hughes *et al*., 2021). Depending on preference and demand, platinum can be supplied in a form of powder, which is also a crucial feedstock in metal additive manufacturing. For additive manufacturing excellent quality spherical powder is needed and it must have exceptional flowability (Żrodowski *et al*., 2021). Current methods for metal powder production include water or gas atomisation. These methods use high velocity jets of gas/water which hit the molten metal as it is being poured through a narrow stream and it then disperses into powder (Sehhat *et al.,* 2022; Richter *et al.,* 2023). The problem with these methods is that they do not always produce very spherical powder and in the case of water atomisation the moisture content is not good enough and requires more processing for 3D printing (Sehhat *et al*., 2022; Richter *et al.,* 2023). They are also limited due to the enormous atomisation towers needed to control the speed of the particles during the process (Żrodowski *et al.,* 2021). Ultrasonic atomisation has not been studied extensively, however it is one of the best methods for powder production. It uses acoustic waves to break up the molten metal that is in contact with the vibrating surface to give powder (Żrodowski *et al.*, 2021). The acoustic waves are created by a vibrating medium which is in most cases a sonotrode. The ultrasonic atomisation machine used at Mintek can produce spherical powder that has little to no oxidation and moisture. The machine not only produces powder but can also be used to recycle scrap and used powder from additive manufacturing.

For this study a known jewellery alloy Pt-5Cu (wt%) (Corti, 2022), previously studied at Mintek,Pt-2.5Ag2.5Au (wt%) was used to make powder which was then analysed for suitability for use in additive manufacturing and characterised to determine if particles were alloyed. Produced spherical powders are used particularly for laser powder bed fusion printing which in addition to spherical particles, requires a particle size distribution of a certain range (30 – 75 microns in general (Anderson *et al.,* 2018)). The Pt-5Cu (wt%) alloy was chosen as it is alloyed with copper (Cu) which is affordable and readily available compared to other alloys such as Pt-Pd, Pt-Ru and Pt-In-Ga which are alloyed with other PGMs and are equally or more expensive than Pt. The previously-studied Pt-2.5Ag2.5Au (wt%) showed promising properties, however with the melting technology available at the time, loss of silver (Ag) in the composition was experienced.

EXPERIMENTAL PROCEDURE

The first alloy was made up using 99.8% pure Pt powder, with pure (99.9%) silver (Ag) and pure (99.8%) gold (Au) pellets. The materials were weighed out to make up 10g samples of the alloy compositions. The second alloy was made using 99.8% pure Pt and 99.9% pure copper (Cu). The two mixed alloy material were separately melted into buttons using the arc melting process on the Amazemet rePowder (Żrodowski *et al*., 2021) machine. Before melting the samples, the chamber was purged three times with argon gas, and a titanium getter was melted to ensure there was no oxygen in the chamber. Ideally the material being atomised should be in a rod form for ease of atomisation. Atomising alloy from a rod entails holding the rod in the machine using a specialised holder and gradually melting by pointing an arc to it. The molten material drops in controlled tiny amounts onto the vibrating sonotrode (Figure 1a). Due to platinum being an expensive material and having limited amounts, it was decided that a button would be used instead of a rod (Figure 1b). A rod would require not less than 100 g of the alloy at a time for each alloy and this would be costly. The ultrasonic arc atomisation technique was used to manufacture the Pt-5Cu (wt%) and Pt-2.5Ag-2.5Au (wt%) powder using the Amazemet rePowder (Żrodowski *et al.*, 2021) machine. The buttons were then atomised by melting onto the vibrating sonotrode which disperses it and produces powder. The arc used in both melting and atomisation can attain temperature up to 3500°C, thus making the system suitable to melt any alloy made from any material. This temperature can be adjusted by controlling the arc current from 5A to 500A. Because the tip of the arc is always at the highest temperature, when using low current, the arc torch is reduced to a small flame that possesses reduced heat or low temperature. Increasing the current increases the arc torch, thus increasing the flame heat. A 40 kHz transducer and relevant sonotrode setup was used as it produces a higher frequency giving a narrower particle size distribution (PSD). (Żrodowski *et al*., 2021).

Inert environment was controlled using argon gas to prevent oxidation. The machine uses a water chiller system to cool the sonotrode and copper hearth to prevent it from overheating.

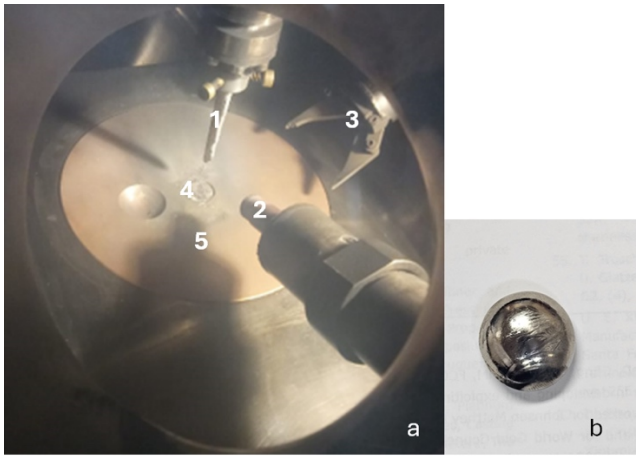


Figure 1. Images showing a) general setup for atomisation using a rod where 1 is rod sample to atomise, 2 is arc electrode holder, 3 is sample manipulating jaw, 4 is a sonotrode and 5 is copper hearth and b) button produced by arc melting.

The produced powder was mounted on conductive tape and analysed using a scanning electron microscope (SEM) to get secondary electron images and composition of the powder using energy dispersive X-ray spectroscopy detector. To determine the PSD and shape the powder was cold-mounted in clear resin and analysed using Tescan Integrated Mineral Analyser on the SEM.

RESULTS AND DISCUSSION

The images of the two ultrasonic atomised powders of Pt-5Cu (wt%) and Pt-2.5Ag-2.5Au (wt%) are shown in Figures 2 and 3, respectively. The particles of Pt-5Cu (wt%) are spherical with no visible satellite particles as shown in Figure 2. The Pt-2.5Ag-2.5Au (wt%) particles (Figure 3) do show some coating around the particles and irregular shapes. During the atomisation process soot is created due to the high temperatures used and ash off the metals with lower melting temperatures (Pt- 1767.2°C, Au-1064.28°C, Ag-961.78°C (Science, 2025)) than the arc with tip temperature of up to 3500°C. The particles of both alloys (Figures 2b and 3b) show dendritic structures. which indicates that the particles were alloyed. Pure metals cannot undergo constitutional undercooling; hence they will show a planar surface (Hogan, 2001).

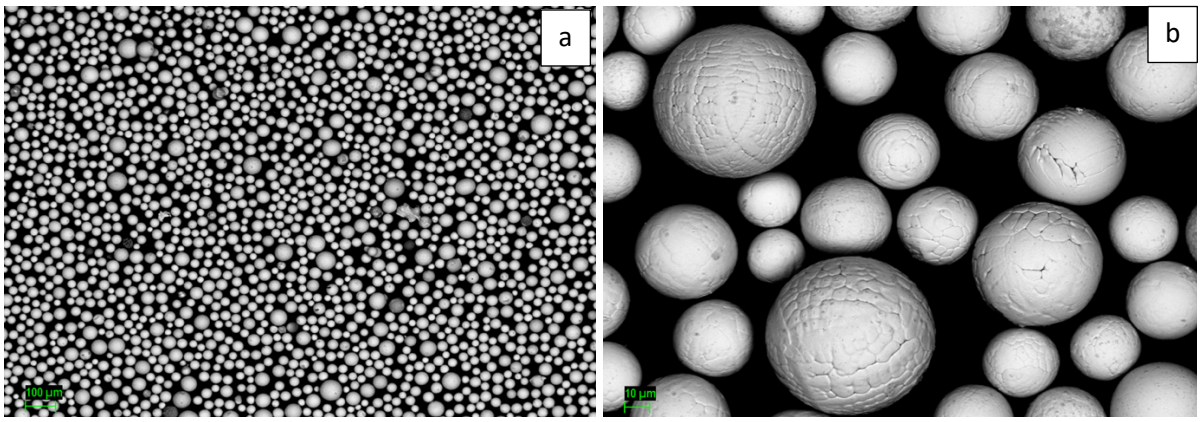


Figure 2. SEM-SE images of atomised Pt-5Cu (wt%) powder at a) low magnification and b) high magnification.

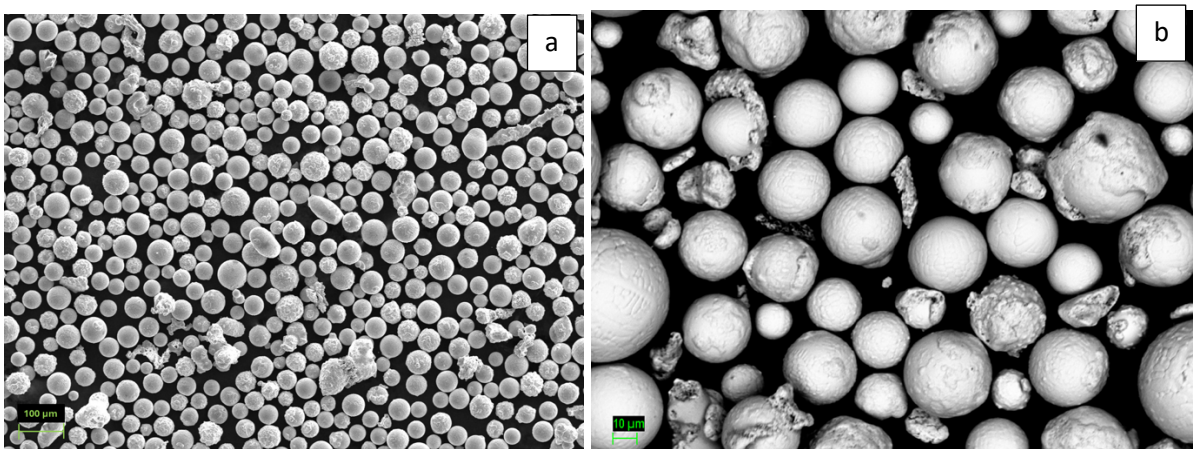


Figure 3. SEM-SE images of atomised Pt-2.5Ag-2.5Au (wt%) powder at a) low magnification and b) high magnification.

The overall compositional analysis for the powders (Table I) show that the Pt-5Cu (wt%) alloy was successfully alloyed as the composition was like the targeted composition. Because of the high heat used during atomisation (up to 300A of the arc current) there are losses of lower melting temperature elements, more Ag and Au was added to the alloy, thus there is an offset from the targeted composition. Again, a small amount of material was used, and with the process of atomisation taking more heat to initiate atomisation, uncontrolled loss of elements is inevitable, which can be balanced off when more material is available for atomisation than just 10 g. The irregular particles had far less platinum and more Au and Ag than the targeted alloy, and some analysed individual particles showed that they were pure Pt and pure Au. The cause of the composition being incorrect could be due to the difference in the melting temperatures of the alloying elements Au and Ag (Pt- 1767.2°C, Au-1064.28°C, Ag-961.78°C (Science, 2025)). Ultrasonic atomisation of alloyed Pt is much more difficult than pure Pt. The process for alloying Pt-2.5Ag-2.5Au (wt%) will need to be optimised. Due to there being a lot of soot in the Pt-2.5Ag-2.5Au (wt%) alloy, it was cleaned with alcohol in an ultrasonic bath. It is possible that cleaning for a longer period may remove the majority of the soot around the spherical particles.

Table I: EDS compositional analysis for Pt-5Cu (wt%) and Pt-2.5Ag-2.5Au (wt%)

	Pt (wt%)	**Cu (wt%)**	
Overall	94.2 ± 1.8	5.8 ± 1.8	
	Pt (wt%)	**Ag (wt%)**	**Au (wt%)**
Overall	83.9 ± 4.0	5.1 ± 9.5	11.0 ± 5.4
Irregular particles	45.2 ± 0.1	28.3 ± 0.1	26.5 ± 0.1

Figures 4-7 show the particle size and shape date for both alloys. The data shows that the majority of the particles lie within the 20-75 µm range. The d90 for Pt-5Cu (wt%) and Pt-2.5Ag-2.5Au (wt%) is 55 µm and 45 µm respectively. The particle range for Pt-2.5Ag-2.5Au (wt%) (Figure 6) is smaller as the majority of the particles range from 20-45 µm, whereas Pt-5Cu (wt%) range from 30-60 µm. The reason for the smaller range for Pt-2.5Ag-2.5Au (wt%) is the high heat used during atomisation and the fact that only 10 g of the alloy was atomised. High heat because the material is difficult to atomise at lower heat. But with more heat and smaller sample, at 40 kHz frequecy of the transducer vibrating the sonotrode, smaller articles are formed. The ellipse ratio in Figures 5 and 7 shows the percentage of particle that are spherical with 0 being not spherical and 1 spherical. For both alloys, the majority of the particles are spherical. Figure 7 shows an intial spike and this is expected as there were some non-spherical particles (Figure 3b), however the majority is spherical.

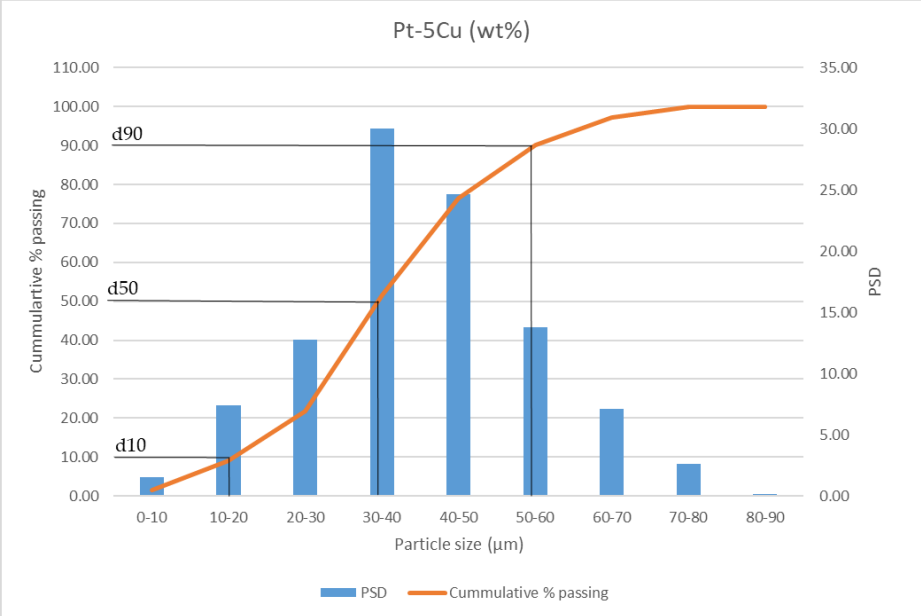


Figure 4. Graph showing the particle size distribution for Pt-5Cu (wt%).

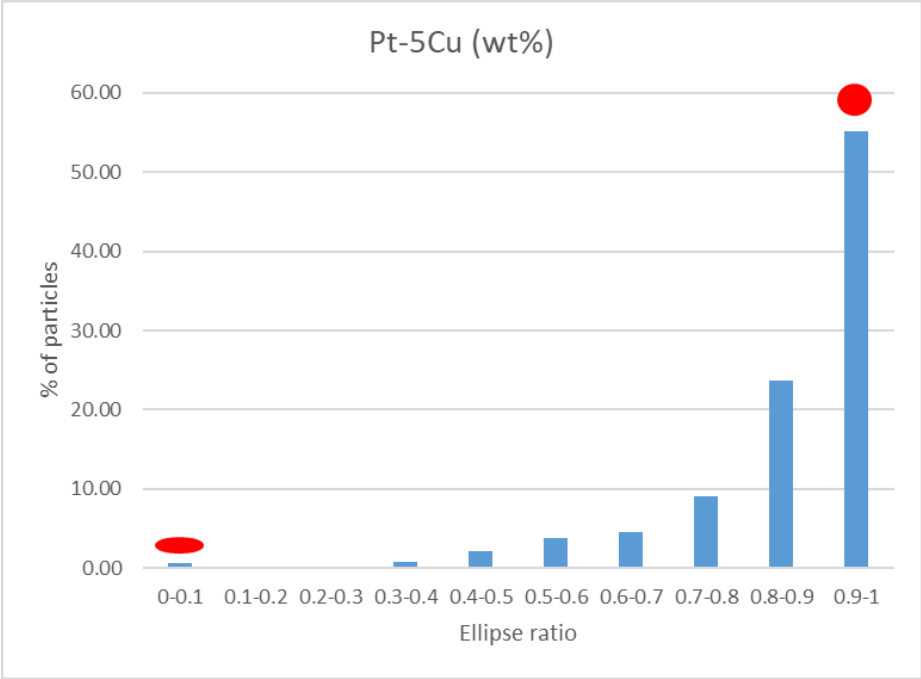


Figure 5. Graph showing the ellipse ratio of the particles (0= not spherical and 1= spherical) for Pt-5Cu (wt%).

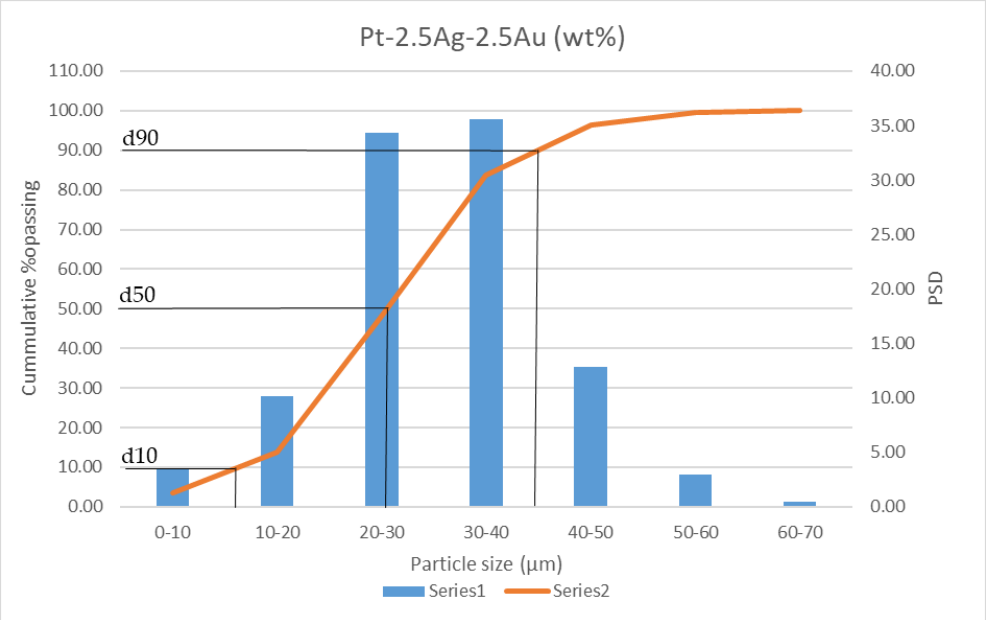


Figure 6. Graph showing the particle size distribution for Pt-2.5Ag-2.5Au (wt%).

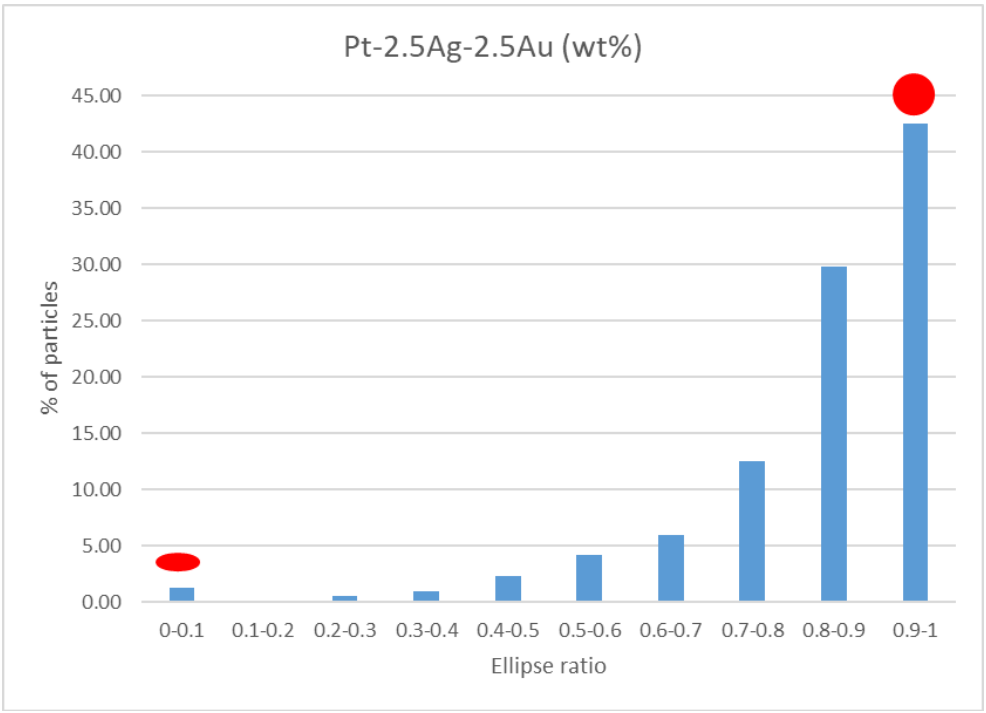


Figure 7. Graph showing the ellipse ratio of the particles (0= not spherical and 1= spherical) for Pt-2.5CuAg-2.5Au (wt%).

CONCLUSION

Each alloy of 10 g was ultrasonically atomised using arc atomisation techniques. It was found that the majority of the particles were spherical and within the 30-75 µm range which is suitable for laser powder bed fusion printing. The method used for Pt-5Cu (wt%) gave alloyed powder with a similar composition to the targeted alloy composition. The Pt-2.5Au-2.5Ag (wt%) alloy particles were mostly spherical and

alloyed but the composition was offset due to elevated temperature and smaller amount of material used. It takes high heat to start atomising Pt-2.5Au-2.5Ag (wt%) alloy, and by the time atomisation start, more soot is already formed, and even smaller particles are formed. It is desirable to note that when atomising, the first material on the sonotrode is used to weld the material on for smoother atomisation going forward. However, with the small amount used, when welding occurred, the same welded material was atomised to form powder. It is on this basis that though the Pt-2.5Au-2.5Ag (wt%) powder composition is off, this atomisation was considered a success. While noting that more material in the future shall be considered for better yield, this also shows that the method used is suitable for producing decent quality Pt-5Cu (wt%) powder and can produce powder within the required particle size range. It will also be beneficial to conduct more tests to further check that the powder is suitable such as density tests and flowabilty tests. With isolated random particle compositions, while alloyed, the produced powder is expected to produce better printed alloy composition and homogeneity compared to in-situ printing.

ACKNOWLEDGEMENTS

The Department of Science, Technology and Innovation (DSTI) and Advanced Materials Initiative (AMI) for funding.

REFERENCES

Anderson, I.E., White, E.M. and Dehoff, R. (2018). Feedstock powder processing research needs for additive manufacturing development. *Current Opinion in Solid State and Materials Science*, **22** (1), pp.8-15.

Corti, C.W. (2022). The evolution of platinum jewellery alloys: from the 1920s to the 2020s. *Johnson Matthey Technology Review*. **66** (4), pp. 418–434.

Fletcher, D. and Cooper, F. (2018), The precious project: polishing and finishing of additive manufacturing (AM) jewelry. In *The Santa Fe Symposium on Jewelry Manufacturing Technology*, Albuquerque, New Mexico, USA: Met-Chem Research, pp. 211–234.

Hogan, L.M. (2001), Crystals, Dendritic Solidification of. *Encyclopedia of Materials: Science and Technology.* Buschow, K.H.J., Cahn, R.W., Flemings, M.C., Ilschner, B., Kramer, E.J., Mahajan, S., Veyssière, P. (ed.). Elsevier, pp. 1913-1918,

Hughes, A.E., Haque, N., Northey, S.A. and Giddey, S. (2021). Platinum group metals: A review of resources, production and usage with a focus on catalysts. *Resources*, 10 (9), p. 93.

Klotz, U.E., Tiberto, D. and Held, F. (2017). Optimization of 18-karat yellow gold alloys for the additive manufacturing of jewelry and watch parts. *Gold Bull.*, **50** (2), pp. 111.

Klotz, U.E., Tiberto, D. and Held, F.J. (2019). Additive manufacturing of gold alloys. *Galvanotechnik*, **110** (8), pp. 1436–1439.

Klotz, U.E. and König, F.R. (2023). Additive manufacturing of platinum alloys. *Johnson Matthey Technology Rev*iew, **67** (3), pp. 303–316.

Nhede, N. (2024). 9 African countries with the most critical minerals. https://energycapitalpower.com/african-countries-most-critical-minerals/#:~:text=South%20Africa%20%E2%80%93%20PGMs&text=The%20country%20contributes%20significantly%20to,chromium%20and%2016%25%20of%20vanadium., Accessed on: 11 August 2025.

Richter, J., Torrent, C.J.J., Krochmal, M., Wegener, T., Vollmer, M. and Niendorf, T. (2023). A comparative study using water atomized and gas atomized powder in laser powder bed fusion–Assessment of the fatigue performance. *International Journal of Fatigue*, 168, p.107468.

Science, Notes and Projects (2025). Free printable periodic tables. https://sciencenotes.org/wp-content/uploads/2014/11/PeriodicTableMeltingPoint.pdf, Accessed on 14 August 2025.

Sehhat, M.H., Sutton, A.T., Hung, C.H., Newkirk, J.W. and Leu, M.C. (2022). Investigation of mechanical properties of parts fabricated with gas-and water-atomized 304L stainless steel powder in the laser powder bed fusion process. *Jom*, **74** (3), pp.1088-1095.

Zito, D., Carlotto, A., Loggi, A., Bortolamei, S., Molinari, A. and Cristofolini, I. (2012). Latest developments in selective laser melting production of gold jewellery. In *The Santa Fe Symposium on Jewellery Manufacturing Technology*, Albuquerque, New Mexico, USA: Met-Chem Research, pp. 537–562.

Zito, D., Carlotto, A., Loggi, A., Sbornicchia, P., Maggian, D., Fockele, M., Unterberg, P., Molinari, A. and Cristofolini, I. (2013). Optimization of the main selective laser melting technology parameters in the production of precious metal jewellery. In *The Santa Fe Symposium on Jewellery Manufacturing Technology*, Albuquerque, New Mexico, USA: Met-Chem Research, pp. 1–20.

Zito, D., Carlotto, A., Sbornicchia, P., Molinari, A., Cristofolini, I., Unterberg, P. and Fockele, M. (2014). Optimization of SLM technology main parameters in the production of gold and platinum jewelry. *In The Santa Fe Symposium on Jewelry Manufacturing Technology*, Albuquerque, New Mexico: Met-Chem Research, pp. 439–470.

Żrodowski, L., Wróblewski, R., Choma, T.,Morończyk, B., Ostrysz, M., Leonowicz, M., Łacisz, W., Błyskun, P., Wróbel, J.S., Cieślak, G., Wysocki, B., Żrodowski, C. and Pomian, K. (2021), Novel cold crucible ultrasonic atomization powder production method for 3D printing. *Materials,* **14,** 2541.



Kiyaasha Dyal Ukabhai

Engineer
Mintek

Kiyaasha Dyal Ukabhai obtained her PhD in Metallurgy and Materials Engineering at the University of the Witwatersrand in 2023. She then worked for a short period as an intern before becoming an engineer at Mintek in the Advanced Materials Division in the physical metallurgy group. She has experience in alloy development, corrosion studies and failure investigations. She is also part of the additive manufacturing team which focuses on producing powder for laser powder bed fusion 3D printing purposes.

Decarbonising the platinum group metals value chain to lower the carbon footprint of energy transition technologies

D. van Wyk, S. Thakurdin

Hatch, South Africa

Platinum group metals (PGMs) are a key material required for the energy transition, with widespread use in several clean technologies' production process. Due to the various processing steps included in PGM production, a full value chain overview was conducted to identify the biggest sources of emissions and develop potential abatement strategies. The PGM value chain has a large carbon footprint due to the high energy requirement across each process step. A large portion of emissions stem from electricity usage across the value chain, due to the South African grid's reliance on coal for electricity generation. There are additional emission sources which includes the use of fossil fuels for powering mining vehicles and machinery, the use of reductants, as well as chemical reagents. The largest emission area in the value chain is at the refining processes; however, this is on an intensity PGM basis. Due to the refining process treating a smaller volume quantity than the upstream areas, on an absolute emission basis this is where the largest emissions stem. Various technologies are available to decarbonise the PGM industry. Abatement opportunities vary from commercially ready, such as deploying electric vehicles, to viable, but supply chain constraints exist such as the case for biofuels, and to ones where technology is demonstrated but not industrially deployed, such as biocarbon reductants. Given the current fluctuating PGM market, lack of policy pressure and government funding opportunities, it is not an ideal environment to implement operational decarbonise measures. However, as countries globally are introducing more stringent carbon legislation such as carbon taxes, as well as taxing imported carbon, the industry risks falling behind and becoming more exposed to carbon prices in the long term. Technologies such as wind turbines and electrolysers which produce green hydrogen are key decarbonisation options for global industry and are produced using PGMs. Although technologies may be called "clean" or "green" they still result in negative environmental impacts if the upstream emissions from input materials are carbon intensive. Therefore, for these energy transition technologies to truly enable a cleaner world, the input PGM material needs to decarbonise to ensure entire lifecycle emissions are reduced.

INTRODUCTION

To keep the planet from warming more than 1.5°C above pre-industrial levels, most countries have set a goal to reach net zero emissions by 2050. Net zero means that all greenhouse gas emissions produced are counterbalanced by an equal number of emissions that are eliminated. To reach this goal, rapid decarbonisation is required. With this goal in mind, companies are tasked with decarbonising their operations to remain compliant with carbon legislation, which is continuously being developed, as well as the public perception regarding companies being sustainable. Various technologies are being investigated and developed to achieve net zero. These technologies include renewable power technologies such as wind power, use of alternative fuels such as green hydrogen and biofuels and carbon capture.

Some of the decarbonisation technologies being investigated such as hydrogen fuel cells as well as battery technologies (Johnson Matthey, 2025) use platinum group metals (PGMs).

In carbon reporting, emissions are classified as direct or indirect. This distinction is based on whether emissions are under control of the reporting organisation. Under the Greenhouse Gas (GHG) protocol, direct emissions are also called scope 1 emissions and indirect emissions are called scope 2 and 3 emissions. Scope 1 emissions are emissions being emitted by the reporting organisation directly, whether from fuel usage or released by the process. Scope 2 refers to purchased electricity or steam by the reporting organisation from a third party. Scope 3 emissions are divided into upstream and downstream emissions. Upstream emissions refer to emissions associated with the production and transport of purchased products and fuels, capital goods and waste generated by the organisation.

Due to the varying scopes that emissions can fall into, it is important to look at the entire production value chain of PGMs to ensure that a scope 1 emission is not being displaced to scope 3 instead of truly being abated.

Due to decarbonisation becoming a key focus for industry, various low carbon products are being positioned to attract a 'green premium' price. This is due to the additional cost associated with purchasing a product which was produced in a more environmentally friendly process than the conventional process. This green premium varies per industry with the iron and steel sector expected to carry premiums of between 150-300 $/ton (Kajrolkar, 2024). The green premium for cement would be between 40-120% of the current cost and costs for low carbon aluminium are estimated to be 40% higher than costs of aluminium produced using traditional methods (Kajrolkar, 2024). Although these percentages are high for producers depending on how costs are passed down, in most cases, consumers would only see an increase in 1-3% final cost price (Kajrolkar, 2024). A survey conducted (Bain & Company, 2024) found that ~50% of consumers said they would pay a sustainability premium of 5% or more today. Only 6% stated that they would not pay any premium. This maximum premium value is expected to increase in the coming years as consumer concerns regarding climate change increase. The survey found that 60% of consumers said that their concerns about climate change have increased during the past two years (Bain & Company, 2024).

Over the past three years, the PGM market has been under price pressure due to decreased demand. The decarbonisation transition might be the market injection the PGM industry needs to mitigate potential demand downside risks going forward. However, the industry risks being excluded from benefitting from this market if the supply chain does not decarbonise. Another lever that is becoming more prominent regarding decarbonisation is carbon policy with various countries introducing a carbon tax, emission targets, and in the case of the European Union (EU), a carbon border adjustment mechanism (CBAM) to put a carbon tax on imported carbon-intensive products. The EU's CBAM is entering its definitive phase in 2026, and countries including the UK, Japan and Canada have expressed plans to introduce similar mechanisms by 2030. Currently, carbon credits can be used to offset some of the regularity pressure from these policies. The United Nations body responsible for setting up a carbon market under the Paris Agreement adopted important new standards to guide how emission-reducing projects measure their impact (United Nations Climate Change, 2025). The Paris Agreement Crediting Mechanism will enable countries and other actors to work together on reducing greenhouse gas emissions by generating high-integrity carbon credits. This would be achieved by introducing rules on how to properly measure a project's actual emission reduction impact. This will guard against companies who may be using low-cost carbon credits, which also tends to be low quality, to limit their carbon exposure without truly decarbonising their operations.

Policy in the South African context includes the Carbon Tax Act and the Climate Change Bill. The carbon tax is currently R236 per ton of carbon dioxide equivalent (tCO_2e), with majority of emissions still, however, being covered by free allowances. It is expected that Phase 2 of the carbon tax would introduce measures to reduce tax free allowances as well as increase the carbon tax rate to R462 per tCO_2e by 2030 (National Treasury, 2024). In March 2025, the Climate Change Bill was signed into law. In its current form, this bill still excludes key items required to stimulate industrial decarbonisation

action; however, these remaining items will potentially be phased in during future revisions. These items include complying with sectoral emission targets, as well as staying within carbon budgets set for various high- emitting industries. Industries under a carbon budget will need to implement an approved greenhouse gas mitigation plan, monitor implementation of the plan and report annually on the progress against the allocated carbon budget.

METHODOLOGY – FLOWSHEET SPECIFICATION

In this paper, the various processing routes being used to produce PGMs were reviewed to determine a representative flowsheet for the industry. PGMs are typically produced using mining, concentrating, smelting and refining process steps. A process overview for each step is given below as context for the emissions calculation methodology.

Mining

For emissions associated with the mining step, a conventional underground South African mine was considered, using diesel equipment and grid electricity, with limited access to renewable power and relying on diesel gensets for auxiliary power. Equipment used on site was considered to include a haul truck fleet, stationary equipment for drilling as well as auxiliary mobile machinery such as loaders. A conventional crushing and ball mill circuit was assumed to be on site for the purposes of this study. Emissions from the mining process were calculated using the benchmarks for fuel and energy consumption as provided in Table I, based on internal project experience.

Table I. Consumption metrics for conventional mines

Benchmark	Unit	Value
Diesel usage	L/t ore	1.75
Electricity usage	kwh/t ore	36.8
Explosives usage	kg/t ore	0.33

Concentrating

For concentrating, it was assumed that the milled PGM ore is treated using gravity separators and flotation cells (Thethwayo, 2018). For flotation reagents, it was assumed that xanthate and a defoamer is used in the flotation cells to produce a sulphide-rich PGM concentrate (Thethwayo, 2018). At the concentrator, most of the energy usage is electrical consumption for the flotation cells and dewatering systems. The consumption benchmarks are given in Table II based on internal project experience.

Table II. Consumption metrics for flotation

Benchmark	Unit	Value
Collector requirement (xanthate)	kg/t ore fed	0.05
Depressant requirement (NaHS)	kg/t ore fed	5.5
Flocculant requirement	g/t ore fed	5
Frother requirement (pine oil)	kg/t ore fed	0.02
Lime requirement	kg/t ore fed	0.5
Modifier requirement (sulfuric acid)	kg/t ore fed	3.5
Steel balls	kg/t ore fed	0.5
Electricity usage	kwh/ t ore fed	3.2

Smelting

For the smelting process, a conventional PGM ore smelter design was assumed, which includes flash drying, electric furnace smelting and Peirce-Smith converting. For the flash dryer, it was assumed to be powered by coal. The smelting process was assumed to use pet coke as a reductant. A diesel allowance was assumed for the mobile machinery associated with the process plant. The benchmarks for fuel and energy consumption are provided in Table III, based on internal project experience.

Table III. Consumption metrics for smelting process

Benchmark	Unit	Value
Coal usage for drying	kg/t concentrate fed	26.62
Reductant consumption	kg/t concentrate fed	8.59
Electrode paste consumption	kg/t concentrate fed	3.52
Electricity usage	MWh/ t concentrate fed	1.49
Diesel allowance	L/t concentrate fed	10.1

Refining – Base Metals

After smelting and converting, the produced matte is sent to a base metal refinery (BMR). Most of the base metals refining facilities in the western world use a sulfuric acid leaching flowsheet to separate the PGMs from the base metals for further processing (Sinisalo & Lundström, 2018). There are various options to produce intermediate nickel products such as nickel sulphate; this flowsheet assumes full nickel metallisation and copper production by electrowinning. The consumption benchmarks as provided in Table IV were used to calculate emissions based on internal project experience.

Table IV. Consumption metrics for base metals refining

Benchmark	Unit	Value
Sulfuric acid consumption	t/t metal in concentrate	0.56
Sodium hydroxide consumption	t/t metal in concentrate	2.91
Electricity consumption	MWh/t metal in concentrate	6.09
Coal usage	t/t metal in concentrate	0.88

Refining – Precious metals

After the BMR, a PGM-rich concentrate is sent to a precious metal refinery for extraction of PGMs. The PGMs can be recovered through a variety of processes such as precipitation, solvent extraction and iron exchange. For this study, a facility using an ion exchange process was modelled to identify emissions associated with this part of the value chain. The benchmark consumption values for this process are given in Table V based on internal project experience.

Table V. Consumption metrics for precious metals refining

Benchmark	unit	Value
Hydrochloric acid consumption	t/t metal in concentrate	0.55
Hydrogen peroxide consumption	t/t metal in concentrate	1.04
Sodium carbonate consumption	t/t metal in concentrate	0.57
Electricity consumption	MWh/t metal in concentrate	0.73
Natural gas usage	m^3/t metal in concentrate	630

METHODOLOGY - CALCULATIONS

The emissions from each emission source were calculated by multiplying the emission factor for the specific fuel, reagent or power source by the consumption of the relevant emission source. The emission factors given in Table VI to Table VIII were used for this study.

Table VI. Scope 1 Emission factors used for this study

Emission Factor	unit	value	Reference
Coal combustion	$kgCO_2e/t$	2.4	(Department for Energy Security and Net Zero, 2024)
Reductant (coke)	$kgCO_2e/t$	3.6	(Department for Energy Security and Net Zero, 2024)
Diesel	$kgCO_2e/l$	3	(Department for Energy Security and Net Zero, 2024)
Explosives	$kgCO_2e/kg$	0.18	(Internal Database)
Natural gas combustion	$kgCO_2e/m^3$	2.04	(Department for Energy Security and Net Zero, 2024)

Table VII. Scope 2 Emission factors used for this study

Emission Factor	unit	value	Reference
South Africa grid electricity	$kgCO_2e/kWh$	0.578	(Department of Forestry, Fisheries and the Environment, 2024)

Table VIII. Scope 3 Emission factors used for this study

Emission Factor	unit	value	Reference
Diesel production	$kgCO_2e/l$	0.62	(Department for Energy Security and Net Zero, 2024)
Explosives production	$kgCO_2e/kg$	4.7	(Wernet et al. 2016)
Steel balls production	$kgCO_2e/kg$	1.26	(Wernet et al. 2016)
Collector (xanthate)	$kgCO_2e/kg$	1.87	(Wernet et al. 2016)
Depressant (NaHS)	$kgCO_2e/kg$	2.22	(Wernet et al. 2016)
Lime	$kgCO_2e/kg$	0.89	(Wernet et al. 2016)
Frother (pine oil)	$kgCO_2e/kg$	1.71	(Wernet et al. 2016)
Modifier (sulfuric acid)	$kgCO_2e/kg$	0.09	(Wernet et al. 2016)
Flocculant	$kgCO_2e/kg$	3.21	(Wernet et al. 2016)
Electrode paste production	$kgCO_2e/kg$	0.4	(Department for Energy Security and Net Zero, 2024)
Reductant production	$kgCO_2e/kg$	0.5	(Department for Energy Security and Net Zero, 2024)
Coal production	$kgCO_2e/kg$	0.42	(Department for Energy Security and Net Zero, 2024)
Hydrogen peroxide production	$kgCO_2e/kg$	1.32	(Wernet et al. 2016)
Sodium hydroxide production	$kgCO_2e/kg$	1.12	(Wernet et al. 2016)
Natural gas production	$kgCO_2e/m^3$	0.34	(Department for Energy Security and Net Zero, 2024)
Hydrochloric acid production	$kgCO_2e/kg$	0.42	(Wernet et al. 2016)
Sodium carbonate production	$kgCO_2e/kg$	1.1	(Wernet et al. 2016)
Electricity generation losses	$kgCO_2e/kWh$	0.09	(Department of Forestry, Fisheries and the Environment, 2024)

RESULTS

Mining

The mining emissions were estimated to be 45 $kgCO_2e/t$ ore. The majority of emissions stem from the electricity usage. Scope 1 emissions are 5.3 $kgCO_2e/t$ ore, Scope 2 emissions are 34.3 $kgCO_2e/t$ ore and Scope 3 emissions are 5.8 $kgCO_2e/t$ ore. The emissions profile for the mining process is given in Figure 1.

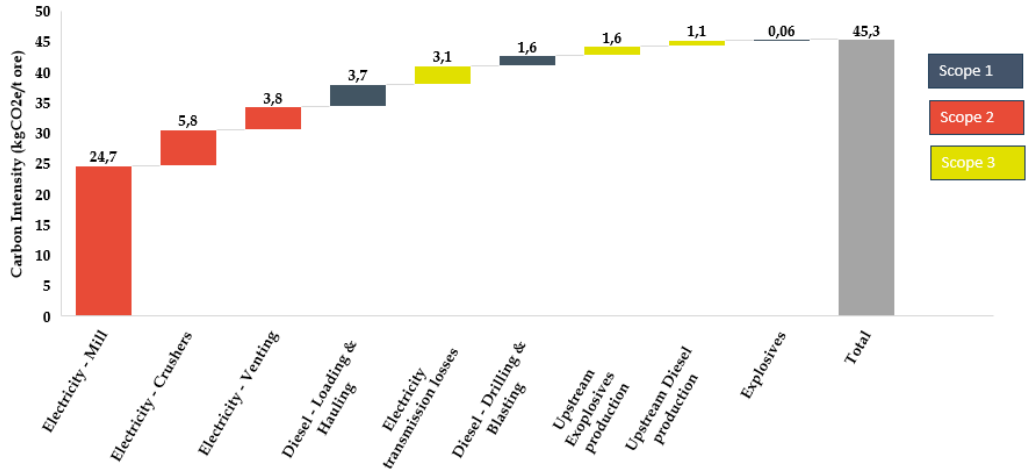


Figure 1. Emissions profile for the mining process.

Concentrating

The concentrator emissions were estimated to be 17 $kgCO_2e/t$ ore fed. The majority of emissions stem from the production of the chemical reagents used for the flotation process. Scope 2 emissions are 3 $kgCO_2e/t$ ore fed, and Scope 3 are 14 $kgCO_2e/t$ ore fed. The emissions profile for the concentrating process is given in Figure 2.

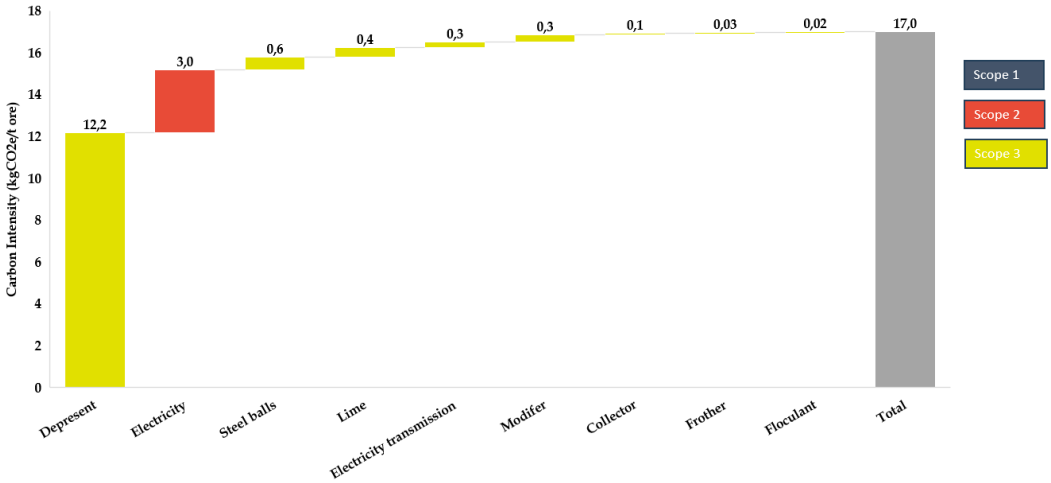


Figure 2. Emissions profile for the concentrating process.

Smelting

The smelting emissions were estimated to be 1540 $kgCO_2e/t$ concentrate fed. The majority of emissions stem from the electricity usage to power the furnace. Scope 1 emissions are 134 $kgCO_2e/t$ concentrate fed, Scope 2 emissions are 1390 $kgCO_2e/t$ concentrate fed, and Scope 3 are 23 $kgCO_2e/t$ concentrate. The emissions profile for the smelting process is given in Figure 3.

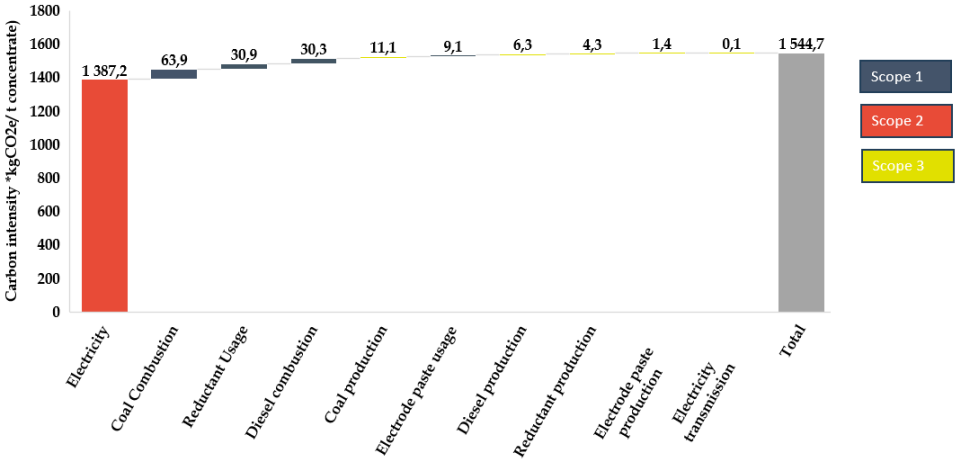


Figure 3. Emissions profile for the smelting process.

Refining – Base Metals

The base metals processing step emissions were estimated to be 12 000 $kgCO_2e/t$ metal in concentrate feed. The majority of emissions stem from the electricity used during refining. Scope 1 emissions are 2120 $kgCO_2e/t$ metal in concentrate feed; Scope 2 emissions are 5670 $kgCO_2e/$ t metal in concentrate feed and Scope 3 are 4200 $kgCO_2e/$ t metal in concentrate feed. The emissions profile for the base metals refining process is given in Figure 4.

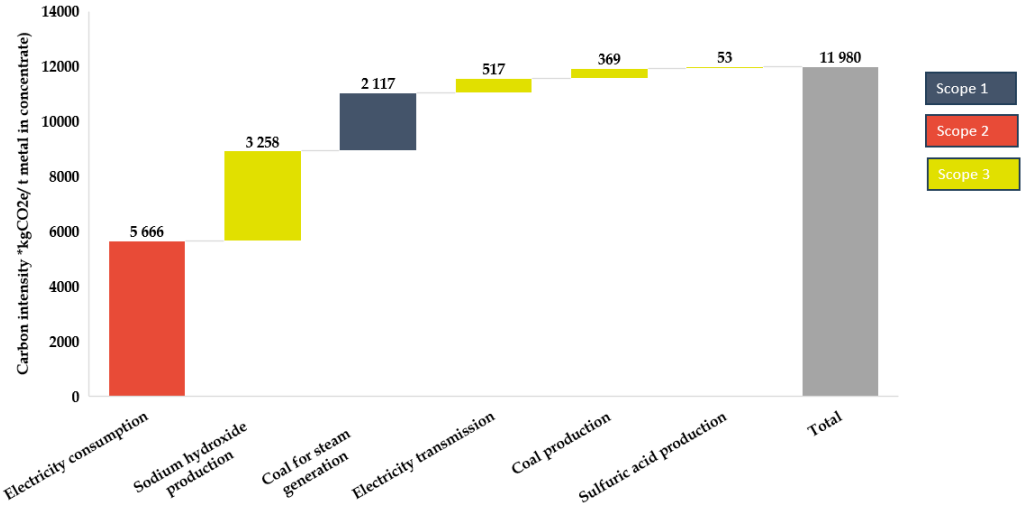


Figure 4. Emissions profile for the BMR process.

Refining – Precious metals

The precious metals processing step emissions were estimated to be 4390 $kgCO_2e/t$ metal in concentrate feed. The majority of emissions stem from the production of reagent used during refining. Scope 1 emissions are 1280 $kgCO_2e/$ t metal in concentrate feed; Scope 2 emissions are 680 $kgCO_2e/$ t metal in concentrate feed and Scope 3 are 2430 $kgCO_2e/$ t metal in concentrate feed. The emissions profile for the precious metals refining process is given in Figure 5.

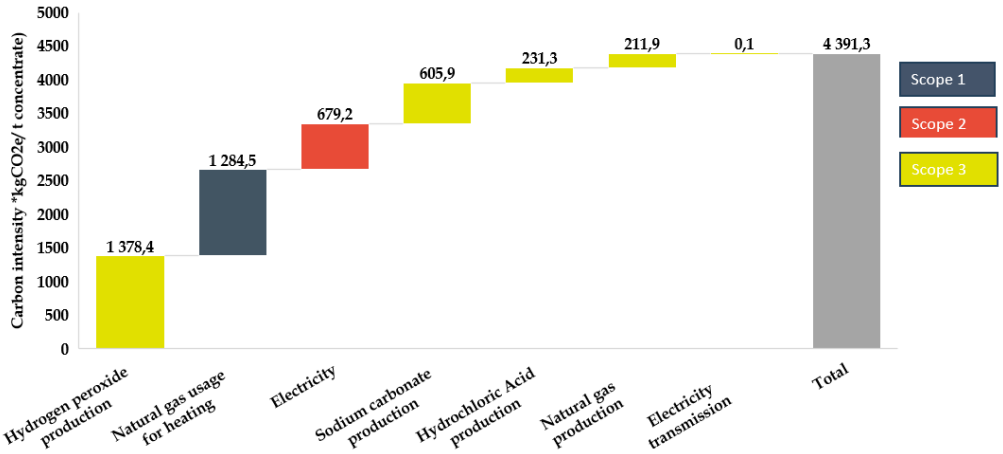


Figure 5. Emissions profile for PMR process.

DISCUSSION

Emissions profile

From the emissions profile analysis, it is seen that a large contributor to emissions across the entire value chain is electricity usage and supply chain purchases. It should be noted that with each step of refining, the amount of PGM purity is increased which means the amount of material being handled decreases between subsequent processing steps. As a result, even though the emissions intensity for the PMR is high, the absolute emissions are far lower than the upstream parts of the value chain.

Abatement Opportunities

Abatement opportunities for the value chain were identified and categorised into the following categories: renewable power, electrification, alternative fuels and supply chain purchases.

Renewable Power

As seen in the value chain emissions profile, the largest emission source is the electricity usage due to the South African grid being largely dependent on coal for electricity generation. For the PGM industry, the first step should be to procure as much renewable power as possible, whether through own generation or a Power Purchase Agreement (PPA). PPAs are an attractive renewable power option since renewable power is simply purchased from a third party owner and operator, and no capital spend is required by the metallurgical plant operator. In South Africa, the rates offered in corporate PPAs are generally lower than the historically escalating Eskom tariffs (FutureEnergyGo, 2024). PPAs can be physical, by direct connection or a mutual grid or virtual, purchasing Renewable Energy Certificates (RECs). In South Africa, there are currently no virtual PPA arrangements available in the market which limits the abatement potential of this opportunity due to the intermittency of renewable power options. For 100% abatement, virtual PPAs would be required so that during times of intermittency, generating assets in other in-country geographical regions/other countries can be used to provide RECs.

Due to the decreasing costs of renewable generation assets and increased demand for renewable energy, the demand for Independent Power Producers (IPPs) available to provide PPAs is growing. In April 2025, Eskom issued an Invitation to Tender for firms to assist them in accelerating the deployment of renewable energy solutions (ESKOM, 2025). The objective for the new subsidiary will be to operate independently of Eskom and to allow for greater governance, competitive market positioning, and enhanced Public-Private Partnerships (PPPs) (ESKOM, 2025). Eskom has an initial pipeline of at least 2 GW of clean energy projects by 2026 and has developed a pipeline for more than 20 GW of clean energy projects (ESKOM, 2025).

Various clients are looking at using aggregators for procuring renewable power. Aggregator traders can be used to decouple power generation from consumption profiles. This allows increased flexibility of supply tenors and profiles for customers, whilst giving IPPs and lenders the comfort of fixed long PPA tenors (Hajduka, 2024). Aggregators work with lenders, IPPs, utilities and customers to standardise transaction documents across the supply value chain and increase efficiencies in project development, project financing and customer acquisition, accelerating transaction processes for renewable energy projects (Hajduka, 2024). The majority of PGM producers in South Africa have already started looking at procuring renewable energy from various sources for a quick win to decarbonise their operations and in some cases save on operating energy costs.

Electrification

Once renewable power is procured, electrification opportunities can be seen as decarbonising initiatives. As seen in the value chain, there are several fossil fuel-powered machines which have electrical counterparts which can be implemented. This includes electrical machinery for mining as well as electrical boilers for heat. A key barrier for this opportunity would be the availability of renewable power since the GHG abatement potential would be highly dependent on the generation source of the power provided to the electrical equipment. Although the cost of electric equipment tends to be higher than their fossil fuel counterparts, there are several use cases where there is a business case for electrification. An advantage of electrification is the reduction in maintenance of equipment, due to elimination of fossil fuel combustion which can clog filters and injectors due to the presence of contaminants found in fuel. Electrical equipment such as electric boilers provides improved safety, ease of installation and faster start-up times when compared to fossil fuel heaters. Electrical alternatives for certain equipment are still being developed, such as for large haul trucks (>400 t). However, these large electric haul trucks are currently being trialled and are generally expected to be ready for large scale deployment by 2030.

Alternative fuels

Across the PGM value chain, fossil fuels are being used, such as diesel at the mines, coal at the dryers and natural gas for steam generation. Alternative fuels such as renewable diesel or renewable natural gas can be used as a drop-in replacement for their conventional counterparts by using the existing refuelling, distribution and transportation infrastructure. The current renewable fuel supply chain is globally constrained. The market is, however, expected to expand drastically due to various policies favouring bioenergy use. In more than 80 countries, regions and subnational states there are policies in place to support liquid biofuels (International Energy Agency, 2024). Several major countries, including Canada and China have announced plans to invest significantly in the research and deployment of biofuels (International Energy Agency, 2024). In South Africa, the Biofuels Industrial Strategy was initiated to foster a supportive policy environment and encourage investment in biofuels (Obileke *et al*., 2024). Drop-in renewable fuels can be gradually phased in as the supply chain develops and becomes more accessible.

Biofuels such as biodiesel cannot completely replace current diesel usage in all equipment but can be used in blends due to the varying energy content of the different fuels. Biodiesel is also not suitable in some operations such as for underground mining equipment since these fuels have increased nitrogen oxide emissions. For a 100% conversion to biodiesel, some equipment replacements or retrofit would be required. Biodiesel also requires special storage facilities and equipment considerations due to being more susceptible to degradation and microbial growth.

Another alternative fuel being considered to decarbonise energy usage of operations is green hydrogen. Although South Africa has a high renewable penetration factor, a limiting factor would be the large water requirement for electrolysis to produce carbon-free hydrogen. In port operations, where water is readily available, hydrogen can be used as an alternative fuel. However, further inland the feasibility of using hydrogen decreases due to the high transport costs.

Supply chain purchases

Supply chain purchases are a large emission source across the entire value chain. Although the

concentrating process has small operational emissions, the scope 3 emissions are significant due to the carbon-intensive production processes for the chemicals used on site. The largest source is the depressant, which was assumed to be NaHS which is generally produced from H_2S derived from a carbon-intensive oil and gas refining route. Due to the chemical production industry being highly carbon-intensive, there are various product routes being developed to lower these upstream emissions for reagents. For example, carbon capture is being investigated for the calcination process of limestone to reduce emissions and create low carbon lime. For NaHS, there does not seem to be a specific company looking to decarbonise the reagent; however, alternative sources of H_2S from wastewater treatment might be explored in future to lower the emissions associated with this reagent.

Something worth considering is that these low carbon products carry a green premium, with low carbon lime, for example, being ~20% more expensive than conventional lime reagent. This premium is expected to decrease as technology develops and becomes more widely adopted. However, the short-term implications of operating costs and trade-off against potential future carbon tax need to be carefully considered when developing the business case.

Market drivers

Customers

As seen from the above emissions calculations, scope 3 emissions can impact a company's emissions profile significantly. After PGM-procuring customers have decarbonised their own operations, they will have to look at decarbonising their supply chains. This will create customer pressure for PGM producers to decarbonise to keep their market share.

Due to an increase in extreme climate events such as floods, droughts and heatwaves, consumers are becoming more concerned regarding climate change and are expecting industry and governments to act accordingly. Consumers are becoming more informed when purchasing products and are starting to prioritise sustainability of their purchases (Bain & Company, 2024) which could impact PGM markets such as platinum jewellery. Recently, there has also been a crackdown in greenwashing claims made by various companies and legislation is developing to ensure companies are open and honest regarding their sustainability metrics advertised to the public.

Policy

The largest driver for decarbonisation would be policy measures such as emissions cap and trade programmes, carbon border mechanisms and carbon taxes. Currently in South Africa, there is not much regulatory pressure on companies to decarbonise their operations. However, carbon policy is developing around the globe and will start to have an impact on export markets. Various countries have implemented a carbon tax, which limits the amount of carbon an industry or operation can release annually. Carbon taxes are region-specific and in South Africa it is currently R236 per tonne CO_2. However, in other countries, the carbon tax fluctuates on a daily or weekly basis such as the EU ETS, with allowances currently priced at 70.88 EUR/tCO_2e as of 24 July 2025. For South Africa to remain competitive globally, an increase in decarbonisation measures is required, with the Climate Act being the first stepping stone.

Current global policy is still in the early development phases with various territories still determining how to implement decarbonisation legislation without hurting their own industries. A key indication of this is the EU developing the Omnibus package legislation which aims to limit the scope and exposure of certain sectors from more stringent carbon regulations. However, the introduction of CBAM is expected to accelerate global carbon policy development, since the funds generated from CBAM would be used to decarbonise EU industries. Under CBAM, the carbon tax paid from the original country can be used to offset CBAM exposure, therefore this will drive countries to implement their own carbon tax to keep money in-country to support their own decarbonisation.

A barrier in South Africa for decarbonisation is the lack of funding mechanisms available to help companies decarbonise and generate an investment environment for decarbonisation. Although further government support is needed, it is up to the industry to pressure government bodies for additional

funding mechanisms and regulatory support to ensure South Africa's industry can stay market-competitive.

Carbon credits

Currently in South Africa, carbon credits can be used to offset up to 10% of annual emissions for carbon tax purposes in South Africa. Carbon credit retirements against South African carbon tax hit record levels in 2025, with buyers flocking to clean cookstoves projects (Johnston, 2025). The carbon credit market is expected to become more constrained due to tightening of carbon credit generation regulations. Due to several false or misleading statements for a variety of carbon credit generating projects issued in the past, there is an increase in calls to only allow carbon credits which are validated under the Paris Agreement. However, at the same time, there are increased calls for Article 6 carbon credits to be included for global trading which would expand and develop the global market further.

CONCLUSION

The PGM industry is a large emitting sector and a valuable contributor to the economic landscape in South Africa. The largest emission source along the value chain is electricity provided by the grid; therefore, the first step for decarbonising the industry should be securing renewable power through own generation or PPAs. Due to the cost of electricity and South Africa's high renewable energy potential, this decarbonising lever would be easy to implement in many cases and be value-accretive; however, decarbonisation efforts thereafter would be more challenging and costly. Electrification would be the most logical step for various equipment across the value chain, given the high technical readiness level of the equipment which would allow for more rapid adoption compared to waiting for alternative fuel supply chains to develop.

Given the current fluctuating PGM market, lack of policy pressure and government funding opportunities, it is not an ideal environment to implement operational decarbonisation measures. However, as countries globally introduce more stringent carbon legislation such as carbon taxes, as well as taxing imported carbon, the industry risks falling behind and becoming more exposed to carbon prices in the long term. In the meantime, companies should work towards identifying pathways to decarbonising operations with a focus on identifying key next steps as well as monitoring decarbonisation markets to ensure they act swiftly if conditions are favourable. Global carbon policy does not stand still and is expected to become more prevalent as extreme climate events become more frequent, causing increasingly devasting effects.

REFERENCES

Bain & Company. 2024. The Visionary CEO's Guide to Sustainability. Johannesburg, South Africa. 5-27 pp.

Department for Energy Security and Net Zero. 2024. Greenhouse gas reporting: conversion factors 2024.
https://www.gov.uk/government/publications/greenhouse-gas-reporting-conversion-factors-2024 [Accessed 24 July 2025].

Department of Forestry, Fisheries, and the environment. 2024. South Africa's 2022 Grid Emission Factors Report.
https://www.gov.za/sites/default/files/gcis_document/202411/51495gon5498.pdf [Accessed 24 July 2025].

Wernet, G., Bauer, C., Steubing, B., Reinhard, J., Moreno-Ruiz, E., & Weidema, B. 2016. The ecoinvent database version 3 (part I): overview and methodology. The International Journal of Life Cycle Assessment, [online] 21(9), pp.1218–1230.

http://link.springer.com/10.1007/s11367-016-1087-8 [Accessed 24 July 2025].

ESKOM. 2025. Eskom accelerates establishment of a separate Renewable Energy Business. https://www.eskom.co.za/eskom-accelerates-establishment-of-a-separate-renewable-energy-business/#:~:text=Eskom%20will%20evaluate%20applicants%20on%20criteria%20that%20includes,Structuring%20Expertise%20and%20technical%20capability%20and%20sector%20knowled [Accessed 25 July 2025].

FutureEnergyGo. 2024. South African PPA Market Evolution: A Quick Deep Dive into the Market Dynamics.
https://futureenergygo.com/south-african-ppa-market [Accessed 25 July 2025].

Hajduka, A. 2024. Aggregation in Reducing the Risks and Costs of Decarbonisation for Industry
https://www.industrialefficiency.co.za/conference/wp-content/uploads/2024/09/3.1-Ana-Hajduka-Sustainable-Industries-Conference-South-Africa-Presentation.pdf [Accessed 25 July 2025].

International Energy Agency. 2024. Bioenergy.
https://www.iea.org/energy-system/renewables/bioenergy#tracking [Accessed 24 July 2025].

Johnson Matthey. 2025. Platinum group metals: the hidden heroes.
https://matthey.com/documents/161599/404086/Platinum+Group+Metals+the+unsung+heroes+of+our+modern+world.pdf/b8dd5367-76e7-3427-1193-859b496c69f5?t=1714051612147 [Accessed 24 July 2025].

Johnston, F. 2025. DATA DIVE: Carbon credit retirements against South Africa tax hit record level in 2025, buyers flock to cookstoves.
https://carbon-pulse.com/412163 [Accessed 24 July 2025].

Kajrolkar, O. 2024. The Green Premium Explained.
https://illuminem.com/illuminemvoices/the-green-premium-explained [Accessed 24 July 2025].

National Treasury. 2024. Carbon Tax Discussion Paper: Phase Two of the Carbon Tax. Pretoria, South Africa. 6 pp.

Obileke, K.C., Mukumba, P., & Lesala, M. (2024). Advancement of Bioenergy Technology in South Africa. Energies. 17. 3823. 10.3390/en17153823.

Sinisalo, P., & Lundström, M. (2018). Refining Approaches in the Platinum Group Metal Processing Value Chain—A Review. Metals, 8(4), 203.
https://doi.org/10.3390/met8040203 [Accessed 24 July 2025]

Thethwayo, B.M. 2018. Extraction of Platinum Group Metals. 10.5772/intechopen.73214.

United Nations Climate Change. 2025. Key Rules Agreed for Credible Climate Project Crediting under UN Carbon Market.
https://unfccc.int/news/key-rules-agreed-for-credible-climate-project-crediting-under-un-carbon-market#:~:text=Known%20as%20the%20Paris%20Agreement%20Crediting%20Mechanism%20%28PACM%29%2C,that%20support%20global%20efforts%20to%20fight%20climate%20change [Accessed 24 July 2025].



Dian van Wyk

Junior Engineer
Company: Hatch

Dian graduated from the North-West University with a bachelor's degree in chemical engineering. Upon graduating, he joined Hatch as a junior process engineer in the Climate Change Business Practice. During his time at Hatch, he has worked on decarbonisation projects for various mining-, mineral processing-, hydrometallurgy-, energy- and port-operations across the world. His focus area is on preparing decarbonization strategies for clients which includes greenhouse gas emissions profiling, opportunity identification and quantification, and decarbonization pathway development. Dian's project experience includes climate change adaptation analysis and risk identification and mitigation. Dian is knowledgeable on global climate change standards, regulations, and carbon credits. His knowledge of carbon regulations includes reporting standards and carbon tax obligations for various global regions to incorporate these levers into a company's decarbonisation strategy.

Implementation of high frequency power supplies and dual flue gas conditioning in particulate matter abatement in the PGM industry

B.P Havenga[1], E. Eichler[2], H. Heller[3]

[1]Impala Platinum, South Africa
[2]Fuel Tech, Inc., United States of America
[3]Lesedi Nuclear Services, South Africa

Industrial processing plants are managed and assessed through various key performance indicators, involving personnel safety, throughput, engineering availabilities, operating factors and legal compliance aspects. Over the course of equipment lifespan, changes in feed material, staff experience and maturity levels of available technology often necessitate adapting control philosophies to meet production targets within the applicable environmental guidelines and legislative requirements.

In order to maintain and ensure continued compliance to Minimum Emission Standards related to particulate matter point source emissions from the Niro spray drying operations at Impala Platinum's Rustenburg smelter operations, relevant primary abatement equipment had to be upgraded. Electrostatic precipitation systems (ESPs) are employed to recover particulates from the spray dryer flue gas outlet streams. The selected upgrade comprises replacement of low voltage transformer rectifier sets with High Frequency Power Supplies, as well as implementation of Dual Flue Gas Conditioning, to improve collection efficiencies of the existing ESPs.

INTRODUCTION

Impala Platinum's Rustenburg operations comprise mining, concentrating and smelting process steps to produce a copper- and nickel-rich converter matte, for refinement into final metal product at the Group's refinery service division. The mine to market process is described by Coetzee (2006), with specific focus on the smelter circuit. Impala remains fully committed to maintain world class environmental performance and adherence to South African Minimum Emission Standards (MES), through continuous improvement and adopting novel technologies in support of this long-standing commitment expressed by Kruger (2004).

Drying operations

Drying of platinum group metals (PGM) concentrate is achieved by means of either of the two drying technologies in operation at Impala's Rustenburg smelter, namely Niro spray dryers, treating slurry feed streams, as well flash dryers for the processing of filter cake feedstock. The spray drying technology dates back to the 1970s and is fairly unique to Impala's flowsheet within the PGM processing sector.

This process involves the evaporation of water from a slurry feed stream using hot gas derived from a coal-fired heat source. Solid particulate carry-over into the flue gas stream is collected in an electrostatic precipitator (ESP). Dryer outlet temperature is controlled between 120˚C - 140˚C, with a preference to the higher end of this range to ensure complete evaporation.

Dried concentrate is recovered in the drying chamber and the ESP, from which it is pneumatically conveyed to storage silos for further processing. A basic process flow diagram is presented in Figure 1.

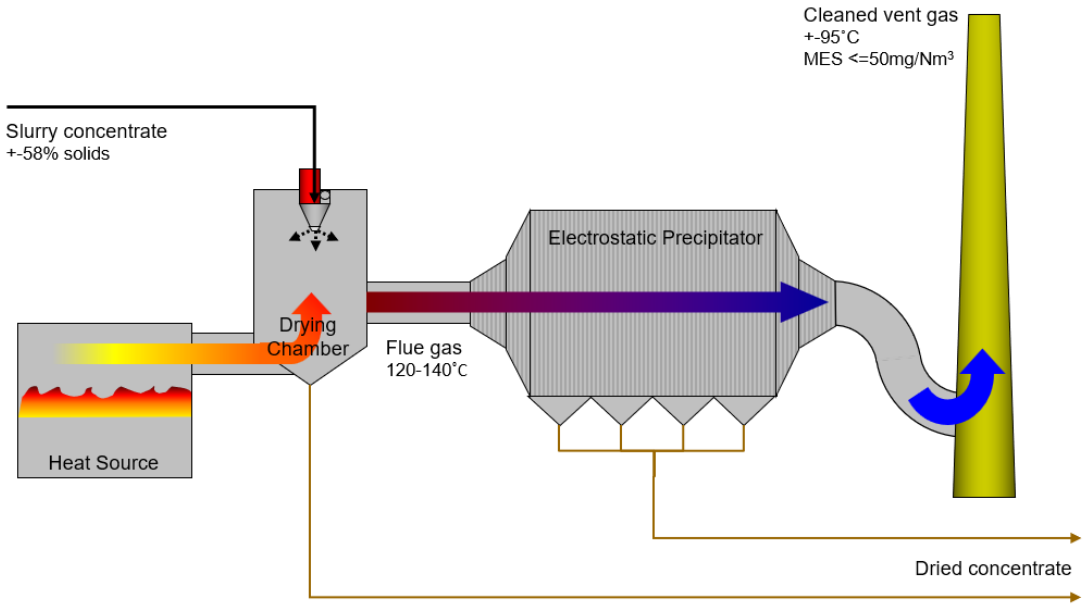


Figure 1: Simplified flow diagram of a typical spray dryer installation at Impala Platinum's Rustenburg Smelter.

Incremental improvements over time have enhanced process efficiency, but the stepped improvement in particulate matter recovery required from flue gas streams to comply with new MES necessitated major modifications to the ESPs attached to the drying plants.

More stringent standards are now applicable to all existing plants, which must operate in compliance with new plant standards (See Table I as contained in the Atmospheric Emission Licence (AEL) issued to the company in terms of the National Environmental Management: Air Quality Act of 2004 (Act no. 39 of 2004).

Table I. Minimum Emission Standards - Subcategory 4.1: Drying and Calcining

Description:	Processes in which sulfide ores are smelted, roasted, calcined, or converted.		
Application:	All installations		
Substance or mixture of substances		**Plant status**	**Mg/Nm³ (101.3kPa / 273K)**
Common name	**Chemical Symbol**		
Particulate matter		Existing New	100 50
Sulfur dioxide (Feed < 5% SO_2)	SO_2	Existing New	3500 1200
Oxides of nitrogen	NO_x *(expressed as* NO_2*)*	Existing New	2000 350

UPGRADE SCOPE AND TECHNOLOGY SELECTION

Pre-feasibility assessments covered several alternative upgrades and technologies which were evaluated on the basis of integration potential, long-term compliance security, cost effectiveness (CAPEX and OPEX) and implementation timeframes.

The rationale for this technology selection involved fulfilment of the following criteria:

- Can be delivered within required timeframes.
- Offers a cost-effective capital investment and acceptable operational cost component.
- Provides long term compliance potential, considering likely changes to feed source characteristics such as particle size distribution and particle resistivity.
- Least invasive installation.

The selected upgrade scope comprised a two-stage ESP upgrade programme, namely:

- Stage 1 – Installation of Switch Mode Power Supplies, also referred to as High Frequency Power Supplies (HFPS)
- Stage 2 – Implementation of Dual Flue Gas Conditioning (DFGC)

High Frequency Power Supplies

HFPS application is a well-established upgrade solution, likely to be recommended or included as standard for any new installation in various applications (Mariscotti, Sandrolini, Liu, & Ye, 2022). The mechanisms related to improved collection of particulates are described by Farmer *et al*., (2018) as an increase in average voltage and improvement in spark response.

The former directly impacts particle migration velocity, the speed at which a charged particle in the electric field moves toward the collector plate's surface. This parameter can be generalised as

$$\omega \sim K_2(kV_{dc})(kV_{peak}) \quad [1]$$

where $K_2 = a/2\pi\theta$ = a constant for a given ESP [2]

and

where ω= particle migration velocity
a = particle radius
θ = gas viscosity or frictional resistance coefficient of the gas
kV_{dc} = output voltage
kV_{peak} = peak voltage

Farmer *et al*., (2018) argues that the particle migration velocity for a given precipitator design can be improved by increasing the product of "kV_{dc} multiplied by kV_{peak}". Both these values are nearly equal for the selected switchmode power supplies, thus increasing particle migration velocity, which in turn is a key parameter in determining ESP collection efficiency.

The second and more subtle mechanism is the improvement in spark response. Krigmont *et al*., (2020) explains that spark response in Silicon Controlled Rectifier devices is line frequency dependent. Conventional power supplies respond to a spark within 16 to 20 milliseconds, depending on the incoming line frequency and processing speed of the controller. HFPS can detect, quench a spark and begin recovery within 4.03 milliseconds, thereby improving average kV input.

Advanced numerical performance modelling predicted that the use of HFPS would benefit drying operation through a reduction in PM emissions of 21% (Krigmont *et al*., 2020). This improvement in isolation can however not guarantee consistent adherence to the new MES.

Equipment description
Both dryer ESPs that received the Stage 1 electrical upgrade are 3-field precipitators. Each electrical field was fitted with a NWL Series 7.5 PowerPlus High Frequency Power Supply, with output as follows:

- Output voltage – 83 kV
- Output current – 1930 mA DC mean
- Switching frequency – 25 kHz
- Output power – 160 kW

These roof- mounted units were installed on the ESP roofs, necessitating minor structural reinforcing to manage the additional load.

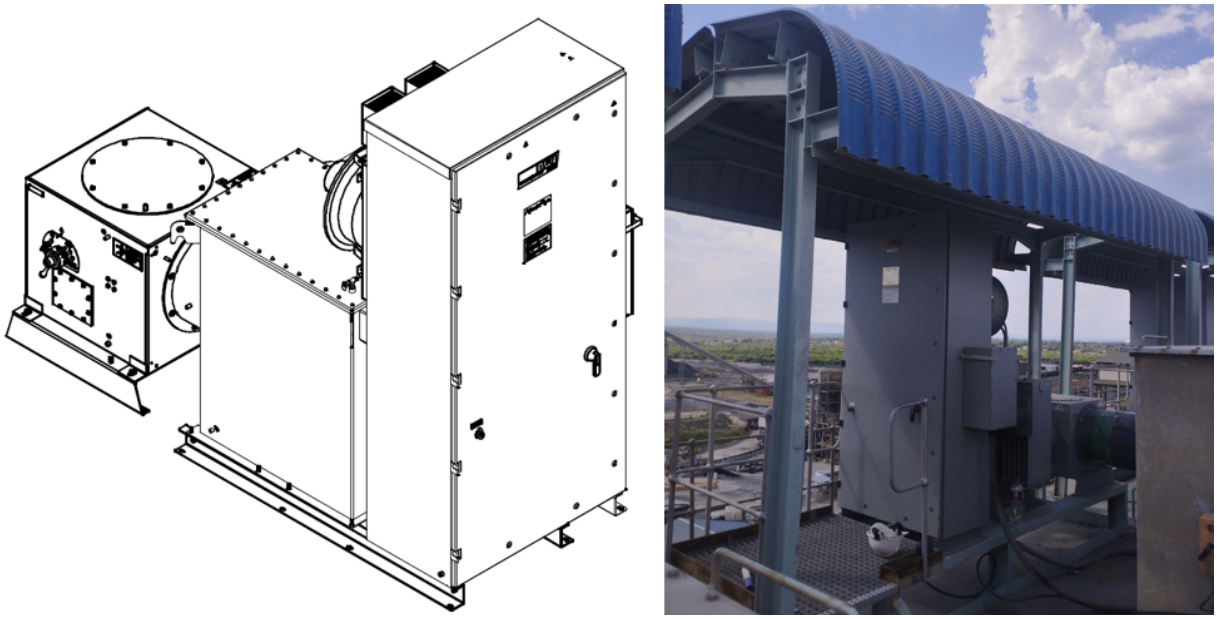


Figure 2: HFPS isometric view (left) and installed in position (right.)

Dual Flue Gas Conditioning
Flue Gas Conditioning (FGC) involves the alteration of physico-electrical properties of particles in a flue gas stream through the injection of chemical additives (Shanthakumar *et al*., 2008). One or more of the following effects, as presented by Shanthakumar *et al*. (2008), and Trivedi and Phadke (2008), are targeted by FGC:

(i) modification of the surface electrical conductivity of the fly ash/dust;
(ii) increasing the inter-electrode space charge; and
(iii) increasing fly ash/dust cohesion to reduce losses during rapping
(iv) reduce back-corona problems.

Trivedi and Phadke (2008) captured the history of flue gas conditioning and note that an increase in SO_3 levels in smelter converter gases was discovered to improve ESP collection efficiency in 1912. These two authors further state that experimental work demonstrated that many non-conductive dusts and fumes could be made collectable by adding SO_3 and/or moisture to the gas stream ahead of the ESP. Many other substances have since been used as conditioning agents, such as ammonia, triethyl amine, and various proprietary chemicals. SO_3 dosing remains the predominate treatment for containing high resistivity ash and ammonia for agglomerating dusts from high ash.

It is surmised that PGM concentrate particulates will behave in a similar fashion, since Trivedi and Phadke (2008) suggest that this technology can be applied to industries outside the proven and tested utility sector, most notably copper processing. Detailed descriptions of the most widely used gas

conditioning circuits are adequately covered by Shanthakumar *et al*., (2008)

A dual FGC solution, involving the injection of both SO_3 and NH_3, was selected to further enhance collection efficiencies of the relevant spray dryer ESPs in operation at Impala's Rustenburg smelter complex.

The mechanisms associated with these two conditioning agents are described by Krigmont (2021), Shanthakumar *et al*., (2008) as well as Krigmont and Ferrigan (2018).

- SO_3 forms sulfuric acid by combining with the moisture vapour in the flue gas, which is then adsorbed on the surface of the particles when the flue gas cools. The particles are thus coated with a thin conducting film, lowering resistivity.
- Ammonia is reported to improve precipitation efficiency of particulates through the phenomena of space-charge effects, as well as an increase in agglomeration and the cohesiveness of fly ash (Krigmont H. , 2021). Krigmont and Ferrigan (2018) further explains that ammonia behaves as a scavenger, selectively seeking out free molecules of SO_3 and/or H_2SO_4 to combine with and produce ammonium salts.

Equipment description

A standard dry sulfur feedstock (also known as sulfur on demand) DFGC system, designed by Fuel Tech, Inc., service two spray dryer ESPs at Impala's Rustenburg Smelter complex. A basic block flow diagram of the system is presented in

Figure .

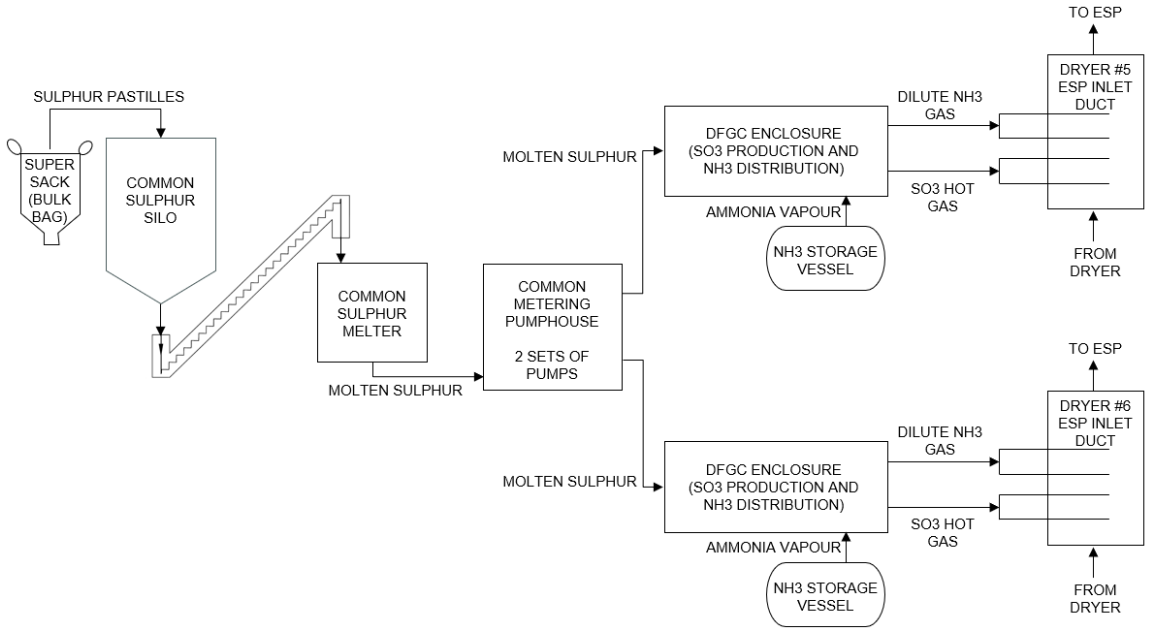


Figure 3: Simplified block flow diagram of the DFGC system installed at Impala Platinum's Rustenburg smelter complex.

Sulfur is delivered and stored in pelletised form, from where it is melted by means of saturated steam coils in a melter vessel. Dry storage and melting equipment are shared between the two dryers. The molten sulfur is pumped to a dedicated refractory lined burner, producing SO_2 which is then converted to SO_3 across a single stage catalytic converter, using vanadium pentoxide catalyst. SO_3 production rates are controlled by adjusting sulfur pumping rates based on feedback from a dryer demand signal linked to production through the dryer.

Anhydrous ammonia is stored as a liquid in dedicated vessels, from where it is vaporised and injected at a fixed ratio to SO_3. NH_3 vapour, delivered at 1 bar pressure, and is thus also controlled by means of a control valve that responds to the dryer demand signal.

INITIAL PERFORMANCE

Stage 1 - High Frequency Power Supplies

The introduction of high frequency power supplies, coupled with the replacement of the inlet screens and introduction of baffle plates in the inlet duct to the ESPs resulted in a significant improvement in final PM emissions. Stable operation saw fairly consistent operation below the MES of 50 mg/Nm^3. This remains highly dependent on process conditions. Flue gas temperature is a major contributing process variable, as shown by the typical trend presented in Figure . The direct relationship between temperature and emission concentration is clearly demonstrated as an increase in flue gas temperature is closely followed by increased particulate emission concentration.

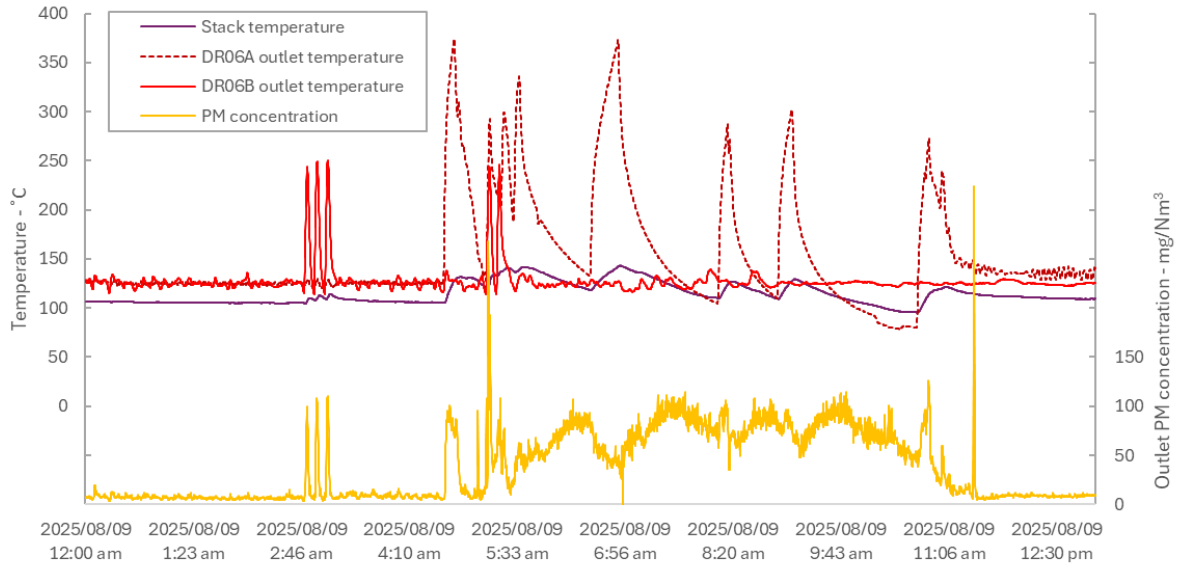


Figure 4: Process temperature and particulate emission trend.

This is due to particle resistivity being a function of temperature. Krigmont and Ferrigan (2025) state that traditional abatement measures, such as ESPs, often struggle with high resistivity fly ash. This is also confirmed by Trivedi and Phadke (2008), who noted that high resistivity dust does not readily accept or release a charge. Dust removal is adversely affected if the particle remains charged, since it may form an insulating layer on the collecting plate, leading to a condition which is known as back corona.

Trivedi and Phadke (2008) further describe this condition as occurring when the layer of collected material on the plates releases the charge into the gas passage instead of the collecting plate, dramatically lowering the field voltage and reducing further charging of the inter-electrode particles. An optimum particle resistivity of 5 x 10^9 to 5 x 10^{10} Ω.cm is suggested, also referenced by Okolo (2019) who listed various ranges as shown in Table II.

Table II. ESP performance vs resistivity, (Okolo, 2019)

Resistivity Ranges	**Classification**	**ESP Performance**
10^4 – 10^8 Ω.cm	Conductive dust or ash	Low Collection Efficiency
10^8 – 10^{10} Ω.cm	Normal resistivity	Moderate Collection Efficiency
10^{10} – 10^{11} Ω.cm	Moderate resistivity	High Collection Efficiency
10^{11} – 10^{13} Ω.cm	High resistivity	Low Collection Efficiency

Particle resistivity of both the Merensky and UG2 ore-type concentrates, the two major constituents of spray dryer feed, across a range of temperature and ambient moisture conditions is shown in Figure 5. Okolo (2019) explains that moisture present in the gas stream results in the formation of a thin layer of surface water on the particles, which reduces surface resistivity. Moisture in the gas stream has been measured at between 2% and 20%, which suggest that the resulting resistivity within operational outlet temperature range of the drying process would remain well above 1 x10^{11} Ω.cm.

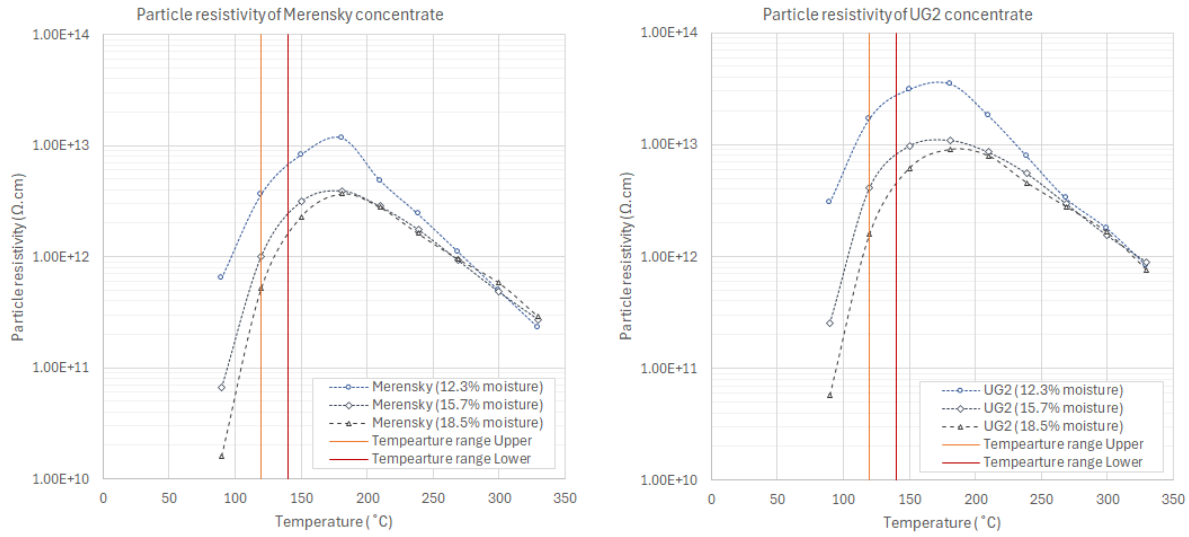


Figure 5: Particle resistivity of Merensky and UG2 concentrates, at 12.3%, 15.7% and 18.5% ambient moisture.

UG2 concentrate displays a significantly higher resistivity, thus leading to the conclusion that an increase in the ratio of UG2 material in the dryer feed blend will likely impact ESP performance. Should future mine production profiles shift towards a higher UG2 ratio, resultant dryer feed and flue gas PM product will become more difficult to collect in the ESP's.

Particle size distribution will also have a bearing on ESP performance, and the likely introduction of additional liberation steps in upstream concentrating circuits could result in a finer feed to the dryers. Krigmont *et al.,* (2020) characterised ESP inlet particles size distribution by a mass median diameter (MMD) and the geometric standard deviation of the particle size distribution (σ). NEP analyses involving various scenarios found that a finer MMD reduces ESP performance within the same particle spread, while a reduction in particle spread could increase ESP performance at the same MMD. It could be theorised that future finer distributions will also have a smaller spread, as only coarser fractions of concentrate streams should be targeted for further liberation.

A conservative view should however be maintained in that finer feed associated with a higher fraction of UG2 type ores will be treated in future, and ESP optimisation projects should take this into account.

Early stages of operation with the newly installed HFPS were hampered due to unstable control and self-limiting response by the power supplies. On-site generation of condition-specific VI curves confirmed that the field stability suffered from back corona discharges. Bacchiega *et al.,* (2004) provides a description of this phenomenon, stating that back-corona is a series of micro-discharges that occur in the air space within a collected layer of high resistivity particulate. These discharges form due to an excessive field being induced by the charge flowing through the surface layer of the collected material.

To counter this, a control methodology termed Intermittent Energising (IE), which actively limits electrical input from the HFPS to reduce spark rates, was instated. The full potential and capacity of the

power supplies are not achieved in this control mode, however field stability could be reached.

Stage 2 – Dual Flue Gas Conditioning

Hot commissioning and performance evaluation of the DFGC circuit was still underway at the time of submission of this paper. This section will thus cover initial observations pertaining to ESP performance with SO_3 injection, as well as key considerations to adopting this technology from lessons learnt.

ESP performance observations

Controlled injection tests of SO_3 were performed without the IE control mode. An improvement in voltage and current was immediately evident, which was expected due to the control system being able to utilise full capacity of the switch mode power supplies. Spark rates of each field reduced substantially, indicating an improvement in field stability and control over the back-corona effect.

SO_3 injection was started at 20% of the maximum injection concentration, followed by a stepped increase to 30%. The latter yielded optimal results with respect to ESP power input and stability, thus suggesting that ideal performance (in this instance at no.5 spray dryer) will be achieved at this injection rate. Cessation of controlled injection resulted in a gradual degradation of electrical performance in the 1st and 2nd electrical fields, as well as increasing spark rates, as can be seen from the trend presented in Figure 6.

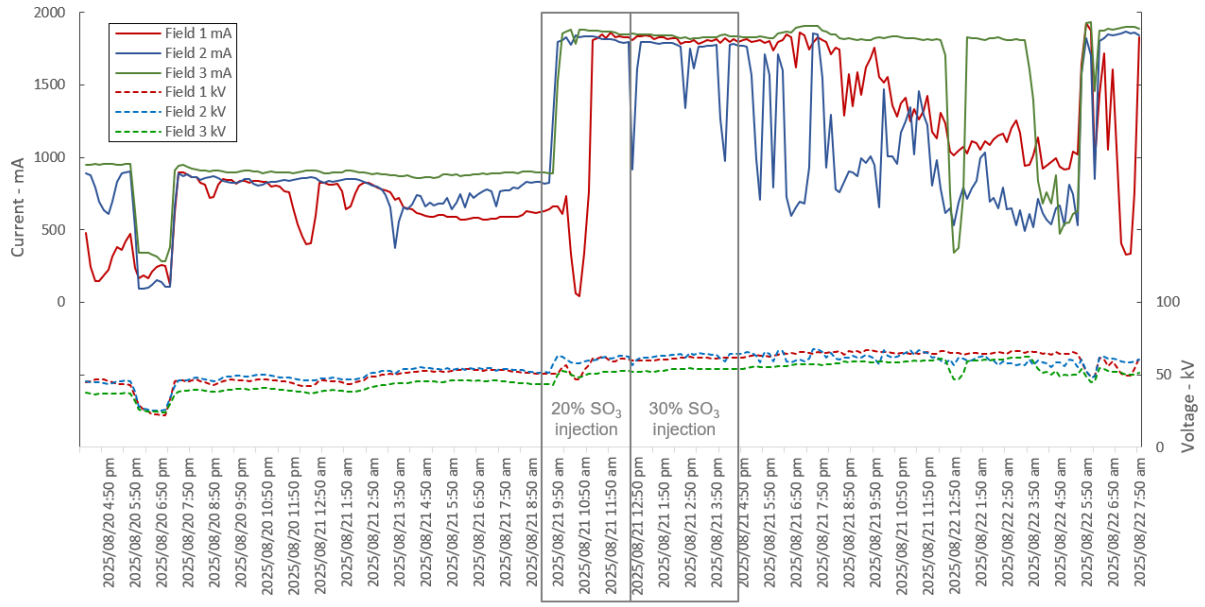


Figure 6: Electrical parameters of No.5 Spray Dryer ESP before, during and after SO_3 injection tests.

Average values of voltage, current, spark rates and power input prior to, during the injection tests, and thereafter, are listed in Table III.

Table III. No.5 Spray dryer ESP parameters prior to, during and after SO_3 injection

Parameter		Unit	Prior to injection	Injection at 20%	Injection at 30%	After injection
Dryer load	**Slurry feed**	*m^3/hr*	32.5	35.1	33.6	30.9
Voltage	**Field 1**	*kV*	45.9	55.0	61.0	63.4
	Field 2	*kV*	47.7	58.5	62.8	60.9
	Field 3	*kV*	39.8	48.9	53.4	56.1
Current	**Field 1**	*mA*	616	1018	1813	1360
	Field 2	*mA*	728	1545	1661	1070
	Field 3	*mA*	852	1566	1837	1644
Spark rate	**Field 1**	*SPM*	15.9	10.3	0.2	7.2
	Field 2	*SPM*	6.9	0.1	1.6	10.1
	Field 3	*SPM*	2.0	0.0	0.0	2.3
Power input	**Field 1**	*kW*	29.4	60.0	111.6	88.2
	Field 2	*kW*	36.2	93.0	106.2	69.2
	Field 3	*kW*	34.9	79.0	99.1	94.4

Similar trends were observed during initial injection at no.6 spray dryer, although the ideal SO_3 injection rate seems to be 50% of the maximum injection concentration for this dryer.

Isokinetic sampling will be performed after commissioning to confirm PM emission improvements. No firm conclusions can be drawn as yet. Ammonia injection test observations are not yet available, although it is expected to aid particulate capturing efficiencies. It is worth noting that ammonia injection will not be done in isolation and is supplementary to SO_3 gas modification.

Lessons learnt

This paper serves to introduce a proven technology in a new industrial sector. Equipment, raw materials and utilities required within the newly implemented circuits have none to very limited pre-existing expertise within Impala and its vendor base. Upfront planning and research assisted preparing for and managing the risks associated with these unknowns, but the following aspects can be shared to benefit future projects of a similar nature.

- Standard equipment or parts, readily available in the USA are uncommon in South Africa. Typical examples of this include construction materials such as weld-on sockets, standard 'off the shelf' pressure vessels (ammonia storage vessels), and various fittings and pipe supports.
- Plant layout and positioning within a brownfields project site face various constraints, and in this instance were impacted by spillage and wastewater control channels. As such, additional control measures and design adjustments were required to manage accessibility and particulate ingress risks.
- Steam generation and steam circuit control is sensitive to correct and complete insulation of the relevant piping and equipment. The placement and positioning of steam traps is also crucial to system operability and maintenance.
- A balance between pre-manufacturing and on-site manufacturing of mechanical components, specifically piping, was required to ensure optimal utilisation of on-site resources. The adoption of a flanged steam cladded pipe design can be considered a success.
- Even though sulfur is readily available within the country, the specification called for in this design is not. Sulfur pastilles of the required quality and form are readily available in US and Asian markets and are therefore an import requirement.

CONCLUSIONS

More stringent MES govern PM emissions from the spray drying operations at Impala's Rustenburg smelter complex. To ensure continuous compliance with the legislated standards, existing abatement equipment was upgraded by replacing older generation electrical components with newer generation High Frequency Power Supplies. Particle resistivity remains a limiting factor, affecting ESP performance at elevated process temperatures. SO_3 injection serves to counter the effects of high resistivity particulate and secure electrical stability within the ESP. Even though limited data is available, initial observations indicate that SO_3 injection into an ESP that recovers PGM concentrate particulate mirror efficiency improvements realised in the utility sector.

The introduction of ammonia as a supplementary conditioning agent in the Dual Flue Gas Conditioning is expected to enhance PM collection efficiencies and further reduce emissions.

Longer term performance in this application, along with operability and maintenance in a mining process plant environment will be included in a future update of this paper.

ACKNOWLEDGEMENTS

The authors would firstly like to thank Impala Platinum Limited for being afforded the opportunity of presenting this paper. Also for the support of senior management at Impala, Lesedi NS and Fuel Tech, Inc. during an extended commissioning period and ongoing finalisation and optimisation of the new plant.

Thank you to the Impala engineering and production staff, for their continued support, especially the development and fine-tuning of control philosophies and systems.

REFERENCES

Bacchiega, G., Gallimberti, I., Arrondel, V., Raizer, P., Lecointre, J., and Hamlil, M. (2004). Static and dynamic back-corona characteristics. *ICESP IX (9th International Conference on Electrostatic Precipitation)*, pp. 1-11. Kruger National Park.

Coetzee, V. (2006). Common-Sense Improvements to Electric Smelting at Impala Platinum. *Southern African Pyrometallurgy 2006*, pp. 43-62.

Farmer, T., Van Wyk, L., and Burger, J. (2018). *Application of Switch Mode Power Supplies on South African Coal.* Bordertown, New Jersey: Unpublished.

Krigmont, H. (2021, September 6). *Ammonia conditioning of flue gases. A White paper*. Retrieved from Alentecinc: https://www.alentecinc.com/papers/ammonia.html

Krigmont, H. V., and Ferrigan, J. J. (2018). Dual Flue Gas Conditioning Processes, Technology and Experience. *ICESP XV*, pp. 1-22. Charlotte.

Krigmont, H. V., and Ferrigan, J. J. (2025). Enhanced emission reduction: Dual flue gas conditioning's impact on mercury and particulate capture. *International Journal of Plasma Environmental Science and Technology*, pp. 1-19.

Krigmont, H., Watson, S., and Van Wyk, L. (2020). *PGM concentrate drier plant – Numerical ESP performance study for ESP emisison enhancement with FGC, DGFC and HFPS technologies.* Tswane: Lesedi Nuclear Services (Pty) Ltd. 43 pp.

Kruger, B. (2004). Recovery of SO2 from low strength off-gases. *International Platinum Conference 'Platinum Adding Value'*, pp. 59-62. Johannesburg: SAIMM.

Mariscotti, A., Sandrolini, L., Liu, S., and Ye, X. (2022). Chapter 3 - Transducers and amplifiers. In V. Majhi, V. K. Pandey, S. Paul, & A. Saikia, *Introduction to Biomedical Instrumentation and Its Applications* pp. 87-167. Academic Press.

Okolo, G. (2019). Resistivity and XRF report on Impala Platinum Limited PGM concentrate samples. Report No. P04502220651. Potchefstroom: North-West University. 50 pp.

Shanthakumar, S., Singh, D. N., and Phadke, R. (2008). Flue gas conditioning for reducing suspended particulate matter from thermal power stations. *Progress in Energy and Combustion Science, Volume 34, Issue 6, December 2008*, pp. 685-695.

Trivedi, S., and Phadke, R. (2008). Flue Gas Conditioning. *11th INternational Conference on Electrostatic Precipitation*, pp. 389-394. Hangzhou.



Bennie Havenga

Process Specialist: Smelting
Impala Platinum Holdings (Pty) Ltd

Bennie holds a Chemical Engineering degree from North-West University, obtained in 2008, whereafter he started his career as a Metallurgist at Impala Platinum. He presently serves as Process Specialist: Smelting within Impala Platinum's Processing Projects department. Bennie has over 15 years' experience in the PGM smelting industry, fulfilling a combination of technical support and project-related roles.

Quantitative spectroscopic analysis of co-existing Platinum Group Metals (PGMs) in iron matrix

T. Ncedo, A. Mkhohlakali, R. Letsoalo, J. Sehata, H. Mabowa, N. Ntsasa, J. Tshilongo

Mintek, South Africa

The simultaneous presence of platinum group metals (PGMs) and iron in geological and industrial samples presents analytical problems and opportunities in mineral processing, metallurgy, and recycling. The nickel sulphide (NiS) fire assay collection method provides an efficient pre-concentration procedure, facilitating precise spectroscopic measurement of PGMs in samples containing iron. This research reports a quantitative spectroscopic methodology employing Inductively Coupled Plasma Optical Emission Spectroscopy (ICP-OES), X-ray Fluorescence (XRF), and Inductively Coupled Plasma Mass Spectrometry (ICP-MS) for enhanced detection and quantification of Platinum Group Metals (PGMs: Pt, Pd, Rh, Ru, Ir). To enhance analytical precision and accuracy, calibration techniques, matrix interferences, and spectral overlaps were examined. The distinct charge densities, ionic radii, and polarities of iron (Fe) and platinum group metals (PGMs) strongly influence their chemical behavior and geochemical partitioning. Iron forms polar oxides capable of adsorbing trace PGMs, while the more noble and less polar PGMs preferentially concentrate in sulfide phases during magmatic differentiation. Iron commonly coexists with platinum group metals (PGMs) in mafic–ultramafic intrusions due to their shared chalcophile and siderophile behavior during magmatic differentiation. The technique's applicability for geochemical exploration and metallurgical evaluation is demonstrated by the results, which show good recovery rates for Pt, Pd, Rh, Ru and Ir in addition to iron. Despite satisfactory recoveries using ICP-OES, ICP-MS proved to be superior. The study highlights how crucial method optimization is for reliable PGM quantification in complex matrices comprising transition metals like iron in spectroscopic analysis.

INTRODUCTION

Platinum Group Metals (PGMs) include platinum (Pt), palladium (Pd), rhodium (Rh), iridium (Ir), osmium (Os), and ruthenium (Ru). These rare, precious metals are geochemically similar and tend to group together in nature in the Earth's crust (Zilibokwe, 2017). The six elements listed above generally occur together (except of osmium, which is more chalcophile) mainly within mafic-ultramafic igneous rocks, iron- and nickel-group associate mostly with sulphides and/or have siderophile behaviour. These six PGMs can be further classified into two sub-groups: - The iridium group (IPGE) consists of iridium, osmium and ruthenium. The elements in this sub-group are refractory, which means that they have high melting points and tend to condense out at high temperatures in the natural environment. The palladium group (PPGE) consists of ruthenium, rhodium, palladium and platinum. The elements in this sub-group are ore minerals in sulphide ore deposits that occur as mineral inclusions in base metal minerals, such as chalcopyrite, pyrrhotite, pentlandite and pyrite, which also tend to tend to condense out at lower temperatures compared to the IPGE members with which they are generally associated. PGMs occur in the Earth's mantle and are formed into ores that are mined worldwide. PGMs are economically and strategically significant due to their catalytic properties and industrial applications. In most geological deposits, PGMs are found in low concentrations, often co-existing with base metals such as iron (Fe).

The Bushveld Complex in South Africa is the world's largest PGM resource, with iron frequently associated in the same ore bodies (Masasire *et al.*, 2022). Accurate quantitative analysis of materials containing PGMs, iron, or both is a vital component of mining operations that extract these metals from raw ores and related materials and for environmental monitoring of these metals in wastes and pollution (Nowinski, 1992).

The high demand for PGMs, especially platinum and rhodium, for various industrial applications stems from their exceptional properties. For example, platinum is extremely resistant to corrosion and oxidation at high temperatures. PGMs serve as catalysts in the automotive industry, petrochemical processing, and fertilizer production. Additionally, they are utilized in semiconductor, electronic, and acoustical industries and play a significant role in jewellery crafting.

From a mining perspective, quantitative analysis provides a basis for measuring PGMs in ores, minerals, and concentrates. It can be used either to track the relative abundance of specific metals in a mineral, or the overall concentration of PGMs at different points in the mining or refining process. Quantitative analyses therefore can inform decisions about the progress of mining, as well as the feasibility of additional mining operations at a particular site. In the same way, such analyses may be used to ensure that certain levels of a metal are not exceeded during processing. Quantitative spectroscopic analysis of the platinum-group metals (PGMs) and iron is a dynamic, fast-moving field with rapid advances appearing almost continuously. Refinement of existing methods, the development of new techniques and instrumentation, and the combination of analytical approaches all provide a great impetus to future work (Handforth, 1999) (Nowinski, 1992). The complex nature of the samples and the low concentration levels of platinum group metals require the use of advanced analytical techniques.

The special prevalence of the platinum group metals in metallurgy and material science offers extensive opportunities for quantitative spectroscopic analyses of these elements, particularly in relation to their coexisting constituents. Detection sensitivity is the highest for the platinum group metals, second highest for gold, and the lowest for iron.

Quantitative spectroscopic methods are essential for the analysis of platinum group metals, particularly in samples where these metals coexist with other elements. This comparative analysis highlights the relative ease of detecting platinum group metals spectroscopically in samples where these elements coexist, thus complementing quantitative analytical methods employed when these metals are present together.

EXPERIMENTAL PROCEDURES

Materials

Two certified reference materials (CRMs) were used in this study as raw material samples. The CRMs used are called AMIS530 (PGMs ore) and AMIS165 (PGMs concentrate). The raw material samples were bought from African Mineral Standard (AMIS).

The certified chemical compositions of the PGMs for each raw material sample are presented in Table 1. The total PGMs concentrations for AMIS530 and AMIS165 are 3.68 ppm and 41.92 ppm respectively.

Table 1: Individual PGM concentrate (ppm)

Element	AMIS530	AMIS165
Au	0.03	1.66
Pd	1	19.1
Pt	1.7	16.9
Rh	0.32	1.72
Ru	0.52	2.02
Ir	0.11	0.52
Total	**3.68**	**41.92**

Sample preparation and procedure

The raw materials were split in a rotary splitter to obtain a representative sample used for the testwork. The representative samples were sized to a particle size range of -75 μm using laboratory sieves.

In a crucible, the sized material was weighed and mixed with a pre-mixed flux containing sodium carbonate, borax, and a nickel-sulfur collector. The charged crucible was then placed in a furnace and fused at high temperatures of 1050°C for a period of an hour. After the completion of fusion, the molten material was poured into an iron mould and allowed to solidify. The resulting products were separated into a matte button and slag.

The matte bead was then crushed using a hydraulic press, placed in a beaker, and mixed with a 37% hydrochloric acid (HCl) solution. The beaker was then placed on a hot plate, and dissolution was allowed to occur for a period of 2 hours. After dissolution, the mixture was allowed to cool down to room temperature before filtration.

The residue from filtration was further digested in a beaker using aqua regia solution. The digested solution was then washed with a 40% HCl solution and transferred to a beaker. The solution was then evaporated using a hot plate. After evaporation, the solution was cooled and transferred into a volumetric flask and filled up using deionized water. The produced solution was used for analysis. Both samples (AMIS 530 and AMIS 165) were prepared five times by different operators. The same solutions were analysed in ICP-OES and ICP-MS.

Spectroscopic analysis

Inductively Coupled Plasma Optical Emission Spectroscopy (ICP-OES) and Inductively Coupled Plasma Mass Spectrometry (ICP-MS) were employed in this study. The ICP-OES used was Agilent 5900 from Chemetrix, while ICP-MS used was Agilent MS HUNTER 7800 also from Chemetrix. A series of calibration standards were prepared from single elemental stock solutions bought from Stargate Scientific. For ICP-MS calibration standards, sample blanks, and samples were spiked with a constant amount of Rhenium (Re) and indium (In) as internal standards to correct for non-spectral interferences.

ICP-OES was used due to its robust multi-element capability and tolerance to matrix effects, while ICP-MS was used for trace PGM determination, taking advantage of its lower detection limits and sensitivity.

The operating parameters for ICP-OES and ICP-MS are presented in Table 2 and Table 3 respectively. The wavelengths and isotopes for individual PGMs used on ICP-OES and ICP-MS methods are tabulated in Table 4 and Table 5. The total of five (5) replicates analyses (n=5) were conducted for each of the analytes (i.e. elements) to ensure the reproducibility and statistically reliability, precision, accuracy of both ICP-MS and ICP-OES result as presented in table 6-9. The chosen number (i.e. n=5) of replicates is considered adequate for assessing both precision and accuracy, as it facilitates the significant statistical assessment measures such as STD and RDS %(CARGNELUTTI FILHO A, 2020).

Table 2: Operating parameters for ICP-OES

Parameters	**Conditions**
RF power (kW)	1.2
Viewing mode	Axial
Stabilization time	15s
Replicates	3
Rinse time	30s
Pump speed (rpm)	12
Nebulizer flow rate (L/min)	0.7
Plasma gas flow rate (L/min)	12
Auxiliary gas flow rate (L/min)	1

Table 3: Operating parameters for ICP-MS

Parameters	**Conditions**
Plasma power (kW)	1 400
Plasma gas	Argon
Plasma gas flow rate (L min-1)	17
Auxiliary gas flow rate (L min-1)	1.4
Nebulizer gas flow rate (L min-1)	0.75
Data acquisition mode	Peak hopping
Sample uptake rate (mL min-1)	0.8
Sampler cone	Cu
Skimmer Cone	Ni
Acquisition time (s)	100
Washout time (s)	120
Number of replicates	3

Table 4: Wavelengths for individual PGMs used in ICP-OES (nm)

Analyte	**Wavelength**
Au	267.594
Pt	299.796
Pd	340.458
Rh	343.489
Ru	349.894
Ir	224.268

Table 5: Isotopes for individual PGMs used in ICP-MS (M/z)

Analyte	Isotopes
Au	197
Pt	195
Pd	105
Rh	103
Ru	101
Ir	191

RESULTS AND DISCUSSION

AMIS 530

The chemical composition and recoveries of individual PGMs using ICP-OES and ICP-MS for the AMIS 530 sample are presented in Table 6 and Table 7. The best recoveries for ICP-OES method were attained for Pd at 98.6% suggesting that the extraction of Pd was efficient. The calculated recoveries for Au were high at >100%, whilst the other PGM recoveries were fairly low at <95%. High recoveries for Au suggest that the measured value was higher than the CRM value, as seen in the results. Low recoveries for Pt, Rh, Ru, and Ir were associated with low measured values when compared to the CRM values. The lowest recoveries of about 85% were attained for Ir. These low recoveries were attributed to spectral interferences. (Potts and Webb, 1992) showed that the emission lines of Ir often match with major matrix elements such as Fe, Ni, and Cu. In complex materials like PGM concentrates or slags, this spectral interference can compromise measurement precision and lead to Ir being reported at lower concentrations than actually present.

Regarding the ICP-MS method, the recoveries were fairly good for most of the PGMs except for Au. The recoveries for Au were high at >105% suggesting that the measured value was higher than the CRM value. These results were satisfactory as compared to those attained from ICP-OES.

Table 6: Chemical composition and calculated recoveries of individual PGMs from the ICP-OES method

AMIS 530	Au(ppm)	Pd(ppm)	Pt(ppm)	Rh(ppm)	Ru(ppm)	Ir(ppm)
1	0.035	0.974	1.561	0.297	0.471	0.080
2	0.030	1.034	1.627	0.314	0.524	0.100
3	0.031	0.968	1.567	0.299	0.483	0.100
4	0.037	0.974	1.550	0.299	0.488	0.093
5	0.034	0.981	1.576	0.303	0.471	0.096
Acc. Value	0.030	1.000	1.700	0.320	0.520	0.110
Mean	0.033	0.986	1.576	0.302	0.487	0.094
STD Dev	0.003	0.027	0.030	0.007	0.022	0.008
RSD	0.001	0.005	0.006	0.001	0.004	0.002
n	5	5	5	5	5	5
Recovery (%)	**111.333**	**98.620**	**92.718**	**94.500**	**93.731**	**85.091**

Table 7: Chemical composition and calculated recoveries of individual PGMs from the ICP-MS method

AMIS 530	Au(ppm)	Pd(ppm)	Pt(ppm)	Rh(ppm)	Ru(ppm)	Ir(ppm)
1	0.031	0.992	1.692	0.311	0.513	0.111
2	0.033	0.999	1.699	0.301	0.532	0.109
3	0.030	0.988	1.697	0.333	0.517	0.108
4	0.032	0.994	1.658	0.316	0.521	0.114
5	0.035	0.996	1.685	0.299	0.516	0.112
Acc. Value	0.030	1.000	1.700	0.320	0.520	0.110
Mean	0.032	0.994	1.686	0.312	0.520	0.111
STD Dev	0.002	0.004	0.017	0.014	0.007	0.002
RSD	0.000	0.001	0.003	0.003	0.001	0.000
n	5	5	5	5	5	5
Recovery (%)	**107.333**	**99.380**	**99.188**	**97.500**	**99.962**	**100.727**

AMIS 165

The measured chemical compositions and calculated recoveries for individual PGMs using ICP-OES and ICP-MS for the sample AMIS 165 are presented in Table 8 and Table 9. The recoveries attained using the ICP-OES method were fairly low at <97% for all PGMs. These low recoveries suggest that the measured values were lower than the CRM values for all PGMs.

The recoveries attained when using the ICP-MS method were significantly high at >96% for all PGMs. These results suggest that there were no major differences between the measured and CRM values.

Table 1: Chemical composition and calculated recoveries of individual PGMs from the ICP-OES method

AMIS 165	Au(ppm)	Pd(ppm)	Pt(ppm)	Rh(ppm)	Ru(ppm)	Ir(ppm)
1	1.546	17.415	16.278	1.577	1.869	0.494
2	1.573	18.218	16.110	1.581	1.931	0.501
3	1.538	17.116	15.405	1.517	1.762	0.458
4	1.552	18.719	16.874	1.658	1.991	0.453
5	1.584	18.235	16.119	1.598	1.947	0.492
Acc. Value	1.660	19.100	16.900	1.720	2.020	0.520
Mean	1.559	17.941	16.157	1.586	1.900	0.480
STD Dev	0.019	0.657	0.524	0.050	0.089	0.022
RSD	0.004	0.131	0.105	0.010	0.018	0.004
n	5	5	5	5	5	5
Recovery (%)	**93.892**	**93.930**	**95.605**	**92.221**	**94.059**	**92.231**

Table 2: Chemical composition and calculated recoveries of individual PGMs from the ICP-MS method

AMIS 165	**Au(ppm)**	**Pd(ppm)**	**Pt(ppm)**	**Rh(ppm)**	**Ru(ppm)**	**Ir(ppm)**
1	1.612	19.164	16.988	1.738	2.046	0.487
2	1.589	19.351	16.794	1.695	1.995	0.513
3	1.599	18.987	16.431	1.689	2.038	0.497
4	1.621	18.996	16.527	1.721	1.989	0.488
5	1.654	18.897	16.668	1.695	2.017	0.522
Acc. Value	1.660	19.100	16.900	1.720	2.020	0.520
Mean	1.615	19.079	16.682	1.708	2.017	0.501
STD Dev	0.025	0.180	0.220	0.021	0.025	0.016
RSD	0.005	0.036	0.044	0.004	0.005	0.003
n	5	5	5	5	5	5
Recovery (%)	**97.289**	**99.890**	**98.708**	**99.279**	**99.851**	**96.435**

Comparisons of the different techniques

The comparison between the ICP-OES and ICP-MS methods for both AMIS 530 and AMIS 165 shows that ICP-MS is the best technique to use for the determination of PGMs. The recoveries from the ICP-OES method were either on a higher (> 110%) or lower (< 95%) side, especially for the Ir. Also, the measured values had higher discrepancies when compared to the CRM values.

The ICP-MS method had significantly good results and the measured values were comparable with the CRM values. These results suggest that ICP-MS is the best technique for measuring individual PGMs in both the ores and concentrate samples.

CONCLUSION

Iron (Fe) and the Platinum Group Metals (PGMs) are transition metals located in the d-block of the periodic table. Although they share metallic bonding and catalytic properties, their distinct charge densities, ionic radii, and polarity strongly influence their chemical reactivity, bonding, and geochemical behaviour (Greenwood et al., 2012). In analytical chemistry, these contrasting chemical behaviours require selective dissolution and collection methods such as the Nickel Sulphide (NiS) collection technique to quantitatively recover PGMs in the presence of abundant iron prior to instrumental analysis by ICP-OES or ICP-MS (Atkins et al., 2010). The analytical results for AMIS 530 and AMIS 165 demonstrate that ICP-MS provides more accurate and reliable determinations of individual PGMs compared to ICP-OES. For ICP-OES, recoveries varied widely: Pd showed efficient extraction (≈98–99%), Au was overestimated (>100%), and Pt, Rh, Ru, and particularly Ir exhibited lower recoveries (<95%), with Ir being the most poorly recovered (~85% in AMIS 530). These low recoveries were largely due to spectral interferences, adsorption, and matrix effects, which are especially problematic for Ir due to overlap with major elements such as Fe, Ni, and Cu. In contrast, ICP-MS achieved consistently high recoveries (>96%) across all PGMs for both samples, with measured values closely matching the certified reference material (CRM) values. This indicates that ICP-MS is the preferred method for quantifying PGMs in complex matrices, ensuring both precision and accuracy.

REFERENCES

Atkins et al. (2010) *Shriver & Atkins' Inorganic Chemistry*. 5th edn. Oxford University Press.

CARGNELUTTI FILHO A, T.M. (2020) 'Sufficient Number of Replicates for Estimation of Dissimilarity Measures Among Maize Cultivars', *Revista Brasileira de Milho e Sorgo*, 19(October), p. 14. Available at: https://doi.org/10.18512/rbms2020v19e1181.

Greenwood et al. (2012) 'Chemistry of the Elements', *Elsevier* [Preprint].

Handforth, D.R. (1999) 'ni ve rs ity of e To w n v s e To w', (March).

Masasire, A. *et al.* (2022) 'A new preconcentration technique for the determination of PGMs and gold by fire assay and ICP-OES', *Journal of the Southern African Institute of Mining and Metallurgy*, 122(1), pp. 29–36. Available at: https://doi.org/10.17159/2411-9717/1638/2022.

Nowinski, P. (1992) 'Microwave digestion methods for preparation of platinum ore Microwave digestion methods for preparation of platinum ore samples for Icp analysis samples for Icp analysis'. Available at: https://digitalscholarship.unlv.edu/rtds.

Potts, P.J. and Webb, P.C. (1992) 'X-ray fluorescence spectrometry', 44, pp. 251–296.

Zilibokwe, N.J. (2017) 'Characterization of the distribution of Platinum Group Elements in Sulphide Ores within the Merensky Reef at Modikwa and Two Rivers Platinum Mines, Eastern Bushveld Complex, South Africa', (April).



Thembakazi Ncedo

Senior Technician
Mintek

Thembakazi is a Senior Technician in the Analytical Chemistry Department at Mintek, where she also serves as an Acting supervisor. With more than 15years of experience in analytical sciences, she has developed strong expertise in laboratory management, method development, and advanced instrumental analysis, including ICP-OES, ICP-MS, XRF, and chromatographic techniques.

In her leadership capacity, Thembakazi provides strategic direction to her department, mentors junior staff, and fosters a culture of accuracy, safety, and innovation. Her role ensures that Mintek's analytical outputs meet the highest standards, supporting critical research and development initiatives in mineral processing and metallurgy.

Academically, she holds a Postgraduate Diploma in Analytical Chemistry and is currently pursuing a Master of Science in Chemistry at the University of the Witwatersrand. Her postgraduate research focuses on the application of analytical techniques to address real-world challenges in materials science and sustainable resource utilization.

Quantification and mineral association of rhodium in low concentration ores using inductively coupled plasma – optical emission spectrometry

R. Letsoalo[1], A. Mkhohlakali[1], J. Sehata[1], N. Ntsasa[1], J. Tshilongo[1,2]

[1]Mintek, South Africa
[2]University of the Witwatersrand, South Africa

Rising global demand for rhodium (Rh) in the automotive industry contributes immensely to the market's growth and it has been predicted to reach over 1.06 million ounces in 2024. Rh is used largely as a catalyst in the automotive industry. Due to the volatile nature and difficulties in analysing the rhodium together with other platinum group metals from lead-based fire assay collection procedures, Mintek has developed a simple and highly selective method for the determination of Rh from low-grade platinum group metals (PGM) using various co-collectors. The recovered prill was subjected to high-pressure dissolution using tubes and incubated at a mild temperature for 8 hrs followed by instrumental analysis using inductively coupled plasma – optical emission spectrometry. This research focuses on quantification of Rh and mineral association in three major layers of Bushveld complex including Merensky (Western Limb), Upper group 2 (UG2, in the Eastern Limb) and Plaatreef (in the Northern Limb) using fire assay methods, utilising the lead oxide collector, palladium stock. Scanning electron microscope coupled with energy dispersive X-ray and X-ray diffraction indicates the silica dominance, with high silica (SiO_2), iron oxide, and magnesium-bearing chromite for UG2 and Platreef whereas Merensky indicates the anorthite ($CaAl_2Si2O_8$) mineral dominance. In addition, the particle size analysis exhibit that 90% of particle size 75 µm correspond to homogeneity of the sample. Using fire assay methodology, Rh recovery was determined using certified reference materials from UG2, Merensky, and Platreef and recovery of 90-110% was obtained. Figures of merit such as accuracy, percentage recovery and reproducibility in the range of 95-103%, precision ranging from 5-10% and detection limit of 0.1 mg/L confirmed that the method was fit for purpose. Rh in PGM-bearing ore samples were analysed using a validated method with concentrations determined between 2.5-65 mg/L.

Keywords: Platinum group metals, Fire assay methods, Bushveld complex, Carius tubes, ICP-OES, Rhodium

INTRODUCTION

Rhodium belongs to the platinum group metals (PGMs), which also includes the heavier trio of platinum, iridium, and osmium, as well as the lighter elements palladium and ruthenium.[1] These elements are currently regarded as the most costly or precious metals available on the open market, with values ranging from $1642 oz–1 for gold, $1599 oz–1 for platinum, and $116 oz–1 for ruthenium.[2] The low natural abundance of these metals in the Earth's crust (0.001 g ton–1), their localised global distribution, and PGM concentrations ranging from 3.0 to 5.5 g ton–1 in the well-known PGM's reef deposits are some of the factors that contribute to their high economic worth.[3]

Rhodium's widespread industrial applications stem from its excellent catalytic properties, high melting point, corrosion resistance, and stable chemical properties, making it crucial for automotive catalysts, jewellery, medicine and chemical processing.[4] Its ability to reduce to reduce harmful nitrogen oxides makes it an indispensable in environmental control, while its use with platinum in alloys creates high-performing materials for specialised equipment in glass and chemical manufacturing industries.[5][6][7][8] According to previous reports, automotive catalysts account for more than 65%, chemical industry 21.26%, jewellery 9.42% and investment accounts for 4%.[4] Figure 1, demonstrates the PGM demands in different industrial sectors.[7]

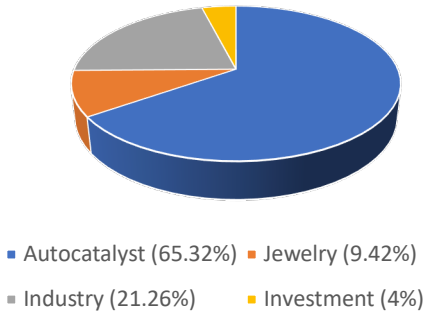


Figure 1: Proportion of PGM's demands in different industrial sectors.

Determining rhodium precisely in geological samples is vital for both geological science and precious metal processing because it enables accurate mineral resource estimation, informs geological models, and supports the economic viability of mining operations by providing data for processing, such as recycling from catalytic converters. However, determining ultra-trace metals is problematic due to their extremely low concentrations, which require sensitive detection methods and careful sample preparation.[9] High volatility complicates sample handling, while its uneven distribution on the Earth's crust makes finding representative samples more challenging.[9]

Rhodium is typically determined in ores by using the fire assay technique to concentrate it into a metal bead, which is then dissolved and analysed using instrumental techniques such as inductively coupled plasma – optical emission spectrometry (ICP-OES), inductively coupled plasma mass spectrometry (ICP-MS) and Atomic Absorption Spectroscopy (AAS). The common fire assay procedure uses lead or nickel sulfide as a collector to concentrate and other PGMs from the ore matrix into a prill or button. This concentrated beat is then chemically dissolved, often in aqua regia and the resulting solution is analysed by a technique like ICP-OES or MS to measure the concentration of rhodium.

Figure 2 depicts the conventional fire assay process, which involves preparation of the sample, heating it at high temperature to melt base metals and concentrate the precious metals into a lead button and other precious metals, and then performing cupellation by slowly oxidising the lead to form a refined precious metal button containing rhodium. This refined button is then dissolved, and the rhodium is quantified using techniques like AAS, ICP-OES and ICP-MS.

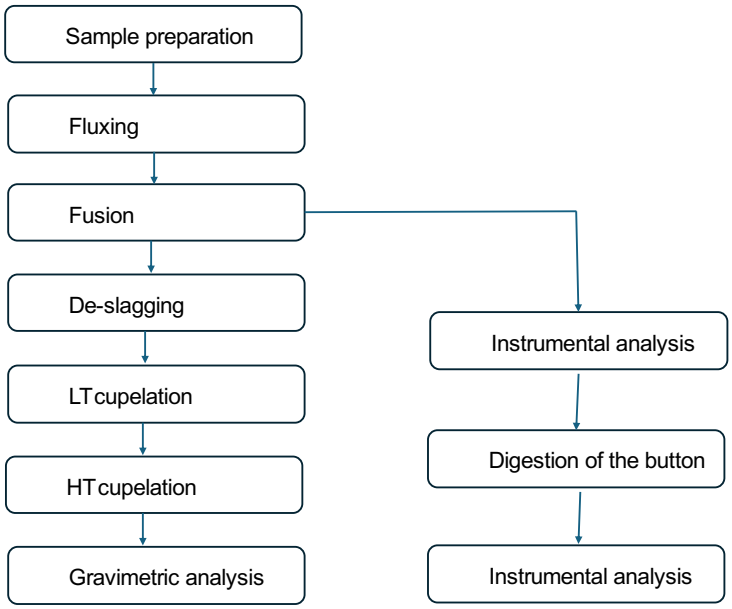


Figure 2: Summary of steps involved in the determination of PGM in fire assay.

Mintek has developed a method to separate rhodium from low-grade PGM bearing ores using co-collectors, followed by a high-pressure dissolution in tubes, mild temperature incubation for overnight and analysis by ICP-OES. This process appears to be a form of metallurgical separation and analysis where rhodium is selectively precipitated, dissolved and then measured with high precision.

Experimental procedure

Fire assay pre-concentration

A well-milled geological sample is mixed with a pre-mixed flux and a collector metal like nickel sulfide (NiS) or lead (Pb). The mixture is heated to over 1000°C in a crucible. During fusion, the PGMs, including rhodium, are collected into a molten NiS or Pb button. The unwanted rock matrix forms a lighter, easily separable slag. The metallic or NiS button, now containing the concentrated PGMs, is separated from the slag and dissolved. The NiS button is dissolved in a strong acid, leaving behind the PGMs as an insoluble residue. This residue is then dissolved in aqua regia (a mixture of nitric and hydrochloric acid) to prepare it for analysis. The lead button is treated in a process called cupellation to remove the lead, leaving a PGM-rich metallic bead that is then dissolved in acid.

Sample dissolution

For the complete dissolution of rhodium, which is inert, digestion is recommended using a combination of acids.

Instrumentation

Agilent ICP-OES 5900 series was used for this exercise. The instrument operating parameters are summarised in Table I.

Table I: Operating parameters for ICP-OES

Parameters	
RF power (kW)	1.2
Viewing mode	axial
Stabilisation time	15s
Replicates	3
Rinse time	30s
Pump speed (rpm)	12
Nebuliser flow rate (L/min)	0.7
Plasma gas flow rate (L/min)	12.0
Auxiliary gas flow rate (L/min)	1.00
Make up gas flow rate (L/min)	0.00

RESULTS AND DISCUSSION

Accurate determination of PGMs, including rhodium, is crucial because these elements are economically valuable and provide insights into geological processes, as well as the origin and evolution of the Earth. Despite their importance, determining their content is challenging due to the very low concentration in many mineral deposits, requiring sophisticated preconcentration techniques for effective analysis. A correct wavelength selection is crucial for the identification and analysis of an analyte because it is a unique spectral 'fingerprint' that identifies the substance. Choosing the right wavelength, often at the peak of an analyte's absorption spectrum allows for a maximum sensitivity and helps differentiate it from other substances in a complex sample.
Wavelength selection for Rh quantification

In this paper qualitative analysis was performed on a certified reference material (CRM) to identify its elemental composition, which is necessary to select an appropriate rhodium wavelength for analysis while minimising spectral interference. According to the data obtained, 343.488 nm was found to be the best line for the quantification of rhodium, with a linearity of r2 = 0.99999 correlation coefficient. This line has minimal interferences from other elements and has high recoveries. Figure 3 shows the wavelength and calibration curve for rhodium.

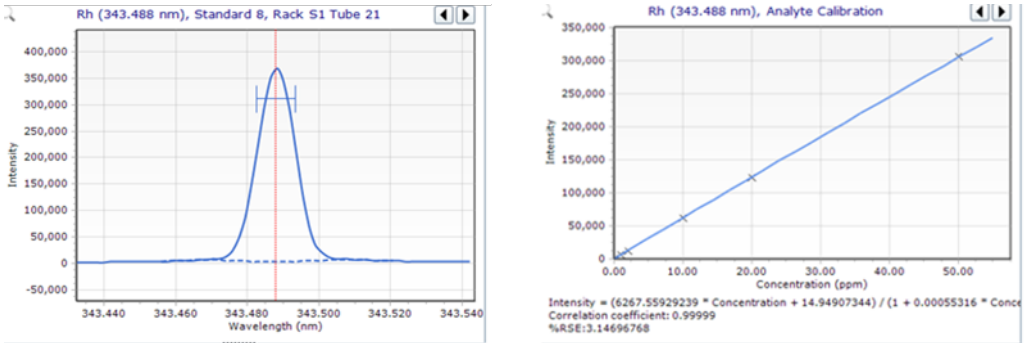


Figure 3: Wavelength and calibration of Rhodium at 343.488 nm.

Having successfully established conditions for the quantification of rhodium using ICP-OES, three CRMs representing the three major layers of Bushveld Igneous Complex (BIC) (Merensky (Amis 314), UG2 (SARM 189), and Platreef (Amis768)) underwent a qualitative investigation to determine the

presence of rhodium and its concentrations. High recoveries (>90% to <110%) (Tables II-IV) were observed in all the CRMs evaluated; showing the robustness of the method for collection and quantification respectively.

Table II: Summary of Rh results and statistical analysis of CRM from Merensky reef

Sample ID	Rh (ppm)
Amis 314/1	1.813
Amis 314/2	1.82
Amis 314/3	1.773
Amis 314/4	1.816
Amis 314/5	1.802
Accurate value	1.89
Recovery%	96.2434
Average	1.819
SD	0.01899
RSD	1.0441

Table III: Summary of Rh results and statistical analysis of CRM from Platreef

Sample ID	Rh (ppm)
Amis 768/1	0.18
Amis 768/2	0.256
Amis 768/3	0.107
Amis 768/4	0.18
Amis 768/5	0.256
Accurate value	0.189
Recovery%	103.5979
Average	0.1958
SD	0.062516
RSD	31.92829

Table IV: Summary of Rh results and statistical analysis of CRM from UG2

Sample ID	Rh (ppm)
SARM 142/1	1.813
SARM 142/2	1.82
SARM 142/3	1.773
SARM 142/4	1.816
SARM 142/5	1.802
Accurate value	0.18
Recovery%	96.2434
Average	0.18516667
SD	0.00872735
RSD	4.71324121

Mineral characteristics
Mineral characteristics of different BIC layers with PGM vary significantly by reef, affecting the PGM recovery. Establishing and understanding of the minerology of the ore is critical for successful quantification.

X-ray diffraction analysis
The X-ray diffraction (XRD) of Merensky shows the anorthite (CaAl2Si2O8) as the predominant mineral, whereas Platreef shows high silica dominance with SiO2, ion oxide and magnesium bearing chromite (Figure 4). These minerals are commonly known to co-exist with the PGM in the ores.

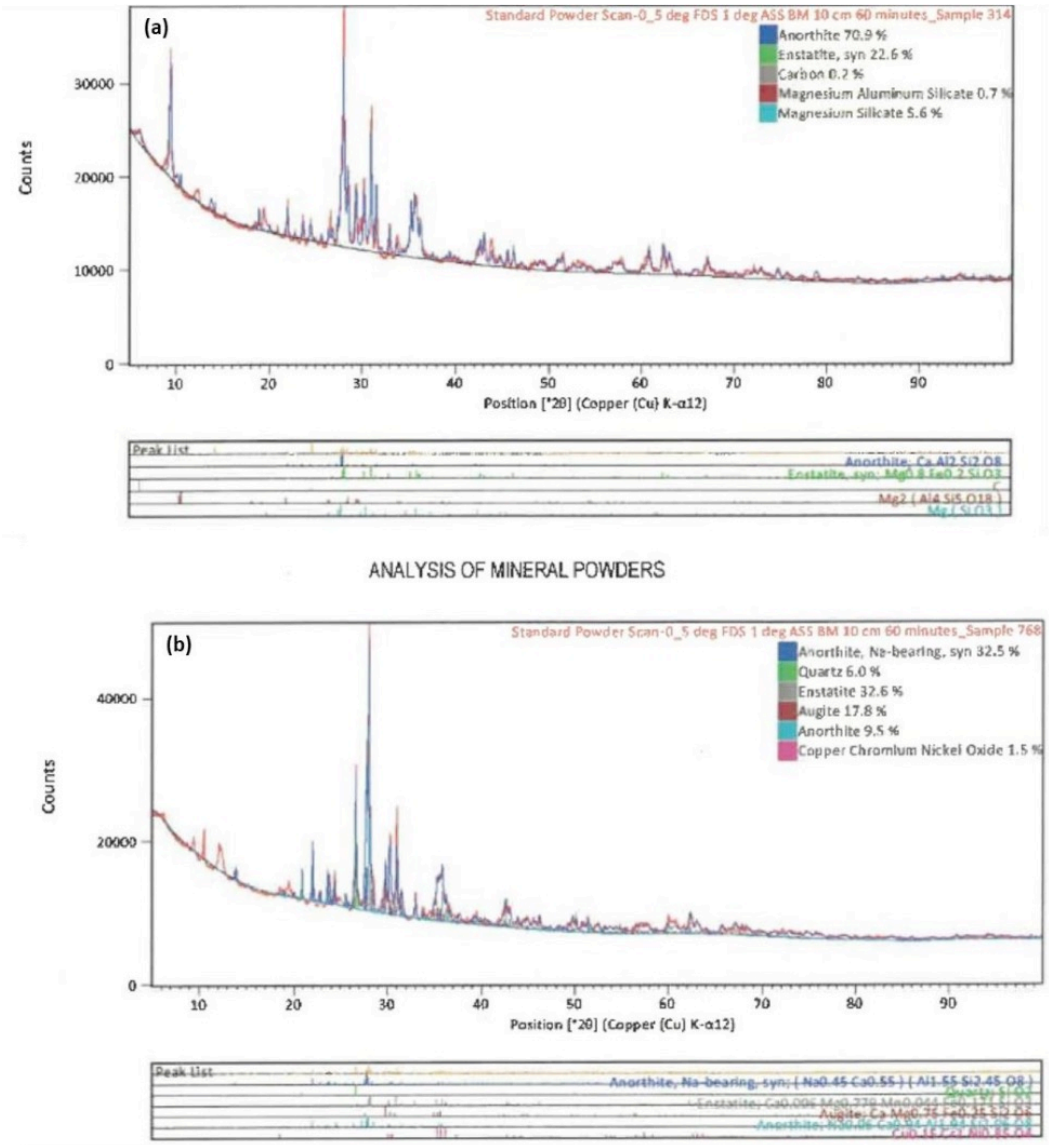


Figure 4: XRD spectra of Amis 314 (a) and Amis 768 (b).

SEM-EDX analysis
Figure 5 displays a scanning electron microscopy with energy dispersive X-ray spectroscopy (SEM-EDX) of PGMs deposits with significant XRD corroboration showing abundant silica (SiO2), ion oxide, and (Mg-bearing chromite) for Platreef; while Merensky reveals the anorthite (CaAl2Si2O8) mineral dominance.

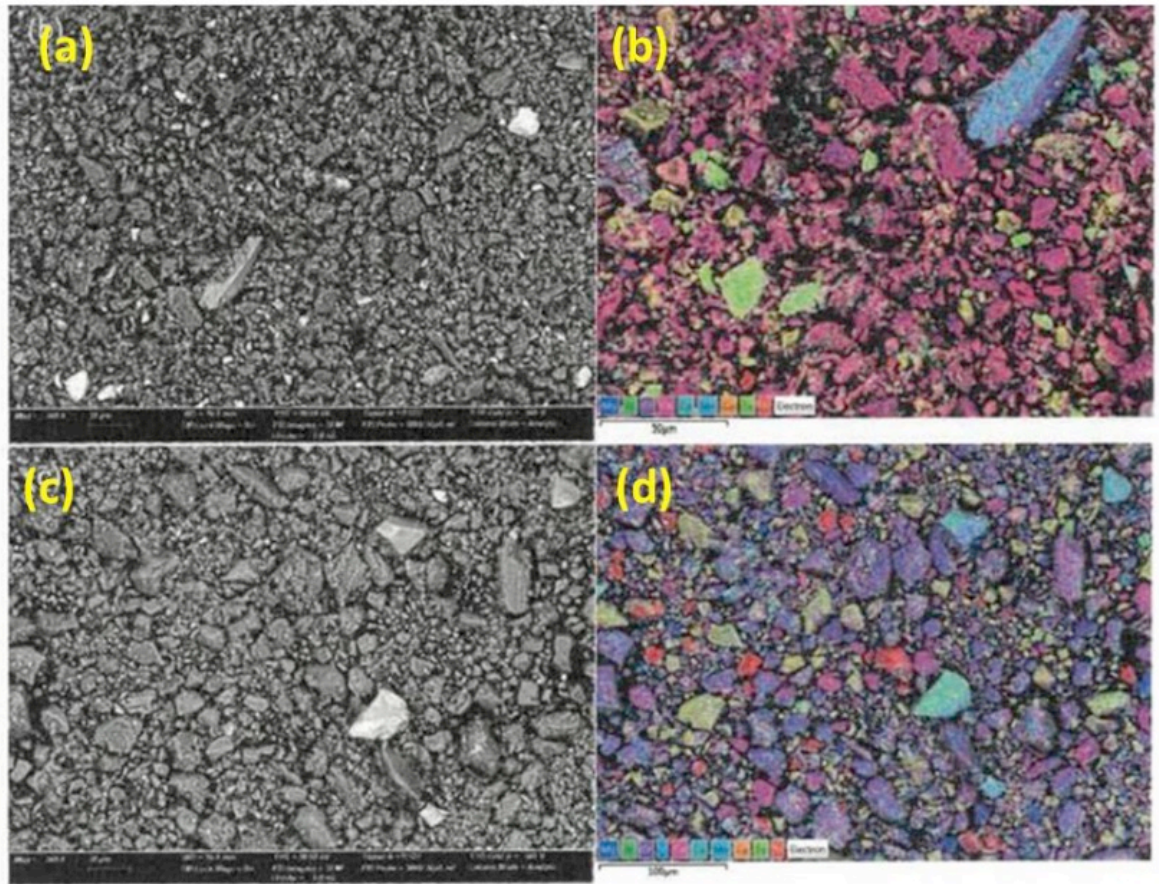


Figure 5: SEM-EDX of Amis 314 (a-b) and Amis 768 (c-d).

CONCLUSION

Rhodium has been successfully isolated and quantified using the conventional fire assay procedure followed by high pressure dissolution and ICP-OES analysis. The procedure demonstrates that this method has great stability and reproducibility. XRD and SEM-EDX comprehensive analysis depicts the presence and distribution key PGM minerals, host gangue (silicates and oxides) and sulfide minerals.

REFERENCES:

[1] A. LeBeau, "Platinum Group Elements: Palladium, Iridium, Osmium, Rhodium, and Ruthenium," Hamilt. Hardy's Ind. Toxicol. Sixth Ed., pp. 187–192, 2015, doi: 10.1002/9781118834015.ch27.

[2] T. T. Chiweshe, W. Purcell, and J. A. Venter, "Quantification of rhodium in a series of inorganic and organometallic compounds using cobalt as internal standard," South African J. Chem., vol. 66, pp. 7–16, 2013.

[3] T. T. Chiweshe, W. Purcell, and J. A. Venter, "Quantification of rhodium in a series of inorganic and organometallic compounds using cobalt as internal standard," South African J. Chem., vol. 66, no. August 2013, pp. 7–16, 2013.

[4] S. Brown and M. Underwood, “Johnson Matthey - PGM market report May 2025,” PGM Mark. Rep., no. May, pp. 1–48, 2025, [Online]. Available: http://www.platinum.matthey.com/services/market-research/pgm-market-reports

[5] H. Tang, Z. Peng, R. Tian, L. Ye, J. Zhang, M. Rao, and G. Li., “Platinum-group metals: Demand, supply, applications and their recycling from spent automotive catalysts,” J. Environ. Chem. Eng., vol. 11, no. 5, p. 110237, 2023, doi: 10.1016/j.jece.2023.110237.

[6] I. Yakoumis, M. Panou, A. M. Moschovi, and D. Panias, “Recovery of platinum group metals from spent automotive catalysts: A review,” Clean. Eng. Technol., vol. 3, p. 100112, 2021, doi: 10.1016/j.clet.2021.100112.

[7] S. Sun, C. Jin, W. He, G. Li, H. Zhu, and J. Huang, “A review on management of waste three-way catalysts and strategies for recovery of platinum group metals from them,” J. Environ. Manage., vol. 305, no. November 2021, p. 114383, 2022, doi: 10.1016/j.jenvman.2021.114383.

[8] H. Tang, P. Zhiwei, L. Zhizhong, M. Yutian, Z. Jian, Y. Lei, W. Liancheng, R. Mingjun, L. Guanghui, and J. Tao, “Recovery of platinum-group metals from spent catalysts by microwave smelting,” J. Clean. Prod., vol. 318, no. November 2020, p. 128266, 2021, doi: 10.1016/j.jclepro.2021.128266.

[9] W. Ni, X. Mao, M. Yao, Q. Sun, X. Guo, H. Zhang, and L. Liu, “Bismuth-Remaining Cupellation Fire Assay Preconcentration Combined with Inductively Coupled Plasma Mass Spectrometry for the Simultaneous Determination of Ultratrace Au, Pt, Pd, Ru, Rh, and Ir in Geologic Samples,” Int. J. Anal. Chem., vol. 2021, 2021, doi: 10.1155/2021/9960673.

Comparison of dissolution methods for ICP-OES analysis of PGMs from printed circuit boards

A. Mkhohlakali[1], J. Sehata[1], N. Ntsasa[1,2], R. Letsoalo[1], M.H. Mabowa[1], J. Tshilongo[1,2]

[1]Mintek, South Africa
[2]University of the Witwatersrand, South Africa

Despite the adoption of appropriate recycling processes, the increasing volume of electronic waste (printed circuit boards (PCBs)) around the globe may jeopardise the development of new technologies while also having a negative impact on the environment if waste is not properly managed. This is because this waste contains large amounts of valuable metals and harmful materials. Identifying and recovering the precious metallic components from such waste PCB is also critical to meeting market demand given restricted resources. Herein, we compare fire assay and microwave acid digestion methods to recover precious metals using inductively coupled plasma optical emission spectrometry (ICP-OES). A PCB head sample was dismantled physically, crushed, milled and pulverised and 90% of particles passed the 75 µm to maintain homogeneity. Various acids mixture was used including concentrated aqua regia (AR), AR + hydrofluoric acid (HF), AR+ hydrogen peroxide (H_2O_2) and AR+HF+ H_2O_2 all assisted with microwave. ICP-OES indicated the higher PGE recovery for lead fire assay (Pb-FA), ranging (Au =134 ppm, Pd =74.78 ppm, Pt =0.264) as compared to microwave-assisted in various conditions ranging from (Au=117ppm, Pd= 59.5 ppm, Pt= 0.233). Moreover, the results showed high accuracy and recovery percent for the fire assay method and microwave-assisted aqua regia and HF. To conduct contextualisation, in this paper a bibliometric analysis on recent literature between 2001-2025 was conducted, revealing how metal recovery through MW aasisted, hydrometallurgy and pyrometallurgy approach is relevant. The interrelation between keyword map highlights the increasing demand for advanced analytical techniques like ICP-OES, SENM EDX and XRD in ensuring eco-friendly recycling of waste-PCBs within the circular economy. Results indicate the opportunity for recycling and repurposing e-waste, particularly waste-PCBs, will be crucial for both economic and environmental benefits. The incorporation of bibliometric analysis in experimental approach indicated the scientific relevance, methodology justified with global research priorities on PGMs recycling, specifically from e-waste.

Keywords; Recycling, Printed circuit boards, Fire assay, Microwave-assisted acid digestion, ICP-OES, Bibliometric analysis

INTRODUCTION

The demand for platinum-group metals (PGMs), such as Pt, Pd, and Rh, is significantly higher than the availability of natural resources worldwide. PGE concentrations are far higher in secondary sources, like printed circuit boards (PCBs), and used-car catalytic converters, than they are in corresponding ore (Yakoumis et al., 2021). Over 57% of PGMs in Europe are reportedly supplied by wasted auto catalytic converters, which is why they are regarded as such an important resource for PGM recovery.

Based on the amount of PGMs consumed in automotive catalysts or the amount of recoverable PGMs in new car sales/registrations, respectively, it is estimated that 195–307 t or 52–478 t of PGMs can be reclaimed from the catalytic convertors each year (Moleko-boyce et al., 2022). Considering the implementation of appropriate recycling techniques, the growing volume of electronic trash such as PCB around the world may jeopardise the development of new technologies while also having a severe influence on the environment if waste is not adequately managed (Jain et al., 2023). This is because this waste contains a considerable number of precious metals PGMs, value-added metals as well as hazardous compounds (Chidunchi et al., 2024). Identifying and recovering precious metallic components from discarded PCBs is also crucial to meeting market demand, given limited resources. There is extensive research on recovery of PGMs from PCBs, some of these methods include hydrometallurgical and pyrometallurgical approaches (Oke & Potgieter, 2024). PGMs are recovered from PCBs) using both hydrometallurgical and pyrometallurgical processes, each having unique advantages and challenges. Recent research has demonstrated the efficiency of these methods in obtaining important metals while resolving environmental issues (Kumari et al., 2024) (Dias et al., 2023). Fire assay as a classical method: Fire assay analysis enjoys its advantages and reputation as the most reliable procedure; the environmental shortcoming receives criticism due to the production of hazardous waste and human exposure to lead(Susanto et al., 2018) (Blyth et al., 2004). Lead gradually accumulates in human bones, although early detrimental effects are detected in the central nervous system, plasma, bone marrow, and kidneys. Additionally, PGMs and heavy metals such as Pb and Ni to name a few, are commonly employed in a variety of applications as abovementioned, resulting in resource scarcity despite significant efforts to safeguard the environment. As a result, it is critical to recirculate the precious metals through recovery and recycling. Furthermore, the driving force for such activities stems from a significant gap between PGM supply, demand, and recycling, as well as the expected rapid depletion of Ni, PGMs, and Pb resources. Thus, recovering PGMs and other essential minerals from waste and secondary sources is of fundamental importance. This study compares microwave-assisted acid dissolution with the classical fire assay approach for the recovery of platinum group elements (PGEs) followed by analysis using Inductively Coupled Plasma Optical Emission Spectroscopy (ICP-OES). Additionally, Bibliometric analysis is a statistical approach of quantitative assessment of published documents from datasets using tools like VOSviewer, Citespace, and bibliometric R:studio (biblioshiny) (Nurvianie & Sundari, 2024), (Aria & Cuccurullo, 2017). Bibliometric analysis is a quantitative analytical tool used in research to identify and evaluate the numerous research trends, inter-relationships, and impacts of publication that have been conducted in the fields of science and engineering (Ananda et al., 2025), The significance of this tool is its ability to strengthen the novelty of the research through providing objectives justification for choosing the analytical approach through visualisation of the global research trends and highlighting the research gaps (i.e, areas of improvement). In this paper, the bibliometric analysis indicated the lack of side-by-side benchmarking of the dissolution methods and pre-concentration method for PGMs in electronic waste, particularly waste-PCBs. Moreover, the work showed the under-explored gaps, revealing that the emphasis of PGMs recovery is on hydrometallurgy and pyrometallurgy process but rarely on preconcentration and dissolution techniques under the homogenised (conformal) analytical conditions.

BIBLIOMETRIC ANALYSIS OF PGMS IN PCBS

Methodology approach

In this paper, Scopus was used for dataset collection using the search keywords such as 'Platinum' and 'Group' and 'Metals'' and 'Printed' and 'Circuit' and 'Boards'. The duration used for the datasets was from 2001 to 2025. The data extraction was performed using a program such as VOSviewer (version 1.6.2.0) and the R package biblioshiny for the bibliometric analysis approach. As illustrated, the approach involves four phases, including (i) setting up R package or VOsviewer, (ii) importing library, biblimetrics::biblioshiny and creating a MA based bibliometric in the case of VOSviwer, (iii) Loading of CSV files on web interface (shiny), (iv) Results which includes analytics matrix: word cloud, co-occurrence network and the leading nations. The outcomes indicate a co-occurrence network, word cloud and authorship by countries. These results enable researchers to identify the correlations between the frequency of co-occurring keywords in the collected articles, co-occurring networks, annual

scientific distribution, authorship by country, as well as the essential future research directions for the themes in this discipline.

Interrelation between the keywords

The bibliometric visualisation is generated using VOSviewer and the R-studio package (i.e., biblioshiny web interface) to visualise databases like Scopus, PubMed, Citespace, and Web of Science (WoS) to display the keywords and interrelationship among the co-occurrence-keywords(Zhao et al., 2024), (Kirby, 2023),(Olatinwo, 2022). Figure 3 (a-b) displays the interrelationship among the keywords using the co-occurrence network map visualisation (2 (a) and word cloud (2(b). which reveals the most frequent search words in the thematic area of PGMs in waste-PCBs. The size of the words ranges from 'printed circuit boards', 'recycling', 'platinum group metals', 'electronic waste', 'metal recovery', 'environmental impact', waste printed circuit boards, and microwave-assisted digestion to name a few. The mapped network represents the different keywords, and lines reflect the association among the keywords. In addition, each node differs in size, which also illustrates the frequency of keyword usage (Ishak et al., 2023). In this regard, the most searched documents included 'platinum group metals' and 'printed circuit boards'. The areas of improvement lie on dissolution methods like microwave-assisted digestion, which show the small size of word cloud. This co-occurrence keywords visualisation is useful for researcher and industry development on recycling of waste PCBs for PGMs recovery, which also enables the quick identification of the emerging areas (Long et al., 2022). The network map visualisation of keywords is displayed in Figure 2 (b), highlighting four major clusters. The first cluster is denoted in green, centres in printed circuit boards, platinum group metals, copper, metal recovery, hydrometallurgy, electronic waste, and recovery of organic pollutants. The second cluster, represented in blue is composed of metal recycling, sustainability, catalysts, chemistry, timing circuits, waste printed circuit boards. The third cluster is denoted in yellow, which includes silver, neobbium, materials waste flow analysis, gold, silver, metallurgy. The red cluster is centred on chemical composition, metals, concentration parametors, ion, aluminium, lanthenides, nickel, zinc,tin, mining

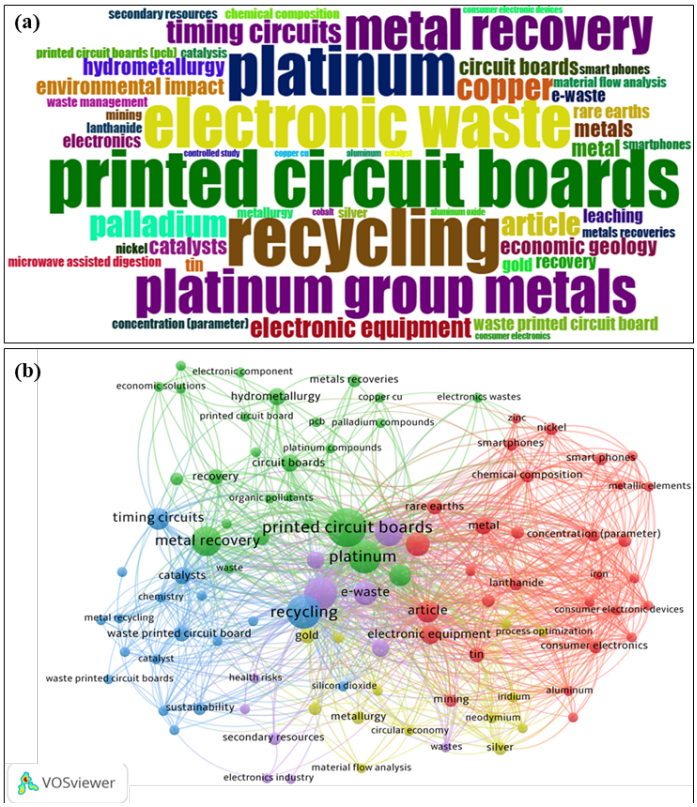


Figure 1. (a) Frequency of key words from R-studio biblioshiny and (b) keywords visualisation from VOSviewer of PGMs in waste-PCBs.

Leading countries
Figure 2 illustrates the top 15 countries globally that are leading in publications in the research area of PGMs recovery in waste-PCBs recycling. It can be seen that France leads with four publications, followed by China and the United States of America with three documents published. Previous study indicates that PGMs recovery originates from China and the USA who collectively published 60% of the publications. Interesting to note, France is the leading country in publications, which may be due to the strong collaboration of France with the European Union. South Africa, which is a developing country, indicates emerging research activities in pyrometallurgical and hydrometallurgical processes due to a strong mining sector which requires improved technologies for metal recovery from mineral ores and e-waste. These countries indicate an increasing number of publications, which may be attributed to strong collaboration through the EU Horizon 2020 funding programme.

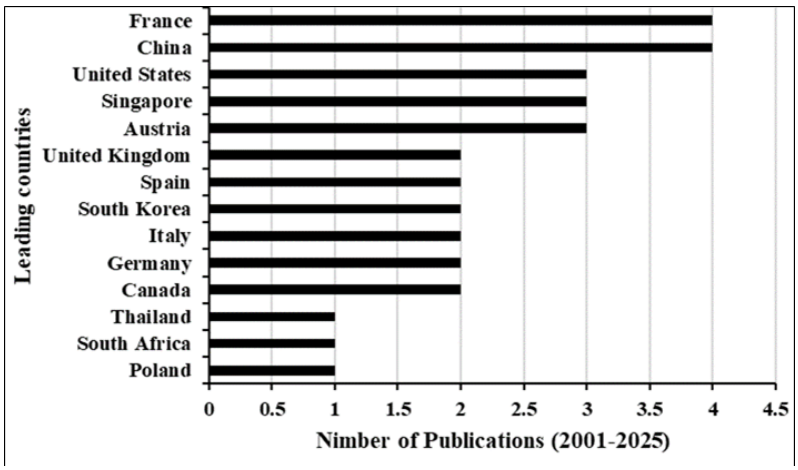


Figure 2. Top 15 countries with research outputs in PGMs from waste-PCBs.

EXPERIMENTAL

Analytical instrumentation
Inductively coupled plasma optical emission spectroscopy (ICP-OES)

Agilent 5900 ICP-OES produced by Agilent Technologies in California, USA, equipped with ICP-Expert software (version:7.5.4.11997) A coupled device detector was utilised to analyse platinum group elements (PGEs). Table 1 summarises the operating conditions used. The Malvern Panalytical particle size analyser was used to analyse particle size distribution of PGE after milling.

Table I. The Agilent 5900: a summary of operating conditions

Parameters	**Conditions**
RF generator	1.20 kW
Plasma gas flow rate	Argon. 15 $Lmin^{-1}$
Auxiliary gas flow rate	1.50 $Lmin^{-1}$
Pump rate	15 rpm
Nebuliser flow rate	0.75 $Lmin^{-1}$

Rinse time	120 s
Sample uptake rate	0.8 $mLmin^{-1}$
Replicate measurement	3

Materials and reagents

All solutions were made from ultra-pure water with a resistance of 18 MΩ cm using a Milli-Q purification system (MilliporeSigma, Bedford, MA, USA). The digestion solvents included 65% (w/w) concentrated nitric acid (HNO_3) (ACS, South Africa), 50 % (w/w) Hydrogen peroxide (H_2O_2), 48% (w/w) hydrofluoric acid (HF) 37% (w/w) Hydrochloric acid (HCl), all manufactured from Merc, Sigma Aldrich. A stock (100 ppm) of multi-platinum group elements (Ir, Os, Rh, Pd, Pt, Au) from VHG labs, Manchester, NH, (USA) was utilised to prepare calibration curves. The standard calibration solutions were prepared in the range of 0.05 ppm to 50 ppm for ICP-OES analysis. The preparation of the working solution was done by diluting 100 ppm stock solution with 0.05% (w/w) of nitric acid to maintain stability and prevent the precipitation of the analyte in the flask. The PCBs were obtained pre-processed from a local e-waste recycler (Desco Electronic Waste Recyclers, located in Pomona, Kempton Park, Gauteng). In brief, the concentrate was created through mechanical and physical beneficiation of discarded PCBs. This is comminution by shredding, gravity, and magnetic separation followed by electrostatic separation to generate a concentrate of coarse metallic grains free of the plastic and ceramic components.

Microwave-Assisted acid digestion

The microwave-assisted acid (MWA) digestion procedure was adapted according to previous studies in (Mceliseni C. Zuma, 2021) with slight modification. MWA studies were carried out using a CEM microwave digestion system (MARSTM 6) with microprocessor control in a 110 mL autoclave-style reactor with PTFE internals and no metallic elements. The PCB samples (PCB-1, PCB-2) masses were 0.25g, weighed using an analytical balance and were transferred in the PTFE vessels. Thereafter, different volumes of aqua regia (3:1) + hydrogen peroxide+ hydrofluoric acid (5, 4, 7 mL) were mixed with PCB samples. Then, the PTFE vessels were fit on a microwave rotor which permitted 13 vessels for each run. The microwave was then pressured to 50 bar to ensure the cap was in the upper part of the PTFE vessel before heating. During the heating, the temperatures were kept at 160˚C, with a hold time of 30 min, ramp time of 20 min, and the power 1030 warts and the digestion reagents were 3 mL HNO_3, 3 mL HCl, 2 mL H_2O_2 and 2 mL HF. Thereafter, the samples were transferred into a 25 mL volumetric flask, and scandium as an internal standard was added and the flask was filled to volume using Milli-Q water.

Classical fire assay method

An appropriate quantity of PCB sample is weighed on an analytical scale and ignited in a muffle furnace at 650˚C until all volatiles have been removed. Furthermore, the ignited sample is homogenised with Lead (Pb) collection flux, silver solution and 20-30g silica before being put into a fusion furnace and heated to 1140˚C for 75 minutes. After the fusion is finished, the crucibles are withdrawn and the contents are poured into the conical iron moulds. After 20 minutes of cooling, the Lead slag are removed from the slag by tipping the mould with a hammer. Thereafter, the excess lead in lead button was further cupelled to the silver bead aa indicated in figure 3 (i.e 5th step) and lead metal converted into PbO according to equation 1, which was treated with concentrated nitric acid o liberate silver (Ag) into $AgNO_3$, according to equation 2 as explained in previous literature (Ireland, 1964), with slight changes. The solution was allowed to cool for 40 min and filtered, and was transferred into a 25 mL flask containing 10% HCl and Scandium (Sc) as an internal standard for analysis with ICP-OES. The summary of the fire assay method, Pb collection is illustrated with a schematic carton diagram in Figure 3.

$$Pb_{(s)} + O_{2(g)} \rightarrow PbO_{(s)} \quad (1)$$

$$AuAgPGM_{\ button} + HNO_{3(conc)} \rightarrow AgNO_{3(aq)} + Au_{residue)} + PGMs_{(residue)} + NO_{x(g)} \quad (2)$$

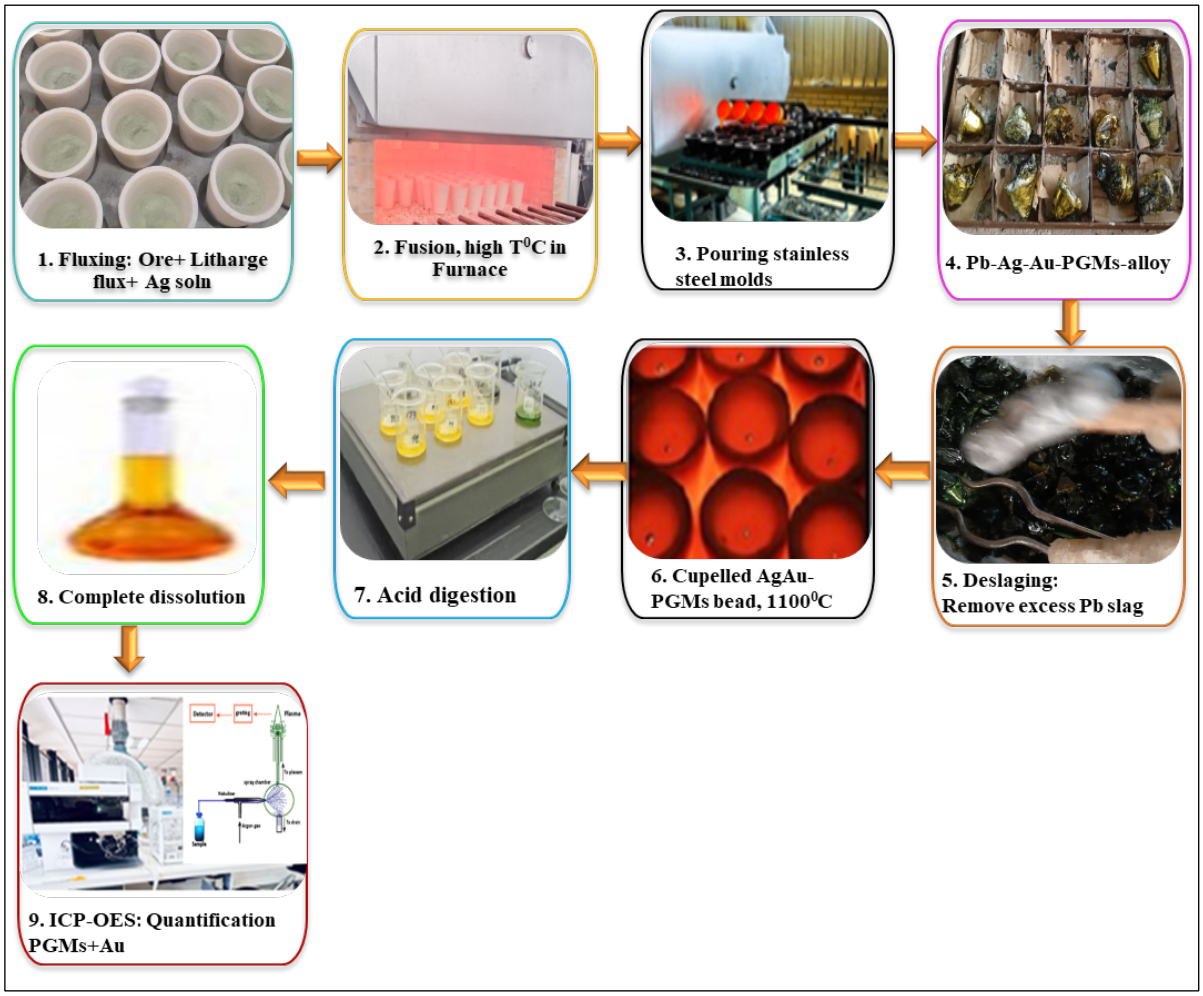


Figure 3. Detailed steps involved in the determination of PGMs by fire assay.

RESULTS AND DISCUSSION

Figure 4 illustrates the calibration plot of PGMs and Au, showing the relationship between signal intensity and concentration (in ppm) for PGMs (Pt ,Au, Rh, Ru) and Au. The linearity of the plot confirms the perfect analytical sensitivity and reliability of the method. The selected and stable wavelengths were 299.296 nm for Pt, 340.458 nm for Pd, 349.894 nm for Ru, 343.488 nm for Rh and 267.594 nm for Au. In addition, the correlation co-efficient (i.e r^2=0999) indicates the strong capability for quantification across the tested concentration range. The plots validate the suitability of method for analysis of multiple PGM elements in waste-PCBs.

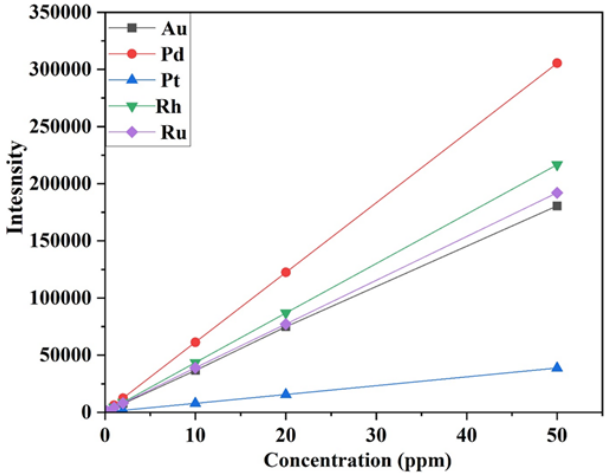


Figure 4. Linear curve indicating of selected PGE+Au (Pd 340.458 and P t 299.296 +Au) calibration.

Figure 5 (a) displays the work for the sample preparation of waste-PCBs. The waste PCB was collected, and the (1) feed into tungsten milling bowls was then comminuted mechanically into powder. This milling/pulverisation process liberates the non-metallic (i.e., resins, plastics, glass fibres) and metallic fractions through breaking the strong bonds of these glass fibres, resins and embedded metals. The milled (i.e., pulverised) material is then (2) introduced into a particle size separator to allow the downstream processing. Figure 5 (b) shows the particle size distribution results from the Malvern particle analyser, it can be seen that most particles fall within micrometre size with a broad distribution, indicating the heterogeneous composition of waste-PCBs

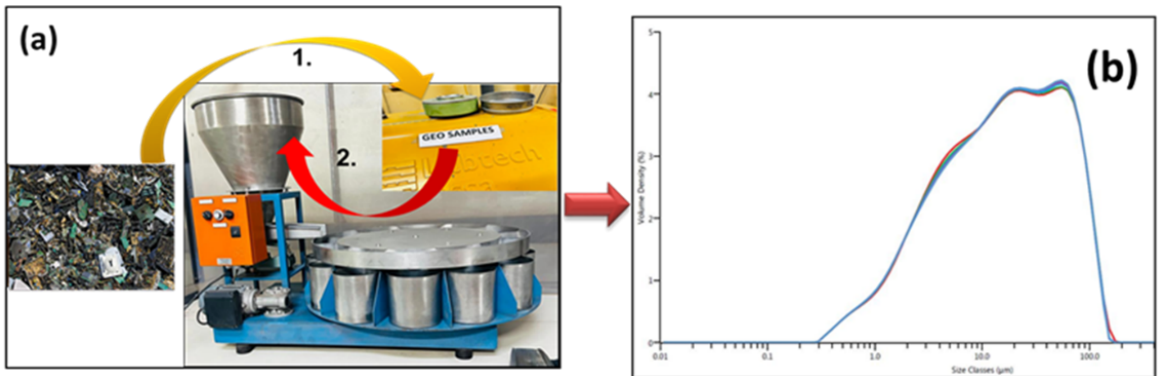


Figure 5. (a) Illustrates the typical spent PCBs, milling, pulverising process, size separation particle size and (b) Particle size distribution.

Table II: Comparative results of microwave-assisted digestion and fire assay process

Fire assay method			
Sample ID	Au	Pd	Pt
PCB-1	134.43	74.78	0.264
PCB-1	127.08	60.83	0.246
PCB-2	169.19	2.75	0.182
PCB-2	135.81	1.41	0.176
RSD %	0.988	1.380	2.05
Microwave-assisted digestion			
PCB-1	117	59.5	0.233
PCB-1	132	61.4	0.609
PCB-2	69.0	0.446	0.155
PCB-2	26.8	0.506	0.105
RSD%	0.95	1.66	1.98

The conventional fire assay and microwave-assisted digestion methods were successful in detecting Au in PCB-2 samples. However, the microwave-assisted digestion method showed significant differences, particularly for Au, compared to the conventional fire assay method. This could be due to the sample's heterogeneity, high base metals, and the presence of a copper nugget, which can interfere with the cupellation process and ICP-OES lines for precious metals. As shown in Table II, the fire assay process showed high recovery for overall PGMs as compared to microwave digestion.

Physicochemical characterisation

X-ray diffraction

Figure 6 illustrates the XRD pattern of waste-PCBs, indicating the mixture of crystalline phases, which is ascribed to metallic phase and amorphous phase, which is due to silicon and non-metallic (i.e., epoxy resins). The metallic phase is indicated by a dominant peak around 2θ= 45˚, 50˚, and 74˚ are related to the characteristic feature of Cu. The peak between 30˚-35˚ can be assigned to Sn compounds and Cu-Sn compounds that usually form in solder joints in PCBs. The amorphous peak is witnessed between 15˚-25˚, and is attributed to the amorphous nature of silicon and epoxy resins**.** The major element is Cu (39.7%), followed by predominant Sn (26.8%), minor Cu-Sn (13.3%), and traces of Pb (1.5%) and Al (0.9%). The XRD pattern is in strong agreement with the reported pattern in the literature (Altansukh et al., 2016)and is assigned according to PCB certificates in the main graphic, analysis view attached as Figure S1 and Figure S2 of the supporting information.

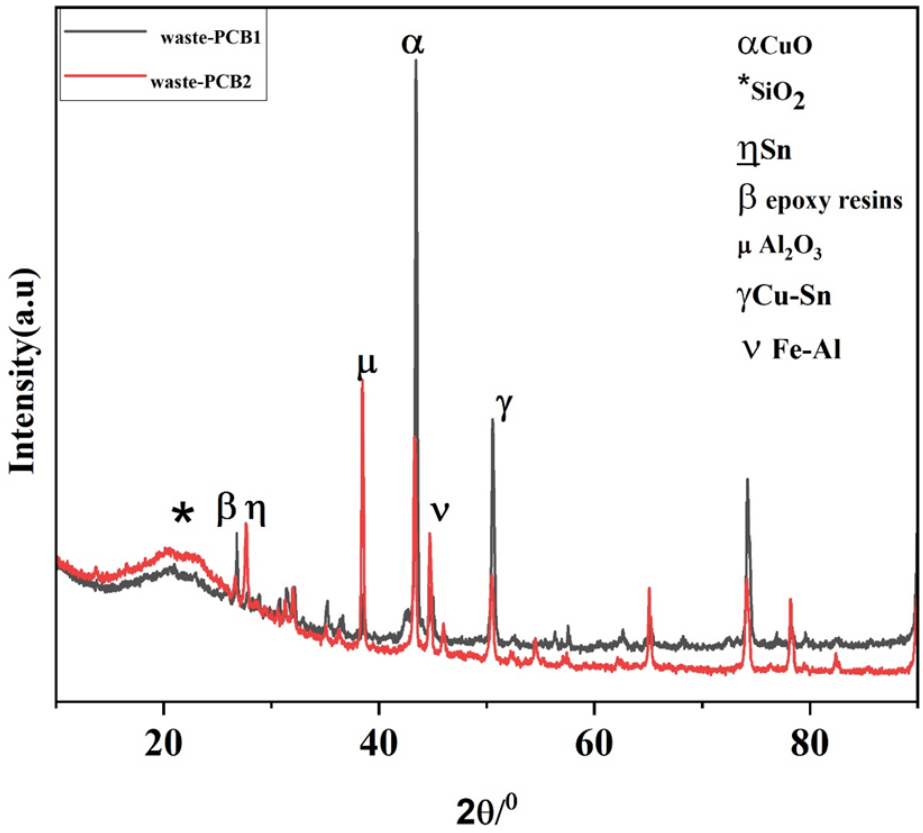


Figure 6. XRD pattern of PCB1 and PCB2.

Scanning electron microscope-energy dispersive Xray (SEM-EDS)

Figure 7 (a) illustrates the SEM micrographs of waste-PCBs, which exhibit a prominent heterogeneous morphological structure, composed of metallic and non-metallic materials. Figure 5a shows the PCB that is delaminated before crushing and milling, while in 5b representing particle size distribution of the crushed waste-PCB. Both SEM images display glassy fibre materials due to the FR-4 substrate, delaminated Cu, Si, Sn, Al traces, and clearly visible fractured epoxy resins, supported by literature (Cui & Forssberg, 2003). The microstructure, with disjointed morphology, indicates recycling challenges as it appears that different fractures are bonded tightly. However, SEM characterisation and the presence of Cu, Si, Sn, confirmed by EDX mapping (Figure 7 (c-d), suggests an opportunity for recycling in strong agreement with literature (Akcil et al., 2015). Interestingly, PGMs are not detected by elemental mapping. The elemental mapping displayed by EDS in Figure 8(c-d) indicates the clear visualisation and existence of heterogeneous composition of waste-PCBs. The elemental distribution of Cu, Al, Fe, alongside Si and calcium, confirms the co-existence of glass fibre reinforced epoxy resins and metallic traces. Figure 7(d) exhibits the complexity of metrics where Cu is embedded with areas that are rich in Al, Mg, which is the nature of PCB's composition. Interestingly to note, PGMs could not be detected by SEM-EDS due to its higher detection of limit (LOD) around 0.1 to 1 wt% which can only analyse at localised micro level and the PGMs are heterogeneously distributed in ppm level in waste-PCBs (Newbury & Ritchie, 2013) (Aamir et al., 2023). Conclusively, the elemental map not only reveals the degradation phases and boundary phases but it also assists with the identification of the critical metals that can be recovered during recycling. In addition, the distribution of metals and morphological characterisation provides crucial information that can help with optimisation of the leaching process, improving the metal recovery efficiency (Martinez-Ballesteros et al., 2023). The combination of microstructure characteristic features with elemental composition obtained from SEM-EDS , makes SEM-EDS a powerful technique to recovery and recycling of metals from waste- PCBs (Priya & Hait, 2017) thereby contributing to the circular economy.

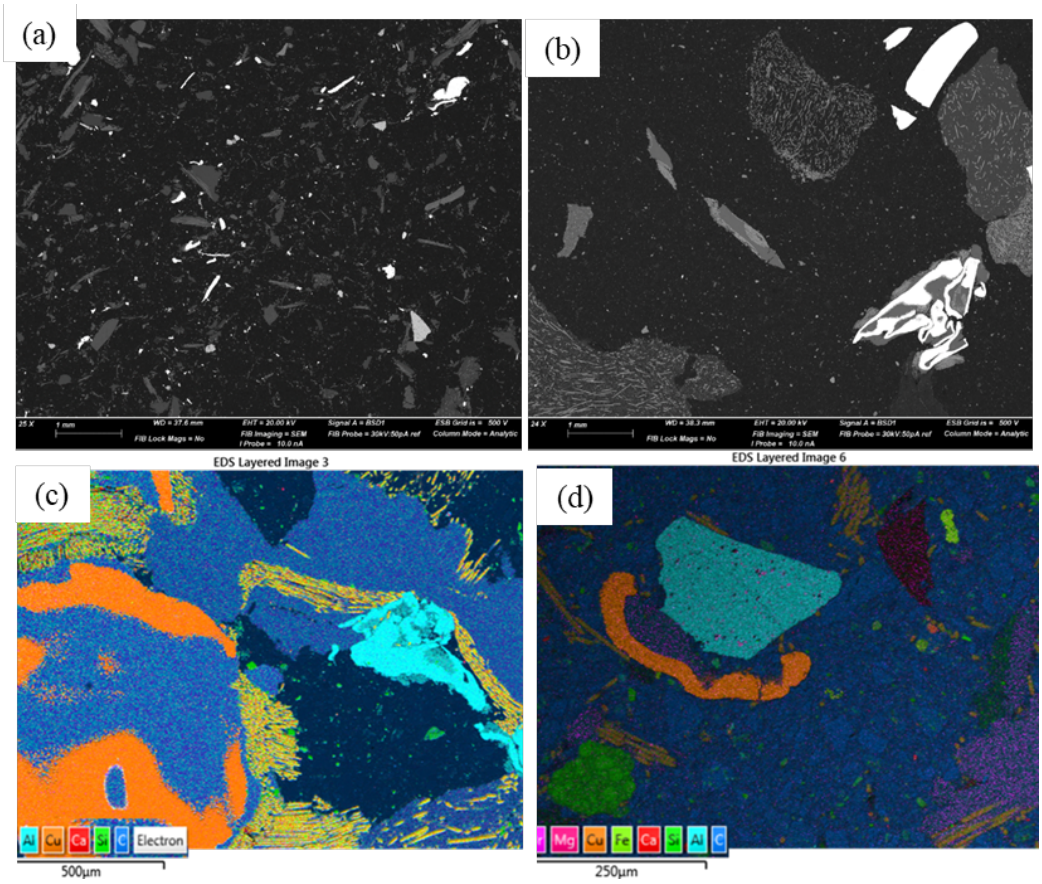


Figure 7. SEM micrographs of waste-printed circuit board (a) Crushed and milled and (b) Crushed only, and (c-d) their corresponding EDX results.

CONCLUSION AND RECOMMENDATIONS

This study successfully compared the MW-assisted acid digestion and classical fire assay for dissolution and preconcentration of PGMs for ICP-OES quantification from waste-PCBs while evaluating the impact of milling (preparation of sample). Classical fire assay obtained the highest PGMs detected in both PCB1 (milled) and non-milled (PCB2) samples, while the MW-assisted acid digestion provided faster dissolution but was challenged with complete dissolution on PCB2 (non-milled). The improved recovery was observed on PBC1 (milled) samples in contrast to PCB2, indicating the importance of milled PCB samples for reliable analytical quantification. SEM-EDS and XRD confirmed the heterogeneous distribution of elements and revealed the crystalline and major phase of Cu, Sn, Cu-Sn, indicating the opportunity for metal recovery, thus contributing to the circular economy. The bibliometric analysis demonstrated the global research trends and interrelation between the keywords, emphasising the hydrometallurgical and pyrometallurgical process, while attention is lacking on samples preparation (i.e., dissolution and analytical benchmarking). The clear research gap is indicated in the milling effect and dissolution methods. Additionally, the work highlights the opportunity to produce PCB-based certified reference materials which support the studies of the fire assay for platinum metals by lead collection methodology in PGMs quantification and recovery from e-wastes.

ACKNOWLEDGEMENT

The authors would like to thank Mintek, project number (ASR-00002533) for their financial assistance.

REFERENCES

Aamir, M. H., Gonçalves, P. P., & Otsuki, A. (2023). Complementary results of non-destructive elemental assay and liberation analysis of waste printed circuit boards. *Non-Destructive Material Characterization Methods*, 767–782. https://doi.org/10.1016/B978-0-323-91150-4.00004-5

Akcil, A., Erust, C., Gahan, C. S. ekha., Ozgun, M., Sahin, M., & Tuncuk, A. (2015). Precious metal recovery from waste printed circuit boards using cyanide and non-cyanide lixiviants--A review. *Waste Management (New York, N.Y.)*, *45*, 258–271. https://doi.org/10.1016/j.wasman.2015.01.017

Altansukh, B., Haga, K., Ariunbolor, N., Kawamura, S., & Shibayama, A. (2016). Leaching and adsorption of gold from waste printed circuit boards using iodine-iodide solution and activated carbon. *Engineering Journal*, *20*(4), 29–40. https://doi.org/10.4186/ej.2016.20.4.29

Ananda, Y., Rizal, E., & Rohman, A. S. (2025). Analisis Bibliometrik Artikel Jurnal Bidang Informartion Quality Pada Database Scopus Menggunakan Vosviewer. *Jurnal Pustaka Budaya*, *12*(1), 89–109.

Aria, M., & Cuccurullo, C. (2017). bibliometrix: An R-tool for comprehensive science mapping analysis. *Journal of Informetrics*, *11*(4), 959–975. https://doi.org/10.1016/j.joi.2017.08.007

Blyth, K. M., Phillips, D. N., & van Bronswijk, W. (2004). Analysis of gold ores by fire assay. *Journal of Chemical Education*, *81*(12), 1780–1782. https://doi.org/10.1021/ed081p1780

Chidunchi, I., Kulikov, M., Safarov, R., & Kopishev, E. (2024). Extraction of platinum group metals from catalytic converters. *Heliyon*, *10*(3). https://doi.org/10.1016/j.heliyon.2024.e25283

Cui, J., & Forssberg, E. (2003). Mechanical recycling of waste electric and electronic equipment: A review. *Journal of Hazardous Materials*, *99*(3), 243–263. https://doi.org/10.1016/S0304-3894(03)00061-X

Dias, J., Silva, A. G. P., de Holanda, J. N. F., Delatorre, F. M., da Conceição, A. O., de Miranda Júnior, G. M., Futuro, A., & Pinho, S. C. (2023). Environmental and Technological Assessment of Operations for Extraction and Concentration of Metals in Electronic Waste. *Sustainability (Switzerland)*, *15*(17). https://doi.org/10.3390/su151713175

Ireland, N. (1964). STUDIES OF THE FIRE ASSAY FOR PLATINUM METALS BY LEAD COLLECTION. *Talanta*, *11*, 1449–1457.

Ishak, N. S., Roslan, M. F., & Abdullah, K. H. (2023). Bibliometric Analysis of Malaysian Authorship: Trends, Patterns, And Prospects. *Asian Journal of Research in Education and Social Sciences*, *June*. https://doi.org/10.55057/ajress.2023.5.2.4

Jain, M., Kumar, D., Chaudhary, J., Kumar, S., Sharma, S., & Singh Verma, A. (2023). Review on E-waste management and its impact on the environment and society. *Waste Management Bulletin*, *1*(3), 34–44. https://doi.org/10.1016/j.wmb.2023.06.004

Kirby, A. (2023). Exploratory Bibliometrics: Using VOSviewer as a Preliminary Research Tool. *Publications*, *11*(1). https://doi.org/10.3390/publications11010010

Kumari, S., Panda, R., Prasad, R., Alorro, R. D., & Jha, M. K. (2024). Sustainable Process to Recover Metals from Waste PCBs Using Physical Pre-Treatment and Hydrometallurgical Techniques. *Sustainability (Switzerland)*, *16*(1), 1–17. https://doi.org/10.3390/su16010418

Long, T., Zhou, Z., Hancke, G., Bai, Y., & Gao, Q. (2022). A Review of Artificial Intelligence Technologies in Mineral Identification: Classification and Visualization. *Journal of Sensor and Actuator Networks*, *11*(3). https://doi.org/10.3390/jsan11030050

Martinez-Ballesteros, G., Valenzuela-Garcia, J. L., Gomez-Alvarez, A., Encinas-Romero, M. A., Mejia-Zamudio, F. A., & Rosas-Durazo, A. de J. (2023). Base Metals Extraction from Printed Circuit Boards by Pressure Acid Leaching. *Minerals*, *13*(1), 1–12. https://doi.org/10.3390/min13010098

Mceliseni C. Zuma, P. N. N. and N. M. (2021). Simultaneous Determination of REEs in Coal Samples Using the Combination of Microwave-Assisted Ashing and Ultrasound-Assisted Extraction Methods Followed by. *Minerals*, *11*, 1–14.

Moleko-boyce, P., Makelane, H., Ngayeka, M. Z., & Tshentu, Z. R. (2022). Recovery of Platinum Group Metals from Leach Solutions of Spent Catalytic Converters Using Custom-Made Resins. *Minerals*.

Newbury, D. E., & Ritchie, N. W. M. (2013). Scanning electron microscopy/energy dispersive spectrometry fixedbeam or overscan x-ray microanalysis of particles can miss the real structure: x-ray spectrum image mapping reveals the true nature. *Scanning Microscopies 2013: Advanced Microscopy Technologies for Defense, Homeland Security, Forensic, Life, Environmental, and Industrial Sciences*, *8729*, 872902. https://doi.org/10.1117/12.2011790

Nurvianie, R., & Sundari, S. (2024). Bibliometric Analysis of Medical Professionals ' Professionalism on Healthcare Service Quality : A Study Using VOSviewer. *Journal of Research in Science Education*, *10*(11), 818–824. https://doi.org/10.29303/jppipa.v10i11.7960

Oke, E. A., & Potgieter, H. (2024). Recent chemical methods for metals recovery from printed circuit boards: A review. *Journal of Material Cycles and Waste Management*, *26*(3), 1349–1368. https://doi.org/10.1007/s10163-024-01944-4

Olatinwo, S. O. (2022). A Bibliometric Analysis and Review of Resource Management in Internet of Water Things : The Use of Game Theory. *Water*.

Priya, A., & Hait, S. (2017). Qualitative and quantitative metals liberation assessment for characterization of various waste printed circuit boards for recycling. *Environmental Science and Pollution Research*, *24*(35), 27445–27456. https://doi.org/10.1007/s11356-017-0351-1

Susanto, A., Putro, E. K., & Purwanto, P. (2018). *Hazardous Waste Identification and Management at Fire Assay Laboratory Based on Indonesian Government Regulation*. *December*, 46–51. https://doi.org/10.5220/0007508900460051

Yakoumis, I., Panou, M., Maria, A., & Panias, D. (2021). Recovery of platinum group metals from spent automotive catalysts : A review. *Cleaner Engineering and Technology*, *3*, 100112. https://doi.org/10.1016/j.clet.2021.100112

Zhao, Q., Zhu, X., Wan, X., Wu, J., Shen, F., & Bian, F. (2024). Mapping research on cognitive impairment in heart failure patients : A bibliometric analysis from 2013 to 2022. *Heliyon*, *10*(19), e38955. https://doi.org/10.1016/j.heliyon.2024.e38955

The integrated mine of the future: How five global trends are driving integrated and intelligent mining operations

C. Bleazard[1], M. Dwyer[2]

[1]Hatch, South Africa
[2]Hatch, Abu Dhabi

Over the next decades, the mining industry is expected to undergo a profound transformation driven by five converging trends: resource constraints, people challenges, a heightened focus on climate change, increased access to data, and the rapid advancement of technology. These forces are reshaping how mines operate and are compelling companies to adopt more deliberate integrated planning and execution strategies. Integrated operations, which brings together people, processes, and technology across the value chain, can be a key enabler in navigating these challenges. This paper explores how these trends are influencing mining operations globally, with examples from recent integrated operations projects, what challenge each project aimed to address, the outcomes and the lessons to be learnt for the future of mining.

INTRODUCTION

Globally, mining operations are facing many changes. Five of these include declining resource quality, changes in the workforce, climate and sustainability pressures, rapid technology changes, and a huge increase in data availability and generation. These changes are creating operational constraints and are influencing long-term planning and daily decision making.

To stay competitive and resilient, many mining companies are considering integrated operations solutions. This means connecting people, processes, and technology across the value chain to break down silos, enable better planning and make faster and more accurate decisions, thereby allowing for more consistency in the operation. Integrated operations thinking is not just about adding more digital dashboards to a video wall, rather it is about aligning the whole value chain to respond intelligently to complex challenges.

This paper explores how these five trends are driving the shift toward integrated and intelligent mining. Through real-world case studies, we discuss what has worked, what needs improvement and how selected mines and operations are addressing their challenges.

RESOURCE CONSTRAINTS

Mines across the world are extracting lower grade ore bodies and this trend is expected to continue. The reduction in grade in extracted ore can be attributed to both the depletion in the grade inherent in the ore bodies themselves (Calvo G, 2016) as well as the improving extractive technology that allows mines to remain profitable longer by extracting more from lower grade material (West, 2011). Regardless of the cause and the long-term trajectory of ore body composition, the net result is that mine operators are required to adjust and plan their day-to-day operations using lower grade ore and still meet quality requirements.

This has led to a greater emphasis on precision planning, efficient resource allocation, and real-time monitoring to maximise yield. Better coordination between exploration, extraction, and processing can ensure that every tonne of ore is mined and processed with maximum efficiency. (Kuvataev, 2020) shows that improved coordination of mining processes and flexibility in planning for operations leads to increased efficiency. As a response to declining quality, a large South African coal miner in 2023 established an integrated operations centre (IOC) focused on quality monitoring and making trade-off decisions to reduce variability in coal quality going to the customer [Case Study 1]. One of the levers required to make this successful was the ability to manipulate colliery production to ensure multiple sections of low grade occurring simultaneously did not disrupt the overall quality blend. The IOC implementation initially struggled to influence the underground production, but with more training and awareness from miners of how their actions influence the overall quality blend, the behaviour has started to change. Additionally, KPIs for collieries to manage and target quality ore, rather than focusing only on tonnes mined has had a positive effect. The IOC is starting to be seen as a valuable partner to help the collieries meet their goals on quality. Long-term, the vision is that the IOC will be able to directly influence work assignments across the different colliery mine plans based on the forecasted coal quality output and the prevailing stockpile blend.

One of the key enablers of this operation has been improving the accuracy and timeliness of the data to know the exact material being placed on the stockpiles. Initial steps taken included surfacing the data from each colliery into the central IOC, making it visible in a prominent location. Additional data sources included blend planning, forecasts, real-time information from sensors and location of stacker/reclaimers. The overall result of the IOC implementation, despite being a fairly small centre with few resources, has shown that a more intelligent holistic planning approach, better and more timely data, and the ability to flexibly react to changes, produces a positive overall result for the mining operation.

CASE STUDY 1: QUALITY MONITORING IOC

Background
The project client is a large South African coal miner. They have been facing challenges with declining ore quality at some of the collieries that they operate, resulting in challenges in their processing plant due to increased variability in the incoming qualities.

Project Objectives
The project objective was to better predict coal quality and to reduce feedstock quality variability entering the plant.

Approach
To achieve this objective, there were several initiatives explored and executed. One of these was to establish a new centralised quality management centre to coordinate mining activities of six collieries, ground transportation and storage of coal, blending and feeding material to the plant. The goal was to orchestrate all activities along the value chain with the aim of delivering a consistent quality product to the processing plant.

The project involved multiple workstreams including focusing on the physical space and equipment for the new centre, updating the business processes and roles, data engineering to ensure systems and analytics needed to support the centre were in place, and a feasibility study for a coal quality optimisation tool.

Implementation
The project was executed between Q1 2023 and Q1 2024. The workstreams were executed in parallel with the new centre opening in Q4 2023. The following scope was executed as part of the project:

Process definitions
Mapping out processes for the new centre and establishing clear decision-making frameworks including RAPID models.
Organisational design
Defining roles, responsibilities and the overall organisational structure for the team.
Implementation Roadmap
Creating a strategic plan for rolling out the centre and effectively managing the change.
Facility and Technology
Advising on the physical layout of the space, necessary technology packages and implementation.
Data warehouse technical support
Providing data engineering services to extract, transform and load mining data from historians, mining plans and databases to a central data warehouse and make it available for analytics.
Visualisation
Developed custom visuals from the data warehouse to communicate the latest status.



Figure 1. Videowall implemented as part of the project showing the data and custom visuals.

Results
The project successfully delivered a quality monitoring IOC space with the new roles defined and the necessary initial data and visualisations implemented. The centre provided a holistic view of operations which has facilitated rapid identification of problems and a more unified approach to solution identification and execution. The ability to show collieries their impact on the overall product quality has been valuable and has started to shift the mindset from 'just mine tons at any cost' to 'I need to produce what the customer is ordering' which includes quality requirements. It is noted that there has been value in colocation of some roles to assist with coordination.

The current implementation has experienced limitations in the levers available to them to change results, and in many cases, people challenges have led to slow adoption of new technologies that would enable better data (for example, shift manager software). There are still many opportunities to improve the quality IOC impact in the future.

Relevance to Research
This project illustrates an example of mining clients addressing declining reserve quality (higher inherent ash and sinks) and greater variation in quality, by implementing an integrated operations centre. It also highlights that many challenges that mines face related to the people implementing the plan. Specifically, software adoption, data stewardship and the need to shift mindsets from how things have been operated in the past, when new challenges arise.

PEOPLE CHALLENGES

As mining and mineral processing operations grow increasingly complex, there are efforts to use software and digital technologies to support decision-making and operational efficiency. This shift toward more 'intelligent' operations is essential, but it introduces a new set of challenges related to the workforce.

One recurring issue is the mismatch between the technological maturity of the systems being deployed and the digital readiness of the workforce expected to use them. In Case Study 1, despite a robust rollout of shift reporting software which was required to enable the integrated quality planning, user adoption has been slow. Similarly, at a Southern African platinum smelter an operations planning software deployed has struggled to gain traction due to frequent turnover of super-users and a reluctance among staff to engage with the system to refine and improve its outputs.

Unlike consumer software, which benefits from extensive usability testing and intuitive design, industrial software is often custom-built and highly specific to the site or process. This means it requires meaningful input from end users to function optimally, which can be frustrating for teams who are already stretched and may not immediately see value in the software.

Compounding this issue is the demographic shift in the workforce. As experienced operators retire, there are attempts to capture their deep domain knowledge with software tools. While this can help mitigate skills loss, it also demands a more technologically sophisticated user base. In many cases, however, the current workforce lacks the digital fluency and training needed to fully leverage these tools, leading to underutilisation and resistance. Globally the mining industry is facing shortages of skilled workers generally (Watts, 2025) and needs to attract more varied talent in order to meet these new demands, including more technologically and data literate staff.

Some operations are addressing these challenges through centralized centres of excellence or technical support hubs, where skilled operators can support multiple sites virtually. This has the added benefit of increasing consistency across similar operations and can provide a central location for software and systems training. Another approach is to improve the attractiveness of mine work, which can be achieved via Integrated Remote Operations Centres (IROCs). IROCs allow resources to spend less time on site and instead operate from safer and more attractive locations in large cities, which can appeal to the new generations of workers. Additionally, many IOC and IROC projects include provision for data analysts and data scientists, increasing the organisations data skills and providing a centralised owner for managing, testing and championing data and software projects.

DECARBONISATION AND SUSTAINABILITY

Further complicating the people and skills challenges are drives for decarbonisation and sustainable mining practices. 44% of mining companies have cited limited expertise and skills shortages as barriers to decarbonisation initiatives (Watts, 2025). However, sustainability and climate change mitigation have become central to mining strategies. Companies are under pressure to reduce their carbon footprint, manage water use, and rehabilitate land.

To reach the goals of more sustainable operations, mines need to incorporate several new technologies. Some of these are: using less or no diesel-powered vehicles, changing electrical energy sources, emissions tracking and capturing, water management and improvements to processing technologies. Adoption and scaling all these initiatives at mines is an unprecedented change for an industry that has been traditionally slow in adopting new technologies.

Integrated operations can assist mines with this change in a three key ways. Firstly, integrated operations projects tend to take a ‘whole mine’ approach which provides a key oversight role in emissions tracking and water usage improvements. This is a perspective that is not easily achieved with traditional siloed views of the mines. Secondly, when well implemented, IOCs allow for decision optimisation that reduces waste. For example, a large bulk miner in Central West Africa found that their IOC was able to make trade off decisions to reduced unnecessary product movement by diesel trucks, when downstream processes did not need product immediately and could instead wait for conveyor belt space [Case Study 2]. Finally, IOCs are well placed to support new technology projects and allow for continuous improvement initiatives in mines.

CASE STUDY 2: VALUE CHAIN TRADE-OFF DECISIONS

Background
The project client is a bulk miner in Central West Africa. They were looking to expand their operation and at the same time, address some of their challenges with siloed operations and lack of coordination across their value chain, which included mine, beneficiation, rail load out, interaction with a third-party rail provider and port operations.

Project Objectives
The project objective was to increase mining production including installing a new ore crushing facility, building a 6.4 km overland conveyor to a beneficiation plant and adding a product stockyard with reclaiming and train loading. As part of this project, during the study phase, the client expressed a desire to be 'digital ready' and several digital packages were explored.

Approach
During the feasibility study, the digital vision that the client had developed previously resulted in six use cases, including an IROC. The IROC scope included the design of a new building, the systems and equipment fit-out, the organisational and change management design and value chain analysis.

Implementation
The project feasibility design phases were completed between Q4 2018 and Q4 2020. Detailed design and execution started in 2021 and the building was commissioned in Q4 2022.

The execution of the project involved a number of design and procurement packages, including process CCTV for remote monitoring of the operations, voice communication systems to interact with sites, networks and ICT equipment, video walls and other displays, and coordinator consoles and furniture for the new building. The building design and construction was performed by a local contractor.
A key part of the project was the design of the operating model of the IROC including role definitions, decision rights via RAPID[1] models and change management planning, including training plans. It also became clear that in order to know which levers the IROC could most effectively influence, an end-to-end value chain analysis for both current and future operations was needed. This resulted in a value chain simulation tool being developed and handed over to the client.

Results
The project successfully delivered a new built IROC to the client, from which the entire operation could be monitored and coordinated. According to feedback from the client, after the commissioning was complete, the centre had contributed to being a central source of truth for the operation and that interactions between parts of the value chain had improved. Unverified estimates by the client, after eight months of implementation, were that they had managed to reduce losses due to inefficient operations by EUR 300,000 and had estimated savings from increasing operational efficiency of EUR 740,000.

The current implementation does still have challenges. Some of the systems needed, such as an integrated planning system, are still in progress. There remains resistance from some sites to rely on the IROC and the change management activities planned have not been fully implemented.

Relevance to Research
This project illustrates a mining company addressing several challenges with an IROC and more intelligent mining operation. The client recognised that they required a more holistic vision of operations to make better trade-off decisions. This has allowed savings due to reduced losses as well as improved operational efficiencies. This case study also highlights a need for additional data to enable the IROC as well as the opportunity an IROC project brings to define a holistic value chain view of the

[1] RAPID model is a framework to help organisations clarify decision making. RAPID stands for Recommend, Agree, Perform, Input and Decide.

operation. Finally, relating to people challenges in mining, the new building was identified as an attractive facility to work from, and the client has showcased it in several press releases and events, adding to its prestige.

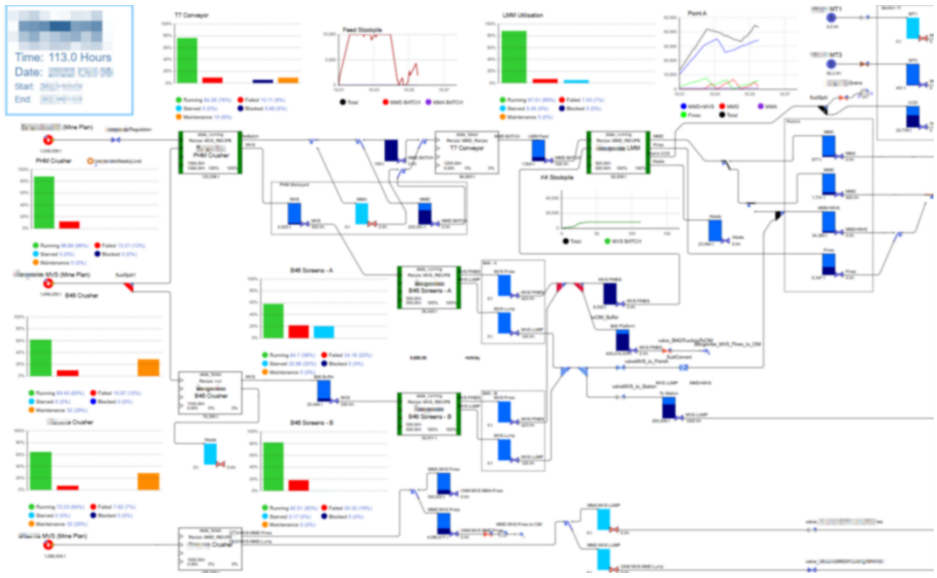


Figure 2: Part of the value chain simulation model developed to explore levers for the IROC.

TECHNOLOGY FOR EFFICIENT PRODUCTION

Along with new technologies being explored in the sustainability space, technological innovation in mining and processing plants is accelerating. Mining and processing operations are testing and deploying increasingly autonomous equipment. Siemens estimates that by 2040, 40% of mining equipment operated on the African continent will be self-driving and that several major operations may be nearly fully automated (Crown Publications, 2025). Most mineral processing plants have some level of automation, and the more advanced ones are moving towards highly automated processing. Additional technologies have been maturing over the past decades, and it is now common to see automated stockpile scanning, drone inspections, and fully automatic sequence controls of plants. Recently, setpoint decision automation is becoming increasingly popular including at a plant in Australia, where a flotation digital twin was implemented in closed-loop control.

All these technologies have the potential to transform the whole mining value chain. However, they need to be effectively orchestrated and planned for as in most cases, these technologies introduce significant changes into the operation's ways of work. Integrated operations thinking provides a central focus to coordinate these technologies across the mine site, broader value chain and beyond. By connecting disparate systems and enabling seamless communication, they unlock new levels of efficiency, safety, and agility.

INCREASED ACCESS TO DATA

The increase of technology adoption on mines and processing plants, along with the proliferation of sensors, automation, and digital initiatives has led to an explosion of data in mining operations. Having visibility across the mining value chain is one of the critical enablers for integrated operations, but it also presents a huge opportunity with the right data becoming available and the right resources providing analyses. Merely having access to more raw data is rarely useful, as value is derived from turning data into actionable insights and using these to drive wins across sites and functions. Intelligent mining operations are starting to leverage advanced analytics, machine learning, and real-time

dashboards to support faster, more informed decision-making. This data-driven approach enhances operational predictability, reduces downtime, and improves compliance with production plans.

CONCLUSION

These five global trends are converging to reshape the mining industry. Integrated and intelligent operations offer a strategic response, enabling mines to optimise performance, enhance decision-making, and remain competitive in a rapidly evolving landscape. By embracing integrated planning and execution, mining companies can unlock new levels of efficiency, sustainability, and resilience, paving the way for the mine of the future.

REFERENCES

Calvo G, M. G. (2016). Decreasing Ore Grades in Global Metallic Mining: A Theoretical Issue or a Global Reality? *Resources*.

Crown Publications. (2025, February 10). *Mining Trends Watch: How African mines will embrace a new era of autonomous, tech-driven mining by 2040*. Retrieved from Modern Mining: https://www.crown.co.za/modern-mining/technology-news/31579-mining-trends-watch-how-african-mines-will-embrace-a-new-era-of-autonomous-tech-driven-mining-by-2040

Kuvataev, A. T. (2020). Improving the Efficiency of a Mining Enterprise. *Vth International Innovative Mining Symposium*. E3S Web of Conferences 174.

Nyasha, V. W. (2024). Technology and growth in the South African mining industry: An assessment of critical success factors and challenges. *Journal of the Southern African Institute of Mining and Metallurgy, 124*, 163-172.

Watts, J. (2025, February 18). Mining's Moment to attract a new generation of talent. *Global Mining Review*.

West, J. (2011). Decreasing Metal Ore Grades: Are They Really Being Driven by the Depletion of High-Grade Deposits? *Journal of Industrial Ecology*.



Claire Bleazard

AIM Regional Lead – Integrated Operations
Hatch

Claire Bleazard brings 15 years of post-qualification experience as a control and automation engineer focused on digital solutions and integrated operations. Her experience includes projects in mining, mineral processing and oil and gas industries for local and international clients. Claire's roles typically include project management and coordination of globally distributed specialist teams, design and implementation of Integrated Remote Operations Centre projects and developing user and functional requirements.

Claire is a professionally registered engineer and holds degrees in electrical and electronic engineering and a BSc. Honours in Mathematics.

Improved control of an electric arc furnace in a PGM smelting operation

J. Siecker[1,2], J. van Rensburg[2], L Mathevula[3], N. Wanblad[3], N. Kotze[3], L. Mukengeshayi[3]

[1]ETA Operations (Pty) Ltd, South Africa
[2]North-West University, South Africa
[3]Valterra Platinum (Pty) Ltd, South Africa

Electric arc furnaces (EAFs) in platinum smelting contribute significantly tor overall electrical energy consumption in platinum group metal mining and processing. Improving operational efficiency and energy productivity at these operations is therefore essential for sustainability. This paper investigates the electrical control techniques used on two identical Six-in-Line EAFs, each rated at 34 MW, to assess the performance of resistance control. The goal of improving electrical control is to enhance overall furnace stability, resulting in lower specific energy consumption and, consequently, less electrical energy usage and costs. After various investigations, audits, and analyses, it was found that the resistance control on these furnaces was inconsistent due to insufficient electrode hydraulic speeds and suboptimal performance of the resistance controllers in the programmable logic control. This was caused by maintenance challenges with the electrodes' hydraulic system and variations in the mineralogy of the concentrate feed blend. The resistance control's performance was evaluated and analysed to determine if the actual resistance remained within the deadband, where the resistances mostly operated outside the upper or lower deadbands, leading to instability. This was resolved by firstly adjusting the electrodes' hydraulic speeds according to their design specifications. Secondly, the resistance controllers were fine-tuned, and the performance impact was evaluated. The results indicated that the resistance was now effectively controlled within the resistance control deadband. These interventions resulted in an annual energy savings of 8.25 GWh and a reduction in specific energy consumption of 3.03 %. This translates to energy cost savings of R 15.17 million per annum, with no capital expenditure required.

INTRODUCTION

The production of platinum group metals (PGMs) is essential to South Africa's economic growth, which has declined over the past century, as mining depths increased and extraction and beneficiation have become more challenging due to lower-quality ore, resulting in higher production costs (Minerals Council South Africa, 2021). Energy expenses, among other factors, are a major contributor to these costs. Electricity prices have risen rapidly over the past decade, making operations increasingly unsustainable (Power Optimal, 2021). This calls for targeted actions to improve operational efficiency and increase energy productivity through energy efficiency initiatives and energy conservation measures. The electrical energy consumption of the various sections at a platinum smelting operation, such as the Waterval smelter, were investigated. In Figure 1, the contribution of the various sections in terms of their energy consumption at the Waterval smelter is illustrated.

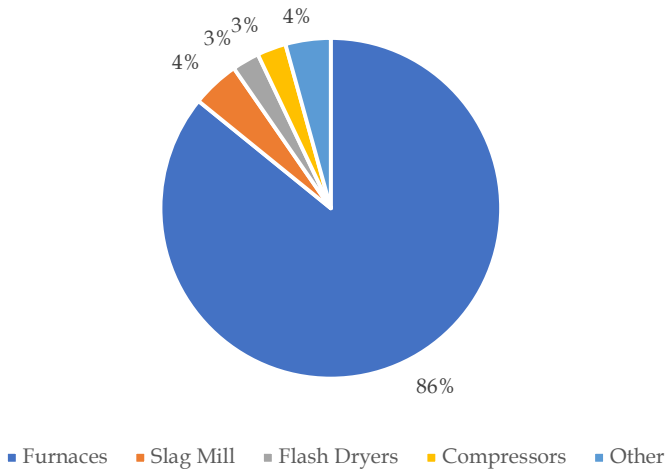


Figure 1. Waterval Smelter electrical energy consumption.

As can be observed from Figure 1, electric arc furnaces (EAFs) in a platinum smelting operation such as the Waterval smelter significantly drive the overall electrical energy consumption. At this smelter, two six-in-line EAFs, each rated at 34 MW, were investigated to assess the performance of these furnaces, with respect to energy efficiency/productivity (Jacobs, 2006). One of the biggest factors driving energy productivity of a furnace is stability and one aspect of stability is derived from the electrical control performance, which is resistance (immersion) and power-controlled (Snodgrass *et al.*, 2024). In this study, the resistance control was investigated to optimise the energy efficiency/productivity of these furnaces.

Few authors have attempted to optimise the resistance control system which includes the electrode hydraulic system and the programmable logic controller (PLC) control system, whereby the electrode hydraulic speeds need to be adjusted according to design specifications, as a first step. The purpose of adjusting the electrode speeds prior to the fine-tuning of the controller is that a ratio between the raise speed and lower speed should be ensured, as only one controller controls both the raise and lower speed of each electrode. Secondly, the resistance controller for each electrode needs to be fine-tuned to ensure improved performance

Hernandez and Onofri. (2022) have developed an optimal control model that aims to find the optimal voltage and impedance setpoints, in order to minimise the radiation losses experienced by the EAF. The results of applying the model to a case study showed a 5% reduction in the electrical energy consumption, which translated to a 2% improvement in energy efficiency.

Nikolaev *et al.*, (2014) developed a mathematical model that analysis the furnace's electrical characteristics, as well as the electrode immersion control dynamics. From the analysis conducted, it highlighted a need to optimise the operating conditions of the furnace during each smelting phase, of which the specific conductivity settings were required to be corrected. This was achieved by making use of the developed mathematical model for the electrical characteristics of the EAF, as well as the electrode immersion control system. Furthermore, the model could identify the smelting phase based on the arc current's harmonics, resulting in improved power consumption.

After reviewing the literature, it is evident that authors have focused on determining the optimal voltage and impedance setpoints to minimise radiation losses. However, it is clear from the literature that electrode immersion control optimisation in EAFs is lacking. Therefore, a need exists to evaluate the performance of the electrode immersion control system in EAFs, which should help identify the areas where the system's performance is inadequate. Understanding these shortcomings should help optimise the control system, leading to an improved resistance stability, and consequently, enhanced power stability.

METHODOLOGY

EAF process description

Waterval Smelter has three EAFs); two 34 MW Six-in-Line furnaces and one 23 MW Slag Cleaning Furnace. Figure 2 shows the SCADA overview of Furnace 2 at the Waterval smelter. The Six-in-Line furnace is referred to where the electrodes are situated next to one another forming a straight line. Electrode 1 is on the left-hand side, where the matte is tapped, and electrode 6 is located on the far right, where the slag is tapped. The matte is the desired product that is processed further, and the slag is the unwanted product. The electrodes are immersed in the slag layer, located above the matte layer. The bone-dry material, referred to as the feed material required to be smelted, is located above the slag layer. Electric current flows from one electrode to another through the slag layer, resulting in heat transfer required for smelting. The freeboard is referred to as the area located above bone-dry material and below the furnace roof. The hearth is referred to as the bottom part of the furnace body.

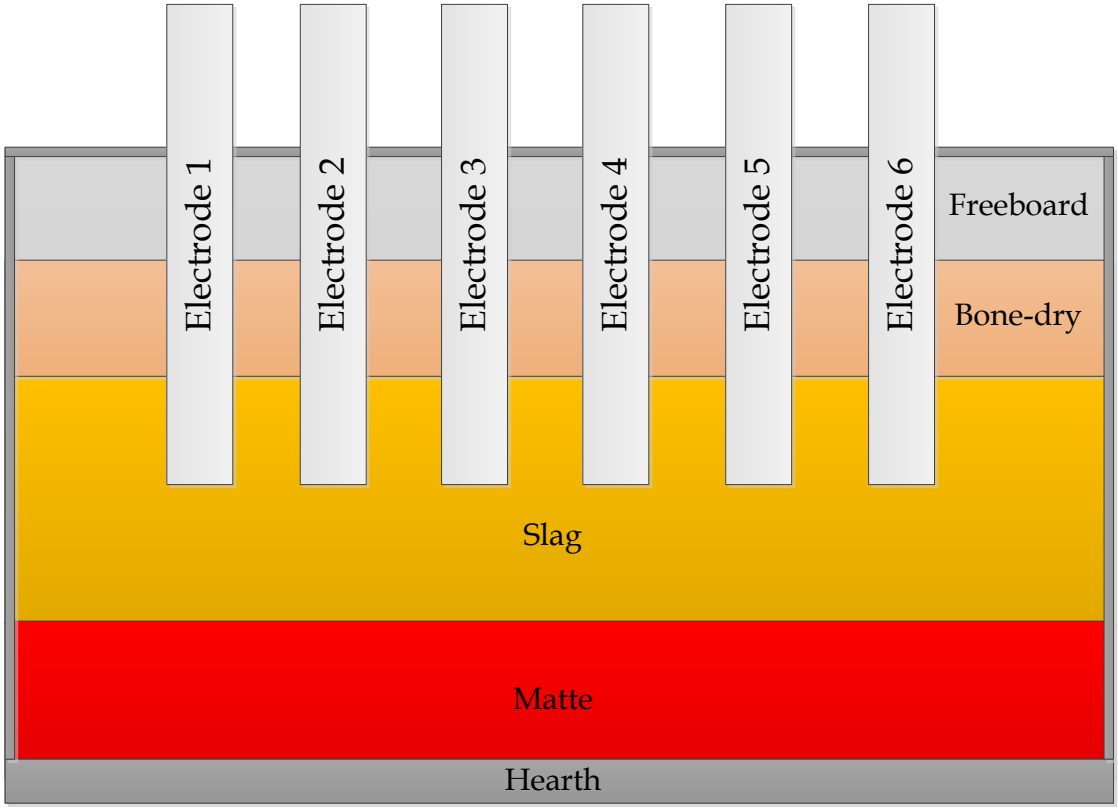


Figure 2. Waterval Furnace 2 SCADA overview.

Methodology (resistance control)

All the Waterval furnaces use resistance (immersion) control and power control. Immersion control works by moving the electrode holder up or down using a hydraulic system. On the other hand, power control is a second priority, where the transformer tap position is increased or decreased, to increase or decrease the voltage on the secondary side of each transformer pair, which increases or decreases the power applied from the electrodes. Regarding the immersion control, the hydraulic system of the Six-in-Line furnaces use pulse control on the hydraulic valves of the six electrodes, through the PLC control system, which is responsible for raising or lowering the electrode holder position.

The speed of the hydraulic valve is set at the valve stand, influencing the speed at which each electrode moves. Each controller forming part of the PLC control system applies pulses at different pulse durations to raise and lower the electrode until the resistance setpoint is reached. Each controller has an

upper and lower deadband of + 0.2 mΩ and – 0.2 mΩ, outside of which the controller will adjust the electrode's position to bring its resistance into the deadband range. Once the resistance falls within the deadband, control action stops until the resistance is out of range again.

This paper examined the resistance control performance of the two Six-in-Line furnaces at the Waterval smelter to determine whether the resistance (immersion) control is working effectively. Power control was excluded from this study because resistance control takes precedence over the power control in the current control philosophy.

Figure 3 presents a generic flow chart outlining all the necessary steps to optimise resistance control on Furnace 1 and 2 at the Waterval smelter.

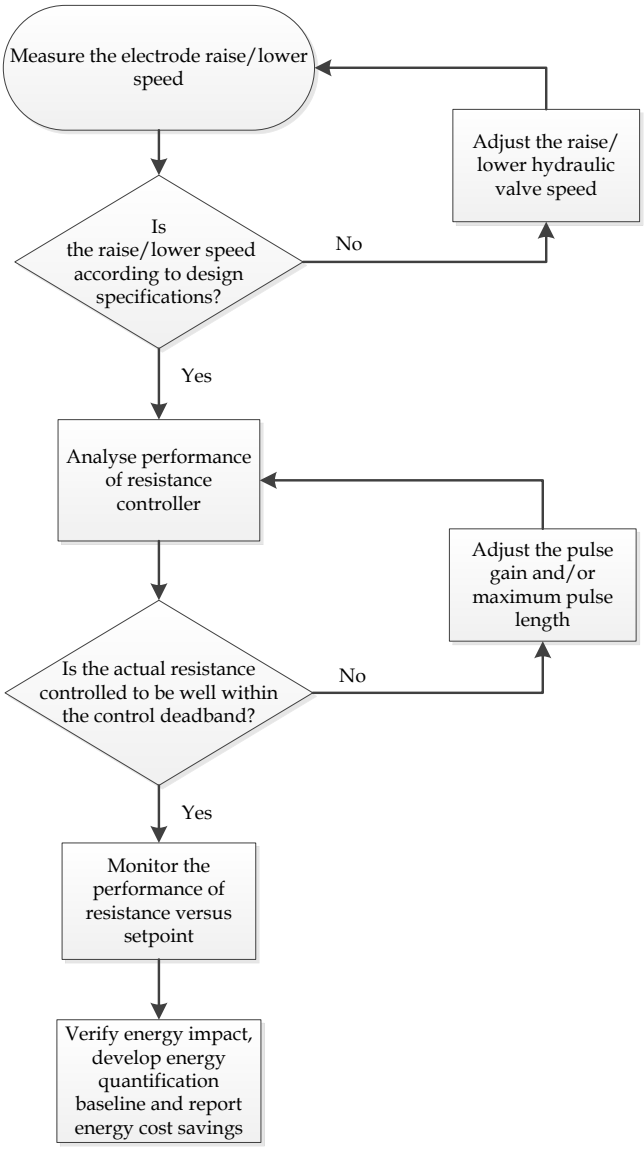


Figure 3. Flowchart to optimise resistance control on Furnace 1 and 2.

The first step in optimising the resistance control for this type of electrode hydraulic system is to measure the actual raising and lowering speeds of each electrode. Once the electrode speeds are measured, it is essential to adjust the hydraulic valve speed for the raising and lowering of each electrode according to the required design specifications.

Once the electrode speeds have been measured and adjusted according to the design specifications, the performance of each electrode's resistance controller should be evaluated to check whether the actual resistance stays within the deadband, as discussed earlier. This analysis helps identify if any controllers are still performing below desired levels — for example, if the actual resistance does not consistently reach its setpoint or if it overshoots the upper and lower limits of the deadband, resulting in a wide control range. When such issues are observed, the affected resistance controller should be reviewed and fine-tuned to ensure the resistance setpoint is reached consistently and maintained within a narrower operating band. The two key parameters that were fine-tuned were the pulse gain and the maximum pulse length. Adjusting the controller gain modifies the strength of the controller's response to the difference between the measured resistance and the resistance setpoint. The maximum pulse length determines the longest duration for which a single pulse can be applied by the controller. Increasing this parameter allows the controller to deliver longer pulses to the electrode, resulting in greater electrode movement. Furthermore, during the fine-tuning of the controllers, the process is iterative by nature, as one is required to evaluate the impact of the changes that were made to the controller until desired performance is achieved.

After optimising the resistance control, the performance of the electrode immersion control needs to be monitored on a weekly basis, to ensure the sustainability of these interventions made. The energy impact also needs to be quantified and verified by analysing the furnace's performance relative to its step change in specific energy consumption. The actual energy impact is then calculated by developing a baseline specific energy consumption (SEC), prior to the initiative being implemented. Regarding the performance tracking period, the developed baseline SEC is multiplied by the concentrate feed during the performance period, to calculate the predicted energy consumption, as seen in Equation 1: (Espindola *et al.*, 2021).

$$E_P = EI_B . P_{PA} \quad [1]$$

Where: E_P is the predicted energy consumption, EI_B is the baseline energy intensity and P_{PA} is the production of the performance assessment month. The actual energy consumption is subtracted from the predicted energy, in order to quantify the actual energy impact of the resistance control optimisation, as seen in Equation 2:

$$E_I = E_P - E_A \quad [2]$$

RESULTS AND DISCUSSION

In this section the performance of the resistance control for each electrode on Furnace 2 is analysed by evaluating the performance prior to the interventions being made, as well as the performance after each significant change, to some of the parameters of the resistance controller of each electrode. Furnace 2 is selected as the case study, as these furnaces are duplicates of each other, which is deemed sufficient to illustrate the impact on the resistance control.

Electrode hydraulic speed adjustments

The first step to optimise the resistance control of Furnace 2 was to measure the current electrodes' hydraulic speed, both the raising speed and lowering speeds. The electrode speeds were physically measured on site, with the results presented in Table I as the baseline measurements. Speed adjustments were necessary to ensure the correct speeds are achieved. In essence the electrode's raising speed should take between 12 and 18 seconds to raise a 100 mm. Conversely, the electrode lowering speed should take between 18 and 25 seconds to lower a 100 mm. These values were defined by a furnace control specialist at the time of the control system's commissioning, with the determined range reflecting the hysteresis characteristics of the hydraulic system. The electrode speeds shaded in red indicate that the speed is not at the required level, while green represents the correct speed levels. Orange indicates that it is not at the correct speed, and the lower speed is adjusted to ensure the correct raising and lowering speed ratio are maintained, such that the fine-tuning of the resistance controllers can commence.

Table I: Furnace 2 electrode speed measurements and adjustments

No	Baseline measurement		1st Adjustment		2nd Adjustment		Comment
Electrode 1	Raise time (s)	17.14	Raise time (s)	18.1	Raise time (s)	18	Didn't adjust raise speed
	Lower time (s)	9.14	Lower time (s)	13.6	Lower time (s)	21.6	Decreased the lower speed
Electrode 2	Raise time (s)	18.08	Raise time (s)	N/A	Raise time (s)	N/A	Didn't adjust raise speed
	Lower time (s)	21.85	Lower time (s)	N/A	Lower time (s)	N/A	Didn't adjust lower speed
Electrode 3	Raise time (s)	32.12	Raise time (s)	30.5	Raise time (s)	31.5	Couldn't increase raise speed. It's at maximum
	Lower time (s)	22.17	Lower time (s)	26.1	Lower time (s)	32	Decreased lower speed
Electrode 4	Raise time (s)	18.09	Raise time (s)	N/A	Raise time (s)	N/A	Didn't adjust raise speed
	Lower time (s)	21.02	Lower time (s)	N/A	Lower time (s)	N/A	Didn't adjust lower speed
Electrode 5	Raise time (s)	33.09	Raise time (s)	34	Raise time (s)	N/A	Couldn't increase raise speed. It's at maximum
	Lower time (s)	18.56	Lower time (s)	36	Lower time (s)	N/A	Decreased lower speed
Electrode 6	Raise time (s)	19.71	Raise time (s)	18.2	Raise time (s)	N/A	Didn't adjust raise speed
	Lower time (s)	16.02	Lower time (s)	24.1	Lower time (s)	N/A	Decreased lower speed

From Table I, it can be observed that adjustments were made to correct most of the electrodes. For some of the electrode speeds it was difficult to set the electrode hydraulic speeds according to the design specifications, due to unanticipated hydraulic system conditions. Therefore, in cases, such as these, the lower speed should at least be slightly slower than the raise speed, which has been done successfully.

Resistance controller optimisation

Once the electrode speeds were set correctly, each electrode's resistance was fine-tuned for optimised resistance control. Figure 4 presents the typical box and whiskers plot for the difference between the actual resistance measured and the resistance setpoint. The range represented by the whiskers part presents the minimum and maximum difference in resistance, which is + 0,4 mΩ and – 0.4 mΩ. The middle line in the box is the average value of all the data, where the desired average is 0 mΩ, which means that the resistance setpoint is consistently obtained. The top and bottom ends of the box plot are the averages of the data in the 1st and 4th quartile respectively, representing the operating band of the resistance versus set-point, which is + 0.2 mΩ and – 0.2 mΩ, respectively.

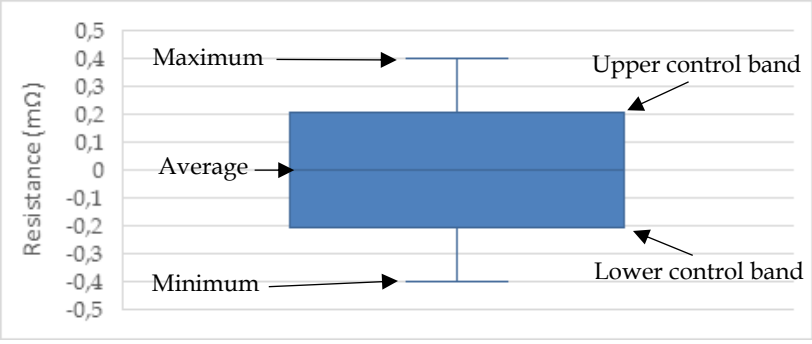


Figure 4. Ideal difference between measured resistance and resistance setpoint box and whiskers plot.

Improved resistance control performance impact

In this section, the box and whiskers analysis for only electrode 6 is shown for illustrative purposes, as all the other electrodes' box and whiskers analysis is conducted in the same manner. However, the results for each electrode will be presented after the box and whiskers analysis (Table II). Figure 5 presents the box and whiskers plot of the difference between the actual resistance and the setpoint of electrode 6.

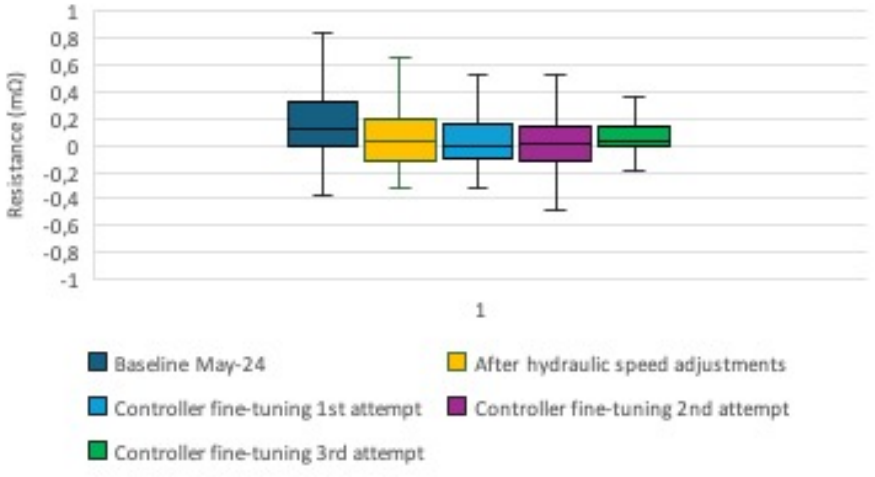


Figure 5. Electrode 6 difference in resistance and resistance set-point box and whiskers.

From Figure 5, it can be observed that the resistance control band was approximately -0.01 to + 0.33 mΩ and an average of + 0.12 mΩ, which illustrates that the control was operating mostly above the upper resistance deadband, which is + 0.2 mΩ. After the electrode speed adjustments were conducted, the control band was – 0.12 mΩ to + 0.19 mΩ and an average of 0.03 mΩ. However, after the third attempt in fine-tuning the resistance controller, the control band is approximately – 0.003 mΩ to + 0.15 mΩ and an average of 0.03 mΩ. Therefore, it illustrates that the resistance control of electrode 6 is operating in the deadband, reaching the set-point consistently, as well as operating in a significantly narrower deadband.

The effect of improved resistance control on power stability is evaluated, where electrode 6 is again chosen for illustrative purposes. Figure 6 presents the box and whiskers plot of the difference between the actual power and the setpoint of electrode 6.

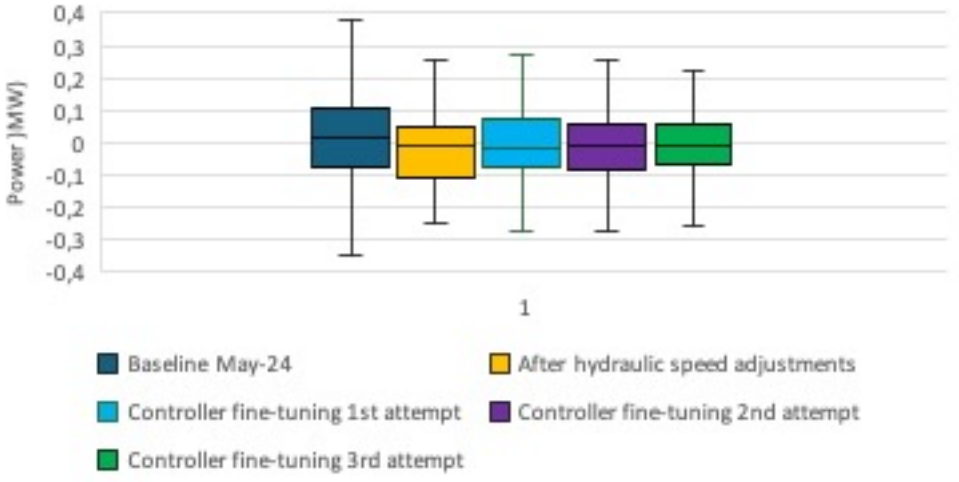


Figure 6. Electrode 6 difference in power and power set-point box and whiskers.

From Figure 6, it can be observed that the power band was approximately -0.08 to + 0.11 MW and an average of + 0.01 MW. After the electrode speed adjustments were conducted, the control band was – 0.11 MW to + 0.05 MW and an average of - 0.005 MW. However, after the third attempt in fine-tuning the resistance controller, the power band is approximately – 0.07 MW to + 0.06 MW and an average of - 0.006 MW. Therefore, it illustrates that the resistance control improvement resulted in a significantly narrower power band.

Table II presents the results of the difference in resistance and setpoint after the fine-tuning of the resistance controllers has been conducted.

Table II: Furnace 2 resistance controllers fine-tuning and adjustments

Electrode no	Maximum resistance versus setpoint (mΩ)	Minimum resistance versus setpoint (mΩ)	Average resistance versus setpoint (mΩ)	Upper band of resistance versus setpoint (mΩ)	Lower band of resistance versus setpoint (mΩ)
1	0.34	-0.26	-0.04	0.08	-0.11
2	0.29	-0.23	-0.04	0.09	- 0.15
3	0.25	-0.34	-0.08	0.03	-0.17
4	0.4	-0.34	-0.11	0.04	-0.21
5	0.48	-0.23	0.03	0.15	-0.09
6	0.36	-0.18	0.03	0.15	-0.003

The performance of the resistance controller for each electrode after the fine-tuning, which is captured in the table above, is evident that the resistance control band for each electrode has been optimised, indicated by the difference in the actual resistance and the resistance setpoint, operating in a significantly narrower band, as well as relatively balanced across the zero axis.

Energy savings impact quantification

The optimised resistance control of both Furnace 1 and Furnace 2, led to an improved power stability, which in turn enhanced furnace stability. This improvement can be observed by the furnace achieving lower SEC. Furnace 2 was selected for illustrative purposes to demonstrate the actual SEC improvement relative to the baseline SEC. In Figure 7, the SEC performance against the baseline SEC, is illustrated.

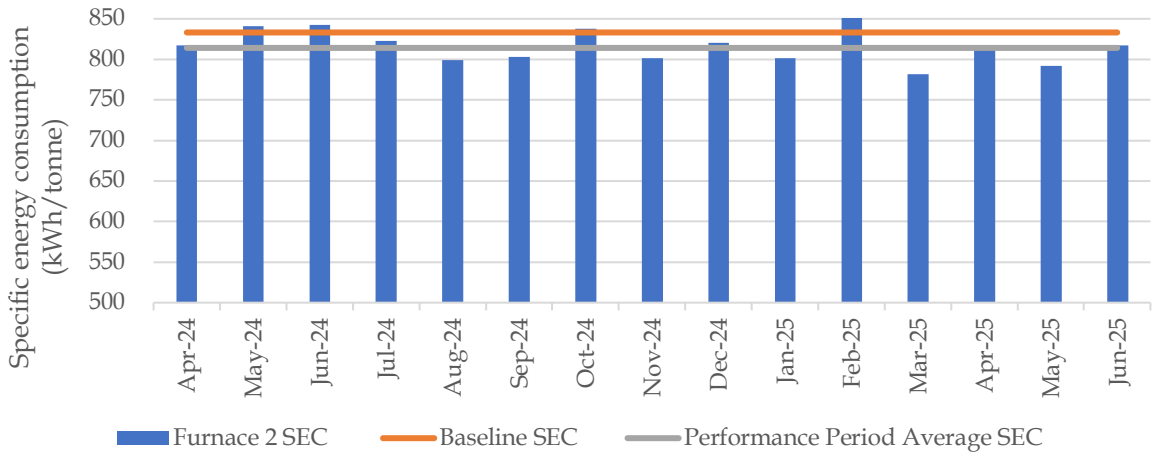


Figure 7. Furnace 2 SEC performance against baseline SEC.

From the figure presented above, it is evident that the actual SEC of Furnace 2 improved when compared to the baseline SEC. The baseline period for Furnace 2 specifically, is from April 2024 to June 2024. The reason for choosing this period for the baseline is that prior to this period, the Waterval smelter underwent an annual shutdown in February 2024 where they struggled in March 2024 to regain stability on the Six-in-Line furnaces. The average SEC during the performance period, was lower compared to the baseline SEC, clearly illustrating an energy improvement. Furthermore, the stability improvement led to an improved energy efficiency on Furnace 1 and Furnace 2, which resulted in an annual energy savings of 8.25 GWh and an SEC improvement of 3.03 %. This translates to energy cost savings of R 15.17 million for Furnace 1 and Furnace 2, without any capital expenditure.

CONCLUSION

In this paper, the proposed improved resistance control strategy is evaluated, based on the little available literature, as very few authors have conducted research in this specific field. The performance of the electrode immersion (resistance) control system was evaluated as a first step, to identify if a sub-optimal performance regime exists.

The initial performance of the resistance and power control operating bands was analysed and evaluated; it was found that the electrode hydraulic speeds were required to be measured, analysed and adjusted. Once the electrode hydraulic speeds were adjusted according to the design specifications, the performance of the resistance control bands were analysed and evaluated. The resistance control bands illustrated sub-optimal performance, as the resistance setpoint for each electrode was not being achieved, which resulted in the fine-tuning of each resistance controller, in order to achieve resistance setpoint consistently, as well as operating within a narrower resistance control band.

The results of the improved resistance control led to enhanced power control stability. These interventions resulted in an annual energy savings of 8.25 GWh and a reduction in specific energy consumption of 3.03 %. This translates to an annual energy cost savings of R 15.17 million, without any capital expenditure.

This paper primarily focused on the resistance control optimisation of an EAF where the aim of this study was to improve the resistance control performance of the current pulse control technique applied to the hydraulic solenoid valves. Further enhancements in resistance control could be achieved through the use of proportional control valves for electrode regulation, enabling more precise and stable control, as opposed to solenoid valves. Furthermore, this paper excluded both the feed control optimisation, which aims to maximise furnace stability, and the power control optimisation, which involves optimising the tap changer control to achieve the power setpoint more consistently. Therefore, further research may be conducted on the feed control and power control optimisation, as these avenues could also potentially yield significant energy savings by improving the furnace stability.

REFERENCES

Espindola, J., Nourin, F.N., Qandil, M., Abdelhadi, A. and Amano, R.S. (2021). Energy Saving Analysis Using Energy Intensity Usage and Specific Energy Consumption Methods. *International Journal of Energy for a Clean Environment*, 22 (1), 15 - 29. DOI: https://doi.org/10.1615/InterJEnerCleanEnv.2020034685

Hernandes, J.D., Onofri, L. And Engell, S.(2022). Energy optimization of the electric arc furnace for operations at a fixed electrical power level. *IFAC PapersOnLine*, 55 (21), 144 - 149. DOI: https://doi.org/10.1016/j.ifacol.2022.09.258

Jacobs, M. (2006). Process Description and Abbreviated History of Anglo Platinum's Waterval Smelter. *South African Pyrometallurgy.* The Southern African Institute of Mining and Metallurgy. Johannesburg. pp. 17 – 28. DOI: https://api.semanticscholar.org/CorpusID:110862132}

Minerals Council South Africa. (2011). Facts and Figures. https://www.mineralscouncil.org.za/industry-news/publications/facts-and-figures [accessed 25 Jun. 2025].

Nikolaev, A.A. Kornilov, G.P. Anufriev, A.V. Pekhterev, S.V. and Povelitsa, E.V. (2014). Electrical Optimization of Superpowerful Arc Furnaces. *Steel in Translation*, 44 (4), 289 - 297. DOI: https://doi.org/10.3103/S0967091214040135

Power Optimal. (2022). Eskom tariff increases vs inflation since 1988 (with projections to 2023) https://poweroptimal.com/2022-update-eskom-tariff-increases-vs-inflation-since-1988/ [accessed 18 Aug. 2025].

Snodgrass, R., Marsden, G., van der Merwe, K. and Shoko, S. (2024). Recent developments at Anglo American Platinum's smelting operations. *South African Pyrometallurgy.* The Southern African Institute of Mining and Metallurgy. Johannesburg. pp. 207 - 220.



Juan Siecker

Technical Specialist Manager and Extraordinary Senior Lecturer
ETA Operations and North-West University

Juan Siecker started working in 2016 as an Electrical Engineer at ArcelorMittal South Africa, where he obtained valuable hands-on experience in the Electrical Engineering discipline. He obtained his PhD degree in Electrical Engineering in 2023. In 2022, he started to work as a Project Engineer for ETA Operations in terms of energy efficiency optimization in the mining and mineral processing sector. He mostly focused on energy efficiency improvements in the platinum smelting and refining processes. Currently, he is working as a Technical Specialist Manager, still focusing energy efficiency improvements on the platinum smelting and refining processes, as well as providing technical support to various other Engineers working in similar processes. Juan is also appointed as a senior extraordinary part-time lecturer at the North-West University.

Comparative study of the interaction of alumina-chrome refractories with PGM smelter slag

N. Fotoyi, Y. Thakurdin, X. Goso, D. Chetty

Mintek, South Africa

This study investigates and compares the corrosion and wear mechanisms of two commercial alumina-chrome (Al_2O_3–Cr_2O_3) refractories—designated Refractory A and Refractory B—during exposure to PGM (Platinum Group Metal) smelter slag at 1550°C in a Top-Blown Rotary Converter (TBRC) furnace. The main objective was to understand how microstructure, mineral phases, and chemical composition influence refractory corrosion behavior in smelting environments. Both refractories were exposed to real PGM smelter slag under dynamic furnace conditions for repeated heating cycles. Post-exposure analyses were carried out using Scanning Electron Microscopy with Energy-Dispersive Spectroscopy (SEM-EDS) to examine slag penetration, phase transformations, and reaction layers. FactSage™ 8.3 thermodynamic simulations were performed to model the slag–refractory interactions and predict phase stability at equilibrium. Results showed that Refractory A, with higher Al_2O_3 and lower Fe_2O_3–MgO contents, developed protective spinel layers of $(Mg,Fe,Ni)(Cr,Al)_2O_4$ and $(Mg,Fe)Al_2O_4$ around alumina grains, restricting slag infiltration. In contrast, Refractory B, richer in Cr_2O_3, Fe_2O_3, and MgO, formed coarse spinel bands that failed to inhibit Al_2O_3 dissolution, leading to extensive grain and matrix degradation. Thermodynamic predictions confirmed that corrosion proceeded primarily through alumina dissolution, with higher dissolution predicted for Refractory B. The findings demonstrate that microstructure and high-temperature phase stability significantly influence refractory performance in PGM smelting, with Refractory A showing superior resistance to slag attack.

INTRODUCTION

Alumina-chrome refractories are prevalent in the metallurgical sector due to their superior mechanical properties, thermal shock resistance, and corrosion resistance [1-4]. However, the interaction of the PGM smelter slag with alumina-chrome bricks is not well reported in the literature or the public domain. On the other hand, literature on the interaction of alumina-chrome refractory with refractory at high temperatures is available for various industries, including waste incinerators, the gasification industry, and other smelting industries [1-10]. Chemical wear from liquid slag is typically the most severe, potentially leading to a loss of structural integrity in the refractory brick, which increases susceptibility to thermal shock, mechanical stresses, and erosion. Chemical wear occurs through three mechanisms: 1) infiltration or penetration of slag into the refractory structure, 2) reaction of the slag with the refractory, forming new phases, and 3) dissolution of the refractory by the slag.

Bennett *et al.* (2009, 2011, 2016) and Kwong *et al.* (2007) studied how chrome-containing refractories react with molten slags during gasification. Their results showed that spinels formed banded zones or layers around the chrome-alumina solid solution in the refractory. The chemical reactions involved iron in the slag reacting with alumina and chrome in the refractory. $FeAl_2O_4$ formed as the first layer at the slag interface, while $FeCr_2O_4$ developed as a second layer interacting with chrome grains. It was noted that $FeCr_2O_4$ formation creates a protective layer that limits further interaction between the refractory and slag.

These reactions deplete the slag of Fe, increasing its viscosity and reducing its ability to penetrate the refractory. Chen *et al.* (2020) performed postmortem analyses to understand how corrosion occurs in chrome-containing refractory within a coal-water slurry gasifier. Different layers formed within the interaction zone, including a $(Mg,Fe^{2+})(Cr,Fe^{3+})_2O_4$ solid solution spinel situated between the slag zone and the reaction layer, and between the reaction layer and the unreacted zone. This spinel formation was attributed to reactions between MgO and Fe_3O_4 in the slag and Cr_2O_3 in the refractory, with alumina not involved in the formation of the spinel. Lui *et al.* (2021) also conducted post-mortem analyses to examine the corrosion of chrome-containing refractory caused by high-sodium slag in an entrained-flow gasifier. The findings showed that slag did not penetrate the refractory; instead, a layer of $(Mg,Fe^{2+})(Al,Cr)_2O_4$ spinel formed on the surface of the aggregate grains. This spinel resulted from reactions between MgO and FeO in the slag with Al_2O_3 and Cr_2O_3 in the refractory, with alumina participating in the spinel formation. Gao *et al.* (2022) theorized that at the slag-refractory interface, wear was caused by FeO and MgO, while at the penetration layer, wear was due to SiO_2, CaO, and Al_2O_3. Cai *et al.* (2018) and Gao *et al.* (2023) investigated the corrosion of high-chromia refractory materials by basic coal ash slag and proposed that the Fe^{2+} in FeO from the slag was the only iron oxide present in the gasification environment and that it participated in $(Mg,Fe^{2+})(Al,Cr)_2O_4$ spinel formation. The studies highlighted the importance of reducing and oxidizing conditions in spinel formation, with the oxidation state of iron varying between the studies: Chen *et al.* (2020) indicated Fe_3O_4 (oxidizing conditions), while Lui *et al.* (2021), Cai *et al.* (2018), and Gao *et al.* (2023) involved FeO (reducing conditions).

In the present work, corrosion experiments of alumina-chrome refractory in interaction with PGM smelter slag were conducted in the TBRC furnace at 1550°C. The objective of the work was to compare the wear mechanisms in two alumina-chrome (Al_2O_3-Cr_2O_3) refractories during their interaction with PGM smelter slag. Thermodynamic simulations to predict the corrosion process were conducted using FactSage™ 8.3 software based on the interface reaction model. It is worthwhile to characterise the effect of this type of slag on alumina-chrome refractories since PGMs are a critical commodity in South Africa and globally.

EXPERIMENTAL PROCEDURE

Materials

The slag used in the current study was obtained from a major PGM smelter in South Africa. Two alumina-chrome (Al_2O_3-Cr_2O_3) refractory bricks that were used in the study were obtained from different commercial suppliers. The slag and refractories were subjected to chemical analysis by Inductively Coupled Plasma Optical Emission Spectroscopy (ICP-OES). Chemical compositions of the slag and refractories are given in Table 1. Refractory A had a relatively higher content of Al_2O_3 and SiO_2 compared to refractory B, while refractory B had relatively higher contents of Cr_2O_3, MgO, and Fe_2O_3.

Table 1: Chemical composition (wt%) of the PGM smelter slag

Al_2O_3	CaO	CoO	Cr_2O_3	Cu_2O	FeO	MgO	MnO	NiO	SiO_2	TiO_2	S	Total
4.10	3.15	0.12	1.51	0.25	25.22	17.58	0.18	0.38	45.56	0.26	0.36	98.67

Table 2: Chemical composition (wt%) of alumina-chrome refractories

	Al_2O_3	CaO	CoO	Cr_2O_3	Fe_2O_3	MgO	SiO_2	Total
Refractory A	88.88	0.07	0.25	7.64	0.97	<0.05	2.19	100.0
Refractory B	82.65	0.10	0.29	10.31	2.76	3.12	0.56	99.79

Refractory Interaction in Top Blown Rotary Converter (TBRC)

Both refractories were exposed to real PGM smelter slag under dynamic furnace conditions for repeated heating cycles. Refractory bricks A and B were installed in the same TBRC shown schematically in

Figure 1. The furnace was heated using an oxygen-propane flame to reach the test temperature, which was 1550°C. The flame stoichiometry was a slightly reducing flame of 95 mol% O_2. Given that the reducing flame was used, incomplete combustion of propane would occur, and the reaction can be presented by equation 1:

$$2C_3H_8 + 9O_2 \rightarrow 4CO_2 + 2CO + 8H_2O + heat \qquad (1)$$

For a runtime of 1 hr and stoichiometry of 95 mol% O_2, about 3.25 kg of propane was combusted with 11.21 kg of oxygen. FactSage software was used to determine the equilibrium amount of CO, CO_2, and H_2O that would be available at the temperature of 1550°C. The partial of oxygen that would be experienced inside the furnace was calculated to be 3.5×10^{-6} atm. It was noted that this partial pressure is higher than the partial pressure reported for smelting of PGM, which is 10^{-9} bar (Nell, 2004). The refractory bricks lining the TBRC shell were arranged in two layers, each layer having about 25 bricks. At first, the refractories in the rotary furnace were heated to 1200°C before slag addition. The furnace temperature was increased to the targeted test temperature (1550°C), with gradual addition of 15 kg of slag. The addition of slag was done every 15 to 20 minutes until a batch of 30kg was fed into the furnace. Once the slag batch was molten and test temperature was reached the slag and refractories were held at 1550°C for one hour, allowing for the refractories to interact with the slag. The slag was removed from the furnace by tilting the furnace and collecting the liquid slag in a ladle. The furnace was then allowed to cool naturally to 600°C. when these temperatures were reached, the furnace was heated again to 1200°C, and a fresh slag batch was fed accordingly. The above process was repeated three times, over three days. The TBRC was used so to allow for slag-refractory interactions to occur under dynamic conditions, and in the end investigate the effect of thermal shock by allowing the refractories to cool down in air just after tapping out the molten slag.

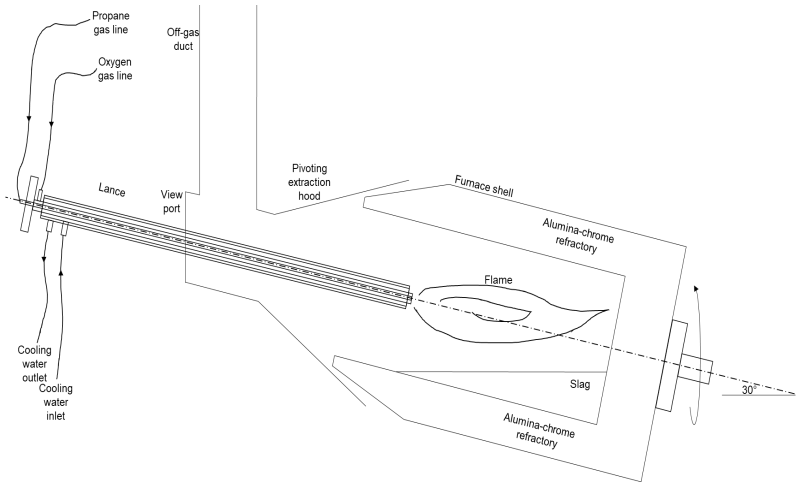


Figure 1: Schematic representation of the Top-blown rotary converter furnace (TBRC)

Scanning Electron Microscopy

After the TBRC testwork, the samples were cross-sectioned to expose the infiltration into the sample and progressively polished. Representative samples of refractory bricks were investigated by mineralogical methods (SEM-EDS). Polished cross-sections of refractory bricks were prepared and subjected to Scanning Electron Microscopy (SEM) analysis using a Zeiss EVO® MA15 SEM equipped with a Bruker energy dispersive X-ray analyser (EDX/EDS). Standard operating conditions included an accelerating voltage of 20 kV and a beam current of 200-500 pA. The results are explained in terms of the degree of slag penetration into the refractory brick, physical changes, and phase chemical compositions of reaction products.

Thermodynamic simulations using FactSage™ software

FactSage™ 8.3 thermodynamic simulations were performed to model the slag–refractory interactions and predict phase stability at equilibrium. Thermodynamic calculations were performed at 1550°C, 1

atm, and a partial pressure of oxygen at $P_{O2}=10^{-9}$ atm, to simulate the PGM smelting conditions. The calculations were performed with the equilibrium module EQUILIB, which is based on the Gibbs free energy minimisation technique. FactSage™ consists of modules that access the thermodynamic databases and perform various calculations. The associated databases applicable to this work were the FToxid (compounds and solutions for oxide systems). The solutions considered in the calculations were FToxid-SLAGA (slag), FToxide-SPINA (spinel solid solutions $FeAl_2O_4$-$FeCr_2O_4$-$MgAl_2O_4$-$MgCr_2O_4$), FToxid-MeO (monoxide solutions, e.g., MgO-CaO-FeO). The slag-refractory interactions were modelled at 1550°C using the interface reaction model. The interface reaction model simulates the interaction process of slag-refractory interface (Berjonnea et al 2009). Figure 2 shows the schematic drawing of the interface reaction model depicting interdiffusion between slag and refractory. In the system, the reaction degree is defined by <A>, which is the ratio R/R+S, where R+S =1. Therefore, the x-axis of the prediction diagrams represents the ratio between the slag and refractory at the interface, where the left side is the bulk slag (A=0), and the right side is the original refractory (A=1). In addition, value A corresponding to the ratio of the fraction of refractory can be described to indicate the corrosion degree of the refractory; thus, as the corrosion progresses, value A decreases gradually.

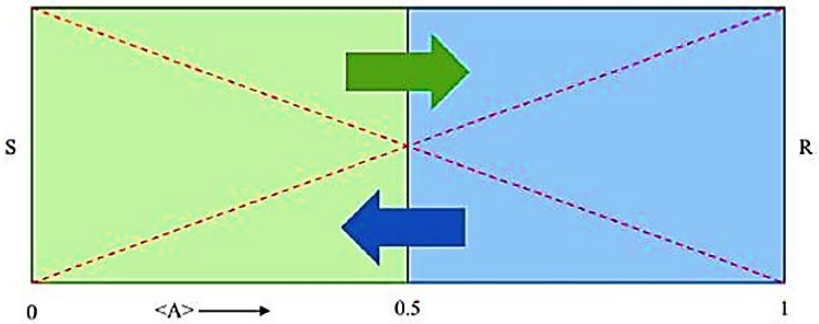


Figure 2: Interface reaction model between slag and refractory as a function of A

RESULTS AND DISCUSSION

As-received refractories

The as-delivered microstructures of refractory A and refractory B are shown in Figures 3 and 4. The EDS analysis results of refractory A are given in Table 3. Refractory A comprised of large (>100 µm) fused alumina grains (spots 1, 2) and small sintered alumina grains situated within the refractory matrix. The fine refractory matrix comprised of Al_2O_3-Cr_2O_3 solid solution (spots 3, 4), which also contained amounts of Si and traces of P. The $ZrSiO_4$ was also sporadically distributed within the refractory matrix as bright phases. P and Na were occasionally found in the refractory structure, supposedly originating from the phosphate binder that is normally used during the refractory manufacturing process. Within refractory B, comparatively larger (up to 1 mm) alumina grains (spots 1, 2) were present, and these displayed boundary rims that contained Cr and traces of Fe (spots 3, 4). The boundary rims were lighter than the grain interior and bound directly into the Al_2O_3-Cr_2O_3 refractory matrix. In this refractory, the matrix that binds the large alumina grains appeared fused compared to that observed in refractory A. The EDS analysis results of refractory B in Table 4 indicated that the refractory matrix also contained spinel-type phase compositions (spots 5, 6), possibly (Mg, Fe)(Al, $Cr)_2O_4$, in certain areas. The major mineral phase in refractory A was the alumina (Al_2O_3) from the grains. In contrast, the corundum (Al,Cr)2O3, forming the refractory matrix, was the intermediate phase, and mullite (Al6Si2O13) was the minor phase. Conversely, in refractory B, the major mineral phase was the corundum solid solution (Al,Cr)2O3 forming the refractory matrix. At the same time, the alumina (Al_2O_3) from the grains was the intermediate mineral phase, and FeCr2O4 was the minor phase in the brick.

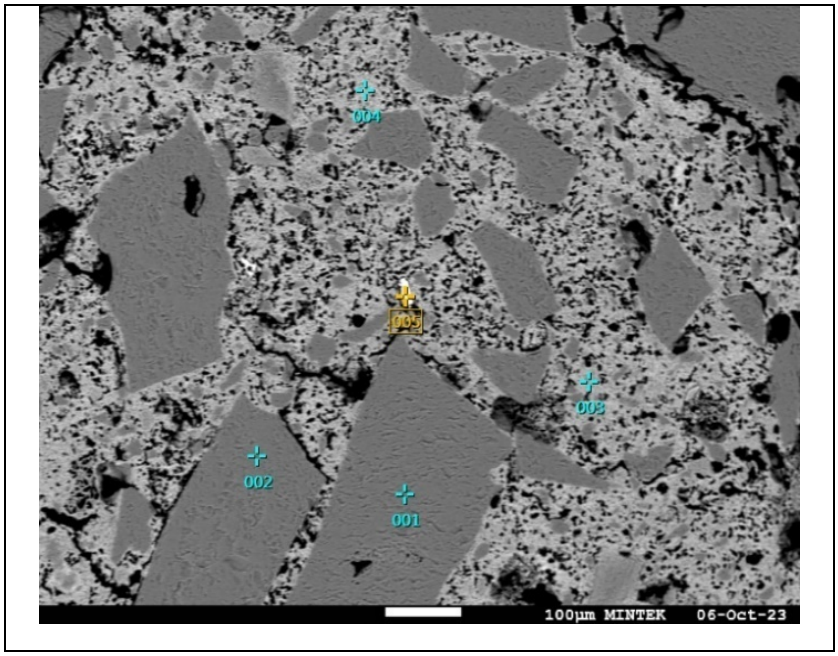


Figure 3: BSE images of as-delivered alumina-chrome refractory A microstructure

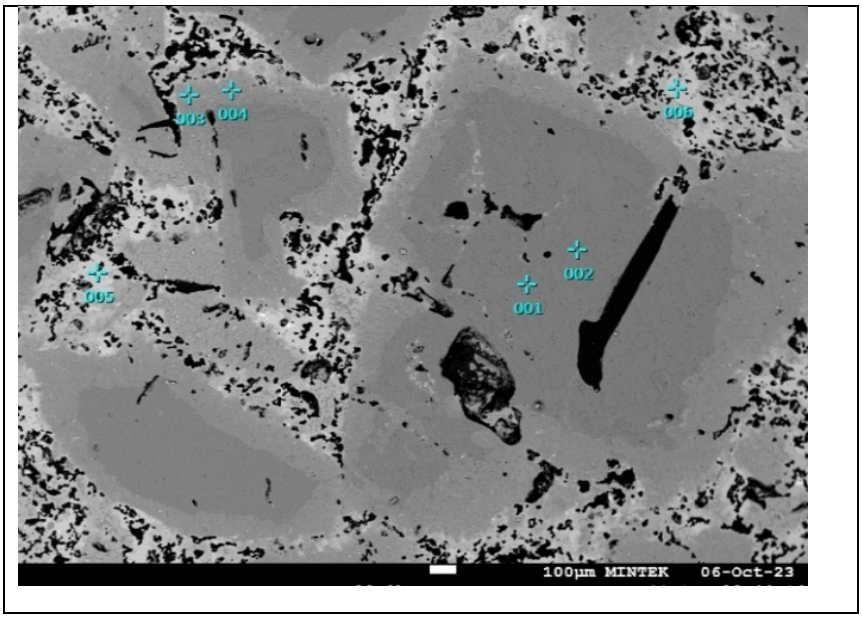


Figure 4: BSE images of as-delivered alumina-chrome refractory B microstructure

Table 3: EDS analysis results of phases in virgin Refractory A

Mass %	O	Al	Cr	Si	P	Zr
Spot 1	54.3	45.7				
Spot 2	40.5	59.5				
Spot 3	46.8	31.9	15.7	5.7		
Spot 4	46.5	28.4	15.54	7.3	1.7	
Spot 5	60.7			16.0		23.4

Table 4: EDS analysis results of phases in virgin Refractory B

Mass %	O	Al	Mg	Fe	Cr
Spot 1	52.2	47.9			
Spot 2	52.4	47.6			
Spot 3	50.1	45.7		0.4	3.8
Spot 4	54.0	43.1		0.52	2.4
Spot 5	44.3	29.2	8.2	4.7	13.6
Spot 6	43.1	22.4	14.6	5.6	14.2

Refractory A

Figures 5 and 6 show the BSE images of the slag zone and the reaction zone of refractory A after interaction with PGM smelter slag. The EDS analysis results of the phases are provided in Table 5. The phases were resolved based on stoichiometry from the EDS analysis results. The first notable feature was the formation of small, numerous, Fe-rich spinel crystals that appear to surround corroded large alumina grains (spot 5, 10). The rounded grain boundary structures of the spinels suggested high-temperature structures. The results indicate that the alumina grains interact with slag to form a solid solution zone with the first layer of $(Mg,Fe,Ni)(Al,Cr)_2O_4$ with high Fe, having a chemical composition tending towards $FeAl_2O_4$. The underlying zone (spots 3, 4) of $(Mg,Fe)Al_2O_4$ formed, limiting further interaction between alumina grains and slag. The underlying zone with high Al had a chemical composition tending towards $MgAl_2O_4$. $MgAl_2O_4$ is thermodynamically stable compared to $FeAl_2O_4$. The uptake of Fe reached 9.8wt%, while that of Mg reached 12.8wt% (spots 3, 4) within the zones. Therefore, the slag reacted with the alumina grains, resulting in element transfer accompanied by corrosion to create complex spinel zones, in agreement with previous work reported by Kwong *et al.* (2007), Bennett *et al.* (2009), and Cai *et al.* (2018). The refractory matrix was completely dissolved by the reaction with the slag, and reprecipitated as large spinel grains (spots 6, 7) within silicate phases. The silicate phases (spots 8, 9) within the reaction zone included pigeonite $(Mg,Fe^{2+},Ca)(Mg,Fe^{2+})Si_2O_6$ and omphacite $(Ca,Na)(Mg, Al, Fe^{2+},Fe^{3+})(Si_2O_6)$-type pyroxenes.

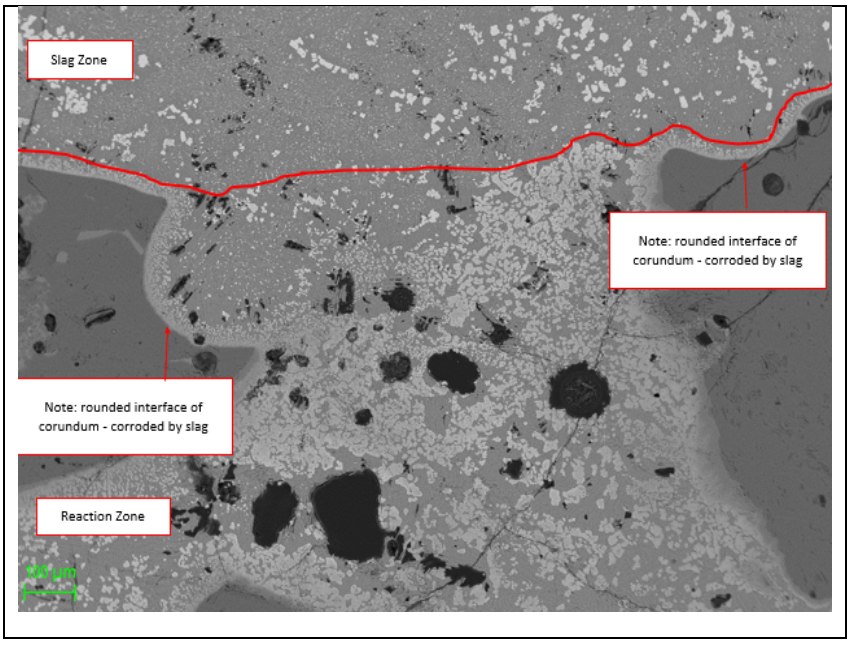


Figure 5: BSE images of Refractory A showing the slag zone and sla-refractory interface after interaction with slag

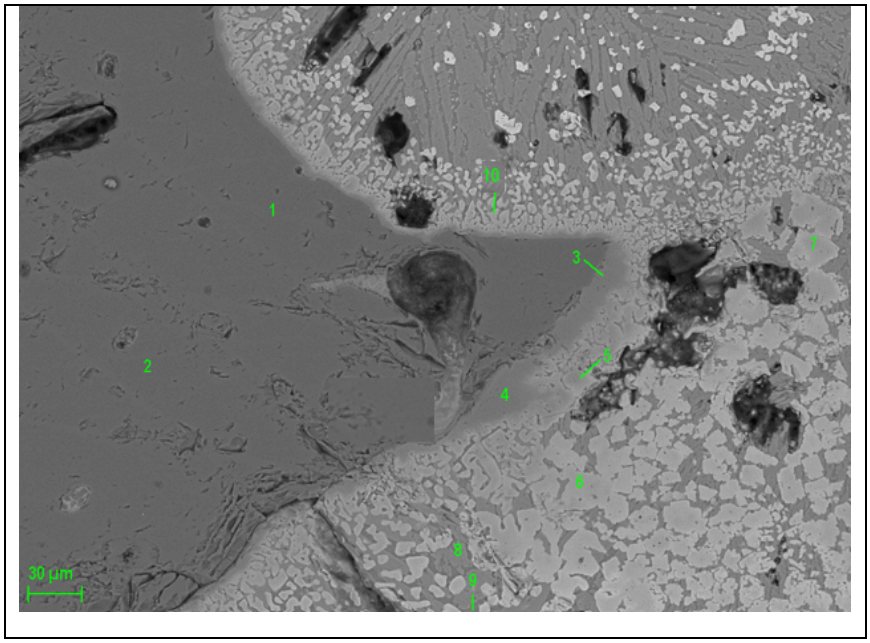


Figure 6: BSE images of Refractory A showing the interface reaction area after interaction with slag

Table 5: EDS analysis results of phases in the reaction zone of Refractory A after interaction with slag

	O	Mg	Al	Si	Ca	Cr	Fe	P	Ni	Phase
Spot 1	45.4		54.6							(Al_2O_3)
Spot 2	45.4		54.6							(Al_2O_3)
Spot 3	41.6	12.4	36.2				9.8			$(Mg,Fe)Al_2O_4$
Spot 4	41.4	12.8	36.6				9.2			$(Mg,Fe)Al_2O_4$
Spot 5	40.6	11.3	24.6	3.5		4.2	15.1	0.1	0.8	$(Mg,Fe,Ni)(Al,Cr)_2O_4$
Spot 6	36.0	9.1	19.4			15.1	19.8		0.6	$(Fe,Mg,Ni)(Cr,Al)_2O_4$
Spot 7	37.2	10.3	23.1			11.8	16.9		0.7	$(Fe,Mg,Ni)(Al,Cr)_2O_4$
Spot 8	43.7	13.9	4.8	21.4	3.6		12.6			$(Mg,Fe^{2+},Ca)(Mg,Fe^{3+})Si_2O_6$
Spot 9	46.5	0.9	12.6	26.5	8.9		4.6			$Ca(Al, Mg, Fe^{2+}, Fe^{3+})(Si_2O_6)$
Spot 10	37.9	9.3	27.3			2.0	22.1		1.4	$(Fe,Mg,Ni)(Al,Cr)_2O_4$

Figure 7 presents the BSE images of the precipitation zone of Refractory A (directly below the reaction zone) after its interaction with PGM smelter slag. EDS results are presented in Table 6. The slag infiltrated the refractory through its pores, filling the spaces between the alumina grains and reacting with the refractory matrix to form secondary phases. The porosity and pore sizes in the penetration zone were lower than those in the reaction zone due to the longer interaction time and adequate supply of corrosive elements from the slag. The secondary phases in the precipitation zone contain Na and P, and exhibit lower Fe content compared to the phases identified in the reaction zone. The phases containing Na and P (spots 13, 14, 15) were identified as an intermediate slag phase, which may broadly comprise a solid solution between cordierite ($(Fe^{2+},Mg)Al_4Si_5O_{18}$) and oligoclase feldspar ($(Na,Ca)(Si,Al,P)_4O_8$)-type compositions. The solid solution product of cordierite suggested a reaction between the Fe and Mg in the slag with the mullite phase in the refractory. The intermediate slag was significantly depleted in Fe (up to 4.2wt%) and Mg (up to 2.8wt%). The resulting change in slag chemistry affected its viscosity, which consequently increased and prevented further slag penetration into the refractory. This was observed in studies by Benette et al. (2011, 2016) and reported to promote the corrosion resistance of the refractory.

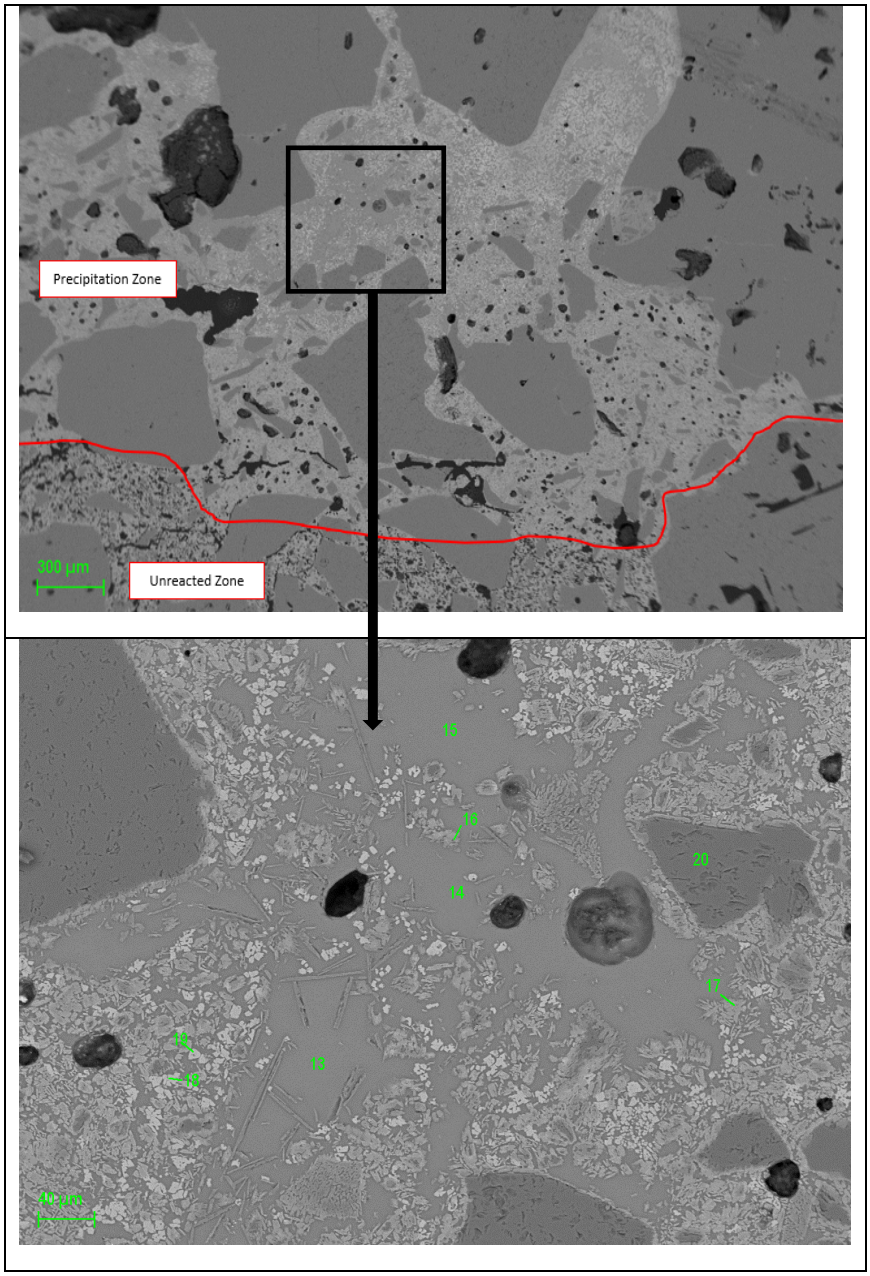


Figure 7: BSE images of Refractory A showing the precipitation zone after interaction with slag. (a) shows an overview of the zones, and (b) shows locations of EDS spot analyses in the rectangular area shown in (a).

Table 6: EDS analysis results of phases in the precipitation zone of Refractory A after interaction with slag

	O	Mg	Al	Si	Ca	Cr	Fe	P	Na	Phase
Spot 13	47.0	2.8	13.5	24.2	4.4		4.2	1.9	2.0	$(Fe^{2+},Mg)Al_4Si_5O_{18}$-$(Na,Ca)(Si,Al,P)_4O_8$
Spot 14	47.0	2.7	14.0	25.2	4.0		3.3	1.5	2.3	$(Fe^{2+},Mg)Al_4Si_5O_{18}$ - $(Na,Ca)(Si,Al,P)_4O_8$
Spot 15	47.2	2.1	13.4	26.2	3.9		3.7	1.3	2.2	$(Fe^{2+},Mg)Al_4Si_5O_{18}$ - $(Na,Ca)(Si,Al,P)_4O_8$
Spot 16	40.9		33.7			24.6	0.8			$(Al,Cr,Fe)_2O_3$
Spot 17	40.9		36.1			23.1				$(Al,Cr)_2O_3$
Spot 18	36.0	8.8	17.1	2.0		20.0	16.0			$(Fe^{2+},Mg)(Cr,Al)_2O_4$
	O	Mg	Al	Si	Ca	Cr	Fe	P	Na	Phase
Spot 19	36.6	8.4	17.6	2.8		18.2	16.5			$(Fe^{2+},Mg)(Cr,Al)_2O_4$
Spot 20	45.7		54.3							Al_2O_3

The refractory matrix (Al_2O_3-Cr_2O_3) reacted to form solid solutions of corundum phases (spots 16, 17), which appeared to precipitate within the slag phase, possibly during cooling. The Al content in the corundum phase was higher than in the refractory matrix phase, which has elevated Cr content. The reaction mix of pyroxene-type matrix with corundum solid solution crystals surrounds the remnant alumina grains of the refractory, which show resorption textures from partial dissolution. These product spinel crystals surrounding the remnant grains helped prevent significant dissolution of alumina grains by the slag. These spinel phases (spots 18, 19) in the precipitation zone are smaller in size and possess higher Cr concentrations compared to those found in the reaction zone. The Mg and Al content within the precipitation zone phases was notably low relative to that in the reaction zone phases. These observations suggest that Fe, Mg, and Al in the slag were depleted through reactions occurring in the reaction zone. Consequently, the Al in the reactions observed in the precipitation zone primarily originated from the refractory matrix and the alumina grains. This indicates that as the slag penetrated the refractory, it became depleted of Fe, Mg, and Al, as these elements were involved in reactions with the alumina grains and refractory matrix within the reaction zone. The residual slag in the precipitation zone contained elevated Na and P levels, implying a reaction with the refractory matrix and the slag. The possible source of the Na and P in the refractory is the binder, which is usually used in refractory manufacturing, and could be distributed unevenly at high temperatures due to volatilization.

Refractory B

Figures 8 and 9 present the BSE images of the slag zone, interface, and reaction zone of refractory B after its interaction with PGM smelter slag. EDS analysis results of the phases are presented in Table 7. The microstructure revealed interconnected, numerous spinel particles that formed a banded structure at the hot face of the refractory after slag reacted with both the alumina grains and the refractory matrix. In comparison to the spinels surrounding alumina grains in refractory A, these showed relatively larger particles. Above the banded spinel structure was a slag zone that contained both the fine and larger spinel crystals that precipitated within the silicate phases. Below the spinel structure was the reaction zone, showing complete dissolution of alumina grains and matrix. The spinel phases had a high Fe content and were identified with the $(Fe,Mg,Ni)(Al,Cr)_2O_4$ structure. At the slag interface (spot 1), the spinel chemical composition tended towards $FeCr_2O_4$, while at the interface with the refractory, the spinel (spot 2) chemical composition tended towards $FeAl_2O_4$. $FeAl_2O_4$ is thermodynamically stable compared to $FeCr_2O_4$.

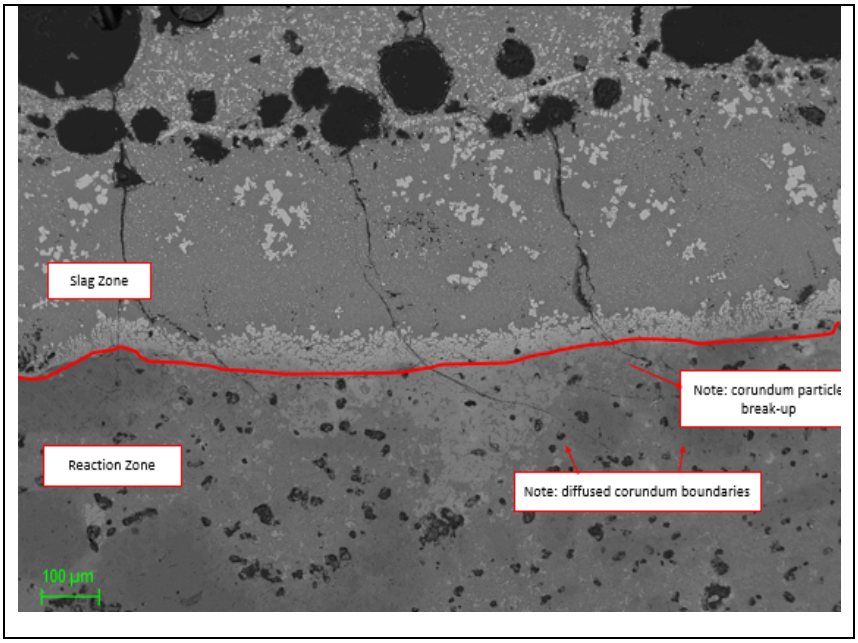


Figure 8: BSE images of Refractory B showing the slag zone, interface, and reaction zone after interaction with slag.

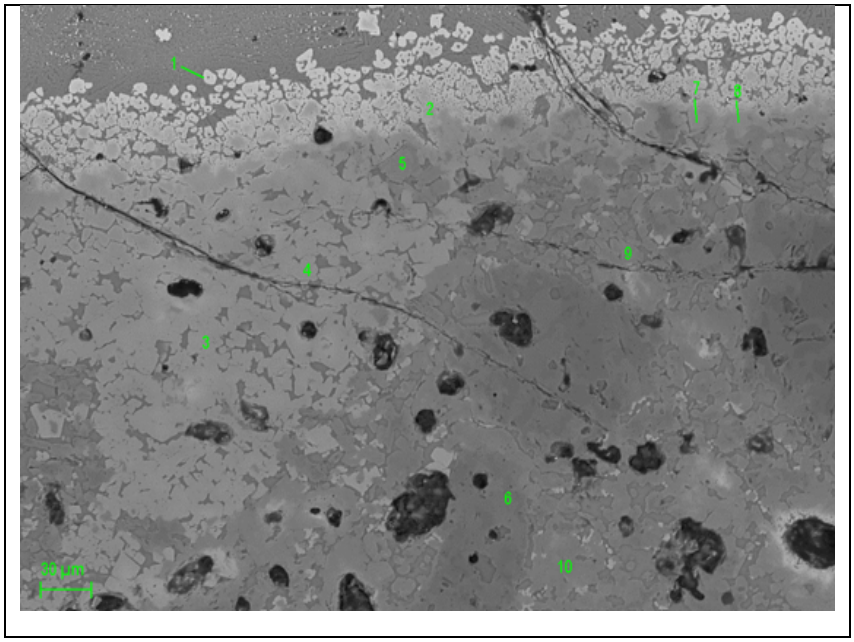


Figure 9: BSE images of Refractory B showing the slag-refractory interface after interaction with slag

Table 7: EDS analysis results of phases in the reaction zone of Refractory B after interaction with slag

	O	Mg	Al	Cr	Fe	Ni	Phase
Spot 1	30.2	5.3	7.7	16.3	39.4	1.1	$(Fe,Mg,Ni)(Cr,Al)_2O_4$
Spot 2	35.3	9.2	18.4	13.1	22.4	1.6	$(Fe,Mg,Ni)(Cr,Al)_2O_4$
Spot 3	36.2	8.8	24.2	16.0	14.7		$(Fe,Mg)(Cr,Al)_2O_4$
Spot 4	36.5	9.3	25.4	14.2	14.6		$(Fe,Mg)(Cr,Al)_2O_4$
Spot 5	40.5		40.4	19.1			$(Al,Cr)_2O_3$
Spot 6	41.8		47.6	10.6			$(Al,Cr)_2O_3$
Spot 7	36.9	11.5	26.9	11.6	13.0		$(Mg,Fe)(Al,Cr)_2O_4$
Spot 8	37.2	11.0	25.9	13.4	12.5		$(Mg,Fe)(Al,Cr)_2O_4$
Spot 9	40.6		40.1	19.4			$(Al,Cr)_2O_3$
Spot 10	41.2		42.9	15.9			$(Al,Cr)_2O_3$

The alumina grains at the refractory hot face in contact with the slag undergo an increase in Cr content up to 19 wt%, changing the Al_2O_3 grains into $(Al, Cr)_2O_3$ solid solution (spot 5). The Cr uptake in alumina grains resulted in the dissolution of the original refractory alumina grains. When comparing spinels formed within similar zones (near the interface between the slag and the spinel), spinel formed within Refractory B showed significantly higher Fe and Mg compared to spinel in Refractory A, and had larger particles. This was attributed to the fact (Table 2) that refractory B had comparatively higher Fe_2O_3 and MgO contents compared to refractory A. These phase compounds tend to promote spinel formation, resulting in larger particles. However, the banded spinel structure formed by the interconnected numerous particles of spinel at the interface with slag did not inhibit infiltration of the slag into the refractory. The spinel phases adjacent to the slag exhibited lower Al content relative to spinels positioned further from the interface. Comparing the microstructure of the virgin refractory (Figure 2 (b)) to that of the refractory after interaction with the slag, it is evident that the alumina grains reacted with the slag at the interface and were completely dissolved, resulting in no identifiable distinct grain boundaries. This textural evidence indicates that the interaction of refractory B with the slag was more extensive than that of refractory A with the slag, since this extensive grain dissolution feature was not observed within the reaction zone of refractory A, in which alumina grain boundaries were still clearly definable. The new refractory matrix consists of spinel phases (spots 3,4) that likely precipitated following the reaction of the prior Al_2O_3-Cr_2O_3 refractory matrix with the slag. The spinel phases were precipitated, possibly at lower temperatures within the refractory matrix and not around the alumina grains as observed in Refractory A. Therefore, it can be suggested that lower temperatures promoted the growth of spinels with larger grains, precipitating within the newly formed matrix. Below the interface, the spinel phases (spots 7,8) had low Fe and high Al contents, which is linked to the new solid solution of the corundum phase, $(Al,Fe,Cr)_2O_3$. Overall, the results indicate that refractory B underwent extensive chemical phase changes wherein the Al_2O_3-Cr_2O_3 refractory matrix reacted both with the slag and the refractory alumina grains.

Figure 10 shows the BSE images of the precipitation zone of Refractory B

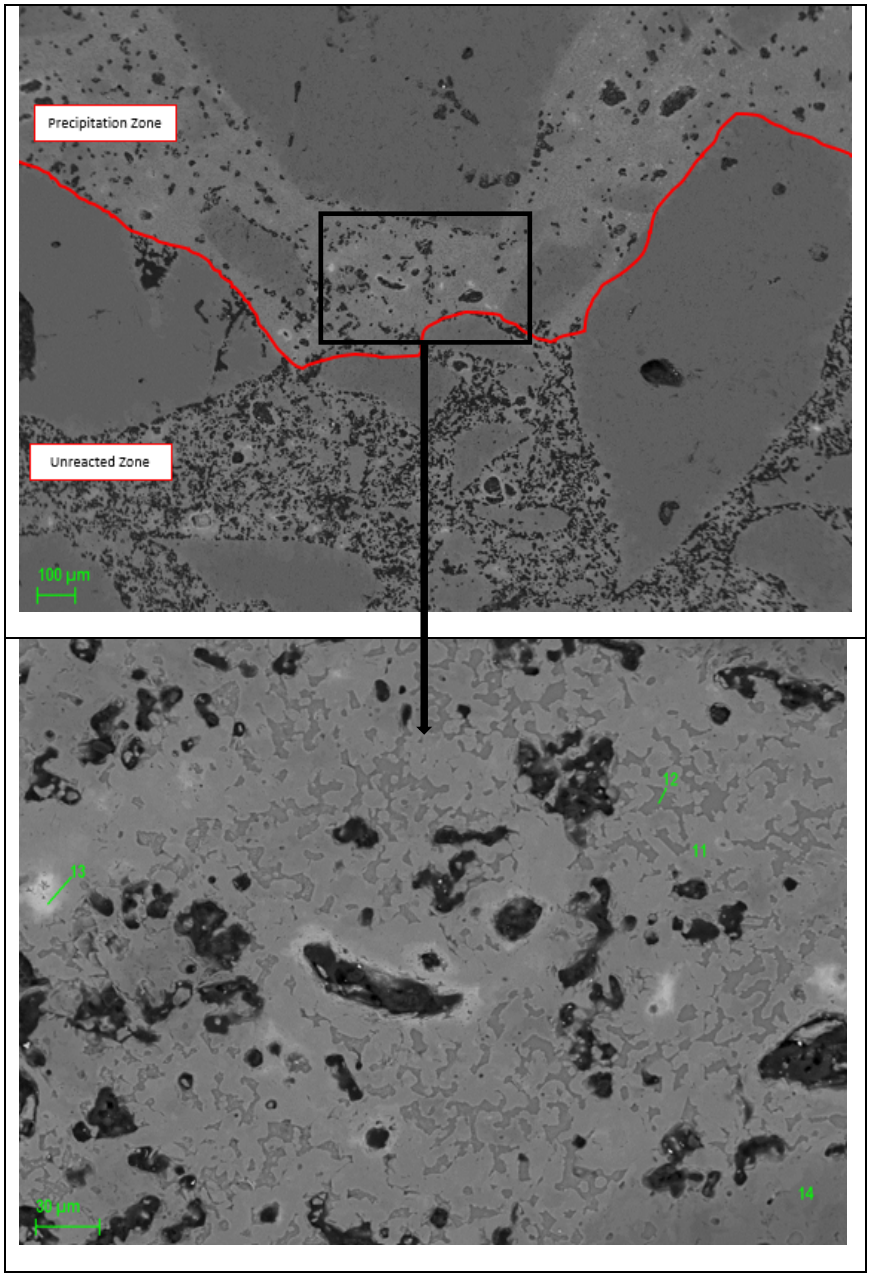


Figure 10: BSE images of Refractory B showing the (a) overview of the precipitation zone and (b) the magnified insert from (a) after interaction with slag.

Table 8: EDS analysis results of phases in the precipitation zone of Refractory B after interaction with slag

	O	Mg	Al	Si	Ca	Cr	Fe	Na	P	Phase
Spot 11	40.3		41.1			18.6				$(Al,Cr)_2O_3$
Spot 12	45.0	1.8	14.2	19.2	4.7	0.9	1.6	6.3	6.4	$(Fe^{2+},Mg)Al_4Si_5O_{18}$ and $(Na,Ca)(Si,Al,P)_4O_8$
Spot 13	32.5		10.3			57.2				$(Al,Cr)_2O_3$-Cr_2O_3
Spot 14	40.2		53.3			6.5				$(Al,Cr)_2O_3$

EDS analysis results of the phases are given in Table 8. In this zone, the individual alumina grains could be observed; however, the rims of corundum solid solution (as observed in the original refractory) were

not encountered. This indicated that the alumina grains and refractory matrix reacted with the infiltrated slag. The refractory matrix contained new phases of silicate and corundum solid solution. Therefore, the corundum phase previous refractory matrix, reacted with the slag, resulting in the corundum phase (spot 11) that was precipitated as (Al,Cr)2O3, thereby creating a new refractory matrix in this region. Variations of this solid solution are evident as sporadic brighter portions in the BSE images (spots 13, 14), containing much higher Cr than Al. Comparing this zone, it can be observed that the corundum phases formed were interconnected structures that grew within the silicate phase, as opposed to the smaller spinel particles observed within refractory A. Additionally, there were no smaller spinel crystal rims surrounding the remaining alumina grains and inhibiting their dissolution by slag, as seen in the precipitation zone in refractory A. New solid-solution silicate phases broadly conform with cordierite ($(Fe^{2+}, Mg)Al_4Si_5O_{18}$) and feldspar ($(Na, Ca)(Si, Al, P)_4O_8$) compositions. The silicate phases in Refractory B had higher Na and P (6.3 wt. % and 6.4 wt. %) compared to those found in Refractory A (1.9 -2.3 wt.%). Smaller Al2O3 grains were also observed within the matrix and reacted with the slag to form the corundum phase.

Figure 11 shows the BSE image of the unreacted zone of Refractory B following interaction with PGM smelter slag nearer the hot face. EDS analysis results of the phases are given in Table 9.

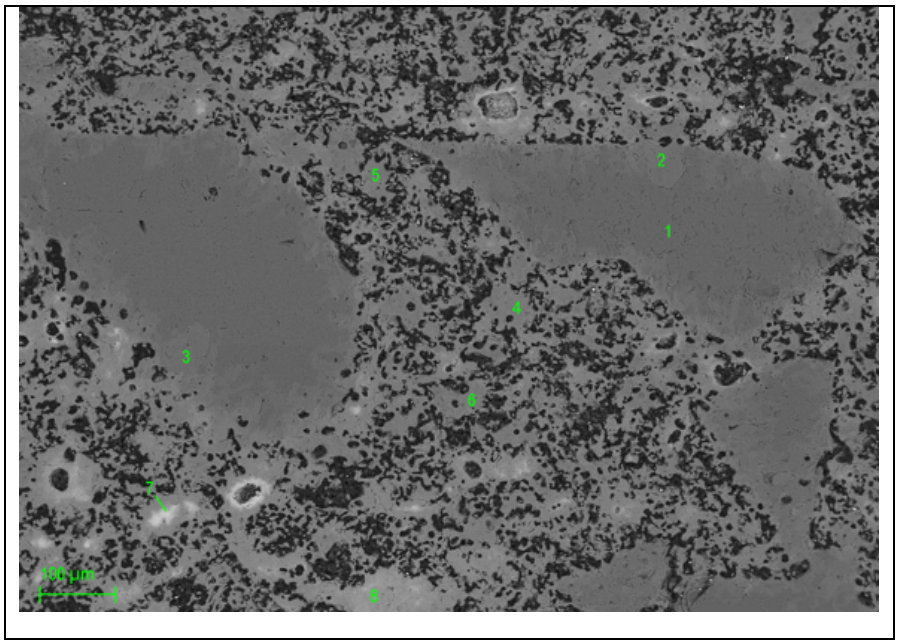


Figure 11: BSE images of Refractory B showing the unreacted zone after interaction with slag

Table 9: EDS analysis results of phases in the unreacted zone of Refractory B following slag interaction

	O	Al	Cr	Phase
Spot 1	43.9	56.1		Al_2O_3
Spot 2	43.3	52.2	4.6	$(Al,Cr)_2O_3$
Spot 3	43.0	49.2	7.8	$(Al,Cr)_2O_3$
Spot 4	40.6	44.0	15.4	$(Al,Cr)_2O_3$
Spot 5	41.9	41.8	16.3	$(Al,Cr)_2O_3$
Spot 6	40.2	43.0	16.8	$(Al,Cr)_2O_3$
Spot 7	29.6		70.4	Cr_2O_3
Spot 8	37.6	29.8	32.6	Al_2O_3-Cr_2O_3

The microstructure revealed a porous refractory structure after the interaction with the slag compared to the virgin refractory, Figure 2(b). The grain boundary rims were still observed, but they contained a higher content of Cr, approximately 8%, compared to the boundary rims surrounding the alumina grains in the original brick, which contained approximately 4%Cr. In addition, the Si content observed in these rims in the original brick was not detected in the rims observed after the interaction with the slag. This suggested that the phase transition towards stable phases continued to occur in the refractory, with the reactions driven possibly by high temperatures. Therefore, the contents of the original refractory continued to react when the brick was exposed to the slag. The EDS phase compositions also indicate that the Al_2O_3-Cr_2O_3 found in the refractory matrix reacted in most parts to form a corundum solid solution. The absence of Mg, Fe, Si, and Ca was observed in the unreacted refractory matrix, indicating that slag had ceased infiltrating the refractory. In other areas of the refractory, bright phases of Cr_2O_3 were observed.

Comparative evaluation of refractories A and B using FactSage™ software

Thermodynamic simulations

Figures 12 and 13 illustrate the predicted phase stability and equilibrium compositions of PGM smelter slag in contact with refractory A (Figure 8) and refractory B (Figure 9).

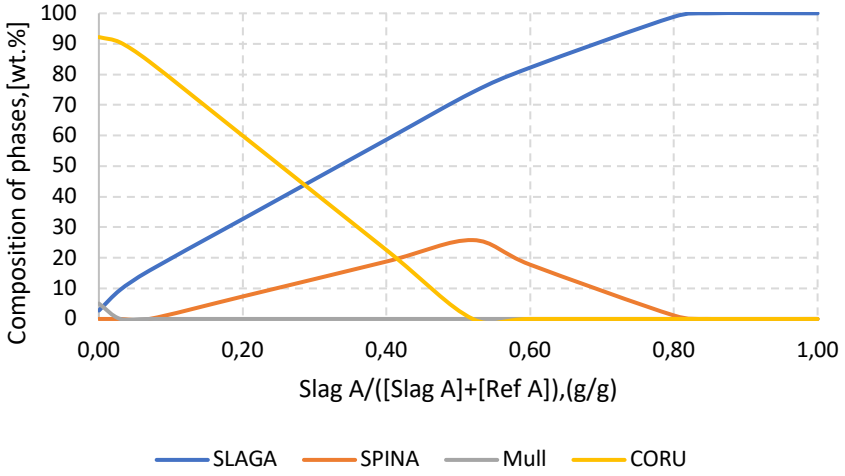


Figure 12: Predicted chemical stability of alumina-chrome refractory A in interaction with PGM smelter slag at 1550°C

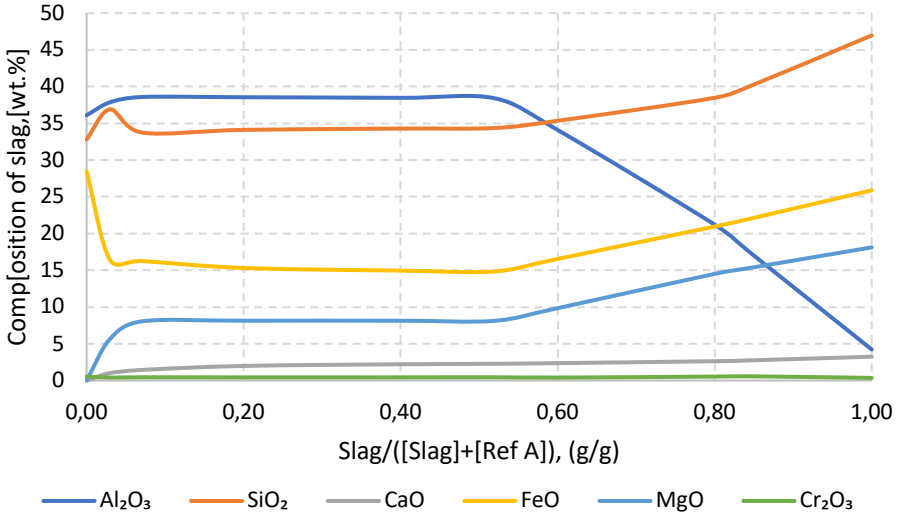


Figure 13: Predicted chemical stability of slag phases at 1550°C

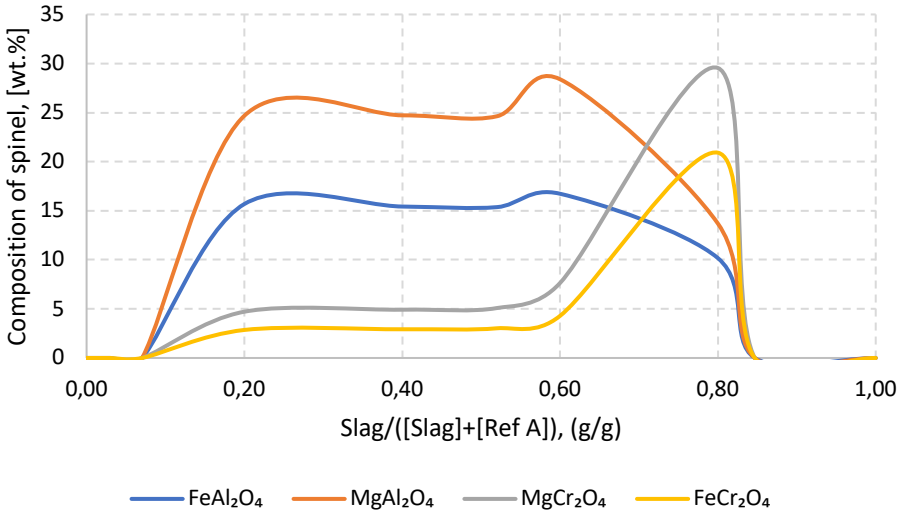


Figure 14: Predicted chemical stability of spinel phases at 1550°C

Figures 12 to 14 show the chemical stability and equilibrium composition of PGM slag in contact with refractory A. The thermodynamic calculations predict the formation of spinel, mullite, slag, and corundum. From Figures 11 and 12, as the fraction of the slag increases, the MgO content in the slag rises until it reaches saturation. The calculated MgO saturation in interaction with refractory A was 8.14 wt.% MgO in slag. The increase in MgO in the slag causes a decrease in FeO in the slag. When the MgO in the slag reaches saturation, it is evident in Figure 12 that spinel starts to become stable. This occurs at a slag fraction of 20%. The spinel phase increases with increasing slag fraction until it reaches a maximum of 25.8%, then decreases significantly to zero as the refractory fraction increases. After the spinel reaches its maximum, a change occurs in the slag phase. The spinel phase peaks when Al_2O_3 in the slag reaches saturation, with an estimated Al_2O_3 content of 38.40 wt.%. This occurs at a refractory fraction of 48%. It can be observed that FeO and MgO contents increase steadily as the spinel phase dissolves into the slag. Simultaneously, the SiO_2 composition rises, making the slag more silica-rich rather than alumina-rich. The results indicate that the slag is unsaturated with respect to both refractory phases, namely the corundum solid solution and the spinel phase. The corundum solid solution dissolves completely until MgO saturation is reached. The spinel phase stabilizes before the corundum phase at a refractory fraction of 52%. Figure 13 shows that the major spinel phases for most of the slag fractions are $MgAl_2O_3$ and $FeAl_2O_3$. $MgCr_2O_3$ and $FeCr_2O_3$ spinel phases are predominant at high slag fractions around 80%.

Figures 15 to 17 depict the chemical stability and equilibrium composition of PGM slag in contact with refractory B. Thermodynamic calculations predict the formation of spinel, slag, and corundum. The results suggest that the slag remains unsaturated with respect to both refractory phases, the corundum solid solution and the spinel phase. As the refractory fraction increases from right to left, the spinel phase rises to a maximum of 37.2%. The corundum solid solution dissolves entirely until the slag reaches Al_2O_3 saturation. The calculated Al_2O_3 saturation point for the slag is 38.10 wt.% and occurs at a refractory fraction of 54%. The spinel in the refractory is stable from the beginning, and Figure 15 shows that MgO content in the slag does not change significantly as the spinel increases with the slag fraction. MgO content in the slag ranged from 9.3 to about 8.1 wt.%, during which the spinel phase increased. After reaching its maximum, as the spinel decreased, MgO in the slag increased markedly, indicating spinel dissolution into the slag phase, which also caused FeO levels to rise. At low slag fractions below 55%, the slag is rich in alumina, whereas at higher fractions, it becomes rich in silica. The later stabilization of corundum compared to refractory A indicates that more refractory dissolves before corundum stabilizes. Figure 16 shows that the major spinel phases for most of the slag fractions are $MgAl_2O_3$ and $FeAl_2O_3$. $MgCr_2O_3$ and $FeCr_2O_3$ spinel phases are predominant at high slag fractions from about 70% to about 80%.

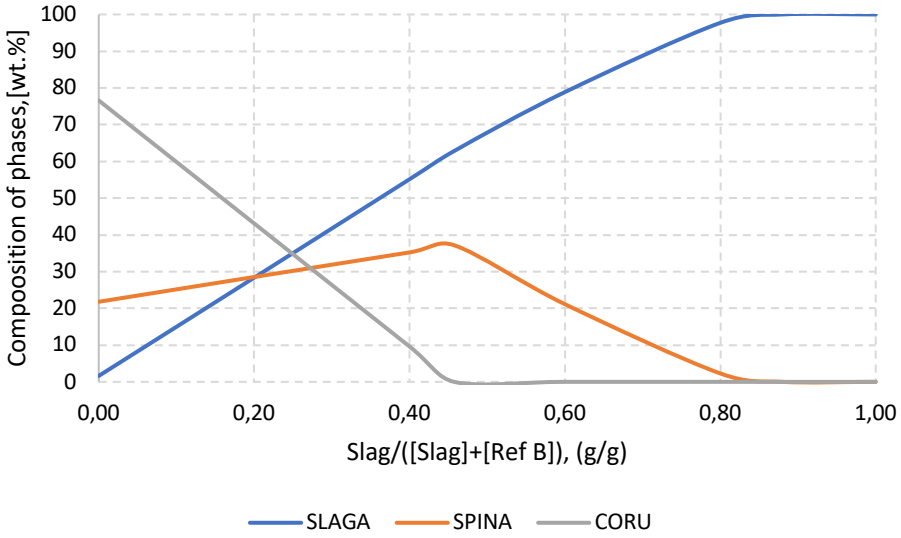


Figure 1: Predicted chemical stability of alumina-chrome refractory B in interaction with PGM smelter slag at 1550°C

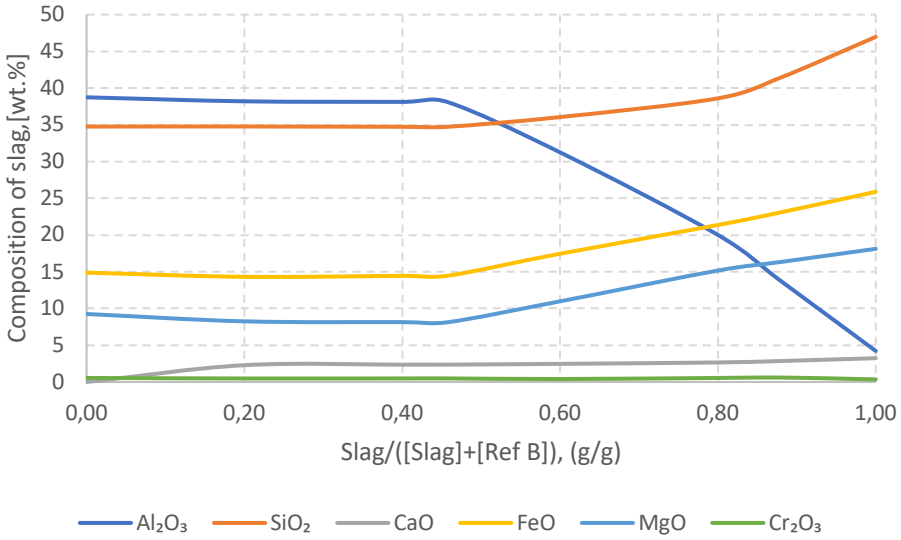


Figure 2: Predicted chemical stability of slag phases at 1550°C

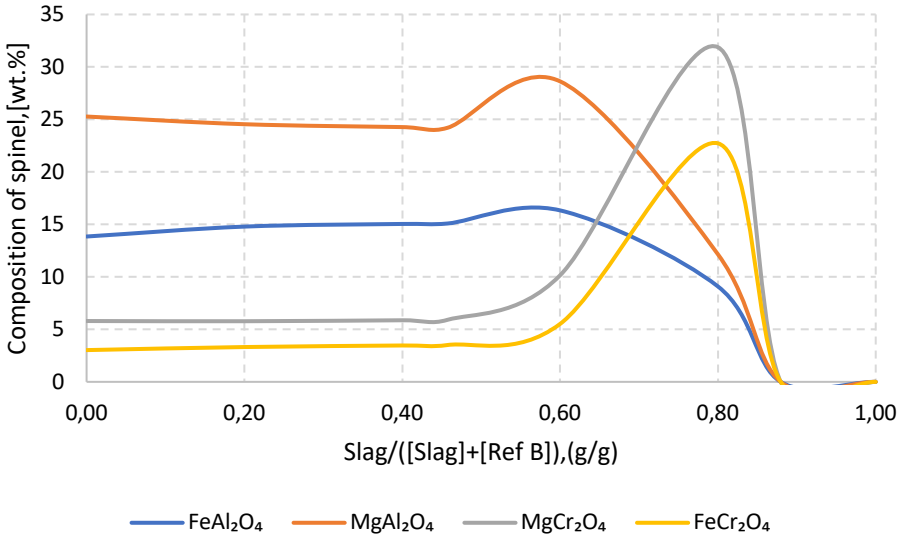


Figure 3: Predicted chemical stability of spinel phases at 1550°C

The predictions indicate that in both refractories, the corundum phase is unstable when in contact with the initial slag, as it is fully dissolved. The corundum dissolved until the Al_2O_3 content in the slags reached saturation. The calculated saturation point for refractory dissolution was 48% for refractory A and 54% for refractory B. This suggests that corrosion should be greatest for refractory B during interaction with the slag. It also indicates that the driving force for refractory dissolution is strongest in refractory B, since the difference between the initial Al_2O_3 content and the amount at equilibrium is the largest. The results imply that the spinel would be present throughout the infiltration path, which was confirmed by SEM observations. From these observations, at the interface of refractory B with the slag, alumina grains were completely dissolved by the slag and enriched with Cr, forming $(Al,Cr)_2O_3$ solid solution. The spinel banded structure formed had varying Fe and Al contents, with chemical composition tending towards $FeCr_2O_4$ at the interface with slag and $FeAl_2O_4$ at the interface with refractory. In refractory A, however, solid solution zones of $(Mg,Fe)Al_2O_4$ tending towards $MgAl_2O_4$, and $(Mg,Fe,Ni)(Cr,Al)_2O_4$ tending towards $FeAl_2O_4$ phases formed at the interface of the alumina grains. The grains were not fully dissolved but resorbed to create concave features, indicating partial dissolution. SEM analysis also showed a high content of MgO and FeO at the refractory's hot face at the slag-refractory interface in refractory A. In contrast, limited amounts of MgO and FeO were found in the precipitation zone. This aligns with the FactSage™ predictions, which indicated that the main phases of spinel are $MgAl_2O_4$ and $FeAl_2O_4$ at decreased slag compositions, while at higher slag compositions, $MgCr_2O_4$ and $FeCr_2O_4$ are the dominant spinel phases.

CONCLUSIONS

The microstructure and phase stability of alumina-chrome refractories significantly determine their corrosion resistance against PGM slag. For refractory B, the infiltrated slag reacted with the solid solution phase (rims) surrounding the alumina grains, thereby altering the composition of the alumina grains and the existing refractory phases. This caused a reaction between the alumina grains and the refractory matrix, forming corundum solid solutions. The boundary rims around the original large alumina grains contributed to their dissolution, with high temperatures likely impacting the extent of reactions with the slag. It can be concluded that, at high temperatures, the complete dissolution of alumina grains by the slag was favored, promoting slag infiltration into the refractory. Consequently, alumina grains dissolved entirely, reacting with the Al_2O_3-Cr_2O_3 matrix to produce a corundum solid solution phase without distinct grain boundaries. The findings suggest the refractory underwent extensive chemical phase changes, with slag reacting with both the refractory matrix and the alumina grains. The spinel phases did not form around alumina grains but instead created a spinel layer at the

interface with the slag, indicating that spinel precipitation was more promoted at lower temperatures. Higher MgO and Fe_2O_3 contents in the refractory led to increased levels of these oxides in the spinel phase compared to refractory A, forming spinel phases $(Fe,Mg,Ni)(Cr,Al)_2O_4$, tending towards $FeCr_2O_4$ at the slag interface, and $FeAl_2O_4$ at the refractory interface. This implies that the spinel layer formed after slag infiltration did not prevent further slag penetration into the refractory. In the reaction zone, after interacting with the slag, the refractory matrix consisted of silicate phases with precipitated spinel. The boundary rims surrounding the alumina grains, as seen in unreacted refractory, were not observed, indicating reaction with infiltrated slag. Conversely, in the unreacted zone, boundary rims around the alumina grains were present, suggesting ongoing phase transformation. Therefore, the contents of the original refractory continued to react when the brick was exposed to the slag, and that, combined with the reactions with the slag, enlarged the extent of corrosion of refractory B by the slag.

Conversely, in refractory A, the numerous spinel smaller particles formed banded spinel structures around the individual alumina grains. The first layer of the $(Fe, Mg, Ni)(Al, Cr)_2O_4$ spinel contained high amounts of Fe, while the second layer of $(Mg, Fe)Al_2O_4$ spinel, directly binding to the alumina grain, contained high amounts of Mg and Al. The chemical composition of the spinel tended towards thermodynamically stable phases of $FeAl_2O_4$ and $MgAl_2O_4$, respectively. The alumina grain boundaries were distinct, but appeared rounded, indicating reaction and partial corrosion caused by the slag. The refractory matrix at the interface consisted of pyroxene-type silicate phases, with larger-grained spinel phases precipitated. Within the precipitation zone, the refractory matrix primarily consisted of cordierite and feldspar-type silicate phases, with smaller grains of spinel phases present, resulting in a dense structure. These results show that the refractory underwent chemical phase changes with its matrix and that spinel phases tended to form spinel zones around the alumina grains. The results suggested that, at high temperatures, slag components participate in forming spinel at the interfaces of alumina grains. The intermediate slag in the precipitation zone was significantly depleted in Fe and Mg. Consequently, the decrease in slag chemical components may have increased the slag's viscosity. The proposed increase in viscosity likely limited further slag infiltration into the refractory. In conclusion, when the spinel solution formed, the matrix structure of the refractory became denser, effectively slowing down slag penetration. Refractory A demonstrated better corrosion resistance to the slag compared to refractory B. The formation of dense, spinel-rich zones and Fe–Mg depletion in the slag were key mechanisms improving slag resistance.

The thermodynamic simulations indicated that for both refractories, the mechanism of corrosion was by dissolution of Al_2O_3 into the slag. In both refractories, the corundum phase is unstable with the initial slag. Thus, the corundum was dissolved until the Al_2O_3 content in the slags reached Al_2O_3 saturation. The refractory dissolution was predicted to be larger in refractory B compared to refractory A, and the results were aligned with SEM observations. From the experimental observations, the spinel phase predicted was formed throughout the infiltration path, which was also corroborated by SEM data. The study emphasizes that refractory selection for PGM smelting applications should be based on microstructural stability and interaction mechanisms, not just bulk composition. Refractories that exhibit stable phases at high temperatures, as in the case of Refractory A, are likely to be less corroded by the slag phase.

REFERENCES

Bennett, J.P. and Powell, C., 2009. Molten slags formed during gasification of carbon feedstock and their interaction with high chrome oxide refractory liners of air-cooled slagging gasifiers. In The VIII international conference on molten slags, fluxes, and salts, Santiago, Chile (pp. 1323-33).

Bennett, J., Nakano, A., Nakano, J. and Thomas, H., 2016. Gasification Slag and the Mechanisms by Which Phosphorous Additions Reduce Slag Wear and Corrosion in High Cr2O3 Refractories. In Advances in Molten Slags, Fluxes, and Salts: Proceedings of the 10th International Conference on Molten Slags, Fluxes and Salts 2016 (pp. 1109-1116). Springer International Publishing.

Bennett, J.P. and Kwong, K.S., 2011. Failure mechanisms in high chrome oxide gasifier refractories. Metallurgical and Materials Transactions A, 42, pp.888-904.

Kwong, K., Petty, A., Bennett, J., Krabbe, R. and Thomas, H., 2007. Wear mechanisms of chromia refractories in slagging gasifiers. International journal of applied ceramic technology, 4(6), pp.503-513

Chen, J., Xiao, J., Zhang, Y., Wei, Y., Han, B., Li, Y., Zhang, S. and Li, N., 2020. Corrosion mechanism of Cr2O3-Al2O3-ZrO2 refractories in a coal-water slurry gasifier: A post-mortem analysis. Corrosion Science, 163, p.108250

Liu, K., Guo, Q., Gong, Y., Chen, X., Wu, T., Wang, S. and Yu, G., 2021. Corrosion of high-chrome refractory materials by high-sodium slag in an entrained-flow gasifier. Ceramics International, 47(21), pp.30648-30656

Cai, B., Li, H., Zhao, S., Sun, H., Li, P., Yan, S., Du, Y., Wang, G. and Cao, Z., 2018. Corrosion of high-chromia refractory materials by basic coal slag under simulated coal gasification atmosphere. Ceramics International, 44(5), pp.4592-4602.

Gao, J., Su, W., Song, X., Lv, P., Yang, J. and Yu, G., 2023. Effect of slag composition on corrosion resistance of high chromia refractory bricks for industrial entrained-flow gasifier. Chinese Journal of Chemical Engineering, 62, pp.139-149.

Gao, J., Su, W., Song, X., Bai, Y., Wang, J. and Yu, G., 2022. Post-mortem analysis of Cr2O3- Al2O3-ZrO2 refractory bricks used in an industrial opposed multi-burner gasifier. Engineering Failure Analysis, 134, p.106017.

Gao, J., Su, W., Wang, X., Song, X., Wang, J., Yang, J. and Yu, G., 2023. Corrosion and degradation mechanisms of high-chromia refractory bricks in an entrained-flow gasifier: experimental and numerical analysis. Journal of Materials Research and Technology, 24, pp.8754-8765.

J. Berjonneau, P. Pringent, J. Poirier, 2009, The development of a thermodynamic model for Al2O3-MgO refractory castable corrosion by secondary metallurgy steel ladle slags, Ceramics International, Vol. 35, pp. 623.

Factors influencing campaign life of PGM furnace hearths

M. Nagorski[2], M. v.d. Merwe[3], G. Mulder[1], M. DeGorter[2], T. Kingsley[1]

[1]Hatch, South Africa
[2]Hatch, Canada
[3]Northam Platinum, South Africa

For a platinum group metals primary concentrate smelting furnace, the campaign of the crucible hearth represents the campaign life of the vessel. A hearth relining requires a complete furnace shutdown and can require three to five months of furnace downtime to complete the reline and recommission of the vessel. The associated sustaining capital costs represent a major contributor to the cost of operation (total cost of ownership). Additionally, the rebuild frequency and duration is a significant component of the furnace's long term operating factor which influences throughput and concentrate stockpile levels. Unplanned failures will exacerbate the business interruption and introduces significant safety risk to operators.

This paper outlines the factors that predominately influence the campaign life of a furnace hearth, including design, process stability, monitoring, and maintenance. Furthermore, this paper provides examples of how knowledge of these factors combined with disciplined decision-making can be used to minimise business interruption and extend furnace hearth campaign life.

Keywords: campaign life, PGM, hearth, smelting, furnace, crucible

INTRODUCTION

The primary purpose of the furnace crucible is to contain the molten materials. The main parts of the crucible are the roof, walls, and hearth. The hearth consists of layers of bricks at the bottom of the crucible which is predominantly in contact with matte containing platinum group metals (PGM). Depending on the design of the crucible and the matte and slag levels, the hearth may be exposed to slag although not preferred.

The campaign of a hearth represents the campaign life of the smelting vessel. For PGM primary smelting operations, the hearth campaign life can range from three years up to 20 years depending on furnace design, process stability, monitoring and maintenance factors. The end of a hearth campaign is typically driven by hearth growth or wear. Hearth growth can lead to the inverted arch geometry becoming unstable or the binding system expansion limits being reached. Hearth wear results in reduced lining thickness and instability of the crucible. The crucible must be monitored closely to understand its condition and identify appropriate interventions (e.g., partial rebuild, full rebuild, process interventions, etc.) to prevent failure.

A furnace hearth relining and recommissioning requires a complete furnace shut. The duration of such relining and recommissioning can vary between three and five months. This operational interruption will (1) affect the cash flow of the operation, (2) may lead to increased concentrate stockpiles, (3) if the rebuild is unplanned can lead to safety risks to the operating team, and (4) contribute significantly to the sustaining capital cost of the operation.

This paper describes the hearth design features, operating practices aimed at process stability, and monitoring and maintenance strategies which influence the campaign life of a PGM furnace hearth with the Northam Platinum Zondereinde smelter as a case study.

DESIGN

Design factors that have the highest influence on hearth performance include process design, hearth geometry, materials, and binding.

Process design

PGM furnaces require concentrate fed to the vessel, wherein smelting of the concentrate forms a slag layer (covered by the concentrate feed) and a denser matte layer within the furnace crucible. PGM concentrate is not roasted as per the copper and nickel sulphide smelting operations. The roasting step adds the benefit of heating and thermally decomposing the concentrate to reduce volatile corrosive material in the furnace operation. In PGM furnaces the corrosive sulphide materials are typically entrained in the slag-concentrate interface which can lead to wear of refractory and copper coolers. Crucible refractory and cooling design has advanced significantly in recent decades to combat these challenges related to corrosive, high intensity pyrometallurgical processes (Donaldson *et al.*, 1992; Shaw *et al.*, 2012 and Voermann *et al.*, 1999).

The typical feed composition of the Northam Zondereinde smelter is illustrated in Table I. The Northam composition aligns well with other UG2 concentrates published (Nell, 2004; Shaw *et al.*, 2012 and Jones, 1999).

Table I: Northam Zondereinde Smelter typical concentrate blend

Element	Formula	Value [wt%]
Concentrate grade	Cu +Ni + Co	1.984
Sulphur	S	2.98
Iron oxide	FeO	11.1
Silica	SiO_2	48.1
Alumina	Al_2O_3	3.99
Magnesium oxide	MgO	22.4
Calcium oxide	CaO	2.64
Chrome (III) oxide	Cr_2O_3	2.02

The matte and slag tapping temperatures achieved at Northam Furnace 1 (F1) are presented in Figre 1 with more detailed statistics provided in Table II. Northam slag temperatures are within the typical slag temperature range of 1,460 and 1,650˚C reported for the PGM industry (Warner *et al.*, 2007). The data shown exhibits a narrow slag temperature distribution which translates to Northam's exceptional process control. This process stability is key to hearth longevity and is covered later in this paper.

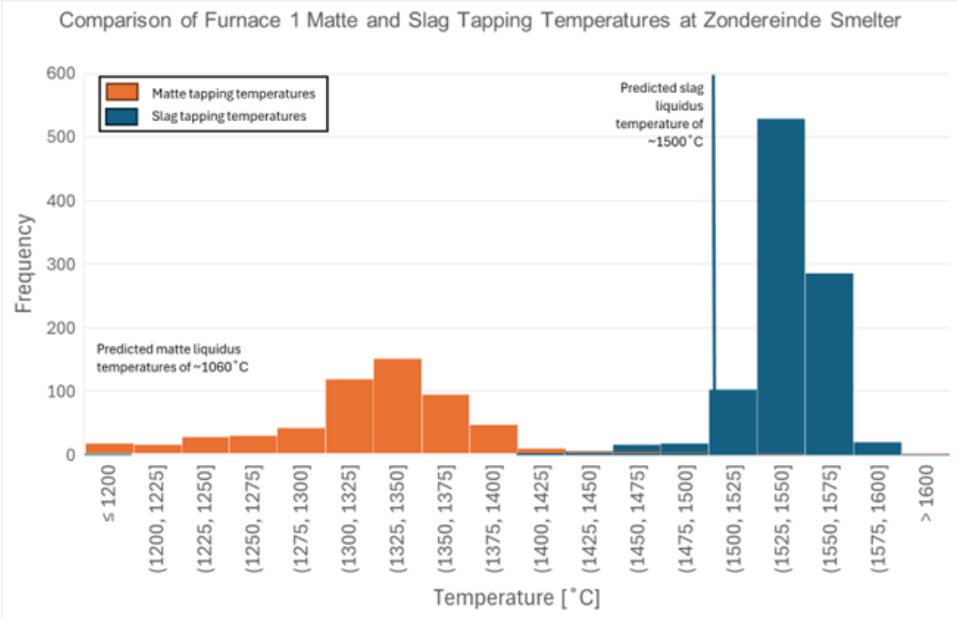


Figure 1: Distribution of Northam Furnace 1 matte and slag tapping temperatures (1-year operating data, liquidus calculated using FactSage).

Table II. Northam Furnace 1 matte and slag tapping temperatures (1-year operating data)

Tapping temperatures (°C)	5th percentile	Median	Average	99th percentile	Standard deviation
Matte	1,207	1,330	1,324	1,454	57.3
Slag	1,500	1,543	1,538	1,585	55.4

PGM concentrates may include chrome and magnesia which raise the slag liquidus temperature, requiring a higher processing temperature and ultimately leads to higher matte superheats. Matte superheats of 300 – 650˚C have been reported within the PGM industry (Shaw *et al.*, 2012). Coupled with higher process intensities, this leads to greater design and operational integrity challenges for the hearth.

Hearth geometry

The hearth is designed as an inverted arch using custom tapered and skew-shaped bricks. Refractory materials have a lower density relative to matte which results in an upwards buoyancy force on the hearth bricks if molten material is present below the refractory lining. The density of PGM matte is in the order of 4.5 g/cm^3 while slag may vary between 2.8 and 3.2 g/cm^3 (Geldenhuis *et al.*, 2004). The inverted arch geometry allows the hearth bricks to resist the buoyancy force and prevent the bricks from floating. Preventing flotation is critical to hearth integrity and molten material containment.

Important geometry parameters include hearth span and radius, hearth thicknesses, and hearth taper. These parameters contribute to the 'hot cumulative taper limit'. Hearth growth due to infiltration beyond the hot cumulative taper limit means that bricks may no longer be geometrically locked by their taper which can lead to lifting or flotation. However, maximising the cumulative taper of the hearth is not an effective design strategy because of the implications on skew elevation which may result in hearth exposure to slag, and increased inventory lockup in the vessel.

Other crucible design features related to geometry and layout that affect hearth integrity include:

- Matte taphole elevation relative to the skew elevation which also affects matte inventory and furnace operating levels. This can lead to the hearth being in contact with slag which, in industries with aggressive slag zone lining wear, becomes an important design trade-off.
- Hearth brick tongue and groove features which lock the hearth bricks together and aid in end-of-life integrity.
- Skew position towards the cold face of the wall. This protects the skew from the hot face conditions and maintains a resultant load transfer from the binding system.

Materials

High-grade refractory materials are used in the crucible, and selection parameters include thermal performance, refractoriness, chemical stability, industry precedence, and cost. In modern hearth designs, the matte solidus isotherm is contained in the working lining (see Figure 2) so that in the event of slow matte infiltration between the hearth bricks, the temperatures should be low enough to freeze the matte and eliminate the buoyancy force which could lead to lifting. Preventing matte infiltration between hearth bricks is especially challenging in PGM furnaces due to the high matte superheat.

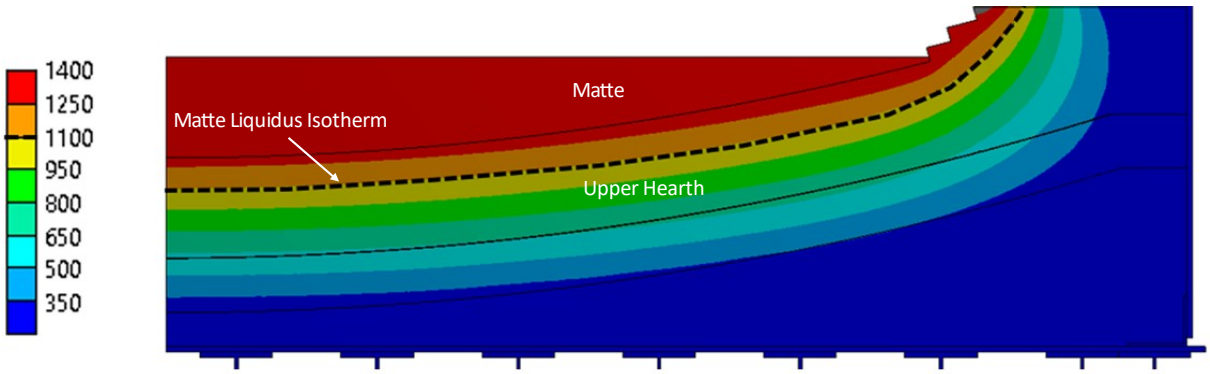


Figure 2: PGM hearth isotherms, indicating matte liquidus isotherm within upper hearth.

Binding

Hearth binding systems are typically sized to overcome frictional forces and ensure that the refractory joints remain tight during all phases of vessel operation. These forces are typically applied through the skews via spring-tie rod systems on rectangular furnaces, and hoop stress in the shell on circular furnaces (Donaldson *et al*., 1992).

Adequate hearth binding is required to maximise campaign life, as insufficient designs, or neglected binding systems can compromise the hearth campaign. As the hearth and furnace grow over time, or contracts during cool down, the loads are adjusted, so that the applied loads remain consistent. The binding system aids in reducing gap formation as the refractory cools and thermally contracts. If these gaps remain open, it increases the likelihood of molten material infiltrating the voids. Subsequent thermal cycles lead to growth, or ratcheting, of the vessel. A well-designed, and well-operated binding system aids in mitigating this growth phenomenon. Ratcheting is discussed later in this paper in more detail.

PROCESS STABILITY

Process stability is critical to hearth integrity and operations teams must therefore be focused on parameters that influence steady furnace feed composition, feed-to-power control, level management and electrode immersion. Each of these factors influence bath temperatures, stirring, freeze lining stability, and ultimately crucible integrity and longevity. Additionally, these factors will affect

throughput and PGM recoveries, requiring disciplined decision-making to minimise business interruption and extend furnace hearth campaign life while maintaining production targets.
The primary levers to achieving process stability include:

- Blending of feed material to maintain key elements, particularly those that impact slag liquidus temperatures, slag viscosity, and the system's electrical properties, within narrower bands.
- Bath levels maintained within operating limits (often dictated by the availability of downstream operating units) and electrode immersion correspondingly maintained towards stable stirring and energy distribution within the slag bath to protect and maintain the freeze lining.
- Feed-to-power ratios consistently balanced to maintain bath temperatures within targeted values and to mitigate against higher heat losses.

Although all the above levers are considered critical to maintain process stability, this paper only elaborates on furnace level control.

Level control

Refractory-slag corrosion is the primary wear mechanism of the crucible lining, and it can be mitigated with cooling elements to manage a slag freeze lining. Refractory-slag corrosion is particularly problematic when slag wears away the hearth or skew bricks where there is naturally less cooling defence. This leads to hearth and sidewall instability and ultimately to a shortening of the campaign. The skews can be protected somewhat by their relative position to the nearest cooling elements; however, the proximity of copper coolers in the skew area is limited by the proximity to maximum matte levels.

The area that is exposed to both matte and slag during operation is referred to as the 'tidal zone'. If the matte temperature is greater than the slag liquidus temperature, then rising matte levels have the potential to melt any frozen slag protecting the refractory, and when matte levels fall the refractory will be directly exposed to molten slag which will lead to accelerated refractory loss. Level control is an important factor in minimising tidal zone wear and maximising hearth campaign life.

Figure 3 shows how Northam Platinum improved their matte level control over time with the aim of protecting the refractory in the tidal zone. The gaps in the data are due to manual operator data entry errors. Table II shows that from January 2022 to June 2022 (initial six months of operating data) the mean matte level was 6.9 cm below the operating matte level with a standard deviation of 3.4 cm. From January 2025 to June 2025 (latest six months of operating data) the mean matte level was only 0.2 cm above the operating matte level and the standard deviation was 1.3 cm which emphasises Northam's operational diligence and disciplined decision-making.

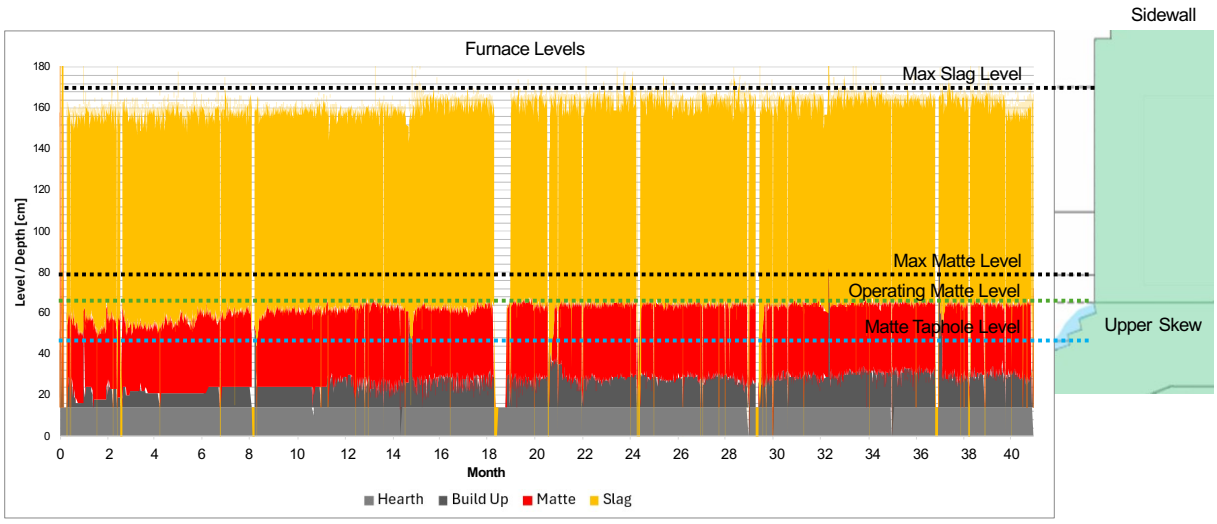


Figure 3. Northam F1 furnace levels relative to typical transverse section.

Table III: Northam F1 matte levels comparison from beginning of campaign to recent operation

Matte levels	Difference between mean level and operating level (cm)	Standard deviation (cm)
January 2022 to June 2022	-6.9	3.4
January 2025 to June 2025	0.2	1.3

Level measurement via soundings

Furnace sounding involves inserting a steel bar through ports in the roof until it contacts the bottom of the crucible to measure matte, slag, and bottom build-up levels. Physical properties of the molten material on the sounding bar are also observed. Material properties such as the adherence, thickness, and colour of the layers are visualised to ensure the furnace is operating in a desirable state. Figure 4 (left) displays how the depth of each layer in the bath can be measured with a sounding bar. Figure 4 (right) shows how the different material properties of each layer in the furnace bath can be visualised to show a clear distinction between layers as well as indicate the state of the furnace.

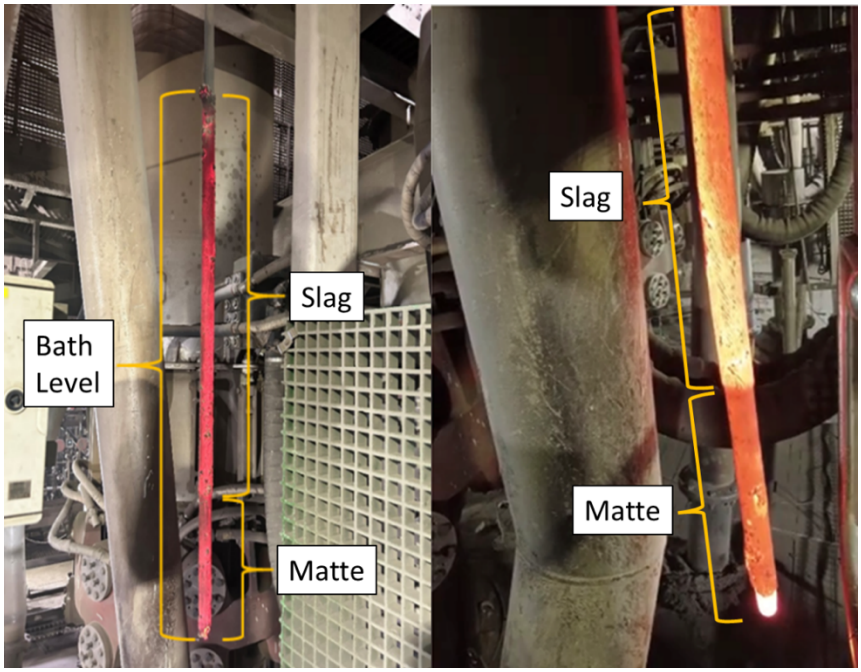


Figure 4. (left) sounding bar measurement (right) slag and matte layers close-up.

HEARTH MONITORING

Furnace monitoring enables data-driven decision-making, such as determining maintenance scope and timing and improving process conditions and stability. Employing the monitoring techniques detailed below generates valuable information which can be used to extend hearth campaign life.

Start-up growth

Furnace start-up involves elevated risk of losing molten material containment as thermal expansion results in brick movements and potential gap formation. Expansion design, heat-up procedures, and binding system adjustments throughout start-up are essential to mitigate this risk.

Buckstay movements are monitored to infer hearth growth. Buckstay positions can be measured manually from fixed reference points (see Figure 5) on a regular basis (e.g., daily during normal operation, once per shift during heat-up and cool-down cycles). Buckstay positions should be surveyed periodically (e.g., annually and after any major shutdown or repair) to validate and calibrate routine

manual measurements. Surveys and manual measurements of buckstay positions in the as-built furnace condition are essential to quantifying start-up growth.

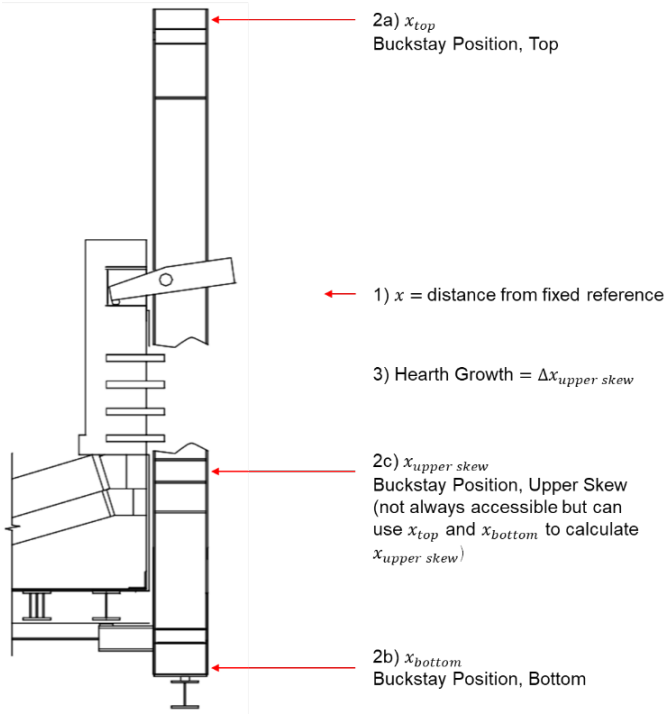


Figure 5. Buckstay position measurements used to monitor hearth growth.

Start-up growth data is valuable in two ways: first, it is used to confirm successful hearth heat-up by comparing measured growth to the design expansion; second, it is used as the baseline for future hearth growth monitoring and comparison toward the hot cumulative taper limit. Figure 6 shows an example of hearth growth monitoring during start-up of Northam F1. After 35 days the hearth growth stabilised around the value determined by the expansion design which provided confirmation that the hearth had successfully completed heat up.

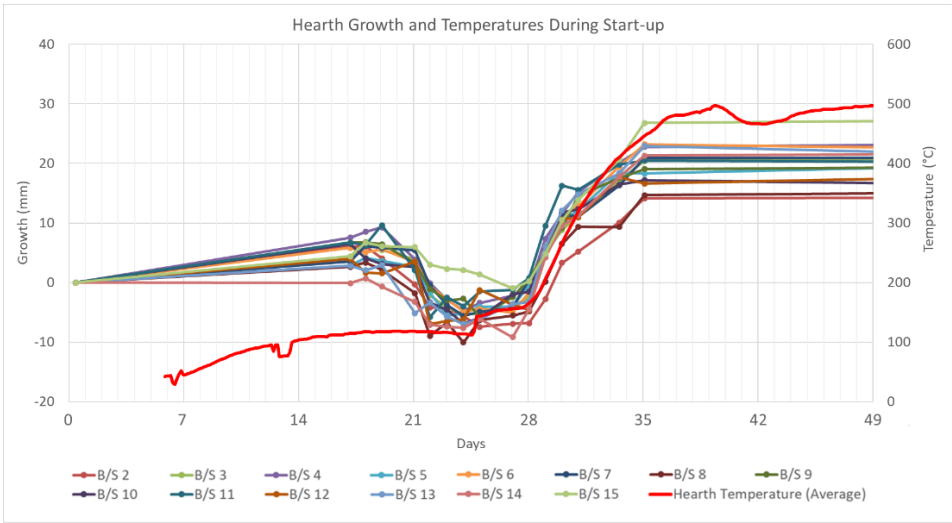


Figure 6. Northam F1 hearth growth and temperatures during start-up.

Ratcheting
Hearth growth may also occur throughout a campaign via a continuous ratcheting mechanism. This is when molten material infiltrates through gaps between the bricks during thermal contraction, then solidifies which results in a net growth when the bricks expand again. This mechanism, when repeated, is responsible for the hearth growth observed throughout a campaign. Minimising ratcheting is therefore considered an effective strategy for extending the hearth campaign life.

Deep thermal cycles occur when hearth temperatures decrease significantly, such as during shutdowns associated with partial relines. Shallow thermal cycles correspond to smaller hearth temperature decreases, such as during shorter shutdowns or during unstable furnace process conditions as detailed earlier in this paper. Figure 9 shows the hearth growth trend and daily cumulative power for Northam F1. Highlighted in green is a period of approximately four months when Northam was able to operate with improved process stability. During this time there was no measurable ratcheting.

Deep thermal cycles almost always result in ratcheting (see Figure 8). This is because it is progressively more challenging to prevent any gaps from forming as the hearth cools down, even with robust binding systems in place. Shallow thermal cycles can also result in ratcheting but, typically will result in less growth per cycle compared to deep thermal cycles. However, the frequency of shallow thermal cycles related to process stability can be such that the hearth growth during operation is greater than shutdown ratcheting over the campaign of a furnace.

Hearth lifting
When setting up a sounding bar during furnace construction it is important to establish a fixed reference point on the sounding platform in line with the top of the sounding bar while the bottom is in contact with the hearth. Then, while sounding during operation, the distance between the top of the sounding bar and the fixed reference point will indicate the position of the top of the hearth plus any bottom build-up. Increasing thickness of the bottom build-up may be evidence of the hearth lifting and therefore can be used as an early failure warning to flotation and hearth failure. Ideally, sounding should be done from multiple ports to mitigate uncertainties in local hearth conditions.

Figure 7 shows sounding measurements from a reference PGM furnace. Hearth lifting started after about 65% campaign duration and progressed until the upper hearth layer was completely lost. Bottom build-up measurements must be interpreted carefully while considering the current hearth growth and taper limit to understand the potential for hearth lifting. This translates to disciplined decision-making within an operating environment.

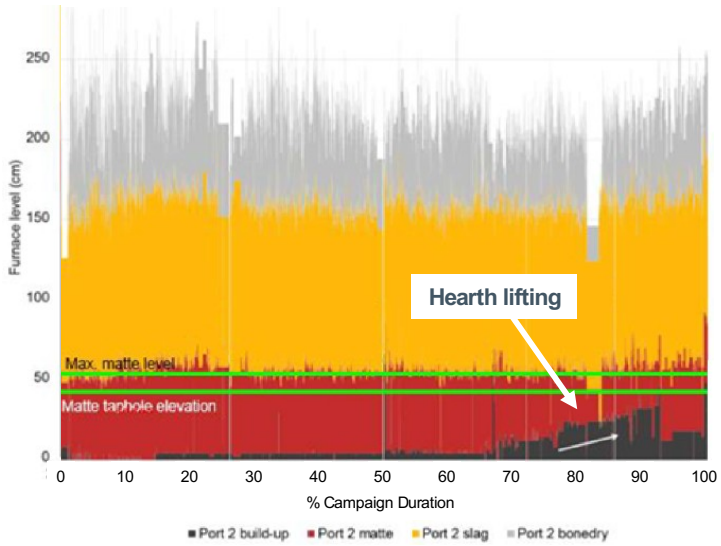


Figure 7. Sounding measurements which reveal hearth lifting starting in Year 6 (reference PGM furnace).

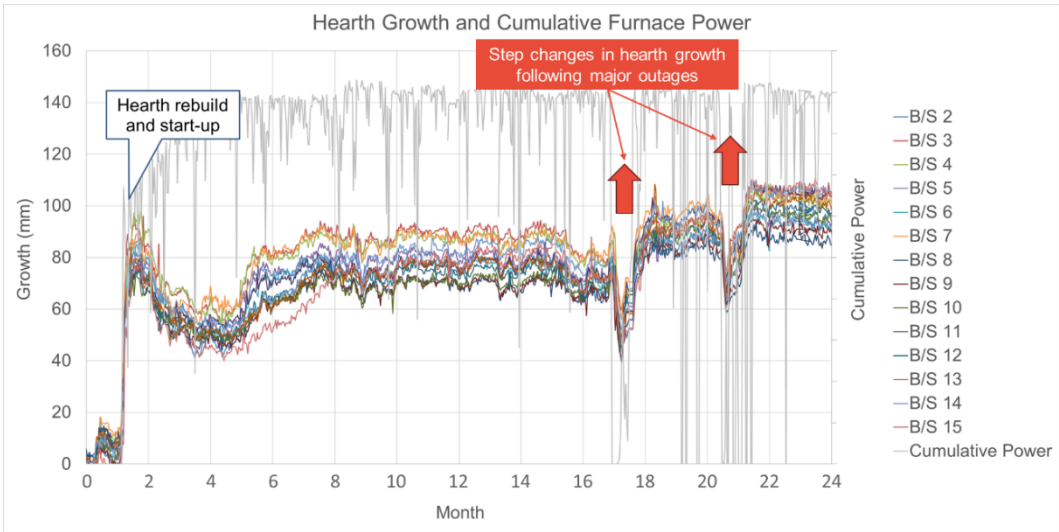


Figure 8. Hearth growth trend and cumulative furnace power highlighting ratcheting after deep thermal cycles (reference PGM furnace).

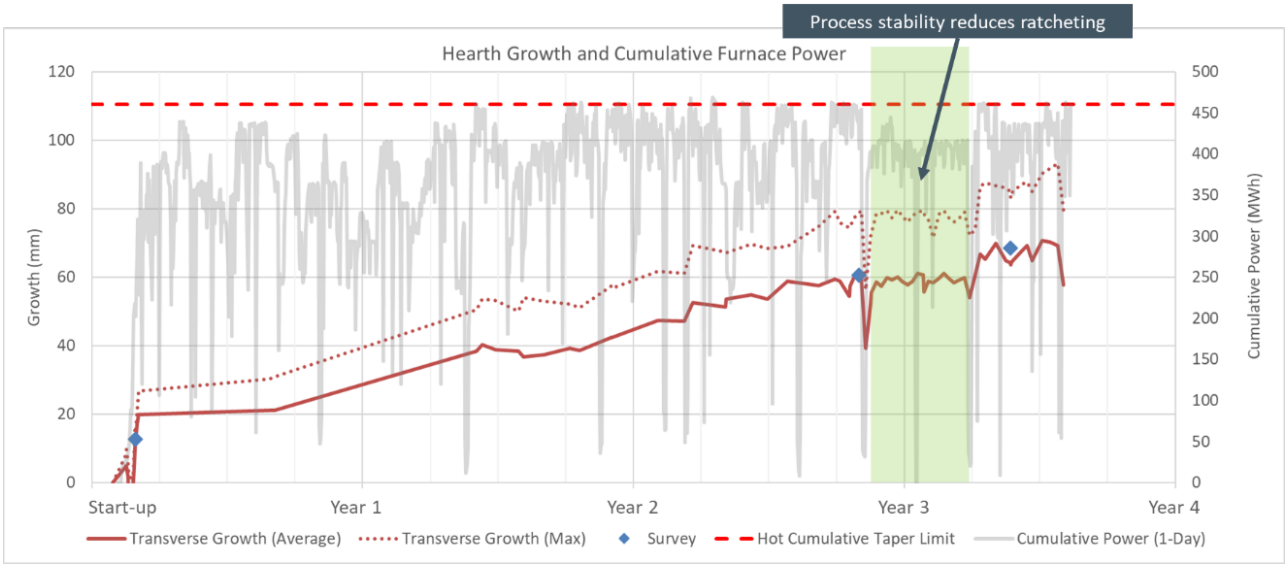


Figure 9. Hearth growth trend and cumulative furnace power highlighting period of power stability and no ratcheting (Northam F1)

Preventing ratcheting is more challenging in PGM furnaces because of the high matte superheat. Additionally, PGM furnace hearths typically do not operate with any frozen build-up on the hearth (Shaw *et al*., 2012), which would act as a protective barrier to infiltration. Strategies to reduce the rate of ratcheting throughout a campaign, as explored in this paper, include:

- Maintaining process stability during normal operation.
- Monitoring and adjusting hearth binding loads during thermal cycles.
- Reducing the number of and the magnitude of hearth temperature decreases during thermal cycles. This can be achieved through well-developed maintenance strategies as detailed later in this paper.

Non-destructive testing and thermal analysis

Refractory wear in the tidal zone can lead to arch instability of the hearth if it occurs near the skew area or upper hearth. For this reason, it is critical to monitor the condition of this area and schedule interventions before the efficacy of a partial reline is compromised.

The refractory condition in the tidal zone can be assessed using non-destructive testing (NDT) and thermal analysis as seen in Figure 10. Hatch's Acousto Ultrasonic-Echo is used to determine the thickness of refractory materials and the presence of anomalies which can indicate changes in material properties, gaps, or cracks in the lining. Thermal analysis involves correlating relevant measured thermal data to a thermal FEA (finite element analysis) model and using predicted isotherms to estimate the remaining refractory thickness. When NDT and thermal analyses are done over an extended period of time, trends can be developed to guide interventions and safely extend hearth campaign life (Sadri *et al.*, 2024).

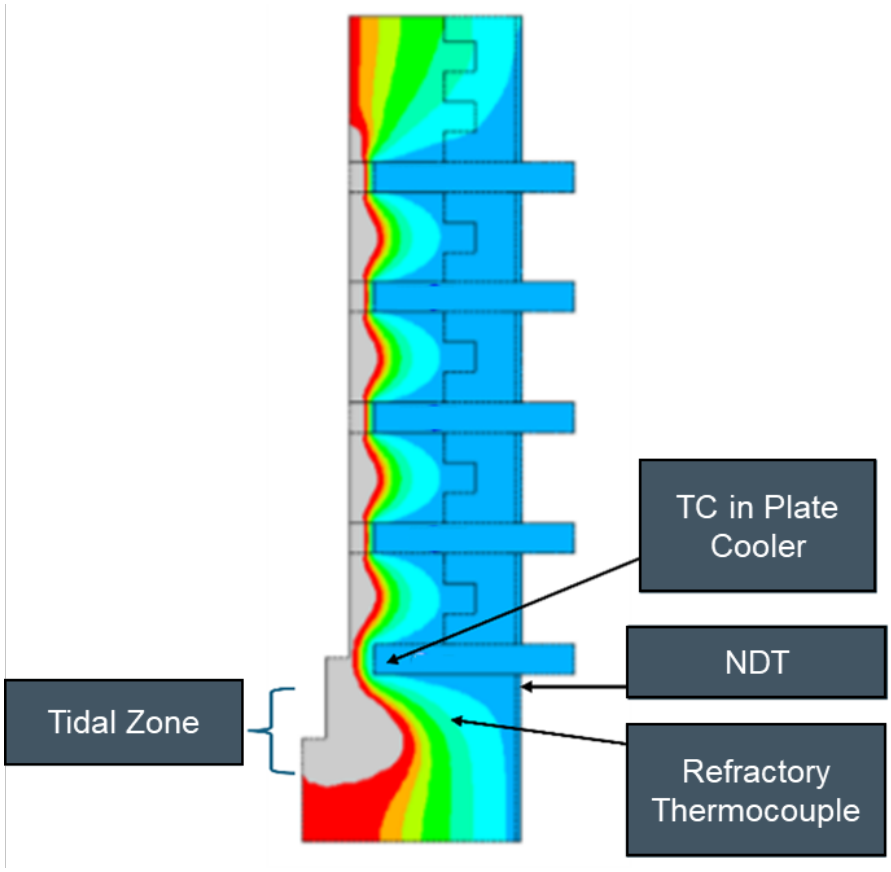


Figure 10. Furnace sidewall thermal model showing locations of temperature monitoring and NDT relative to tidal zone.

MAINTENANCE

Maintenance strategies that can extend hearth campaign life are particularly focused on reducing hearth growth due to ratcheting.

Factors that affect ratcheting resulting from a given thermal cycle include:

- Binding spring adjustment frequency. During partial relines, load should be always maintained on the hearth through regular adjustments of the binding system. Any maintenance to the

binding system during a shutdown should be coupled with procedures and engineered solutions to ensure loads are maintained.

- Magnitude of hearth temperature change. During 'hot shutdowns', furnace power is reduced, but not off, to maintain molten slag pools, benefiting the furnace restart process. Ratcheting can be reduced during a hot shutdown due to hearth temperatures being maintained and contraction being reduced. However, hot shutdowns alone do not eliminate ratcheting.
- Rate of change of hearth temperatures. The rate of increase in hearth temperature will be described in a startup or heat-up curve that is aimed at allowing sufficient time to ensure heat passes to the hearth and gaps close before the frozen material on the hearth liquidises and can infiltrate openings.

Maintenance synchronisation

Synchronisation of maintenance during major furnace shutdowns (i.e., endwall, sidewall, and hearth relines) will reduce the number of thermal cycles by avoiding other stoppages. Ensuring the balance of the plant is well maintained will further improve availability of those systems and improve operations capacity to stabilise operation.

CONCLUSIONS

The furnace hearth campaign can be a major contributor to the smelter cost of operation as the end of the hearth campaign will typically trigger a full reline which can represent downtime of between 25% and 50% of the financial year. The production and stockpiling impact of this disruption invariably has a major impact on the business affected. Hearth campaign life extension therefore has major value and should be treated with the appropriate level of attention. The furnace hearth is ultimately a system impacted by a number of factors outlined in this paper. This includes the design itself, which should be appropriate for the application and focused on mitigating factors like slag corrosion and matte infiltration. Secondly, the operation of the vessel toward its design parameters should have a particular focus on bath levels and thermal stability as potential life impacting factors. Thirdly, by using advanced monitoring and NDT techniques, operations can make use of inhouse knowledge and consultants to influence operational or partial reline decisions that can further extend hearth campaign life.

ACKNOWLEDGEMENTS

The authors would like to thank Northam Platinum Ltd. and Hatch for permission to publish the information provided in this paper.

REFERENCES

Donaldson, K.M., Ham, F.E., Francki, R.C. and Schofield, J.G. (1992). Design of Refractories and Bindings for Modern High-productivity Pyrometallurgical Vessels. *The Proceedings of the International Symposium on Non-Ferrous Pyrometallurgy: Trace Metals, Furnace Practices and Energy Efficiency*. The Metallurgy and Materials Society of CIM. Edmonton, Alberta. pp. 491–504.

Geldenhuis, J.M.A., Millar, D., van Beek, B., Ndlovu, J. and Hara, K.T. (2004). Development of Alternative Techniques for Matte Level Measurements in Sulphide Smelting Furnaces. *Proceedings of the First International Platinum Conference*. The Southern African Institute of Mining and Metallurgy. Sun City, South Africa. pp. 25–32.

Jones, R.T. (1999). Platinum smelting in South Africa. *South African Journal of Science*, 95 (11), 525–534.

Nell, J. (2004). Melting of Platinum Group Metal Concentrates in South Africa. *Journal of the South African Institute of Mining and Metallurgy*, 104 (7), 423–428.

Sadri, A., Cornett, H., Mosnier, M., Ying, W.L. and Ferrer, B. (2024). Furnace Refractory Lining Barrier Monitoring Tools and Techniques. *Proceedings of the 63rd Annual Conference of Metallurgists, COM 2024.* The Canadian Institute of Mining, Metallurgy, and Petroleum. Halifax, Nova Scotia. pp. 793–802.

Shaw, A., de Villiers, L.P.vS., Hundermark, R.J., Ndlovu, J., Nelson, L.R., Pieterse, B., Sullivan, R., Voermann, N., Walker, C., Stober, F. and McKenzie, A.D. (2012). Challenges and solutions in PGM furnace operation: high matte temperature and copper cooler corrosion. *Proceedings of the Fifth International Platinum Conference*. The Southern African Institute of Mining and Metallurgy. Sun City, South Africa. pp. 193–216.

Voermann, N., Ham, F., Merry, J., Veenstra, R. and Hutchinson, K. (1999). Furnace Cooling Design for Modern High-Intensity Pyrometallurgical Processes. *Proceedings of Copper 99: Volume V–Smelting Operations and Advances*. George, D.B., Chen, W.J., Mackey, P.J. and Weddick, A.J. (eds.). The Minerals, Metals & Materials Society. Phoenix, Arizona. pp. 573–582.

Warner, A.E.M., Díaz, C.M., Dalvi, A.D., Mackey, P.J., Tarasov, A.V. and Jones R.T. (2007). JOM World Nonferrous Smelter Survey Part IV: Nickel: Sulfide. *Journal of Metals*, 59 (4), 58-72.



Michael Nagorski

Asset Performance Specialist, Furnaces
Hatch

Michael is a mechanical engineer in Hatch's Asset Performance Management (APM) group focusing on pyrometallurgical furnaces. The APM group provides services to help clients optimize the performance of their operational assets. Michael's furnace engineering experience includes: site inspections, modelling, and data analysis to assess condition, remaining campaign life, and planned maintenance interventions; root cause investigations to assess equipment performance and identify opportunities for technology improvements, and operations support in the form of condition monitoring and technical advisory to improve reliability, productivity, and safety.

Michael graduated from the University of Waterloo in Canada with a Master of Applied Science specializing in radiation heat transfer. Michael's research developed the field of quantitative optical gas imaging (QOGI) using mid-wavelength infrared (MWIR) cameras to image and quantify greenhouse gas emissions, particularly methane from upstream oil and gas production. Michael's contributions demonstrated the advantages of multispectral infrared imaging in species differentiation and quantification on non-ambient temperature gases, and the challenges with uncooled multispectral filters and velocimetry algorithms.

Challenges in crucible- and pilot-scale refining of a PGM-bearing iron alloy

M.S. Moholwa[1], S.P. Tsebe[1], E. Matinde[1,2]

[1]Mintek, South Africa
[2]The University of the Witwatersrand, South Africa

Platinum group metals (PGMs) have a wide range of applications, primarily due to their catalytic properties and resistance to corrosion. The secondary production of these metals typically involves recycling of secondary resources such as spent automotive catalysts (autocats). The process normally involves smelting of spent autocats with a reductant, fluxing reagents, and a source of collector alloy. An investigation was undertaken to evaluate the technical feasibility of refining a PGM-containing iron alloy recovered from recycled spent autocats. The study involved investigating the technical feasibility for upgrading the PGMs' content of the alloy from 3% to 20% through oxygen refining. The chemical composition of the start alloy comprised of approximately 90% Fe, 5% Cu, 0.6% Ni, 0.2% Co, and 3.4% PGMs. The test work involved a series of preliminary converting tests at crucible scale followed by tests at pilot scale in a top blown rotary converter (TBRC). The tests were conducted in three stages. Stage 1 tests were carried out in an induction furnace to establish optimum processing conditions such as oxygen delivery rate, operating temperature, and flux addition. Stage 2 tests were also carried out in an induction furnace to estimate deportment of PGMs and base metals to product alloy and slag. Stage 3 tests were carried out in a TBRC to facilitate preparation of 1–2 kg of the final upgraded alloy with the desired PGMs grade. The results showed that it was not technically feasible to extensively refine the alloy at the crucible scale due to consistent premature crucible failure. Tests at pilot scale produced excessively oxidised alloys due to lack of reliable method of measuring the oxidation efficiency.

INTRODUCTION

Platinum group metals (PGMs) such as platinum (Pt), palladium (Pd), rhodium (Rh) and ruthenium (Ru) are considered precious metals due to their scarcity and high prices (Q. Yang *et al*., 2023). PGMs are used in the petrochemical and automobile industry as catalyst due to their excellent catalytic performance (Li *et al*., 2025). Governments around the world have become increasingly strict about environmental protection, with several strict regulations declared on the emissions from automobile exhaust (Qin and Gao, 2022). Automotive catalysts (autocats) play a crucial role in converting toxic NO_x, CO and hydrocarbon gases released by internal combustion engines into non-toxic gases such as N_2, CO_2 and H_2O (Yakoumis *et al*., 2021; D. Yang et al., 2023). In 2024, it was reported that the demand for Pt and Pd are 91.5 and 224.7 t, respectively (Alison, 2024). Almost 42% Pt and 84% Pd out of the total demand is used in the automotive industry according to the report. PGMs resources must be recycled due to their short supply and uneven distribution (Q. Yang *et al.,* 2023). PGMs content in spent autocats is much higher than that of mineral resources (content in primary resources is less than 0.01g/t) (Li *et al.*, 2025). The higher PGMs content in spent autocats combined with the uneven distribution and scarcity of PGMs necessitate recycling of secondary resources. PGMs can be recovered from spent autocats through mild reductive smelting. This is done by smelting a fluxing reagent, reductant and spent autocats in the presence of copper or iron as PGMs collector.

The study by McCullough et al (2008) studied the pyrometallurgical removal of iron and other impurities (Si, Ca and Cr) from a PGM-containing alloy by oxygen converting. The study examined the converting behaviour of an iron-rich alloy at a laboratory scale and successfully demonstrated removal of iron to <5% in the final alloy. Yang et al (2023) studied the removal of impurities (Si, Al, Mg, Ti and Ca) from a PGM-containing alloy through green slag refining process. The study reported a successful removal of impurities through a slagging treatment of PGM-containing alloy. The review article by Sarkar and Sohn (2018) discussed the interaction of alumina-based refractories with iron melts and slags. The study by Kwack et al (2023) studied the dissolution of Al_2O_3 non-metallic inclusions in FeO containing slag. The study focused on the effect of FeO concentration in slag and reaction temperature on Al_2O_3 dissolution into the slag. The study reported a linear increase of Al_2O_3 dissolution in slag with FeO and temperature.(Q. Yang *et al.*, 2023).

There is limited literature related to refining of PGM-containing iron alloy produced from secondary resources available in the public domain. The current study investigated the technical feasibility of upgrading the PGM-containing alloy produced from recycling of spent autocats from 3% to 20% PGMs.

EXPERIMENTAL METHOD

Raw materials

The test work utilised four raw materials, namely (i) PGM-containing alloy, (ii) silica (SiO_2), (iii) lime (CaO) and (iv) alumina (Al_2O_3). The CaO, Al_2O_3 and SiO_2 were chemical grade with >98% purity. the composition of the alloy used is shown in Table 1. The samples were analysed with inductively coupled plasma optical emission spectroscopy and fire assay to determine base metals and PGMs, respectively. The alloy was milled to 100% passing through 1 mm sieve.

Table 1. Chemical composition of the PGM-containing iron alloy (%)

Element	Fe	Pd	Rh	Pt	Cu	Ni	Co	Zn	PGMs	Total
%	90.2	1.97	0.22	1.23	5.10	0.64	0.19	0.02	3.42	99.5

Equipment description

Two types of furnaces were used in the test work, namely (i) an induction furnace, and (ii) a top blown rotary converter (TBRC). Each equipment is described in detail in the next sub-sections.

Crucible tests

The induction furnace facility was equipped with a few components; (i) the control panel and power supply, (ii) a chamber with induction coils, and (iii) cooling water supply for the induction coils. The heating chamber was connected to a 60 kW power supply with a digital controller to enable control of power input. The heating chamber was lined with a ceramic cast crucible and a graphite susceptor crucible. The cooling-water circuit cooled the induction coils during operation of the furnace. The schematic of the induction coil furnace chamber is shown in Figure 1.

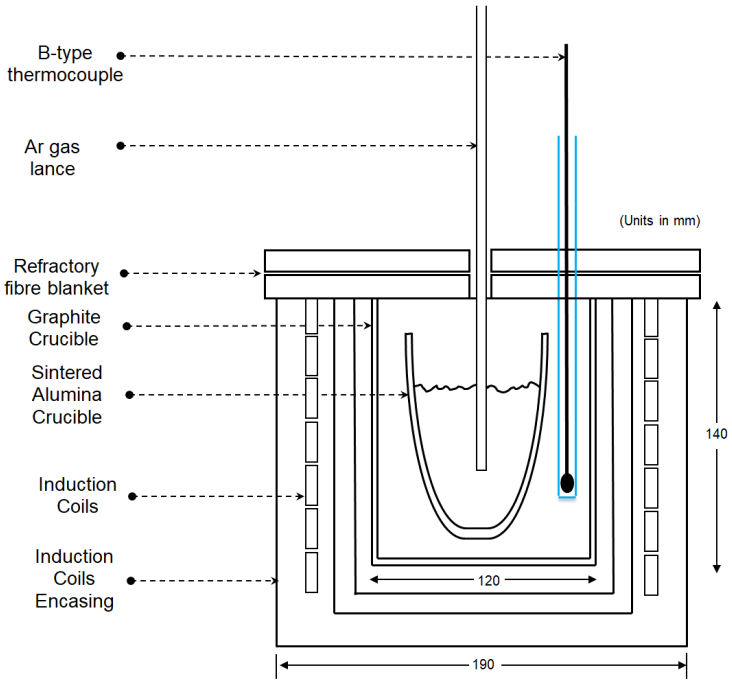


Figure 1. Schematic diagram of the induction coil furnace set-up during converting test.

TBRC tests

The TBRC facility consists of three main sections, namely: (i) gas supply train, (ii) rotary furnace, and (iii) off-gas handling system. The furnace was heated with an oxygen-propane burner equipped with flowrates controllers. The oxygen (O_2) and propane (C_3H_8) flowmeters used floats to give a maximum flow of 30 Nm^3/h (at 200 kPa(gauge)) and 5.6 Nm^3/h (at 50 kPa(gauge)). The burner had a power rating of 120 kW with four concentric pipes (two for cooling water, one for oxygen and one for propane). Figure 2 shows the cross-sectional view of the TBRC vessel during operation. The rotary furnace vessel comprised a cylindrical mild steel shell with a diameter of 600 mm x 585 mm. It had a conical shape tapering from 600 mm to 400 mm. The shell was lined with a high-quality alumina (93% Al_2O_3) castable. The vessel was tilted by hydraulic pistons operated from a portable hydraulic pressure pack. A 0.37 kW variable speed motor enabled the vessel to be rotated between 2–11 rpm.

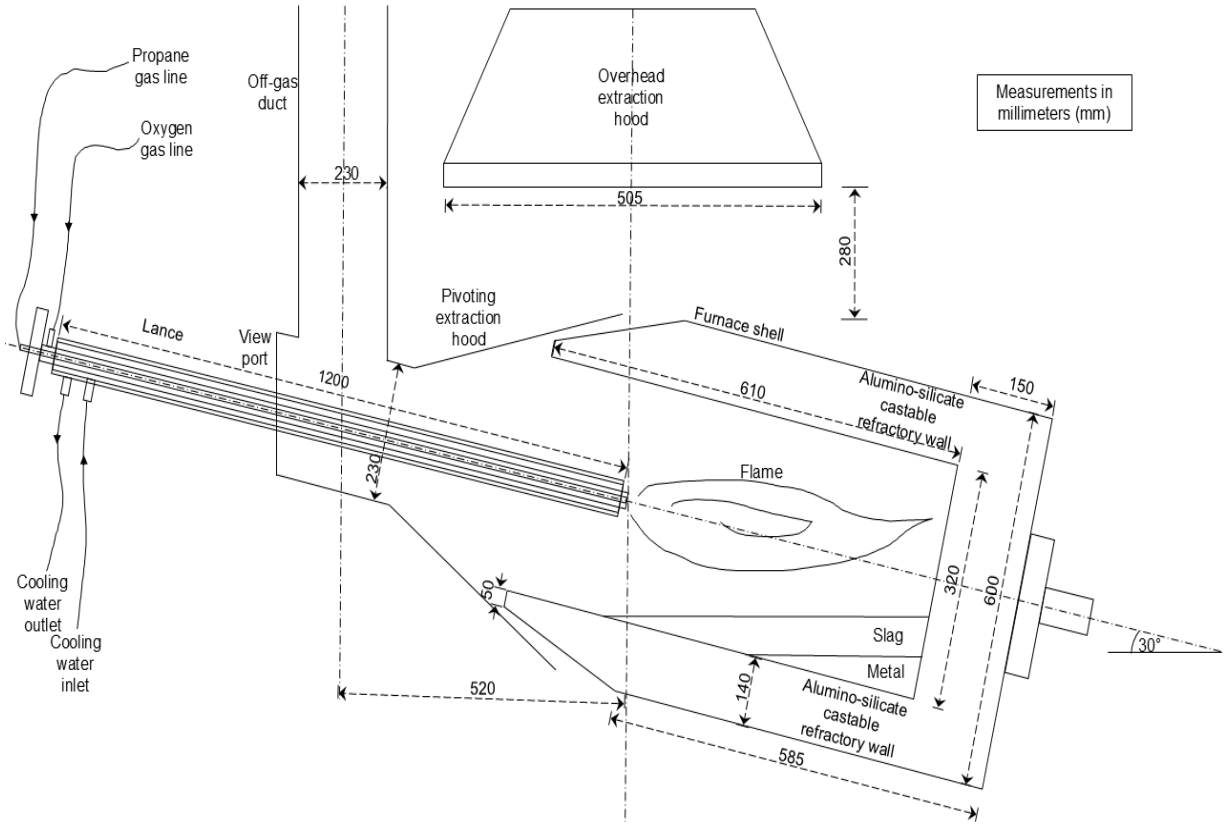


Figure 2. Schematic overview of the TBRC vessel (source: Tsebe and Steenkamp (2024)).

Operating procedure

Crucible tests

A pre-determined mass was packed in a sintered alumina crucible, and the crucible was placed in a graphite susceptor. The furnace was switched on to slowly heat the alloy at 10°C/min to 1450°C under inert argon (Ar) atmosphere. The temperature was monitored with a B-type thermocouple inserted into the susceptor as shown in Figure 1. Once the alloy was molten, oxygen was injected into the melt through an alumina-based gas lance. A mixture of Al_2O_3, CaO and SiO_2 were weighed and thoroughly mixed before being added to the melt as fluxing reagents. Addition of fluxes was based on visual observations of the physical state or condition of the bath. The test was terminated once the crucible was full by removing the gas lance and switching off the furnace to allow the products to cool. The cooled products were removed from the furnace, weighed, carefully separated and prepared for chemical analysis.

TBRC tests

Furnace warmup for the TBRC was initiated using a neutral flame stoichiometry over a period of 2.5 h. The pre-determined mass was divided into four bags while the furnace warm up was in progress. The vessel walls were heated to a temperature of 1400°C before the first bag of alloy was fed into the furnace to melt. Once the alloy was molten, another bag was fed until all four bags were charged to the furnace. Temperature was taken using an optical pyrometer before switching to an oxidising flame to start oxidising the alloy. A mixture of Al_2O_3, CaO and SiO_2 with varying quantities for different tests was charged to the furnace at pre-determined intervals. The slag was skimmed off to open the bath for further oxidation when large slag volumes had accumulated. The furnace was tapped by tilting the vessel and pouring the melt into a ladle once the desired degree of conversion was achieved. Samples were collected in the molten state and granulated. The collected samples were prepared and submitted for chemical analysis.

RESULTS AND DISCUSSION

Stage 1

Stage 1 tests sought to understand the behaviour of the alloy in terms of a suitable operating temperature and the nature of the slag generated at different levels of conversion. Establishing the necessary fluxing strategy to maintain a liquid slag throughout the converting process was also the aim of stage 1 tests. Six tests were conducted in this stage and three tests (test 1, 2 and 6) out of the six were stopped prematurely due to crucible failure. The operating conditions of the six tests are presented in Table II. The percentage of the oxygen delivered was calculated as (oxygen delivered in g)/(stoichiometric amount of oxygen required to oxidise all the Fe in the sample) multiplied by 100. The alloy mass loss was calculated as (starting alloy mass – final alloy mass)/ (starting alloy mass) multiplied by 100. It was established that the alloy was molten at temperatures above 1470°C.

Table II. Operating conditions for stage 1 tests

Test	Start alloy mass, g	Temp before blow, °C	Oxygen delivered, g	Oxygen delivered, %	Final alloy mass, g	Alloy mass loss, %	Al_2O_3 added, g	CaO added, g	SiO_2 added, g
1	102	1510	8.14	7.98	39.6	61.3	-	-	-
2	100	1466	8.14	8.14	-	-	2	2	2.0
3	90.0	1524	5.57	6.19	33.0	63.3	-	-	-
4	182	1503	9.86	5.42	128	29.9	2	-	4.0
5	186	1509	18.7	10.1	98.9	46.9	6	-	18
6	200	1525	9.86	4.93	-	-	4	-	12

The two crucibles used in this stage are shown in Figure 3. The crucible in Figure 3(a) had an internal diameter (ID) and internal height (IH) of 50 mm and 40 mm respectively. The crucible in Figure 3(b) had an ID and IH of 25 mm and 60 mm respectively. Crucible (a) was used for test 1 and test 2 while crucible (b) was used from test 3 to test 6. The decision to change the crucible was due to the need to increase the height of the alloy to allow gas injection without the tip of the lance touching the base of the crucible. The results of the gas injection lance touching the base of the crucible can be clearly seen in Figure 3(c). The oxidation reaction is highly exothermic as indicated in the study by Mich et al (2024), which means that temperature at gas lance tip was the highest. The reaction temperature exceeded the service temperature of the alumina crucible which led to premature crucible failure. The narrower ID of the cylindrical crucibles provided a deeper metal bath height that mitigated against premature failure of the crucible due to leaks through the crucible bottom. (Mich et al., 2024)



(a) (b) (c)

Figure 3. Crucibles used in stage 1 tests.

The chemical composition of the products obtained from stage 1 tests are shown in Table III and Table IV. Due to the crucible leakages experienced, slag sample from some of the tests (test 2 and test 6) were

not recovered. All the products from test 2 were lost due to the location of the leak at the bottom of the crucible. This is why no composition is reported for test 2. The highest percentage of oxygen delivered at this stage was achieved in test 5. But the alloy chemical composition results show that the highest PGMs content was achieved in test 1. During the crucible failure in test 1 there was an uncontrolled ingress of air into the molten alloy which further oxidised the sample. This explains the higher PGM grade obtained even when the controlled oxygen delivered was less than that of test 5. Test 5 was the only test completed without crucible failure, but the alloy was only upgraded to 5.15% PGMs. This indicated that to refine the alloy to the required PGM grade of 20%, it was necessary to blow the alloy multiple times. The significant volume of slag generated rendered the process impractical to achieve the desired alloy PGM grade through a single pass.

Table III. Chemical composition of the final alloy from stage w tests (%)

Test	Fe	Pd	Pt	Rh	Cr	Cu	Ni	Si	PGMs	Total
1	82.0	3.89	2.58	0.51	0.37	8.27	1.37	0.44	6.98	99.4
3	89.5	2.24	1.32	0.22	0.22	4.82	0.55	0.88	3.78	99.8
4	89.0	2.35	1.40	0.22	0.23	4.91	0.55	0.87	3.97	99.5
5	86.2	3.07	1.76	0.32	0.28	5.99	0.73	0.82	5.15	99.1
6	84.6	3.30	1.85	0.34	0.29	6.21	0.78	0.80	5.49	98.2

Table IV. Chemical composition of the slags from stage 1 tests (%)

Test	FeO	Al_2O_3	Cr_2O_3	CuO	NiO	SiO_2	Total
1	81.0	14.7	0.89	0.40	0.21	0.91	98.0
3	83.5	8.21	0.91	0.42	0.22	0.86	94.1
4	82.5	10.6	0.91	0.41	0.17	5.60	100
5	77.5	16.9	0.90	0.48	0.23	3.39	99.4

All the tests in stage 1 had their individual issues. As mentioned earlier test 1, test 2 and test 6 were stopped due to crucible failure. This was due mainly to chemical erosion of the crucible by the FeO-containing slag. This observation was supported by the findings in literature (Kwack *et al.*, 2023; Sarkar and Sohn, 2018). The two studies mentioned indicated that FeO containing slag is highly corrosive towards alumina based refractories and increased FeO in the slag lead to increased rate of refractory corrosion Test 3 was terminated due to insufficient metal bath height; as a result the starting alloy mass for test 4 was doubled as observed in Table II. Test 4 was stopped due to freezing of slag in the crucible. The reason for slag freezing was due to insufficient fluxing and operating the furnace at lower temperatures (<1 500°C). Test 5 was terminated due to the crucible being full. This test was also the one with the highest percentage of oxygen delivered. Although there was no crucible leakage, there was considerable discoloration in the wall of the crucible as shown in Figure 4. Despite the numerous challenges encountered, it was established that (i) an operating temperature of >1550°C was required to maintain a molten slag, (ii) the oxidation efficiency was very high (>99%), and (iii) the ensuing slag required frequent addition of fluxes and additions in large quantities in order to dilute the high concentration of FeO in the slag. Frequent additions of fluxes in large quantities were not practical at this scale due to limited crucible volume and disturbing the thermal balance in the crucible leading to freezing of the slag.

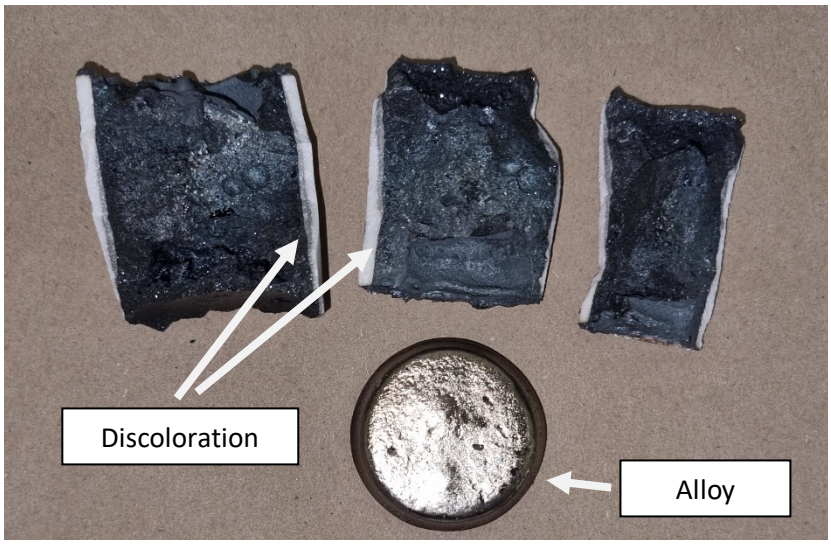


Figure 4. Products from test 5.

Stage 2

Stage 2 tests sought to evaluate the deportment of elements of interest between the metal and slag products at different levels of conversion. Eight tests were conducted in this stage and six tests (test 1,2,3,4,7 and 8) out of the eight were prematurely terminated due to crucible failure. The operating conditions of the tests conducted in this stage are shown in Table V. Due to some of the alloy leaking out the crucible, it was not possible to accurately calculate the mass loss for tests 1,2,3,4,7 and 8.

Table V. Operating conditions for stage 2 tests

Test	Start alloy mass, g	Temp before Blow, °C	Oxygen delivered, g	Oxygen delivered, %	Final alloy mass, g	Alloy mass loss, %	Al_2O_3 added, g	CaO added, g	SiO_2 added, g
1	1090	1496	23.3	8.30	931.4	-	4.0	-	12
2	970.0	1503	26.4	10.6	862.6	-	34	-	42
3	500.0	1496	38.6	29.9	323.2	-	48	68	68
4	701.0	1480	27.5	15.2	455.1	-	68	72	72
5	701.0	1489	32.2	17.8	574.4	18.1	72	80	80
6	747.0	1478	30.7	16.0	633.7	15.2	56	64	64
7	713.0	1497	25.0	13.6	617.0	-	56	64	64
8	617.0	1509	26.4	16.6	198.1	-	56	64	64

The chemical composition of the products obtained from stage 2 tests are shown in Table VI and Table VII. Once again due to crucible failure slag samples from some of the tests were not recovered. The contents of the crucible leaked on the side wall of the crucible for all tests which enabled recovery of alloy samples for analysis. Test 1 to 5 and test 8 used fresh alloy, test 6 used final alloy from test 1 and test 2 and the final alloy from test 6 was re-used in test 7. The highest percentage of oxygen delivered in stage 2 was delivered in test 3 (29.9%) and highest PGMs grade was also obtained in this test (for tests that used fresh alloy). The crucible failures were due to a chemical interaction between the content of the crucible (slag) and the crucible wall. A discolouration of the crucible wall was observed when the crucible was broken down to collect products remaining in the crucible. The same was observed in stage 1 tests and it was also observed in literature *(Kwack et al.*, 2023; Sarkar and Sohn, 2018). Pictures of products from test 5 are shown in Figure 5. The degree of upgrade was still not sufficient in this stage;

the highest grade achieved was 4.95% PGMs. Due to the crucible failure there was not enough time to inject a significant amount of oxygen to upgrade the alloy. There was an attempt to blow the same alloy over multiple tests to achieve the desired grade, but it was deemed impractical due to the number of tests that would have to be conducted to achieve the grade. It was hypothesised that the desired grade could be quickly achieved if the oxygen was injected at a high flow rate. This could be easily done at stage 3 scale; for this reason it was decided to proceed to the next stage besides the challenges experienced.

Table VI. Chemical composition of alloys from stage 2 tests (%)

Test	Fe	Pd	Pt	Rh	Cr	Cu	Ni	Si	PGMs	Total
1	90.5	1.88	1.20	0.22	0.21	5.11	0.60	0.59	3.30	100
2	90.9	1.78	1.24	0.22	0.29	4.88	0.64	0.61	3.24	101
3	88.1	2.44	1.47	0.27	0.26	6.41	0.81	0.58	4.19	100
4	89.4	2.20	1.35	0.25	0.25	5.59	0.74	0.51	3.80	100
5	89.4	2.13	1.31	0.24	0.31	5.50	0.70	0.52	3.68	100
6	89.3	2.23	1.37	0.25	0.33	5.70	0.88	0.55	3.85	101
7	86.4	2.87	1.76	0.32	0.39	7.01	1.01	0.63	4.95	100
8	87.1	2.70	1.67	0.30	0.35	6.73	0.90	0.55	4.67	100

Table VII. Chemical composition of slags from stage 2 tests (%)

Test	FeO	Al_2O_3	Cr_2O_3	CuO	NiO	CaO	SiO_2	Total
3	67.1	8.65	0.31	0.15	0.01	11.8	11.5	99.5
5	63.1	7.44	0.19	0.14	0.03	17.8	10.9	99.6
6	64.2	7.39	0.09	0.33	0.03	16.1	11.7	99.9



(a) (b) (c)

Figure 5. Test 5 pictures showing (a) crucible pictures after breaking (b) crucible piece attached to slag (c) enlarged section showing discoloration.

Stage 3

Three tests were attempted in this stage using a larger crucible and larger induction coil furnace. The aim was to produce 1-2 kg of alloy containing 20% PGMs. Unfortunately, all three tests failed dismally. In test 1 and 2, the crucible leaked before oxygen could be blown into the melt. This signified that the crucible wall integrity was compromised before any oxygen was introduced to the system. In test 3, the crucible failed 10 min into blowing oxygen into the melt. No samples were collected for analysis in this stage due to the premature crucible failures. Given the exacerbated rapid premature failures of the crucibles at the larger crucible scale, it was decided to conduct further tests in a TBRC. The use of sintered MgO crucibles was discussed but calculations completed with Factsage showed that the high FeO slags produced will severely erode the MgO crucible as well.

Crucible failure investigation

Seeing that the crucibles failed at the larger crucible scale before oxygen could be introduced, an investigation was initiated to confirm whether the premature failures of the crucibles were a result of interaction of the molten alloy with the crucible wall. The investigation involved re-melting of the PGM-containing alloy and mild steel in crucibles of the same grade under the same conditions. The tests made use of 500 g of each alloy. These alloys were respectively packed into two separate sintered alumina crucibles. The crucibles were then placed in an induction furnace and heated to 1550°C under an inert Ar atmosphere. The alloys were kept at temperature for an hour and allowed to cool. After cooling the crucibles were broken and the crucible pieces were analysed. Pictures of the crucibles after the re-melt test are shown in Figure 6. Crucible wall discolouration was only observed on the crucible containing the PGMs alloy.

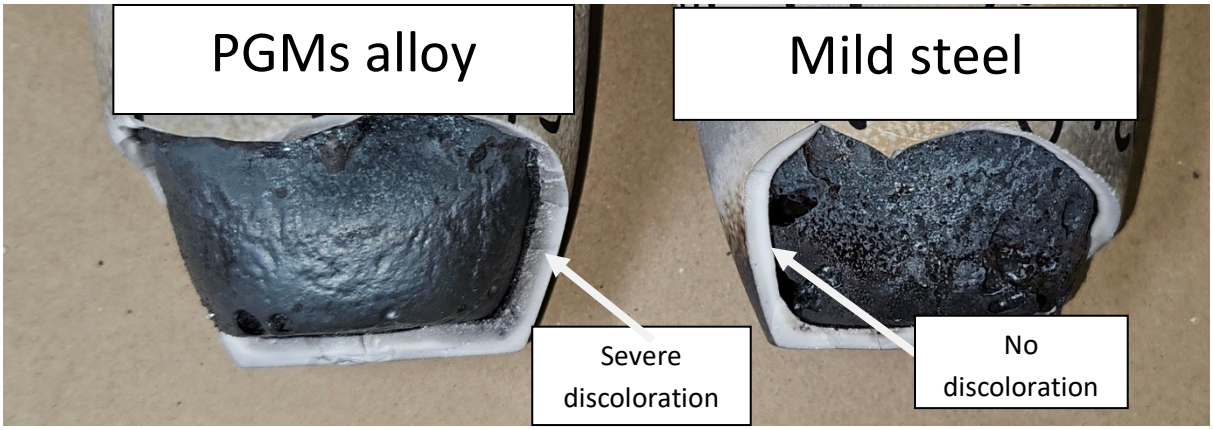


Figure 6. Evidence of severe discoloration on the walls of the crucible in which the PGM-containing alloy was re-melted while no discoloration was observed on the walls of crucible in which mild steel was re-melted.

The crucible pieces were examined with a scanning electron microscope (SEM) and analysed with energy dispersive spectroscopy. The analyses and SEM images (see Table VIII and Figure 7) showed the presence and wide distribution of Al-Fe oxide and Al-Fe alloy inclusions in the walls of the crucible in which the PGM-containing alloy was re-melted. These inclusions were not observed in the wall of the crucible in which the mild steel was re-melted. It is not clear why the PGM-containing alloy penetrated and reacted with the crucible wall to form these inclusions. According to a review completed by Sarkar and Sohn (2018), no discoloration was observed on the wall of the crucible that contained steel because the steel forms a hercynite ($FeAl_2O_4$) protective layer which prevents further penetration of the steel into the crucible wall. The PGM-containing alloy does not form the protective hercynite layer on the alumina

crucible wall which resulted in severe penetration of the alloy into the crucible wall leading to compromised crucible integrity and premature failure.

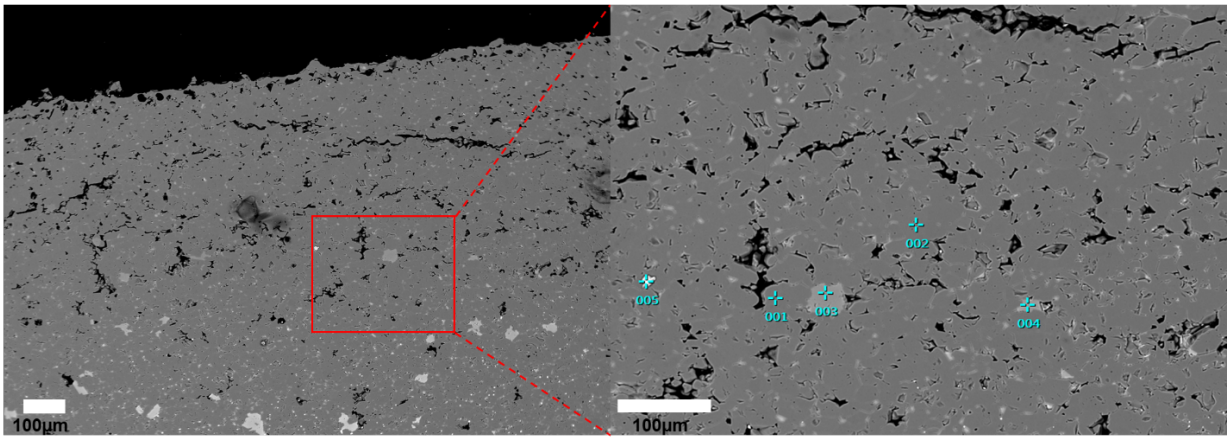


Figure 7. Backscattered electron images from SEM of crucible wall that re-melted PGM-containing alloy.

Table VIII. EDS spot analysis of crucible wall from re-melting of PGM-containing alloy

Spot	Al	Cr	Mg	Fe	O	Total	Comment
1	58.31	-	-	-	41.69	100	Alumina
2	58.77	-	-	-	41.23	100	Alumina
3	45.28	0.08	8.35	12.59	33.71	100	Al-Fe-O
4	45.07	0.08	8.43	12.82	33.59	100	Al-Fe-O
5	86.27	-	-	13.73	-	100	Al-Fe

TBRC Converting tests

A total of four tests were conducted in this stage, with a primary objective of producing 1-2 kg of final alloy containing 20% PGMs. The tests utilised the TBRC facility. Mintek pilot TBRC was successfully used in the past to carry out oxidative refining tests as detailed in the study by McCullough (2008) and Tsebe and Steenkamp (2024). The quantities of raw materials and products, composition of alloy and slag from the TBRC tests are shown in Table VIII, Table IX and Table X, respectively. The alloy in test 1 was oxidised for a duration of 60 min under a flame stoichiometry of 140 mol% O_2. The temperature of the bath was taken using the optical pyrometer and dip B-type thermocouple every 15 min during the oxidation duration. The pyrometer and dip thermocouple recorded average temperatures of 1717°C and 1800°C respectively after the first 15 min. The temperatures were measured again at a 30 min mark, and the readings were 1710°C and 1680°C for dip thermocouple and pyrometer respectively. Due to the high price of B-type thermocouples, an operational decision was made to only use the optical pyrometer. The temperatures recorded during the TBRC tests are shown in Figure 8. All the four (4) tests reported a spike in temperature during the first 15 min of oxidation. The temperature spike was due to the exothermic oxidation reactions taking place. The temperature then drops as oxidation rate is reduced by formation of the slag covering the metal bath. Due to difficulty in controlling the oxidation efficiency, all the alloy was oxidised. It was decided to increase the quantities of the fluxes to reduce consumption of the TBRC vessel lining. The consumption of the alumina lining was expected as it was observed in literature (Kwack *et al.*, 2023; Sarkar and Sohn, 2018) and tests from previous stages.

The alloy in test 2 was oxidised for a duration of 110 min under a flame stoichiometry of 140 mol% O_2. The higher slag volume owing to increased quantities of fluxes effectively covered the pool of metal and resulted in a lower oxidation efficiency. The PGM grade of the alloy obtained was 5.40% with a low alloy mass loss of 29.1%. After test 2 more refractory wear was observed due to the higher operating temperatures (>1600°C) as observed in Figure 8. This agrees with literatures as it was shown that increased operating temperatures resulted in increased dissolution of Al_2O_3 in FeO containing slag (Kwack *et al.*, 2023). The alloy in test 3 was oxidised for 50 min under a flame stoichiometry of 160 mol% O_2. Due to decreased flux quantities and increased flame stoichiometry the alloy was over-oxidised to a grade of 60% PGMs. The increased oxidation efficiency was expected as less slag volume provided better contact between the oxygen gas and the surface of the alloy pool. The over-oxidation in test 3 led to a decision to reduce the flame stoichiometry. The alloy in test 4 was oxidised for 60 min under a flame stoichiometry of 140 mol% O_2. The alloy was over-oxidised to a PGMs grade of 82%. Refining of the alloy at pilot scale in a TBRC was effective but there was poor control of the oxidation rate and lack of a reliable method to measure the oxidation efficiency. Aggressive addition of fluxes to dilute the FeO in the slag leads to formation of large volumes of slag which negatively impacts on the oxidation efficiency. Similar future test work on refining PGM-containing alloy will require a better refining strategy that considers the rate of oxygen delivery, the frequency and quantity of flux additions, rate of slag formation and impact on oxidation efficiency, reliable and robust method to measure oxidation efficiency, and regular sampling and a quick turn-around-time method to analyse the slag and alloy.

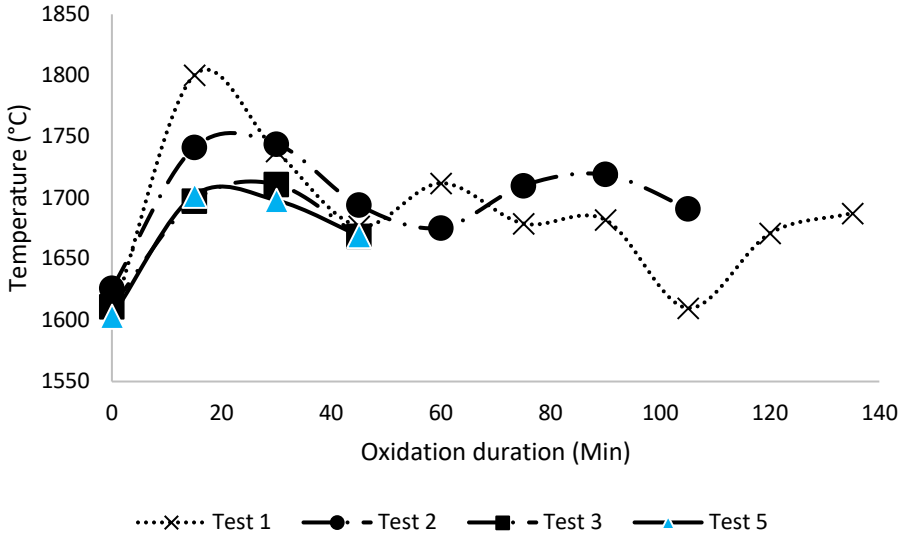


Figure 8. Temperatures during the TBRC tests

Table VIII. Quantities of raw materials and products from the TBRC tests

Test	Start alloy mass, kg	Final alloy mass, kg	Alloy mass loss, %	Al_2O_3 added, kg	CaO added, kg	SiO_2 added, kg	Slag produced, kg
1	10.0	-	100	1.5	1.5	1.5	18.6
2	9.25	6.55	29.1	2.1	2.1	2.1	8.45
3	9.25	0.18	98.1	0.8	0.8	0.8	9.16
4	7.25	0.30	95.0	0.8	0.8	0.8	8.86

Table IX. Composition of the alloy obtained from TBRC tests (%)

Test	Fe	Pd	Pt	Rh	Cu	Ni	Si	PGMs	Total
2	85.2	3.06	2.00	0.37	4.20	0.59	2.33	5.4	97.7
3	22.3	30.1	24.1	3.76	8.10	0.59	9.23	58	98.2
4	1.30	44.0	32.3	5.72	11.1	0.10	3.81	82	98.3

Table X. Composition of the slag produced from TBRC tests (%)

Test	FeO	Al_2O_3	Cr_2O_3	CuO	NiO	SiO_2	CaO	Total
1	35.2	35.8	0.09	1.60	0.34	6.72	6.42	85.7
2	7.11	47.6	0.11	0.13	0.06	31.7	11.8	98.4
3	21.7	55.9	0.10	0.40	0.31	9.90	11.0	99.3
4	23.9	50.4	0.10	0.50	0.62	12.0	11.0	98.6

CONCLUSION

The crucible scale test work encountered severe premature failures of high-quality alumina crucibles due to chemical attack by both the slag and the alloy. This prevented the refining process to progress long enough to demonstrate refining of the alloy to the target PGMs grade. Further tests were conducted at pilot scale in a TBRC whereby high oxidation efficiencies were obtained but could not be accurately controlled, leading to over-oxidation of the alloy and production of final alloys with PGM grades of more of more than 80%. Therefore, the refining of this particular PGM-bearing alloy was not technically feasible at the crucible scale due to consistent premature failures of the alumina crucibles. The refining of the alloy at pilot scale in a TBRC was effective but there was poor control of the oxidation rate and lack of reliable method to measure the oxidation efficiency which resulted in over-oxidised alloys. While the target grade was not reached, the work provides valuable insights into crucible behaviour, slag chemistry, and oxidation control. Further studies are recommended to evaluate alternative refractories, fluxing strategies and oxidation efficiency measurements methods.

REFERENCES

Alison, C., 2024. PGM market report. Johnson Matthey.URL: https://matthey.com/documents/161599/509428/PGM-Market-Report-24.pdf/4d557d3b-47d1-d975-c4af-5df1c81000f0?t=1715228936090

Kwack, T., Um, H., Chung, Y., 2023. Activation Energy of Alumina Dissolution in FeO-Bearing Slags. Metals 13, 1702. https://doi.org/10.3390/met13101702

Li, T., Bingguo, L., Fang, X., Yuwen, C., Hou, K., Chen, W., Liu, X., Guo, S., Zhang, L., 2025. High-Value Utilization of Steel Slag and Red Mud: Recovery of Platinum from Spent Aluminum-Based Catalyst by Pyrometallurgy. https://doi.org/10.1016/j.jece.2025.116748

McCullough, S.D., Geldenhuys, I.J., Jones, R.T., 2008. Pyrometallurgical iron removal from a PGM-containing alloy. Presented at the Third International Platinum Conference 'Platinum in Transformation, Sun city, South Africa.

Mich, J., Da Silva, A.K., Ning, D., Li, T., Raabe, D., Böhm, B., Dreizler, A., Hasse, C., Scholtissek, A., 2024. Modeling the oxidation of iron microparticles during the reactive cooling phase. Proceedings of the Combustion. Institute. 40, 105538. https://doi.org/10.1016/j.proci.2024.105538

Sarkar, R., Sohn, H.Y., 2018. Interactions of Alumina-Based and Magnesia-Based Refractories with Iron Melts and Slags: A Review.Metallurgical and Materials Transactions B 49B. https://doi.org/10.1007/s11663-018-1300-1

Tsebe, S.P., Steenkamp, J.D., 2024. Development of an Integrated Process Flowsheet to Recover Valuable Metals from Waste Cathode Ray Tubes and Printed Circuit Boards. J. Sustain. Metall. 10, 224–240. https://doi.org/10.1007/s40831-023-00775-1

Yakoumis, I., Panou, M., Moschovi, A.M., Panias, D., 2021. Recovery of platinum group metals from spent automotive catalysts: A review. Clean. Eng. Technol. 3, 100112. https://doi.org/10.1016/j.clet.2021.100112

Yang, D., Yang, Q., Ma, W., Ma, X., Wang, S., Lei, Y., 2023. Characteristics of spent automotive catalytic converters and their effects on recycling platinum-group-metals and rare-earth-elements. Sep. Purif. Technol. 308, 122977. https://doi.org/10.1016/j.seppur.2022.122977

Yang, Q., Lei, Y., Yang, D., Ma, W., Ma, X., 2023. A harmless slagging treatment to separate key impurities from Fe-PGMs alloys for improving the recovery ratio of PGMs from spent auto-catalysts. J. Environ. Chem. Eng. 11, 110669. https://doi.org/10.1016/j.jece.2023.110669



Matale Samuel Moholwa

Senior Engineer: Techology Demonstration Group
Mintek

Matale Samuel Moholwa is a senior engineer under the technology demonstration group in the pyrometallurgy division at Mintek. He holds a master's degree in chemical engineering and has been employed at Mintek since 2018. In his current role, Sam conducts research on pyrometallurgical process involving various commodities and different smelting technologies. His experiences and interests are but not limited to research & development, project and people management, process engineering design, equipment selection, process optimization, commissioning of new and modified plants, feasibility studies and business development. Sam has presented at international conferences which include the 4th Manganese school and TMS conference.

Evaluation of an alternative furnace cooling medium for enhanced operational safety

K.C. Maluleke[1], H. Joubert[1], P. Jonker[1], G. Tawane[2], X.C. Goso[2]

[1]Tenova Pyromet, South Africa
[2]Mintek, South Africa

Many modern furnace designs incorporate coolers made from steel or copper to stabilise the refractory and promote the formation of a protective slag freeze layer. Typically, water is used as the cooling medium in these systems, although a few installations have adopted synthetic oils as an alternative. Water-cooled systems integrated into the furnace crucible pose safety risks in the event of unintended water leakage. Such leaks can cause equipment damage, physical injuries, and even fatalities, due to explosions caused by hot liquid metal or matte being mixed with water. To mitigate these risks, alternative cooling media have been proposed in industry, including ionic liquids and mono-ethylene glycol (MEG). In this study, Tenova Pyromet, in collaboration with Mintek, evaluated the cooling performance and safety characteristics of a 70% MEG, 30% water mixture (MEG70). A pilot-scale copper test cooler was operated under controlled flow conditions at bulk temperatures of 68°C and 83°C to measure heat flux, copper temperature, and heat transfer coefficients. Explosion trials were also conducted to compare the behaviour of MEG70 and water when in contact with molten matte. The results showed that MEG70 provides comparable cooling performance to water, though requiring higher flow velocities. At elevated bulk temperatures, MEG70 demonstrated improved heat transfer but with increased hydraulic losses. Importantly, safety trials confirmed that, unlike water, MEG70 does not trigger violent explosions with molten matte; instead, it burns in a controlled manner. These findings demonstrate that MEG offers a technically viable and significantly safer alternative to water for deep furnace cooling applications.

INTRODUCTION

The use and demand for cooling systems in high-wear areas for industrial electric arc furnaces, such as the slag zone or tap-hole areas have dramatically increased in the last few decades due to the increased productivity demands on furnace operations. Cooling elements are widely incorporated in modern furnace designs as an effective method for stabilising the refractory and creating a freeze-lining of slag inside the furnace (Joubert & Mc Dougall, 2019). Utilising cooling elements allows for increased operational intensity and longer campaign lives, resulting in increased process throughput. Typical cooling elements are constructed using steel and/or copper and normally utilise water as a cooling medium (Kennedy, *et al*., 2016; Kennedy, *et al*., 2015; Filzwieser, *et al*., 2014).

Water is commonly used as a cooling medium due to its abundance, low cost, and acceptable heat transfer properties (Kennedy, *et al*., 2016). Utilising water as a cooling medium in the vicinity of molten material introduces risk; a leak on the cooling element has a high probability of resulting in powerful boiling liquid expanding vapour explosions, which can cause furnace and equipment damage, and major incidents leading to physical injuries and even fatalities (Filzwieser, *et al*., 2020; Kennedy, *et al*., 2015).

Significant work has been done to improve and optimise furnace cooling elements and design durable tap-holes (Joubert, *et al*., 2024; Joubert, *et al*., 2022; Mc Dougall, 2014; Nelson & Hundermark, 2014). Various preventative measures have been suggested, such as the use of coatings in aluminium casting pits, the use of sufficient depth of water, and the use of alternative coolants to combat incidents related to steam explosions (Crivits, *et al*., 2021). Several alternative coolants to water have also been proposed in literature, including ionic liquids and mono-ethylene glycol (MEG), as solutions for avoiding steam explosions (Kennedy, *et al*., 2016).

Tenova Pyromet has conducted finite element analysis modelling to evaluate MEG and ionic liquid as alternative cooling mediums in its MAXICOOL copper cooling elements. Modelling was conducted at coolant bulk velocities of 2 and 4 m/s through the cast-in Monel tubing. The convective heat transfer coefficient between the coolant and the inside of the cooling channel is directly related to the square of the coolant bulk velocity. The results showed that, for MEG, a velocity of 4 m/s is required to maintain the copper element temperature below the 400°C design limit when considering extreme operating conditions in a typical primary copper smelting furnace. The results showed that for ionic liquids, the copper element temperatures are above the design limit for the same velocity and conditions. Further work was recommended to confirm the cooling efficiency, and the perceived safety advantages of using MEG or ionic liquid as alternative cooling media (Joubert, *et al*., 2019). Tenova Pyromet subsequently conducted test work to assess the cooling performance of MEG and its potential to reduce explosion risks when in contact with molten platinum group metal (PGM) matte, compared with conventional water cooling. The outcomes of this evaluation are presented in this paper.

EXPERIMENTAL PROCEDURE

This study utilised two experimental approaches to evaluate the performance and safety characteristics of the cooling medium, i.e., cooling efficiency tests and controlled explosion tests, discussed in this section.

Raw Materials

A sample of high-grade PGM matte was obtained from a major South African PGM smelter for use in the laboratory test work. The sample was representative of typical industrial furnace operating conditions. MEG of industrial grade, DOWCAL 100 heat transfer fluid, was used to prepare a 70% MEG and 30% water mixture (MEG70) for cooling tests. Rand tap water was used as a baseline coolant for comparison. Argon gas (AFROX) was used to maintain inert conditions during selected experiments.

Cooling efficiency tests

Cooling efficiency tests were conducted to compare MEG with water as a cooling medium for furnace sidewall copper coolers. For the test programme, a mixture of 70% MEG and 30% water (hereafter referred to as MEG70) was selected to balance thermal performance with favourable flow characteristics. The addition of water reduces the viscosity of pure MEG, thereby limiting pressure losses and lowering the pumping power required. The key physical properties of MEG70 relative to water are summarised in TableI.

Table I: Relative properties of MEG70 and water.

Property	Unit	Water at 58°C	MEG70 at 68°C	MEG70 at 83°C
Density	kg/m^3	984	1077	1069
Specific heat	J/kgK	4179	3223	3290
Thermal conductivity	W/mK	0.65	0.354	0.348
Kinematic viscosity	mm^2/s	0.5	2.49	1.85

A pilot-scale copper cooler was fabricated for the test work, based on Tenova's high-intensity MAXICOOL cast copper cooler design for furnace sidewall applications. Tenova's MAXICOOL cast copper coolers have been successfully employed in furnace sidewalls containing various pyrometallurgical processes, including nickel and PGM primary smelting and slag cleaning, copper slag

cleaning and converting, and autocatalyst recycling (Joubert, *et al.*, 2005; Joubert, *et al.*, 2022). The test cooler incorporated Monel piping cast into the copper body to form three independent cooling circuits. Three thermowells were embedded between the Monel pipes and the hot face to enable temperature measurements during operation. These were positioned at the top left corner, centre, and bottom right corner of the cooler. Figure 1 shows the schematic diagram of the test cooler setup used for the cooling efficiency experiments.

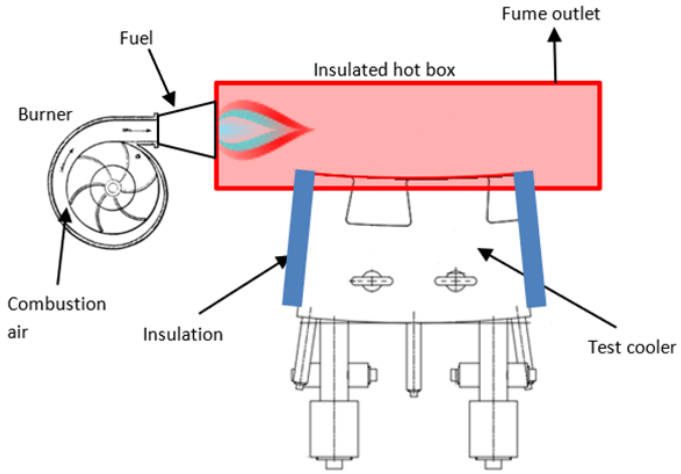


Figure 1: Schematic diagram of the test cooler setup.

High-alumina refractory castable was applied to the hot face of the test cooler, ensuring alignment with the copper star hot face to simulate an extreme operating condition, such as the dislodgement of a freeze lining. The insulated hot box base was constructed from alumina bricks measuring approximately 750 x 1200 mm. The test cooler was positioned within the side of the hot box to achieve a tight fit, with no more than 50% of the cooler's star or castable section depth exposed to the internal atmosphere. A positive seal was applied along the sides to minimise heat loss, and thermal insulating blanket material was placed on the top and side external surfaces to establish an adiabatic boundary condition.

Thermocouples were installed within the copper casting, extending to the front of the thermowell holes, while additional thermocouples measured the gas temperature inside the hot box. Resistance temperature detectors were inserted in the cooling medium piping to monitor inlet and outlet temperatures. All measurements were recorded over time using a data logger. Figure 2 illustrates the hot box, test cooler, burner, and data logger setup.



Figure 2: Hot box, test cooler, burner and data logger setup.

Figure 3 shows the pump station, including pumps for circulating the cooling medium through the copper cooler and a holding tank. The same pumping system was used for both water and MEG70 to enable direct comparison of cooling efficiency. Flexible supply and discharge hoses connected the system, and the cooling medium was initially circulated at 8 m^3/h (133 L/min) prior to starting the burner, maintaining continuous flow throughout the tests.



Figure 3: Photograph of pumping station for coolant of experimental setup.

The gas burner was ignited and checked for leaks, and the heat inside the hot box was gradually increased. For the first run, the gas temperature was held at 200°C for 3 hours to ensure proper drying of the castable refractory, followed by a 4-hour hold at 500°C to complete curing. Subsequently, the gas temperature was increased to 900°C and maintained at 900°C ± 20°C by adjusting the burner. Prior to each test run, temperatures of the hot box, test cooler, and cooling medium were allowed to stabilise at 900°C.

Each test run started with a cooling medium flow rate of 8 m^3/h (133 L/min), corresponding to a bulk velocity of 8 m/s in the cooler channels. The flow rate was then gradually reduced to a minimum of 2.5 m^3/h, yielding a bulk velocity of approximately 1.25 m/s. At least three runs were performed for each cooling medium, covering a range of average cooling medium temperatures. For MEG70, the lowest and highest average temperatures tested were 68°C and 83°C, respectively.

During testing, the following parameters were continuously recorded: cooling medium inlet (supply) temperature, outlet (return) temperature, supply pressure, return pressure, flow rate, three internal test cooler temperatures, furnace box internal temperature (for burner control), and test cooler refractory hot face temperature (measured with a thermocouple positioned within 10 mm of the castable surface).

The cooling efficiency of the test cooler was evaluated by processing the recorded measurements from each run. From these measurements, the average hot face heat flux over the hot face of the cooler was calculated based on the temperature difference between the cooling medium inlet and outlet, the specific heat of the medium, and the measured flow rate. The convective heat transfer coefficient within the cooler channels was determined using the cooling medium bulk temperature, flow rate, and corresponding fluid properties, with bulk temperature and fluid property values updated for each data point to account for variations during testing.

Explosion tests

Explosion tests were conducted to investigate the interactions between various MEG/water mixtures with molten material compared to water, which is used as a standard coolant in industrial furnaces. The tests were conducted at Mintek in South Africa (MINTEK, 2024). Two experimental setups were employed to investigate the interactions:

- Test setup 1: Adding or pumping the MEG/water coolant into the molten matte
- Test setup 2: Adding the molten matte to the coolant.

Test setup 1: Adding or pumping the MEG/water coolant into the molten matte
Explosion tests involving adding coolant into the molten matte were conducted in a steel-caged induction furnace. The steel cage served to protect the surrounding furnace laboratory equipment from potential damage. A peristaltic pump and gas cylinder were placed outside the laboratory to minimise risks to personnel.

Each test was conducted using 1600 g of PGM furnace matte, which was measured and transferred into an alumina crucible, filling it to approximately three-quarters of its volume. The crucible was positioned inside a graphite susceptor, resting on a bed of alumina bubbles. Additional alumina bubbles were packed into the space between the crucible and the susceptor to provide stability. A schematic representation of the induction furnace setup is shown in Figure 4.

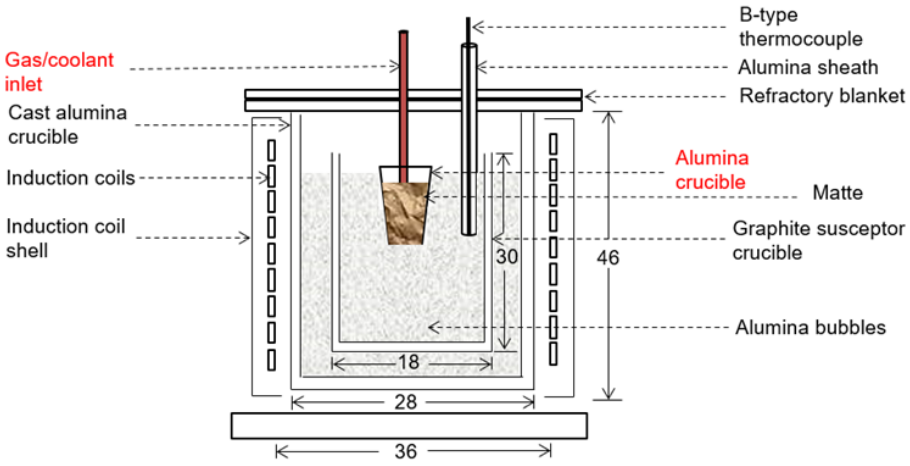


Figure 4: Schematic diagram of the induction furnace setup (test setup 1).

An inert atmosphere was maintained by continuous argon (Ar) gas flow throughout the experiment to prevent oxidation of both the matte and the graphite susceptor. The furnace was manually controlled by increasing the input power to heat the sample at an average rate of 10°C/min to a target temperature of 1600°C. Upon reaching this temperature, a pre-heated quarter-inch alumina sheath was inserted approximately 10 cm into the molten matte. The coolant was introduced into the matte using a peristaltic pump at a constant flow rate of 85 mL/min for all the tests, with a total coolant volume fixed at 100 mL per test. During each test, the procedure was recorded using a video camera, and sound levels were monitored with a sound meter to capture the dynamic interactions between the coolant and the molten material.

Six tests, including duplicates, were conducted. The test matrix and corresponding parameters are summarised in Table II.

Table II: Test matrix for test setup 1 – pouring coolant into molten matte

Test	Cooling agent	% MEG addition	% Water addition
1	MEG100	100	0
2	MEG100-1*	100	0
3	MEG70	70	30
4	MEG70-1*	70	30
5	MEG0	0	100
6	MEG0-1*	0	100

(*) indicates repeated tests

Test setup 2: Addition of molten matte to the coolant

Explosion tests investigating the interactions between molten material and coolant using test setup 2 were conducted. Each test was performed using a predetermined mass of matte, which was weighed and transferred into an alumina crucible, filling approximately three-quarters of its volume. The crucible was placed inside a gas-tight furnace chamber. Argon gas was continuously supplied to purge air and maintain an inert atmosphere throughout the heating of the matte. The furnace was programmed to heat the sample at a rate of 10°C/min to a target temperature of 1600°C, holding it at this temperature for 30 minutes.

After the soaking period, the crucible was removed from the furnace and secured on a rotating stand using a clamp. The molten matte was then poured directly into the coolant, which was positioned beneath the stand. Figure 5 and 6 show the schematic diagram and image of the explosion tests using test setup 2. A camera mounted on a tripod was used to record the interaction at the coolant-matte interface, while a sound meter simultaneously measured and recorded sound data generated during the process.

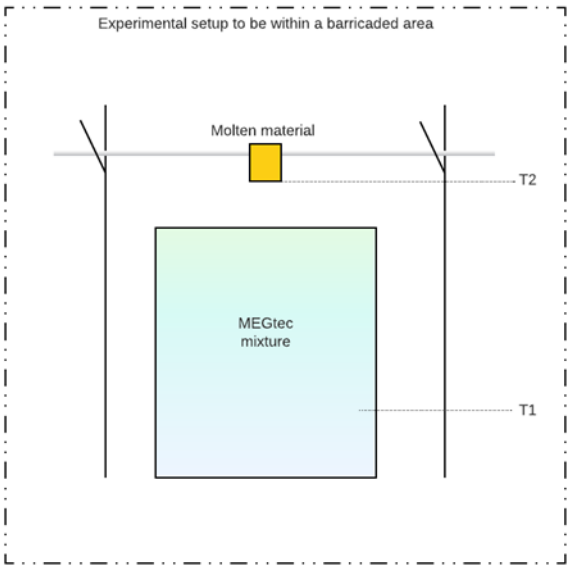


Figure 5: Schematic diagram for the test setup 2.

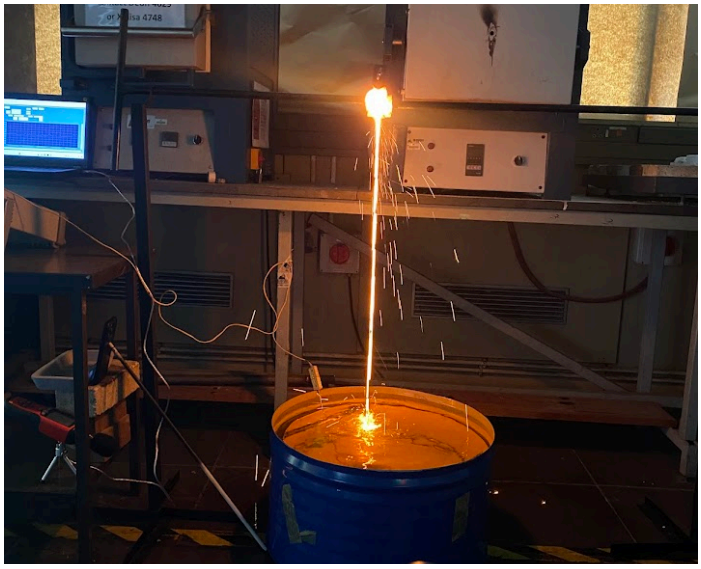


Figure 6: Image showing test setup 2.

Five tests, including duplicates, were conducted. The test matrix and corresponding parameters are summarised in Table III.

Table III: Test matrix for test setup 2- adding molten matte to coolant

Test	Cooling agent	%MEG addition	%Water addition	Matte: coolant ratio	Height, mm
1	MOLT70	70	30	500 g: 10 L	400
2	MOLT70*	70	30	500 g: 10 L	400
3	MOLT30	30	70	200 g: 65 L	800
4	MOLT0	0	100	200 g: 600 mL	250
5	MOLT0*	0	100	200 g: 600 mL	250

(*) indicates repeated tests

RESULTS AND DISCUSSIONS

Cooling efficiency tests

Figure 7 shows a graphical comparison of the heat flux, test cooler copper temperatures, and cooling medium heat transfer coefficients for MEG70 (average bulk temperature 83°C) and water (average bulk temperature 58°C), plotted as a function of bulk velocity in the cooler channels. At equivalent flow rates or bulk velocities, the heat removal capacity, as indicated by heat flux, was higher for water than for MEG70. This difference was attributed to the lower heat transfer coefficients achieved with MEG70 under the same flow conditions. For example, the heat flux obtained with MEG70 at a bulk velocity of 4 m/s (~200 kW/m²) was comparable to that achieved with water at 2–2.5 m/s. These findings are consistent with earlier finite element modelling results (Joubert *et al.*, 2019), which indicated that achieving equivalent cooling performance with MEG70 requires higher bulk velocities than with water.

For MEG70, the measured copper temperatures in the test cooler were consistently higher than those for water. At a bulk velocity of 4 m/s, the centre thermocouple (positioned in front of the cooling channels) recorded a copper temperature of approximately 115°C for MEG70, compared to 81°C for water at 2 m/s. This difference reflects the higher bulk operating temperature of MEG70 during testing. The average refractory hot face temperature was 684°C for MEG70 and 665°C for water.

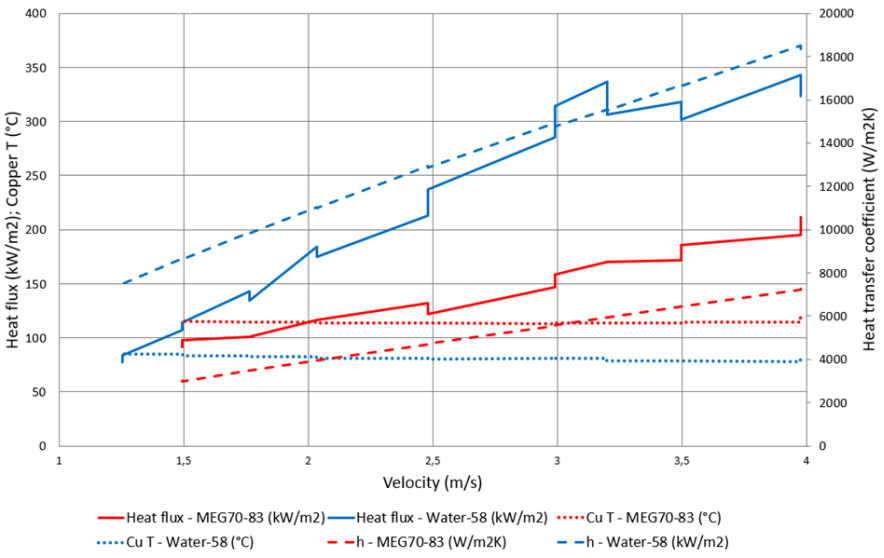


Figure 7: Heat flux, test cooler copper temperatures, and cooling medium heat transfer coefficient for MEG70 relative to water.

Figure 8 shows a graphical comparison of the heat flux, copper temperature, and heat transfer coefficient for MEG70 at average bulk temperatures of 83°C and 68°C. At equivalent bulk velocities, the higher-temperature MEG70 exhibited greater heat flux, indicating an increased heat removal capacity for the test cooler. This improvement is attributed to the higher heat transfer coefficients achieved at elevated temperatures, resulting from reduced viscosity and increased specific heat (see Table I). Conversely, the copper temperature in the test cooler was lower for the lower-temperature MEG70, reflecting both the reduced heat flux into the cooler and the lower operating temperature of the cooling medium.

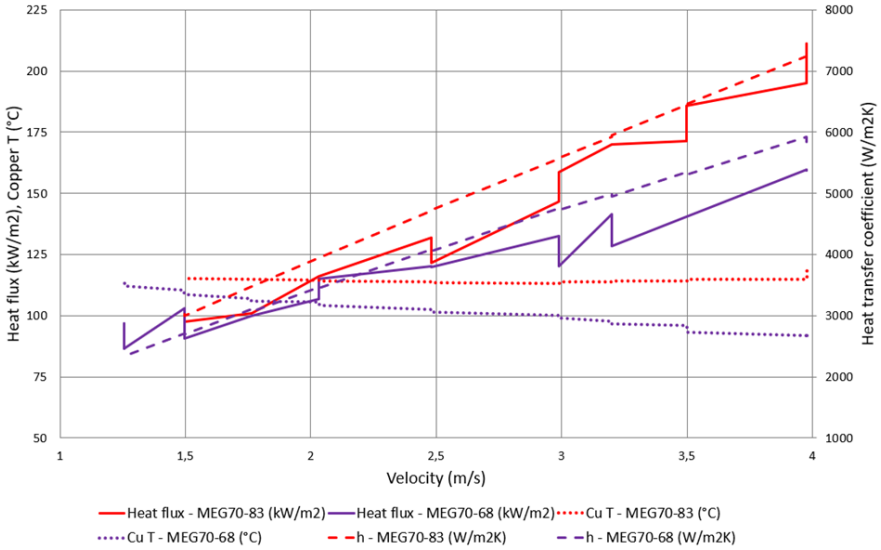


Figure 8: Heat flux, test cooler copper temperatures, and heat transfer coefficient for MEG70 at higher and lower temperatures.

Figure 9 presents the differential pressure measured across the test cooler and supply piping for MEG70 and water. The pressure drop was found to be similar for MEG70 at an average temperature of 83°C and water at 58°C, with slightly higher values recorded for MEG70 at 68°C. However, the difference becomes significant when accounting for the higher velocity required for MEG70 to achieve a comparable cooling efficiency to water. At a bulk velocity of 4 m/s, MEG70 exhibited a pressure drop of 1.16 bar, compared to 0.26 bar for water at 2 m/s. These higher flow rates and associated pressure losses for MEG70 must be taken into account when designing the pumping and piping system.

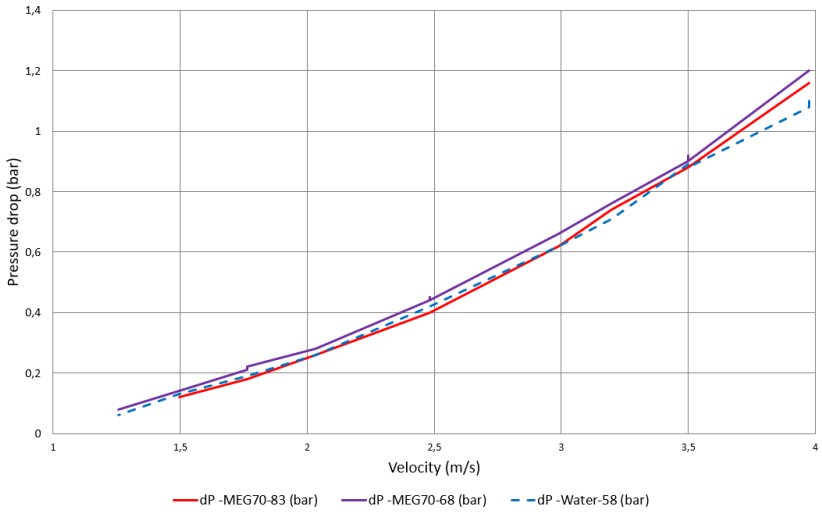


Figure 9: Differential pressure across the test cooler and piping.

Explosion tests

Test setup 1: Addition of coolant into the molten matte

This section presents the observations, images from video footage, and sound recordings captured during the tests (including repeated trials) in which coolant was pumped into the molten matte. It should be noted that the sound measurement results were inconclusive, largely due to inconsistent background noise from operational equipment and extraction systems in the working area.

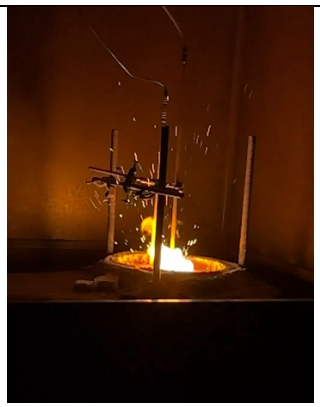
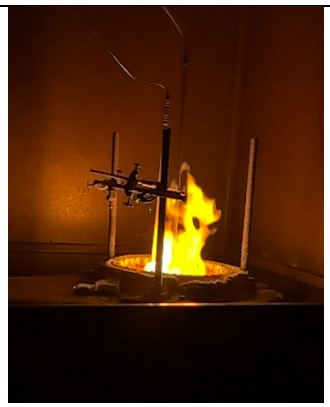
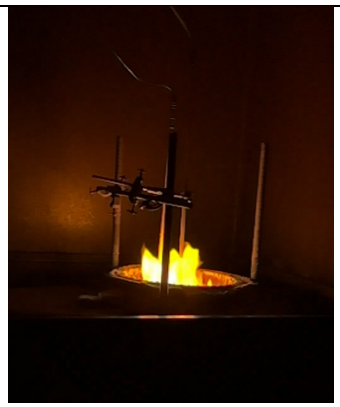
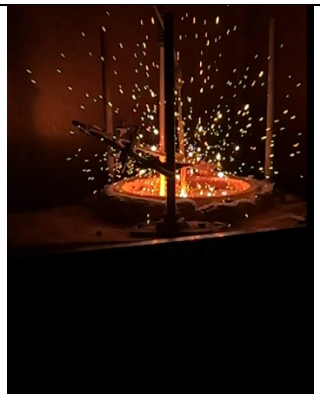
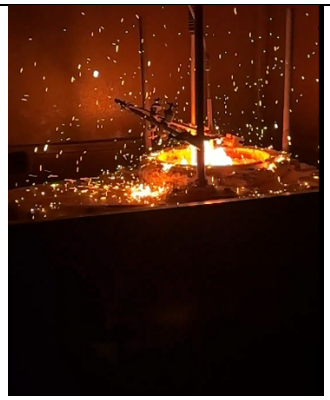
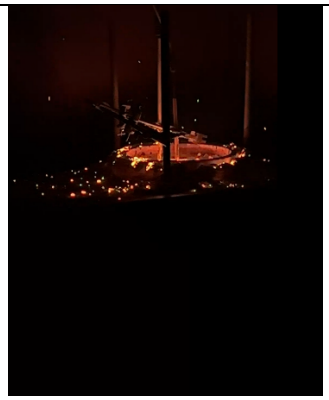
Table IV provides a summary of the results obtained from the test involving the addition of coolant into the molten matte (test setup 1). Introducing 100% MEG (Test 1 and 2 – MEG100) into the molten matte produced a flame with no matte sparks and explosive sound. Small sparks were observed upon contact, which, upon further inspection, were found to be fumes from the MEG burning and not matte prills.

A moderate-sized flame with some sparks was observed during the MEG70 tests (Tests 3 and 4). The sparks were less intense compared to those observed with the 100% MEG tests. The findings suggest that increasing the MEG content in the cooling mixture leads to a higher degree of flames and sparks observed.

The addition of 100% water (Tests 5 and 6, MEG0) into the molten matte resulted in a violent and explosive reaction accompanied by a loud sound/ bang, causing nearly half of the molten matte to splash out of the crucible. Matte prills were observed around the furnace upon completion of the experiment. These observations were consistently noted in the repeat test.

The results indicate that increasing the MEG content in the cooling mixture enhances the propensity for flame generation, while the use of pure water as a coolant leads to an explosive reaction when interacting with molten matte. The presence of the flame in both the ME100 and MEG70 tests was mainly attributed to the combustible nature of MEG, an organic reagent, which automatically ignites at temperatures above 398°C (BASF, 2025). The test results demonstrate that, in comparison with water (MEG0), a MEG-water mixture has a lower risk of causing explosions when in contact with molten matte.

Table IV: Summary of results - adding/pumping the MEG/water coolant into the molten matte

Test	Upon contact	During flow	After 60 sec	Observations
MEG100				Intense flame, no bang.
MEG70				Moderate flame, no bang.
MEG0				Rapid explosion with a loud bang. No flame. Matte prills outside the furnace.

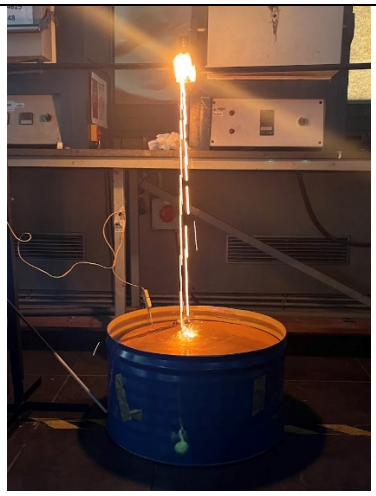
Test setup 2: Addition of molten matte to the coolant

This section presents the observations, images from video footage, and sound recordings captured during the tests (including repeated trials) in which molten matte was poured into the coolant (test setup 2). It should be noted that the sound measurement results were inconclusive, largely due to inconsistent background noise from operational equipment and extraction systems in the working area.

Table V summarises the results of five tests conducted by pouring molten matte into the coolant. The MOL70 tests (i.e., Test 1 and 2) produced a flame with slight bubbling on the surface of the cooling mixture. No explosions or sparks were observed, and the flame extinguished after approximately 30 seconds, leaving a bubbling mixture. The MOLT30 test showed no explosion and no sound during the experiment. The MOLT0 (water) test resulted in a rapid and loud gas eruption/explosion when the

molten matte came into contact with water, causing vigorous splashing of matte prills into the surrounding area.

Table V: Summary of results - adding molten matte to coolant

Test	Upon contact	End of test	Observations
MOLT 70			Flame with no explosive behaviour
MOLT 30			No explosion no flame
MOLT 0			Rapid explosion with significant bang sound. Matte prills around container.

CONCLUSIONS

The cooling performance of MEG and various MEG–water mixtures was evaluated against that of water for a typical furnace copper cooling element. Results show that MEG70, when operated at higher bulk velocities, can achieve heat removal rates comparable to water. A bulk velocity of 4 m/s for MEG70 provided similar cooling performance to water at 2 m/s. Cooling efficiency improved at elevated coolant temperatures, with average bulk temperatures of 83°C outperforming 68°C due to lower viscosity and higher specific heat. However, these higher velocities resulted in greater pressure drops—1.16 bar for MEG70 at 4 m/s compared to 0.26 bar for water at 2 m/s—requiring careful consideration in pumping and reticulation system design.

Explosion risk testing showed that water in contact with molten matte produced violent explosions, whereas MEG70 eliminated such events. When exposed to molten matte, MEG70 ignited and burned, but no explosive reactions occurred. These findings demonstrate that MEG70 offers both effective cooling performance and significantly reduced explosion risk compared to water.

Based on these results, MEG70 is recommended as a coolant for critical furnace sidewall and taphole cooling elements, with system designs adapted to accommodate its higher flow and pressure requirements.

ACKNOWLEDGEMENTS

The authors wish to thank Thos Begbie & Company (Pty) Ltd and Elite Refractory Services (Pty) Ltd for accommodating the efficiency test work in their facilities, and Mintek for the explosion risk test work conducted at their facilities. The authors furthermore wish to thank Tenova Pyromet for granting permission to publish the work.

REFERENCES

BASF, 2025. *https://download.basf.com.* [Online].

Crivits, T. et al., 2021. *A qualitative study on matte/slag/copper alloy interactions with water/MEG.* s.l., The 11th International Conference on Molten Slags, Fluxes and Salts.

Filzwieser, A. et al., 2020. *ILTEC Technology-New Pathways Towards Safe and Effective Cooling.* s.l., Springer International Publishing, pp. 683-694.

Filzwieser, A., Konetschnik, S. & Dreyer, E., 2014. *METTOP's ionic liquid cooling technology: the safest way of furnace tapping.* Muldersdrift, The Southern African Institute of Mining and Metallurgy, pp. 217-222.

Joubert, H., De Villiers, G., Mbedzi, P. & Davis, J., 2024. *Composite Copper-Graphite Cooler for PGM Furnace Sidewall.* Orlando, The Minerals, Metals & Materials Society, pp. 51-65.

Joubert, H. & Mc Dougall, I., 2019. *Designing furnace lining/cooling systems to operate with a competent freeze lining.* San Antonio, Springer International Publishing, pp. 1181-1195.

Joubert, H., Mc Dougall, I. & de Villiers, G., 2019. *Design of copper cooling systems for copper smelting and converting furnaces.* Vancouver, Conference of Metallurgists.

Joubert, H. et al., 2022. *Design, construction and performance of the copper cooling system installed in the first ISACONVERT copper converting furnace.* Santiago, The Chilean Institute of Mining Engineers.

Joubert, H. et al., 2022. *Design, construction and performance of the copper cooling system installed in the first ISACONVERT copper converting furnace.* Santiago, The Chilean Institute of Mining Engineers.

Joubert, H., Nourse, B. R., Masters, b. & Hundermark, R., 2005. *Copper cooling design, installation and operational results for the slag cleaning furnace at waterval Smelter, Rustenburg Platinum, South Africa.* Calgary, s.n.

Kennedy, M. W. et al., 2015. *Some considerations for safer furnace cooling.* s.l., The Canadian Institute of Mining, Metallurgy and Petroleum, pp. 1-15.

Kennedy, M. W., Nos, P., Bratt, M. & Weaver, M., 2016. Alternative coolants and cooling system designs for safer freeze lined furnace operation. *Ni-Co 2013,* pp. 299-314.

Mc Dougall, I., 2014. *Water-cooled tap-hole blocks.* Muldersdrift, The Southern African Institute of Mining and Metallurgy, pp. 183-191.

MINTEK, 2024. *Cooling of matte using alternative coolant, Report no. 8655, CONFIDENTIAL,* Randburg: MINTEK.

Nelson, L. R. & Hundermark, R. J., 2014. *'The Tap-hole' - key to furnace performance.* Muldersdrift, The Southern African Institute of Mining and Metallurgy, pp. 1-32.



Kgomotso Charlotte Maluleke

Technical Sales Engineer
Tenova Pyromet

Kgomotso Maluleke is a Metallurgical Engineer with BSc and MSc in Metallurgical Engineering from the University of the Witwatersrand and over five years hands-on pyrometallurgy base metals experience. Kgomotso holds a BSc and MSc in Metallurgical Engineering from the University of the Witwatersrand, and currently works as a Technical Sales Engineer at Tenova Pyromet. Kgomotso began her career at Mintek as a Process Engineer, where she focused on process development and optimisation in both pyrometallurgical and hydrometallurgical environments. In this role, she gained hands-on experience with a broad range of commodities, including PGMs, base metals, vanadium, rare earth elements, manganese, and autocatalytic converters. In 2023, Kgomotso joined Pyromet as a Technical Sales Engineer, where she supports customers across the base metals sector by preparing technical and commercial proposals, developing cost estimates, and advising on process improvements and equipment solutions. This role enables her to leverage her practical background in extractive metallurgy to help clients tackle their unique operational challenges. Her ongoing client engagements and exposure to diverse projects offer valuable insight into the evolving requirements of the industry, allowing her to contribute to continuous improvement and innovation in the solutions delivered by Pyromet.

Optimising reverts addition in PGM smelting: Strategies for enhanced furnace stability and efficiency

C. Sikiotis[1], G. Mulder[1], J. Bezuidenhout[1], S. Matutu[2], T. Sisya[2]

[1]Hatch, South Africa
[2]Selous Metallurgical Complex, Zimbabwe

Processing and recycling of reverts in platinum group metal (PGM) smelters is essential for the recovery of PGMs and base metals. However, if reverts are recycled directly to the furnace, the feed methodology and rate of reverts addition can significantly influence process stability, energy efficiency, and refractory longevity. The process and electrical impacts of batch vs continuous reverts feeding strategies have been investigated for the Zimplats Selous Metallurgical Complex, with the key findings summarised in this paper.

The results indicate that a localised batch feeding strategy can lead to process instabilities and increased operational risk. In contrast, implementing a continuous and well-distributed reverts feed strategy can lower slag operating temperatures, resistivity, and viscosity, while supporting overall process stability. The findings provide a practical framework for optimising reverts handling systems in PGM smelters.

INTRODUCTION

In the context of platinum group metal (PGM) smelting, reverts refer to process-derived materials such as ladle and launder skulls, aisle spillages, and Peirce-Smith converter rebuild material. Reverts contain valuable materials and therefore are recycled (1) directly back to the furnace or converters or (2) with concentrate (typically after being processed in a slag plant). Reverts are often reintroduced not only to recover entrained PGMs that may otherwise be lost to waste streams, but also to temper furnace or converter temperatures (Shaw *et al*., 2014).

Reverts typically comprise predominantly converter slag, which contains large amounts of iron oxide (Sohn, 2014; Warner *et al*., 2007). Reverts therefore often act as a flux, reducing the liquidus temperature of the slag, and altering other key slag properties such as slag viscosity and resistivity. It is therefore essential to consider not only the process implications, but also the electrical implications of PGM reverts processing.

The Selous Metallurgical Complex (SMC), operated by Zimbabwe Platinum Mines (Zimplats) commissioned their 38 MW Furnace 2 (F2) in 2024. This has led to an increased reverts generation, prompting the need to determine the maximum reverts feed rate to the new furnace within the F2 operational constraints. The findings from the detailed analysis conducted for SMC have been used as the basis to provide a general framework applicable to reverts processing in the PGM industry. The work detailed in this paper leverages process engineering fundamentals, Metsim mass and energy balance modelling, FactSage modelling, industry benchmarking, and literature reviews.

REVERTS HANDLING AND FEED PHILOSOPHIES IN THE PGM INDUSTRY

Other PGM smelter reverts handling and feed philosophies were compared to SMC as detailed in the paragraphs that follow. The following bookends have been identified: batch, localised in contrast to continuous, well distributed reverts feeding philosophies.

Zimplats' current reverts handling and feed philosophy (case study)
At SMC, reverts are sorted into high-grade (converter matte) and low-grade reverts (converter slag and furnace matte). High-grade reverts are returned to converters, whereas low-grade reverts are recycled to the furnace. The reverts fed to the converters are fed via boats, uncrushed, with larger chunks broken using a rock breaker if necessary. Reverts recycling to the furnace is the focus of this paper, with no further investigation towards the converter heat balance and reverts addition philosophy.

The low-grade reverts are collected in a kibble, which is transported to the furnace lift-well area. The lift-well crane hoists the kibble to the electrode paste floor. The paste addition crane then transfers the kibble to the reverts feed hopper, where it is emptied. The vibrating feeder discharges the reverts into the feed chute leading to the furnace. Currently, the low-grade reverts are fed to the furnace in batches, dictated by the logistics associated with reverts crushing and transporting, the reverts' kibble size and the logistical inefficiencies of the hoisting system. The reverts are batch-fed to the centre of the furnace on either side of the middle pair electrodes, as illustrated by the black dots in Figure 1.

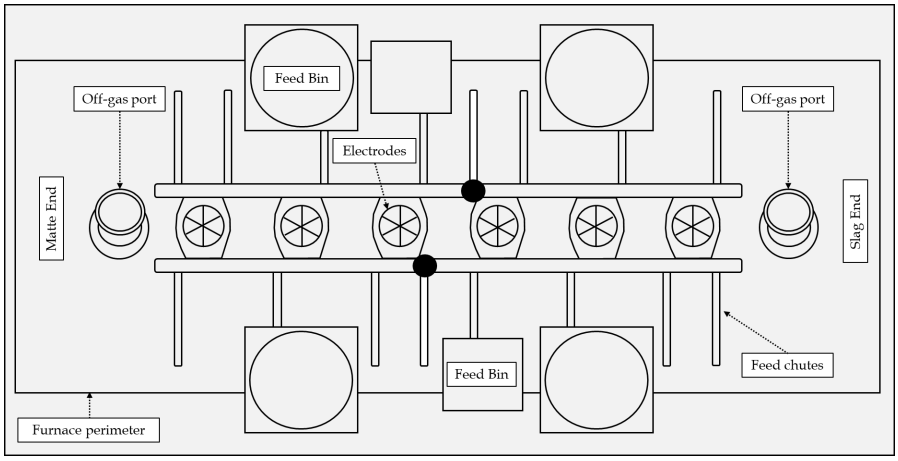


Figure 1. SMC Furnace 2 reverts addition location.

Sibanye Stillwater Marikana smelter
Reverts are repulped in a mill located within the slag plant section. The resulting repulped reverts are combined with slag concentrate from the flotation circuit, and the mixture is then thickened before being transferred to the blending section, in line with the established blending plan. (Eksteen *et al*., 2011). This ensures a well blended feed is consistently received at the furnace.

Sibanye Stillwater Columbus smelter
The concentrate is pneumatically transferred into a storage bin, while reverts are moved to a separate bin. A batching system then transfers materials from these bins into a weigh bin on load cells according to a predetermined recipe. Once the batch is prepared, it is conveyed via a bucket elevator to the furnace feed bin. From this bin, the blended feed is continuously introduced to the furnace at the target feed rate (Roset *et al*., 1992). This is another example of a well-blended, continuous-feed philosophy.

BACKGROUND

Reverts flow pattern

Ritchie and Eksteen (2011) demonstrated that there are inherent fluid flow patterns within the furnace, making it essential to consider the reverts mixing dynamics within the bath. Figure 2 (a) presents a snapshot of a tracer model developed by Ritchie and Eksteen (2011) for a circular furnace, illustrating the flow patterns originating from an electrode. The flow model shows that the material in the bath rises from beneath the electrode where it is heated, then is pushed towards the sidewall where it cools. The material will subsequently sink and return to the electrode, forming a recirculation loop as illustrated in Figure 2 (b). This loop occurs in all directions from all electrodes.

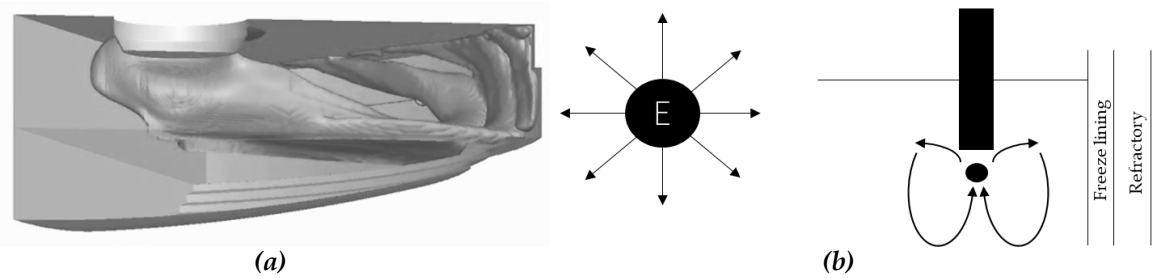


Figure 2. Flow patterns from furnace electrodes shown using (a) a slag tracer model by Ritchie and Eksteen (2011) and (b) a cross-sectional view of the recirculation loop (right). Recirculation loops occur in all directions from an electrode (left).

Batch, centralised vs continuous, well distributed feed philosophies

Two feed patterns were considered and compared for the purpose of this paper i.e., batch, centralised (or localised) and continuous, well-distributed feed patterns. The continuous, well-distributed feed profile assumes reverts are fed continuously to the furnace and is spread (with concentrate feed) throughout the entire bath. This feed profile assumes a reverts-concentrate blend that is completely homogenised upon smelting.

The batch, centralised feeding strategy assumes reverts are only fed to the centre of the furnace (such as the SMC feeding philosophy). Batch reverts feeding of variable amounts, charge durations, and frequencies will have an impact on the furnace bath dynamics due to the instantaneous changes in feed chemistry. If resistance and power setpoints are maintained, electrode immersion will vary in response to changes in bath resistance. Batch reverts addition will therefore require close management of the power-to-feed ratio to prevent process excursions that could cause damage to the crucible.

To quantify the impact of batch feeding for the SMC case study, the bath has been assumed to be divided into three feeding regimes, i.e., the first and last receiving no reverts and the centre receiving all the reverts (Figure 3). The central area therefore experiences a localised reverts feed rate equivalent to three times the true reverts feeding rate. Additionally, the batch reverts feed rate will result in higher instantaneous feed rates needed to achieve the required daily reverts processing rates.

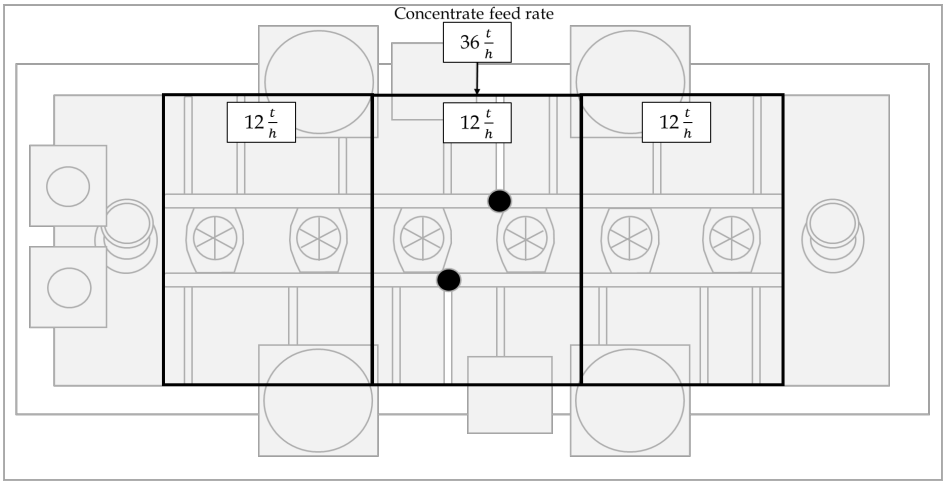


Figure 3. Impact of localised feeding (SMC case study).

A comparison of the different feed strategies for the 3% reverts addition case is illustrated in Table I.

Table I: Comparison of the different feed strategies for the 3% reverts addition case

Description	Unit	Base case	Batch, centralised	Continuous, well-distributed
Reverts addition	tpd	0 (0 % of feed)	26.4 (3 % of feed)	26.4 (3 % of feed)
	tph	0	3.3	1.1
Reverts feeding time	h	0	8	24
Localised feed rate	tph	0	9.9	1.1

METHODOLOGY

To determine the maximum possible reverts addition to the furnace, the considerations in Table II are investigated.

Table II: Impacts of furnace reverts addition investigated

Electrical and Process Limitations		Mechanical Limitations
Impact on electrical operation:	• Slag bath resistivity • Electrode pair resistance and electrode immersion • Power-voltage-current (PVI) operating window	Current design of reverts feed system
Impact on slag composition and properties:	• Slag temperatures (liquidus, operating temperatures, and superheats • Slag viscosity	
Impact on the mass and energy balance:	• Furnace power and specific energy consumption (SEC) • Furnace matte production	

Modelling method and analysis approach
Metsim modelling was used to simulate various reverts addition scenarios. The scenarios ranged from

3% to 50% reverts addition relative to the concentrate feed rate as detailed in Table III. Scenarios up to 50% were investigated to simulate potential localised conditions within the bath. The operating parameters for SMC without reverts addition (base case) are presented in Table III.

Table III: Modelling basis and reverts addition scenarios

Description	Unit	Value		
Reverts composition	% split	77% converter slag, 21% furnace matte, 2% converter matte		
Reverts FeO content	wt%	34		
Reverts addition quantities		Values in ( ) represent assumed localised SMC effect		
Scenario 1	% of concentrate feed rate	3 (9 %)		
Scenario 2		5 (15 %)		
Scenario 3		10 (30 %)		
Scenario 4		15 (45 %)		
Scenario 5		20 (60 %)		
Scenario 6		30 (90 %)		
Scenario 7		40 (120 %)		
Scenario 8		50 (150 %)		
SMC operating data *(base case, 0% reverts addition)*		Minimum	Average	Maximum
Concentrate Fe content	wt%		12	
Slag bath resistivity	Ω.cm	5.0	3.5	2.6
Electrical resistance at 30% immersion	mΩ	10	7.2	5.3
Slag bulk (90%) liquidus temperature	˚C		1389	
Slag tapping temperature	˚C	1,450	1550	1650
Slag superheat	˚C	61	161	261
Slag viscosity	Poise	5.3	3.1	1.9
SEC	kWh/t_{conc}		754	
Furnace power	MW		25	
Furnace matte production	tpd		252	

The SMC concentrate contains 12 wt.% Fe in line with others in the PGM industry (reported as 18 wt.% for Merensky type concentrate and 15 wt.% for UG2 type concentrate, Nell (2004)). The SMC F2 has a relatively low SEC of 754 kWh/t_{conc} (reported as 900 kWh/t_{conc} for SMC F1 by Mabiza (2006)) compared to others in the PGM industry (680 to 1,044 kWh/t_{conc}, Warner *et al.*, (2007)). The SMC slag temperatures are considered well within the temperatures reported for the PGM industry i.e., 1460 and 1750˚C (Warner *et al.*, 2007; Mabiza, 2006). Typically, UG2 concentrates contribute to higher slag temperatures due to the high MgO and Cr contents (Nell, 2004). As presented in this paper, higher slag temperatures can also be attributed to increased FeO content.

RESULTS AND DISCUSSIONS

The changes in slag chemistry with increasing reverts addition are indicated in Figure 4. Iron oxide in slag increases with increasing reverts addition due to reverts being predominantly converter slag.

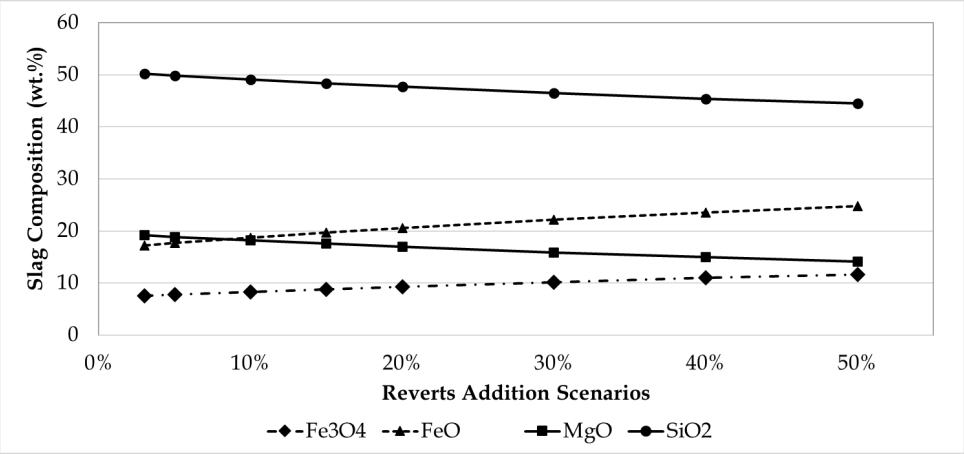


Figure 4. Impact of reverts addition on slag composition.

Electrical and processing limitations, as well as the effect of reverts on the mass and energy balance, considering the changes in slag properties, have been considered in the sections below.

Electrical limitations

The increase in iron oxide drives slag behaviour. The effect of this increase in FeO on slag bath resistivity, electrode pair resistance, electrode immersion and the PVI operating window has been investigated.

Slag bath resistivity

Electrical conductivity of the slag was calculated using the Hundermark unified equation (Equation 1) (Hundermark, 2003). With increasing reverts addition, the slag's electrical conductivity increases, resulting in a reduced resistivity (inverse of electrical conductivity) (as shown in Figure 5). Iron oxide boosts conductivity by facilitating electron exchange between Fe^{2+} and Fe^{3+} ions. Figure 5 illustrates that slag resistivity decreases at higher temperatures due to increased ion mobility, making the slag more electrically conductive (Van der Colf and Howat, 1979).

$$\ln \kappa = \left(19.9 - \frac{47348}{T}\right).X_{Al_2O_3} + \left(15.4 - \frac{24087}{T}\right).X_{CaO} + \left(9.2 - \frac{14151}{T}\right).X_{MgO} + \left(-0.5 - \frac{7478}{T}\right).X_{SiO_2} + \left(10.0 - \frac{9140}{T}\right).X_{FeO.Fe^{2+}} + \left(65.4 - \frac{82447}{T}\right).X_{FeO^2.Fe^{2+}.Fe^{3+}} + \left(-2.6 - \frac{6642}{T}\right).X_{FeO.Fe^{3+}} \quad [1]$$

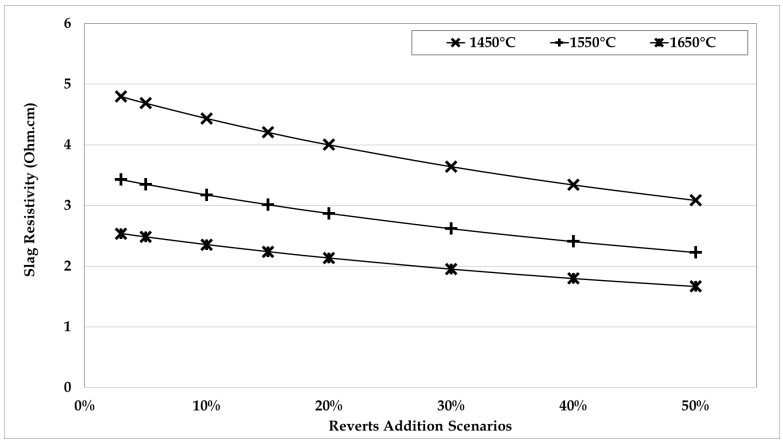


Figure 5. Impact of increasing reverts addition on slag resistivity.

Electrode pair resistance and immersion

As a result of decreasing slag resistivity, the slag bath resistance, and hence, the electrode pair resistance decreases if the electrode immersion remains constant. The decrease in electrode pair resistance with increasing reverts addition at immersion depths of 10%, 15%, and 30% is illustrated in Figure 6. It is evident that electrode pair resistance is temperature dependent, with higher slag operating temperatures resulting in lower electrode resistance at the same immersion depth.

As electrode immersion increases, resistance decreases. If resistance and power setpoints remain unchanged as reverts are fed to the furnace, the associated electrode pair will become shallower (as illustrated in Figure 7). Shallow electrode immersion can result in the following:

- Reduced slag stirring, which negatively impacts heat transfer (Eric, 2004), resulting in lower matte temperatures (Shaw *et al.*, 2014) and the upper slag layer becoming excessively superheated.
- The reduced stirring may lead to the accumulation of chrome spinels (Shaw *et al.*, 2014) but may improve prill settling to the matte (Eric, 2004).
- Brush arcing (Shaw *et al.*, 2014) and concentrate bed sintering, which can cause crust formation resulting in more frequent furnace freeboard positive pressure events (i.e., excursions in freeboard pressure resulting in off-gas expulsion).
- A thinner black top, increasing freeboard and off-gas temperatures.
- Potential to lose electrode contact, which would result in a loss of the electric arc between the electrode and the bath, leading to a loss of power transfer. This may lead to electrode wear due to repeated lowering and restriking of the arc.

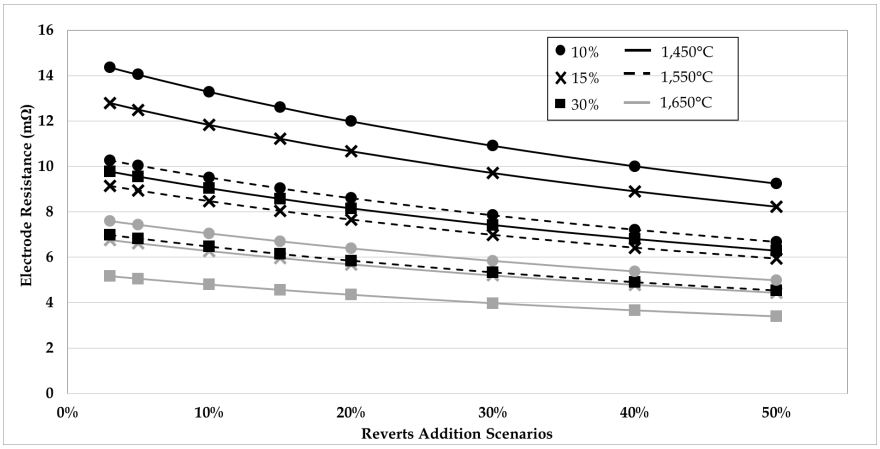


Figure 6. Electrode pair resistance as a function of increasing reverts addition at 10%, 15%, and 30% immersion.

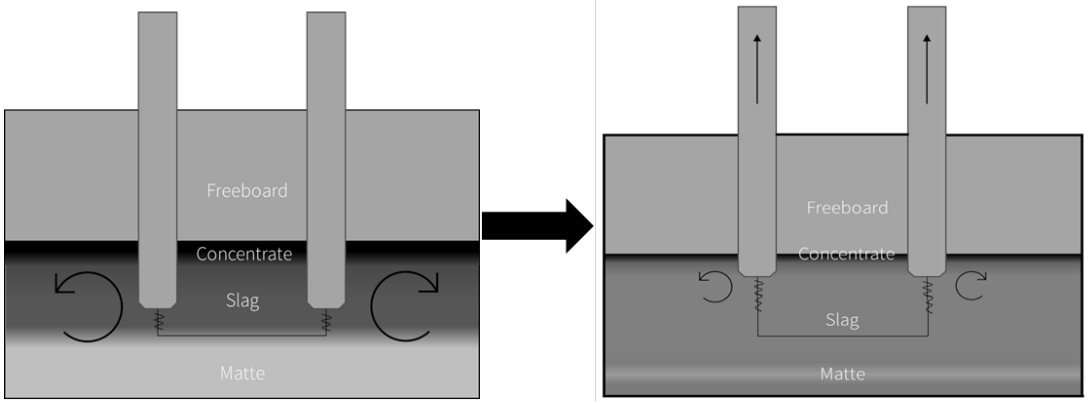


Figure 7. Impact of reverts addition on electrode immersion (if resistance and power setpoints are maintained).

PVI operating window
The electrode pair resistances should be considered on the furnace PVI diagram to determine the maximum allowable amount of reverts addition to the furnace at different immersion depths based on the furnace transformer capacity. If the reverts addition moves the operating point beyond the maximum allowable current boundary, the furnace will trip to protect the transformer. The following is noted:

- Higher operating temperatures will result in less electrical capacity to process reverts.
- More reverts can be processed at lower immersions, constrained by the risks of shallow immersion operation highlighted in the previous section.

Process limitations
The slag temperatures and viscosities have been evaluated to identify any process limitations with increasing reverts addition.

Slag temperatures (liquidus, operating temperatures, and superheats)
Reverts have fluxing properties which can lower the furnace slag liquidus temperature (as shown in Figure 8). The liquidus temperatures for the various compositions have been calculated using FactSage. If the liquidus temperature continues to vary over time, it may compromise the furnace freeze lining and integrity (Fallah-Mehrjardi *et al.*, 2014). However, continuous, well-mixed reverts addition will reduce the slag liquidus, thereby allowing for lower operating temperatures, which can lead to improved furnace integrity and a larger electrical operating window for reverts processing.

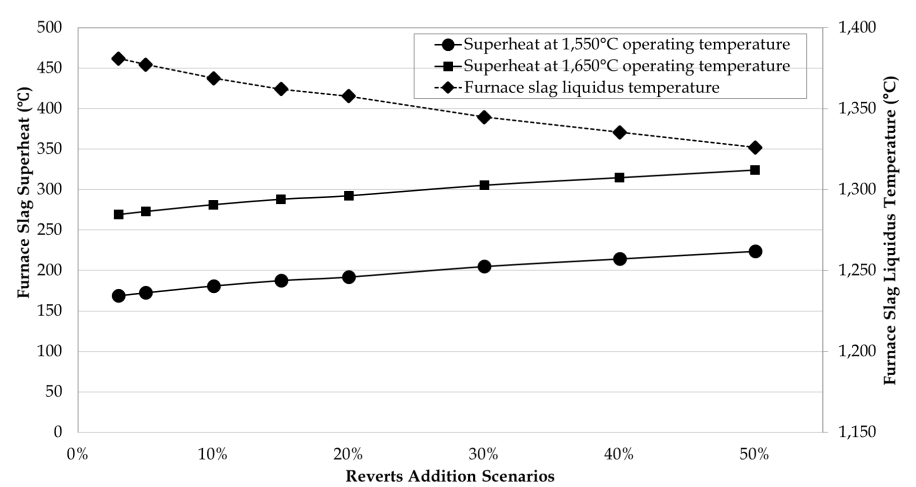


Figure 8. Impact of reverts addition on furnace slag liquidus temperature (90% bulk liquidus) and slag superheat (if high operating temperatures are maintained at 1550 °C and 1650 °C).

Slag viscosity
Iron oxide acts as a network modifier, disrupting the silicate network structure and reducing slag complexity and polymerisation (Mills, 2011). The increase in iron oxide can be seen to lower the system's slag viscosity as illustrated in Figure 9. Decreased slag viscosity will result in the following effects:

- An increased slag velocity, which can result in ease of tapping and improved matte-slag separation but may lead to increased mechanical erosion of the freeze lining and refractory (Munroe, 1986).
- Lower losses of PGMs to slag due to less entrainment of matte (Nell, 2004).

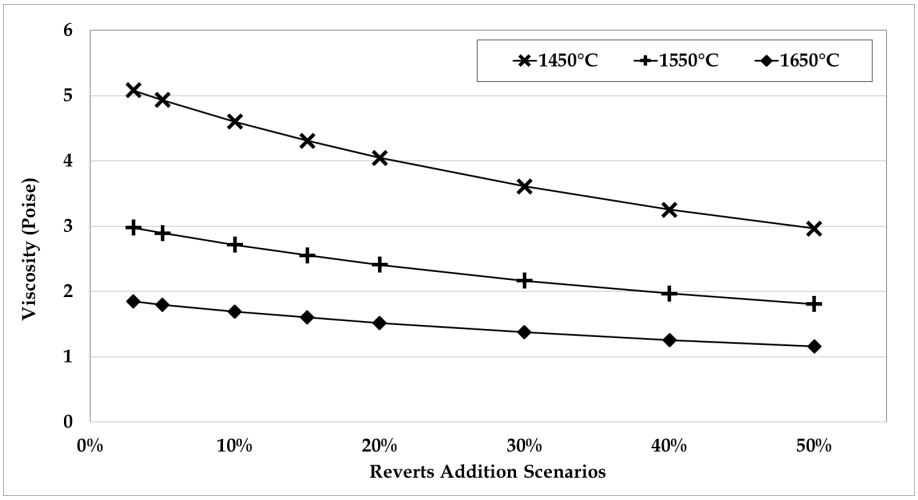


Figure 9. Impact of reverts addition on slag viscosity.

Impact on the mass and energy balance

The mass and energy balance have been evaluated to identify any further process limitations with increasing reverts addition.

Furnace power and SEC

The impact of reverts addition on furnace power and SEC is illustrated in Figure 10. An increased amount of reverts returned to the furnace would require an increase in furnace power, and as a result, an increased SEC. This is because of (1) more material requiring smelting, (2) more energy required to melt cold reverts material and (3) increased chemical reaction energy required.

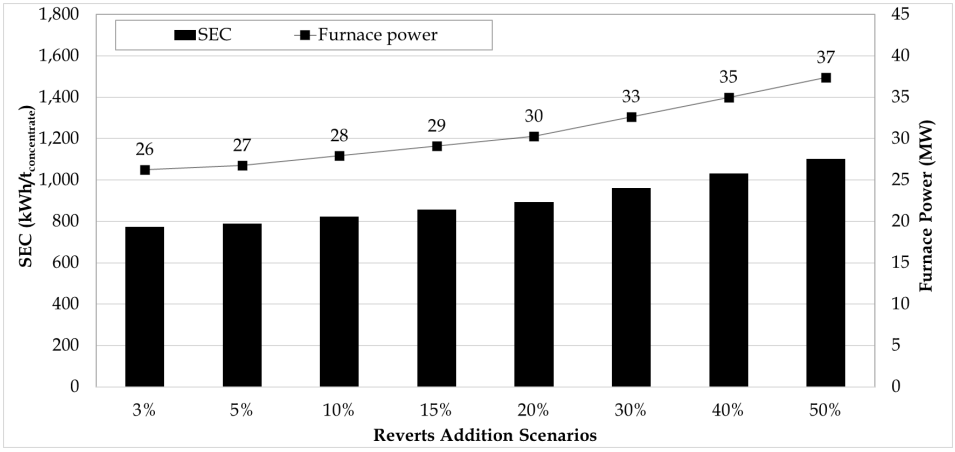


Figure 10. Impact of reverts addition on furnace power and SEC.

Furnace matte production

Reverts addition increases matte production as illustrated in Figure 11. This is attributed to matte-forming components within the reverts. Due to this, the amount of reverts that can be added may be limited by installed converter capacity as well as taphole integrity concerns.

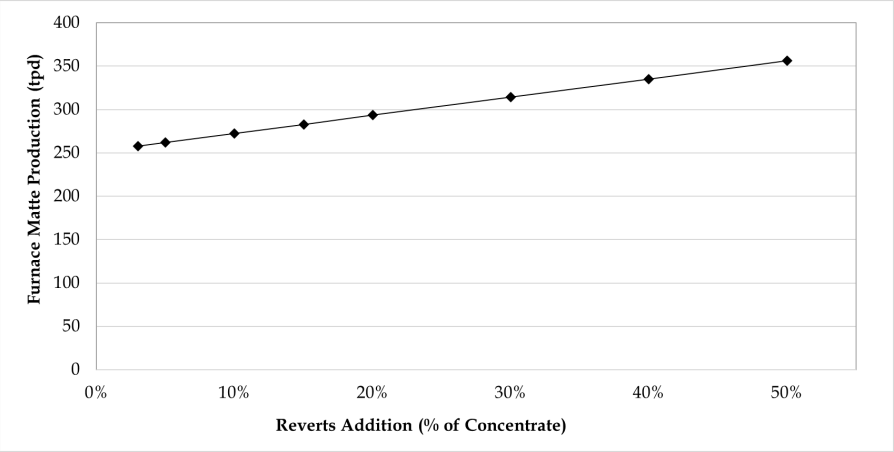


Figure 11. Impact of reverts addition on matte production.

CONCLUSION

From the work summarised in this paper it is evident that the high FeO content in reverts significantly affects the properties of the slag. This study underscores the necessity to define a reverts feed strategy to promote operational stability. Table IV shows a summary comparison of the results for the two feed strategies.

Table IV: Comparison of the results for the different feed strategies for the 3% reverts addition case

Parameter	Unit	Base case	Batch, centralised	Continuous, well-distributed
Reverts addition	tpd	0	26.4 (3 % of feed)	26.4 (3 % of feed)
	tph	0	3.3	1.1
Reverts feeding time	h	0	8	24
Localised feed rate	tph	0	9.9	1.1
Localised FeO contents	wt%	16.6	18.5	17.3
Slag bath resistivity at 1550˚C tapping temperature	Ω.cm	3.5	3.2	3.4
Electrical resistance at 30% immersion and 1550˚C tapping temperature	mΩ	7.2	6.5	7.0
Slag bulk (90%) liquidus temperatures	˚C	1,389	1,371	1,381
Slag superheat at 1550˚C tapping temperature	˚C	161	179	169
Slag viscosity at 1550˚C tapping temperature	Poise	3.1	2.8	3.0
SEC	$kWh/t_{conc.}$	754	816	774
Furnace power	MW	25	28	26
Furnace matte production	tpd	252	270	258

When reverts are fed localised, the effect on the slag properties will be concentrated at the reverts feed area. This will result in different slag properties in the bath. This effect will be exacerbated when feeding in batch mode since the reverts feed rate will vary throughout the day, causing constant changes in bath chemistry.

Additionally, electrode immersion stability will be compromised with non-homogeneous slag resistivities requiring different electrode positions throughout the furnace. These effects may increase the risk of freeze lining wear and lead to power-to-feed imbalances.

In contrast, a continuous, well-distributed reverts feed strategy will reduce the slag liquidus temperature and enable lower operating temperatures. The benefit of lower operating temperatures should however be carefully balanced against (1) higher energy requirements, (2) higher slag velocities (decreased viscosities) which may lead to increased taphole and freeze lining wear and (3) the impact on furnace matte production, which may be limited by the converter capacity.

The paper recommends a continuous, well-distributed reverts feed philosophy. If the reverts handling and feed system is constrained and prevents distributing reverts across the entire furnace bath, it is recommended that reverts are not fed in batch mode. The amount of reverts fed needs to be carefully considered after the evaluation of the effects on the properties discussed in this paper.

ACKNOWLEDGMENT

The authors would like to thank Zimplats and Hatch for permission to publish the information provided in this paper.

NOMENCLATURE

tph	Mass flowrate measured in tonnes per hour
tpd	Mass flowrate measured in tonnes per day
h	Time measured in hours
wt.%	Composition measured in weight percentage
Ω.cm	Resistivity measured in Ohm centimetres
mΩ	Electrode resistance in milliohms
◦C	Temperature measured in degrees Celsius
$kWh/t_{conc.}$	Specific energy consumption measured in kilowatt hours per tonne of concentrate
MW	Furnace power measured in megawatts
κ	Electrical conductivity
X_y	The weight fraction of component y
T	Temperature

REFERENCES

Eksteen, J.J., Van Beek, B. and Bezuidenhout, G.A. (2011). Cracking a hard nut: an overview of Lonmin's operations directed at smelting of UG2-rich concentrate blends. *Journal of the Southern African Institute of Mining and Metallurgy*, 111(10), pp. 705-716.

Eric, R.H., 2004. Slag properties and design issues pertinent to matte smelting electric furnaces. *Journal of the Southern African Institute of Mining and Metallurgy*. vol. 104, no. 09, pp. 499–520.

Fallah-Mehrjardi, A., Hayes, P.C. and Jak, E., 2014. Understanding Slag Freeze Linings. JOM, 66, pp.1654–1663.

Geldenhuys, I., Jones, R.T., McCullough, S. and Fotoyi, Z., 2010. Refractory erosion during reductive PGM matte smelting. Mintek, Randburg, South Africa. Available at: pyrometallurgy .co.za/Mintek/Files/2010Geldenhuys.pdf [Accessed 14 Aug. 2025].

Shaw, A., de Villiers, L.P.v.S., Hundermark, R.J., Ndlovu, J., Nelson, L.R., Pieterse, B., Sullivan, R., Voermann, N., Walker, C., Stober, F. and McKenzie, A.D., 2014. Challenges and solutions in PGM furnace operation: high matte temperature and copper cooler corrosion. *Journal of the Southern African Institute of Mining and Metallurgy*, 113(3), pp.233–242.

Hundermark, R., 2003. The electrical conductivity of melter type slags. Master's thesis, UCT.

Mabiza, L. 2006. An overview of PGM smelting in Zimbabwe – Zimplats operations. Presented at the Southern African Pyrometallurgy 2006 International Conference, South African Institute of Mining and Metallurgy, Johannesburg, pp. 63–76.

Mills, K.C., 2011. The estimation of slag properties. Presented at the Southern African Pyrometallurgy 2011, 7 March 2011. Department of Materials, Imperial College London.

Munroe, M.M., 1986. Refractory erosion index in electric arc furnaces. JOM, 38, pp.51–52.

Nell, J. (2004). Melting of Platinum Group Metal Concentrates in South Africa. *Journal of the South African Institute of Mining and Metallurgy*, 104 (7), 423–428.

Ritchie, S. and Eksteen, J.J. (2011). Investigating the effect of slag bath conditions on the existence of multiphase emulsion zones in PGM smelting furnaces using computation fluid dynamics. Minerals Engineering, Volume 24, Issue 7, June 2011, Pages 661-675.

Roset, G., McNeill, T.J., Millard, L.M. and Roset, G.K., 1992. Electric furnace operation at the Stillwater Mining Company's precious metals smelter. *Proceedings of the International Symposium on Non-ferrous Metals, Trace Elements, Furnace Practices and Energy Efficiency*, pp.279-287.

Sohn, H. 2014. Non-ferrous process principles and production technologies. Treatise on Process Metallurgy, p. 533. Elsevier.

Warner, A.E.M., Díaz, C.M., Dalvi, A.D., Mackey, P.J., Tarasov, A.V. and Jones, R.T., 2007. JOM World Nonferrous Smelter Survey Part IV: Nickel: Sulfide. JOM, 59(4), pp.58–72.

Van der Colf, J. and Howat, D.D., 1979. Viscosities, electrical resistivities, and liquidus temperatures of slags in the system CaO-MgO-Al_2O_3-TiO_2-SiO_2 under neutral conditions. *Journal of the Southern African Institute of Mining and Metallurgy*, 79(9), pp.255–264.



Christella Sikiotis

Process Engineer, Pyrometallurgy
Hatch Africa (Pty) Ltd

Christella is a chemical engineer with experience in the pyrometallurgical industry, focusing on PGM smelter design and process development. Her work includes operational support, process control and optimisation, techno-economic evaluations/trade-offs, Metsim and FactSage™ modeling, development of mass and energy balances, sizing and scheduling of furnaces and Peirce-Smith converters, and analysis of operational data to drive performance improvements. Christella has also been involved in the development of SO_2 fixation flowsheets, as well as technology, performance, and safety risk reviews for novel metallurgical processes. She has conducted various pyrometallurgical studies for operational smelters and has contributed to smelter process control and optimisation through the development of a smelter process control model that supports plant optimisation and operational efficiency.

Reductive matte smelting of UG2 concentrate using Al, FeSi, and SiC reductants

S.B. Nkosi, X.C. Goso

Mintek, South Africa

Merensky Reef, in the Bushveld Complex of South Africa, has been used as the primary source of platinum group metals (PGMs) over the years; however, this resource is becoming depleted. Pyrometallurgical extraction of PGMs from a Merensky concentrate has been conducted through the conventional matte smelting process, which is designed for concentrates with high sulfur and low chrome contents. Upper Group 2 (UG2) Reef in the Bushveld Complex is an alternative PGM resource, but has lower sulfur and high chrome contents, which make this resource challenging for processing using the conventional process. In the this paper, metallothermic reductive matte smelting of UG2 concentrate was investigated using Al, FeSi, and SiC as reductants for increasing the matte fall to compensate for lower sulfur content and improving the solubility of chrome in the slag. FactSage thermochemical simulations and experimentation were conducted to complete the investigations. Smelting blends of UG2 concentrate and respective reductants at 100:1 and 100:5 mass ratios were processed at 1600°C, in an inert (argon) atmosphere. Empirical smelting products, i.e., slags, mattes and matte-alloys were subjected to chemical and mineralogical characterisation. Both simulation and empirical results showed an increase in matte fall with reductant addition. Higher reductant additions resulted in the highly undesirable formation of both matte and alloy, with PGMs primarily deporting to the iron-rich alloy. Simulation results showed that a chrome-spinel [$(Mg)(Cr,Al)_2O_4$] was stable in the slag at 0% to 4% reductant additions, above which the spinel dissolved. Mineralogical analysis results showed that chrome-spinel in the slags produced using Al reductant, and FeSi at 1% addition was generally stable. The observed stabilisation of the spinel was attributed to the formation of Al_2O_3 during the aluminothermic smelting. Spinel was not detected in the slags produced using SiC reductant. The results show that SiC (and FeSi, to a lesser extent) can be effectively used for smelting UG2 concentrate, resulting in increased matte fall and solubility of chrome-spinel in the slag. Further work is recommended to optimise SiC (and FeSi) reductant additions to avoid the complication of producing separate matte and alloy during the smelting. Phase relations in the slags produced from reductive matte smelting of UG2 concentrate using these reductants should also be investigated to understand the conditions that promote the solubility of the spinel in the slag.

INTRODUCTION

The Bushveld Complex (BC) in South Africa is the world's largest source of platinum-group metals (PGMs), accounting for over 80% of global reserves. Traditionally, the majority of PGMs have been extracted from flotation concentrates of the Merensky Reef, which has historically provided an ore feed of favourable mineralogy for conventional pyrometallurgical processing. The Merensky ore contains abundant base-metal sulfides such as pentlandite, chalcopyrite, and pyrrhotite. These minerals play a vital role as natural collectors of PGMs during smelting because they readily form a nickel–copper matte phase that efficiently collects PGMs (Jones, 2005; Nell, 2004).

The gangue minerals in Merensky concentrates consist mainly of feldspathic and pyroxenitic silicates with only minor chromite content. This mineralogical balance enables stable furnace operation, since the low Cr_2O_3 levels in the slag (<1.5 wt.%) prevent excessive spinel precipitation and ensure fluidity of the molten slag. Consequently, furnace slags are manageable, and matte grades are stable, leading to efficient recoveries of PGMs into the matte phase. Over several decades, the process flowsheet of drying, smelting in electric furnaces, converting, and hydrometallurgical refining has been optimised for Merensky ores and remains one of the most reliable industrial approaches for PGM recovery.

As reserves of Merensky ore have declined, mining has increasingly shifted toward the Upper Group 2 (UG2) reef, a geologically distinct horizon in the BC. UG2 ore differs from Merensky ore, both mineralogically and metallurgically. UG2 is dominated by Fe–Cr spinel (chromite) and contains relatively low concentrations of sulfide minerals (Nell, 2004; Cramer, *et al.,* 2004).

While UG2 often carries equal or even higher PGM contents compared to Merensky, its mineralogy introduces significant challenges for smelting operations. The high chromite content in UG2 results in slags that have high Cr_2O_3 contents. The Cr_2O_3 content in feed material must be controlled to avoid spinel precipitation (Jones, 2015; Eksteen, 2011). These spinels are highly refractory and stable, creating multiple metallurgical problems such as:

1. The viscosity of the slag becomes higher, which hinders the separation of the matte, alloy, and slag phases.
2. PGMs become trapped as metal droplets in the spinel phase, resulting in lower recoveries.
3. Refractory linings in the furnace get damaged, as spinels stick to the bricks. This may cause refractory erosion, unexpected furnace downtime, and higher maintenance (Shaw, *et al.,* 2013; Eksteen, 2011; Barnes & Newall, 2006).

In addition, the limited sulfur content in UG2 ore prevents the formation of sufficient quantities of the matte phase. As the matte serves as the main phase for concentrating the PGMs, insufficient sulfides reduce the overall effectiveness of the smelting process. In the absence of adequate sulfides, PGMs are likely to report to the slag or to become incorporated within the spinel phase, which further decreases the PGMs recoveries. (Jones & Geldenhuys, 2011).

A variety of methods have been investigated to address the challenges of smelting UG2 concentrates. The most common industrial practice has been the blending of UG2 with Merensky concentrates. Merensky concentrate supplies additional sulfur that promotes matte formation while lowering the chromite content from the UG2 concentrate. This blending strategy has enabled smelters to process higher proportions of the UG2 concentrate without experiencing major furnace complications. Since the depletion of the Merensky is ongoing, this smelting approach is no longer viable (Jones, 2005).

Technologies such as column flotation and other fine particle separation techniques have been applied to reduce chromite entrainment in concentrates. These methods can significantly lower the Cr_2O_3 content in the furnace, improving slag chemistry and reducing spinel precipitation. Nonetheless, such advanced beneficiation steps increase processing costs and require additional water and energy inputs, which limit their adoption across the industry (Hay & Roy, 2010).

Hydrometallurgical solutions such as the Kell process have been proposed to bypass smelting altogether. The Kell process involves oxidative leaching of base metals and PGMs under controlled conditions, thereby avoiding the problems caused by chromite-rich slags (Liddell & Adams, 2012). Similarly, bioleaching has been investigated as a pre-treatment step to selectively remove base metals before smelting. While these approaches appear promising, they remain largely experimental or at a pilot scale, and commercial adoption has been limited.

One of the most significant technological innovations in this field is the ConRoast process, developed by Mintek. ConRoast was designed to treat high-chromite UG2 concentrates. The process involves dead-roasting the concentrate to remove sulfur, followed by smelting the calcine in a DC arc furnace. This yields a base-metal alloy enriched in PGMs and a chromium-tolerant slag, avoiding the traditional

matte–slag system that is sensitive to Cr_2O_3 levels. ConRoast can successfully treat 100% UG2 concentrate while maintaining high PGM recoveries and offering environmental advantages such as a sulfur-free off-gas stream (Jones, 2002). In parallel with blending and ConRoast, increasing attention has been directed toward reductive smelting strategies that employ strong reductants to control chromite-related problems. The principle of reductive smelting is to use chemically active reductants to destabilise spinel phases and reduce oxides, thereby improving slag fluidity and enhancing matte and alloy formation (Jones, 2002).

The ongoing transition from Merensky to UG2 concentrates has exposed the South African PGM industry to severe metallurgical constraints. Blending and ConRoast have demonstrated partial success, but long-term sustainability and cost-effectiveness remain uncertain. Reductive matte smelting represents a promising pathway forward, offering the potential to:

- Improve chromite management by reducing spinel precipitation
- Enhance matte formation even with low sulfide feed
- Increase PGM recoveries by minimising slag entrapment
- Lower furnace energy consumption through exothermic reduction reactions

Jones and Geldenhuys (2011) reviewed the principles, benefits, and limitations of reductive matte smelting for UG2 concentrates. They noted that the process can improve PGM recovery from high-chromium, low-sulfur ores by lowering slag viscosity and enhancing phase separation, which also reduces refractory wear and produces cleaner collector phases. However, they emphasised that excessive reduction can lead to contamination of the metal or matte phase, difficulties in process control, and high energy requirements. Most importantly, they highlighted the significant risk of furnace failure under conditions where both alloy and matte occur together, and documented how a highly superheated high-sulfur alloy caused a failure near the alloy tap-hole of the pilot-plant furnace and resulted in a series of highly dangerous metal-water explosions. Overall, their work underlines that reductive matte smelting can be an effective strategy for processing challenging UG2 concentrates, provided that slag composition and process conditions are carefully managed to optimise both recovery and product quality (Jones & Geldenhuys, 2011).

Malan *et al.*, (2015) investigated the use of silicon carbide (SiC) as a reductant in smelting low-grade UG2 concentrates, which are difficult to treat by conventional matte smelting. Their results showed that SiC promoted the formation of an iron alloy phase that effectively collected PGMs, achieving over 85% recovery of Ir and Pd and about 60% recovery of Pt. This study has proved that the use of SiC results in higher PGMs recoveries and that SiC can be used as an alternative reductant to carbon (C).

Continued laboratory-scale and pilot-scale research is therefore essential to validate the feasibility of reductive smelting and to determine its role in complementing or competing with established solutions such as ConRoast. By addressing the key challenges of UG2 processing, reductive smelting using reductants such as aluminium (Al), ferrosilicon (FeSi), and silicon carbide (SiC) could provide a scalable and industry-compatible approach to sustaining South Africa's position as the world leader in PGM production.

EXPERIMENTAL PROCEDURES

Thermochemical Simulations

Thermochemical simulations for the reductive matte smelting of the UG2 concentrate were conducted using FactSage 8.3 software. The databases employed included FactPS (pure substances), FToxid (oxide phases), FTsulf (sulfide phases), and SGTE (alloys). All solution phases in the respective databases were active. Stable phases were determined by the software, shown by an activity of unity. The simulation of the smelting of UG2 concentrate was conducted at 1600°C, with varying additions of Al/ FeSi/ SiC reductant from 0% to 20%. Considering that slag solution databases do not typically include all the PGMs, the calculated deportment of the PGMs between product phases was anticipated to be distorted. However, simulation results were anticipated to provide reliable results regarding the slag phases,

which would assist to shed light on the stability of the detrimental chrome spinel phase in the reviewed range of conditions. Simulation results were useful in guiding the experimental work.

Raw Materials
The UG2 concentrate used in this study was provided by one of the major PGM smelters in South Africa. The as-received UG2 concentrate was split into 20 representative samples of about 2 kg using a rotary splitter. The reductants used in these experiments were Al, FeSi, and SiC. These raw materials were subjected to chemical analysis using the techniques described below.

Chemical analyses of the concentrate, reductants, and smelting products were conducted using:

- A Varian Vista-PRO CCD simultaneous inductively coupled plasma optical emission spectrometer (ICP-OES) for the determination of Al, Ca, Co, Cr, Cu, Fe, Mg, Mn, Ni and Si,
- CS744 LECO combustion instrument for the determination of S,
- Fire assay (6E) coupled with ICP-OES for the determination of PGMs and Au, and
- Bruker D8 advanced X-ray diffractometer (XRD) and a JEOL JXA-8230 electron probe microanalysis (EPMA) for the determination of chemical phases in the slag products.

Empirical Smelting Testwork
Bench-scale reductive matte smelting tests were conducted using a 100 kVA tilting induction furnace equipped with a SiC susceptor crucible, using a 3 kg sample. The crucible was preheated to 1600°C under argon, and UG2 and reductant blends were charged using a steel scoop. After reaching full melt, the charge was held at temperature for 60 minutes. The furnace was tilted to tap the molten products into a ladle. After cooling, the products were weighed and separated.

Collected slags were subjected to XRD analysis to identify crystalline phases and were also prepared for EPMA analysis to provide microstructural and compositional information. Simulation results showed that at low reductant additions, spinel crystals occurred in the slag at 1600°C. However, higher additions of >3% for all three reductants resulted in significant reduction in quantities of spinel phase. Hence, two reductant additions at high and low spinel crystallisation zones were selected for each of the reductants. As the behaviour in terms of spinel formation was similar for all three reductants, the same addition pointes of 1% and 5% to the mass of concentrate were used for all reductants.

RESULTS AND DISCUSSION

Chemical analysis of raw materials
Chemical compositions of raw materials, i.e., UG2 concentrate, Al, FeSi, and SiC reductants, are presented in Table I to Table III. To facilitate effective simulation of the smelting process, sulfur and chromium in the samples were expressed in terms of their typical mineral phases, such as chalcopyrite ($CuFeS_2$), pentlandite (NiS), pyrite (FeS_2) and chromite ($FeCr_2O_4$). The UG2 chemical composition resembles the typical UG2 concentrate from the Bushveld Complex, with relatively low contents of sulfide phases and high chromite.

Table I: Chemical composition of the UG2 concentrate (mass %)

Al_2O_3	CaO	Co	$FeCr_2O_4$	$CuFeS_2$	FeS_2	Fe_3O_4	MgO	MnO	NiS	SiO_2	TiO_2	C	PGMs+Au	Total
4.66	2.50	<0.05	4.02	2.69	2.80	9.46	22.45	0.14	2.94	45.60	0.31	0.28	0.06	97.92

Table II: Individual PGM concentrations (ppm)

Au	Pd	Pt	Rh	Ru	Ir	**Total**
1.99	126.33	271.33	51.83	83.80	15.24	**550.53**

Table III: Chemical compositions of the reductants (mass %)

Reductant	Al	Fe	Mn	Si	C
Al	99.31	0.25		0.44	
FeSi	0.32	15.4	0.13	85.7	0.03
SiC				70.05	29.95

Thermochemical simulations

100% UG2 with Al reductant

Thermochemical simulation results of smelting the UG2 concentrate with Al as a reductant at 1600°C predicted the formation of alloy, matte, slag, and spinel phases, as shown in Figure 1 (a). The alloy production began to increase from about 5% Al addition, while matte yield peaked around 6% before declining at higher Al additions. The slag showed a steady increase in mass from 0% to 15% Al additions, suggesting the formation of Al_2O_3 that reports to the slag phase. The spinel was present at low Al reductant levels (0–3%), disappeared between 4–14% Al additions, and reappeared from 15% onwards. The recovery of PGMs+Au to the alloy at different Al additions is shown in Figure 1 (b). The result showed low recoveries between 0% and 3% Al additions, which may be associated with spinel that formed at low Al additions. After 3% Al additions, the PGMs+Au recoveries increased significantly up to 4% Al additions. These high recoveries were associated with no spinel formation within the Al addition range. The slight decrease in the PGMs+Au recoveries to the alloy after 4% Al addition was associated with the PGM distribution between the matte and the alloy phases.

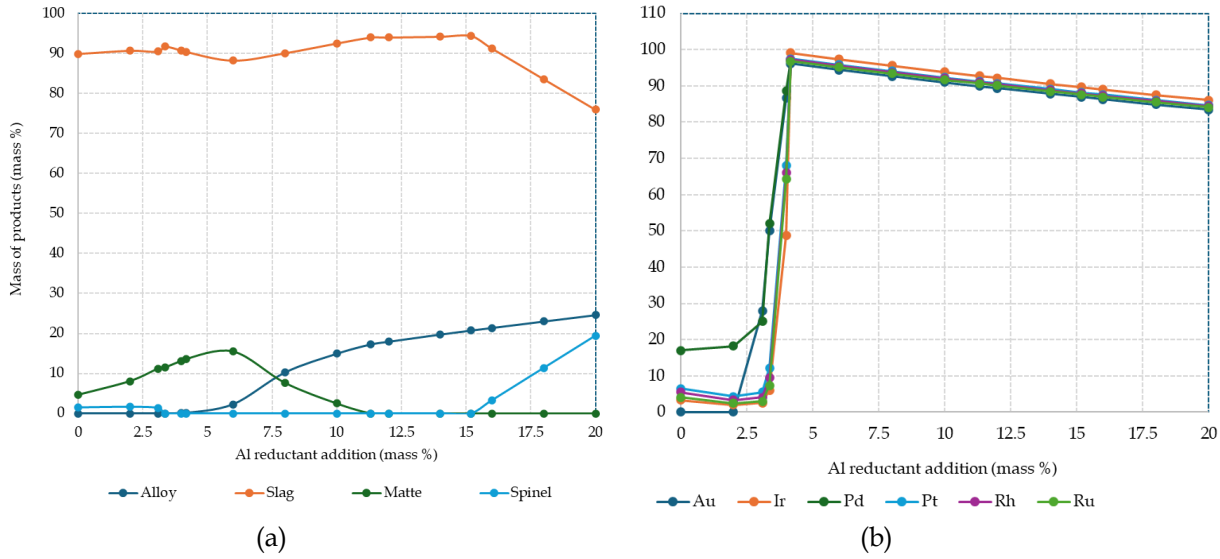


Figure 1: (a) Calculated masses of the products produced after smelting UG2 concentrate with Al reductant, (b) Recoveries of PGMs+Au to the alloy after smelting UG2 concentrate with Al reductant.

100% UG2 with FeSi reductant

Masses of alloy, matte, slag, and spinel obtained from reductive smelting of UG2 concentrate with varying FeSi additions at 1600°C are presented in Figure 2 (a). The slag mass remained relatively constant across all FeSi levels. The matte mass increased with FeSi additions from 0% to 5%, after which it decreased as the alloy mass increased. Spinel mass remained consistently low (<1%) for all FeSi additions examined. Figure 2 (b) presents the recoveries of PGMs and Au to the alloy. The recoveries were low between 0 and 3% FeSi addition, then significantly increased between 3% and 4% FeSi additions. After 4% FeSi additions, the recoveries for all PGMs+Au to the alloy started to decrease, indicating a distribution of PGMs+Au between the matte and alloy phases.

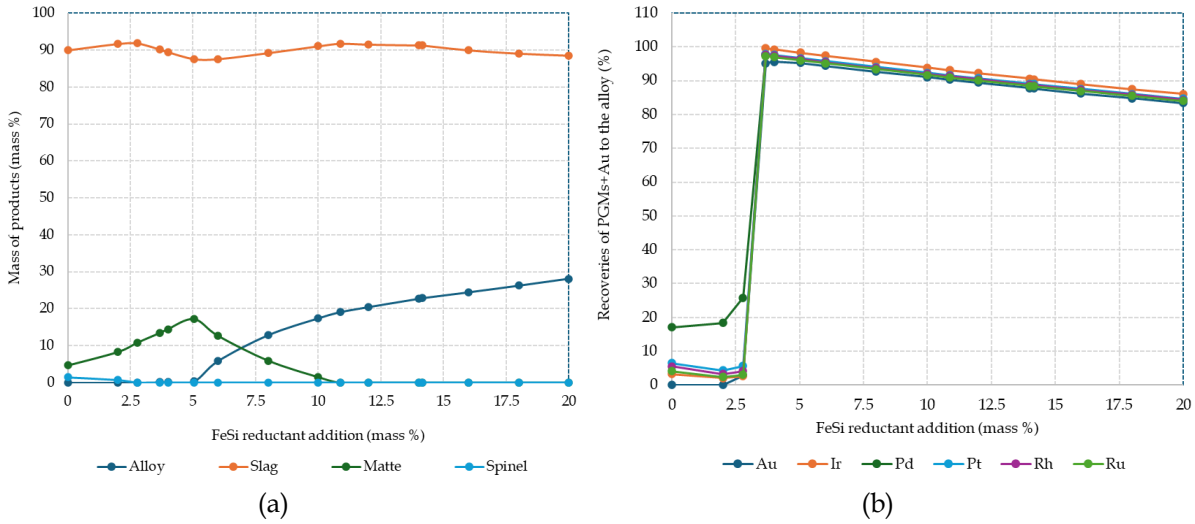


Figure 3: (a) Calculated masses of the products produced after smelting UG2 concentrate with FeSi reductant, (b) Recoveries of PGMs+Au to the alloy after smelting UG2 concentrate with FeSi reductant.

100% UG2 with SiC reductant

The masses of alloy, matte, slag, and spinel obtained from smelting UG2 concentrate with SiC reductant at 1600°C are shown in Figure 3 (a). The slag mass decreased progressively with increasing SiC addition. The matte mass increased between 0% and 4% SiC addition but declined thereafter. In contrast, the alloy mass began to increase beyond 4% SiC addition, while the spinel mass remained consistently low across the entire range of reductant additions. The PGMs+Au recoveries to the alloy are illustrated in Figure 3 (b). PGM recoveries increased with SiC additions from 0% to 3%, after which the recoveries slightly decreased. Au recoveries to the alloy increased between 2% and 6% SiC addition, remained steady between 6% and 8%, and then declined at higher SiC levels. The slight decline in PGMs recoveries were visible when the mass of the alloy started to increase, suggesting the distribution of the PGMs between the matte and the alloy. It should be noted that the partitioning of the PGMs between the product streams is anticipated to be distorted due to the lack of PGMs in some slag and matte databases.

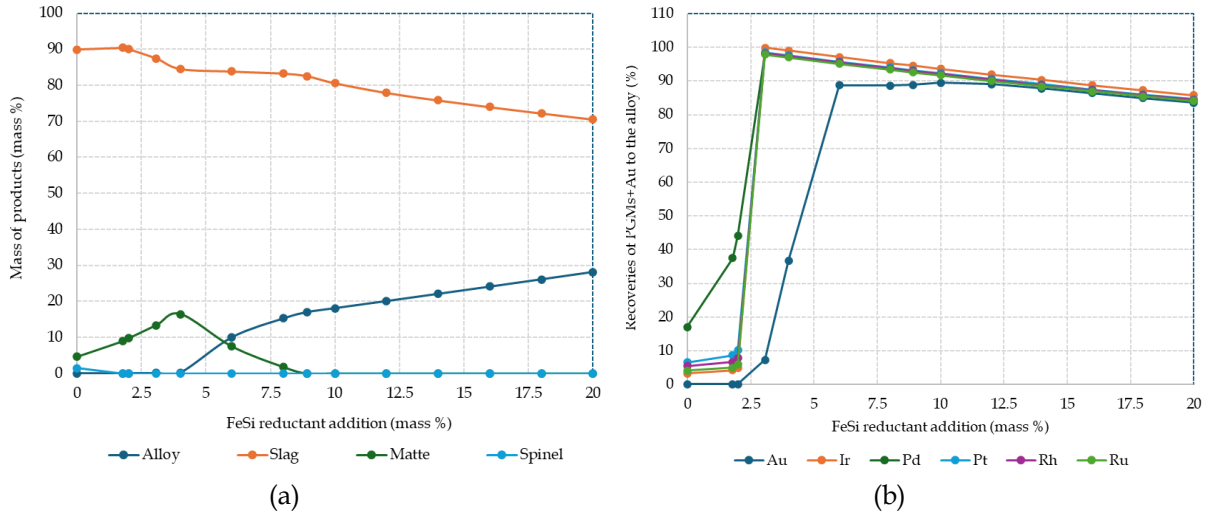


Figure 3: (a) Calculated masses of the products produced after smelting UG2 concentrate with SiC reductant, (b) Recoveries of PGMs+Au to the alloy after smelting UG2 concentrate with SiC reductant

Empirical Smelting Testwork

Smelting product masses

Smelting product masses produced from the mini-pilot tests are presented in Table IV. The results show an increase in the alloy fall with increasing reductant additions. The highest alloy fall of 7.5% was attained when 5% FeSi was used as a reductant. The slag masses generally decreased with increasing Al and SiC reductant additions. These results were supported by the thermochemical simulation results, which showed an increase in alloy slag masses with increasing reductant additions. Though simulation results predicted the formation of matte at 1% and 5% reductant additions, matte could not be effectively separated from the slag and alloy. According to the simulation results, the mass of matte was higher than the alloy mass at 1% and 5% additions of the respective reductants. Thus, the lack of accounting for the matte had a potential to distort the results of the study.

Table IV: Bench-scale smelting product masses

	Feed masses, kg				Product masses, kg		Product masses, %		
Test	UG2	Al	FeSi	SiC	Alloy	Slag	Alloy	Slag	Loss
1	3.01				0.12	2.88	3.94	90.71	5.34
2	3.02	0.03			0.19	3.92	4.51	93.19	2.30
3	3.01	0.15			0.16	2.77	5.36	90.43	4.20
4	3.03		0.03		0.12	2.92	3.92	87.84	8.24
5	3.03		0.15		0.20	2.49	7.54	90.66	1.80
6	3.04			0.03	0.18	2.87	5.77	93.26	0.98
7	3.02			0.15	0.20	2.81	6.58	87.99	5.42

Chemical compositions of the slags

Chemical compositions of the slags are presented in Table V. Total PGMs+Au contents in the slags were generally high, mainly due matte entrainment. The results did not show a specific trend likely due to smelting product separation challenges.

Table V: Chemical compositions of the slags (mass %)

Test	Al_2O_3	CaO	Cr_2O_3	FeO	MgO	MnO	SiO_2	TiO_2	PGMs+Au (ppm)
1	7.06	2.75	1.11	2.75	24.80	0.13	56.40	0.33	71.30
2	8.43	2.72	1.15	5.35	24.20	0.13	54.60	0.32	23.86
3	15.70	2.80	0.95	1.39	24.40	0.12	53.30	0.33	23.59
4	6.99	2.59	0.96	2.21	24.90	0.13	54.40	0.33	71.60
5	6.97	2.73	0.92	2.76	24.70	0.14	56.30	0.37	91.78
6	9.21	2.78	0.75	1.74	33.70	0.14	44.80	0.43	42.64
7	11.40	3.00	0.80	1.79	25.20	0.18	54.40	0.53	45.16

Chemical compositions of the alloys

Chemical compositions of the alloys are presented in Table VI. The results show that the alloys mainly comprised Fe, Si, Ni, Cr, and Cu. S contents in the alloys were <1%. Alloy chemical compositions also did not show conclusive results regarding the effect of different additions of Al, FeSi, and SiC reductants. However, these results show that the PGMs and Au were significantly concentrated in the alloy phase.

Table VI: Chemical compositions of the alloys (mass %)

Test	Co	Cr	Cu	Ni	Si	Fe	S	PGMs+Au (ppm)
1	0.36	6.04	3.47	12.10	10.15	64.85	0.91	4165
2	0.37	6.65	3.99	12.50	7.84	62.30	0.91	4407
3	0.39	4.70	3.24	13.40	10.20	64.70	0.75	4022
4	0.32	7.79	3.89	11.00	10.60	63.00	0.56	3180
5	0.31	8.33	4.45	10.50	13.70	61.20	0.44	3357
6	0.35	8.63	4.13	10.73	9.64	65.42	0.43	2327
7	0.29	9.53	4.82	10.15	12.00	61.35	0.30	2225

PGMs+Au recoveries and distributions

Total PGM recoveries were calculated using Equation [1] based on the slag chemical analysis results and are presented in Table VI. PGM recoveries to the alloy were generally low and were also inconclusive about the effect of different additions of the tested reductants. These adverse phenomena were attributed to the product separation challenges, which resulted in non-accountability for the matte stream. However, these results are conclusive in that reductive matte smelting of UG2 concentrate using Al, FeSi, or SiC results in PGMs and Au primarily reporting to the alloy stream.

$$\text{Recovery} = \left(1 - \frac{\text{mass of PGEs+Au in slag}}{\text{mass of PGEs+Au in feed}}\right) \text{x } 100 \qquad [1]$$

Table VII: Recoveries of PGMs+Au based on the slag chemical compositions

Test	**Recovery**
1	**88.6**
2	**94.8**
3	**96.4**
4	**88.5**
5	**87.4**
6	**93.3**
7	**93.0**

Mineralogical characterisation of furnace slags

The different phases detected from XRD are presented in Table VIII. XRD patterns of the slags produced from the different tests show that the slags are primarily crystalline silicates belonging to the pyroxene and olivine mineral groups. This observation is in line with previous studies on PGM smelting slags, which identified pyroxene (clinopyroxene/orthopyroxene) and olivine (forsterite–fayalite solid solutions) as the dominant crystalline phases (Nell, 2004). Spinels were not identified by the XRD, which might be due to their concentration falling below the detection limit of XRD.

Table VIII: Different phases detected by XRD.

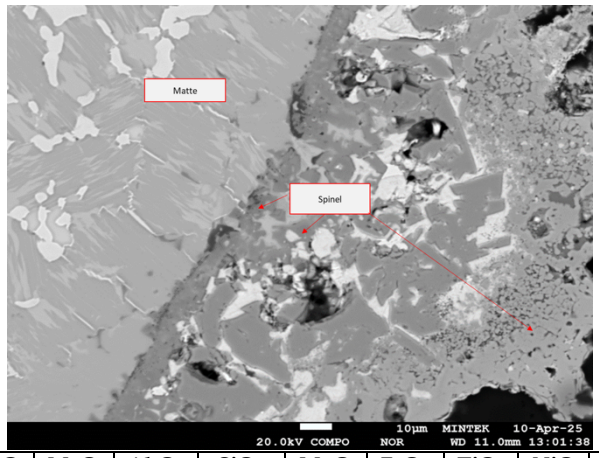
Phase	Test 1	Test 2	Test 3	Test 4	Test 5	Test 6	Test 7
Clinopyroxene	*****	*****		*****	*****		***
Orthopyroxene	***	****	***	****	***	***	****
Olivine			*****			*****	****
Periclase					**		
Iron silicon					*		*
Quartz							*
***** predominant, **** major, *** intermediate, ** minor, *trace							

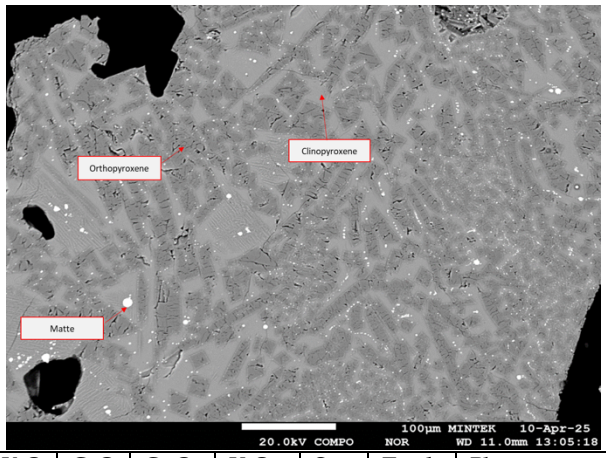
EPMA results are shown from Figure 4 to Figure 10. Microstructures show significant presence of matte phases occurring across the slag matrix. Thus, the missing masses of mattes in the product mass distribution in Table IV are confirmed to be entrained in the slags. Lack of separation of matte from the slag was attributed to possible high viscosities of the slags, which also had unconventionally lower FeO content.

EPMA results confirmed the presence of small spinel grains, mainly at slag–matte interfaces. This spatial distribution indicates that spinel crystallisation occurred preferentially at interfacial zones, where Cr and Fe were locally enriched, and oxygen gradients can promote nucleation. The fact that spinels are scarce in bulk slag but more common at interfaces aligns with observations by Schouwstra *et al.*, (2010), who noted that chromite and related spinels segregate into boundary regions during subsequent processing. The spinels identified are polymorphic, with both high-Cr and low-Cr contents. The cation distribution shows variable proportions of Mg, Fe, and Mn, but notably low Al concentrations. The absence of Al-rich spinels suggests that Al is preferentially incorporated into silicate phases rather than spinels. EPMA confirmed elevated Al and Si in the pyroxene and olivine phases. This agrees with Park and Min (2005), who demonstrated that silicate melts with high Al_2O_3 stabilise Al substitution into pyroxene rather than spinel crystallisation.

A particularly interesting observation was the presence of eskolaite (Cr_2O_3) in some slags. This indicated that under certain conditions, Cr did not enter the spinel lattice but instead crystallised as a simple oxide. The presence of eskolaite is industrially significant because it is highly refractory and can accumulate in furnace linings, causing operational challenges. In the current study, eskolaite could have formed during cooling outside of the furnace.

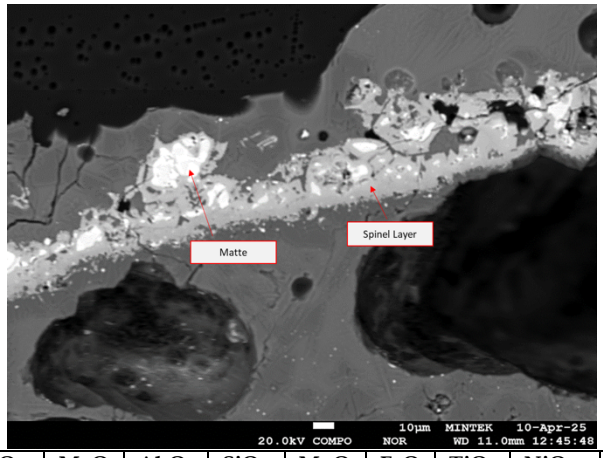
High Al and Si concentrations in silicate phases compared to stoichiometric pyroxenes and olivines point to significant substitution mechanisms. Augite and omphacite structures (clinopyroxene) allow substantial Al-for-Si and Ca-for-Mg substitution, while orthopyroxenes (enstatite) also tolerate Al substitution at the tetrahedral site. The non-stoichiometric compositions observed here reflect these substitutions and suggest that silicates act as a major capture for Al in the slag system. The limited presence of Al-bearing spinel could be attributed to the preferential stabilisation of Al within the silicate matrix, which reduced the thermodynamic favourability of its incorporation into the spinel structure.

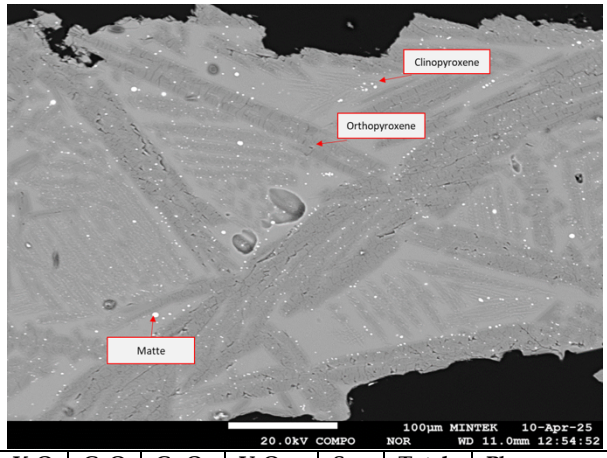




Na_2O	MgO	Al_2O_3	SiO_2	MnO	FeO	TiO_2	NiO	K_2O	CaO	Cr_2O_3	V_2O_5	S	Total	Phase
0.05	0.09	0.05		0.06	0.54	1.68	0.09	0.01	0.02	96.10	1.03	0.19	99.92	Eskolaite
0.05		0.04		6.79	24.32		0.04	0.01	0.02	66.97	0.10	0.39	98.72	Cr-Fe Spinel
0.07	14.61	0.11	0.24	1.48	6.32	3.23	0.24	0.01	0.05	68.09	1.03	2.10	97.57	Cr-Mg Spinel
2.26	13.11	12.91	62.77	0.11	0.10	0.50	0.03	0.34	6.25	0.39	0.04	1.61	100.42	Clinopyroxene
0.36	38.32	1.41	59.72	0.06	0.11	0.19	0.01	0.04	0.37	0.44	0.04	0.39	101.48	Orthopyroxene
1.14	27.49	6.90	60.58	0.10	0.16	0.29	0.02	0.19	2.74	0.53		1.20	101.34	Glass
0.05	0.14	0.13	100.32		0.06			0.01	0.03			0.03	100.78	Quartz

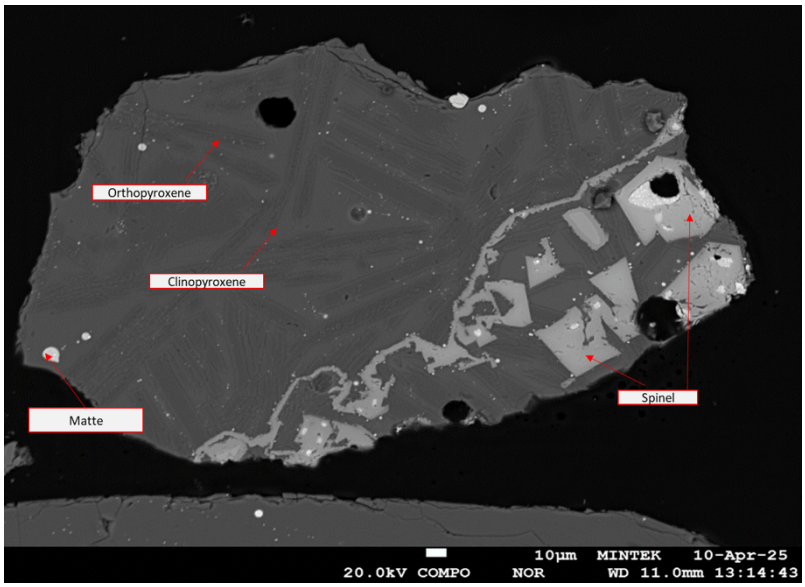
Figure 4: EPMA results of Test 1 slag.





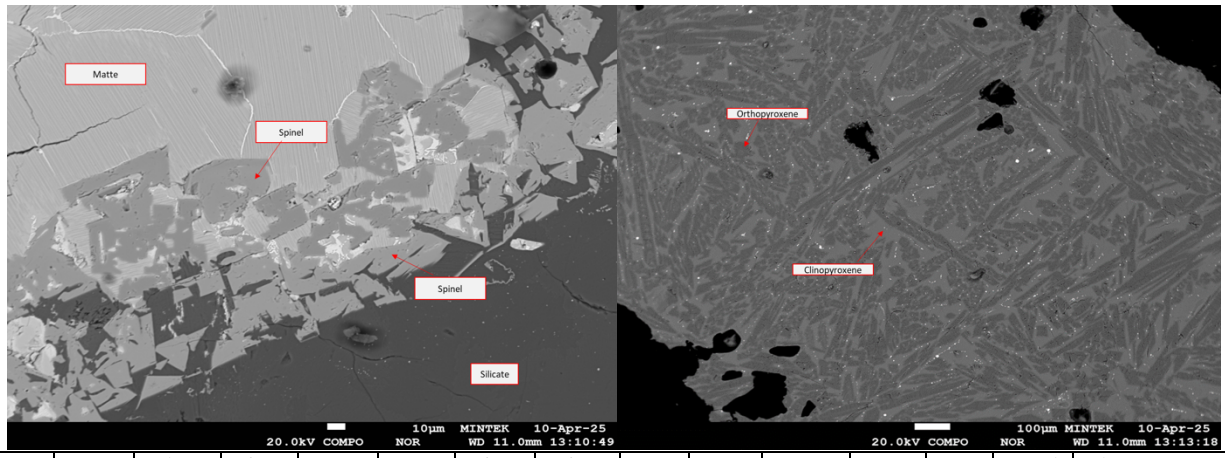
Na_2O	MgO	Al_2O_3	SiO_2	MnO	FeO	TiO_2	NiO	K_2O	CaO	Cr_2O_3	V_2O_5	S	Total	Phase
0.09	13.12	0.24	0.52	1.17	9.97	2.05	0.05	0.01	0.07	69.95	0.79	0.44	97.96	Low Cr-Spinel
0.12	0.05	0.05		0.06	0.62	0.90	0.06		0.03	95.27	1.58	0.18	98.92	Eskolaite
1.31	14.57	15.44	60.33	0.12	0.10	0.40		0.28	5.91	0.41		1.54	100.42	Clinopyroxene
0.12	38.61	1.89	59.40	0.06	0.09	0.19	0.01	0.03	0.37	0.34	0.04	0.19	101.15	Orthopyroxene
0.91	24.85	9.70	59.52	0.10	0.08	0.33		0.18	3.63	0.52		0.97	100.79	Glass

Figure 5: EPMA results of Test 2 slag.



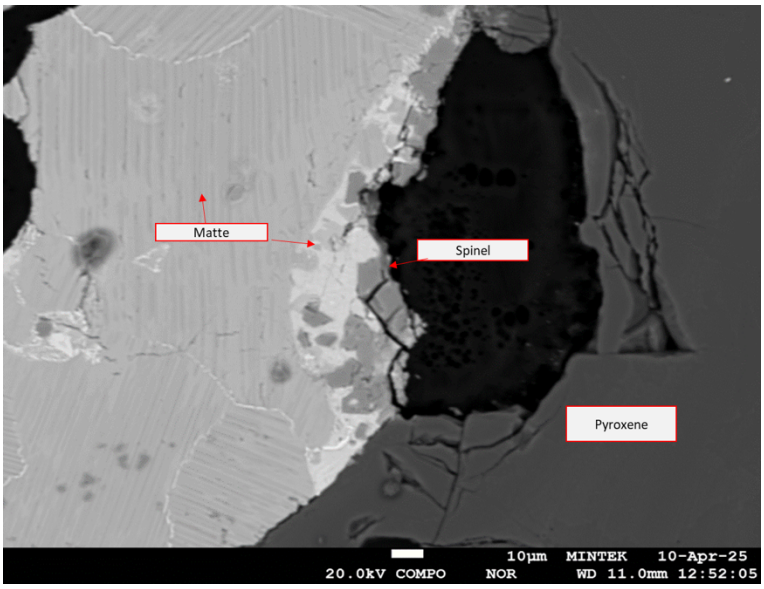
Na_2O	MgO	Al_2O_3	SiO_2	MnO	FeO	TiO_2	NiO	K_2O	CaO	Cr_2O_3	V_2O_5	S	Total	Phase
0.03	5.07	0.06		2.39	20.12	0.65	0.03	0.01	0.06	69.60	0.61	0.31	98.93	Low Cr-Spinel
	0.08	0.09		0.08	1.30	3.22		0.01	0.11	93.06	1.20	0.02	99.17	Eskolaite
0.03	10.08	0.12		1.67	13.25	0.81	0.02	0.01	0.11	71.11	0.63	0.22	98.05	High Mg Spinel
0.25	47.11	4.99	46.66	0.05	0.14	0.14		0.08	0.90	0.38	0.04	0.54	101.24	Olivine
0.09	35.76	10.13	53.63	0.07	0.13	0.31	0.01	0.03	0.40	0.52		0.14	101.13	Orthopyroxene
0.44	19.38	19.12	56.28	0.11	0.09	0.38	0.02	0.12	3.47	0.50	0.04	1.40	101.31	Glass

Figure 6: EPMA results of Test 3 slag.



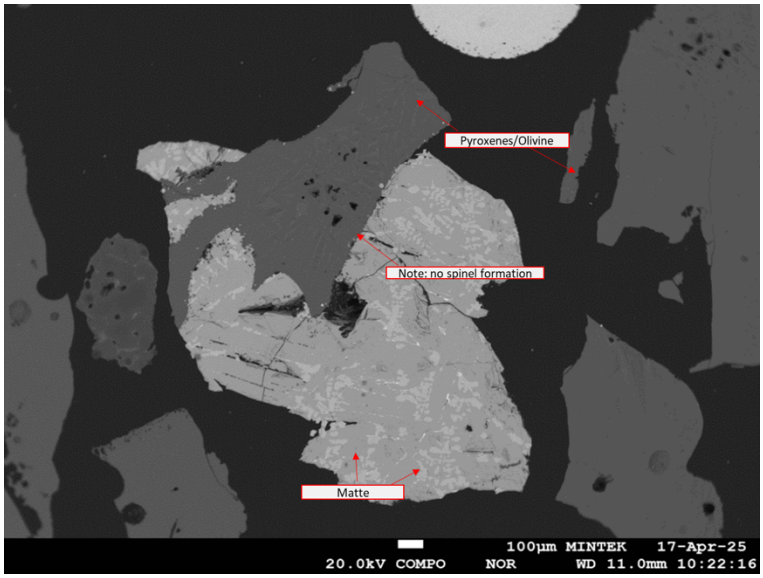
Na_2O	MgO	Al_2O_3	SiO_2	MnO	FeO	TiO_2	NiO	K_2O	CaO	Cr_2O_3	V_2O_5	S	Total	Phase
0.07	1.38	0.05		3.88	24.35	0.11	0.08	0.01	0.03	68.94	0.39	0.40	99.29	Cr-Fe Spinel
0.03	0.13	0.08		0.08	0.79	0.38	0.03		0.02	96.65	0.95	0.46	99.34	Eskolaite
1.08	17.40	12.55	58.77	0.07	0.04	0.38		0.25	6.02	0.22		3.14	99.89	Clinopyroxene
0.04	38.85	1.10	58.53	0.05	0.02	0.22	0.03	0.01	0.16	0.27		0.15	99.30	Orthopyroxene

Figure 7: EPMA results for Test 4 slag.



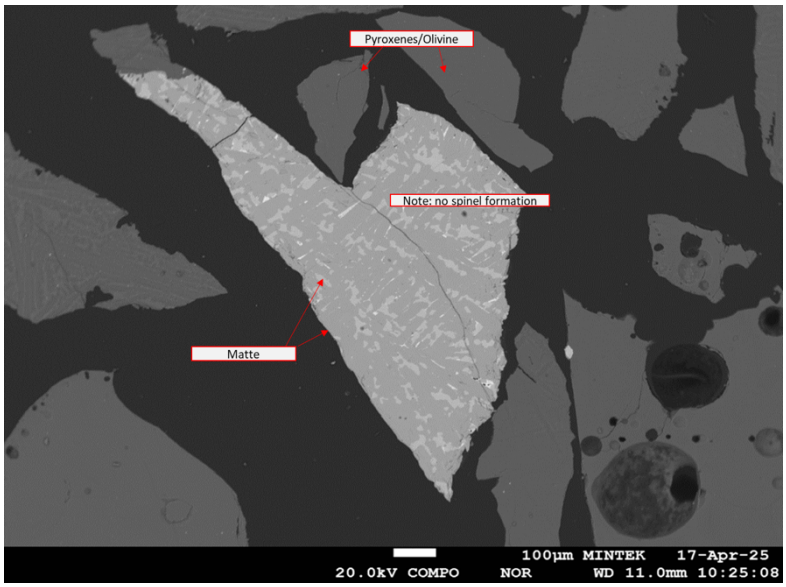
Na_2O	MgO	Al_2O_3	SiO_2	MnO	FeO	TiO_2	NiO	K_2O	CaO	Cr_2O_3	V_2O_5	S	Total	Phase
0.05	0.18	0.04		3.57	28.29	0.30	0.07	0.00	0.01	64.64	0.28	1.33	98.58	Chromite
0.02		0.04		0.04	1.03	0.16	0.07			98.33	0.37	0.11	100.18	Eskolaite
0.07	39.23	0.97	59.38	0.04	0.02	0.18	0.02	0.02	0.25	0.21		0.19	100.43	Orthopyroxene
0.56	27.98	6.53	59.76	0.12	0.05	0.27	0.01	0.13	2.54	0.42		2.21	100.54	Clinopyroxene 1

Figure 8: EPMA results for Test 5 slag.



Na_2O	MgO	Al_2O_3	SiO_2	MnO	FeO	TiO_2	NiO	K_2O	CaO	Cr_2O_3	V_2O_5	S	Total	Phase
0.51	23.35	12.82	57.77	0.14	0.04	0.59		0.23	3.78	0.36		2.03	101.60	Clinopyroxene
0.03	57.54	0.11	42.65	0.06	0.02	0.10	0.01	0.01	0.06	0.15	0.04		100.72	Orthopyroxene
0.33	43.10	4.90	50.41	0.08	0.03	0.25		0.18	1.04	0.23		0.74	101.28	Forsterite
0.60	27.91	10.81	55.74	0.15	0.04	0.51		0.26	3.23	0.37		1.78	101.40	Silicate

Figure 9: EPMA results for Test 6 slag.



Na_2O	MgO	Al_2O_3	SiO_2	MnO	FeO	TiO_2	NiO	K_2O	CaO	Cr_2O_3	V_2O_5	S	Total	Phase
0.73	18.03	16.05	58.12	0.09	0.04	0.35	0.02	0.44	5.11	0.12	0.05	3.10	102.16	Clinopyroxene
0.22	31.50	7.75	52.66	0.17	0.04	0.42	0.01	0.13	1.47	0.22	0.04	1.22	94.18	Orthopyroxene
0.27	47.71	3.64	47.92	0.09		0.12		0.17	0.84	0.07		0.71	101.54	Forsterite

Figure 10 EPMA results for Test 7 slag.

CONCLUSION

This paper demonstrated that reductive matte smelting of UG2 concentrate using Al, FeSi, and SiC reductants offers a viable pathway to address the metallurgical challenges posed by the high-chromite, low-sulfide mineralogy of UG2. Both thermochemical simulations and experimental results confirmed that reductant additions improve alloy fall, with SiC and FeSi showing a particular promise in enhancing chromium solubility in the slag while limiting refractory spinel precipitation. Aluminium, although effective at increasing alloy fall, was associated with persistent spinel formation.

Empirical results also highlighted the trade-offs between reductant addition and alloy fall. High additions of reductant of 5% resulted in substantial alloy formation, which would likely complicate the furnace operation through the formation of both matte and alloy (in the tests, the matte occurred within the slag). It is also essential to control the sulfur levels in the feed and the levels of reductant addition, to avoid the formation of superheated molten phases in the furnace that could raise the risk of furnace explosions.

Notably, SiC exhibited the most favourable behaviour, with minimal spinel formation, making it a strong candidate for further optimisation.

Overall, reductive matte smelting represents a promising alternative or complement to blending strategies and advanced processes such as ConRoast, particularly as reliance on Merensky feed continues to decline. Future work should focus on refining reductant dosages, assessing phase equilibria in slag systems, and scaling the process to pilot and industrial levels to validate its robustness and economic feasibility. By improving chromium management and sustaining PGM recoveries, reductive smelting using SiC and FeSi could play a key role in ensuring the long-term viability of UG2-based PGM production in South Africa.

REFERENCES

Barnes, A. R. & Newall, A. F., 2006. *Spinel removal from PGM smelting furnaces.* Johannesburg, South African Institute of Mining and Metallurgy, Southern African Pyrometallugy 2006, pp. 77-88.

Cramer, L. A., Basson, J. & Nelson, L. R., 2004. *The extractive metallurgy of South Africa's platinum ores.* Cape Town, South Africa, Proceedings: Tenth International Ferroalloys Congress, INFACON X: 'Transformation through Technology', pp. 47-59.

Eksteen, J. J., 2011. A mechanistic model to predict matte temperatures during the smelting of UG2-rich blends pf platinum group metal concentrates. *Minerals Engineering,* Volume 24, pp. 676-587.

Hay, M. P. & Roy, R., 2010. A case study of optimising UG2 flotation performance. Part 1: Bench, pilot and plant scale factors which influence Cr2O3 entrainment in UG2 flotation. *Minerals Engineering,* Volume 23, pp. 855-867.

Jones, R. T., 2002. *ConRoast: DC arc smelting of deadroasted sulphide concentrates.* Seattle, Washington, USA, TMS Annual Meeting (The Minerals, Metals, & Materials Society), p. 435–456.

Jones, R. T., 2005. An overview of Southern African PGM smelting. *The Journal of the South African Institute of Mining and Metallurgy,* 105(6), pp. 389-396.

Jones, R. T., 2015. *Fundamental aspects of alloy smelting in a DC arc furnace,* Johannesburg: University of the Witwatersrand.

Jones, R. T. & Geldenhuys, I. J., 2011. *The pros and cons of reductive matte smelting for PGMs.* Falmouth, Precious Metals '10, pp. 495-498.

Liddell, K. S. & Adams, M. D., 2012. Kell hydrometallurgical process for extraction of platinum group metals and base metals from flotation concentrates. *The Journal of The Southern African Institute of Mining and Metallurgy,* Volume 112, pp. 31-36.

Malan, W., Akdogan, G., Bradshaw, S. & Bezuidenhout, G. A., 2015. The recovery of platinum group metals from low-grade concentrates to an iron alloy using silicon carbide as reductant. *The Southern African Institute of Mining and Metallurgy,* 115(5), pp. 375-383.

Nell, J., 2004. Melting of platinum group metal concentrates in South Africa. *The Journal of The South African Institute of Mining and Metallurgy,* 104(9), pp. 423-428.

Schouwstra, R. & Kinloch, E. D., 2000. A short geological review of the Bushveld Complex. *Platinum Metals Review,* 44(1), pp. 33-39.

Shaw, A., de Villiers L. P., Hundermark, R. J., Ndlovu, J., Nelson, L. R., Pieterse, B., Sullivan, R., Voermann, N., Walker, C., Stober, F. & McKenzie, A. D., 2013. Challenges and solutions in PGM furnace operation: high matte temperature and copper cooler corrosion. *The Journal of The Southern African Institute of Mining and Metallurgy,* Volume 113, pp. 251-261.



Sanele Nkosi

Scientist
Mintek

Sanele Nkosi holds an MSc in Chemical Engineering from the University of Cape Town. In her career, Sanele has been involved in many projects for the beneficiation of different resources including ferrous minerals, industrial minerals and precious materials, base and technology metals-bearing primary and secondary materials, and energy minerals like coal. Her research interests include extractive metallurgy of titaniferous magnetite for vanadium, steel and titania production; coal characterisation and carbonaceous reductant reactivity testing; general chemical, thermal, and mineralogical characterisation of materials; and high temperature experimentation including reaction kinetics and mechanisms in gas-solid systems, smelting and refining. She is currently working on a PGM research project involving the investigation of alternative reductants that can be used in the PGM matte smelting process. This project involves thermochemical simulations, 200 g laboratory-scale smelting tests, and 15 kg smelting tests in a 100 kVA induction furnace.

Commissioning the Zimplats smelter expansion

M. Crafford[1], M. Monobe[1], G. Erasmus[1], S. Matutu[2]

[1] Hatch, Johannesburg, South Africa
[2] Zimplats, Selous, Zimbabwe

Zimplats, in collaboration with Hatch, undertook a fast-tracked expansion of its Selous Metallurgical Complex smelter to triple its processing capacity. The project included the installation of a new 38 MW six-in-line Hatch electric furnace, flash dryer, Peirce-Smith converters, and auxiliary systems. Commissioning was completed late 2024, achieving stable production within months of initial matte tapping. This paper presents the commissioning strategy, challenges encountered, and solutions implemented under tight schedule constraints and overlapping operational activities.

Key issues such as compressed air system overload, deferred SO_2 abatement integration, and slag granulation inefficiencies were resolved through data-driven diagnostics, practical implementation of solutions, and collaborative engineering. The commissioning methodology and outcomes offer valuable insights for future smelter projects, particularly in balancing operational continuity with aggressive execution timelines. The project sets a benchmark for PGM smelting projects, with implications for industry-wide practices in utility design, emissions control, and commissioning under constrained conditions.

Keywords: Smelter expansion, commissioning, collaboration

INTRODUCTION

Zimplats operates the largest platinum group metals (PGM) smelter in Zimbabwe, at their Selous Metallurgical Complex (SMC), south-west of Harare. Smelting operations at SMC commenced in 1997 (Mabiza, 2006).

The Smelter Expansion and SO_2 Abatement project ('the Project') was undertaken to increase the plant throughput threefold, which included Zimplats' internal growth expansion and the toll treatment of third-party concentrates. Hatch provided full engineering, procurement and construction management services for the project.

The expanded smelter flow diagram depicting the main processing steps is shown in Figure 1. Before the expansion, the smelter operated a 25 t/h concentrate flash dryer, a 12.5 MW circular electric furnace (Furnace 1 - F1), two small (10'x15') Peirce-Smith converters (PSCs) and a converter matte granulation plant. PGM-containing concentrate is dried and smelted in the furnace to generate a furnace matte and water granulated furnace slag. The furnace matte is tapped into ladles and transferred via the overhead aisle crane into PSCs for further processing. Iron is removed from the furnace matte in the converters by blowing air through tuyeres. This generates a converter slag which is returned hot to the furnace for metal recovery. The PGM-rich converter matte is water granulated, bagged and trucked to the Implats Base Metal Refinery (BMR) in South Africa.

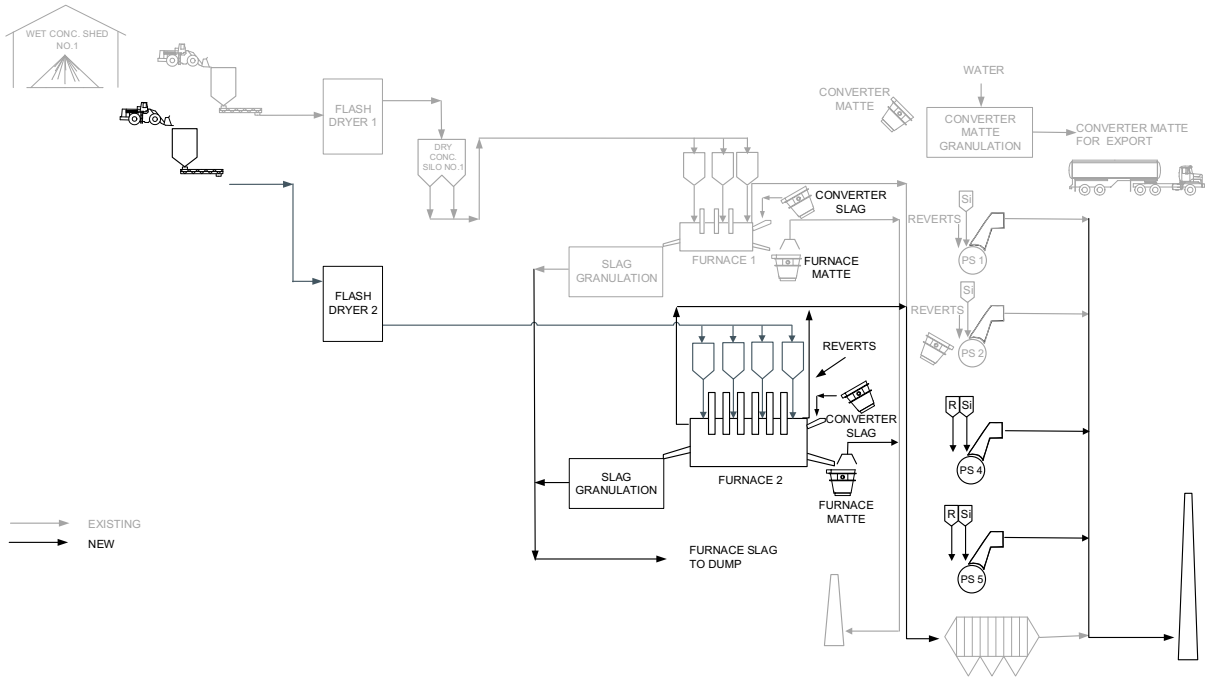


Figure 1. Smelter expansion flow diagram.

The smelter expansion scope included the installation of a new 45 t/h concentrate flash dryer, new 38 MW Hatch rectangular electric furnace (Furnace 2 – F2) with water slag granulation system, two new larger (12'x24') PSCs and primary and secondary off-gas handling systems including a 160 m tall concrete stack to serve the old and new furnaces and converters. Water and compressed air utility systems were established to service the expanded smelter as well as the SO_2 Abatement plant.

The existing converter aisle was extended to the west and a new overhead crane installed to service the new furnace and PSCs. Minimal disruption to the operation of the existing smelter was achieved by designing for hot bypass of the off-gas systems, utilising the existing furnace and converters and tie-in during planned shutdowns.

The project initially included the upgrade and re-start of the mothballed SMC BMR and installation of a new SO_2 Abatement plant (wet gas cleaning and sulphuric acid plants) to treat the furnace and converter primary off-gas. Due to PGM market conditions and subsequent client cash flow constraints, the BMR and SO_2 Abatement portions of the project were deferred during the detailed design phase.

The client's target for increased smelting capacity was December 2024. The feasibility study for the project was undertaken by Hatch during 2021, together with early detail engineering and procurement for early earthworks and infrastructure as well as long lead packages (technology packages, substations, etc.). The demolition of existing structures commenced in March 2022; construction of new civil foundations starting in August 2022 and commissioning started in July 2024. The first F2 matte was successfully tapped on 7 October 2024 (meeting the P80 probabilistic schedule date) which marked a significant milestone not only for the project but also for Hatch and Zimplats, who have been collaborating on the possibility of an expansion of the smelter since 2002. The timeline of commissioning milestones in 2024 to first matte tap is shown in Figure 2

Figure .

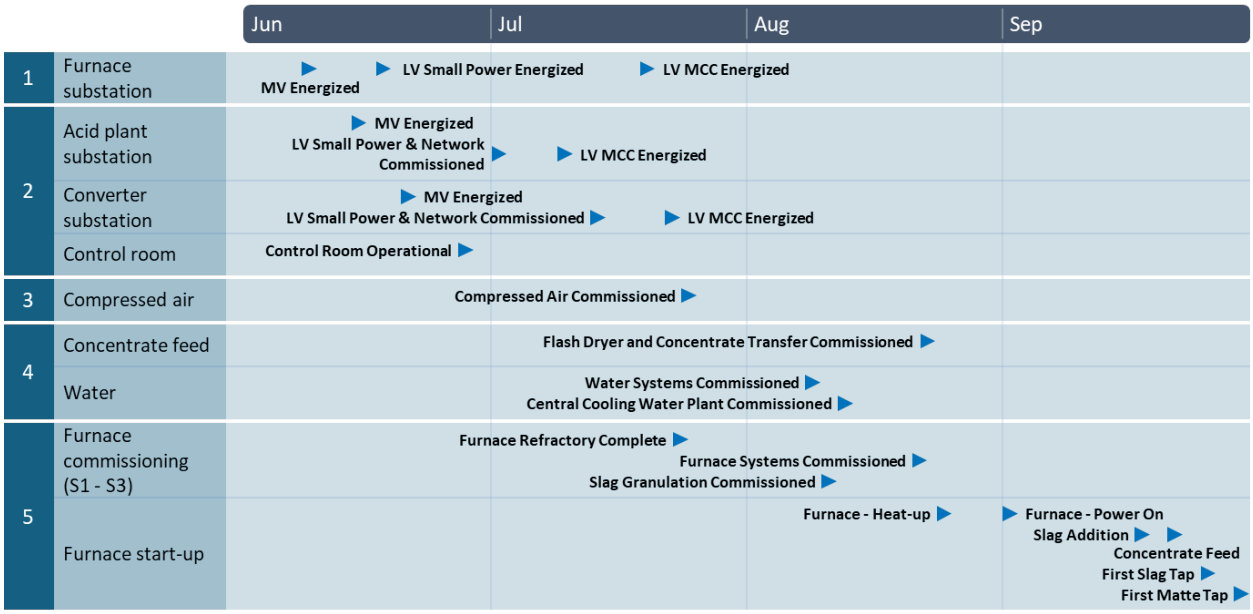


Figure 2. Furnace 2 first matte tap timeline.

The overlapping of design, construction and commissioning phases on this project required significant integration and collaboration between the teams responsible for each of these phases. This paper provides a description of the smelter operation and presents some of the challenges faced and their solution. Challenges resulted from the strict timeline, scope changes and ramp-up of the smelter.

OPERATING DESCRIPTION

This section describes the flowsheet of the smelter expansion, which was designed to operate independently from the existing operation, from the main process units to utilities and control systems (networks: programmable logic controller (PLC) and supervisory control and data acquisition (SCADA). An overview of the historical Zimplats operation is described by Mabiza (2006). The design, operation and start-up of F2 will be addressed in a separate paper.

Concentrate drying and transfer

Concentrate from external concentrators arriving by truck are weighed by weighbridge and sampled before off-loading and stockpiled in an existing concentrate shed and then blended.

Wet concentrate is reclaimed via front-end loader (FEL) for discharge into a hopper. A variable speed feeder extracts concentrate from the hopper for transfer to the new flash dryer via a series of conveyors. The new flash dryer is a Drytech design, similar to the existing flash dryer. The operation of two flash dryers in parallel improves the availability of the drying section. Each dryer has a storage silo from where dry concentrate can be pneumatically transferred to both F1 and F2.

Furnace feed

The furnace feed system receives dry concentrate, electrostatic precipitator (ESP) dust return, crushed reverts and cold dope for feeding the furnace during startup and under normal operation. Concentrate and dust return from the ESP are pneumatically conveyed into roof bins, while crushed reverts and cold dope are hoisted using a hoist crane and a kibble into hoppers.

Feeders extract the material from the roof storage for discharge through feed pipes. The furnace is fed through several feed ports on each side of the electrode centreline and the end wall.

The concentrate bins are equipped with load cells and loss-in-weight methodology is used to determine total furnace feed rate and track the power-feed ratio of the furnace. The concentrate feeders use variable speed drives to adjust feed rate as required.

Furnace cooling water
The furnace water-cooling system is a closed loop system that consists of multiple circuits. The water is continuously pumped throughout the various coolers that are located within the furnace sidewalls, tap blocks and launders. The heated water is cooled in plate heat exchangers, with the cold side water received from the central cooling water plant.

To ensure optimum heat transfer, safe operation and longevity of the cooling system piping and coolers, the system has been designed as a closed-circuit system with continuous blowdown and make-up with demineralised (demin) water.

Additives are dosed to the cooling water circuit to aid in prevention of scaling, corrosion and biofouling. To remove solid impurities, a side stream of closed-circuit cooling water is passed continuously through a cartridge filter.

Closed-circuit cooling water returned from the furnace crucible circuits are routed to the furnace cooling water collection tank. The cooling water supply pumps transfer water through the plate heat exchangers and back to the furnace cooling elements and the low voltage (LV) bus cooling water tank. The LV bus cooling water overflows to the furnace cooling water collection tank.

The emergency cooling water tank is continuously supplied with water from the cooling water collection tank and overflows back to the furnace cooling water tank via gravity. The occurrence of continuous supply to and overflow from the emergency water tank ensures that the tank is always filled and ready to drain to the furnace crucible in the event of an emergency.

In the event of a power loss or low circulating flow, the emergency head tank drains water to the furnace crucible cooling circuits to maintain furnace integrity while the operator attends to the emergency.
The furnace transformers and hydraulic power unit (HPU) circuits are supplied with cooling water directly from the central cooling water plant as the cooling water to these users should be as cold as possible.

Furnace off-gas
The furnace off-gas system aims to maintain a slight negative pressure in the furnace freeboard such that the process off-gas can be extracted (and hygiene can be maintained in the furnace building) and delivered to the downstream ESP, where the bulk of the off-gas dust is removed. The primary off-gas from F1 and F2 are combined prior to entering the ESP. Dilution air is added (if needed) to reduce the off-gas temperature to ensure the maximum design temperature of the ESP is not exceeded. Two primary off-gas fans, located downstream of the ESP, provide the motive force to extract the off-gas from the furnace freeboard through the system. Due to the deferred SO_2 Abatement plant, furnace primary off-gas is routed to the new 160 m stack.

Furnace slag handling
Molten slag is tapped from F2 through three tap holes (one or two simultaneously). The tapped slag is guided by the slag launders and water granulated by spray nozzles at the tip of the launders. The granulated slag and water land in the granulation pond. The water and fines make their way via overflow to the connected fines settling pond.

There are two sets of pumps at the end of the settling pond. One set provides the pressurised granulation water. The other set circulates the warmed granulation water to the slag granulation cooling tower. The water is cooled by induced draft evaporation created by three fans in the tower and drains by gravity into the granulation pond. The fans are switched on or off depending on the temperature of the granulation water.

In the event of a power loss or pump failure, an emergency head tank drains water to the slag granulation nozzles, to provide time for an operator to close the tapholes.

There are two clamshell cranes to reclaim granulated slag from the ponds. The cranes drop the slag into a hopper which then discharges onto the first of two conveyors that transfer the slag to a holding silo. Slag from the silo is discharged into dump trucks that transport the material to the slag dump for discard.

Converters
The existing two small (10′ x 15′) PSCs will be in use together with the new large (12′ x 24′) PSCs. The capacity of the two small PSCs is similar to that of a single large PSC. During the interim period after the F2 first matte tap and prior to the completion of construction and commissioning of the large PSCs, the small PSCs , sometimes blowing simultaneously, were required to treat the F2 matte. The combination of the large and small PSCs provides the smelter with wide operational flexibility to match varying furnace matte production.

To turn the PSC into the desired position, the PSCs are equipped with an electric drive for normal conditions and a pneumatic drive in the event of a power failure.

Two blowers supply the air required for the large PSCs tuyeres (32 installed). The blowers pull in filtered ambient air for compression and discharge into a common header line, which feeds the large PSCs. The blowers are water-cooled with cooling water from the central cooling plant.

The large PSCs are also equipped with an emergency blast air line to supplement the blast air with compressed air from the dedicated air receivers should the blast air flow fall below the required minimum setpoints or in the event of blower failure. The emergency blast air capacity is sufficient to allow safe turn out of the PSC from the blowing position.

All PSCs are equipped with Gaspe-type manual punchers that clears one pair of tuyeres at a time. The clearing is required as the blast air tends to cool and solidify the molten material in front of the tuyere which may cause blockage if not cleared.

Converter feed
During converting operation silica flux and reverts ('cold dope') are added intermittently to maintain the slag chemistry and operating temperatures respectively. Three bunkers are available for storage of silica flux, high quality reverts and low quality reverts. One type of material is loaded by means of a FEL to a series of conveyors that deliver the material into the converter building, for discharge into the silica or reverts roof bins.

The silica and reverts bins are shared between the large PSCs. Each bin has two outlets that discharge onto two weigh feeders that measure the weight of material fed. The weigh feeders discharge onto a vibratory feeder which drops material through the hoods and into the mouth of the PSC while it is blowing.

Converter off-gas
The large PSCs are fitted with primary and secondary off-gas hoods. Primary off-gas collected from the new PSCs are cooled by spray coolers before combining with the primary off-gas from the small PSCs. The combined off-gas is then sent to the 160 m stack using an induced draft fan.

Extraction on the primary converter hoods is maintained at a slightly negative pressure to ensure evacuation of the PSC mouth gas and enable an allowable amount of ambient air ingress into the hood. The large converters are fitted with close-sealing water-cooled primary hoods to enable close-capture of high-SO_2 bearing off-gas (which is important for eventual acid plant operation).

Hot off-gas flows into evaporative spray coolers to control temperatures suitable for downstream equipment. This is done by atomising water, using high pressure instrument air, into fine droplets that need to be fully evaporated before the off-gas leaves the spray cooler. Dust fall-out in the spray cooler is safely removed and recycled from the bottom of the vessel.

The secondary hoods capture emissions during converter charging, skimming and matte transfer events, as well as fugitive emissions that escape the primary hood during blowing.

Converter primary hood cooling
The large PSC hoods are water-cooled, as the tight-fitting hoods allow less ambient ingress that can cool the mouth gas and hood surfaces, resulting in higher heat loads experienced when compared to the small PSC hoods.

The primary hoods are composed of various panels that contain channels through which the cooling water flows. The demin water circulating through the hoods is cooled by indirect heat exchanges in plate heat exchangers with cooling water from the central cooling tower.

A head water tank ensures circulating water remains pressurised to prevent nucleate boiling and cavitation in the system. The cooling water supply temperature is maintained to minimise acid dewpoint condensation on the inner surface of the primary hood.

Water storage and distribution
Raw and potable water are required by several users. Raw water and potable water are received from existing plant systems for storage in dedicated tanks. Raw water is termed process water after it leaves the raw water storage tank, and it is used as make-up to the central cooling tower and slag granulation pond. Potable water is currently mostly used for the PSC spray coolers and as feed to the demin water plant, where demin water is prepared by a reverse osmosis process and provides make-up water to the furnace crucible and converter hood closed cooling water circuits.

Central cooling water
The central cooling water plant consists of a multi-cell concrete cooling tower with a basin connected to recirculation pumps that supply cooling water to the following equipment:

- Crucible heat exchangers
- Furnace transformers and HPUs
- Converter blowers
- Convertor primary hood heat exchangers.

The hot returning cooling water is distributed over the cooling tower cells and cooled down by contact with ambient air induced by the cooling tower fans and by partial evaporation of a portion of the cooling water. The cooled water collects in the basin.

A portion of the circulating flow is circulated through sand filters to remove suspended solids. The sand filters are backwashed intermittently with the backwash discharged to the slag granulation pond. A portion of the cooling water is also continuously bled to the slag granulation pond to prevent the build-up of salts and other impurities within the cooling water system. Water treatment consists of dosing the basin at pre-specified intervals with anti-scalant, corrosion inhibitors and biocide chemicals.

Compressed air
The plant compressed air system consists of four compressors, each with an associated dryer and filtration fan, that feed three plant air receivers through a common header. The air is dried to instrument air quality standard. The air receivers act as a buffer and storage medium between the compressors and the consumption system for peak load demand. The compressor supplier's proprietary central controller will start the compressors individually and control their load if the air supply pressure drops below the setpoint.

COMMISSIONING METHODOLOGY AND SEQUENCE

Commissioning of the plant followed a nested, bottom-up staged approach, for which a simplified process is presented in Figure 3. Individual equipment is inspected, energised and tested and is then grouped into subsystems and systems in order to be tested as a functional unit, initially with no load and then with inert material. Only then can process materials be introduced in the systems and the plant tested, ramped-up and optimised as a whole (Bailey, 2005).

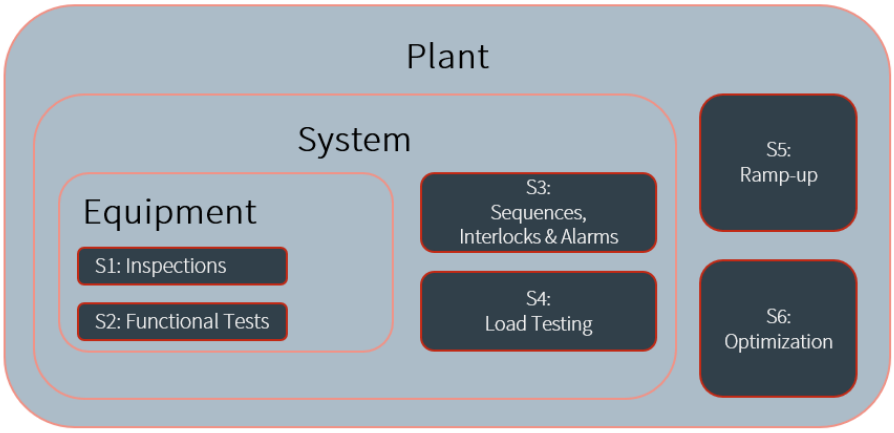


Figure 3: Commissioning approach.

In June 2024 the pre-commissioning of the smelter commenced. A progressive turnover of access to facilities from the construction team to the pre-commissioning team, or handover of facilities from pre-commissioning to Zimplats Operations was planned, where Hatch covered responsibilities between S1 and S3 and thereafter handed over to the owner (Zimplats) to complete the S4 to S6 activities. However, due to the significant time constraints and tight schedule there were large overlaps between these phases during the implementation of the project.

Error! Reference source not found. Figure 4 provides a high-level sequence for the commissioning of the various functional areas. The priority was driven by the start-up readiness for the furnace. The basis for the sequence is to start-off with power supply, followed by utilities, and then upstream and downstream auxiliaries to the furnace. Depending on construction progress in specific areas, some systems were partially commissioned before formal handover.

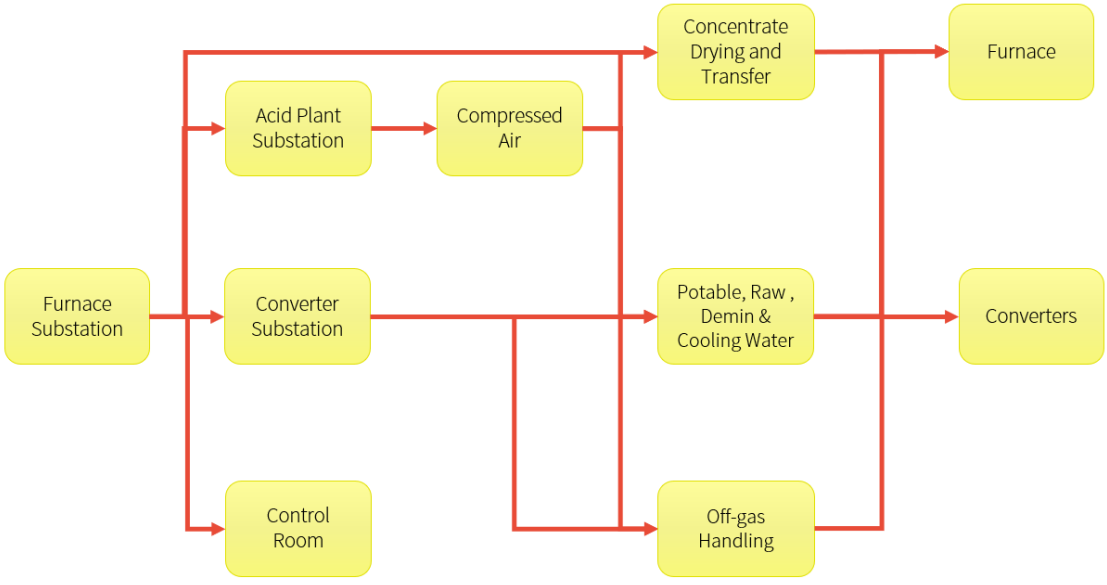


Figure 4. High-level expansion commissioning sequence.

COMMISSIONING CHALLENGES AND SOLUTIONS

In total 5,143 S1 check sheets, 4,192 S2 check sheets and 33 S3 check sheets had to be completed to successfully commission the new smelter and its auxiliary systems. This included pre-commissioning of more than 3000 new IO, 11 new PLCs and their SCADA integration, construction and commissioning of three new substations.

During the height of commissioning, between 16 July 2024 and 17 August 2024, 6,707 check sheets were completed by the construction and commissioning teams. These teams consisted of close to 70 Hatch employees involved in the construction, commissioning and start-up activities. Furthermore, the Zimplats instrument technicians and operational personnel assisted with the pre-commissioning checks to ensure the new furnace can be started on schedule.

The accelerated project schedule placed significant pressure on the construction, commissioning and start-up teams. To meet the 'Power-On' date, the teams worked in close collaboration, keeping track of the work completed by submitting the check sheets completed on a daily basis to an online system. This allowed updated tracking of the completed systems and alignment on the outstanding areas on a daily basis between the various teams. The daily check sheets completed during the commissioning and start-up of the new furnace are indicated in Figure 5. Key dates are also indicated, illustrating the fast-tracked furnace start-up, moving from commissioned furnace systems on 21 August to 'Power-On' on 1 September 2024.

During the S2 and S3 commissioning, each area presented different challenges. Some of the major challenges and solutions are discussed below.

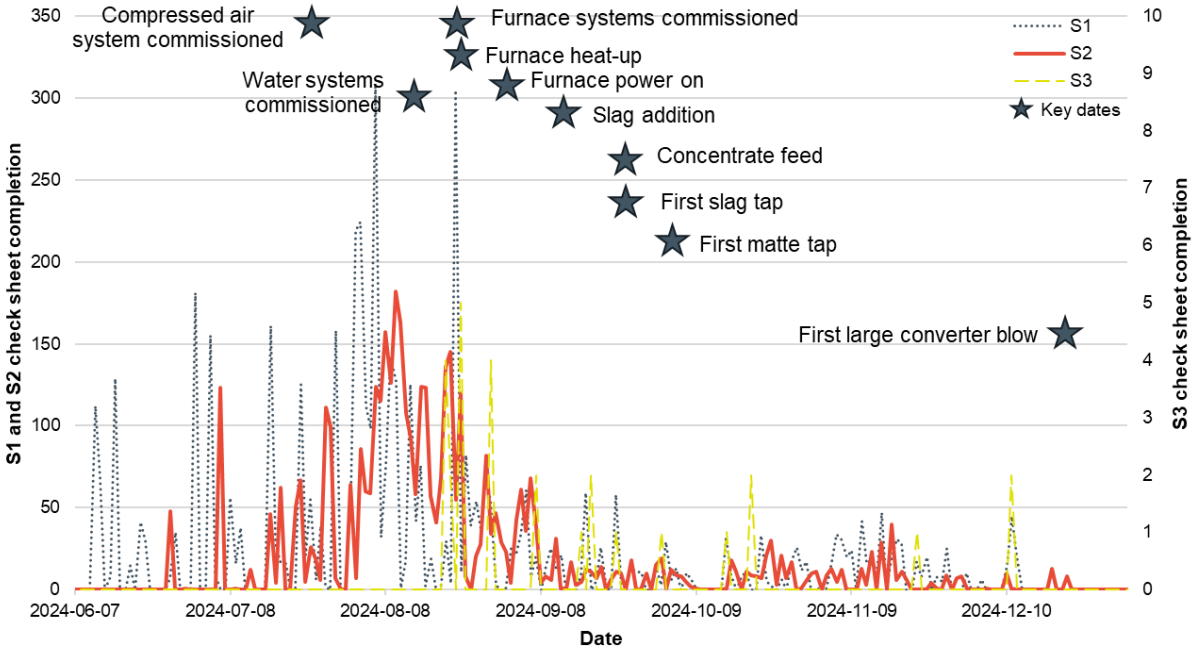


Figure 5: Daily check sheets completed.

Challenges due to a fast-tracked schedule

Scope changes

Due to the overall fast-tracked project schedule and smart risk-taking initiatives taken during the earlier project phases, late design changes were inevitable. These changes had to be incorporated while construction and commissioning activities were taking place. Furthermore, changes were often influenced by increased involvement from operators and the availability of updated information.

One example of such a design change was the removal of the potable water lines to the furnace cooling water tanks. Potable water supply lines were added in the initial designs to serve as short-term emergency back-up should demineralised water not be available for an extended period of time. The cooling water system should have been flushed with demineralised water once available again to displace any added potable water.

Analysis of potable water samples were received towards the end of the detail engineering design and showed to be of poor quality. Poor cooling system performance leading to furnace downtime and possible damage to the cooling system could result if the furnace cooling water system is operated with potable water make-up for an extended period of time.

To eliminate this risk completely and to ensure that the emergency cooling water supply tank remains supplied with demineralised water, the potable water supply lines to the various tanks had to be removed, and overflow and supply lines between tanks had to be rerouted to ensure supply of high quality water to all three tanks and no wastage of the high quality water.

This change was approved days before the targeted Burners-On date and required a risk analyses of the design changes and collaboration between the site and office-based engineering teams to produce a new design and layout, while considering swift construction. The changes required updates to the control philosophy and functional descriptions. These updates in turn had to be implemented in the PLC and the SCADA layouts had to be updated based on the new flowsheets.

Deferred scope
The deferment of the SO_2 Abatement plant resulted in difficulties on the commissioning of the shared utilities and on the emission control systems.

The SO_2 Abatement plant would have accounted for about 60% of the cooling water requirements of the smelter expansion. The cooling water supply flow and pressure were to be maintained by automatic speed adjustment of two running pumps, with another on standby. During commissioning, the control philosophy had to be updated to require only one running pump at any given time to match the lower demand. This update required reprogramming of the duty-standby controller, considering the various interlocks impacted by the requirement for only one pump to be running, changing the start-up and shut down sequence, and optimising (by trial and error) the pump speed and discharge valve to achieve the target supply flow within a suitable supply pressure range.

Deferment of the SO_2 Abatement plant possibly had the largest impact on the off-gas system. The primary off-gas had to be routed to the 160 m stack, which was originally meant to be dedicated to the converter secondaries. This off-gas configuration meant that the overall system could not be placed in automatic mode and had to be operated manually in order to balance suction at the various points, which was a significant learning curve for the operations.

Commissioning handover
The ideal commissioning scenario involves plant operators in the cold commissioning activities to familiarise themselves with the new system in preparation for S4 commissioning and minimise handover delays. However, the furnace start-up schedule pressure coupled with construction and commissioning activities overlapping with existing smelter operation impacted the effective handover of systems.

To manage the impact of this overlap, close collaboration between the Hatch and Zimplats teams was required. Once the burners were switched on, the operations team were involved with the operation of both F1 and F2. Consequently, they did not have capacity for extensive involvement with the commissioning of the remaining systems and areas. In turn, the plant operators were not familiar with the new systems. This required the commissioning team to assist with the S4 commissioning and run certain portions of the plant to allow the operations team to become familiar with the newly

commissioned systems. This collaboration between the Hatch and Zimplats team continued as the plant was ramped-up to reach nameplate production and stability.

Ramp-up and optimisation challenges

Converter blast air blowers

The converter blowers were designed to use cooling water flowing through a shell and tube heat exchanger to cool the pressurised air and thereby reduce the (actual) volume of the air, in turn reducing the duct size and system pressure drop. During operation of these blowers, some of the tubes were damaged, with water leaking into the air side, which resulted in downtime of the blower and converters. To mitigate this, the removal of the cooling water was investigated to prevent future loss of production due to similar damage and leaks. The risks of hotter air on the ductwork and process were investigated. It was concluded that the air coolers be removed from the blowers.

Compressed air

It is inevitable that operators will tie-in to the system, introducing added 'unaccounted' usage of compressed air during normal operation or maintenance activities. This causes significant dips in the system air pressure and hence functionality of plant air and instrument air users. During commissioning, this caused delays to the dry concentrate transfer and converting operations, as their operating sequences are related to the air pressure signal. However, as the plant was still new and in the process of ramping up, little stable operating data was available to determine when and where the problems were first encountered. A practical approach was followed, supported by operating data, to identify the problem area.

This approach is illustrated in Figure 6 where it was observed three compressors at full load failed to maintain the 6 bar design pressure. Isolation of the Flash Dryer Area via its main valve resulted in an immediate pressure recovery, confirming excessive air consumption in that area. A systematic branch isolation identified a major consumer – a line added to fluidise wet coal due to insufficient pressure from the fluidising fan. This modification overloaded the system, requiring all four compressors and compromising stability. The identified line was closed, and with all other consumers online, only two compressors operated at low load, with the system stabilising at one compressor during low demand periods. The compressed air system was not designed for this additional load, and its continued use would prevent reliable pneumatic concentrate transfer to the furnace at the required 50 t/h feed rate for 38 MW operation.

It requires effort to identify all the unaccounted tie-ins and take necessary action to raise the plant air pressure. To minimise the effort and impact on operations, the following are recommended for future projects.

- Addition of flow meters at the main branches to help with accounting for air leaks or pressure losses, and allow for isolation of main and sub-branches to facilitate ease of maintenance.
- Provision of sufficient capacity buffers on a combined plant and instrument air supply network, especially when this network supplies air to an entire plant, by including dedicated compressors and air receivers for large or critical consumers.

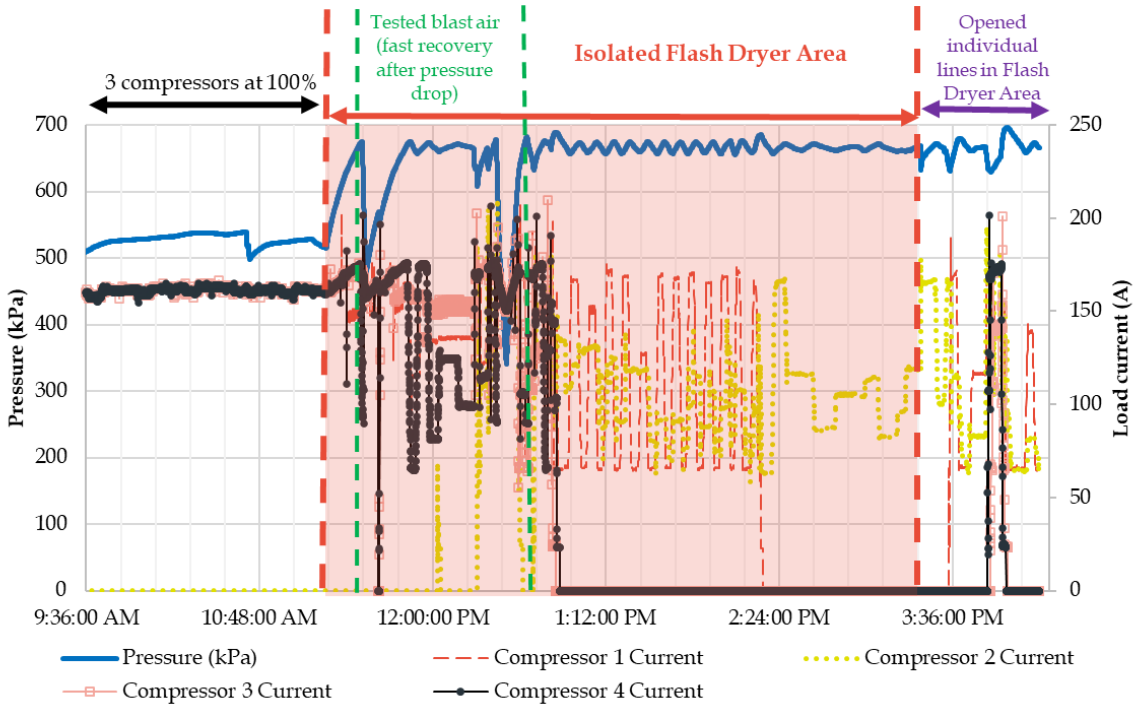


Figure 6: Systematic evaluation of the compressed air system.

Furnace slag handling

Initially, the slag granulation system worked well-enough, however, at some point the granulated slag started accumulating within the system due to blockage of the granulated slag transfer hopper. Upon physical inspection, it was found that the granulated slag now contained significant amounts of fibres or 'angel hair'. Consequently, the slag had to be dropped next to the slag pond and removed via front end loaders and dump trucks. Two avenues of solving this problem are available: chemical changes such as changing the slag properties, where this requires more research and experiments on the formation of fibres during slag granulation, and physical updates, such as changing water flow rates, water-to-slag ratios or equipment designs (Van Hooff et al., 2006). The slag chemistry was evaluated and it was hypothesized that the decrease in FeO coupled with the increase in basic and acidic oxides (MgO, CaO, Al_2O_3, and SiO_2) could contribute to the wool formation due to increased viscosity and increase slag liquidus. However, changing the slag properties to prevent wool formation is no simple task. Physical updates were deemed as the first step and easier to implement solution.

The smelter trialled lower granulation flowrates, systematically decreasing the flow rate from 1400 m^3/h to 1200 m^3/h, and reduction in the fibres was noted. The granulated hopper transfer chute was also redesigned. These actions allowed the slag transfer and conveying system to be fully commissioned and utilised.

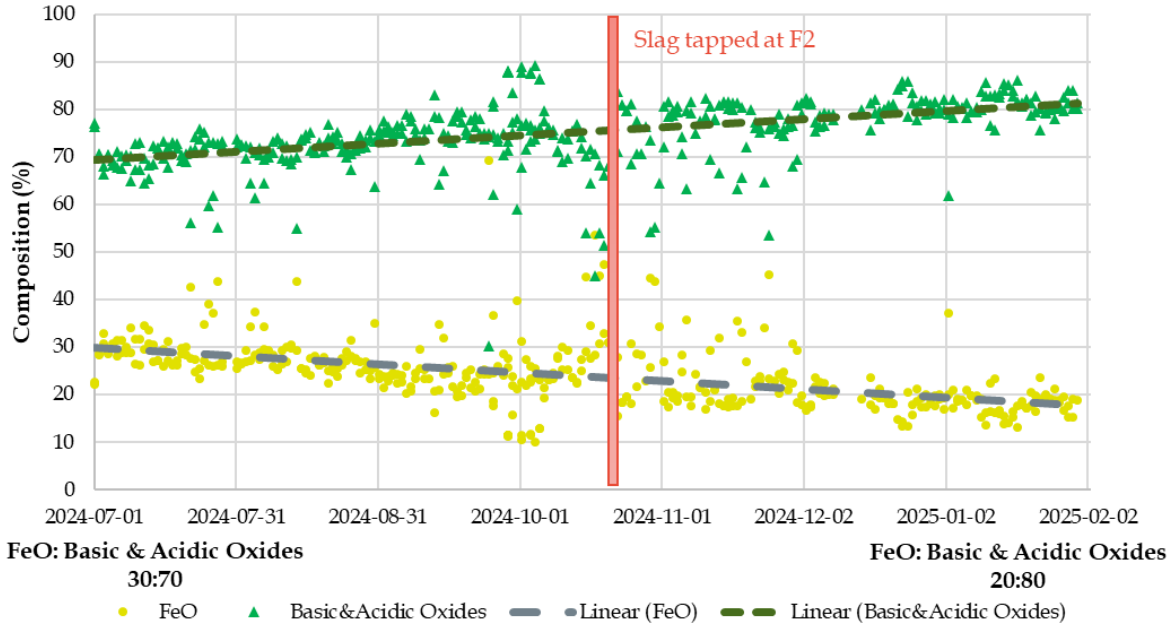


Figure 7: Furnace slag FeO and Basic and Acidic Oxides composition over time.

CONCLUSION

The project moved from a fast-tracked feasibility study in 2021 to execution in less than a year and completed the final hot commissioning in December 2024 (less than three years execution). The construction and commissioning effectively proceeded in parallel to ensure that the client's milestone matte tapping date and ultimately increased production requirement was met. The first furnace matte was tapped on 7 October 2024, within weeks of energising the new furnace on 28 August 2024. The new furnace matte was treated in the existing small converters while the new converters were still under construction and commissioning. The first blow on the large converter was conducted on 25 December 2024, marking the completion of commissioning of the new expanded smelter, less than six months after the first commissioning activities started.

Despite the commission challenges encountered, the integrated Hatch and Zimplats teams achieved a safe, efficient, and sustainable handover to operations of the expanded smelter. Challenges were addressed using a combination of technical expertise, data-driven analysis, and practical engineering interventions. Decisions were supported by benchmark data and operational experience to ensure safe, effective, and reliable implementation. Following the successful project delivery and fast furnace start-up, this project has become a benchmark for new PGM smelting projects. Lessons learned from this expansion, particularly around system flexibility, operator integration, and risk management can inform industry-wide practices and contribute to more resilient and efficient smelter commissioning frameworks.

REFERENCES

L. Mabiza *An Overview Of PGM Smelting In Zimbabwe - Zimplats Operations*. The Southern African Institute of Mining and Metallurgy, 2006.

B. Bailey. (2005). *Commissioning – The Interface Between Construction and Operations*. First Extractive Metallurgy Operators' Conference.

Van Hooff, W., Greiveldinger, B. & Wenner, M. (2006). Evolution of granulation technology. *Proceedings of the EPD Congress*. The Minerals, Metals and Materials Society (TSM).



Minèt Crafford

Process Engineer
Hatch

Minèt has been involved in various gas handling and metallurgical processing plant design projects. Where the gas handling projects primarily focused on designing, evaluating and debottlenecking of off-gas systems and SO_2 abatement plants. Minèt has worked on projects ranging from desktop studies to execution phase projects. As process engineer she has experience in developing process deliverables, operating cost estimates, functional specifications and control philosophies for a wide variety of operations.

Most recently, Minèt was involved in the commissioning of the new 38 MW furnace and its wraparound facilities as part of the Zimplats Smelter Expansion project.

An overview of pyrometallurgical research on PGMs at Mintek: from conceptualisation to demonstration

X.C. Goso, S.P. Tsebe, B.S. Xakalashe, E. Matinde

Mintek, South Africa

Mintek's pyrometallurgical research, development and innovation (RDI) on the production of platinum group metals (PGMs) was reviewed to provide insights on testing capabilities and flagship technologies. Pyrometallurgical RDI is conducted through a dedicated Pyrometallurgy Division, which implements Mintek's strategy for conducting RDI that promotes responsible and sustainable production of PGMs. Mintek has been providing high-impact and cutting-edge pyrometallurgical RDI to support the South African and global PGM industry since the early 1970s. Thermochemical simulation software and computational modelling tools, high temperature laboratories equipped with world-class RDI infrastructure, and a range of pilot-scale electric arc and rotary furnaces are utilised for developing pyrometallurgical PGM projects from conceptualisation to full demonstration, i.e., moving from TRL 1-7/8 on the global Technology Readiness Level index. Towards supporting the sustainability of the PGMs industry, Mintek developed and demonstrated the flagship ConRoast process up to the 3 MW DC arc furnace scale. Cutting-edge RDI has also been conducted towards the development of sustainable processes for secondary PGM-bearing resources, including the recycling of automotive catalysts and electronic waste. Pyrometallurgical RDI at Mintek is backed up by extensive analytical chemistry and mineralogical analysis support.

INTRODUCTION

Platinum group metals (PGMs) refer to a group of six elements, namely platinum, palladium, rhodium, ruthenium, osmium and iridium, which possess unique chemical and physical properties suitable for applications in a variety of technologies. PGMs are found in many applications, including automotive converters, hydrogen fuel cells, electronic components, chemical and petrochemical refineries, dental and medical equipment, alloy fabrication, and jewellery. PGM applications continue to grow, as the new advancements and technologies also involve PGMs, including smartphones and automated robots. The demand for PGMs is projected to be sustained, and even increase steadily, long into the future (Zhang, 2024; Gibson, *et al.*, 2023; Kruger, 2022; Glaister & Mudd, 2010). The growing hydrogen economy and general ambition towards clean and renewable energy are expected to be other significant drivers of the demand for PGMs (Zhang, 2024; Minerals Council South Africa, 2023).

South Africa holds approximately 88% of the world's known PGM reserves (Mudd, 2010), and is by far the largest producer of PGMs in the world (Zhang, 2024; Afreximbank, 2024). South African PGM deposits are found in the Bushveld Complex, mainly within the Merensky Reef, Platreef, and Upper Group 2 (UG2). The three deposits have distinct chemical and mineralogical compositions, with the Merensky Reef and the smaller size Platreef deposits being similar, hence they are treated following a similar process. Merensky Reef is a sulfidic ore that is characterised by high PGM and base metal (BM) contents, while the UG2 has comparable PGM contents to Merensky Reef, but lower BM and sulfur (S) contents and high chromite contents.

Valterra Platinum (formerly Anglo-American Platinum), Sibanye Stillwater (formerly Lonmin), Impala Platinum, and Northam Platinum are the major PGM producers in South Africa (Valterra Platinum, 2025; Sibanye Stillwater, 2025; Implats, 2025; Northam Platinum, 2025).

Historical PGM production technology in South Africa has been based on the processing of the preferred Merensky Reef. The conventional process involves comminution and flotation to produce a concentrate for pyrometallurgical processing, which is critical in the overall process flowsheet. The first pyrometallurgical stage is matte smelting, conducted using conventional rectangular six-in-line submerged-arc furnaces or circular three-electrode submerged-arc furnaces. The produced PGM-bearing furnace matte is typically subjected to converting to produce a converter matte for successive processing at the base metals refinery (BMR) and precious metal refinery (PMR) sections (Thethwayo, 2018; Eksteen, 2011; Hundermark, 2011; Cramer, 2008; Jones, 2005). The converter slag is typically recycled to the smelting furnace (Thethwayo, 2018; Jones, 2005; Nell, 2004) or processed separately in a slag cleaning furnace.

Due to declining Merensky Reef reserves, pyrometallurgical exploitation of the UG2 ore increased in the past two decades. Pyrometallurgical processing of UG2 and UG2-rich concentrates with high Cr_2O_3 contents requires special considerations (Eksteen, 2011; Barnes & Newall, 2006; Jones, 2005; Nell, 2004). In addition to challenges presented by the changing PGM smelter feed, the PGM pyrometallurgy sector is also under pressure due to, among others, high costs and unreliable supply of electricity in South Africa, and stringent global regulations to minimise the environmental impact and costs associated with high energy consumption, greenhouse gas emissions, and excessive waste generation (Kruger, 2022; Glaister & Mudd, 2010).

PGM recycling from end-of-life and secondary resources, including automotive converters and electronic waste, is another source of PGMs for supplementing current primary PGM production. Recycled PGMs account for about 60% of new PGM products every year. PGM recycling option has advantages over the primary production processes, including a reduction of carbon intensity by 97%, curbing the need for extensive ore mining while extending the life of PGM mining in South Africa, and superior PGM recovery yields (Johnson Matthey, 2025). Though PGM recycling has obvious advantages and needs to meet the growing demand, it is faced with some challenges, which include social factors such as a lack of responsible parties for PGMs throughout the product life cycle and scrap metal collection inefficiencies, as well as the underdevelopment of technologies for effective recycling of PGMs (Zhang, 2024; Tang, *et al.*, 2023).

Primary and secondary production of PGMs is required to meet the current and projected PGM demand. Research, development and innovation (RDI) is key for addressing the technical challenges facing the primary and secondary PGM production industries. In addition to the opportunity for optimising the flotation process to reject more chromite, RDI pyrometallurgy-based processes for dealing with high chromium concentrates need to be investigated. Thus, fundamental project development principles, involving conceptualisation, laboratory- and demonstration scale testwork, are essential to mitigate risks and uncertainties before implementing new processes or changes in industrial operations, which can be costly (Zietsman & Weitz, 2024; Geldenhuys & Jones, 2011).

Mintek has been providing high-impact and cutting-edge pyrometallurgical RDI to support the South African and global PGM industry since the early 1970s. This paper presents an overview of Mintek's world-class RDI infrastructure and capabilities, and flagship technologies pertaining to the pyrometallurgical processing of PGMs. A critical review of conventional and non-conventional PGM pyrometallurgical process flowsheets and technology projections is also provided.

RDI INFRASTRUCTURE AND CAPABILITIES

Mintek has considerable infrastructure and capabilities for completing pyrometallurgical RDI on PGMs, from conceptualisation to demonstration, towards commercialisation to support the sustainability of

the PGMs industry. PGM pyrometallurgical RDI at Mintek typically involves desktop studies through computational modelling and thermochemical simulations for developing preliminary process flowsheets with mass and energy balance, feasibility testing at laboratory and bench scale, and subsequently pilot-scale testing for demonstrating the viability of proposed technical solutions. Empirical work is supported by extensive analytical chemistry and mineralogical characterisation capabilities.

Mintek's Pyrometallurgy Division (PMD) comprises three functional groups, namely, New Technology, Technology Development, and Technology Demonstration, for conducting relevant RDI, including the development of PGM projects. PGM technology conceptualisation, development, and demonstration at Mintek follows the globally accepted benchmarking tool, Technology Readiness Level (TRL) index, with a scale of 1 – 9. The TRL index provides the means for tracking technology maturity and supporting development from New Technology or blue-sky research using theoretical tools (TRL 1-3), to Technology Development involving empirical feasibility studies at a laboratory scale (TRL 3-5), and to Technology Demonstration involving testing using an integrated system in a relevant environment (TRL 5-7). Development stages at Mintek generally complement each other.

PMD employs a total of 44 staff, 27 of whom have university qualifications as scientists, engineers and technologists (SET). Of the 27 SET staff members, 34% and 31% have master's and doctoral degrees, respectively. The qualification profile of the PMD SET staff, with 65% staff complement having post-graduate qualifications, is testament to Mintek's endeavours to improve their service offering and provide quality RDI to support the minerals industry, especially the pyrometallurgy PGM industry.

Analytical Chemistry and Mineralogical Analysis Support

PGM pyrometallurgical RDI at Mintek is supported by extensive analytical chemistry and mineralogical characterisation expertise, providing a 'one-stop shop' for complete development of a PGM project. The Analytical Chemistry Division operates under ISO 17025 accreditation and has the capacity to analyse PGM process samples using conventional and unconventional analytical techniques and methods. The conventional fire assay method used for determining PGMs in ores, concentrates, slags and other solid samples is typically coupled with modern instrumentation analytical techniques such as Inductively Coupled Plasma Optical Emission Spectroscopy (ICP-OES) and or Inductively Coupled Plasma Mass Spectrometry (ICP-MS) for simultaneous determination of PGMs at minor or trace concentration levels. Direct acid dissolution of PGM-bearing alloys and mattes using a microwave or hotplate, followed by analysis using ICP-OES and/ or ICP-MS, is typically conducted for determining PGM concentrations in these samples. ICP-OES, ICP-MS, and Laboratory Equipment Corporation (LECO) combustion techniques are also used for determining the concentrations of other elements in the feed and processed materials during RDI of a pyrometallurgical PGM project (Mintek, 2025a). Most of the analytical chemistry work is conducted for commercial clients; hence, it is not readily available in the public domain.

The Mineralogy Division (MND) uses modern analytical techniques to provide qualitative and (semi)quantitative mineralogical analysis results of mainly PGM ores and concentrates, and to a lesser extent, PGM smelter slags and matte. MND hosts the conventional instrumentation, such as X-Ray Diffraction (XRD) and Scanning Electron Microscopy coupled with Energy Dispersive Spectroscopy (SEM-EDS), as well as modern analytical techniques, such as Electron Probe Micro Analysis (EPMA), micro-X-Ray Fluorescence (micro-XRF), and automated SEM techniques, including Mineral Liberation Analyser (MLA), Quantitative Evaluation of Minerals by SCANning electron microscopy (QEMSCAN), and TESCAN Integrated Mineral Analyser (TIMA). Mineralogical characterisation using the identified techniques is particularly important in the high-temperature study of the interaction of furnace refractory and PGM process materials, such as PGM smelter slag/ matte and converter slag and matte. Some of the mineralogical analysis work is published in the literature (Carelse, *et al.*, 2022; Chetty, 2009), while most of the work has been conducted for clients and could not be published.

New Technology and Concept Development through Modelling and Simulation

Mintek has capacity to undertake RDI in this area from conceptualisation using thermochemical

software, feasibility studies at laboratory and bench scales, and demonstration using large pilot furnaces. To support laboratory and pilot scale test work related to PGMs, PMD offers desktop and theoretical modelling studies, including process and flowsheet modelling, mass and energy balances as well as process optimisation and troubleshooting as follows:

- Thermochemical and process simulations are undertaken using FactSage, HSC Chemistry, and Pyrosim.
- Mathematical modelling and computer simulations of different flow-regimes in PGMs processing – material flow modelling and heat transfer, multiphysics modelling for simultaneous evaluation of heat transfer, mass transfer and chemical reaction phenomena, models for scaling up laboratory experiments to higher TRLs
- Arc modelling work to support the electric arc furnace testing work.

Desktop and theoretical modelling studies can investigate a wide range of conditions at a relatively low cost and fast turnaround time compared to experimental work. The results obtained from such studies are used to evaluate the feasibility of the concept of interest from a fundamental basis.

Technology development through laboratory testwork

PGM smelters, like other industrial operations, apply caution to minimise risk before commissioning new operations or implementing new technologies and significant step-changes in their operations. Even with positive theoretical concept development, empirical testwork at laboratory scale is still important to validate the preceding theoretical work and to understand the process performance under strictly controlled conditions. Laboratory/bench-scale testwork is generally adopted for testing the robustness of the proposed technology or process, as a wide range of test parameters under strictly controlled conditions can be evaluated at relatively lower costs and minimal risk (Geldenhuys & Jones, 2011).

Pyrometallurgical laboratory testwork at Mintek typically involves material property measurements and smelting and converting process testing and development.

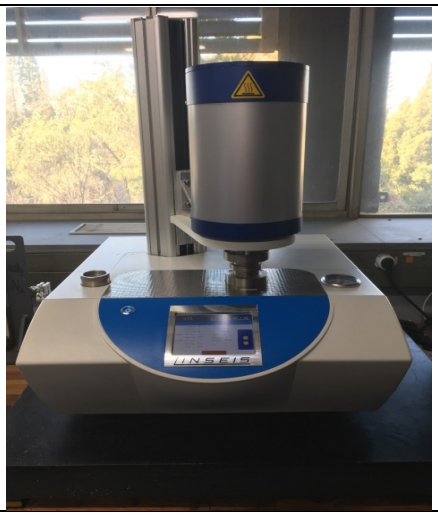
Material property measurements

The high temperature laboratories at Mintek have the equipment capacity for measuring different thermochemical and physicochemical properties of materials, including slags, matte, and alloys involved in PGM processes, to support up-scale demonstration work and industrial operations. Equipment that is available for material property measurement is described in the following points, with the photographs of some of the actual equipment shown in Figure 1.

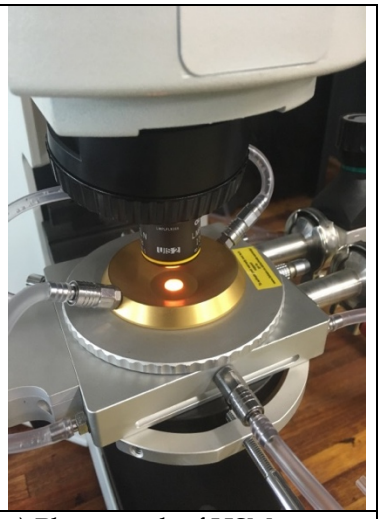
a) Conventional equilibration-quench tube furnace coupled with mineralogical analysis using EPMA, SEM-EDS, and/ or AutoSEM techniques. This equipment is used for determining the liquidus, sub-liquidus/solidus and solidus temperatures of slags and phase relations of chemical systems. This furnace has an upper operational temperature of 1700°C, under a controlled atmosphere, i.e., tests can be conducted in specific atmospheres such as inert using argon/ nitrogen gas, specific oxygen partial pressure (pO_2) controlled by CO/CO_2 or H_2/H_2O, or other atmospheres.
b) Differential Scanning Calorimetry coupled with Thermogravimetric Analysis (DSC-TGA) for determining the liquidus temperatures and other thermochemical properties, including heat capacity of different materials, including slags, matte, and alloys. This unit can operate at temperatures of up to 1600°C under an inert atmosphere.
c) Hot-Stage Microscopy (HSM) for determining the liquidus temperatures of materials and recording the phase transformation images and footage for different materials, including slags, matte, and alloys. HSM can operate at temperatures of up to 1500°C under an inert atmosphere.
d) In an effort to improve the service offering, Mintek and the National Research Foundation are collaborating on the procurement of a Furnace Rheometer System (FRS) for determining the viscosity and electrical conductivity of molten materials, including slags, matte, and alloy. This national equipment will be located at Mintek. An FRS 1800 system, with an upper sample temperature of 1730°C under inert conditions, is being procured.



a) Photograph of equilibration-quench furnace



b) Photograph of DSC-TGA



c) Photograph of HSM

Figure 1: Photographs of the available property measurement equipment, a) equipment-quench furnace, b) DSC-TGA, and c) HSM

PGM smelting and converting process development

Pyrometallurgical testwork requirements typically involve the evaluation of client concentrates for processing by conventional matte smelting to recover PGMs and BMs in the matte while deporting the gangue to the slag. As a solution for processing low-sulfur and high-chromium oxide ores like UG2, Mintek developed a smelting process called the ConRoast process, which is essentially a dead-sulfur roasting of a concentrate and carbothermic smelting process to recover PGMs and BMs in an iron-rich alloy. So, typical laboratory testwork conducted at Mintek supports conventional and unconventional matte and alloy smelting options. For ConRoast process testing, dead-roasting testwork is typically conducted at temperatures of up to 1000°C. Conventional matte smelting and unconventional carbothermic alloy smelting testwork is conducted at high testing temperatures in the order of 1600°C under a controlled atmosphere to avoid unintended oxidation of sulfur required for matte formation or carbon reductant in the case of alloy smelting. For smelting tests, either alumina or magnesia sintered crucibles are used. Parameters during the PGM smelting work include flux and reductant additions.

PGM-bearing matte or alloy product is typically subjected to converting to remove mainly iron to the converter slag, while concentrating the PGMs and BMs in the corresponding converter matte or alloy. Converter slag composition, varied by flux type and addition, is the typical parameter during converting testwork.

Equipment that is used at Mintek for PGM matte and alloy smelting and converting testwork is described in the following points, with photographs of some of the equipment shown in Figure 2.

a) Rotary kiln furnace for dead-sulfur roasting testwork, at temperatures of up to 1200°C under semi-controlled atmospheric conditions. This kiln can process a PGM concentrate of up to 5 kg per batch. Temperature control is supported by a K-type thermocouple.
b) Quartz tube reactor with a silica frit, fitted in a vertical tube furnace for dead-sulfur roasting testwork in a fluidised or static bed mode, at temperatures of up to 1000°C (measured by a K-type thermocouple) under semi-controlled atmospheric conditions. This set-up can process concentrates of up to 200 g.
c) Gas-tight/ atmosphere-controlled chamber furnace for completing smelting tests at 100 – 200 g, at temperatures of up to 1700°C, measured using a B-type thermocouple.
d) Semi-atmosphere-controlled induction furnace for completing smelting tests. Different scales of induction furnaces allow for smelting tests to be completed at scales of up to 30 kg (using the

largest 100 kVA induction furnace), at temperatures of up to 1700°C, measured using a B-type thermocouple.



a) Photograph of an atmosphere-controlled chamber furnace



b) Photograph of a semi-atmosphere-controlled induction furnace (25 kW power rating)

Figure 2: Photographs of the available smelting furnaces, a) atmosphere-controlled chamber furnace, b) semi-atmosphere-controlled induction furnace.

Typical outcomes of laboratory testwork

PGM pyrometallurgical testwork at laboratory-scale typically allows for the evaluation of the effect of different test parameters on the objective of the testwork, which is generally the maximum recovery of PGMs (and BMs) to the matte/ alloy products at both smelting and converting stages of the process flowsheet. These tests allow for the evaluation of a wide range of parameters and, thus, allow for a good understanding of the dependence of the PGM smelting and converting processes on the parameters. These results generally suffice to indicate the feasibility or otherwise of a proposed process, including the evaluation of the quality of product streams. They are generally achieved within a reasonable budget and time period, using a relatively small sample and synthetic additives (fluxes and reductants). All this work is possible at a laboratory scale because these experiments can be controlled with some confidence (Geldenhuys & Jones, 2011).

However, by their very nature, laboratory-scale tests are indicative as they are also conducted in batch mode, while industrial operations are conducted in continuous mode. At a low TRL of 5 or less, laboratory-scale PGM pyrometallurgical testing would not be able to test processes under relevant conditions and environment to industrial operations. For example, a pilot-scale demonstration test would be essential to understand the roasting, smelting, and converting behaviour of PGM resources using real fluxes and reductants, using pilot furnaces that closely mimic the target or current industrial furnaces.

Technology demonstration utilising pilot furnaces

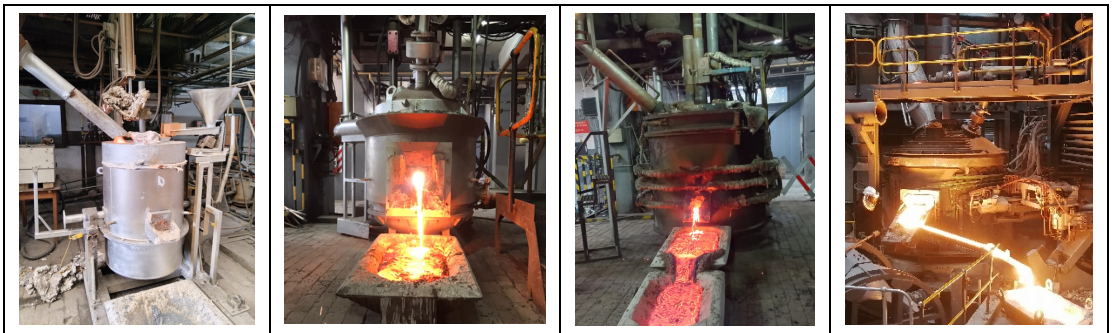
Importance of upscaling laboratory-scale tests

The inherent technical and commercial risks associated with upscaling new processes to an industrial scale warrant a systematic approach to any pyrometallurgical technology development (Zietsman & Weitz, 2024). Tests conducted at laboratory scale can sometimes provide the best-case scenario of a process owing to the well-controlled nature of the experiments, including quality of the raw materials, accurate batch feed masses, accurate temperature measurements, uniform temperature distribution, and intimate mixing of reactants. When the same process is demonstrated at pilot scale or implemented at industrial scale, there may be differences in the process efficiencies obtained. This is mainly why scaling up from small scale tests is generally perceived as high risk, especially when applying a new technology where limited references or industry standards are available (Geldenhuys & Jones, 2011).

To de-risk uncertainties associated with the introduction of a new technology, processing of new raw material or the application of existing technology to a different process chemistry, rigorous testing at the appropriate pilot scale is imperative.

Available furnace capacity – from 30 kW to 2 MW

Mintek recognised the uniqueness and importance of addressing different process design challenges at different pilot scales for different technological developments. To this end, significant investment was dedicated, over the years, to developing a versatile pyrometallurgical research infrastructure hinged predominantly on the application of a range of electric arc furnaces, especially DC arc furnaces, for the processing of critical minerals and metals of strategic importance to the South African economy, such as PGMs, iron and steel, and ferroalloys. Piloting capabilities to test recovery of PGMs from primary resources via the ConRoast process and secondary resources such as recycled spent autocats include DC arc furnaces at small, medium, and large pilot scale with operating power from 30 to 2000 kW (see Figure 3). For example, the 1 m shell diameter DC arc furnace (Figure 3(b) can be operated at powers up to 200 kW and voltages of up to 150 V at currents of 1300 A. This furnace can process total feed batches of 150 kg, which may include PGM concentrate, reductant, fluxes, and other additives such as a source of collector alloy (e.g., hematite during smelting of autocats) to achieve a daily throughput of 1 t/day of PGM concentrate.



(a) (b) (c) (d)

Image	-	(a)	(b)	-	(c)	-	(d)
Current type	DC	DC	DC	AC	AC	DC	DC
Power, kW	30	50	200	200	250	1500	2000
Current, kA	0.4	0.5	≤1.3	≤1.3	≤1.4	≤5	≤6.6
Voltage, V	≤80	≤100	≤150	≤150	≤180	≤300	≤300
Shell diameter, m	0.35	0.45	1	1	1.5	2.5	2.5
Shell cooling	Forced	None	Film	Forced	Forced	Forced	Forced
Total batch size, kg	30	50	150	150	250	1500	1500
Throughput (t/day)	≤0.2	≤0.4	≤1	≤1	≤1.7	≤10	≤15

Figure 3. Mintek's range of electric arc furnaces available for testing at small, medium, and large pilot scale, including the (a) 50 kW DC, (b) 200 kW DC, (c) 250 kW AC, and (d) 2000 kW DC furnaces, and their associated typical operating parameters.

The ConRoast process (and spent autocat smelting process) produces iron-rich alloys containing the PGMs and BMs. Mintek also has piloting capabilities to refine the iron-rich PGMs collector alloy in either a small- or medium-sized pilot scale top blown rotary converter (TBRC), shown in Figure 4. The 600 kW natural gas burner TBRC has capacity to demonstrate refining of up to 4 t of alloy a day.



(a)



(b)

Image	(a)	(b)
Power source	Gas burner	Gas burner
Power, kW	120	600
Oxidant gas	Oxygen	Oxygen
Fuel gas	Propane	Natual gas
Shell diameter, m	0.6	1.5
Total batch size, kg	50	650
Throughput (t/day)	≤0.4	≤4

Figure 4. Mintek's (a) 120 kW oxy-propane burner TBRC, and (b) 600 kW oxy-natural gas burner TBRC for testing at small and medium pilot scale, and their associated typical operating parameters.

Typical outcomes of demonstration studies

The framework of the main activity groups of managing a pilot smelting campaign at Mintek involves project management, procurement, raw materials preparation and characterisation, facility preparation and commissioning, pilot smelting campaign, decommissioning of plant, and technical report writing. Table I provides a brief description of the systematic approach to the general activities undertaken and the output delivered from each activity group. The outcome of the pilot test work is the successful delivery of the project without any safety, health, environment, and quality incidents at the agreed time, quality, and cost. This is underscored by key outputs such as on-time delivery of correctly specified goods and services, demonstration and delivery of all agreed project and process objectives, furnace operating data and process information, and complete plant data and all material masses and analytical data diligently compiled in a written technical report.

Table 1. A framework for executing a pilot smelting campaign outlining the general activities and outputs

Activity group	**Activity**	**Output**
Project management	Project planning & administration, SHEQ risk assessments & management, resource planning, external contractor management, quality control & monitoring, logistics, client interaction, project financial management, communication with all stakeholders, and appropriate filing of all project records.	Delivery of project without any SHEQ incidents at agreed time, quality, and cost.
Procurement	Contact suppliers, compile specifications, raise purchase requisitions, send out RFQ, receive quotes, technical evaluation, issue PO, delivery of order, confirm quality, and invoice payment.	On-time delivery of correctly specified goods and services.
Raw materials preparation & characterisation	Moisture analysis, bulk drying, crushing, blending and sub-sampling, chemical and phase chemical analysis, particle size distribution, density measurement, and LOI test.	Data set of all characterisation results.
Facility preparations & commissioning	Mechanical modifications & installations, electrical installations & testing, field instrument wiring and signal testing, control system software configuration, furnace refractory installation, power supply pre-inspection & testing, measurement instrument	Fully prepared pilot facility with a GMR2 inspection report and approval.

	calibrations, checking and testing of quality of utilities (electricity, compressed air, natural gas, oxygen gas, de-ionised water).	
Pilot smelting campaign	Detailed thermochemical calculations. Refinement of process simulations, experimental design and plan, process control philosophy, furnace operating parameters, campaign safety briefing, plant management, safe operation of plant equipment, health and safety of shift teams, problem solving, people management, sample management, plant data management, quality management, interaction with support service divisions, communication of plant information, project file management, environmental management, continuous improvement.	Demonstration and delivery of all agreed project & process objectives. Furnace operating data & process information.
Decommissioning of plant	Refractory wear assessment & measurements, furnace dig-out, emptying of hoppers, baghouse & plant cleanup, collect & file all logsheets and other SHE documentation, update campaign workbook & follow up on all missing material and furnace operating data. Ensure all samples are labelled and stored appropriately. Overall project audit & verification.	Complete plant data & all material masses and analytical data.
Technical report writing	Plant data collation, process information organisation & visualisation, analysis & interpretation, mass & energy calculations, technical report writing with detailed discussions on materials, method, equipment, process results & efficiencies, conclusions & recommendations.	Official final approved technical report.

RDI ACTIVITIES AND TECHNOLOGY OUTPUT

Overview of PGM Pyrometallurgical RDI work

Using the PGM RDI infrastructure and capabilities described above, Mintek has been involved in key technological research and development to support the local and global PGMs industries. When in the 1970s the demand for PGMs was anticipated to surge exponentially due to newly found additional applications in, amongst others, the automotive sector for emission controls, Mintek got involved by contributing RDI for producing UG2 concentrate using a flotation process (Deeplaul & Bryson, 2004). The UG2 concentrate was characterised by low S and high Cr_2O_3 contents, which presented challenges for processing using the conventional sulfide/ matte smelting process. Mintek embarked on RDI involving conceptualisation up to demonstration using large pilot furnaces and subsequently produced the novel ConRoast process. ConRoast is an integrated process that essentially involves the removal of S from the concentrate through oxidative dead-roasting and direct current arc furnace carbothermic smelting process for collecting PGMs and BMs in an iron-based alloy. ConRoast process was later commercialised by Braemore Platinum, which was acquired by Jubilee Metals Group (Phillips, 2008).

To support the downstream process for effective and efficient extraction of PGMs from the iron-based alloy produced from the ConRoast process, Mintek researched and developed a converting process. Converting process aims to remove iron and concentrate the PGMs and BMs in the remaining alloy to facilitate effective and economical extraction of the PGMs by the downstream hydrometallurgical process (McCullough, 2008). This converting process can be applied to secondary processing of end-of-use PGM- and BM-bearing alloys.

The commercialisation of the ConRoast process did not take off at the pace that was initially anticipated, as the available Merensky Reef resources still allowed for smelting of their blends with UG2 ores using the current installed furnace capacity. To maximise the processing of Merensky-UG2 blends and exclusive UG2 concentrates, Mintek investigated a reductive matte smelting process. During reductive matte smelting, some iron oxides are reduced to the metallic state, and the chromium oxides from UG2 concentrate are reduced to CrO to increase the matte/alloy fall and PGM recoveries and also improve the solubility of chrome-spinel in the slag. Reductive matte smelting and the ConRoast processes have similar advantages; however, the reductive matte smelting process can, to some extent, use the current installed furnace capacity by the major PGM smelters.

To support the current and projected PGM demand, extend the lifespan of primary PGM resources, and mitigate against environmental challenges presented by the primary PGM smelting processes, Mintek has also been active in the research of pyrometallurgical solutions for extracting PGMs from secondary resources. Most of the work conducted in this area has been in collaboration with the private sector.

Flagship PGM RDI capabilities and technologies

Overview of the ConRoast process

ConRoast process is one of the flagship processes developed by Mintek to support the global PGMs industry. This novel process was developed for the treatment of low sulfur and high chrome PGM ores like UG2, which are not readily amenable to processing using the conventional matte smelting process. ConRoast process, shown in Figure 5, is essentially an integrated oxidative roasting and carbothermic smelting process. The first stage is for dead-roasting for the removal of sulfur and conversion of BM sulfides to oxides, allowing for the direction of the produced sulfur dioxide (SO_2) to a sulfuric acid plant. Roasting, which can be conducted using a fluidised-bed roaster, is typically conducted at 1000°C. The dead-roast/calcine is fed to a smelter for carbothermic reductive smelting, where a carbonaceous reductant is added for the formation of an iron-rich alloy that collects the BMs and PGMs. This process was developed and demonstrated up to 3 MW DC arc furnace scale at Mintek.

ConRoast process was licensed to Braemore Platinum for commercialisation using a 35 MW DC arc furnace for smelting. Braemore Platinum was later acquired by Jubilee Platinum.

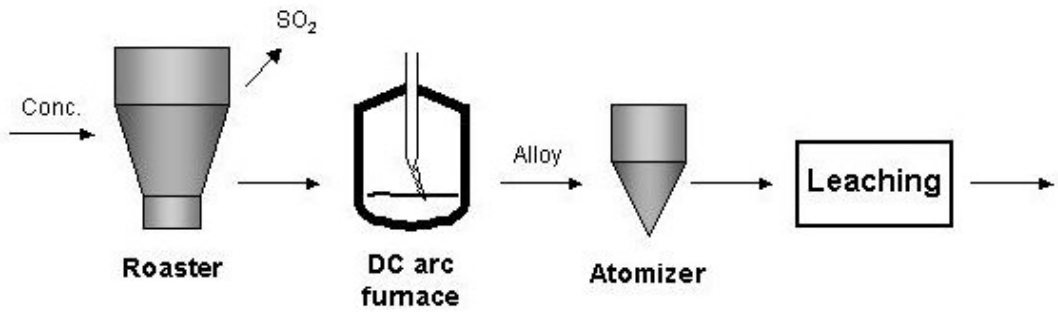


Figure 5: Overview of the ConRoast process.

Converting work for the extraction of PGMs from the Fe-rich alloy

ConRoast process produces a PGM-bearing iron-rich alloy, with about 80% Fe content, that can be atomised and fed directly into a leaching stage for BM and PGM extraction and refining. During leaching, iron is leached into solution and subsequently rejected by precipitation as hematite, while the acid lixiviant is ideally recycled. The acid can also be neutralised with lime, followed by further precipitation of residual iron as goethite, which would be disposed of . However, due to high Fe content in the alloy, acid consumption during leaching is generally high. McCullough *et al*. (2008) developed a converting process for lowering the Fe content in the feed to the downstream hydrometallurgical process, thereby lowering the acid consumption for leaching iron. The pyrometallurgy-based converting process involves iron removal from the alloy by blowing either air or oxygen into the molten alloy, coupled with appropriate fluxing for the collection of iron oxide in the Fe-Si-O (fayalite slag) or Fe-Si-Ca-O (olivine-type slag) system. At bench-scale, Fe content was decreased from about 80% in the starting alloy to <5% Fe in the final alloy, with minimal losses of BMs and PGMs to the slag stream (McCullough, 2008). This converting work has also been conducted at a larger scale using Mintek's 120 kW oxy-propane burner TBRC, with a molten alloy volume of 20 L, in collaboration with the private sector.

Alternative collectors for PGMs

ConRoast process essentially results in the production of PGM- and BM-bearing iron-rich alloy, with about 80% Fe content. In collaboration with the private sector and academia, Mintek is involved in RDI

for alternative collectors of PGMs, from iron-based alloy, to maximise the economics of the ConRoast process. Similar to iron-based alloy collection, Pt (and other PGMs) dissolves readily in Cu and Ni-based alloys, as shown in Figure 6. The approach involves the co-smelting of chrome-rich dead-roasted PGM concentrate, like Merensky-UG2 blend or UG2-only, and Cu and/ Ni primary/ secondary source like spent petroleum catalysts. In this process, PGMs are collected in Cu- and/ Ni-rich alloys, which are subjected to hydrometallurgical BM and PGM extractions without pre-converting. Mintek has capacity to undertake RDI in this area from conceptualisation using thermochemical software, feasibility studies at laboratory and bench scales, and demonstration using pilot furnaces. Most of the work conducted in this area has been in collaboration with the private sector and/or academia.

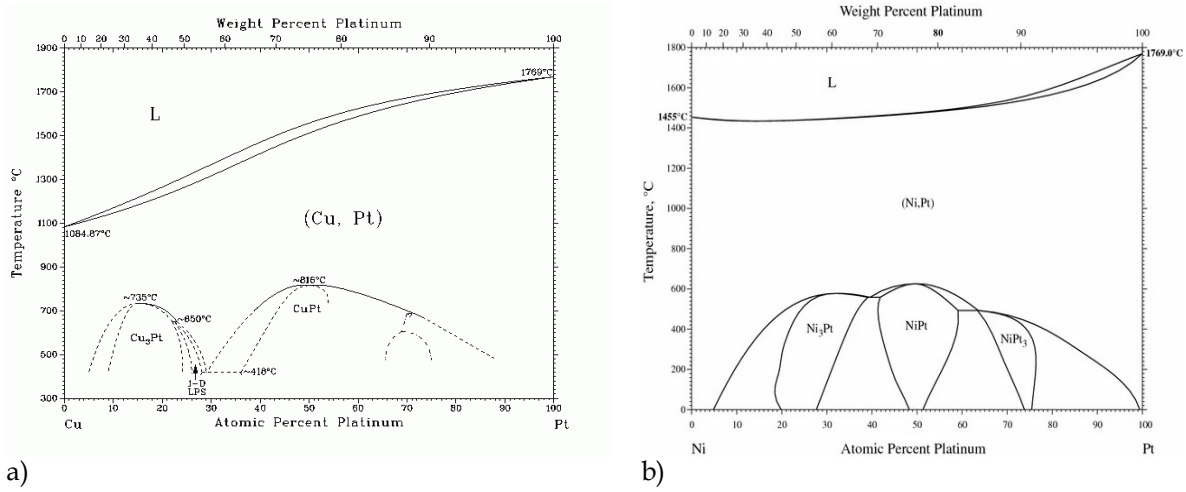


Figure 6: Binary phase diagrams for a) Cu-Pt, and b) Ni-Pt (Okamoto et al.*, 2016).*

Secondary PGM resources

The projected increase in the demand for PGMs long into the future, the desire to prolong the lifespan of primary PGM resources, and the stringent global regulations mitigating against environmental attack by emissions from industrial smelting operations are some of the factors that contribute to the strong initiatives for the production of PGMs from secondary resources. Already, recycled PGMs account for over 60% of new PGM products every year. Increased efficiency in the collection of secondary resources and development of efficient technologies, amongst others, have the potential to grow the contribution of recycled PGMs to the global PGM production. Mintek has been conducting cutting-edge research and development towards the development of sustainable processes for secondary PGM resources, including spent automotive catalysts (autocats) and electronic waste (e-waste). One of the pyrometallurgical-based approaches for recycling PGMs from autocats and e-waste involves co-smelting of each of these secondary materials with a metal collector source like hematite, a reductant for reducing hematite, and flux for effective slagging. Most of the work conducted in this area has been in collaboration with the private sector.

CRITICAL REVIEW OF CONVENTIONAL PGM PYROMETALLURGY PROCESS FLOWSHEET AND TECHNOLOGICAL PROJECTIONS

The PGMs industry is well-established. The projected increase in the demand for PGMs long into the future for current and new applications provides assurance about the future of the industry. The main application of PGMs is in the production of autocats for environmental control in vehicles. The introduction of electric vehicles creates both risk, in terms of losing application in a complete electric vehicle, and opportunity when hybrid vehicles are used. As South Africa is home to the majority of global PGM reserves, most PGMs are primarily produced in South Africa. The conventional matte smelting process for producing PGMs, shown Figure 7, is well established, with high throughputs and

proven flowsheet and downstream integration.

Major technical and operational challenges facing the conventional matte smelting process include:

- Changes in the feed mineralogical and chemical compositions with increasing chromite content and decreasing sulfur content as more UG2 concentrate is added in the feed blend. High chromite content in the feed blend results in the stabilisation of the chrome-spinel in the slag, compromising PGM recoveries and the build-up on the furnace refractory lining, resulting in the reduction of furnace working volume and premature furnace shutdown that adversely affects the throughput of the operation. Low sulfur content in the feed results in low matte falls and overall PGM and BM recoveries.
- Process containment challenges as a consequence of operating with a highly superheated furnace matte at about 500°C superheat temperature, which generally result in high wear rate and degree of damage to the refractory lining. This is a consequence of large differences between the matte and slag liquidus temperatures.
- Environmental and regulatory challenges presented by the inherent emission of SO_2 from the primary smelting furnaces and converters. Additional capex is generally required to manage the off-gas streams from the smelters and converters.
- Energy intensity of the process and vulnerability to energy crisis in South Africa. As major PGM producers are in South Africa, the energy costs and availability are a serious risk facing the PGM industry.

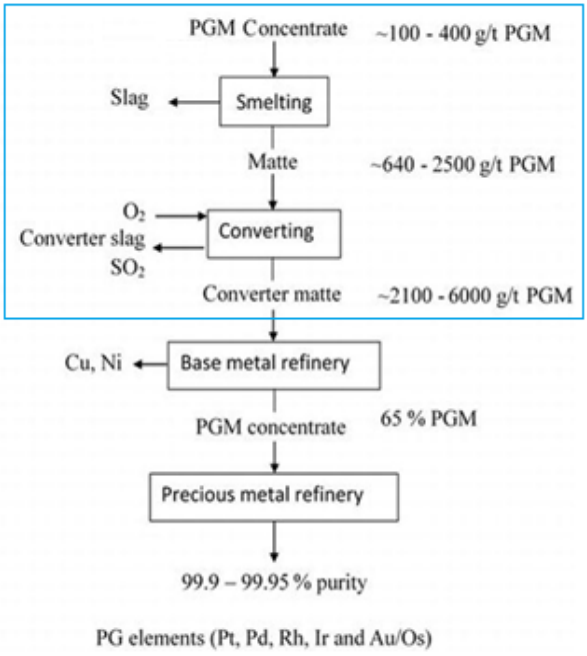


Figure 7: Overview of the matte smelting process flowsheet for production of PGMs (adapted from Thethwayo, 2018).

Reductive matte smelting of the UG2-rich smelter feed has been proposed as an alternative to the conventional matte smelting process. This alternative allows for the utilisation of the installed furnace capacity, with only a limited modification, if any. This approach is able to address the challenges presented by UG2-based feeds with high chromite and low sulfur contents, as some iron is reduced to the metallic state and gets incorporated into the PGM-bearing matte-alloy stream, thereby increasing the matte-alloy fall. Moreover, reducing conditions support the reduction of chromium oxide in the feed to CrO, which is readily soluble in the slag. A reductive matte smelting furnace would operate at relatively low oxygen partial pressures, thus more sulfur would be retained as matte, resulting in more

matte fall, and less sulfur would deport to the off-gas stream. Despite these advantages, this approach is still prone to process containment challenges presented by the highly superheated PGM furnace matte and energy issues experienced in South Africa. The environmental challenges become more complex in the reductive matte smelting process, as more CO/CO_2 is incorporated into the off-gas stream. Reductive matte smelters would not be immune to energy issues faced by the conventional matte smelting operations in South Africa. Moreover, excessive reductant additions in the smelter feed would result in the production of a separate alloy stream, which would complicate the process from the PGM distribution between matte and alloy, and furnace operational viewpoints.

Complete alloy smelting process, like Mintek's ConRoast process, would require a substantial capex investment to change from the current installed capacity or for a new operation. CO/CO_2 management would also require attention, similar to other carbothermic smelting operations. ConRoast process is conducted in a fluidised bed roaster and DC arc furnace. Environmental challenges relating to the management of the SO_2 emissions are better in this process, as high-temperature processing of sulfur-bearing charges would occur during roasting only. Moreover, high chromite and low sulfur contents in the PGM concentrate are not an issue in this process. Considering that an iron-rich alloy with a liquidus temperature similar to that of an operating slag, neither the alloy nor the slag would be super-heated, thus avoiding process containment challenges.

The imminent depletion of the conventional Merensky PGM deposit has compelled PGM smelters to review their current operations while using the installed furnace capacity. Considering that the PGMs industry is becoming more reliant on the UG2 ore, Mintek's ConRoast process will provide support for sustaining the global pyrometallurgy industry. Fortuitously, pyrometallurgical RDI capabilities, including the bench-scale and piloting infrastructure at Mintek, for producing PGMs, are established at Mintek to support project development from conceptualisation to demonstration, towards commercialisation. Downstream hydrometallurgical processing capabilities of PGM-bearing alloy or converter alloy are also available at Mintek. All these developments are supported by well-equipped analytical chemistry and mineralogy laboratories.

CONCLUSIONS

In view of the presented challenges facing the current PGM producers utilising the conventional matte smelting process, Mintek's pyrometallurgical RDI activities and infrastructure are well-suited to support the PGM industry in intensifying the current operations and also to explore alternative processes like the ConRoast process. A combination of theoretical approaches involving computational modelling and thermochemical modelling and simulations, feasibility studies at laboratory and bench scales, and subsequently demonstration at scale are unique capabilities that exist at Mintek to start and/ or support initiatives towards sustaining the PGMs industry. Mintek can provide support for the development of PGM projects from conceptualisation to demonstration of responsible and resilient PGM processes, i.e. from TRL 1 – 7/8 in the global Technology Readiness Level index. This is completed with on-site chemical and mineralogical analysis support.

ACKNOWLEDGEMENTS

This paper is published by permission of Mintek.

REFERENCES

Afreximbank. (2024). *Platinum Group Metals (PGMs) - Analyzing Recent Price Trends.* Afreximbank.

Barnes, A. R., & Newall, A. F. (2006). Spinel Removal from PGM Smelting Furnaces. (pp. 77-88). Cradle of Humankind: Southern African Pyrometallurgy 2006 International Conference.

Carelse, C., Manuel, M., Chetty, D., Taguta, J., Safari, M., & Youlton, K. (2022). The flotation behaviour of liberated Platinum Group minerals in Platreef ore under reduced reagent conditions. *Minerals Engineering, 190*, 1-8. doi:https://doi.org/10.1016/j.mineng.2022.107913.

Chetty, D., Gryffenberg, L., Lekgetho, T. B., & Molebale, I. J. (2009). Automated SEM study of PGM distribution across a UG2 flotation concentrate bank: implications for understanding PGM floatability. *The Journal of The Southern African Institute of Mining and Metallurgy, 109*, 587-593.

Cramer, L. A. (2008). What is your PGM concentrate worth? (pp. 387-394). Sun City: Third International Platinum Conference, Platinum in Transformation, The Southern African Institute of Mining and Metallurgy.

Deeplaul, V., & Bryson, M. (2004). Mintek, a national resource of minerals processing expertise for platinum ores. (pp. 9-14). Sun City: International Platinum Conference 'Platinum Adding Value', The South African Institute of Mining and Metallurgy.

Eksteen, J. J., Van Beek, B., & Bezuidenhout, G. A. (2011). Cracking a hard nut: an overview of Lonmin's operations directed at smelting of UG2-rich concentrate blends. *The Journal of the Southern African Institute of Mining and Metallurgy, 111*, 681-690.

Geldenhuys, I. J., & Jones, R. T. (2011). What scale should your smelting testwork be done at, and what do you get for the money you spend? *6th Southern African Base Metals Conference 2011.* Palaborwa, South Africa, 18-21 July 2011: Southern African Institute for Mining and Metallurgy.

Gibson, B. A., Nwaila, G., Manzi, M., Ghorbani, Y., Ndlovu, S., & Petersen, J. (2023). The valorisation of platinum group metals from flotation tailings: A review of challenges and opportunities. *Minerals Engineering, 201*, 1-24. doi:https://doi.org/10.1016/j.mineng.2023.108216.

Glaister, B. J., & Mudd, G. M. (2010). The environmental costs of platinum–PGM mining and sustainability: Is the glass half-full or half-empty? *Minerals Engineering, 23*, 438-450. doi:doi:10.1016/j.mineng.2009.12.007.

Hundermark, R. J., Mncwango, S. B., de Villiers, L. P., & Nelson, L. R. (2011). The smelting operations of Anglo American's platinum business: an update. (pp. 295-307). Sun City: 4th International Platinum Conference, Platinum In Transition 'Boom or Bust', The Southern African Institute of Mining and Metallurgy.

Implats. (2025). *Implats at a glance*. Retrieved August 25, 2025, from https://www.implats.co.za/implats-at-a-glance.php

Johnson Matthey. (2025). *The PGMs: a circularity success story.* Johnson Matthey.

Jones, R. T. (2002). ConRoast: DC arc smelting of dead-roasted sulphide concentrates. *3rd International Sulfide Smelting Symposium* (p. pg22). Seattle, Washington, USA: TMS Annual Meeting.

Jones, R. T. (2005). An overview of Southern African PGM smelting (pp. 147–178). Nickel and Cobalt 2005: Challenges in Extraction and Production, 44th Annual Conference of Metallurgists, Canadian Institute of Mining, Metallurgy and Petroleum.

Jones, R. T. (2009). Towards commercialisation of Mintek's ConRoast process for platinum smelting. In J. Liu, J. Peacey, M. Barati, S. Kashani-Nejad, & B. Davis (Ed.). Sudbury, Ontario, Canada: Proceedings of the 48th Annual Conference of Metallurgists of CIM, Pyrometallurgy of Nickel and Cobalt 2009, Met Soc.

Jones, R. T., & Geldenhuys, I. J. (2011). The pros and cons of reductive matte smelting for PGMs. *Minerals Engineering, 24*(6), 495-498. doi:https://doi.org/10.1016/j.mineng.2011.03.007.

Kruger, J. (2022). PGM mining and processing in the circular economy: A framework towards circularity. (pp. 23-32). Sun City: 8th International PGM Conference, The Southern African Institute of Mining and Metallurgy.

McCullough, S. D., Geldenhuys, I. J., & Jones, R. T. (2008). Pyrometallurgical iron removal from a PGM-containing alloy (pp. 169-176). Sun City: Third International Platinum Conference, Platinum in Transformation, The Southern African Institute of Mining and Metallurgy.

Minerals Council South Africa. (2023). *Comprehensive facts and figures.* Johannesburg: Minerals Council South Africa.

Mintek. (2025a). *Analytical Chemistry.* Retrieved July 20, 2025, from https://mintek.co.za/clusters/divisions/analytical-chemistry.html

Mudd, G. M. (2010). Platinum group metals: a unique case study in the sustainability of mineral resources. (pp. 113-120). Sun City: The 4th International Platinum Conference, Platinum in transition 'Boom or Bust', The Southern African Institute of Mining and Metallurgy.

Nell, J. (2004). Melting of platinum group metal concentrates in South Africa. *The Journal of The South African Institute of Mining and Metallurgy*, 423-428.

Northam Platinum. (2025). *Annual integrated report for the year ended 30 June 2025.* Northam Platinum.

Okamoto, H., Schlesinger, M. E., & Mueller, E. M. (Eds.). (2016). *Alloy Phase Diagrams* (Vol. 3). ASM International. https://doi.org/10.31399/asm.hb.v03.9781627081634.

Phillips, R. E., Jones, R. T., & Chennells, P. (2008). Commercialization of the ConRoast process (pp. 141-148). Sun City: Third International Platinum Conference, Platinum in Transformation, The Southern African Institute of Mining and Metallurgy.

Sibanye Stillwater. (2025). *About us.* Retrieved August 25, 2025, from https://www.sibanyestillwater.com/about-us/.

Tang, H., Peng, Z., Tian, R., Ye, L., Zhang, J., Rao, M., & Li, G. (2023). Platinum-Group Metals: Demand, Supply, Applications and Their Recycling from Spent Automotive Catalysts. *Journal of Environmental Chemical Engineering, 11*(5). doi:DOI: 10.1016/j.jece.2023.110237.

Thethwayo, B. M. (2018). Extraction of Platinum Group Metals. In M. S. Seehra, & A. D. Bristow (Eds.), *Noble and Precious Metals - Properties, Nanoscale Effects and Applications* (pp. 393-403). IntechOpen. doi:http://dx.doi.org/10.5772/intechopen.69142.

Valterra Platinum. (2025). *What we do.* Retrieved August 25, 2025, from https://www.valterraplatinum.com/about-us/what-we-do.

Zhang, S., He, X., Ding, Y., Shi, Z., & Wu, B. (2024). Supply and demand of platinum group metals and strategies for sustainable management. *Renewable and Sustainable Energy Reviews, 204*, 1-15. doi:https://doi.org/10.1016/j.rser.2024.114821.

Zietsman, J. H., & Weitz, H. (2024). Navigating uncertainty - Advancing pyrometallurgy through reliable new technology developments (pp. 33-42). *Southern African Pyrometallurgy 2024.* Johannesburg, South Africa, 11-14 March 2024: Southern African Institute for Mining and Metallurgy.



Xolisa Goso

Head: Technology Development, Pyrometallurgy
Mintek

Dr Xolisa Goso completed an MTech degree in chemistry at the University of Johannesburg (UJ) and a PhD in Chemical Engineering at the University of Cape Town (UCT). He has been with Mintek for over 17 years and currently works as Head: Technology Development in the Pyrometallurgy Division.

Dr Goso is a member of SAIMM, a published author of journal and conference papers, and has presented at local and international conferences. In his career, he has been involved in many projects for the beneficiation of various resources, including ferrous minerals, industrial minerals and chemicals, precious metals, base and technology metal-bearing primary and secondary materials, and energy minerals. His research activities include: extractive metallurgy of titaniferous magnetite for vanadium, steel and titania production; pyrometallurgical extraction of PGMs from primary and marginal/ secondary ores; thermochemistry of materials; phase relations and pyro-hydrometallurgical beneficiation of primary and secondary materials; coal characterisation and carbonaceous reductant reactivity testing; general chemical, thermal, and mineralogical characterisation of materials; and high-temperature experimentation including refractory-material interaction studies, and reaction kinetics and mechanisms in gas-solid systems, smelting and refining.

The influence of impeller geometry on stirred media mill performance

C. Lekgoro[1,4], S. Nkwanyana[1], N. Lameck[1], I. Govender[1,2,3], T. Moodley[1], M. Ramakokovhu[4]

[1]Mintek, South Africa
[2]University of Cape Town, South Africa
[3]University of KwaZulu-Natal, South Africa
[4]Tshwane University of Technology, South Africa

The flow behaviour of a granular ensemble in stirred mills is influenced by operating conditions such as the tip speed, filling level and bead size distribution. The flow behaviour is also influenced by the stirred mill design features such as rotor/impeller geometry and liner wall of the chamber. The flow behaviour creates the collision environment, which effectively drives the size reduction of mineral ores mainly by attrition breakage. Stirred media mills are common in platinum group metals (PGM) minerals processing plants for fine/ultrafine grinding purposes. It is envisaged that the PGM industry will see more installation of stirred media mills for tailing treatment purposes in the future. The size reduction ratio and the efficiency of energy utilisation of a stirred mill are influenced by the collision environment inside the mill. Discrete element method simulations were conducted (using Ansys ROCKY) to explore the collision environment in stirred mills fitted with pin disc impellor, perforated disc impellor and modified disc impellor.

INTRODUCTION

South Africa has large amounts of ore tailings that are a source of platimun group metals (PGMs. The tailings are from the main PGMs ore sources (Merensky reef, UG2 reef and Platreef) and from the chromitite reefs (MG and UG1) processing plants. Studies conducted at Mintek and elsewhere (Rule, 2011; Buys *et al.*, 2004) have shown that these tailings require additional grinding steps to fine/ultrafine sizes to liberate the PGMs that were lost into them due to incomplete liberation and/or flotation and plant instability inefficiencies.

The energy requirements in grinding increase sharply with product fineness (Wang and Forsberg, 2007; Hukki, 1961). In view of the significant contribution of comminution energy to the total energy consumption of a mineral processing operation (Napier-Munn, 2012), choosing equipment with a superior efficiency of energy utilisation is of critical importance to the viability of a new venture where fine/ultrafine grinding is required. Stirred mills are known to be superior in terms of efficiency of energy utilisation than ball mills in fine and ultra-fine grinding (Naeimi *et al.*, 2025; Ntsele and Allen, 2010; Brisset, 2010; Shi *et al.*, 2009; Nesset, 2006; Lichter and Davey, 2006; Yan *et al.*, 1995).

Most stirred mills, except for TowerMill and Vertimill, use inert ceramic grinding media. Ceramic beads are preferred over steel beads when concentration is through flotation; this is because with the steel beads, the iron hydroxide precipitation and coatings on particle surfaces inhibit the floatability of valuable mineral particles (Zhang *et al.*, 2021; Greet, 2004; Cullinan *et al.*, 1999). The benefits of ceramic beads in this regard have also been reported in the flotation of PGM ores (Song *et al.*, 2018; Greet, 2009).

A feed with a narrow particle size distribution (PSD) is often desirable in a flotation process as the entrainment of gangue reduces the concentrate grade. Stirred mills can produce a narrower PSD compared to ball mills (Naeimi *et al*., 2025; Larson, 2019; de Waal *et al*., 2018; Xiao *et al*., 2012; Buys *et al*., 2004). Stirred mills are therefore the better equipment option to deliver the grinding duty required in retreatment projects of ore tailings that are a source of PGMs.

The common stirred mills in the minerals processing industry are the Nippon Eirich TowerMill and Metso Vertimill (gravity induced stirred mills), the Metso SMD, FLSmidth VXPmill, Metso HIGmill and Glencore IsaMill (fluidised stirred mills). In terms of the design, these mills differ in the main by the geometry of the stirrer and by the feed and discharge arrangement (Martins and Qiu, 2025; Ndimande *et al*., 2019; Reddick *et al*., 2011; Keikkala *et al*., 2018; de Waal *et al*., 2013). In terms of operating conditions, they differ in the main by the range of tip speeds and bead sizes, which often overlap and determine the suitable feed top size range and achievable product PSD (Can and Altun, 2023; Ford, and Naude, 2021; Larson, 2019; Ntsele and Allen, 2010; Erb *et al*., 2016; Allen, 2013; Keikkala *et al*., 2015; Reddick *et al*., 2011).

The flow behaviour of the beads in stirred mills is influenced by operating conditions and the stirrer geometry. The flow behaviour creates the collision environment, which effectively drives the size reduction of mineral ores. For retreatment projects of tailings that are a source of PGMs, in cases where the feed size is suitable for processing in all fluidized stirred mills, and the target product size is achievable in all stirred mills, how do the vertically orientated fluidised stirred mills compare in terms efficiency of energy utilization? The efficiency of energy utilization can be inferred from the collision environment inside the mill. To compare the efficiency of energy utilization in different fluidised stirred mills, discrete element method (DEM) simulations were conducted (using Ansys ROCKY®) to explore the collision environment created by pin disc impellor, perforated disc impellor and modified disc impellor at typical tip speeds for fluidised stirred mills.

DEM SIMULATIONS

Simulation set up

Table I shows the dimensions of the batch mill simulated and the operating conditions. The mill is at Mintek, and it is used for test-work for generating signature plots and fine ground samples for leaching and flotation batch tests. The ceramic beads used in the simulation had a narrow size distribution, which was normally distributed about the mean size of 5 mm with a maximum deviation of 0.05 mm.

Table I. Simulation set up

Mill dimensions (D×L)	18 cm × 23 cm
Tip speed	5.8 - 12 ms^{-1}
Mill loading	45%
Bead density	2700 $kg.m^{-3}$

The mill chamber and the impellers (pin disc, perforated disc and modified disc) were drawn on Autodesk Maya and imported into Ansys ROCKY® platform. Figure 1 shows the 3D images of the impellers. The impellers have identical dimensions, i.e. the shaft length of 235 mm, and the disc diameter of 144 mm. The material properties of the discs, shafts and grinding chamber cylinder were defined by three parameters, which were the density = 7850 $kg.m^{-3}$, Young's modulus = 1×1011 $N.m^{-2}$ and Poisson's ratio = 0.3.

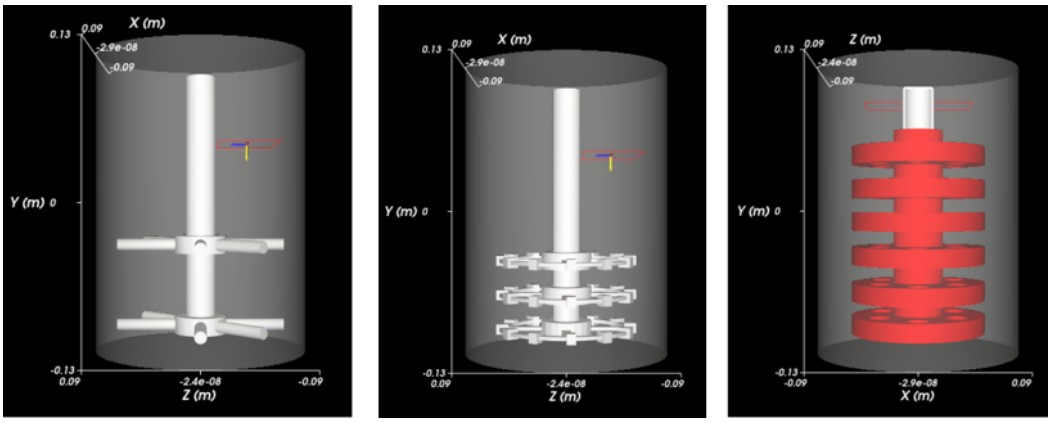


Figure 1. 3D images of the pin disc, modified disc and perforated disc impellers

The Hertzian spring-dashpot law was chosen to model the normal contact force, and the Mindlin-Deresiewicz law was chosen to model the tangential contact force. These contact force laws have been used widely in simulation studies that had energy dissipation as a parameter of interest (Bbosa *et al.*, 2016; De Carvalho & Tavares, 2013; Weerasekara *et al.*, 2016). The following is a list of the material contact parameters used in the simulations: coefficient of restitution = 0.6 and coefficient of friction of 0.4 for ceramic-ceramic collisions, and a coefficient of restitution = 0.5 and coefficient of friction of 0.3 for ceramic-steel boundary collisions. These material contact parameters were used on a similar DEM study conducted by Ndimande *et al.*, (2019) but may need to be optimised for this research project.

COLLISION ENVIRONMENT

The primary source of energy dissipation during a collision is related to the inelastic nature of the contact force F_c. The dissipation work done by this force (W^{diss}) and power (P^{diss}) are calculated using Equation (1) and (2). The integral is defined over the entire collision interval (loading and unloading):

$$W^{diss} = -\int F_c . v_c^{rel} dt \tag{1}$$

$$P^{diss} = \frac{\sum_{k=1}^{k}(W^{diss})}{\Delta t_{out}} \tag{2}$$

Where v_c^{rel} is the instantaneous relative velocity at the contact point, k is the number of collisions occurring within the time interval Δt_{out}. The total contact force is given by Equation (3):

$$F_c = F_n . \hat{n}_c + F_t \tag{3}$$

Where F_n and F_t are, respectively, the normal and tangential components of the contact force. Additionally, $\hat{n}_c$ is the normal unit vector of the contact.
The shear work (W^{shear}) is calculated using Equation (4):

$$W^{shear} = -\int F_t . ds_t \tag{4}$$

Where d_s^t is the sliding distance, i.e., the displacement parallel to the tangential plane of the contact. The difference of Equation (1) and (4) gives the impact work (the normal component).

RESULTS AND DISCUSSION

Figure 2 shows the stirred mills' power draw curves. During the first 3 seconds of the simulation, the beads were released and loaded into the mill. At 4 seconds, the rotation of the stirrer was started. Steady state was reached after 2 seconds from the start of stirrer rotation (depicted by the steady power draw curves). The analysis presented in this paper is from the data collected starting from 6 seconds simulation time to 10 seconds simulation time.

In minerals processing, when comparing the performance of grinding equipment, it is a standard practise to have the equipment supplied with the same specific energy. Specific energy is the ratio of power draw to tonnage processed per unit time. For the same grinding chamber dimension, same grinding time and mass of ore, to achieve the same specific energy input the mills must be configured to draw comparable power. In the case of the stirred mills simulated, comparable power draw was achieved by operating at different tip speeds as shown in Figure 2. The pin disc at 5.8 ms^{-1} tip speed draws comparable power as modified disc at 6.6 ms^{-1} and perforated disc at 9.3 ms^{-1}. The pin disc at 7.0 ms^{-1} tip speed draws comparable power as modified disc at 8.2 ms^{-1} and perforated disc at 12 ms^{-1}.

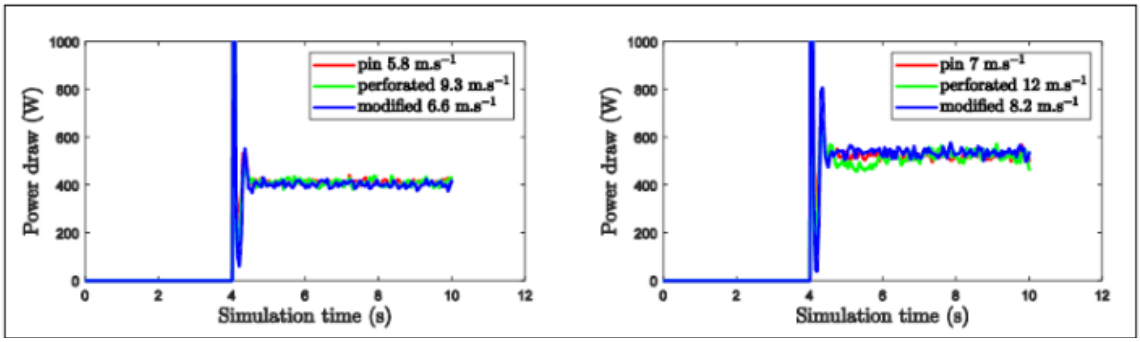


Figure 2. Power draw time plots.

In this paper, the collision environment is defined by the distribution of power dissipated in collisions across different energy levels, between the shear and the normal components of collisions, and spatially across the mill. These three aspects are examined.

Figures 3 show the energy spectra from the different impellers, which demonstrate the distribution of power dissipated in collisions across different energy levels.

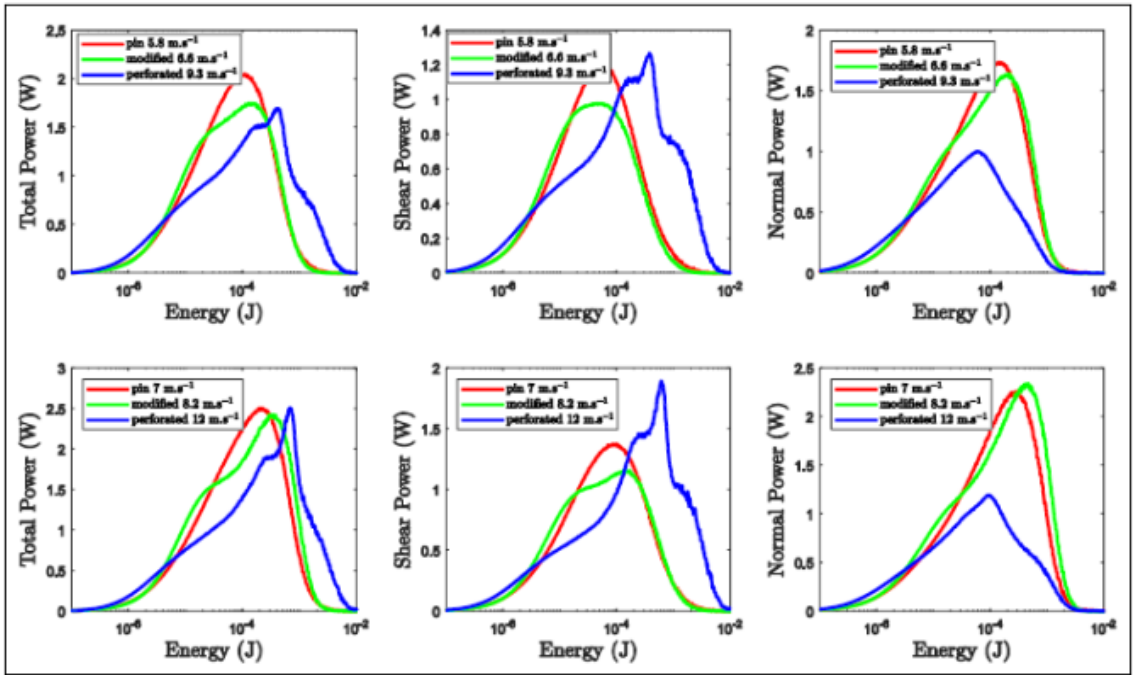


Figure 3. Collision energy spectra.

The total power dissipation curves presented in Figure 3 show that collision dissipated energies range from about 10^{-7} J to 10^{-2} J. The peak total power in all the impellers corresponded to collisions that dissipated energies of between 10^{-4} J and 10^{-3} J. The shapes of the total power dissipation curves for the pin disc and modified disc are similar. From the standpoint of the total power dissipation curves, it can be argued that the pin disc and modified disc impellers should give similar product PSDs for the same specific energy input (kWh/t). The perforated disc impeller can be expected to give a slightly finer product PSD because the curve is positioned slightly to the right relative to the pin disc and modified disc impeller curves.

The total power is the sum of the power dissipated by the normal and shear components of collisions; it is also important to analyse the power dissipation curves from these components. The shear energy spectra from the pin disc and modified disc impellers run close to each other, and the energy level contributing the most to power dissipation is also comparable. The shear energy spectra from the perforated disc impeller are shifted to the right, higher energy levels, which suggests that for a mill fitted with the perforated disc impellor, the shear components of collisions dissipate higher energies than the mills fitted with modified disc and pin disc impellers. The normal energy spectra also show that the perforated disc impellor creates a different collision environment compared to the pin disc and modified disc impellers. The normal energy spectra of the perforated disc have a significantly lower power peak relative to the normal energy spectra from the modified disc and pin disc impellers. The data suggest that for comparable mill power draw, the pin disc impeller and perforated disc impeller can be expected to give similar product PSDs. However, the product PSD from a perforated disc impeller can be expected to be different/ coarser due to reduced breakage events that are attributed to normal components of collisions and potentially high shear energy wasted on disc wear.

Figure 4 shows the distribution of the power dissipated by the normal and shear components of collisions. Table II shows the proportions from each component of collision. It is evident from the data presented in Figure 4 and Table II that the shear components of collisions dissipate more power than the normal components. The perforated disc impeller stands out to have the highest power dissipated by the shear component of collisions, which is about 75% of the total power dissipated. Figure 4 and Table II reinforce the arguments derived from the data presented in Figure 3.

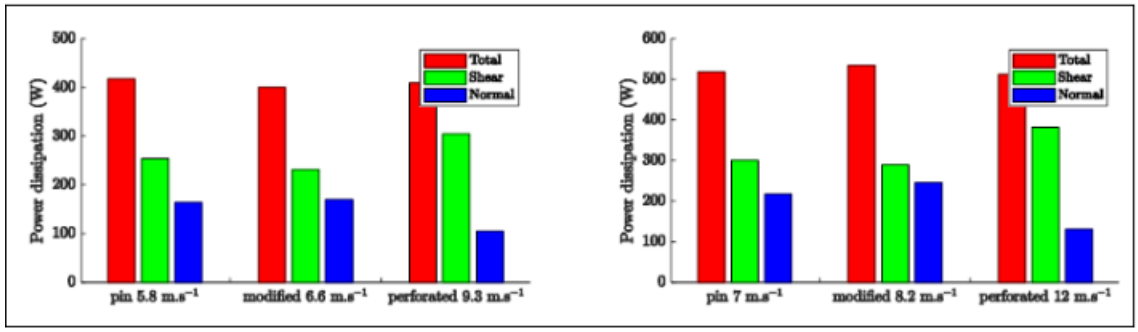


Figure 4. Distribution of dissipated power between normal and shear components of collisions.

Table II: Distribution of dissipated power between normal and shear components of collisions.

	pin disc	perforated disc	modified disc
	5.8 m/s	9.3 m/s	6.6 m/s
Shear power dissiation	65	75	64
Normal power dissipation	35	25	36
	7 m/s	12 m/s	8.2 m/s
Shear power dissiation	63	75	60
Normal power dissipation	37	25	40

Figures 5 and 6 show the spatial maps of total power dissipation in the stirred mills simulated. Colour bars alongside each map indicate the value in a voxel, with the range of low to high quantities depicted using hues from blue to red, respectively. The regions of high-power dissipation, and arguably where there is a high probability of particle breakage, are marked by the red, yellow, green and cyan hues. The swirling motion created by the pin disc and the modified disc impellers create a vortex around the impellor shaft, which is depicted by the white regions in Figure 5.

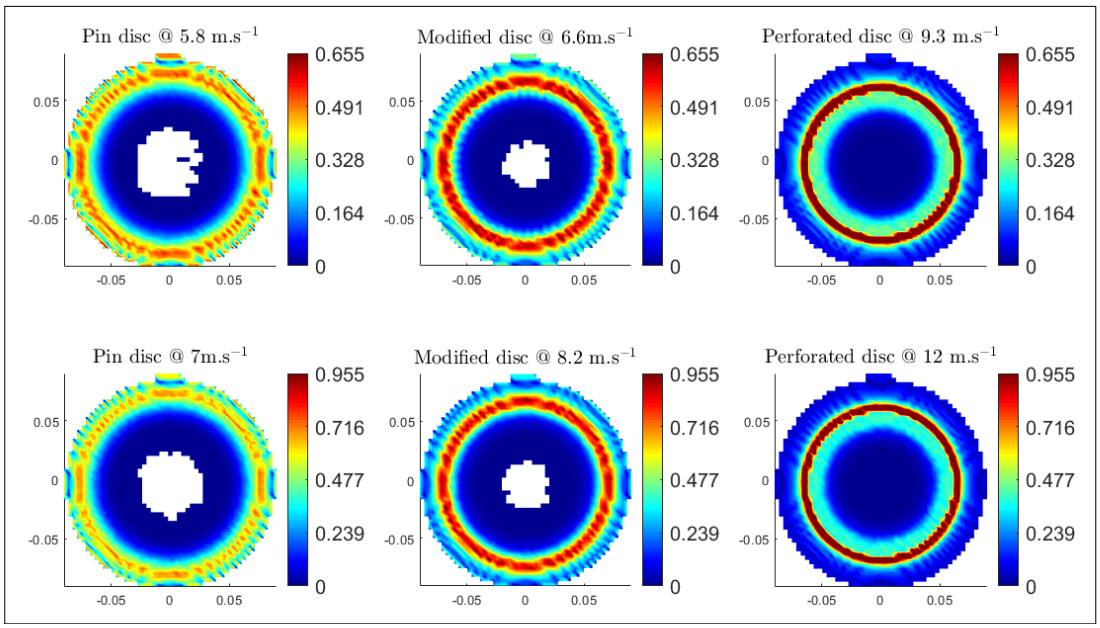


Figure 5. Spatial maps of total power dissipation in the stirred mills simulated, top view.

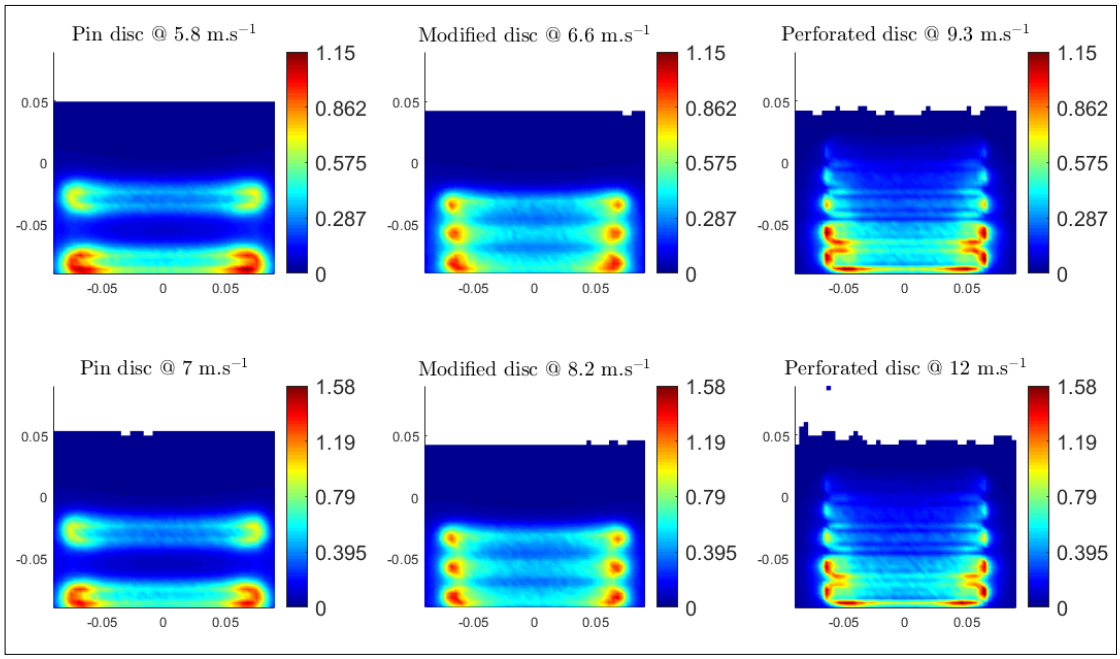


Figure 6. Spatial maps of total power dissipation in the stirred mills simulated, side view.

It is eident in Figures 5 and 6 that, for the mills fitted with pin disc and modified disc impellers, the region of high-power dissipation is between the grinding chamber wall and a few millimetres away and inside the disc diameter. Figure 6 shows that the modified disc impeller has a greater number of regions of high-power dissipation than the pin disc impeller, which are relatively smaller. This may make the modified disc slightly better than the pin disc because of the more regions where ore particles can experience breakage.

Figures 5 and 6 show that for the mill fitted with a perforated disc impeller, the region of high-power dissipation is within the disc holes and on the surface between the disc hole and the disc edge. This makes the perforated disc impeller highly susceptible to wear.

It is also evident in Figure 6 that the regions of high-power dissipation are largest near/around the lowest discs, where the lowest disc is the one near the grinding chamber floor. The regions of high-power dissipation gradually become smaller near/around the discs at higher heights, and this is true for all the impellers. It is notable on the perforated disc impeller that disc 3, 4, 5 and 6 above the grinding chamber floor create negligible high-power dissipation regions.

Figure 5 shows that in terms of wear of surfaces (cylinder wall and impeller), the perforated disc is most susceptible, given that the larger surface area of the disc exposed to the charge. The pin impeller follows, given the proximity of the high-power dissipation zone to the cylinder wall.

CONCLUSIONS

- A mill fitted perforated disc impellor requires more discs to achieve comparable power to a mill fitted with a castellated or pin disc impeller.
- The shear and normal components of collisions dissipate significant power and hence it can be argued the two are both important in grinding.
- It is expected that the ranking of the wear of the internals, from highest to lowest, will be perforated disc – pin disc – modified disc.

- For comparable specific energy input, it is expected that the in terms of efficiency of energy utilization from the impellors, the pin and modified disc impellor may be similar.
- For comparable specific energy input, it is expected that the perforated disc impellor may have a poorer performance relative to the pin disc and modified disc impeller.
- The disc diameter should be large enough to maximise power draw, but should be carefully reduced, when necessary, to ensure that the region of high-power dissipation does not reach the grinding chamber wall.

REFERENCES

Allen, J., 2013. Stirred milling machine development and application extension. http://www.ceecthefuture.org/wp-content/uploads/2014/03/Allen.pdf.

Bbosa, L.S., Govender, I., Mainza, A., 2016. Development of a novel methodology to determine mill power draw. Int. J. Miner. Process. 149, 94–103. https://doi.org/ 10.1016/J.MINPRO.2016.02.009.

Brissette, M. Energy saving and technology comparisons using small grinding media. XXX International Mineral Processing Congress, Brisbane, Queensland, Australia, September 2010.

Buys S, Rule C.M, & Curry D (2004). The application of large-scale stirred milling to the re-treatment of Merensky platinum tailings; CIM 2004, Montreal, Canada.

Cullinan, V.J., Grano, S.R., Greet, C.J., Johnson, N.W. and Ralston, J., 1999. Investigating fine galena recovery problems in the lead circuit of Mount Isa Mines Lead/Zinc Concentrator part 1: Grinding media effects. Minerals engineering, 12(2), pp.147-163.

De Carvalho, R.M., Tavares, L.M., 2013. Predicting the effect of operating and design variables on breakage rates using the mechanistic ball mill model. Miner. Eng. 43–44, 91–101. https://doi.org/10.1016/J.MINENG.2012.09.008.

De Waal, H., Gurnett, I. and Stieper, G., Stirred Circuit Design: Open Circuit or Closed Circuit? 2023. Proceedings of Comminution 2023, Organised by Minerals Engineering International.

Erb, H., Cronje, C., Mahlangu, T., Ebell, B., Hanuman, Y., Smit, F., and Lehto, H. 2016. Impact of the stirred mill grinding mechanism on grinding performance and media consumption. Proceedings of Comminution 2016, Organised by Minerals Engineering International.

Ford, E. and Naude, N., 2021. Investigating the effect on power draw and grinding performance when adding a shell liner to a vertical fluidised stirred media mill. Minerals Engineering, 160, p.106698.

Greet, C.J., 2009. The significance of grinding environment on the flotation of UG2 ores. *Journal of the Southern African Institute of Mining and Metallurgy*, *109*(1), pp.31-37.

Greet, C.J., Small, G.L., Steinier, P. and Grano, S.R., 2004. The Magotteaux Mill®: investigating the effect of grinding media on pulp chemistry and flotation performance. Minerals Engineering, 17(7-8), pp.891-896.

Hukki, R. T. (1961) 'Proposal for a solomnic settlement between the theories of von Rittinger, Kick and Bond', Transactions SME/AIME, 220.

Keikkala, V., Lehto, H. and Roitto, I., 2015. Recent progress of regrinding circuits with Outotec HIGmills. Cuprum: czasopismo naukowo-techniczne górnictwa rud.

Larson, M., 2019. A review of published full-scale stirred mill results. Proceedings of SAG conference 2019

Lichter, J.; Davey, G. 2006. Selection and sizing of ultrafine and stirred grinding mills. In Advances Comminution; 2006; p. 69.

Lichter, J.K.H. and Davey, G. 2002. Selection and sizing of fine and ultrafine grinding mills. Mineral Processing Plant Design, Practice, and Control Proceedings. Mular, A.L., Halbe, D.N., and Barratt, D.J. (eds). Society for Mining, Metallurgy, and Exploration (SME), Littleton, Colorado, 2002. pp. 783-800.

Naeimi, M., Behrad Vakylabad, A., Hosseini, S.M., Hassanzadeh, A., Rahmanian, A., Asgari, K., Duan, C. and Nazari, S., 2025. A Critical Review of Innovations in Stirred Mill Technology for Enhancing Energy Efficiency. Mineral Processing and Extractive Metallurgy Review, pp.1-16.

Napier-Munn, T., 2012. Comminution energy and how to reduce it. CEEC workshop 2012. http://www.ceecthefuture.org/wp-content/uploads/2014/03/Allen.pdf.

Nesset, J.E.; Radziszewski, P.; Hardie, C.; Leroux, D.P. Assessing the performance and efficiency of fine grinding technologies. In Proceedings of the 38th Annual Canadian Mineral Processors Conference, Ottawa, ON, Canada, January 2006; pp. 17–19.

Ntsele, C.; Allen, J. Technology Selection of Stirred Mills for Energy Efficiency in Primary and Regrinding Applications for the Platinum Industry. South. Afr. Inst. Min. Metall. 2012, 781–808.

Rule, C.M (2010). Stirred milling—new comminution technology in the PGM industry. The 4th International Platinum Conference, Platinum in transition 'Boom or Bust', The Southern African Institute of Mining and Metallurgy, 2010.

Rule C. M. (2011). Stirred milling in Anglo American Platinum. Proceedings of SAG conference 2011.

Shi, F., Morrison, R., Cervellin, A., Burns, F., and Musa, F. Comparison of energy efficiency between ball mills and stirred mills in coarse grinding. Minerals Engineering, vol. 22, no. 7-8, 2009. pp. 673 – 688

Song, Z.G., Corin, K.C., Wiese, J.G. and O'Connor, C.T., 2018. Effect of different grinding media composition on the flotation of a PGM ore. Minerals Engineering, 124, pp.74-76.

Shi, F., Morrison, R., Cervellin, A., Burns, F. and Musa, F., 2009. Comparison of energy efficiency between ball mills and stirred mills in coarse grinding. Minerals Engineering, 22(7-8), pp.673-680.

Wang, Y. & Forssberg, E. 2007. Enhancement of energy efficiency for mechanical production of fine and ultra-fine particles in comminution. China Particuology, 5, 193-201.

Weerasekara, N.S., Liu, L.X., Powell, M.S., 2016. Estimating energy in grinding using DEM modelling. Miner. Eng. 85, 23–33. https://doi.org/10.1016/j. mineng.2015.10.013

Xiao, X., Zhang, G., Feng, Q., Xiao, S., Huang, L., Zhao, X. and Li, Z., 2012. The liberation effect of magnetite fine ground by vertical stirred mill and ball mill. Minerals Engineering, 34, pp.63-69.

Yan, D.S.; Dunne, R.C.; Freeman, M.E. Efficiency of stirred ball mills. In Proceedings of the XIX International Mineral Processing Congress, San Francisco, CA, USA, October 1995

Zhang, X., Qin, Y., Han, Y., Li, Y., Gao, P., Li, G. and Wang, S., 2021. A potential ceramic ball grinding medium for optimizing flotation separation of chalcopyrite and pyrite. Powder Technology, 392, pp.167-178.



Collins Machiri Lekgoro

Metallurgical Technician
Mintek

Collins is a Metallurgical Engineering Technician in the Comminution Group within the Mineral Processing Division at Mintek. He holds a National Diploma in Metallurgical Engineering from the Vaal University of Technology and a B-Tech degree in Metallurgical Engineering from the Tshwane University of Technology. He has worked for Anglo American Research for two years and Anglo Platinum Operations (Concentrator) in the production department for two and a half years before joining Mintek in November 2023.

Comminution behaviour of the middle group ores

P.C. Siwela, M.M. Ramakokovhu, M.L. Teffo

Tshwane University of Technology, South Africa

The Middle Group chromitite ores are a significant source of chromium and platinum group metals. However, their complex mineralogy and variable texture pose challenges for efficient comminution and downstream processing. This study investigates the comminution behavior of four MG ore types (MG1, MG2, MG3, and MG4A) using Bond Work Index, Uniaxial Compressive Strength, Abrasion Index, and JK Drop Weight Test. Results indicate that MG ores exhibit challenging comminution characteristics, evidenced by high Bond Work Indices and variable impact breakage behavior. These findings align with observations by Mwanga et al. (2017), who emphasized the importance of understanding ore characteristics for comminution optimization. Notably, MG1 exhibits the lowest energy requirements for comminution, while MG2 and MG3 demand more energy-intensive processing. These variations underscore the need to tailor comminution circuits to ore-specific properties. Recommendations include optimizing crusher selection, configuration, and operating parameters to minimize energy consumption and wear. Future research should explore alternative comminution methods, such as high-pressure grinding rolls or stirred media mills, and investigate the correlation between mineralogy, JK parameters, and other comminution properties for a comprehensive understanding of MG ore breakage behaviour.

Keywords: Comminution, Chromitite, Platinum Group Metals, Bond Work Index, Middle Group ores, Bushveld Complex

INTRODUCTION

The Middle Group chromitite ores represent a valuable resource for chromium and platinum group metals. However, their complex mineralogy and variable texture present significant challenges for efficient comminution and downstream processing. Understanding the breakage characteristics of these ores is crucial for optimizing grinding circuits and maximizing metal recovery.

Comminution is an essential operation for the mining and mineral processing industry . In the mineral industry, the liberation of valuable minerals from the gangue is a fundamental requirement for all subsequent separation or extraction operations, and this process involves multiple stages of crushing and grinding to liberate the desired minerals (Fuerstenau and Abouzeid, 1991).

Schönert (1979) estimated that minerals comminution consumes 3% of all the energy produced by industrialized countries, in line with former studies (Austin and Klimpel, 1964). More recent evaluations estimate that comminution operations are responsible for 3–5% of energy consumption at a global scale (Deniz and Ozdag, 2003). Moreover, in terms of OPEX in mineral processing plants, comminution operations amount to 40–50% of the energy consumption.

Considering the above, any gain in efficiency can significantly impact the plant operating costs and the consequent conservation of resources (Fuerstenau and Abouzeid, 1991). In this sense, an improvement in knowledge of ore grinding behavior can allow modification of the operation and control strategies of the grinding operations, resulting in significant energy savings. This would increase the competitiveness of operations and reduce emissions.

It is common to process multicomponent ores, made up of at least two mineralogical components with differences in their physical and physicochemical properties. Some authors (Menéndez-Aguado et al., 2005; Coello Velázquez et al., 2008) show that disregarding the variability of the feed mineralogical composition produces large deviations in the planned metallurgical efficiency, along with problems in the treatment of the ores with such characteristics. On the other hand, between the initial exploration work for the design of any mineral beneficiation plant and the reaching of its full operating regime, and even after reaching it, there will be variations in the plant feed composition, implying substantial changes in mineral properties. Therefore, it would be advisable to adjust the operating and control conditions of the treatment plant in general and the size reduction section in particular.

The energy–size relationships in comminution processes have been an object of research since the first industrial revolution (Nikolić and Trumić, 2021). Rittinger (1867) proposed the first law of comminution, supposing that the amount of created surface is proportional to the specific energy consumption in grinding operations, as expressed in Equation (1):

$$E = K_R \cdot \left(\frac{1}{P} - \frac{1}{F} \right) \tag{1}$$

where E is the specific energy consumption [kWh/t], K_R is the proportionality coefficient and P and F are the particle sizes of the product and feed, respectively [µm].

Kick (1885), in the second law of comminution, argued that according to his calculations, the specific energy consumption would be proportional to the volume reduction, as expressed in Equation (2), where K_K is a different proportionality coefficient.

$$E = K_K \cdot \left(\frac{1}{\ln(P)} - \frac{1}{\ln(F)} \right) \tag{2}$$

The differences between the Rittinger and Kick models lasted for years, until the proposal of the third theory of comminution by F. Bond (1943), (1961) and (1952) which is summarized in Equation (3),

$$E = K_B \cdot \left(\frac{1}{\sqrt{P}} - \frac{1}{\sqrt{F}} \right) \tag{3}$$

where $K_B = 10\, w_i$, and w_i is expressed in kWh/t.

Subsequent studies (Hukki, 1961) explained that the three laws derive from a generalized comminution differential equation, each one best applied to a different size range (Rittinger's law for fine grinding; Bond's law for coarse grinding and secondary/tertiary crushing; and Kick's law for primary crushing). The novelty in the third law's proposal was the procedure for determining w_i in the case of crushing, rod milling and ball milling (Bond, 1961) and (Deister, 1987). The practical interest of w_i is unquestionable. From a technical perspective, it constitutes the most reliable method of characterizing ore grindability when designing the necessary tumbling mills to process that ore. (Bearman et al., 1997) showed that other mechanical characterization tests are insufficient when predicting the grinding ore behaviour.

A logical reasoning process should suggest finding some correlation among mechanical parameters [hardness, Young's modulus, uniaxial compression strength (UCS), etc.] and the ore grinding behavior. Several researchers (Deniz & Ozdag, 2003), (Bearman et al., 1997) and (Ram Chandar et al., 2016) followed that inspiration, but no generalizable results have been obtained since grindability behavior is usually evaluated under closed-circuit conditions, which means that not only breakage but breakage plus classification operations are involved. Moreover, we can easily find ores with high hardness and high grindability values, but among the highest grindability values, we can find quite soft ores (graphite or mica group minerals). On the other hand, diamond mineral shows modest grindability values. Thus, it is worth emphasizing that the Bond work index tries to characterize the ore grinding behavior in a closed circuit, encompassing the ore mechanical behavior before the mill action (i.e., whatever the type of the mill and its characteristics of action), but also the screening or classification stage involved in the closed circuit, which is greatly influenced by product size and shape.

Due to the fact that Bond's proposal was undoubtedly linked to a market-dominant firm, i.e., Allis Chalmers, which even owned the patent of the standard mill, several proposals soon emerged to define alternative test approaches, which can be grouped in the following types:

- Indirect work index determination in other lab mills (Berry & Bruce, 1966; Yap et al., 1982; Bonoli & Ciancabilla, 1992; Chakrabarti, 2000; Menéndez-Aguado et al., 2005; Nikolić & Trumić, 2021)
- Specific energy determination from correlations in different devices (Napier-Munn et al., 1996; Mwanga et al., 2017; Faramarzi et al., 2020)
- Work index calculation through lab tests and simulation (Karra, 1981; Lewis et al., 1990; Aksani & Sönmez, 2000; Ciribeni et al., 2020)

This study investigates the comminution behavior of different MG ore types (MG1, MG2, MG3, and MG4A) using a series of standard tests, including Bond Work Index, Uniaxial Compressive Strength, Abrasion Index, and JK Drop Weight Test. These results are further contextualized with insights from existing literature, such as the work of Mwanga (2014), to provide a comprehensive understanding of the comminution behavior of MG ores.

Materials and Methods

Figure 1 illustrates the flowsheet overview of the testwork program conducted. This flowchart outlines the main steps and tests involved in the research project, from sample preparation to data analysis and conclusion.

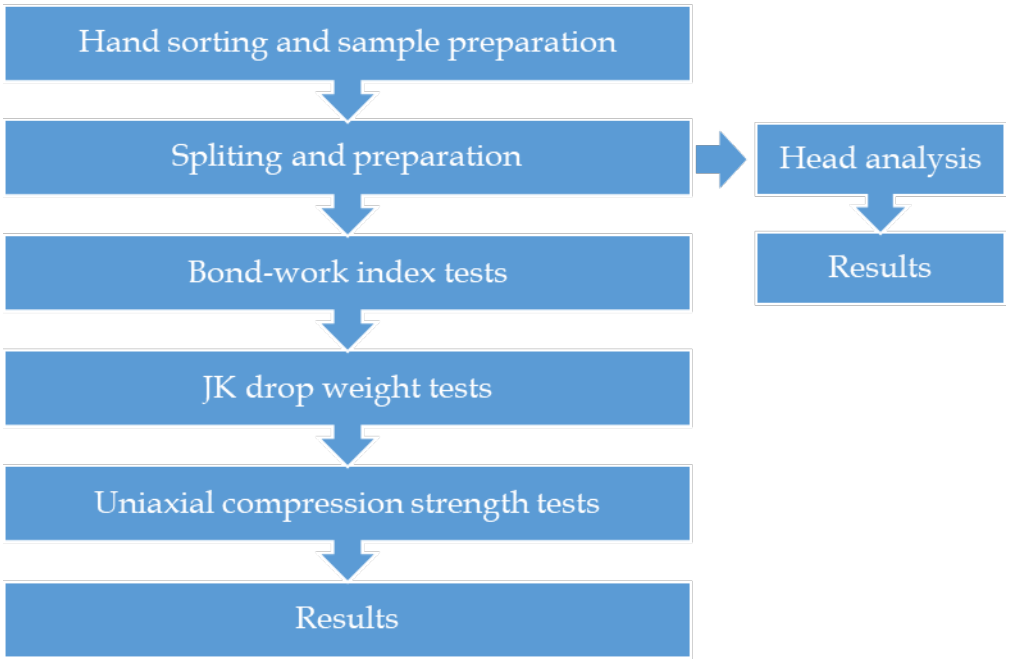


Figure 1: Representation of Flowsheet Overview for the Testwork Program

Sample Preparation and splitting
Hand-sorted bulk samples of 100% passing 20mm MG ores classified into four distinct ore types: MG1, MG2, MG3, MG4A**.** Diamond saw used to prepare quartered core particles for SMC test**.** Classified samples were split into two halves:

- One half for chemical head analysis

- Second half for chemical head analysis and potential further testing

Comminution Tests

- **Bond Work Index:** The Bond Ball Work Index was determined at closing screens of 106 and 212 microns, while the Bond Rod Work Index was conducted at a limiting screen of 1180 microns. The Bond Crushability Work Index was also determined for each ore type.
- **Uniaxial Compressive Strength:** UCS tests were performed to assess the ore's resistance to compressive forces.
- **Abrasion Index:** The Ai was determined to evaluate the abrasiveness of each ore type.
- **JK Drop Weight Test:** The JK Drop Weight Test was conducted to assess the impact breakage behavior of the ores.

Data Analysis and Conclusion

- Analysis of comminution test results
- Determination of breakage characteristics for each ore type
- Drawing conclusions based on testwork outcomes

RESULTS AND DISCUSSION

Head samples

Table 1 presents the chemical analysis of head samples from four different ore types (MG1, MG2, MG3, MG4A), focusing on Platinum Group Elements (3E+Au) and Chromium Oxide (Cr2O3) content as depicted below.

Table 1: Head sample analysis on different MG ores

Ore type	Pt(g/t)	Pd(g/t)	Rh(g/t)	Au (g/t)	3PGE+Au (g/t)	Cr2O3 (%)	Cu (%)	Ni (%)	SiO2 (%)
MG1	0,32	0,2	0,11	0,004	0,634	32,1	0,002	0,077	22,54
MG2	0,98	0,28	0,15	0,004	1,414	19,33	0,002	0,061	41,83
MG3	0,6	0,35	0,15	0,005	1,105	17,99	0,003	0,047	35,11
MG4A	0,4	0,15	0,12	0,003	0,673	24,85	0,003	0,066	29,95

PGE Distribution

MG2 exhibits the highest overall PGE grade with 0.98 g/t Pt, 0.28 g/t Pd, and 0.15 g/t Rh, MG2 stands out with the highest concentration of valuable PGEs, resulting in a significant 3PGE+Au grade of 1.414 g/t. MG1 and MG3 show moderate PGE grades, both ore types contain notable amounts of Pt and Pd, with MG3 having a slightly higher Pd content. However, their overall PGE grades are lower compared to MG2. MG4A possesses the lowest PGE content, this ore type displays the lowest concentrations of all PGEs analyzed, resulting in the lowest 3PGE+Au grade.

Cr_2O_3 Content

From table 1 above, there is an inverse relationship between Cr2O3 content and PGE grades. MG2, with the highest PGE grade, has the lowest Cr2O3 content (19.33%). Conversely, MG4A, exhibiting the lowest PGE grade, possesses the highest Cr2O3 content (24.85%).

Cu and Ni Content

All ore types exhibit low Cu and Ni grades, ranging from 0.002% to 0.003% for Cu and 0.047% to 0.077% for Ni. MG1 displays the highest Ni content: At 0.077%, MG1 stands out with a slightly elevated Ni concentration compared to the other ore types. Limited economic significance at current levels: The low Cu and Ni grades suggest these metals are unlikely to be primary recovery targets based solely on these head sample analyses.

Bulk density

The average density for each ore type set is presented in the Table 2, whereas the detailed graph is shown in figure 1 below.

Table 2: Average solid density on different MG ores

Ore type	Average density (g/cm3)
MG1	3.84
MG2	3.61
MG3	3.47
MG4A	3.74

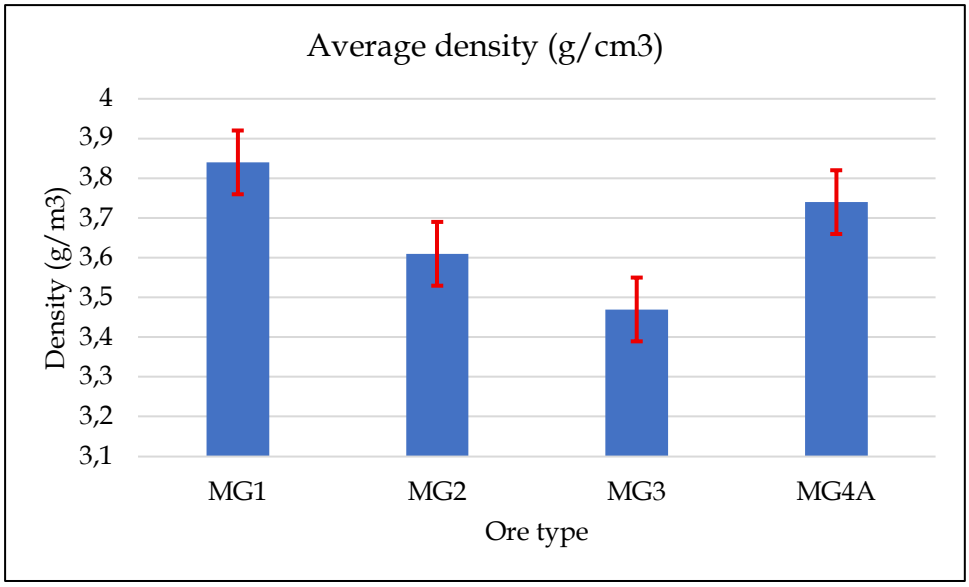


Figure 1: Average solid density on different MG ores

MG1 is the densest at 3.84 g/cm^3, indicating a more compact or mineralogically heavy composition. MG3 is the least dense at 3.47 g/cm^3, which suggest a more porous structure or a higher proportion of lighter minerals. MG2 (3.61 g/cm^3) and MG4A (3.74 g/cm^3) have intermediate densities, with MG4A being closer to MG1 and MG2 closer to MG3.

Bond Work Indices

The Bond Ball Work Index results, summarized in Table 3 and figure 2, indicate that MG1, MG2, MG3 and MG4A ores are relatively hard and require significant energy for grinding.

Table 3: Bond Ball Work Index on different MG ores

Rock type	Limiting screen (microns)	F80 (microns)	P80 (microns)	Net generation (g/rev)	Work Index (kWh per metric ton)
MG2	106	2497.71	83.73	1.19	16.33
	212	2497.71	158.36	2.12	13.02
MG3	106	2532.44	89.58	1.22	16.68
	212	2532.44	157.15	1.93	13.94
MG1	106	2510.24	90.46	1.97	11.30
	212	2510.24	161.89	5.85	5.74
MG4A	106	2515.08	90.98	1.26	17.33
	212	2515.08	165.64	2.12	13.88

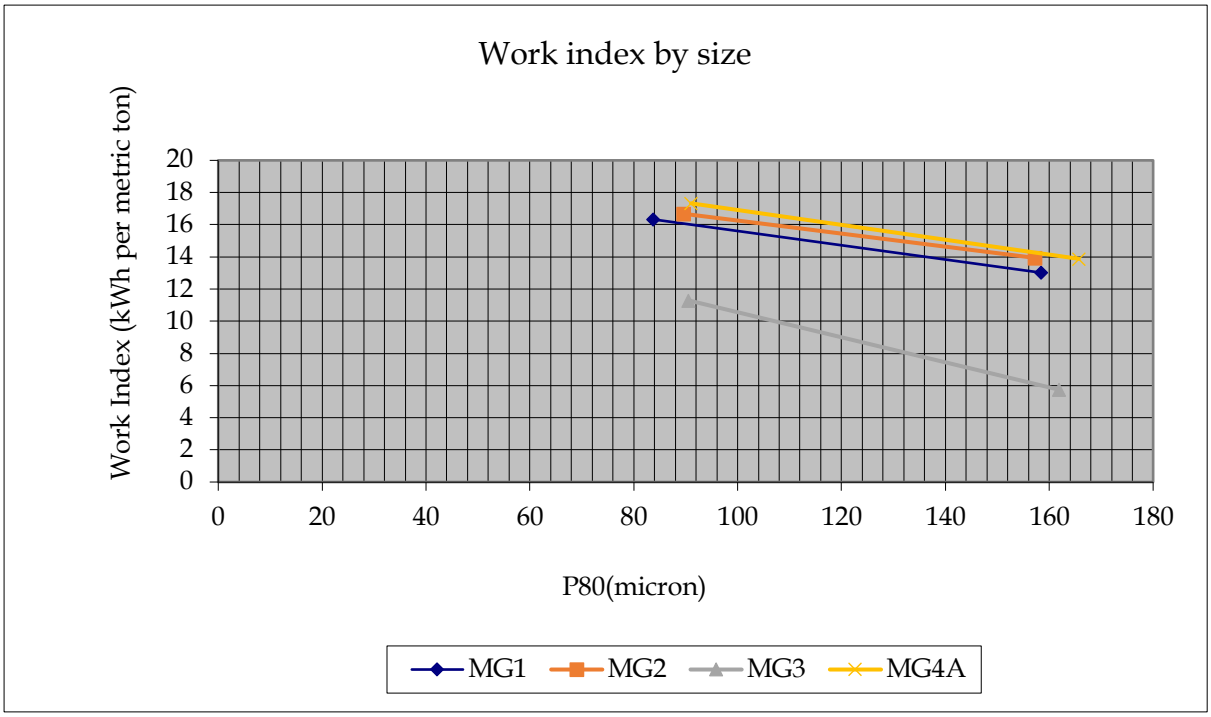


Figure 2: Wok index of different ores by size

The BWI values ranged from 5.74 kWh/t for MG1 at a 212-micron closing screen to 17.33 kWh/t for MG4A at a 106-micron closing screen. These values are generally higher than those reported for other chromite deposits, highlighting the challenging nature of MG ores in terms of comminution.

The Bond Rod Work Index results, presented in Table 4 and figure 3, further confirm the hard and abrasive nature of MG ores. The test was conducted at a limiting screen of 1180 microns.

Table 4: Bond Rod Work Index on different MG ore types

Rock type	Limiting screen (microns)	F80 (microns)	P80 (microns)	Net generation (g/rev)	Work Index (kWh per metric ton)
MG2	1180	8332.00	804.96	9.12	13.91
MG3	1180	8865.64	713.64	6.74	15.20
MG1	1180	9627.67	606.46	10.27	9.91
MG4A	1180	8598.82	759.3	7.93	14.57

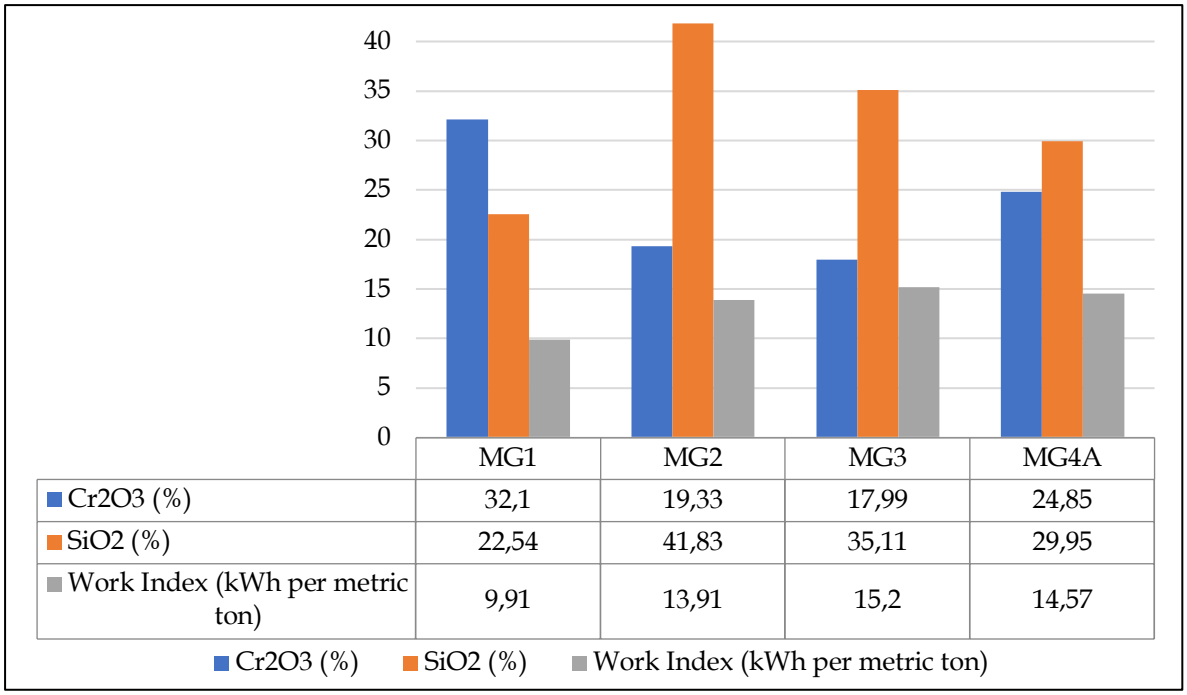


Figure 3: Work index vs Cr2O3 vs SiO2 of different MG ore types

The RWI values ranged from 9.91 kWh/t for MG1 to 15.20 kWh/t for MG ores. These values are indicative of the significant energy required for primary crushing stages.

The Bond Crushability Work Index results, shown in Table 5, provide insights into the energy required for crushing MG ores. The CI values ranged from 7.0 kWh/t for MG1 to 16.3 kWh/t for MG2. These results suggest that MG ores require robust crushing circuits and careful selection of crusher types to achieve efficient size reduction.

Table 5: Bond Crushability Work Index on MG ore type

Rock type	Work Index (kWh per metric ton)
MG2	16.3 ± 2.7
MG3	12.4 ± 1.9
MG1	7.0 ± 1.4
MG4A	14.35± 2.3

Uniaxial Compressive Strength

The UCS results, summarized in Table 6, demonstrate the high strength of MG ores.

Table 6: Bond Crushability Work Index on MG ore type

Rock type	UCS Strength (Mpa)
MG2	88 ± 21
MG3	72 ± 10
MG1	78 ± 24
MG4A	81 ± 21

The UCS values ranged from 72 MPa for MG3 to 88 MPa for MG2. These high UCS values are consistent with the observed high Bond Work Indices and highlight the need for robust comminution equipment.

Abrasion Index
The Abrasion Index results, presented in Table 7, indicate that MG ores are moderately abrasive.

Table 7: Abrasion Index results for different rock type for MG ore

Rock type	Abrasion Index (g)
MG2	0.3114 0.2671
MG3	0.2710 0.2890
MG1	0.3760 0.4546
MG4A	0.2912 0.2781

The Ai values ranged from 0.2671 g for MG2 to 0.4546 g for MG1. These values suggest that wear protection measures, such as the use of wear-resistant liners and grinding media, are essential to mitigate wear and tear on comminution equipment.

JK Drop Weight Test
The JK Drop Weight Test results, summarized in Table 8, provide insights into the impact breakage behavior of MG ores.

Table 8: Abrasion Index results for different rock type for MG ores

Rock type	JK parameters			
	A	b	A*b	Ta
MG2	69.3	0.93	64.45	0.51
MG3	62.3	0.95	59.19	0.73
MG1	72.7	1.4	101.78	0.98
MG4A	65.8	0.94	61.82	0.62

The A*b parameter, which represents the overall breakage propensity, varied significantly among the ore types, ranging from 59.19 for MG3 to 101.78 for MG1. This indicates that MG1 has the highest impact breakage resistance, while MG2, MG3, and MG4A exhibit relatively similar and average breakage behaviour.

DISCUSSION

The comminution test results highlight the challenging nature of MG ores in terms of comminution. The high Bond Work Indices, UCS values, and variable impact breakage behaviour necessitate careful consideration during the design and operation of comminution circuits.

The findings of this study are consistent with the observations made by Mwanga (2014), who emphasized the importance of understanding ore characteristics for optimizing comminution processes. Mwanga highlighted that the selection of appropriate comminution tests and the interpretation of test results are crucial for developing efficient and cost-effective comminution, this was further expanded by Morrell (2004) who asserted that the selection of appropriate comminution tests is guided by the targeted particle size range, encompassing crushing for coarse particles, grinding for intermediate sizes, and ultra-fine grinding for very fine particles

CONCLUSION

The comminution and strength test results suggest that the four MG ore types possess distinct grindability and breakage characteristics. MG1, being the softest and easiest to grind, might require less energy during comminution. In contrast, MG2 and MG3, with their higher work indices and UCS values, demands more energy-intensive processing. These variations highlight the importance of considering ore-specific properties when designing and optimizing comminution circuits.

RECOMMENDATIONS

The relatively high Work Indices for MG2, 3 and 4A ore types suggest that significant energy is required for comminution, whereas MG1 appears to be less energy-intensive. Furthermore, it indicates the need for robust crushing circuits, signaling an optimal comminution equipment selection, configuration, and operating parameters to minimize energy consumption and wear, by considering factors like crusher and mill type, speed, and liner design to improve energy efficiency.

FUTURE RESEARCH

Investigate alternative comminution methods, such as high-pressure grinding rolls or stirred media mills, which might be more energy-efficient for these hard ores. Conduct detailed mineralogical analysis of each ore type and correlate it with the BWI values to understand the influence of specific minerals on crushability and grindability. Study the correlation between JK parameters and other comminution properties, such as BWI and UCS, to develop a more comprehensive understanding of impact breakage behavior.

REFERENCES

Aksani, B.; Sönmez, B. Simulation of Bond grindability test by using Cumulative Based Kinetic Model. Miner. Eng. **2000**, 13, 673–677.

Austin, L.G.; Klimpel, R.R. The Theory of Grinding Operations. Ind. Eng. Chem. 1964, 56, 18–29.

Bearman, R.A.; Briggs, C.A.; Kojovic, T. The Application of Rock Mechanics Parameters to the Prediction of Comminution Behaviour. Miner. Eng. **1997**, 10, 255–264.

Berry, T.F.; Bruce, R.W. A simple method of determining the grindability of ores. Can. Min. J. **1966**, 87, 63–65.

Bond, F.C.; Maxson,W.L. Standard grindability tests and calculations. Trans. AIME Min. Eng. **1943**, 153, 362–372.

Bond, F.C. Third theory of comminution. Trans. AIME Min. Eng. **1952**, 193, 484–494.

Bond, F.C. Crushing and grinding calculations. Br. Chem. Eng. **1961**, 6, 378–385.

Bonoli, A.; Ciancabilla, F. The Ore Grindability Definition as an Energy Saving Tool in the Mineral Grinding Processes. In Proceedings of the 2nd International Congress "Energy, Environment and Technological Innovation", Rome, Italy, 12–16 October 1992.

Chakrabarti, D.M. Simple approach to estimation of the work index. Transactions of the Institutions of Mining and Metallurgy, Section C. Miner. Process. Extr. Metall. **2000**, 109, 83–89.

Ciribeni, V.; Bertero, R.; Tello, A.; Puerta, M.; Avellá, E.; Paez, M.; Menéndez-Aguado, J.M. Application of the Cumulative Kinetic Model in the Comminution of Critical Metal Ores. Metals **2020**, 10, 925.

Coello Velázquez, A.L.; Menéndez-Aguado, J.M.; Brown, R.L. Grindability of lateritic nickel ores in Cuba. Powder Technol. **2008**,182, 113–115.

Deister, R.J. How to determine the BondWork Index using lab ball mill grindability tests. Eng. Min. J. **1987**, 188, 42–45.

Deniz, V.; Ozdag, H. A new approach to bond grindability and work index: Dynamic elastic parameters. Miner. Eng. 2003, 16,211–217.

Faramarzi, F.; Napier-Munn, T.; Morrison, R.; Kanchibotla, S.S. The extended drop weight testing approach—What it reveals. Miner. Eng. **2020**, 157, 106550.

Fuerstenau, D.W.; Abouzeid, A.-Z.M. Effect of fine particles on the kinetics and energetics of grinding coarse particles. Int. J.Miner. Process. **1991**, 31, 151–162.

Hukki, R.T. Proposal for a solomonic settlement between the theories of von Rittinger, Kick, and Bond. Trans. AIME **1961**, 220, 403–408.

Karra, V.K. Simulation of the Bond grindability test. CIM Bull. **1981**, 74, 195–199.

Kick, F. Das Gesetz der Proportionalen Widerstände und Seine Anwendungen; Arthur Felix: Leipzig, Germany, 1885.

Lewis, K.A.; Pearl, M.; Tucker, P. Computer Simulation of the Bond Grindability Test". Miner. Eng. **1990**, 3, 199–206. [CrossRef]

Morrell, S. (2004). A new autogenous and semi-autogenous mill model for scale-up, design and optimisation. Minerals Engineering, 17(3), 447–451

Menéndez-Aguado, J.M.; Dzioba, B.R.; Coello-Velázquez, A.L. Determination of work index in a common laboratory mill. Miner. Metall. Process. **2005**, 22, 173–176.

Mwanga, A.; Rosenkranz, J.; Lamberg, P. Development and experimental validation of the Geometallurgical Comminution Test (GCT). Miner. Eng. **2017**, 108, 109–114.

Mwanga, (2014) Mwanga, A.. Test Methods for Characterising Ore Comminution Behavior in Geometallurgy. In Proceedings of the Geometallurgy 2014 Conference (pp. 64-72). Australasian Institute of Mining and Metallurgy.

Narayanan, S.S., Whiten, W.J. (1983). Breakage characteristics for ores for ball mill modelling. In: Proceeding of the Australasian Institute of Mining and Metallurgy, vol. 286, pp. 31–39.

Nikoli´c, V.; Trumi´c, M. A new approach to the calculation of Bond work index for finer samples. Miner. Eng. **2021**, 165, 106858.

Napier-Munn, T.J.; Morrell, S.; Morrison, R.D.; Kojovic, T. Mineral Comminution Circuits: Their Operation and Optimisation University of Queensland; Julius Kruttschnitt Mineral Research Centre: Indooroopilly, Australia, 1996.

Ram Chandar, K.; Deo, S.N.; Baliga, A.J. Prediction of Bond's work index from field measurable rock properties. Int. J. Miner. Process. **2016**, 157, 134–144.

Rittinger von, P.R. Lehrbuch der Aufbereitungskunde; Ernst und Korn: Berlin, Germany, 1867.

Russell, A.R., Muir Wood, A. (2009). Point load tests and strength measurements for brittle spheres, International Journal of Rock Mechanics and Mining Sciences 46 (2009), pp. 272 – 280.

Schönert, K. Aspects of the physics of breakage relevant to comminution. In Proceedings of the 4th Tewksbury SymposiumFracture, February, Melbourne, Australia, 12–14 February 1979; University of Melbourne: Melbourne, Australia, 1979; p. 3.

Yap, R.F.; Sepulveda, J.L.; Jauregui, R. Determination of the Bond Work Index Using Ordinary Laboratory Batch Ball Mill. In Design and Installations of Comminution Circuits; Mular, A.L., Jergensen, G.V., Eds.; AIME: New York, NY, USA, 1982; p. 176.



Phumlani Siwela

Process Superintendent
Minopex

I am a seasoned metallurgical environmental professional with 16 years of experience in the mining industry. Starting as a student, I demonstrated unwavering dedication and perseverance, rising through the ranks to attain the esteemed position of Superintendent.

Throughout my illustrious career, I have gained extensive expertise in various commodities, including Platinum Group Metals (PGM), chrome, and coal. This diverse experience has equipped me with a unique understanding of the complexities and challenges associated with different mining operations.

A holder of two master's degrees, I have earned an Mtech in Metallurgical Engineering and an MBA. This exceptional academic background has provided me with a strong foundation in both the technical and business aspects of the industry.

As a respected leader, I continue to drive innovation and excellence in metallurgical environmental management, leveraging my expertise to optimize processes, ensure sustainability, and foster growth in the mining sector.

Improving PGM recovery through optimised solid liquid separation

M. Hove[1], N. Nhleko[2], T. Moretsele[2], S. Mhlongo[3], K. Tshenye[3], C. Mtileni[2]

[1]Anglo American-Technical Solutions, South Africa
[2]Valterra Platinum, South Africa
[3]Solenis, South Africa

As the platinum metals group (PGMs) market faces challenges of demand, it is imperative that refinery operations must ensure continuous improvement in process efficiency and reduce metal losses. This paper presents a comprehensive approach to a technical evaluation and optimisation of a PGM refinery solid-liquid separation process of an effluent stream. The study was conducted in two parts: bench-scale laboratory test work to identify the flocculant chemistry, and a full-scale plant validation trial of the flocculant chemistry.

Initial bench-scale laboratory test work showed that Magnafloc 10 was the flocculant of choice for improving settling rates, underflow density, and overflow clarity. Magnafloc 10 consistently delivered superior performance over different feed samples, compared to other flocculants. It achieved overflow turbidity clarity below 100 NTU, and underflow density improvement of up to 5%. Dosing profiles and settlement rate analysis validated Magnafloc 10 for suitability for full scale plant trials.

Full-scale plant trials, firstly focused on plant operational readiness for Magnafloc 10 flocculant make-up and identifying an effective dosing philosophy. The plant make-up unit was identified as functional but requiring minor maintenance and calibration due to the use of an incompatible product prior to Solenis. The findings from the plant assessment also revealed critical limitations arising from a lack of flow meters, and monitoring tools such as turbidity and density meters. To address these challenges, screw feeder calibration and settling rate protocols, and dosing strategies were investigated. The second part of the full-scale plant trial focused on optimisation of the Magnafloc 10 dosage. The full-scale plant trial results achieved a suspended solids percentage removal 97% and underflow density of 1.15 g/L at a dose rate of 2.2 g/T. The full-scale plant application of Magnafloc 10 revealed there were additional benefits in the dewatering filter plant cake moisture content.

This paper contributes valuable insights into the practical challenges and solutions associated with improving PGM recovery from solid-liquid separation processes within refinery operations using a flocculant.

INTRODUCTION

Platinum Group Metals (PGMs) are mostly found in ore bodies of ultramafic and mafic igneous rock formation in South Africa, Canada, Zimbabwe, and Russia; globally PGMs reserves are estimated to range from 69300 – 90700 tonnes (Ndlovu, 2021; Hughes *et al.*, 2021). Figure 1 shows the PGMs world reserves distribution, wherein South Africa has the world's largest known reserves over 80% (Mvokwe *et al.*, 2025).

Moreover, Ndlovu (2021) states that 60% of newly mined PGMs and over 80% of platinum come from South Africa. Industrial mining of PGMs in South Africa began in the early 1900s; while globally it started around the 1800s (Mineral Council for South Africa, 2019).

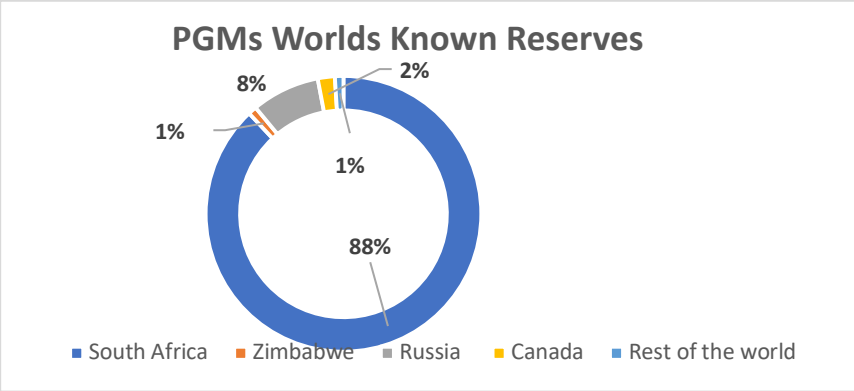


Figure 1: PGMs globally-known reserves adapted from Ndlovu (2021)

In South Africa, mining of PGMs occurs entirely in the Bushveld Ignesous Complex (BIC), making it the largest global source of PGM-bearing ore. This region is commonly divided into three parts; Eastern limb, Northern limb and Western limb. However, the region consists of three distinct mineral-bearing reefs: Merensky reef, UG2 reef, and Platreef (O'Connor & Alexandrova, 2021; Hughes *et al.*, 2021). There are several studies on the mineralogy and geology of the BIC, in particular the mineral-bearing reefs (O'Connor & Alexandrova, 2021):

- Merensky reef – it is named after the geologist, Hans Merensky, and it is one of the first known PGM-bearing sulfide ore in South Africa. It contains relatively higher PGM grades ranging from 0.04 to 2.7 g/T (refer to Table I), and the PGMs are typically contained in base metal sulfide grains.
- UG2 reef – it is a PGM-bearing chromite rich ore, with a lower head grade of PGMs ranging from 0.13 to 2 g/T.
- Platreef – it is located on the northern limb of the BIC, with a low head grade range of 0.04 to 1.9 g/T and it contains high concentrations of base metals when compared to the other reefs.

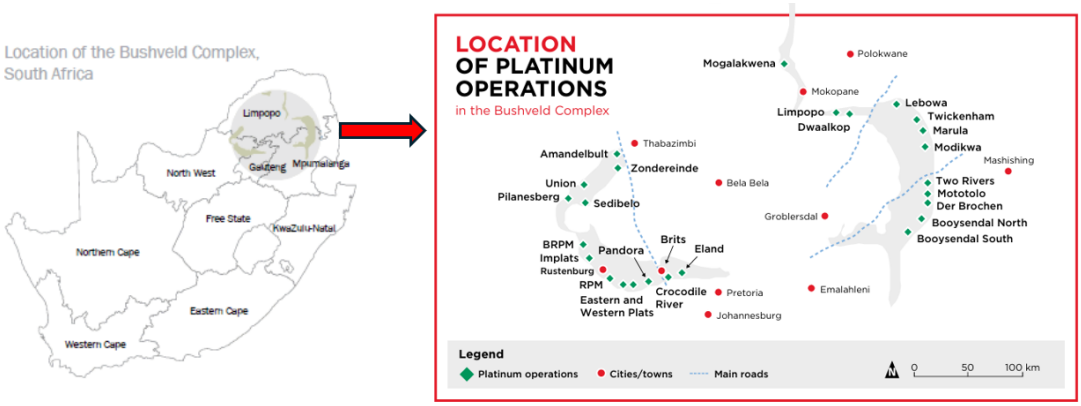


Figure 2: Location of PGMs mining activity within South Africa adapted from Hughes et al., (2021) and Mineral Council of SA (2019).

Table I: PGM concentration in g/T for the Bushveld Igneous Complex ore bodies adapted from Hughes et al., (2021).

Ore Body	Pt g/T	Pd g/T	Rh g/T	Ru g/T	Ir g/T	Os g/T	Total PGM g/T
Merensky Reef	2.7	1.4	0.16	0.33	0.05	0.04	4.68
Platreef	1.9	1.9	0.12	0.14	0.04	0.03	4.13
UG2	2	1.3	0.34	0.45	0.13	0.05	4.27

In South Africa, Valterra Platinum Ltd. is the leading producer of PGMs, and it is the world's largest vertically integrated producer of platinum-based metals; as such, the company focuses its operations on exploring, mining, processing and refining precious metals. As explained by Ndlovu (2021) the operations of the company are integrated and comprise of 6, four smelter plants, and two refineries (base metals refinery and precious metals refinery). This paper aims to improve the process efficiency through increasing the recovery of PGMs in the Precious Metals' Refinery.

The PGM refinery process consists of PGM extraction and dissolution, and precipitation. These processes generate an effluent stream that contains dissolved PGMs chlorides; as such, the residual PGMs are to be recovered through pH neutralisation and precipitation followed by a solid-liquid gravity separation process utilising a high-rate thickener (HRT). The clear thickener overflow is pumped to the evaporation dams (ponds) whilst the thickener underflow is further concentrated using a plate and frame filter press. The HRT was identified as not complying with its processing target of < 300 mg/L for the overflow and 1.15 specific gravity for the underflow. As a a result a significant amount of PGMs, averaging 11% were lost to the evaporation dams (ponds). Thus the main objective of this study was to reduce the PGMs' losses by optimising the operations of HRT.

HRT operates on the sedimentation process, where gravitational force is used to separate suspended solids from a liquid suspension by making the density of the solids exceed the density of the liquid. The differences in density result in the solids settling within the liquid suspension. The particle size also plays a crucial role in the settling of the solids; in general coarse particles (> 75 µm) tend to settle with ease while fine particles (<75 µm) settle slowly. HRTs is primarily designed to handle high feed throughput with the addition of flocculant helping to achieve higher solids settling rates and underflow density.

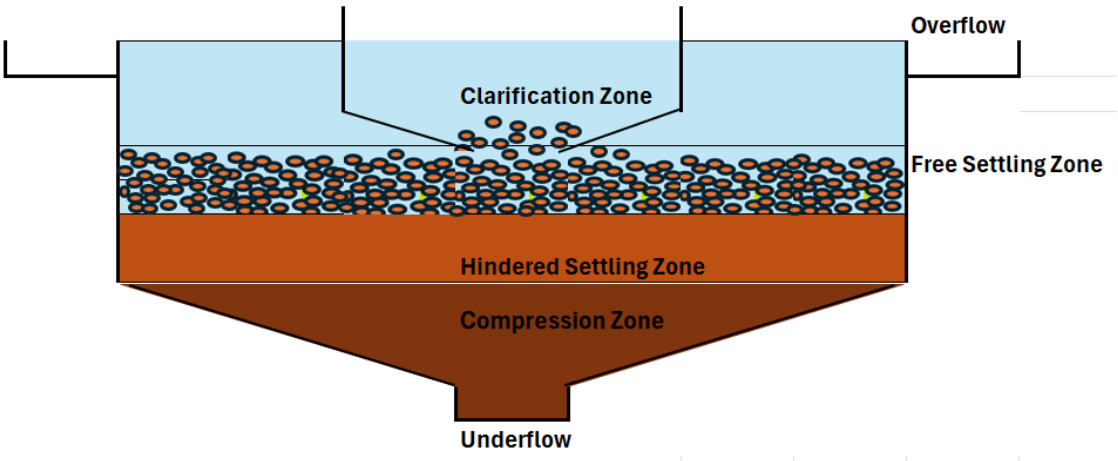


Figure 3: Overview of thickener settling zones.

Flocculants are polymers with long-chain molecules that agglomerate solid particles into flocs, and the dense flocs settle faster. In practice, the determination of the optimum flocculant dosage is determined empirically on the plant. It is well documented in literature (Bista, 2022) that overdosing of flocculant in thickener has adverse effects such as disposition of solids on the thickener wall, floating flocs, and a fluffy underflow bed. As such the optimisation of the HRT process was twofold; firstly, identifying a suitable flocculant, and secondly determining the appropriate flocculant dosage rate that will enable faster solids settling, resulting in increased recovery of PGMs.

Methods and Materials

Laboratory evaluation of flocculants was conducted by collecting a 20-litre thickener slurry sample from PMR. The thickener slurry feed sample was homogenised by stirring it to ensure consistent solids and randomised aliquots of the feed were sampled into 500 mL transparent cylinders.

The thickener slurry feed was characterised by measuring its pH, percentage solids, and relative density – listed in Table II.

Table II: Characteristics of thickener slurry feed sample

Slurry SG (gcm^{-3})	Slurry solids %	pH
1.068	11.58%	11.50

Typical slurry solids particle size distribution is shown in Table III.

Table III: Slurry solids particle size distribution

Particle size	Percentage passing
10 micron	25-40% passing
25 micron	75% passing
53 micron	>90% passing
300 micron	>98% passing

Standard solutions of Solenis' solid-grade flocculants were prepared at 0.5% m/m using deionized water. Stock solutions were diluted to 0.05% v/v using the thickener overflow, following plant practice. A standard plunger settling test method was utilised which consists of five plunger strokes to effectively disperse the flocculent after addition into the thickener slurry feed and letting the slurry settle for 30 minutes while recording the settling time, liquid-solid interface and turbidity. All flocculent chemical samples were Solenis laboratory-grade samples. The turbidity and pH meters used were Lovibond and Hanna, respectively.

Shortly after laboratory evaluation of the flocculants, a plant visit was carried out with the aim to conduct a process audit. The process audit covered assessment of the plant flocculent makeup unit, dosing pumps, dosing points, mixing regime, and plant instrumentation and control philosophy. Subsequently, a plant trial was carried out to determine the performance of the selected flocculant in improving the recovery of PGMs by reducing the overflow suspended solids concentration to below the specification of <300 mg/L as per the HRT manufacturer's design specification.

RESULTS AND DISCUSSION

This section will be divided into three parts: results and discussion of the laboratory test work, results and discussion of the plant readiness assessment, and results and discussion of the plant trial.

Laboratory Test work

Various anionic flocculants were tested using the cylinder settling tests at a constant dose of 8,2 g/T. As indicated in Figure 4, the tested flocculants were able to achieve satisfactory results compared to the

blank feed sample which exhibited slow settling, higher turbidity, and the lowest underflow density, requiring longer residence time. Magnafloc 10, Magnafloc 155, and Magnafloc 338 were the best performing flocculants because they were able to respectively improve clarity by 60%, 66% and 77%. These flocculants also displayed exceptional improvements of the settling rate and underflow density; 20m/h and 800g/L for Magnafloc 10, 35 m/h and 750 for Magnafloc 155, and 25 m/h and 780g/L for Magnafloc 338.

The best performing products in terms of settling rate were selected for dose profiling. Dose profiling was done to further investigate the settling at a certain dose. Figure 2 indicates that all three products are suitable to settle the slurry as they perform similarly in all doses used, considering the plant variation is minimal. However, it must be noted that the variation in feed solids density (which was constant in these tests) will also influence the dose required.

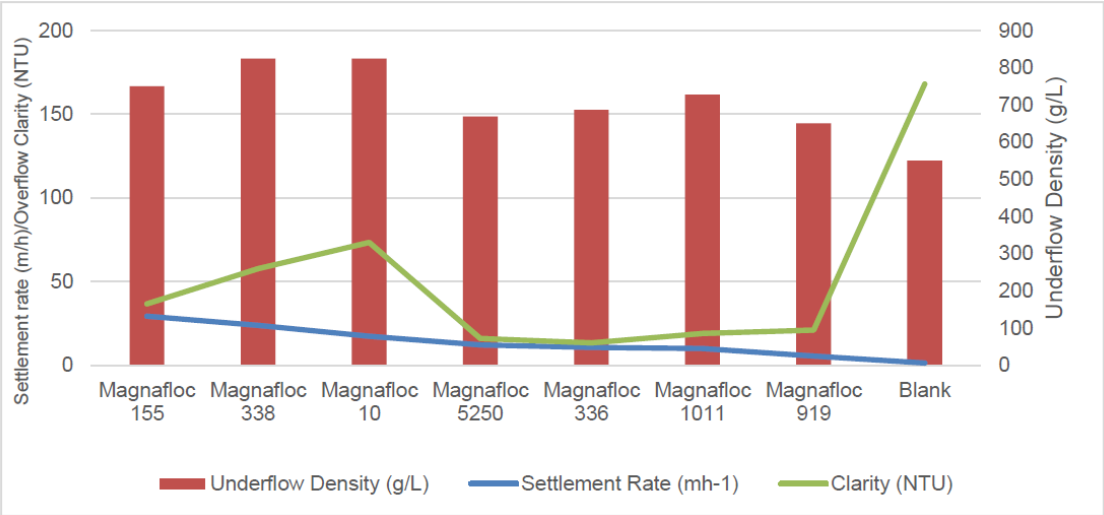
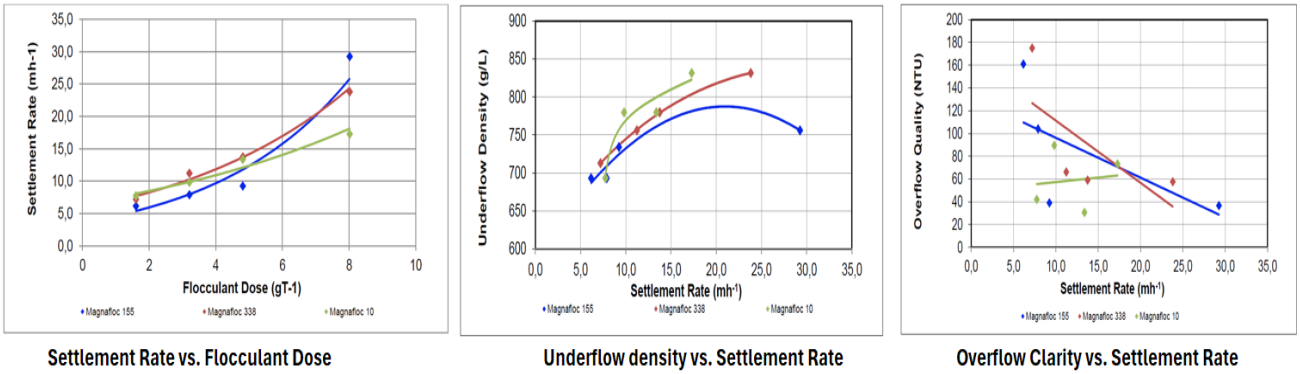


Figure 4: Single point screening of flocculents at 8,02g/T dosage.

Further dosage optimisation tests were conducted with Magnafloc 10, Magnafloc 155, and Magnafloc 338 with the aim of determining the agile flocculent. The agility of the flocculent was based on conducting dose profiling to investigate its effect on settling rate, underflow density, and overflow clarity. Figure 5 indicates that all three products are suitable to settle the slurry as they perform similarly in all doses used. In terms of the underflow density, Magnafloc 10 achieve higher underflow density as compared to Magnafloc 338 and Magnafloc 155. At the settlement rate of 10m/h, Magnafloc 10 achieves an underflow density of 4% and 5% higher than Magnafloc338 and Magnafloc 155 respectively. Furthermore, the test work results revealed that Magnafloc 10 offers the lowest turbidity for the overflow clarity. All products can give the turbidity below 200 NTU; however Magnafloc 10 offers turbidity below 100 NTU at all dosages tested. The flocculent screening test results indicate that Magnafloc 10 demonstrates the best overall performance in terms of underflow density, and overflow clarity.



Settlement Rate vs. Flocculant Dose | Underflow density vs. Settlement Rate | Overflow Clarity vs. Settlement Rate

Figure 5: Flocculent dosage profiles effect on settling rate, underflow density and overflow clarity.

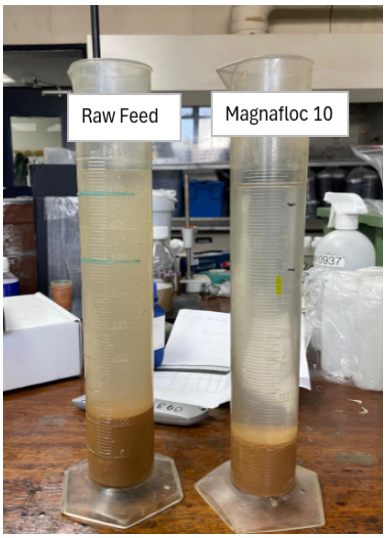


Figure 6: Comparison picture of raw feed natural settling against the addition of Magnafloc 10.

Plant readiness assessment

The assessment consisted of examining the plant state of readiness to dose a flocculent and to ensure that the proposed flocculant, Magnafloc 10, is compatible with the plant equipment. The site has one HRT (~4.5m radius) that treats the effluent after precipitation of PGMs. It was determined that the plant had functional flocculant dosing pumps that can achieve the desired flowrates range up to 500 l/hr. Furthermore, it was determined that the flocculant dosing flow rotameter was no longer visible, thus need replacement.

The flocculant make-up unit on site was for a powder-dry flocculent meaning that Magnafloc 10 would be suitable for use with the existing equipment. However, the flocculant make-up unit was poorly maintained and had an unknown product that had blocked the screw feeder. It was also discovered that the screw feeder had no means of measuring the amount of flocculant consumed. After the screw feeder underwent maintenance; it was calibrated to ensure that it was dosing a consistent flocculant mass that allowed for a 0.04% $^{m}/_{v}$ concentration of flocculant. Table IV shows the calibration results of the screw feeder.

Table IV: Flocculant screw feeder calibration of mass discharged

Screw Feeder Calibration	
Time seconds	**Mass of Magnafloc 10 pumped**
30	475 grams
120	1735 grams

The results show that the screw feeder was to be set for 30 seconds to ensure that it discharged the appropriate amount of Magnafloc 10 that will make up the desired concentration of 0.04% $^{m}/_{v}$. Based on visible inspection, the plant dosing point for the flocculent was appropriate since it had moderate mixing thus no shearing of flocs would occur. Furthermore, it was evident that one dosing point of the flocculant will be sufficient to aggregate the slurry solids to achieve the desired settling rate. Lastly, the assessment revealed that the plant had no monitoring tools for the effectiveness of the HRT such as a turbidity and density meter.

It was also noted that the HRT also had a settling rate controller and bed level measurement installed previously which are no longer functional. The settling rate control system functions by periodically measuring the slurry solids settling rate to ensure that it is within the plant operating setpoint. Similarly, the bed level measurement functions by measuring the slurry solids bed level within the HRT to ensure smooth operational efficiency, especially with the underflow density specifications. Figure 7 shows a typical unit for a settling rate system – Alcotech - that offers the benefits of:

- Consistent solids settling velocity.
- Consistent underflow density.
- Prevention of solids carryover in the overflow stream.
- Optimised flocculant addition.

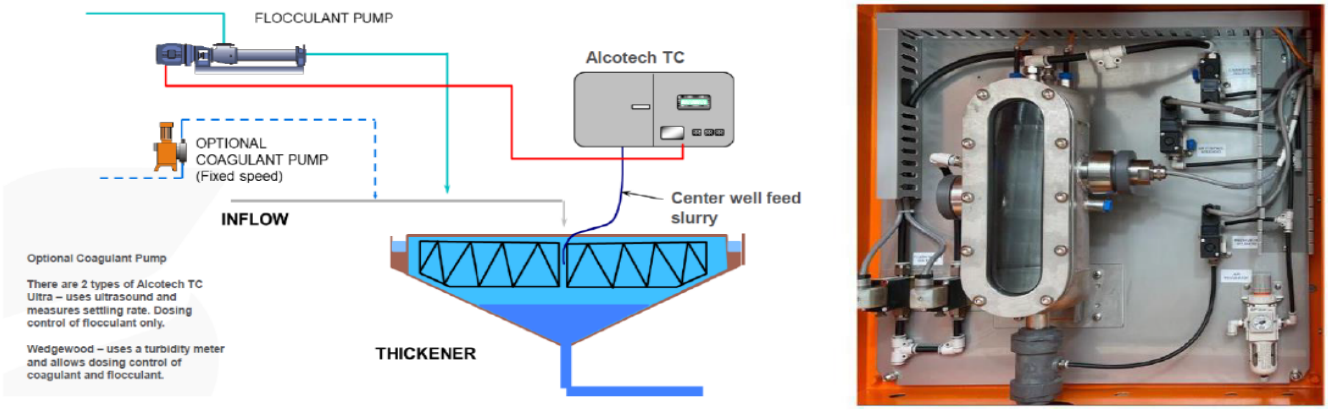


Figure 7: Overview of operating philosophy and installation of Alcotech TC.

Plant Trial

The full-scale plant trial focused on optimisation of the Magnafloc 10 dosage. The full-scale plant trial results achieved a suspended solids percentage removal of more than 97%, and an underflow density of 1.15 g/L at a dose rate of 2.2 g/T. A weeklong plant trial was conducted to assess the efficacy of dosing a flocculent.

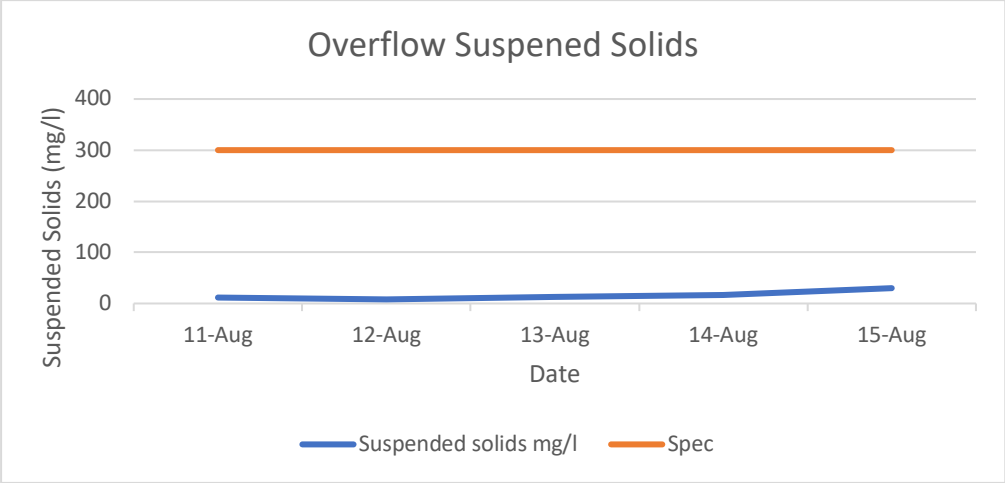


Figure 8: Magnafloc 10 overflow suspended solids at optimum dosage of 2.2 g/T.

The full-scale plant application of Magnafloc 10 revealed there were additional benefits on the dewatering filter plant cake moisture content. Literature (Bista, 2022) and Solenis (date) experience validates that dosing of a flocculent in a thickener to improve sedimentation rate not only reduces suspended solids in the overflow stream and increases underflow density but it also assists with improving dewatering capabilities.

For the work of optimisation to continue smoothly, other variables need to be monitored and documented, such as:

- Feed slurry flow rate – ml/min units
- Feed slurry density – kg/L
- Feed slurry % solids - %
- Flocculant dosed – ml/min
- Flocculent make up strength - % units
- Underflow density – kg/L
- Overflow clarity turbidity – NTU units
- Flocculent level on screw feed hopper - %



Figure 9: Thickener overflow clarity during plant trial.

CONCLUSIONS

A systematic approach in improving the recovery of PGMs of the refinery from its HRT proved to produce exceptional results. The laboratory screening test method was able to identify Magnafloc 10 as the best performing the flocculant. –The plant trial using Magnafloc 10 at 2.2 g/T resulted in more than 97% PGMs recovery (much better than specification), less than 40 NTU turbidity (far less than the specification), and undeflow SG of 1.15 as specified for this particular thickener.

RECOMMENDATIONS

The installation of a settling rate controller and bed level measurement equipment that will allow for automation and monitoring within the HRT are highly recommended. Furthermore, the plant needs to obtain basic monitoring equipment such as turbidity and density meters. It is important to point out that, as much as the solid liquid separation process has been optimised at the HRT, focus now needs to be directed at ensuring high plant utilisation, and stable and consistent operation of the plant to prevent any PGM losses.

ACKNOWLEDGEMENT

The successful completion of this project on optimising the HRT was made possible by many team members from Anglo American Technical Solutions, Valterra Platinum and Solenis.

REFERENCES

Bista, S., 2022. Tailings dewatering: thickening followed by filtration.

Hughes, A.E., Haque, N., Northey, S.A. and Giddey, S., 2021. Platinum group metals: A review of resources, production and usage with a focus on catalysts. Resources, 10(9), p.93.

Minerals Council South Africa. (2019). National Platinum Strategy for South Africa. [PDF] Available at: https://www.mineralscouncil.org.za [Accessed 09 Sep. 2025].

Mvokwe, S.A., Oyedeji, O.O., Agoro, M.A., Meyer, E.L. and Rono, N., 2025. A Critical Review of the Hydrometallurgy and Pyrometallurgical Recovery Processes of Platinum Group Metals from End-of-Life Fuel Cells. Membranes, 15(1), p.13.

Ndlovu, J., 2021. Overview of PGM processing. Anglo Platinum. Available online: http://www. angloamericanplatinum. com/~/media/Files/A/Anglo-American-Platinum/investor-presentation/standardbankconference-anglo-american-platinum-processing-111114. pdf (accessed on 31 May 2017).

O'Connor, C. and Alexandrova, T., 2021. The geological occurrence, mineralogy, and processing by flotation of platinum group minerals (PGMs) in South Africa and Russia. Minerals, 11(1), p.54.

Investigating the impact of stirred milling to improve the fineness of the grind for PGM tailings reprocessing - IsaMill case study

K.I. Mohapi[1], M. Becker[1], K.C. Corin[1], D. Makhubele[2], T. Pienaar[2], A.N. Mainza[1]

[1]University of Cape Town, South Africa
[2]Tailings Technology (Pty) Ltd, South Africa

IsaMills have been used in the Mill-Float circuits in the platinum industry to ensure that the platinum group minerals (PGM) are liberated and available for the subsequent flotation stages. A growing trend of reprocessing tailings to recover both chromite and PGMs in the UG2 ore, one of the local platinum-bearing ores, has been observed. The tailings are either reprocessed without any milling stage or a ball mill is used as a preparatory stage for minimal grinding to polish the particle surfaces. Due to the fine-grained nature of PGMs, achieving adequate liberation often requires grinding below 45 µm. High energy consumption is required to grind to the appropriate levels of fineness using ball mills, and the product often has a significantly high amount of slimes, which leads to high losses of valuable minerals downstream. This paper presents the results of tests performed using the IsaMill to produce products with P80 values of 71, 52, and 28 µm, which were subjected to batch flotation tests to evaluate the effects of grinding the tailings before reprocessing on recovery, along with the associated energy-grind relationships. 4E recoveries in the order of 70% were obtained from the tests where stirred milling was applied in the preparation stage, compared to 25-30% for the tests that did not involve milling or the tests that had a ball mill (P80=83 µm and 45 minutes grinding time) before the flotation stage. The high recoveries observed were largely due to the enhanced liberation of PGM-bearing phases. The study indicates that stirred milling is a viable strategy for PGM tailings reprocessing, provided that operational conditions are tuned for energy efficiency.

Keywords: IsaMill, Tailings, Liberation, Recovery, Reprocessing

INTRODUCTION

Comminution plays a critical role in the mineral processing industry. It is responsible for ensuring that sufficient particle size reduction is achieved to liberate valuable minerals from the surrounding gangue, preparing them for downstream separation. This process is highly inefficient in energy utilisation and is one of the largest energy consumers in the mineral processing industry (Napier-Munn, 2015). Traditional tumbling mills often fail to deliver the fine particle sizes (<45 µm), which is often required for adequate liberation of platinum group minerals (PGMs) embedded in silicate and chromite matrices for the Upper Group 2 (UG2) ore (Rule, 2010; Leroy *et al.,* 2011; Baloyi *et al.*, 2024). Consequently, tailings from platinum group metal (PGM) concentrators processing UG2 ore can contain significant unrecovered PGMs. Tailings reprocessing is increasingly being recognised as a viable strategy for additional value recovery, primarily because the major capital and operational expenditures associated with hard rock mining and initial processing have already been incurred. However, conventional approaches for milling in tailings reprocessing are limited because of the high energy demands associated with grinding finer.

The development of stirred media mills, including the IsaMill, has been a breakthrough in addressing this challenge. Initially developed for pigment and pharmaceutical applications, stirred mills have been increasingly applied to process complex base and precious metal ores that require fine and ultra-fine grinding (Jankovic *et al*., 2003; Kwade & Schwedes, 2007). Compared to tumbling mills, they provide higher energy efficiency, narrower particle size distributions (PSD), and improved mineral liberation at fine grind sizes (Allen & Ntsele, 2012). Stirred mills have been installed across at least nine different commodities, including base metals and precious metals (Gurnett *et al*., 2021).

The stirred milling process employs a drive shaft connected to multiple agitators (rotors) housed within a stationary mill chamber. As the stirrers rotate, they fluidise the grinding media, initiating particle breakage predominantly through attrition and shear forces. The choice of grinding media, ranging from sand and ceramic to steel or glass, is influenced by the application and characteristics of the feed material (Becker *et al*., 2001; Jayasundara *et al*, 2012; Gupta & Yan, 2016). These mills are versatile, capable of handling both wet and dry feeds, and are particularly effective in producing ultrafine particles in the 1–10 μm range (Hogg & Cho, 2001; Gupta & Yan, 2016).

The IsaMill was first developed in the early 1990s to address the processing challenges of ultrafine-grained lead–zinc deposits at Mount Isa and McArthur River mines in Australia (Pease *et al*., 2005) that were uneconomic to treat with conventional technologies available at the time. The IsaMill is a horizontally-oriented stirred mill, equipped with a motor and gearbox from which the grinding shaft is mounted laterally. Along the shaft, a series of rotating discs act as agitators, imparting energy to the grinding media and promoting intense particle comminution. Feed slurry enters the shaft at one end and exits under pressure further downstream in the horizontal direction. Each gap between consecutive discs functions as an individual grinding stage, effectively creating multiple grinding chambers in series and thereby improving efficiency (Glencore Technology, 2023). A distinguishing feature of the IsaMill is its patented internal product separator, which ensures precise particle size distributions without requiring external classification. This separator centrifuges the grinding media outward against the chamber walls, while allowing the finer mineral slurry to flow centrally toward discharge (de Waal *et al.,* 2013).

The study by Rule & Schouwstra (2012) demonstrated that PGM losses to UG2 tailings typically occurred in two forms: (i) fine grains locked within larger gangue particles and (ii) liberated PGMs smaller than 10 μm, which were lost due to flotation inefficiencies. This understanding was critical in showing where finer grinding would most effectively improve recovery. To address these challenges, Anglo Platinum (now Valterra Platinum) adopted the stirred milling technology, specifically the IsaMill. The application of this technology enhanced mineral liberation and improved separation of valuable minerals from gangue, with the Amandelbult UG2 concentrator serving as a prominent case study: before IsaMill installation, tailings contained 0.8-1.0 g/t 4E platinum group elements but after its integration, the 4E tailings grades fell to 0.5-0.6 g/t and recoveries exceeded 88% (Rule, 2010; Rule & Schouwstra, 2012).

This study evaluates the efficacy of IsaMill technology for PGM tailings reprocessing, with emphasis on energy-grind relationships, flotation performance, and mineralogical constraints.

Materials and Methods

A bulk sample of UG2 tailings was provided by Tailings Technology (Pty) Ltd., which runs a tailings reprocessing plant servicing Impala Platinum Mine in Rustenburg. The bulk samples were cut at regular intervals by directing the discharge hose pipes from the tail stream of the adjacent chromite recovery plant into 220 L drums. The drums were left overnight for the solids to settle, and clear water was decanted; the process was repeated for several days until sufficient samples for the test work were collected. In total, five drums of the UG2 tailings, weighing approximately 420 kg each, were received for the test work. The tailings were sun-dried, then de-lumped and manually blended. The sample was split 10 ways using a rotary splitter and recombined to culminate into five representative lots, which were stored in separate drums. The blended sample from each drum was then sequentially split using a 10-way rotary splitter until 10 kg representative sample aliquots were produced in preparation for the grinding tests. The 10 kg aliquots were then packed and sealed in labelled plastic bags and stored.

Experiments were conducted using an M4 IsaMill test rig at the University of Cape Town (UCT), comprising a 4 L horizontal stirred mill driven by a 5.5 kW motor. Grinding was conducted in semi-continuous (pendulum) mode using 3.5 mm ceramic grinding media. Slurry feed was prepared at 45 wt.% solids, with staged passes through the mill. For testing purposes, the M4 is equipped with a digital control panel that enables real-time monitoring of operational variables, including rotor speed, mill feed pressure, and discharge temperature, to ensure safe operation and consistent results. Rotor speed and pump speed are independent variables, initially set to predetermined values at the onset of each test work.

The experimental program employed the UCT 8-L modified Leeds flotation cell for the batch flotation tests, with each test replicated for error analysis. A standard reagent suite was used, consisting of sodium isobutyl xanthate (SIBX) as the collector and Senfroth 516 as the frother, both dosed according to the Standard UCT flotation procedure (Wiese, 2009). No depressant was added for these experiments, as the focus of tailings reprocessing is on PGM recovery; improving the grade falls outside the scope of this paper. The feed, flotation tails and concentrate samples were analysed for Pt, Pd, Rh, and Au (fire assays and ICP-OES finish) at an external accredited laboratory. Characterisation of the feed included determination of the bulk mineralogy of the feed ore using the QEMSCAN bulk mineral analysis method, validated with quantitative X-ray diffraction (QXRD) and X-ray fluorescence major element oxides (XRF).

The research approach applied in this study is outlined in Figure 1. It comprised characterisation of the tailings material, after which different routes were taken to determine the flotation response as follows: (i) base case, where no regrinding was done; (ii) ball mill, primarily used to repolish the mineral surfaces; and (iii) IsaMill, operated at varied grinding durations and rotor speeds. In the semi-continuous configuration, the product of one pass becomes the feed to the next pass. During each pass, two 100 ml samples were collected for particle size distribution (PSD) analysis, and a single tray sample was collected to confirm the moisture content of the sample. For the flotation response, a pair of 8 L samples was collected. As soon as the flotation samples were collected, they were stored in sealed buckets to minimise oxidation before flotation. The time of collection for each sample was recorded to guide the flotation sequence, ensuring that each test was conducted after a comparable waiting period following milling.

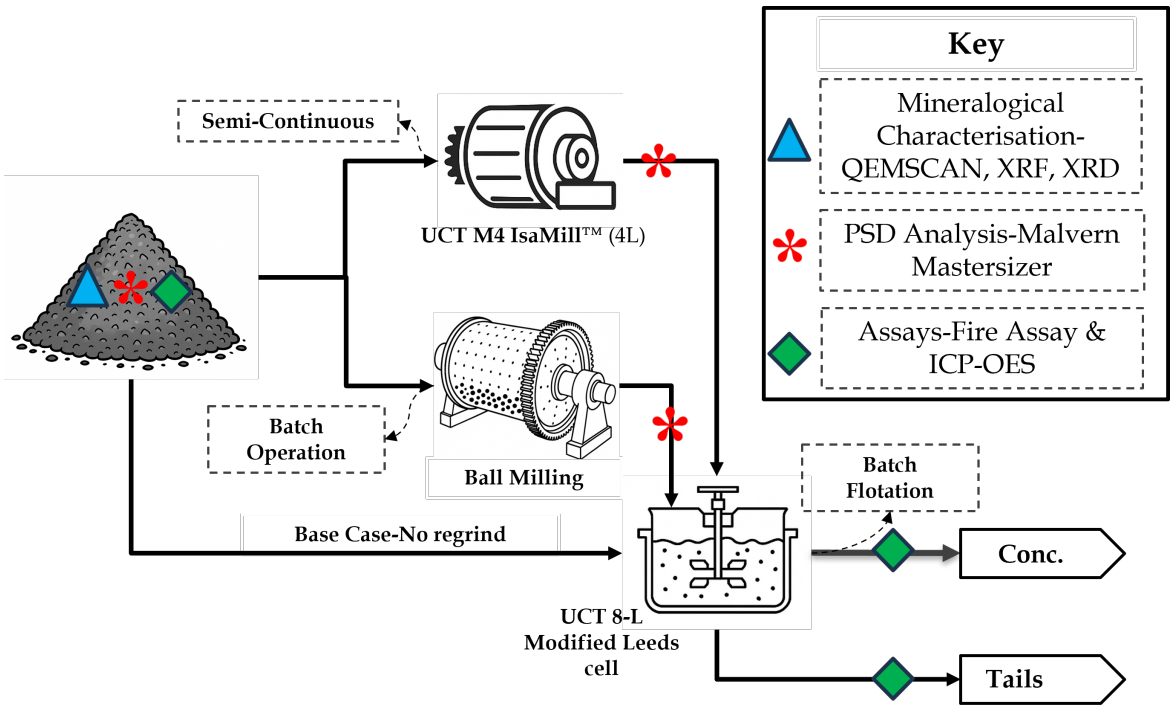


Figure 1. Research approach with the analytical techniques employed, shown

RESULTS AND DISCUSSION

The bulk mineralogical composition determined by QEMSCAN (Table I) shows that the sample is primarily composed of silicate minerals such as orthopyroxene (35.6%), plagioclase (21.7%), and clinopyroxene (4.2%), as well as chromite (28.6%). Of the phyllosilicate minerals present, including chlorite, mica, and serpentine, the abundance of talc (4.6%) would be the most concerning due to its natural hydrophobicity and froth-stabilising effects. Sulfide minerals, including chalcopyrite (0.4%) and pentlandite (<0.1%), are present in low concentrations but are of economic importance, particularly if they show an association with the PGMs.

Table I. Bulk mineralogy of the flotation feed, determined with QEMSCAN

Mineral Group	Mineral	Weight %
Base Metal Sulfides	Chalcopyrite	0,4
	Pentlandite	<0,1
	Pyrrhotite and Pyrite	0,1
Pyroxenes	Orthopyroxene	35,6
	Clinopyroxene	4,2
Phyllosilicates	Mica	0,6
	Talc	4,6
	Serpentine	<0,1
	Chlorite	1,8
Other Silicates	Amphibole	1,0
	Plagioclase	21,7
	Quartz	0,6
Oxides	Chromite	28,6
Carbonates	Calcite	0,2
Other		0,6

The QEMSCAN analysis also detected several trace PGMs, occurring as inclusions within silicate and chromite matrices, as shown in Figure 2. This mineralogical background is significant because chromite and silicate minerals are non-floatable, and their encapsulation of PGMs prevents reagent access to the valuable mineral surfaces. Consequently, any improvement in metallurgical performance is likely to depend on targeted regrinding designed to enhance exposure of the PGM while minimising the negative effects of slime coatings from the phyllosilicates.

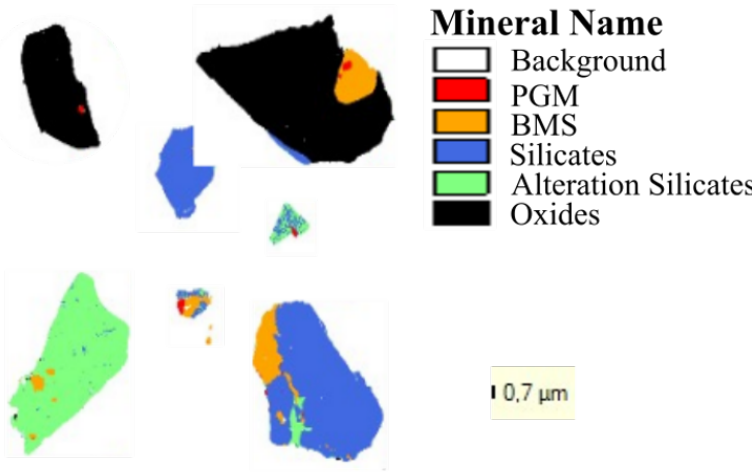


Figure 2. QEMSCAN false colour images of selected PGM particles in the feed prior to fine grinding.

Investigation of the stirred milling performance in terms of the change in PSD with grinding showed that, as the rotor speed increases, higher size reduction is achieved at the coarse end of the distribution than the fine end (Figure 3). These results confirm that rotor speed has a significant influence on size reduction in stirred milling. By manipulating the rotor speed, it is possible to tailor the grind to meet specific processing requirements, such as achieving the desired target grinds that can enhance the liberation of the valuable minerals. The particle size distributions produced under various experimental conditions investigated exhibited steep curves, highlighting the ability of stirred milling to produce narrow particle size distributions. Increasing rotor speed raised the agitation, which accelerated breakage, particularly in the coarse fractions, where repeated particle-media contacts are known to preferentially fracture coarser particles (Fuerstenau et al., 2003; Kwade & Schwedes, 2007). This is because larger particles shield the fine particles from contacting the media, and the coarser particles have more distinct crystallographic weak points, which promote particle breakage (Fuerstenau et al., 2003).

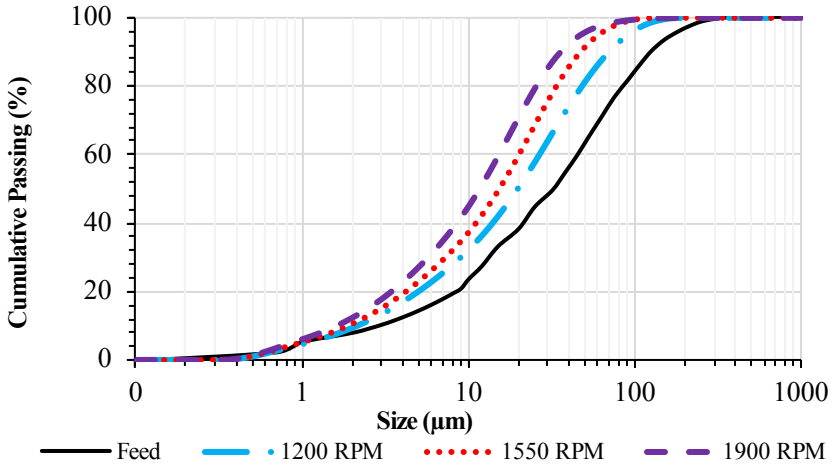


Figure 3. PSDs for varied rotor speeds.

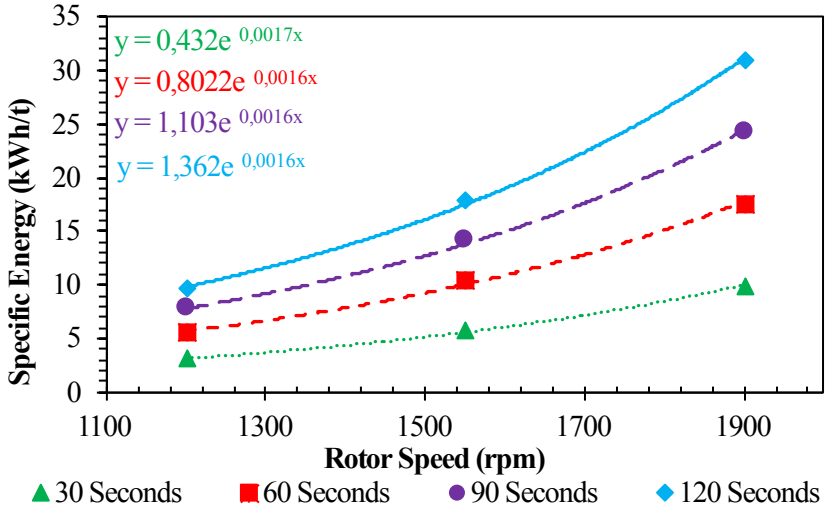


Figure 4. Relationship between rotor speed and specific energy, measured at different grinding times, with the corresponding exponential regression models shown.

The performance of the grinding process was evaluated by examining the relationship between rotor speed, grinding time, and specific energy. The relationship between the specific energy and rotor speed

at different grinding times is shown in Figure 4. The plots show energy demand variations with operating conditions and scale-up with increasing grinding intensity. The trends show a similar pattern of an exponential increase in specific energy with increasing rotor speed for all the different grinding times. The exponential increase shows that the increase in rotor speeds leads to a disproportional increase in specific energy, making it a major factor in determining optimum operating conditions. This is consistent with the Jankovic's, (2003) findings from the test work on stirred media milling, where elevated tip speeds intensify particle-media contacts but at the cost of disproportionately higher energy input (Jankovic, 2003). Grinding time also exerts a strong influence on energy, showing that for a given shaft speed, longer grinding durations consistently lead to higher specific energy values. It reflects the cumulative energy absorbed by the system, as particles remain exposed to repeated media-particle contacts over time, i.e. grinding longer at a high rotor speed result in much higher specific energy compared to what is observed at low rotor speeds.

Figure 5 shows the relationship between the specific energy and the product size represented by the P80 marker, commonly referred to as a signature plot. All the curves follow a strong negative power relationship: specific energy rises as particle size decreases. This is consistent with the fundamental comminution theory, including Rittinger's and Bond's laws, which predict that the energy to generate new surface area increases as size decreases (Bond, 1952; Hukki, 1961). The magnitude of the decay factor decreases with increasing shaft speed; this is shown by the slope of the plots decreasing with increasing shaft speed. It shows that for coarser product requirements, low rotor speed is the preferred operation, and for finer grind requirements, a high rotor speed leading to high energy intensity is a preferred method of operation.

Importantly, the variation in exponents across different operating conditions illustrates that the efficiency of size reduction is not constant but dependent on mill settings. High exponents reflect steeper energy–size relationships, indicating less efficient grinding at fine sizes, while gentle steepness correspond to more gradual energy increases, implying more favourable energy utilisation. Such differences underline the importance of identifying operational windows where sufficient liberation is achieved without incurring excessive energy costs, whilst being cognisant of the high wear rate associated with high rotor speed operations.

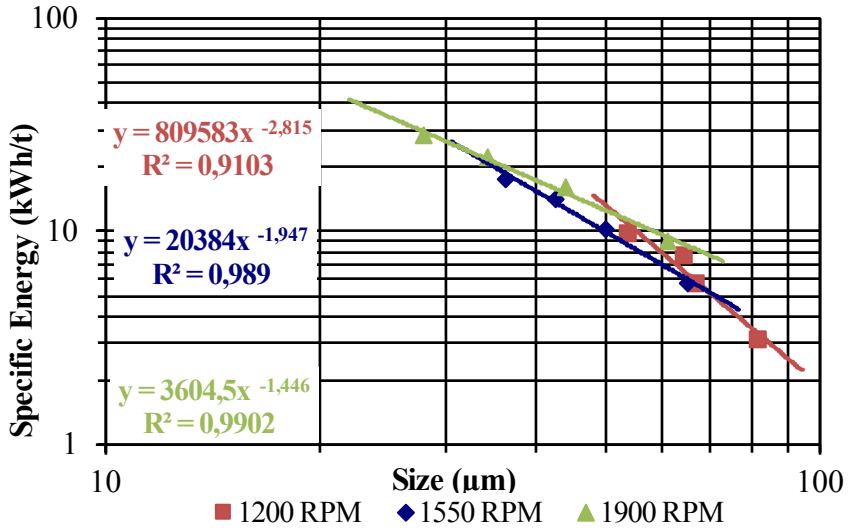


Figure 5. Signature plots associated with the different rotor speeds.

Table II shows the specific energy values corresponding to the stirred milling target grinds used for flotation response in this study (P80 = 28, 50, and 74 µm). These specific energy requirements for the target grinds were determined based on the signature plots shown in Figure 5.

Table II. Specific Energies from Signature Plots for Flotation Test Targets

Rotor Speed	**Specific Energy (kWh/t)**		
rpm	***P80 = 74 µm***	***P80 = 50 µm***	***P80 = 28 µm***
1200	4.43	13.36	68.31
1550	4.68	10.03	31.02
1900	7.14	12.59	29.12

The flotation results demonstrated an improvement in 4E recovery with an increase in the fineness of the ground product, as shown in Figure 6. In these experiments, the tailings were floated without carrying out any grind to establish a base case, and another float was performed with the material ground using a ball mill to a nominal P80 of about 80 microns, which is conventionally applied for most of the grinds in the PGM industry. A consistent trend emerges: as the grind gets finer, the gradient of the curve increases, which implies an improved selectivity, recovering more valuable PGEs per fraction of solids recovered. The 4E recovery versus solids recovery plots in Figure 6 show the positive effect of finer grind sizes on metallurgical performance. The target grind to P80 = 28 µm, achieved recoveries approaching 70%, compared to <25% for the base case and <35% for ball milling for the same flotation residence time. Further analysis on the flotation performance is shown in the upgrade ratio versus recovery curves shown in Figure 7. On this graph, the P80 = 50 µm shows the highest upgrade ratio as recovery increases, although the final recovery is higher on the finest grind (P80 = 28 µm). The base case and ball mill data remain clustered in the low-upgrade ratio, low-recovery region.

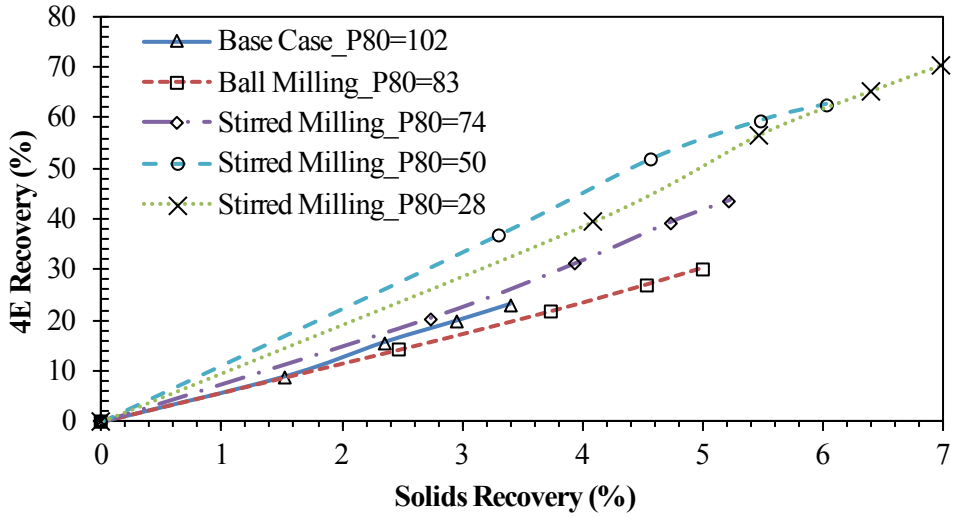


Figure 6. 4E PGE flotation recovery versus solids recovery.

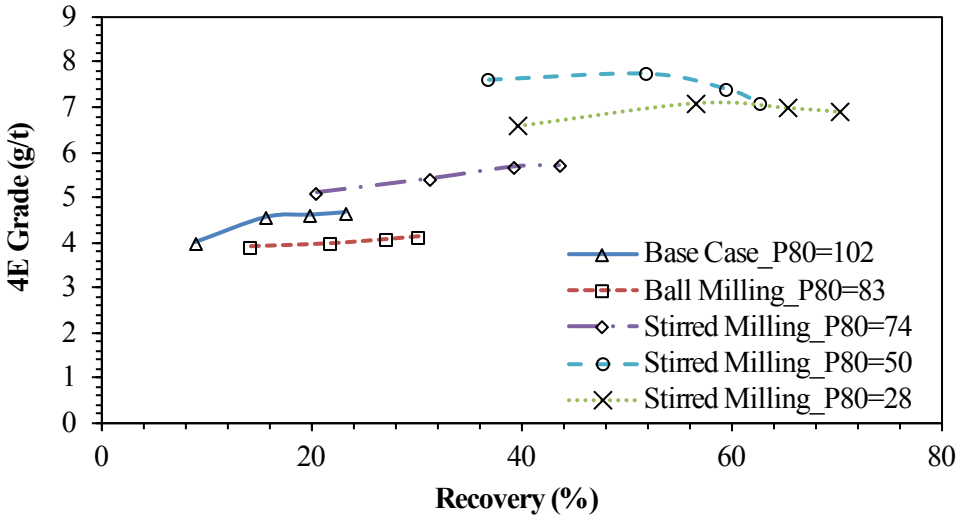


Figure 7. Flotation upgrade ratio versus 4E recovery, where the upgrade ratio is the 4E grade of the concentrate divided by the 4E grade of the feed.

Figure shows that the upgrade ratios increased significantly through regrinding, exceeding 10 for the finest grinds, while the base case and ball milling remained below 7. These improvements infer that fine grinding, which is faster and more energy efficient using the stirred milling technology, enhances the liberation of PGM surfaces previously locked in gangue, as indicated by the feed analysis in Figure 2. They align with findings in the fine particle flotation literature, which emphasise the importance of liberation and addressing fine particle effects when seeking enhanced valuable mineral recoveries (Pease *et al*., 2010; Rule C & Schouwstra R, 2016). These researchers determined that, when necessary, ultra-fine grinding increases the liberation of PGMs locked within gangue phases and improves recoveries but also warn of issues such as entrainment and increased reagent costs if grinding is too fine. It is worth noting that the upgrade ratio-recovery curves show a relatively constant upgrade ratio with increasing recovery, which is atypical for this type of curve. The nature of the ore used influences this, being the tailings, where most of the fast-floating minerals have already been recovered through primary processing, leaving the slow-floating PGMs.

These results, coupled with those in Table II, show the impact of enhanced energy input and stirred media dynamics on reduced particle size and flotation selectivity, offering valuable insight into the role of fine grinding in improving downstream beneficiation efficiency. The feed characterisation results back this premise (Table II; Figure 2), which provides an important context for interpreting flotation performance and highlights the limitations of conventional comminution technologies in liberating PGMs. Furthermore, Table II shows that at lower rotor speeds, relatively modest energy inputs (4–7 kWh/t at P80 = 74 µm) corresponded to lower recoveries. In contrast, the substantial increases in specific energy at finest grinds (P80 = 28 µm), which can be as high as 68 kWh/t when grinding is done with a rotor speed of 1200 rpm, directly align with the enhanced upgrade ratios and recoveries observed in Figure 7. This trend shows the strong dependence of flotation performance on particle size, indicating the degree of mineral liberation in this context. Also, it highlights the increasing energy intensity required to achieve ultrafine particle sizes. Thus, while regrinding with the IsaMill improves recovery, practical application demands careful optimisation to balance metallurgical benefits against energy efficiency and operational costs, which are outside the scope of this study.

CONCLUSIONS

Regrinding the tailings in the IsaMill can liberate minerals that remain locked in gangue minerals after primary processing of the ore, leading to increased recovery potential for the material. The tests performed in this study that involved grinding the tailings using a stirred milling technology

substantially enhanced the reprocessing potential of the UG2 ore tailings by addressing the liberation deficit from primary processing, where conventional mills were used in the milling circuit (*Pease et al*., 2010). By producing feeds with more suitable particle size distributions and which increased mineral exposure, using the IsaMill led to enhanced flotation performance. The identification of a mid-range particle size distribution (P80 = 50 µm) that yielded the highest upgrade ratios in the flotation testwork highlights the importance of controlled regrinding strategies to minimise excessive energy usage or compromised flotation selectivity by creating slimes in the milling stage. Future studies should incorporate detailed mineralogical analyses to verify improvements in PGM liberation and extend testing across multiple tailings samples to account for ore variability. In addition, scale-up considerations and cost–benefit evaluations are essential to fully establish the industrial viability of IsaMill regrinding in PGM tailings reprocessing.

ACKNOWLEDGEMENTS

This work was partially funded by Tailings Technology Pty Ltd, along with Impala Platinum Rustenburg. The authors would like to acknowledge the support and assistance of the Tailings Technology personnel at the Tailings Scavenging Plant at the Impala Platinum Rustenburg concentrators. The entire Centre for Minerals Research Laboratory personnel are thanked for their contributions in different capacities in the set-up and their assistance in conducting the experimental work.

REFERENCES

Allen, J. & Ntsele, C. 2012. Technology selection of stirred mills for energy efficiency in primary and regrinding applications for the platinum industry. In Platinum 2012: Fifth International Platinum Conference. South African Institute of Mining and Metallurgy. 781–808. Available: http://www.saimm.co.za/Conferences/Pt2012/

Baloyi, N.P., Nheta, W., Sibanda, V. & Safari, M. 2024. Mineralogical Insights into PGM Recovery from Middle Group (1–4) Chromite Tailings. Minerals 2024, Vol. 14, Page 924. 14(9):924. DOI: 10.3390/MIN14090924.

Becker, M., Kwade, A. & Schwedes, J. 2001. Stress intensity in stirred media mills and its effect on specific energy requirement. International Journal of Mineral Processing. 61(3):189–208. DOI: 10.1016/S0301-7516(00)00037-5.

Bond, F.C. 1952. The third theory of comminution. Trans. AIME, Min. Eng. 193:484–494.

Fuerstenau, D.W., Kapur, P.C. & De, A. 2003. Modelling breakage kinetics in various dry comminution systems. KONA Powder and Particle Journal. 21(March):121–132. DOI: 10.14356/KONA.2003015.

Glencore Technology. 2023. IsaMillTM. Available: https://www.glencoretechnology.com/en/technologies/isamill/ [2023, April 20].

Gupta, A. & Yan, D. 2016. Stirred Mills – Ultrafine Grinding. In Mineral Processing Design and Operations. Elsevier. 287–316. DOI: 10.1016/B978-0-444-63589-1.00010-1.

Gurnett, I., De Waal, H. & Stieper, G. 2021. The IsaMillTM - 25 years of Stirred Milling. Vancouver: Canadian Insti.

Hogg, R. & Cho, H. 2001. Grinding. Encyclopedia of Materials: Science and Technology. (January, 1):3652–3658. DOI: 10.1016/B0-08-043152-6/00652-5.

Hukki, R.T. 1961. Proposal for a solomonic settlement between the theories of von Rittinger, Kick and Bond. Trans. AIME. 220(5):4.

Jankovic, A. 2003. Variables affecting the fine grinding of minerals using stirred mills. Minerals Engineering. 16(4):337–345. DOI: 10.1016/S0892-6875(03)00007-4.

Jankovic, A., Valery, W. & Rosa, D. La. 2003. FINE GRINDING IN THE AUSTRALIAN MINING INDUSTRY. In 3rd International Conference on Recent Advances in Materials, Minerals and Environment (RAMM 2003). Malaysia.

Jayasundara, C.T., Yang, R.Y. & Yu, A.B. 2012. Effect of the size of media on grinding performance in stirred mills. Minerals Engineering. 33:66–71. DOI: 10.1016/J.MINENG.2011.10.012.

Kwade, A. & Schwedes, J. 2007. Chapter 6 Wet Grinding in Stirred Media Mills. In Handbook of Powder Technology. V. 12. Elsevier Science B.V. 251–382. DOI: 10.1016/S0167-3785(07)12009-1.

Leroy, S., Dislaire, G., Bastin, D. & Pirard, E. 2011. Optical analysis of particle size and chromite liberation from pulp samples of a UG2 ore regrinding circuit. Minerals Engineering. 24(12):1340–1347. DOI: 10.1016/J.MINENG.2011.06.006.

Napier-Munn, T. 2015. Is progress in energy-efficient comminution doomed? Minerals Engineering. 73:1–6. DOI: 10.1016/J.MINENG.2014.06.009.

Pease, J., Young, M. & Curry, D. 2005. Fine grinding as enabling technology-the IsaMill. In Proc. VIth Annual Conf. "Crushing and Grinding 2005". Perth, Australia. 1–20. Available: http://www.isamill.com/EN/Downloads/Downloaded Technical Papers/FineGrindingasEnablingTechnology_TheIsaMill.pdf.

Pease, J.D., Young, M.F., Curry, D. & Johnson, N.W. 2010. Improving fines recovery by grinding finer. Mineral Processing and Extractive Metallurgy. 119(4):216–222. DOI: 10.1179/037195510X12816242170852.

Rule, C. 2010. Stirred milling – new comminution technology in the PGM industry. In The 4th International Platinum Conference, Platinum in transition `Boom or Bust´. The Southern African Institute of Mining and Metallurgy. 71–78.

Rule, C. & Schouwstra, R.P. 2012. Process mineralogy delivering significant value at Anglo Platinum concentrator operations. In Proceedings of the 10th International Congress for Applied Mineralogy (ICAM). Springer. 613–621.

Rule C & Schouwstra R. 2016. Increasing Platinum Recovery by Fine Grinding. In Process mineralogy / M. Becker, E. M. Wightman and C. L. Evans (editors). 6th ed. Becker M., Wightman E.M, & Evans C.L, Eds. Indooroopilly, Queensland: Julius Kruttschnitt Mineral Research Centre. 323–343.

de Waal, H.S., Barns, K. & Monama, J. 2013. From base metals and back – IsaMills and their advantages in African base metal operations. In The Southern African Institute of Mining and Metallurgy-Base Metals Conference. 55–64.

Wiese, J.G. 2009. Investigating depressant behaviour in the flotation of selected Merensky ores. University of Cape Town. Available: http://hdl.handle.net/11427/11181 [2025, September 26].



Kabeli Irvin Mohapi

MSc Chemical Engineering Student
University of Cape Town-Centre for Minerals Research

Kabeli Irvin Mohapi is a dedicated Chemical Engineering graduate and postgraduate researcher, currently pursuing a Master's degree in Chemical Engineering at the University of Cape Town with the distinguished support of the Mastercard Foundation Scholars Program. With a strong emphasis on sustainable resource recovery and process optimisation, Mr. Mohapi is passionate about utilising science and technology to tackle some of the most urgent challenges in the mining industry, particularly in waste valorisation and circular economy principles.

As a Mastercard Foundation Scholar, Kabeli Mohapi has demonstrated exceptional academic ability, leadership, and a clear commitment to making a transformative impact on their community and the broader African continent. This prestigious scholarship has provided both the platform and inspiration to pursue high-impact research in mineral processing and to develop solutions that promote inclusive and sustainable growth.

Kabeli's current research focuses on the reprocessing of Platinum Group Minerals (PGM) tailings, evaluating the effect of fine grinding technologies on mineral liberation and flotation performance. His work specifically investigates

the use of stirred media mills, namely the IsaMill and HIGMill, under varying energy input conditions. Through a systematic study of comminution parameters such as stress intensity, stress energy, and specific energy, the research offers valuable insights into how fine particle breakage mechanisms influence downstream flotation efficiency, selectivity, and concentrate grade.

Key outcomes of the project include the development of energy-based models for optimising grind size, the application of stress models to quantify mechanical environments within mills, and the use of kinetic data to predict flotation behaviour. These findings are intended to support industry efforts to recover value from tailings and improve the sustainability of PGM extraction.

In addition to technical expertise in flotation, comminution, and metallurgical testing, Kabeli has gained practical experience in laboratory-scale experimentation, data analysis, and mineralogical interpretation. His approach combines experimental design with engineering analysis to solve complex metallurgical problems, with an emphasis on reproducibility, scalability, and environmental responsibility.

Kabeli has actively contributed to academic seminars. He is deeply interested in knowledge exchange between academia and industry and aspires to play a bridging role by translating research insights into applied technologies that can be adopted by mining operations across Africa and beyond.

Beyond research, Kabeli Irvin Mohapi is an advocate for youth empowerment and equitable access to education. As a Mastercard Foundation Scholar, he has been involved in mentorship programs and STEM outreach initiatives aimed at inspiring the next generation of African scientists and engineers.
With a long-term vision of contributing to sustainable mineral development and technological innovation in Africa, Kabeli intends to pursue a career in process optimisation, research and development, or technical consulting within the mineral processing and metallurgical sectors.

Blower system energy cost improvement in platinum group metal concentrators

H. Janse van Vuuren[1,2], W.H. Sterrenberg[1], J. Siecker[1,2], J.H. Marais[2]

[1]ETA Operations (Pty) Ltd, South Africa
[2]North-West University, South Africa

The South African platinum mining sector relies on energy-intensive processes to extract, concentrate, and refine minerals. A significant portion of this energy is consumed during mineral concentrate processing. To remain competitive, mining companies must implement energy management systems that reduce their energy consumption, whilst maintaining production performance.

This paper presents an integrated solution to reduce energy consumption in flotation circuit aeration blower systems. A practical methodology was developed and implemented to guide the investigation, classical analysis, and simulation where necessary. This approach also supported the testing and roll-out of energy-efficiency initiatives. The method draws from current operating principles in compressed air management in large underground mines.

Implementation resulted in control strategy adjustments that enhanced energy efficiency, reducing mean electricity costs over the case studies by R500 000 during the first six months of the year. Following the current trend, overall cost savings of R4 million are expected for the year.

The results underscore the potential for significant energy- and cost-savings through targeted control improvements, demand and supply matching, and demand reduction through network maintenance in aeration systems across varying orebody types.

Keywords: Energy, Cost Improvement, Concentrators, Flotation, Blowers, Positive Displacement, Centrifugal

INTRODUCTION

Over 90% of the world's platinum group metal (PGM) reserves are located in South Africa (U. S. Geological Survey, 2019), making the country the largest global producer of PGMs, accounting for 70% of the world's refined platinum in 2019 (World Platinum Investment Council, 2020). This industry plays a crucial role in South Africa's economic growth, with PGMs contributing 22% of the country's total mining revenue in 2024 (Pricewaterhouse Coopers, 2024).

Despite its critical importance, PGM production declined from 280 tonnes in 2021, following the Covid-19 pandemic, to 240 tonnes in 2024 (Minerals Council South Africa, 2024a). The mining sector's contribution to nominal GDP has steadily declined since 2022, falling from 7.3% to 6.1% in 2024 (Minerals Council South Africa, 2024b). Furthermore, for the first time since 2020, PGMs have been surpassed by coal as the largest contributor to total mining sector sales (Minerals Council South Africa, 2024a).

Several factors have contributed to this decline, including rising operational expenses, falling mineral prices, and global trade disruptions caused by the Covid-19 pandemic (Pricewaterhouse Coopers, 2024, Minerals Council South Africa, 2024a, Minerals Council South Africa, 2024b). The combination of decreasing production and increasing costs has led to lower profit margins for many mining operations, with some mines being forced to shut down (Marais *et al.*, 2021).

As price takers, mining companies cannot adjust commodity prices to improve profitability and must instead sell at global market rates. To remain financially sustainable, PGM mining operations must focus on reducing operational costs (Neingo *et al.*, 2018, Zietsman, 2020, Krogscheepers and Gossel, 2015). Utilities rank as the third-largest expense in mining operations, following labour and supplies (Schroeder, 2009). For platinum mines to maintain financial stability and long-term sustainability, implementing energy-saving measures is essential (Shaw *et al.*, 2019).

Significant efforts have been made to reduce shaft energy consumption, through demand-side management (DSM) initiatives (Zietsman *et al.*, 2019). However, processing plants, which consume approximately 30% of the investigated area's electricity, have received far less attention in terms of energy cost-saving measures. Despite their substantial contribution to overall energy usage, initiatives aimed at optimising energy efficiency in these facilities remain underexplored (Jordaan, 2007). Addressing this gap presents an opportunity to enhance operational efficiency, reduce costs, and improve the sustainability of mining operations. A detailed breakdown of the electricity usage for the various business units operated by Mine X, can be seen in Figure 1.

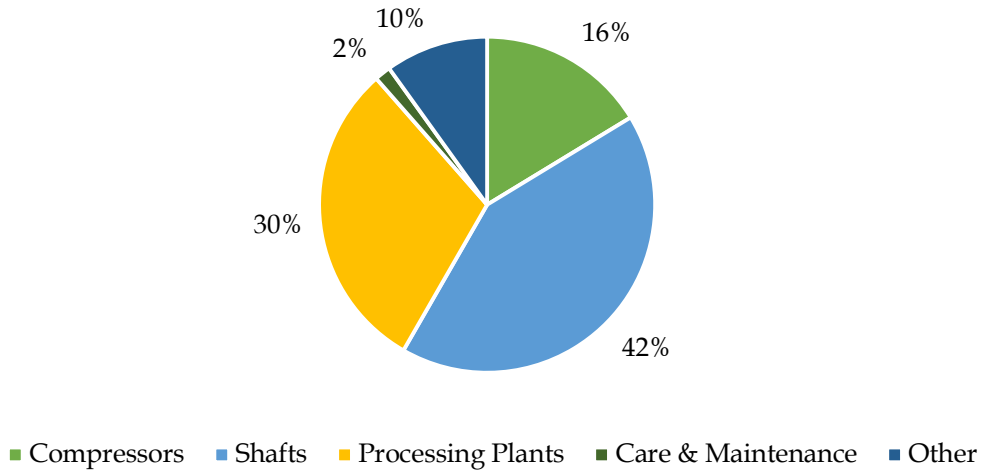


Figure 1. Electricity usage for Mine X.

This research gap is likely due to the inherent challenges of implementing energy-saving measures in continuous operations, where process interruptions can lead to production losses and operational inefficiencies (Jordaan, 2007, Hamer, 2014). Unlike intermittent processes that allow for flexible energy management strategies, continuous operations require innovative approaches to reduce energy consumption without disrupting production. Addressing this challenge presents a valuable opportunity for the industry to enhance cost efficiency, reduce environmental impact, and improve overall energy management practices in platinum mining.

There is significant potential to achieve energy savings by optimising auxiliary systems commonly found in mineral processing plants, including platinum concentrators. Key systems with high energy consumption include compressed air equipment (such as blowers, compressors, and fans), material handling systems (e.g., conveyors), and various pumping systems (including sump and tailings pumps) (Cordeiro, 2022).

In addition to compressors, platinum processing plants also utilise blower systems as part of their compressed air infrastructure. One of the primary applications of blowers is in flotation circuits, where they are used to inject air into flotation cells. This aeration promotes the formation of air bubbles, creating the appropriate hydrodynamic conditions for the effective flotation of fine particles (Deglon, 2005). Blowers used in this application typically have motor ratings ranging from 10 kW to 90 kW (Hamer, 2014). A typical blower setup can be seen in Figure 2.

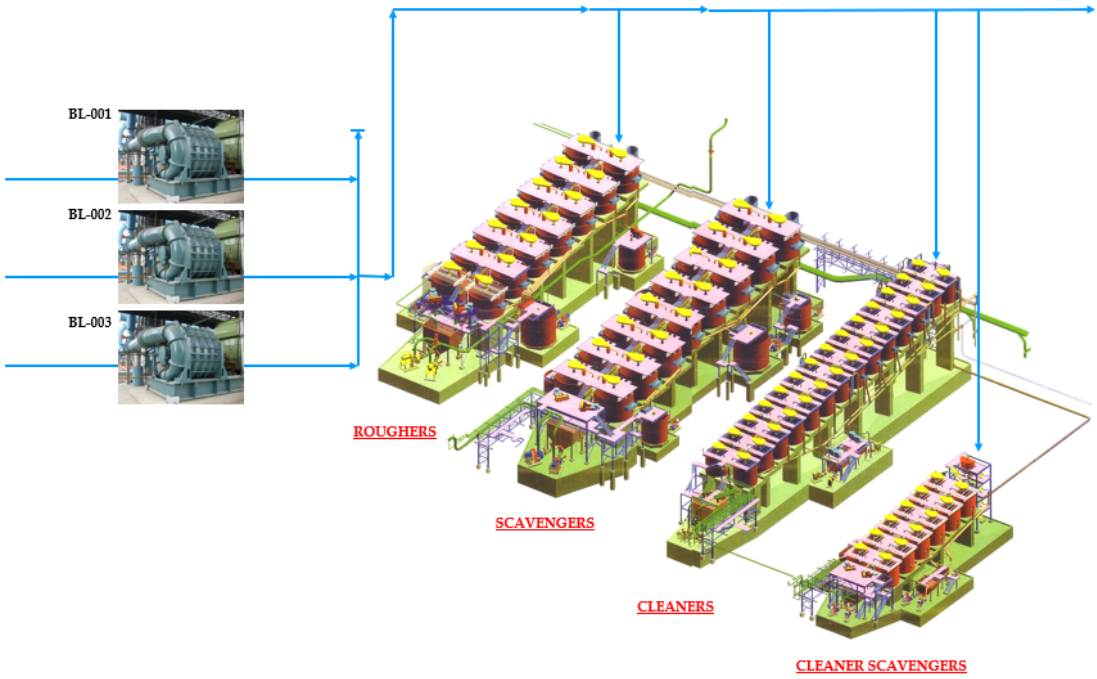


Figure 2. Typical flotation air distribution.

Typically, the systems investigated consist of multiple blowers connected to a single manifold. This manifold has a pressure setpoint, which is controlled by a blow-off valve opening and closing as needed to maintain the required pressure. In theory, this configuration allows for flexible operation by running different combinations of blowers to meet varying demand. However, energy wastage frequently occurs when larger blowers than required are operated, or when too many blowers run simultaneously for the actual demand. This inefficiency is characterised by a blow-off valve that remains at a consistently high opening percentage, indicating excess air generation that must be vented to maintain the setpoint pressure rather than being productively used in the process.

Blowers are also employed during the matte converting process, where they supply oxygen-enriched air to facilitate the oxidation of sulfur and its removal as sulfur dioxide. The blowers used in this stage are significantly larger than those in the flotation circuits, with installed capacities of up to 600 kW (Jones, 2005, Cramer, 2008). Given their continuous operation and high energy demand, these systems represent a key opportunity for energy savings and performance optimisation in platinum processing operations.

Despite the energy-intensive nature of these systems, there is currently no established methodology, specifically focusing on the identification and implementation of energy efficiency measures for blower systems in platinum concentrators. This gap presents an opportunity for targeted research and development to enhance energy performance and reduce operational costs.

This research focused on identifying energy-saving opportunities in blower operations, with the goal of reducing energy consumption without disrupting continuous production processes.

The investigation started with a comprehensive audit of electrical consumption data, accompanied by a review of blower performance curves to assess if any energy savings may be realised. Additionally, historical performance data was analysed to assess the current efficiency of the blower systems, with particular emphasis on key variables, such as blow-off valve flow rate and valve position. If any potential savings are identified, system simulations were conducted as a secondary verification step. The proposed solutions also underwent physical testing to validate their practicality. This iterative process continued until either no further savings can be identified, or an effective energy-saving solution is implemented. Ultimately, this paper aimed to offer practical insights for optimising blower operations and improving energy efficiency in industrial settings.

METHOD

To date, no standardised method exists for improving the electrical cost efficiency of blower systems within platinum concentrator operations. However, techniques used in mining DSM can be applied to deliver input to the optimal method (Marais, 2012). There is therefore a clear need to develop a tailored approach to address this gap. A high-level methodology is outlined below and forms the foundation of the current investigation. Following implementation, its effectiveness will be assessed using relevant case studies.

Method:

(1) Data acquisition: obtain site layouts; gather detailed blower system specifications; conduct a system audit; and collect historical operational data.
(2) Analysis: identify key operating parameters; validate system behaviour against blower performance curves; and, where inefficiencies are found, develop appropriate solutions.
(3) Implementation: design a test procedure for the proposed solutions; implement the solution if validated, otherwise revise as necessary; and confirm energy savings through continuous monitoring and reporting.

Data acquisition

The initial phase of the study involved obtaining site layouts and detailed specifications of the blower systems, including blower performance curves. This foundational information provides critical insights into system design, operating conditions, and potential areas for improvement.

To validate the received data and identify any discrepancies, a comprehensive system audit was conducted. This process not only verifies the accuracy of the provided specifications; it also encapsulates additional operational insights that may not be readily available from existing documentation.

Historical operational data was collected to establish a baseline for analysis, with key parameters including:

- Manifold pressure
- Total air flow produced by the blowers
- Blower operation combinations (i.e., which and how many blowers typically run at a given time)
- Power consumption of each blower

Additionally, the air demand from consumers is considered as part of the assessment. However, optimising the air requirement itself falls outside the scope of this paper, as the focus remains on improving the efficiency and cost-effectiveness of blower supply operation.

Analysis

The operating parameters of each blower system are required, using historical data to establish typical performance trends. This analysis assisted in identifying energy wastage, particularly in the form of excess air that is vented or blown off unnecessarily.

To verify the extent of this wastage, the findings were cross-checked against blower performance curves. If the blower curves confirm that the identified excess air aligns with system capabilities and expected

inefficiencies, the need for optimisation is validated, confirming the existence of energy-saving opportunities.

Once inefficiencies are established, a tailored solution is developed based on each system's unique characteristics. The optimisation strategy may involve (Marais, 2012):

- Turning off unnecessary blowers to reduce excess energy consumption.
- Adjusting the manifold pressure setpoint to match actual process demand more efficiently.
- Reconfiguring the default blower operation setup, such as modifying the combination of blowers that run at a given time to improve efficiency.
- A combination of the above approaches, depending on the specific conditions of each site.

By implementing these targeted adjustments, the aim is to reduce energy consumption whilst maintaining or improving system performance, leading to measurable cost savings.

Implementation

A test procedure was designed, based on the proposed optimisation strategy, outlining the exact steps required for implementation and evaluation. This test is planned to be conducted on the blower system at a time acceptable to plant personnel, ensuring minimal disruption to operations. A basic overview of the test procedure can be seen in Figure 3.

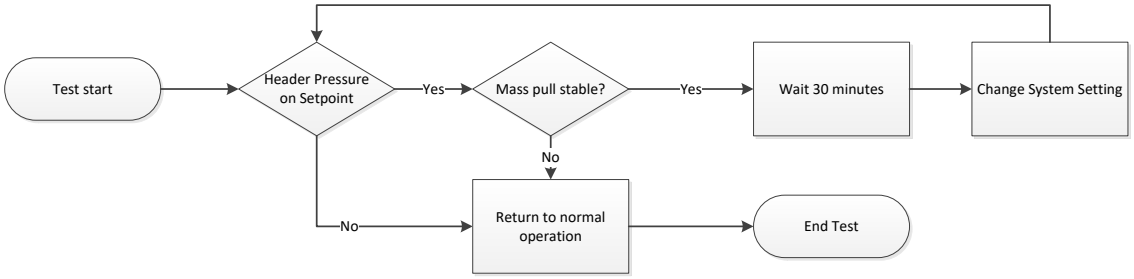


Figure 1. Test procedure.

If the test proves successful, the recommended changes can be permanently implemented. However, if unexpected factors emerge during testing, a revised solution needed to be developed based on the new insights gained. This iterative approach ensures that all potential challenges are addressed before final implementation and commissioning.

Once a solution was in place, the resulting energy savings were verified through continuous energy monitoring and reporting, ensuring that the improvements lead to consistent, measurable reductions in energy consumption over time.

A critical requirement of this process was that all optimisations were implemented without negatively impacting platinum production. This was verified by monitoring the mass pull, a key performance indicator (KPI) used by site personnel to assess flotation efficiency. The adequacy of air delivery was confirmed by checking that individual cell setpoint requirements were met, through visual inspection of the froth characteristics in the cells. Throughout the implementation phase, the system was required to maintain operational efficiency whilst achieving the targeted energy savings.

Finally, the knowledge and insights gained throughout this study were used to develop a standardised, practical methodology that can be applied to other blower systems in platinum concentrators. This provided a structured approach for identifying, testing, and implementing energy-saving measures, enabling wider adoption across the industry.

RESULTS AND DISCUSSION

Four case studies were conducted as part of this paper. The first case study is discussed in detail below, whilst the remaining three are summarised. Table I provides a comparative summary, highlighting the differences and the unique challenges associated with each case.

Table I. Case study characteristics

Case study	Reef processed	Plant capacity (t/d)	Type	Differentiating system characteristics	Blower type	Operating pressure (kPa)
A	Merensky & UG2	7 500	Fresh Ore	Self-aspirating flotation cells retrofitted to work with blowers.	Positive displacement	30
B	Merensky & UG2	16 000	Fresh Ore	Significant leaks, multiple blow-off valves.	Positive displacement	56
C	Merensky & UG2	17 000	Tailings	Frequent pressure setpoint changes.	Positive displacement	53 – 55
D	Plat Reef	29 000	Fresh Ore	Centrifugal blowers	Centrifugal	65

A common feature across Case Studies A – C is their connection to a shared air header. This air header is equipped with one or more blow-off valves. Depending on the pressure setpoints of each valve, one or more of them function as pressure regulators by venting excess air to the atmosphere. The flotation circuits differ across the case studies, comprising various types of flotation cells and operating under varying daily throughput conditions. At all case study sites, blower operation is manually controlled to maintain header pressure at its setpoint. The control strategy also permits setpoint adjustment to optimise flotation performance under varying conditions. Increasing the header pressure setpoint raises mass flow to the cells without requiring additional volumetric flow, and vice versa. If the margin required to switch off a blower is sufficiently small, a minor adjustment to the pressure setpoint may be adequate to achieve the desired outcome.

Case Study A

Data acquisition

The investigation began by gathering information about the site layout. The system consists of six blowers that supply air to both the A and B stream rougher flotation circuits. These blowers are connected to a common air header, where the pressure is maintained at a setpoint using a control valve that vents excess air to the atmosphere. A simplified layout is shown in Figure 4.

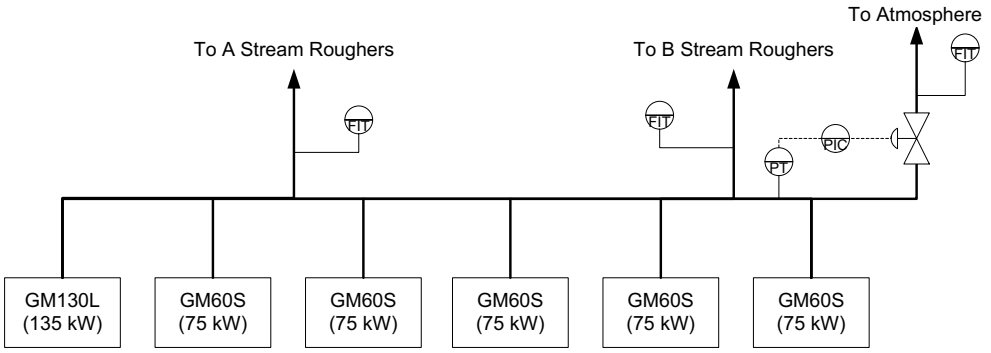


Figure 4. Blower air reticulation for case study A.

The blower configuration includes one GM130L unit operating as the baseload blower, supplemented by five GM60S units acting as trim blowers.

The flotation cells supplied by the blowers are retrofitted self-aspirating units. The existing control philosophy allows for the header pressure to reduce to 0 kPa, which would occur if all blowers were to trip. In such cases, the control valve on the common header is designed to fully open, while non-return valves at the rougher banks open as well, enabling ambient air to flow directly to the cells.

For the initial phase of this investigation, historical data related to blower operation and flotation cell performance was reviewed over a three-month period, from 1 April 2024 to 1 July 2024. During this time, the common header pressure setpoint remained constant at 30 kPa.

Analysis

Over the three-month analysis period, the fewest blowers were operated during May, where four blowers were active for the most part of the month. In contrast, six blowers were typically in operation throughout April. Figure 5 presents the blower running statuses overlaid with the control valve position. Despite variations in the number of active blowers, the header pressure setpoint remained constant at 30 kPa and was consistently maintained.

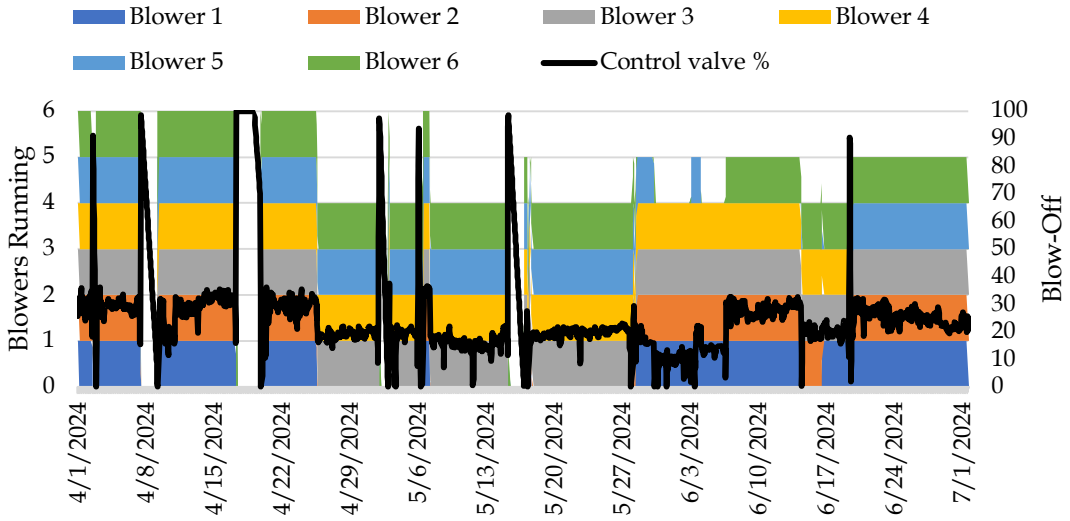


Figure 2. Running status and control valve (blow-off) position for case study A.

Figure 5 illustrates that the control valve opens further when an additional blower is brought online, maintaining the header pressure at the setpoint by venting the excess air to atmosphere. Since flow is driven by the pressure differential, the amount of air reaching the flotation cells does not significantly increase when an extra blower is added. Instead, the surplus air is diverted, preventing a rise in cell air flow. This imbalance between increased air supply and relatively unchanged demand is summarised in Table II.

Table II. Blown air demand and supply comparison for case study A

Month	**Average Demand (m^3/min)**	**Average Supply (m^3/min)**
April	206	330
May	187	269
June	190	299

Table Table highlights a significant disparity between the air supplied—estimated using blower performance curves—and the air reaching the flotation cells (average demand), particularly during April when six blowers operated for most of the month before being reduced to four during the final week. According to the original equipment manufacturer (OEM) blower curves, at a header pressure of 30 kPa, the GM130L blower delivers approximately 109 m^3/min, while each GM60S unit provides around 61 m^3/min. These values could not be directly verified due to the absence of flow metering on site, but they offer a useful estimate for comparison.

Based on these figures, the combined output of the GM130L and two GM60S blowers should be sufficient to meet the observed demand. This suggests a potential inefficiency in the current operation. As a result, the proposed adjustment is to limit blower operation—under similar demand conditions—to just three units: one GM130L and two GM60S blowers.

Implementation
To test the proposed configuration under real conditions, a site test was conducted. The test involved switching off one or more blowers under stable operation and monitoring pressure, mass pull, and air addition to the flotation cells.

The test procedure:

(1) Under stable operation, one GM60S blower was turned off.
(2) System response was monitored for at least 10 minutes, up to 30 minutes.
(3) If the blow-off valve percentage was high and setpoint (SP) was maintained, another blower was turned off.
(4) If pressure reduced below SP or only three blowers remained, blowers were cycled (one stopped, one started) after the system was given 10 – 30 minutes to respond.
(5) The test was repeated across setpoints from 30 kPa up to 35 kPa in 50 mbar increments.
(6) The test ended when all blowers were cycled or if operational impacts prompted site personnel to request early termination.

At the start of the test, five blowers were running, with one GM60S on standby. The test data is shown in Figure 6.

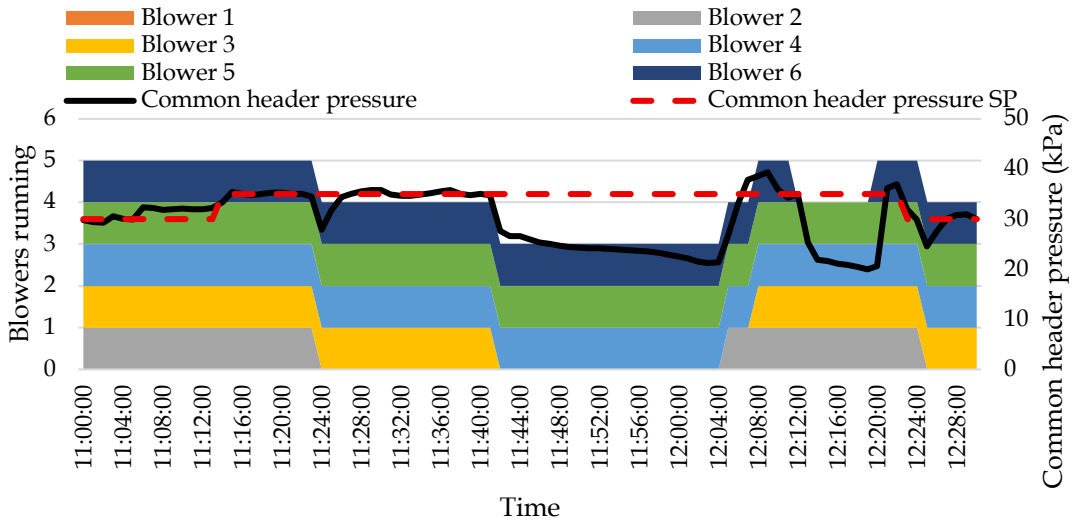


Figure 6. Test data for case study A

At 11:14, the pressure setpoint was increased from 30 kPa to 35 kPa. At 11:23, a GM60S (Blower 2) was stopped. After pressure stabilised, Blower 3 was stopped at 11:41. With only the GM130L and two

GM60S units running, the SP could not be met—the pressure dropped to 20 kPa. All blowers were restored by 12:09. At 12:11, the GM130L was switched off to test the equivalency of four GM60S units versus the GM130L plus two GM60S units. Pressure again dropped to 20 kPa. At 12:18, the system was restored.

Later, with the SP returned to 30 kPa, another GM60S was switched off, and the system remained stable.

The test confirmed that four blowers can maintain a 35 kPa SP, validating that under standard operating conditions, fewer blowers are required. It also showed that blowers are sometimes added unnecessarily, even when the control valve is already venting excess air.

The test results show that our proposed solution of one GM130L and two GM60S' is not feasible due to not being able to reach the pressure setpoint, and instead one GM130L and three GM60S' are required to be used. Therefore, the proposed solution was insufficient, due to it not being able to reach the required pressure. This could be due to a variety of reasons, such as leaks, worn motors, blocked air intakes, etc.

The case study highlights the importance of considering blow-off valve position when evaluating blower operation. A high blow-off valve percentage indicates an oversupply of air and can serve as a trigger to reduce the number of operating blowers. However, it cannot be directly correlated to a specific volume of air wasted.

To support long-term optimisation, a baseline operating profile was developed in collaboration with site personnel. This baseline comprises the historical running status and amperage data of the blowers prior to implementation of the changes. By utilising this data, the power consumption of the blowers was determined, and the average operating conditions before intervention were compared with actual post-intervention performance, excluding anomalous periods such as plant shutdowns. This difference in energy consumption was combined with the applicable Eskom Megaflex tariffs to calculate the savings value. Site personnel were instructed to start additional blowers only when the blow-off valve closed completely and were provided with the revised standard operating procedure for blower quantities as determined through testing. Figure 7 shows the actual vs baseline average daily performance.

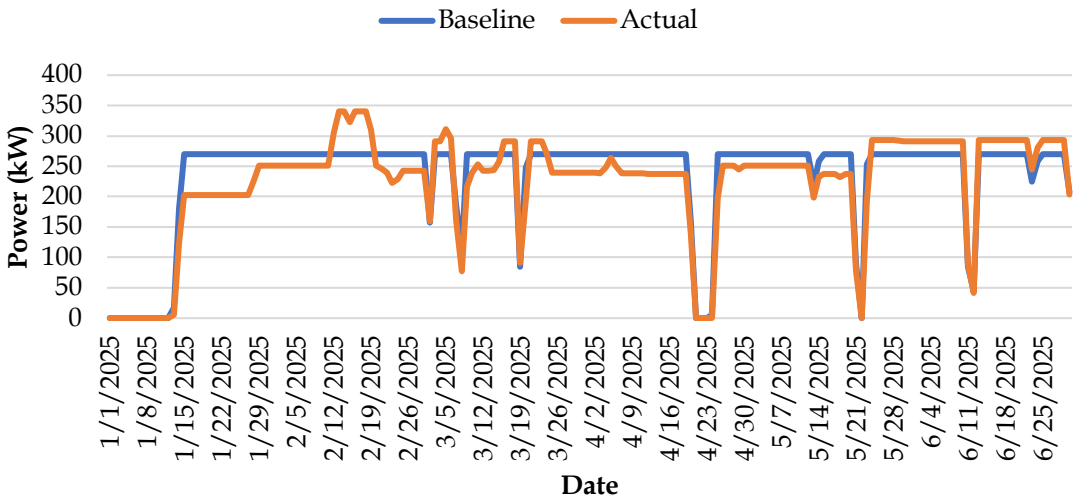


Figure 3. Daily profile of project performance for case study A.

As of 1 July 2025, savings of R80 000 had been achieved year-to-date; however, this was lower than anticipated. This was primarily due to operators starting up unnecessary blowers at the beginning of their shifts, as well as equipment failures on the plant. Operator KPIs are not always aligned with energy

efficiency objectives, as their primary focus is on maintaining stable plant operations and meeting production targets.

Summary of other case studies

The results of the four case studies are consolidated in Table III, which provides an overview of the blower configurations, pressure setpoints, key analytical findings, implementation outcomes, and cost savings achieved. The table also highlights the main lessons learned in each case, offering insights into how different operational strategies and site conditions influence blower system efficiency.

Table III. Summary of other case studies

Case study	Blower configuration	Pressure setpoint (kPa)	Analysis findings	Implementation outcome	Six-month savings (as at 1 July 2025)	Key lessons learned
A	1 × GM130L 5 × GM60S	30–35	Historical data showed air supply consistently exceeded demand, with high blow-off valve activity. Based on OEM curves, 1 GM130L + 2 GM60S should theoretically meet demand.	Site tests demonstrated that this combination could not maintain the setpoint; 1 GM130L + 3 GM60S was required instead. A baseline operating profile was developed, although operator behaviour sometimes limited savings.	R80 000	Blow-off valve position is a valuable indicator of oversupply, but it does not directly quantify air wastage. Operator alignment with efficiency targets is critical.
B	7 × GM90S	56	Average demand was significantly lower than supply; calculations suggested five blowers should suffice. However, pressure stability problems and suspected leaks forced higher utilisation.	Tests confirmed six blowers could maintain pressure once leaks were partially addressed. Leak audits improved performance and allowed the plant to avoid unnecessary use of all seven blowers.	R170 000	Air leaks can distort perceptions of demand, leading to excess blower use. Regular audits are essential to enable operation with fewer blowers.
C	6 × GM80L of mixed motor sizes: 2 × 132 kW 1 × 185 kW 2 × 110 kW 1 × 132 kW.	53–55	Analysis indicated demand could be met by three blowers. The 185 kW unit was often run instead of more efficient options. OEM data showed each blower delivered ~82.5 m^3/min.	Site testing confirmed that 3 blowers (preferably 1 × 132 kW + 2 × 110 kW) could meet demand under most conditions. A new prioritisation sequence was introduced to favour smaller units.	R750 000	Proper sequencing of blowers reduces energy use. Nameplate ratings may be inaccurate; auditing installed motor sizes can reveal hidden optimisation opportunities.
D	3 × GD 2400 centrifugal blowers	65	Two blowers normally operated. Blow-off activity was high, and surge control was inactive with the setpoint incorrectly configured (34.35 kPa vs. OEM 29 kPa).	Surge control was re-enabled and reset to OEM specification. This reduced blow-off activity and improved pressure stability. Further optimisation is possible through improved surge management.	R1 000 000	Correct surge control configuration improves both stability and efficiency. Manufacturer design specifications should be verified and restored when deviations are found.

Limitations
As a result of limitations in instrumentation, the amount of air wasted was estimated using the blow-off control valve percentage, which proved to be grossly inaccurate. Furthermore, blower specifications provided by the OEM or site personnel were not consistently accurate. In practice, blowers often did not perform to specification due to factors such as open vents, faulty discharge points, and manifold leaks. Additionally, flotation air flow meters do not account for variations in air density.

There exists an equilibrium point that defines the maximum mass flow achievable in a manifold, governed by the manifold design and the duty/standby configuration of the blowers. Therefore, when planning plant modifications to accommodate increased tonnage, it may be more effective to split the manifolds and relocate the blowers, or alternatively resize the manifold, rather than simply bringing an additional blower online.

CONCLUSION

This study set out to explore a practical and low-risk method to reduce energy use in blower systems at platinum concentrators, without negatively impacting production. By applying a structured, data-driven method—combining classical analysis and controlled site testing—it was possible to identify and implement realistic optimisation opportunities tailored to the specific conditions of each case study.

The investigation found that the existing blower system configurations setups across all four sites frequently operated with excess capacity. In multiple instances, unnecessary blowers were running while blow-off valves vented surplus air to the atmosphere, indicating a clear mismatch between supply and demand. This not only resulted in wasted energy, but also masked inefficiencies in blower selection, control philosophy, and system maintenance.

Adjustments to control strategies, such as refining pressure setpoints, optimising blower combinations, implementing operating priorities based on motor efficiency, and enabling surge protection, resulted in measurable improvements in energy performance. In total, energy cost savings exceeding R2 million were realised across the four sites during the six-month period from 1 January 2025 to 1 July 2025, with further potential identified through continued optimisation. Extrapolation of current trends indicates that total energy cost savings of R4 million could be achieved over a full 12-month period.

The results demonstrate that even in the complex, high-risk environment of continuous mineral processing, energy savings are achievable through targeted control improvements and minimal capital intervention. These improvements are implementable without compromising flotation performance or plant stability.

However, the paper also highlighted key limitations, such as instrumentation accuracy, data reliability, and challenges in aligning operator behaviour with energy-saving goals. These constraints underscore the importance of involving operations personnel in the optimisation process and developing clear, operationally-relevant baselines and standard procedures.

This paper provides a replicable high-level methodology that can be applied to blower systems in the platinum sector, and potentially more broadly in mineral processing, to drive meaningful reductions in energy consumption and operating costs.

ACKNOWLEDGEMENTS

I would like to thank my study leader, Juan Siecker, for his guidance and support throughout this project. I am also grateful to ETA Operations (Pty) Ltd, South Africa for sponsoring and enabling this work. A special thanks to my colleagues Brendan Kriel, Niël Muire and Liam Sterrenberg for their valuable assistance during the project.

REFERENCES

CORDEIRO, B. 2022. *Developing an electrical cost saving methodology for platinum plant auxiliary systems.* M.Eng Dissertation, North-West University.

CRAMER, L. A. 2008. What is your PGM concentrate worth? *Third International Platinum Conference 'Platinum in Transformation'.*

DEGLON, D. A. 2005. The effect of agitation on the flotation of platinum ores. *Minerals Engineering,* 18**,** 839 - 844.

HAMER, W. 2014. *Analysing electricity cost saving opportunities on South African gold processing plants.* M.Eng Dissertation, North-West University.

JONES, R. T. 2005. An overview of Southern African PGM smelting. *44th Annual Conference of Metallurgists.*

JORDAAN, N. 2007. *New Demand Side Management Opportunities in the Precious Metals Industry.* PhD Thesis, North-West University.

KROGSCHEEPERS, C. & GOSSEL, S. J. 2015. Input cost and international demand effects on the production of platinum group metals in South Africa. *Resources Policy,* 45**,** 193 - 201.

MARAIS, J. H. 2012. *An integrated approach to optimise energy consumption of mine compressed air systems.* PhD Thesis, North-West University.

MARAIS, L., CLOETE, J. & DENOON-STEVEN, S. 2021. Firms' approach to mitigating risks in the platinum group metals sector. *Mineral Economics,* 34**,** 383 - 404.

MINERALS COUNCIL SOUTH AFRICA 2024a. Facts and Figures 2024. *Facts and Figures.* Johannesburg, South Africa.

MINERALS COUNCIL SOUTH AFRICA 2024b. Integrated annual review 2024. *Annual Reports.* Johannesburg, South Africa.

NEINGO, P. N., THOLANA, T. & NHLEKO, A. S. 2018. A comparison of three production rate estimation methods on South African platinum mines. *Resources Policy,* 56**,** 118 - 124.

PRICEWATERHOUSE COOPERS 2024. SA Mine 2024. *SA Mine.* Johannesburg, South Africa.

SCHROEDER, F. W. 2009. *Energy efficiency opportunities in mine compressed air systems.* M.Eng Dissertation, North-West University.

SHAW, W. G., MATHEWS, M. J. & MARAIS, J. H. 2019. Holistic analysis of the effect on electricity cost in South Africa's platinum mines when varying shift schedules according to time-of-use tariffs. *Journal of Energy in Southern Africa,* 30**,** 26 - 40.

U. S. GEOLOGICAL SURVEY 2019. Mineral Commodity Summaries 2019. *Mineral Commodity Summaries.* Reston, VA, USA.

WORLD PLATINUM INVESTMENT COUNCIL 2020. Platinum Quarterly Q3 2020. *Platinum Quarterly.* London, United Kingdom.

ZIETSMAN, L. N. 2020. *Novel solutions for compressed air demand management on deep-level mines.* PhD Thesis, North-West University.

ZIETSMAN, L. N., MARAIS, J. H. & SCHOEMAN, W. 2019. A Practical Method for Compressed Air Leak Localisation in Deep-Level Mines. *AIUE Proceedings of the 17th Industrial and Commercial Use of Energy (ICUE) Conference.* Cape Town, South Africa.



William Henry Sterrenberg

Engineer and PhD candidate
ETA Operations and North-West University

Liam Sterrenberg is a Senior Project Engineer with a strong track record in energy management, process optimization, and engineering execution within the South African mining industry. He has contributed to a range of greenfield projects and operational improvement initiatives across both underground and mineral processing environments, with a focus on platinum group metals. Liam's expertise includes utility cost reduction, compressed air optimization, power factor correction, and ISO-aligned energy strategies. He applies a data-driven, practical approach to improve operational performance, reduce energy costs, and support long-term sustainability goals in energy-intensive mining operations.

Revisiting the role of pH modifer and process water ions in platreef Cu-Ni-PGM ore flotation: What's the matter with choosing a pH modifier?

M.S. Manono

University of Cape Town, South Africa

In sulfide mineral flotation, pH control is traditionally regarded as a fundamental operating parameter, commonly adjusted using inorganic pH modifiers such as lime, caustic soda, or soda ash – there exist arguments in the literature that some collectors also exhibit pH modification effects owing to residual components from the collector synthesis processes. However, in the context of water recirculation, ion build-up, the choice of pH modifier and the resulting electrolyte interactions and speciation, may introduce not only a desired pH shift but also a distinct suite of inorganic electrolytes into flotation. These inorganic electrolytes whether calcium from lime or sodium from caustic soda can influence the electrochemical properties of mineral surfaces in the pulp phase, particularly under high ionic strength conditions typical of modern mineral concentrators with closed water circuits. This paper investigates whether the type of alkaline pH modifier affects flotation performance for a selected Platreef Cu-Ni-PGM ore, beyond its role in achieving target pH. Batch flotation experiments were conducted at the natural pH of the slurry (~pH 9), pH 11 and pH 12 in synthetic process water with an ionic strength typical of concentrator process water (0.0241 mol.dm^{-3}) and in synthetic process water of a higher-than-normal process water ionic strength (0.241 mol.dm^{-3}). Alkaline pH modifiers in the form of slaked lime ($Ca(OH)_2$) and caustic soda (NaOH) were used for pH adjustments. This work explored how these chemically distinct modifiers affect sulfide mineral recovery and selectivity in a complex sulfidic Cu-Ni-PGM ore from the Platreef. The broader motivation arises from previous work highlighting specific ion effects and ionic strength variations in synthetic process waters and their influence on flotation chemistry. By isolating the role of the pH modifier as an electrolyte contributor, this research aims to deepen our understanding of reagent-mineral-water interactions. Findings from this work are expected to inform both fundamental flotation research and operational strategies for optimising reagent selection in recirculated process water environments where pH modification is a key operating factor.

Keywords: Divalent ions, entrained gangue, floatable gangue, ionic strength, water quality

INTRODUCTION

Froth flotation is the most widely employed process for the beneficiation of sulfidic Cu–Ni–PGM ores, where the selective recovery of valuable sulfide minerals depends on carefully orchestrated interactions between reagents, mineral surfaces, and the pulp environment. Among the suite of operating parameters, pulp pH has long been considered a critical control variable (Wills and Finch, 2016). Adjustment of pH is traditionally achieved using alkaline modifiers such as slaked lime ($Ca(OH)_2$), caustic soda (NaOH), and, less commonly, soda ash (Na_2CO_3)(Bulatovic, 2007).

These modifiers are applied to depress the floatability of naturally hydrophobic gangue, to promote collector adsorption onto sulfide minerals, and to minimise deleterious reactions that compromise selectivity. Historically, lime has been the preferred choice in many industrial circuits due to its availability, cost-effectiveness, and ability to produce stable operating conditions (Rao and Finch, 1989; B Wang and Peng, 2014). Yet, this conventional view of pH control as a simple adjustment of proton activity fails to capture the full chemical complexity introduced by pH modifiers. Each reagent introduces not only hydroxide ions but also a distinct ionic background; lime contributes Ca^{2+}, caustic soda introduces Na^{+}, and soda ash contributes both Na^{+} and CO_3^{2-}. These species do not remain inert. Rather, they participate in solution speciation, mineral surface modification, and interfacial phenomena that profoundly influence flotation chemistry (Manono *et al.*, 2018a). For example, Ca^{2+} can adsorb onto silicate gangue minerals, promoting coagulation or altering their surface charge, while also precipitating as $CaCO_3$ or $CaSO_4$ under process water conditions (Manono *et al.*, 2019). Similarly, Na^{+}, although less strongly adsorptive, influences ionic strength and electrical double-layer compression, thereby modifying collector–mineral interactions (*October et al.*, 2021). The carbonate species introduced by soda ash contribute to buffering capacity and alter equilibria through complexation or precipitation reactions (Corin and Wiese, 2014). Consequently, pH modifiers cannot be treated as interchangeable tools for achieving a target pH; their impact must be considered in the broader pulp chemistry context of the flotation system.

This question is made more urgent by the increasing reliance on water recirculation in modern concentrators. Driven by water scarcity, environmental regulations, and economic pressures, most Cu–Ni–PGM operations now operate in closed or near-closed water circuits (Corin *et al.*, 2011; Le *et al.*, 2020). Recycled water inevitably undergoes quality deterioration with each cycle, leading to progressive increases in ionic strength and the accumulation of dissolved solids such as Ca^{2+}, Mg^{2+}, Na^{+}, Cl^{-}, SO_4^{2-}, and NO_3^{-} (Harrison *et al.*, 2018; Slatter *et al.*, 2009). The consequences for flotation performance are significant. A large body of work has shown that ions in recycled process water can alter mineral hydrophobicity, interfere with collector adsorption, and destabilise froths, often leading to reduced recoveries and grades (Corin *et al.*, 2011; Manenzhe *et al.*, 2023; Manono *et al.*, 2018b, 2012; October *et al.*, 2019, 2021, 2020; Bo Wang and Peng, 2014; B Wang and Peng, 2014). Synthetic plant waters have been widely used to mimic these conditions, allowing controlled studies of how specific ion types and concentrations affect flotation. These studies consistently report that gangue behaviour, particularly entrainment and natural floatability, is strongly influenced by solution chemistry (Dzingai *et al.*, 2021, 2020; Manono *et al.*, 2018b, 2020; Moimane *et al.*, 2016).

What emerges from this body of research is that the effects of recycled water are not generic but ion-specific. Divalent cations such as Ca^{2+} and Mg^{2+} tend to have more pronounced effects on mineral surface chemistry and froth stability compared to monovalent ions such as Na^{+} or K^{+} (Dzingai *et al.*, 2020; Manono *et al.*, 2020, 2016; Manono and Corin, 2022). Anions such as SO_4^{2-} and NO_3^{-} have also been shown to influence collector adsorption indirectly, through competitive adsorption, changes in surface charge, or modification of the hydration environment at the mineral–solution interface (Dzingai *et al.*, 2021; Mhonde *et al.*, 2021b, 2021a). The recognition of such specific ion effects challenges the assumption that water chemistry can be managed solely through bulk ionic strength or pH adjustments. Instead, the chemical identity of the ions and their interactions with both reagents and minerals must be considered. In this context, the choice of pH modifier becomes central to flotation strategy. The ions introduced by pH modifiers do not operate in isolation; rather, they are superimposed on the existing ionic matrix of recycled water. For example, the addition of lime into a system already rich in sulfate may promote gypsum precipitation, consuming both Ca^{2+} and SO_4^{2-}, altering ionic speciation, and potentially reducing the activity of free Ca^{2+} available for surface interactions. Conversely, in a chloride-rich environment, the addition of NaOH will increase Na^{+} activity, contributing to double-layer compression and potentially enhancing entrainment of fine gangue. Moreover, carbonate equilibria introduced by soda ash can shift depending on pH, ionic strength, and dissolved CO_2, generating

species such as HCO_3^- and CO_3^{2-} that alter buffering capacity and solution saturation indices. At the mineral–solution interface, these solution chemistry shifts manifest in altered adsorption and precipitation pathways (October *et al.,* 2020). Divalent cations such as Ca^{2+} can bridge between negatively charged silicate gangue surfaces and polysaccharide depressants such as carboxymethyl cellulose (CMC), enhancing gangue rejection but simultaneously destabilising froths at high concentrations (Burdukova *et al*., 2008; Manono *et al.,* 2020; Wiese, 2009). Monovalent cations, while less strongly adsorptive, still influence interfacial water structure and bubble–particle attachment kinetics (Manono and Corin, 2022; October *et al*., 2021). The net effect is that flotation performance is not solely a function of pH level but of the electrolyte composition associated with pH control strategies.

While the literature on water chemistry effects is extensive, relatively few studies have explicitly interrogated the role of pH modifiers as electrolyte contributors (Manono *et al*., 2024, 2017; Muzenda *et al.*, 2011). Most investigations treat lime, caustic soda, and soda ash as equivalent means to the same end, achieving a target pulp pH. The potential for these reagents to introduce fundamentally different chemical species, interacting with recycled process waters of varying ionic strengths has not been systematically addressed. This oversight represents a critical gap in our understanding of flotation chemistry, particularly in Cu–Ni–PGM circuits where water recirculation is unavoidable and mineralogies are complex.

This study addresses this gap by examining the performance of lime $Ca(OH)_2$ and caustic soda [NaOH] as pH modifiers in the flotation of a Platreef Cu–Ni–PGM ore under controlled process water conditions. By comparing their effects in synthetic process waters of both typical and elevated ionic strengths, the study isolates the role of pH modifiers as sources of distinct ionic species, beyond their conventional role in pH adjustment. The central question posed is not simply "what is the optimal pH?" but rather "how does the choice of pH modifier, through its contribution to solution speciation and electrolyte chemistry, influence flotation response?" By situating pH control within the broader framework of pulp chemistry and specific ion effects, this work addresses a long-standing assumption in flotation practice. It recognises that the type of pH modifier cannot be divorced from the ionic environment into which it is introduced, and that its chemical consequences extend beyond hydrogen ion activity. Findings from this investigation are expected to provide not only fundamental insights into reagent–mineral–water interactions but also practical guidance for operational strategies in concentrators where water recirculation and pH control intersect as key operating realities.

Materials and Methods

Ore Milling and Synthetic Plant Water Preparation

A Platreef ore sourced from the South African Bushveld Igneous Complex (BIC) was crushed and ground to a particle size of -1 mm using a terminator jaw crusher model JCT#1AL. The ore was thereafter homogenised and split using a Dickie & Stockler 10 pot rotary splitter into portions of 1.3 kg, packed and sealed into airtight plastic bags which were stored at room temperature. Using synthetic plant water (SPW) of an ionic strength of 0.0241 mol.dm^{-3} (1 SPW) and 0.0723 mol.dm^{-3} (10 SPW), 66% solids slurry samples were milled in a laboratory scale stainless steel rod mill to a grind size of 60% grind passing 75 µm. The compositions of the SPW used are shown in Table I. Synthetic plant waters were prepared using inorganic salts of analytical grade, supplied by Merck.

Table I. Composition of SPW

Water type	Ca^{2+} mg/L)	Mg^{2+} (mg/L)	Na^+ (mg/L)	Cl^- (mg/L)	SO_4^{2-} (mg/L)	NO_3^- (mg/L)	CO_3^{2-} (mg/L)	TDS (mg/L)	Ionic Strength [M]
1 SPW	80	70	153	287	240	176	17	1023	0.0241
10 SPW	800	700	1530	2870	2400	1760	170	10230	0.2410

Batch Flotation

A 3 L Barker flotation cell was used with a volume of 35% solids by adjusting the slurry from the mill using the required SPW. The pulp level in the cell was controlled manually with the cell operating at a variable speed drive and an impeller speed of 1200 rpm. A constant airflow of 7 L/min and froth height of 2 cm were sustained throughout. The cell's slurry height or pulp level was corrected to 2 cm by the addition of the respective SPW continuously. The froth was scraped into four distinct collecting pans (C1, C2, C3 and C4) every 15 s at the respective times of 2, 6, 12 and 20 min to collect four concentrates. Water usage was monitored throughout the experimental test work. Feed and tailings samples were collected at the start and end of each experimental test. The collected feed, tailings and concentrates samples were filtered, dried, and weighed. Cu and Ni assays from the dried concentrate, feed and tailings samples were determined using an Olympus Vanta Handheld-XRF Analyser at the University of Cape Town (UCT). Flotation tests were conducted in duplicates for each experimental condition to minimise error and ensure reproducibility of the results. The standard error was generally within 5%.

Reagents

Sodium isobutyl xanthate (SIBX) of a purity of 97%, supplied by AECI Mining Chemicals, was used as a collector at a dosage of 150 g/t and was dosed directly into the mill prior to milling. Senfroth 200, supplied by AECI Mining Chemicals, was used as a frother, and was added into the flotation cell at a dosage of 45 g/t. A polysaccharide in the form of sodium carboxy methyl cellulose (CMC), Sendep 30E, supplied by AECI Mining Chemicals, was used as a depressant, dosed into the flotation cell at 100 g/t. Calcium hydroxide ($Ca(OH)_2$) and sodium hydroxide (NaOH) were used to adjust the slurry inside the batch flotation cell to pH 11 and 12 whilst other flotation experiments were conducted at the natural pH of the slurry which is ~pH 9.

RESULTS AND DISCUSSION

The Effect pH Modifier and Process Water Ions on Solids and Water Recoveries

Figure 1 illustrates the effect of pH, pH modifier type and synthetic plant water ionic strength on solids and water recoveries.

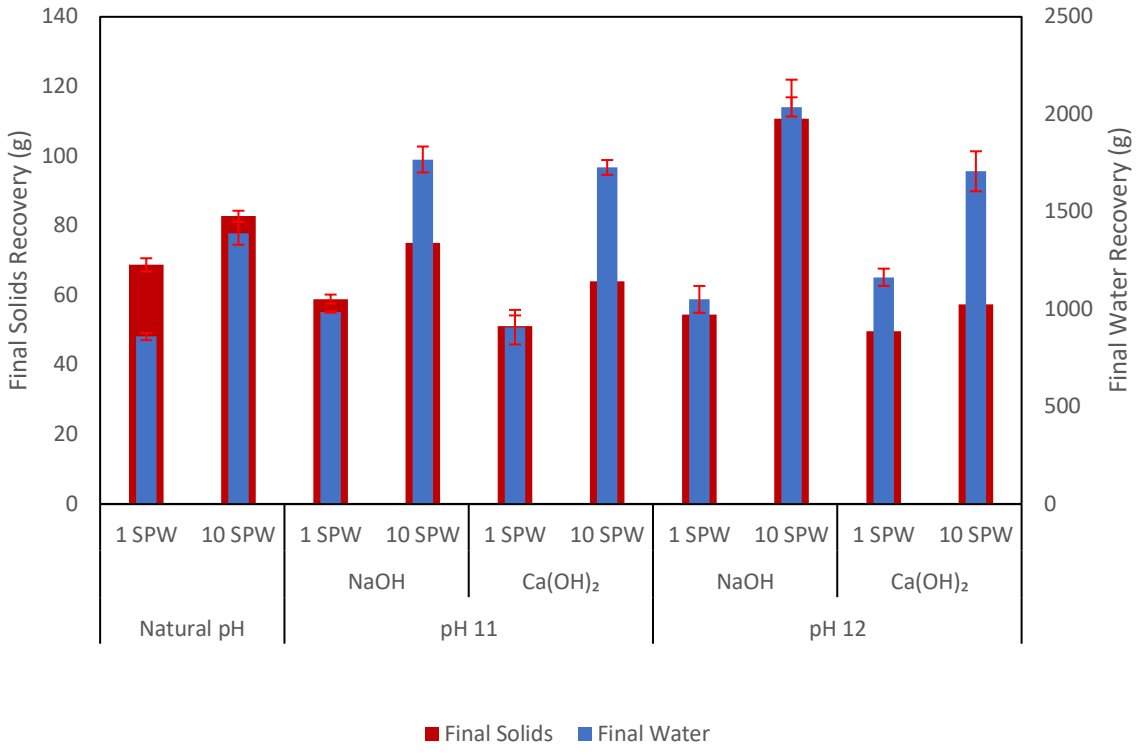


Figure 1. Total solids and water recoveries for all conditions tested.

At natural pH, recoveries of both solids and water were significantly higher in 10 SPW compared to 1 SPW, reflecting the role of elevated ionic strength of process water in stabilising froths and promoting entrainment. This outcome is consistent with previous findings that increases in ionic strength of synthetic plant water can reduce bubble coalescence, thereby enhancing froth stability and water recovery (Corin and Wiese, 2014; Manono *et al*., 2018b, 2013). The simultaneous increase in solids recovery under these conditions is indicative of greater reporting of both valuable and gangue material to the concentrate, suggesting that ionic strength of process water enhances mass pull at natural pH.

When the pH was increased to 11, clear differences between the two alkaline pH modifiers were evident. In NaOH systems, solids and water recoveries were markedly higher at 10 SPW than at 1 SPW, indicating a strong ionic strength of process water effect under sodium-dominated chemistry. In contrast, lime ($Ca(OH)_2$) produced notably lower recoveries, especially at 1 SPW, suggesting that the introduction of Ca^{2+} had a froth-destabilising effect. Calcium ions are known to compress the electrical double layer and promote hetero-coagulation of gangue particles, thereby reducing froth stability and entrainment (Manono *et al.,* 2020; Manono and Corin, 2022). At higher ionic strength (10 SPW), some recovery was regained in $Ca(OH)_2$ systems, but values remained lower than those with NaOH. This highlights a fundamental difference in the way monovalent (Na^+) and divalent (Ca^{2+}) cations influence froth stability while both increase ionic strength, divalent ions have a stronger propensity to interact with mineral and gangue surfaces, potentially suppressing their flotation.

At pH 12, the trends became even more pronounced. In NaOH systems, solids and water recoveries in 10 SPW reached the highest levels across all conditions tested, exceeding 2000 g of water recovery. This reflects the synergistic effect of high ionic strength and elevated alkalinity under sodium chemistry, which appears to stabilise froths and facilitate high entrainment of water and fine solids. Conversely, under lime addition, both solids and water recoveries were suppressed relative to NaOH at the same ionic strength, confirming the inhibitory role of Ca^{2+}. Such results reinforce that not all pH modifiers are equivalent: although both NaOH and $Ca(OH)_2$ achieve the same nominal pH, the ions they introduce produce markedly different flotation outcomes.

The results of this work demonstrate that both ionic strength and the type of pH modifier have a strong bearing on flotation hydrodynamics. Elevated ionic strength (10 SPW) generally promoted higher water and solids recoveries, reflecting greater froth stability and entrainment. However, the choice of pH modifier determined the extent to which this effect was expressed. NaOH consistently promoted higher solids and water recoveries compared to $Ca(OH)_2$, particularly at elevated ionic strength. These findings align with broader literature on specific ion effects, where monovalent cations such as Na^+ are associated with weaker surface interactions but enhanced froth stability, while divalent cations such as Ca^{2+} suppress froth stability and entrainability by binding to gangue surfaces or interacting with depressants (Corin *et al.,* 2011; Corin and Wiese, 2014; Manono *et al*., 2018b, 2020, 2012).

From an operational perspective, these results suggest that the selection of pH modifier cannot be made solely on the basis of cost or availability but must consider the broader solution chemistry implications. Under water recirculation regimes with high ionic strengths, the introduction of additional Ca^{2+} via lime may exacerbate froth destabilisation and decrease mineral recoveries, whereas NaOH may sustain higher recoveries but at the expense of increased entrainment of gangue. Thus, the role of pH modifiers must be understood not simply as pH adjusters, but as co-determinants of solution speciation and flotation performance.

The Effect pH Modifier and Process Water Ions on Copper Recoveries and Grades

Figure 2 illustrates the effect of pH, pH modifier type and SPW ionic strength on Cu recoveries and grades.

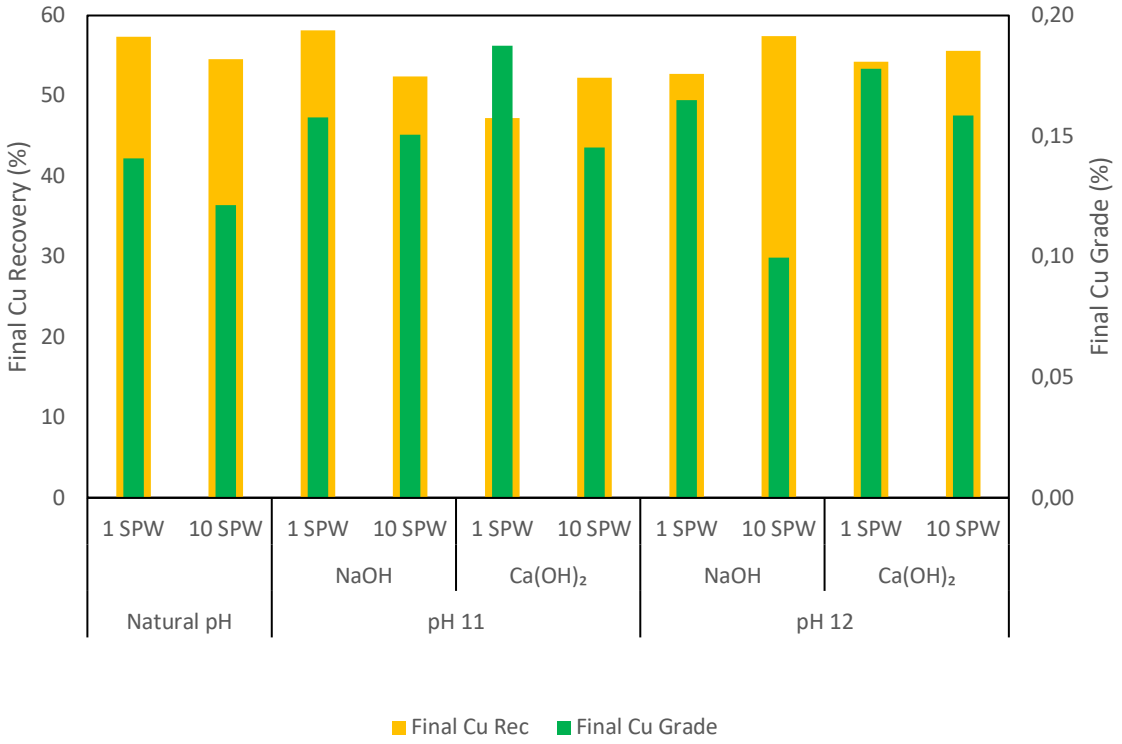


Figure 2. Total Cu recoveries and grades for all conditions tested.

At natural pH, Cu recoveries were reasonably high in both 1 SPW and 10 SPW, with slightly higher values in 1 SPW. However, grades were lower in 10 SPW compared to 1 SPW, indicating that elevated ionic strength promoted entrainment of gangue without a commensurate improvement in copper selectivity. This mirrors the solids and water recovery trends (Figure 1), where froth stability under higher ionic strength of SPW led to greater mass pull but poorer concentrate quality. Similar behaviour has been reported in Merensky and UG2 ores, where ion build-up in process waters reduces selectivity by increasing the recovery of naturally floatable gangue (Corin *et al*., 2011; Manono *et al*., 2018b, 2012).

At pH 11, the contrasting roles of the two pH modifiers became more apparent. Under NaOH addition, copper recoveries remained moderate, with grades improving slightly at 1 SPW compared to 10 SPW. This suggests that Na^+ addition, while enhancing froth stability at elevated ionic strength, did not strongly promote Cu selectivity, resulting in a trade-off between recovery and grade. In contrast, lime addition produced a notably higher Cu grade at 1 SPW, even though recoveries were lower than those with NaOH. The higher Cu grade indicates that Ca^{2+} ions likely contributed to enhanced depression of silicate gangue, consistent with their stronger adsorption and double-layer compression effects (Manono *et al*., 2019, 2020). At 10 SPW, however, both Cu recoveries and grades declined under $Ca(OH)_2$ addition, suggesting that excess Ca^{2+} in an already ion-rich environment led to froth destabilisation and possible precipitation reactions, which compromised Cu recovery and selectivity.

At pH 12, Cu recoveries again increased under NaOH in 10 SPW, reaching some of the highest values across all conditions. However, the corresponding Cu grade dropped sharply, reflecting extensive entrainment of gangue under these highly alkaline, sodium-dominated conditions. By contrast, lime addition at the same pH maintained higher Cu grades than NaOH, albeit at somewhat lower Cu recoveries. These results emphasise the dual role of Ca^{2+}: while it suppresses froth stability and reduces mineral recoveries, it can improve concentrate quality by depressing gangue relative to Cu-bearing sulfides.

The results of this work indicate a clear divergence between NaOH and $Ca(OH)_2$ systems. NaOH favours higher Cu recoveries, particularly under elevated ionic strength, but does so at the expense of

the concentrate grade in respect to Cu due to increased entrainment of gangue. Lime, on the other hand, decreases both recovery and water carryover but tends to yield higher Cu grades under moderate ionic strength conditions. This divergence highlights the importance of considering not only target pH but also the chemical species introduced by the chosen pH modifier. From an operational standpoint, these findings suggest that NaOH may be advantageous when maximising recovery is prioritised, whereas lime may be preferable when concentrate quality and gangue rejection are critical.

The Effect pH Modifier and Process Water Ions on Nickel Recoveries and Grades
Figure 3 illustrates the effect of pH, pH modifier type and synthetic plant water ionic strength on Ni recoveries and grades.

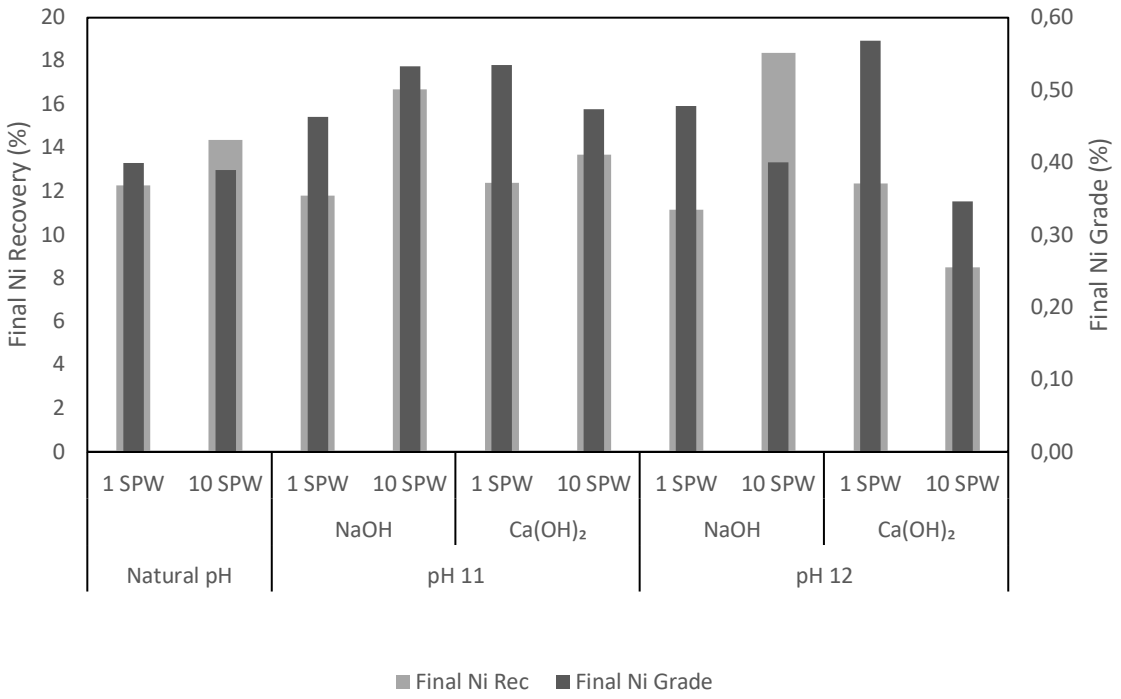


Figure 3. Total Ni recoveries and grades for all conditions tested.

At natural pH, Ni recoveries were modest (≈13–14%) across both 1 SPW and 10 SPW, with slightly higher grades in 1 SPW. The lower Ni grades observed in 10 SPW suggest that increased ionic strength promoted greater entrainment of gangue minerals into the concentrate, diluting Ni content. This trend mirrors the behaviour seen for Cu at natural pH (Figure 2) and reinforces that elevated ionic strength of SPW can stabilise froths but reduce selectivity (Corin *et al.*, 2011; Manono *et al.*, 2018a).

At pH 11, Ni recoveries improved relative to natural pH, particularly in NaOH systems where values approached 18% in 10 SPW. Grades under NaOH addition remained moderate, again suggesting that sodium chemistry promotes higher mass pull but does not significantly enhance selectivity. In contrast, lime addition resulted in slightly lower Ni recoveries but higher Ni grades, especially in 1 SPW. This implies that Ca^{2+} ions acted to depress gangue more strongly than Na^{+}, leading to cleaner concentrates. The observed trade-off between recovery (favoured by NaOH) and grade (favoured by $Ca(OH)_2$) is consistent with the dual role of pH modifiers in shaping both froth stability and gangue–mineral interactions (Manono *et al.*, 2020).

At pH 12, the divergence between the two pH modifiers became clearer. Under NaOH, Ni recoveries in 10 SPW were among the highest measured across all conditions, exceeding 18%. However, Ni grades under these conditions were suppressed, consistent with extensive gangue entrainment under highly alkaline, sodium-dominated chemistry. Conversely, $Ca(OH)_2$ addition produced lower Ni recoveries

but consistently higher Ni grades, particularly in 1 SPW, where Ni grade approached 0.5%. This reflects Ca^{2+} induced gangue depression and froth destabilisation, yielding concentrates of superior quality despite reduced Ni recovery.

The results of this work show that nickel flotation performance is highly sensitive to the combined effects of pH modifier chemistry and process water ionic strength. Sodium-based pH control promotes higher Ni recoveries under elevated ionic strength but compromises Ni grade through gangue entrainment. Calcium-based pH control suppresses overall Ni recovery but enhances concentrate grade through gangue depression. From an operational perspective, the choice of pH modifier therefore represents a strategic trade-off: NaOH may be advantageous when maximising Ni recovery is the priority, while lime may be better suited when concentrate grade and gangue rejection are critical. Importantly, these trends reinforce that pH modifiers should not be viewed as equivalent reagents, since their ionic contributions fundamentally alter flotation outcomes.

CONCLUSIONS

Based on the results of this study, it was seen that for the selected ore:

- Although both NaOH and $Ca(OH)_2$ achieve the same target pH, they introduce different ionic species (Na^+ vs. Ca^{2+}) that profoundly affect flotation performance, froth stability, and selectivity.
- Elevated ionic strength (10 SPW) generally promoted higher solids and water recoveries, with NaOH systems showing the strongest entrainment effects. Lime, by contrast, suppressed recoveries, reflecting Ca^{2+}'s froth-destabilising role at elevated pH.
- NaOH improved Cu recoveries, particularly under high ionic strength, but often at the expense of the concentrate grade due to entrainment. Lime produced lower valuable mineral recoveries but cleaner concentrates, especially at moderate ionic strength.
- Ni recoveries were maximised in NaOH at high ionic strength, while $Ca(OH)_2$ consistently yielded higher Ni grades. This demonstrates a trade-off between recovery (favoured by NaOH) and concentrate quality (favoured by lime).
- The results of this work highlight that flotation performance cannot be explained by pH alone. The chemical identity of the ions introduced by pH modifiers interacts with baseline process water chemistry, influencing both surface chemistry and froth behaviour, so, specific ion effects are important.
- In water-recycling concentrators, where ionic strengths are elevated, pH modifier choice becomes a critical operating decision.
- NaOH-based pH control may maximise throughput and recovery, but risks increased gangue entrainment and dilution of concentrate grades, particularly at elevated ionic strengths of process water..
- Lime-based pH **control** may suppress recovery but provides better concentrate quality through stronger gangue depression.
- A 'one-size-fits-all' approach to pH adjustment is insufficient, operators must evaluate not only target pH but also the ionic contributions of modifiers within the context of their specific water circuits.
- These findings call for integrated water–reagent management strategies, where the choice of pH modifier is optimised alongside process water recycling practices to balance mineral recovery, selectivity, and downstream smelting requirements.

ACKNOWLEDGEMENTS

The author would like to acknowledge Thabang Shamukuni for conducting the experimental test work. Thanks go to AECI Mining Chemicals for supplying the reagents. Members of the Centre for Minerals Research's Reagent Research Group are also acknowledged.

REFERENCES

Bulatovic, S.M., 2007. Handbook of flotation reagents, chemistry, theory and practice: flotation of sulphide ores. Elsevier Science & Technology Books.

Burdukova, E., Van Leerdam, G.C., Prins, F.E., Smeink, R.G., Bradshaw, D.J., Laskowski, J.S., 2008. Effect of calcium ions on the adsorption of CMC onto the basal planes of New York talc – A ToF-SIMS study. Miner Eng 1020–2025.

Corin, K.C., Reddy, A., Miyen, L., Wiese, J.G., Harris, P.J., 2011. The effect of ionic strength of plant water on valuable mineral and gangue recovery in a platinum bearing ore from the Merensky reef. Miner Eng 24, 131–137. https://doi.org/10.1016/j.mineng.2010.10.015

Corin, K.C., Wiese, J.G., 2014. Investigating froth stability: A comparative study of ionic strength and frother dosage. Miner Eng 66, 130–134. https://doi.org/10.1016/j.mineng.2014.03.001

Dzingai, M., Manono, M., Corin, K., 2020. Simulating the Effect of Water Recirculation on Flotation through Ion-Spiking: Effect of Ca2+ and Mg2+. Minerals 10, 1033. https://doi.org/10.3390/min10111033

Dzingai, M., Manono, M.S., Corin, K.C., 2021. Probing the Effect of Water Recycling on Flotation through Anion Spiking Using a Low-Grade Cu–Ni–PGM Ore: The Effect of NO3−, SO42− and S2O32−. Minerals 11, 340. https://doi.org/10.3390/min11040340

Harrison, S.T.L., Slatter-christie, K., Broadhurst, J., 2018. Integrating competing water needs of mining and mineral processing with the environment , community and economic activity in a mining-dominated catchment.

Le, T., Schreithofer, N., Dahl, O., 2020. Dissolution Test Protocol for Estimating Water Quality Changes in Minerals Processing Plants Operating With Closed Water Circulation. Minerals 10, 653. https://doi.org/10.3390/min10080653

Manenzhe, R.M., Manono, M.S., Wiese, J.G., Musuku, B., Corin, K.C., 2023. Exploring the effects of different process water sources on xanthate adsorption and flotation performance. Miner Eng 204, 108376. https://doi.org/10.1016/J.MINENG.2023.108376

Manono, M., Corin, K., Wiese, J., 2019. The effect of the ionic strength of process water on the interaction of talc and CMC: Implications of recirculated water on floatable gangue depression. Minerals 9. https://doi.org/10.3390/min9040231

Manono, M., Corin, K., Wiese, J., 2018a. Perspectives from literature on the influence of inorganic electrolytes present in plant water on flotation performance 54, 1191–1214. https://doi.org/10.5277/ppmp18157

Manono, M., Corin, K., Wiese, J., 2018b. Water quality effects on a sulfidic PGM ore : Implications for froth stability and gangue management 54, 1253–1265. https://doi.org/10.5277/ppmp18181

Manono, M.S., Corin, K.C., 2022. Considering Specific Ion Effects on Froth Stability in Sulfidic Cu-Ni-PGM Ore Flotation. Minerals 12. https://doi.org/10.3390/min12030321

Manono, M.S., Corin, K.C., Wiese, J.G., 2020. The Behavior of Gangue During the Flotation of a Sulfidic PGM-Bearing Ore in Response to Various Monovalent and Divalent Ions in Process Water. Front Chem. https://doi.org/10.3389/fchem.2020.00079

Manono, M.S., Corin, K.C., Wiese, J.G., 2016. The influence of electrolytes present in process water on the flotation behaviour of a Cu-Ni containing ore. Miner Eng 96–97. https://doi.org/10.1016/j.mineng.2016.06.015

Manono, M.S., Corin, K.C., Wiese, J.G., 2013. The effect of ionic strength of plant water on foam stability: A 2-phase flotation study. Miner Eng 40. https://doi.org/10.1016/j.mineng.2012.09.009

Manono, M.S., Corin, K.C., Wiese, J.G., 2012. An investigation into the effect of various ions and their ionic strength on the flotation performance of a platinum bearing ore from the Merensky reef. Miner Eng 36–38. https://doi.org/10.1016/j.mineng.2012.03.035

Manono, M.S., Matibidi, K., Thubakgale, C.K., Corin, K.C., Wiese, J.G., 2017. Water Quality in PGM Ore Flotation : The effect of Ionic Strength and pH 777–784.

Manono, M.S., Matibidi, K.M., October, L.L., Thubakgale, C.K., Corin, K.C., 2024. Increasing Ionic Strength and Oxyhydroxo Species in Process Water on the Floatability of Chalcopyrite and Pentlandite for a Selected Cu–Ni Bearing Ore Flotation. Recovery of Values from Low-Grade and Complex Minerals: Development of Sustainable Processes 65–85. https://doi.org/10.1002/9781119896890.CH3

Mhonde, N., Johansson, L.-S., Corin, K., Schreithofer, N., 2021a. The Effect of Tetrathionate Ions on the Surface Chemistry and Flotation Response of Selected sulphide Minerals. Mineral Processing and Extractive Metallurgy Review 1–14. https://doi.org/10.1080/08827508.2021.1998044

Mhonde, N., Pitkänen, L., Corin, K., Schreithofer, N., 2021b. The Solution Interaction of Tetrathionate Ions and Sodium Isobutyl Xanthate and Its Effect on the Flotation of Galena and Chalcopyrite. Minerals 11, 204. https://doi.org/10.3390/min11020204

Moimane, T.M., Corin, K.C., Wiese, J.G., 2016. The effect of varying pulp reagent chemistry on the flotation performance of a South African PGM ore. Miner Eng 95, 155–160. https://doi.org/10.1016/j.mineng.2016.07.002

Muzenda, E., Afolabi, A.S., Abdulkareem, A.S., Ntuli, F., 2011. Effect of pH on the Recovery and Grade of Base Metal Sulphides (PGMs) by Flotation. Proceedings of the World Congress on Engineering and Computer Science 2011 Vol II II, 19–22.

October, L., Corin, K., Schreithofer, N., Manono, M., Wiese, J., 2019. Water quality effects on bubble-particle attachment of pyrrhotite. Miner Eng 131. https://doi.org/10.1016/j.mineng.2018.11.017

October, L.L., Corin, K.C., Manono, M.S., Schreithofer, N., Wiese, J.G., 2020. A fundamental study considering specific ion effects on the attachment of sulfide minerals to air bubbles. Miner Eng. https://doi.org/10.1016/j.mineng.2020.106313

October, L.L., Manono, M.S., Corin, K.C., Schreithofer, N., Wiese, J.G., 2021. The Influence of Specific Ions and Oxyhydroxo Species in Plant Water on the Bubble-Particle Attachment of Pyrrhotite. ACS Omega 6, 28496–28506. https://doi.org/10.1021/acsomega.1c01152

Rao, S.R., Finch, J.A., 1989. A review of water re-use in flotation. Miner Eng 2, 65–85. https://doi.org/10.1016/0892-6875(89)90066-6

Slatter, K.A.; Plint, N.D.; Cole, M.; Dilsook, V.; De Vaux, D.; Palm, N.; Oostendorp, B., 2009. Water Management in Anglo Platinum Process Operations: Effects of Water Quality on Process Operations. International Mine Water Conference, Pretoria, South Africa, 19th – 23rd October 2009 Proceedings ISBN Number: 978-0-9802623-5-3 46–55.

Wang, B, Peng, Y., 2014. The effect of saline water on mineral flotation – A critical review. Miner Eng 13–24.

Wang, Bo, Peng, Y., 2014. The interaction of clay minerals and saline water in coarse coal flotation. Fuel 134, 326–332. https://doi.org/10.1016/j.fuel.2014.05.085

Wiese, J.G., 2009. Investigating Depressant Behaviour in The Flotation of Selected Merensky Ores. MSc.Eng Thesis, Faculty of Engineering & the Built Environment, University of Cape Town.

Wills, B.A., Finch, J.A., 2016. Froth Flotation. Wills' Mineral Processing Technology 265–380. https://doi.org/10.1016/B978-0-08-097053-0.00012-1



Malibongwe S. Manono

Associate Professor of Chemical Engineering & Deputy Dean of Undergraduate Studies in the Faculty of Engineering & the Built Environment
University of Cape Town

Malibongwe Manono is an Associate Professor in the Department of Chemical Engineering and the Deputy Dean of Undergraduate Studies in the Faculty of Engineering and the Built Environment at the University of Cape Town. He holds a PhD in Chemical Engineering specialising in Minerals Processing. His research interests are in the areas of froth flotation, water within flotation, dewatering of flotation products and value recovery from minerals and metallurgical processing waste. He has supervised many final-year Chemical Engineering projects, 13 MSc(Eng) students and 2 PhD to completion. He is currently supervising 15 MSc(Eng) students and 1 PhD candidate. His publication record boasts over 20 articles in globally recognised journals and significant participation in international and local conferences. He also stands as a reviewer for esteemed journals in his research field and has lent his expertise to conference organising committees for international conferences as a scientific committee member.

Beyond recovery: Rethinking reagent strategies for sustainable middle group ore processing

P.C. Siwela, M.M. Ramakokovhu, M.L. Teffo

Tshwane University of Technology, South Africa

The economic extraction of platinum group metals from Middle Group ores has historically been deemed challenging. Yet, due to the depletion of more conventional ore sources like UG2 and Merensky, these ores are increasingly processed in metallurgical plants. However, reagent addition strategies, originally developed for UG2 and Merensky ores, are often directly applied to Middle Group ores without full consideration of their unique mineralogical properties. This study addresses the resulting knowledge gap surrounding xanthate and depressant interactions within Middle Group ore processing.

This research, titled "Beyond recovery: rethinking reagent strategies for sustainable middle group ore processing", critically examines and aims to improve beneficiation strategies for Platinum Group Metals from Middle Group chromitite. It acknowledges the environmental challenges and limited selectivity associated with traditional xanthate-based flotation schemes. The primary objective was to optimize a xanthate-based reagent suite to achieve enhanced valuable mineral grades and recoveries comparable to established industry benchmarks.

The methodology involved systematic batch flotation tests in a Denver flotation cell. While the frother (Betachem 436 at 25 g/t) and activator (copper sulfate at 80g/t) dosages were kept constant, the depressant and collector dosages were varied to investigate and optimize their impact on separation. PGM content was determined using fire assay coupled with Inductively Coupled Plasma-Optical Emission Spectrometry, and bulk chemistry and modal mineralogy were analyzed by X-ray Fluorescence and X-ray Diffraction, respectively. Ore samples, sourced from the Bushveld Complex in South Africa, were blended chromitite, and a milling curve analysis determined that 40 minutes of grinding achieved an 80% passing 75 microns particle size.

Key findings from the chemical dosage optimization revealed that the highest metal recovery of 79.06% was achieved with a combination of 200 g/t SIBX and 150 g/t CMC, underscoring the crucial role of both SIBX and CMC dosages in maximizing recovery. Variations in CMC dosages significantly altered recovery for fixed SIBX concentrations, indicating an optimal range for each reagent. Mineralogical analysis of the feed demonstrated a dominance of Chromite (74.4%), followed by Pyroxene (15.9%) and Plagioclase (8.6%). Notably, common sulfide minerals, often PGM hosts, were absent, suggesting PGMs are associated with chromite or other silicate minerals rather than sulfides. The flotation process dramatically enriched Pyroxene in the concentrate, increasing its proportion from 15.9% in the feed to 73.4%, while effectively rejecting a significant portion of Chromite from the concentrate (from 74.4% in feed to 19.3%) to the tailings (56.1%). Amphibole also showed enrichment in the concentrate (from 0.1% to 2.6%), contributing to gangue. The study further illustrated the classic grade-recovery trade-off, where increasing cumulative recovery (up to 75.59%) typically led to a decrease in concentrate grade.

In conclusion, this research successfully optimized a xanthate-based reagent suite for the froth flotation of Middle Group chromitite, achieving significant metal recovery. The process demonstrated high selectivity of Pyroxene while effectively rejecting Chromite, highlighting the challenge of reduced concentrate grade for PGM extraction. The findings contribute valuable insights into developing more sustainable and efficient beneficiation routes for PGM recovery from complex ore types, emphasizing the importance of tailored reagent strategies and understanding mineralogical associations in optimizing metallurgical performance.

Keywords: froth flotation, reagent strategies, Middle group ore, xanthate, CMC, PGM recovery.

INTRODUCTION

Chromite layers within the Bushveld Complex are widely recognized as significant potential sources of Platinum Group Metals (Yudovskaya and Kinnaird, 2010). Historically, the economic extraction and recovery of PGMs from the main chromite layers have been challenging due to their relatively low grades, with past research often focusing on these lower concentrations (Junge et al., 2016). However, as higher-grade PGM deposits become increasingly depleted, there is growing interest in identifying alternative sources and developing more effective beneficiation routes for PGM recovery (Oberthur et al., 2016; Langa et al., 2021).

In recent years, the recovery of chromite from the Middle Group in South Africa's Bushveld Complex has garnered increased attention, driven by the escalating demand for chromium and the necessity for more sustainable mineral processing practices (Sefako et al., 2017). Within the Bushveld Complex, the Upper Group 2 chromitite layer and the Merensky Reef are particularly significant PGM ore horizons, both situated in the upper portion of the Critical Zone. Numerous other chromitite strata also exist, broadly classified into three groups—Lower, Middle, and Upper Groups—based on their stratigraphic position within the critical zone (Corin et al., 2021).

The Middle Group itself is located at a critical boundary between the Lower Critical Zone and the Upper Critical Zone as shown in Figure 1 below. This geological interface is characterized by the juxtaposition of an ultramafic (pyroxenite) assemblage with a more mafic rock assemblage comprising pyroxenite, norite, and anorthosite. This boundary specifically marks chromitite layers 2 and 3 of the MG on the eastern limb and is notably defined by the first appearance of cumulus plagioclase (Murthy et al., 2011; Ghorbani et al., 2023).

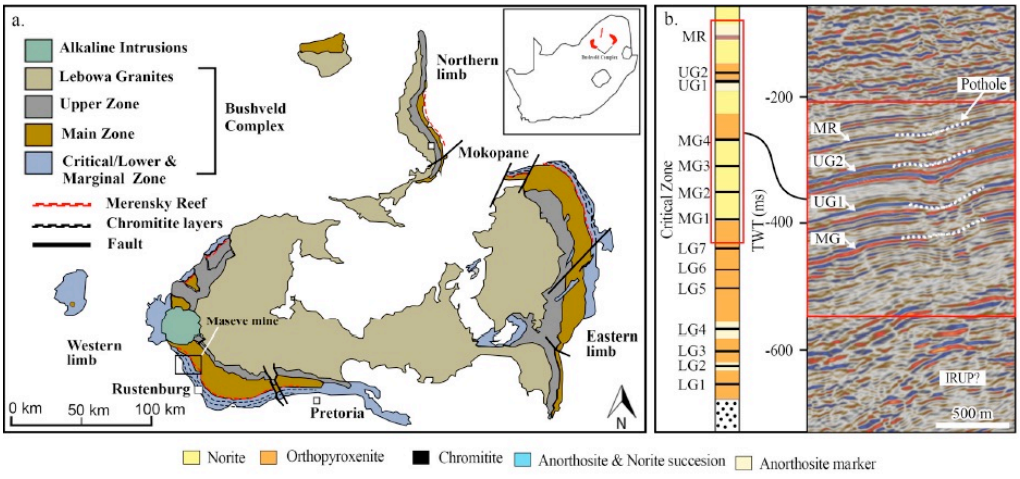


Figure 1. Geological map of the Bushveld Complex, showing the location of the Bushveld Complex within South Africa.

The PGMs in the Bushveld Igneous Complex are extracted through froth flotation. Froth flotation stands as one of the most versatile and widely adopted mineral processing techniques. Its efficacy lies in its ability to selectively separate valuable minerals from gangue (waste minerals), particularly in low-grade, complex (polymetallic) ores characterized by particle sizes too fine for other processing methods to handle effectively (Rahman et al., 2012; Wills and Finch, 2015).

According to Wills et al., flotation primarily operates through three key mechanisms:

1. **Selective Attachment:** Valuable mineral particles selectively adhere to air bubbles.

2. **Entrainment:** Mineral particles are carried into the froth layer by the water phase as air bubbles ascend.

3. **Aggregation:** Mineral particles accumulate and are retained within the froth phase.

Particle size plays a critical role in the flotation process, influencing several fundamental interactions. It directly impacts the probability of mineral particles colliding with air bubbles, their subsequent ability to attach to these bubbles, and crucially, their capacity to remain attached once the bubbles enter the froth phase (Feng & Aldrich, 1999; Norori-McCormac et al., 2017). Each specific ore typically exhibits an optimum particle size range for efficient mineral extraction.

An ideal scenario often involves a blend of finer and coarser particles. Very fine particles, while possessing a large surface area, are susceptible to excessive reagent adsorption and increased entrainment. Conversely, coarse particles can aggregate, potentially leading to increased drainage of fine particles from the froth phase. Therefore, a balanced mix of fine and coarse particles can enhance froth stability and improve overall recovery. However, the optimal particle size distribution for froth flotation must be thoroughly investigated and optimized for each specific ore type. Following comminution, a specific suite of chemical reagents is essential for modifying the flotation system and mineral surfaces to enhance the selective separation of valuable minerals from gangue. These reagents are typically categorized into collectors, frothers, depressants (also known as suppressants), activators, and pH modifiers.

Collectors are surfactants designed to adsorb onto selected mineral surfaces, thereby increasing their hydrophobicity (Maree et al., 2017; Pearse, 2005). This process involves forming a mono- or multi-layer 'bubble' that destabilizes the hydrated layer between the air bubble and the mineral surface, facilitating attachment.

Frothers primarily function to modify the properties of air bubbles within the flotation system. They aid in bubble formation and control bubble size, stabilize the froth layer, and prevent bubble coalescence (Chipfunhu et al., 2019; Wills & Finch, 2015).

Depressants chemically act to render gangue minerals (or sometimes secondary valuable minerals) hydrophilic, similar to how collectors modify surfaces. By reducing the entry of unwanted minerals into the froth layer, depressants significantly contribute to the selective flotation of low-grade ores (Liu et al., 2021; Wills and Finch, 2015; Xuemin et al., 2020).

Activators modify mineral surfaces to amplify the effect of collectors, making them more receptive to becoming hydrophobic.

Lastly, the role of **pH modifiers** is both complex and critical. An alkaline medium is frequently preferred in the mining industry, not only to mitigate equipment corrosion but also to establish a stable chemical environment for the reagents. pH profoundly influences flotation selectivity, as each mineral possesses a critical pH value beyond which its flotation is hindered. Therefore, precise control of pH, in conjunction with reagent dosages, is paramount for achieving optimal grades and recoveries.

While xanthate reagent schemes are commonly employed in base metal sulfide ore flotation processes due to their effectiveness as universal collectors, they pose environmental challenges. Xanthates are

anionic thiol collectors with known environmental toxicity; for instance, they have been shown to inhibit microbial and enzyme activities in soil and exhibit acute oral and dermal toxicity to animals. Furthermore, their limited selectivity can compromise the grade of valuable minerals in the concentrate. These limitations underscore the pressing need for innovation in either the application or type of flotation reagents to meet the evolving demands of the mineral processing industry. Copper sulfate, often used as an activator with xanthates, substantially increases valuable mineral recovery but shares the disadvantage of environmental toxicity (Finkelstein and Allison, 1976; Lai et al., 2019; Wills and Finch, 2015). Typically, methyl isobutyl carbinol and carboxymethyl cellulose are utilized as frother and depressant, respectively (Bicak et al., 2007; Wang et al., 2022). Ultimately, optimizing the dosages of all chemical reagents is essential for enhancing the recovery, grade, selectivity, and overall economics of the flotation process.

Building upon the recognized potential of the Middle Group chromitite and the challenges associated with PGM recovery, the primary objective of this study is to optimize a xanthate-based reagent suite for the froth flotation of Middle Group ore**.** This optimization aims to achieve valuable mineral grades and recoveries comparable to established industry benchmarks for similar ore types, thereby addressing the ongoing need for improved beneficiation strategies for lower-grade PGM resources.

MATERIALS AND METHODS

Sample Preparation

Chromite samples (MG 1, MG 2, MG 3, and 4A) were acquired from a South African chromite beneficiation plant located in the western limb of the Marikana area. This plant utilizes a gravity concentrator with water as the processing medium for chromite beneficiation. Upon receipt, the samples underwent air-drying, de-lumping, and blending. Subsequently, they were riffle-split into 10 kg aliquots and stored in sample bags. These four distinct samples were then combined to form a blend, with each contributing 25% by weight as shown in Table 1 below.

Table 1. Middle group blending ratio

Sample ID	Blending ratio (%)
MG1	25
MG2	25
MG3	25
MG4A	25
TOTAL	100.00

A subsample from this blend was then extracted for comprehensive chemical and mineralogical analysis. The head grade of platinum, palladium, and rhodium (3E) plus gold in the as-received material was quantified using fire assay followed by inductively coupled plasma-optical emission spectrometry. The prepared blend was further divided into multiple samples for subsequent flotation test work.

Flotation experiments and reagents used

All batch flotation tests were conducted using a Denver flotation cell, a standard laboratory-scale unit designed for mineral processing studies. To ensure consistent mixing and aeration conditions throughout the experiments, the rotor speed of the cell was precisely maintained at 1200rpm. The chemical regime for the flotation tests involved specific concentrations of several key reagents. The frother, Betachem 436, was maintained at a constant dosage of 25g/t. Concurrently, copper sulfate, acting as an activator for the target minerals, was applied at a consistent dosage of 80g/t across all batch tests. In contrast, the dosages of the (CMC) depressant and the collector, sodium isobutyl xanthate, were systematically varied. This deliberate variation allowed for the investigation and optimization of their respective roles in selectively separating the desired minerals from the gangue.

Froth collection was performed meticulously to obtain kinetic data and maximize recovery. The froth was scraped from the cell every 15 seconds over a total flotation period of 20 minutes. Custom-made paddles were employed for this process, designed specifically to scrape just above the froth-pulp interface, thereby minimizing mechanical entrainment of pulp into the concentrate. As froth was removed, the resulting concentrates were collected, and their solids and water masses were accurately recorded for subsequent mass balance calculations. To maintain a constant pulp level within the flotation cell throughout the test – a critical factor for consistent hydrodynamic conditions – water was added after each scraping interval. The precise amount of water added during the scraping process was determined by recording the initial and final masses of the spray water bottle

PGMs Characteristics

The precious metal content, specifically Platinum Group Metals and gold, was precisely determined using a fire assay method. This robust technique involves high-temperature fusion to collect precious metals into a lead button, followed by cupellation, and then analysis of the resulting prill via highly sensitive methods like ICP-OES.

Bulk Chemistry and Modal Mineralogy

The samples underwent comprehensive analysis to determine their major and minor metal content, as well as their mineralogical composition. Chemical composition was precisely measured using wavelength dispersive X-ray Fluorescence on a Rigaku SSX Primus IV instrument. For mineral identification and quantification, a Rigaku X-ray diffraction Ultima IV was employed. Furthermore, the analysis of platinum group metals (3E PGM) plus gold was conducted utilizing the fire assay nickel sulfide collection method. The final quantification of these precious metals was performed using an Agilent 5900 Inductively Coupled Plasma Optical Emission Spectroscopy system.

RESULTS AND DISCUSSIONS

Milling curve

A milling curve was determined for the composite material by milling 1kg samples at 1.7mm size using a rubber lined laboratory ball mill at different time intervals. The milling curve is shown in Figure.

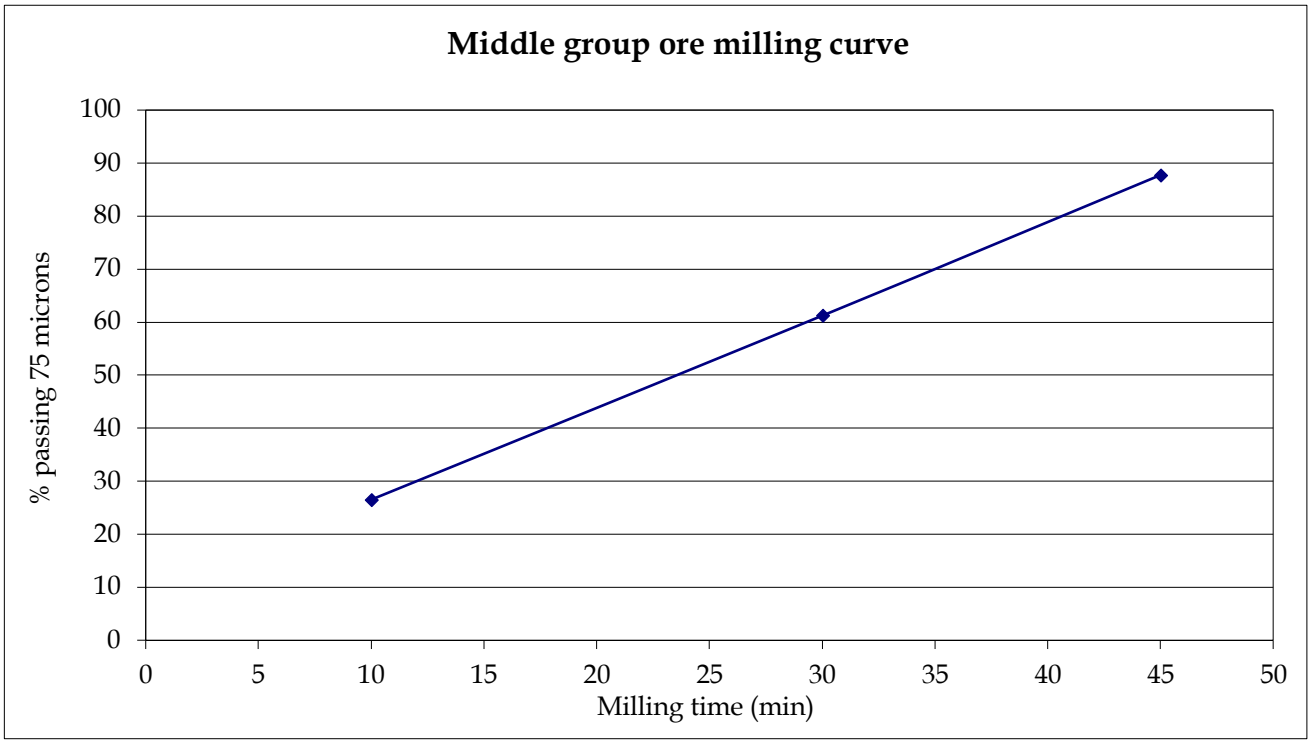


Figure 2: Composite milling curve

To achieve an 80% passing 75 microns grind, the sample required 40 minutes of milling, as shown by the milling curve in figure 2.

Bulk modal mineralogy

From Table 2 below, the Feed column clearly shows that the ore is overwhelmingly dominated by Chromite at 74.4%, making it the primary mineral phase. Pyroxene (15.9%) and Plagioclase (8.6%) are the next most abundant minerals. Notably, all listed sulfide minerals, which are often primary hosts for PGMs, are present at 0.0% in the feed. This suggests that Middle group ore PGMs are hosted within the chromite or other silicate minerals, they are not rich in sulfide-associated PGMs.

Table 2. Bulk modal mineralogy (mass %)

Bulk Modal Mineralogy (Mass %)			
Mineral	**Feed**	**Concentrate**	**Tailings**
Pentlandite	0.0	0.0	0.0
Millerite	0.0	0.0	0.0
Pyrite	0.0	0.0	0.0
Pyrrhotite	0.0	0.0	0.0
Chalcopyrite	0.0	0.0	0.0
Pyroxene	15.9	73.4	30.3
Plagioclase	8.6	3.8	12.8
Chromite	74.4	19.3	56.1
Olivine	0.3	0.1	0.1
Talc	0.0	0.2	0.0
Amphibole	0.1	2.6	0.1
Mica	0.0	0.1	0.1
Quartz	0.2	0.3	0.3
Calcite	0.0	0.0	0.0
Rutile	0.0	0.0	0.0
Prehnite	0.3	0.0	0.0
Kaolinite	0.0	0.0	0.0
*Other	0.2	0.3	0.1
Total	**100.0**	**100.0**	**100.0**

*other includes chlorite, ankerite, titanite and Fe oxide

The flotation process has dramatically enriched Pyroxene, increasing its proportion from 15.9% in the feed to a substantial 73.4% in the concentrate. This indicates that despite this reagent suite being optimal, it renders pyroxene highly floatable, leaving areas of improvement. In contrast to pyroxene, Chromite is significantly depleted in the concentrate, dropping from 74.4% in the feed to only 19.3%. This is a critical observation, suggesting that the current flotation conditions are effectively chromite rejection. Amphibole shows a notable enrichment in the concentrate, increasing from 0.1% in the feed to 2.6%. This indicates that amphiboles are also floating, contributing to the gangue content and supporting the earlier observation. As expected, Chromite remains a major component of the tailings at 56.1%, confirming its rejection. Other Gangue Minerals like Olivine, Talc, Amphibole, Mica, Quartz and Prehnite are present in minor amounts in the feed and remains low in both concentrate and tailings.

Chemical dosage optimization

The highest metal recovery observed in this dataset is 79.06%, achieved with a dosage combination of 200 g/t SIBX and 150 g/t CMC as shown in figure 3 below. The results show that both SIBX and CMC dosages play a crucial role in achieving maximum PGM (3E+Au) recovery.

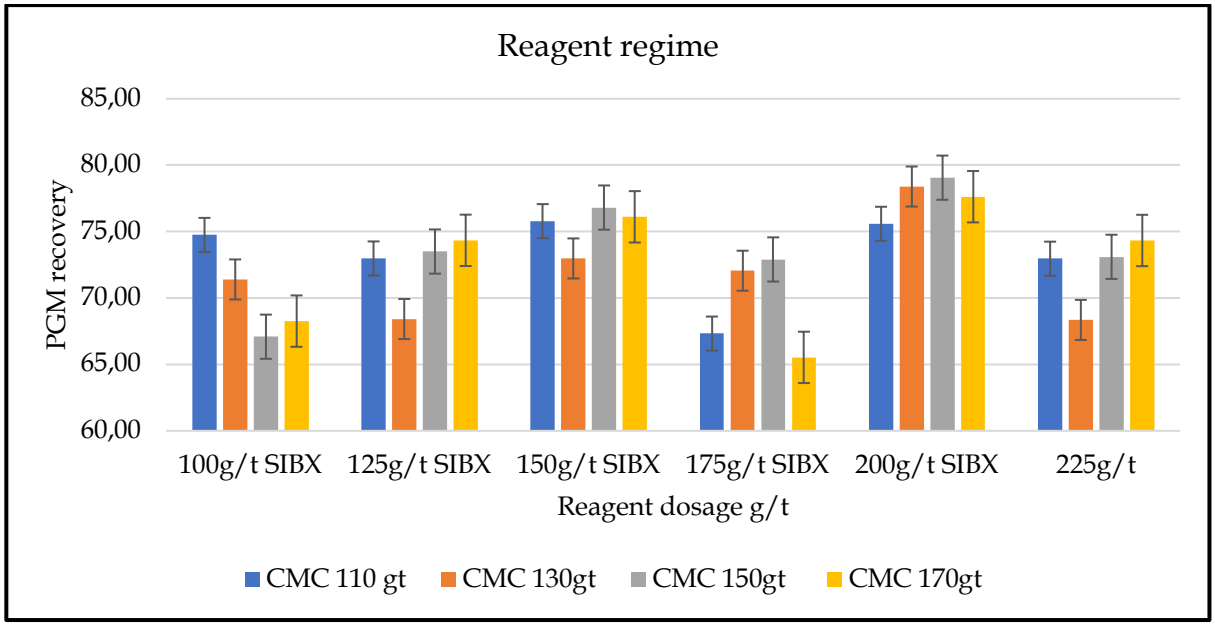


Figure 3. PGM recovery

At lower CMC dosages (e.g., 110 g/t), increasing SIBX generally leads to higher recovery, with a peak at 150 g/t SIBX (75.79%) and 200 g/t SIBX (75.59%). For a fixed SIBX dosage, varying CMC can significantly alter recovery. For instance, at 200 g/t SIBX, recovery improves from 75.59% (CMC 110 g/t) to 79.06% (CMC 150 g/t), then slightly drops to 77.63% (CMC 170 g/t). This suggests an optimal CMC dosage range.

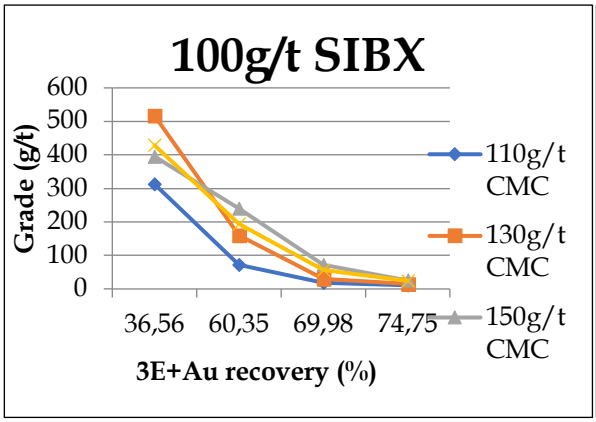


Figure 4(a) grade recovery curve at 100g/t SIBX

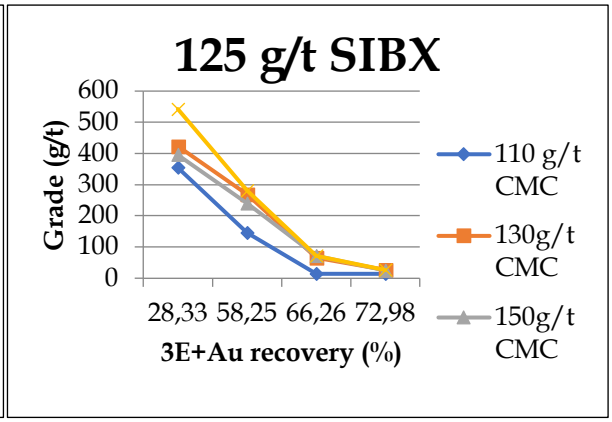


Figure 4(b) grade recovery curve at 125g/t SIBX

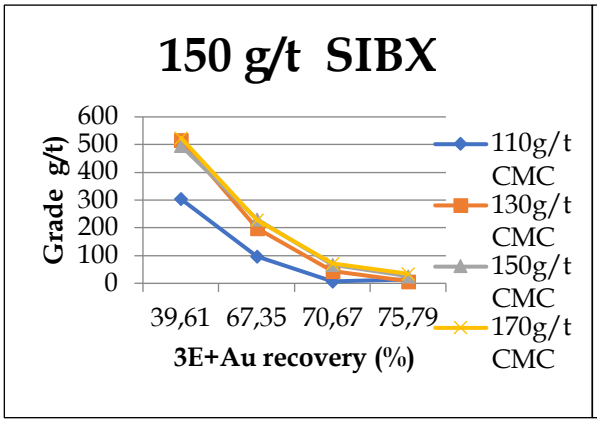


Figure 4(c) grade recovery curve at 150g/t SIBX

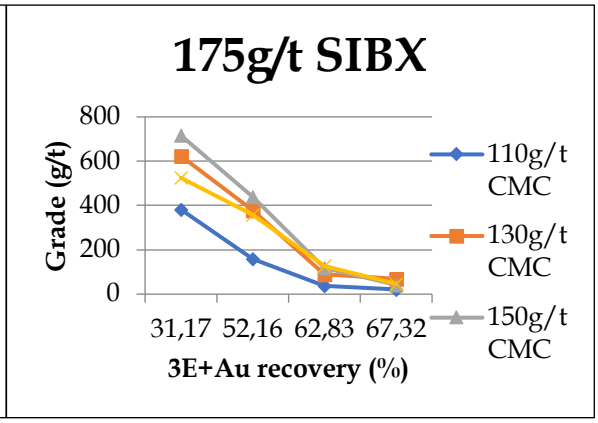


Figure 4(d) grade recovery curve at 175g/t SIBX

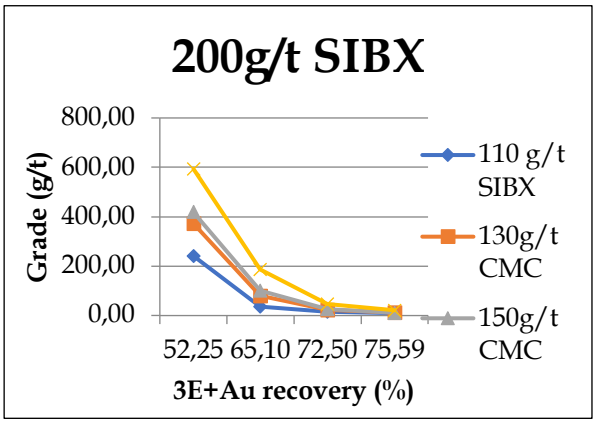


Figure 4(e) grade recovery curve at 200g/t SIBX

In Figure 3 the graphs are as follows:

- Figure 3(a) grade recovery curve at 100g/t SIBX
- Figure 3(b) grade recovery curve at 125g/t SIBX
- Figure 3(c) grade recovery curve at 150g/t SIBX
- Figure 3(d) grade recovery curve at 175g/t SIBX
- Figure 3(e) grade recovery curve at 200g/t SIBX

From figure 3 graphs above, high Initial Grades with moderate recoveries are observed. At a cumulative recovery of 52.25%, the grades (354.55g/t, 381.95g/t & 241.40g/t) are exceptionally high, such high numbers typically suggest a very selective but perhaps not yet fully optimized recovery process in the initial stages. As the cumulative recovery increases (from 52.25% to 75.59%), there's a clear and significant decrease across all dosage grades. The highest cumulative recovery achieved in this set is 75.59%. This comes at the expense of the lowest grades (14.18g/t, 21.33g/t & 9.76g/t). This again demonstrates the classic grade-recovery relationship where pushing for higher recovery often dilutes the concentrate grade.

CONCLUSIONS

The study aimed to optimize a xanthate-based reagent suite for the froth flotation of Middle Group ore, acknowledging the environmental challenges and limited selectivity associated with traditional xanthate schemes. The research successfully identified an optimal chemical dosage combination for

metal recovery, achieving the highest metal recovery of 79.06% with 200 g/t SIBX and 150 g/t CMC. This highlights the crucial role of both SIBX and CMC dosages in maximizing recovery. However, this optimization demonstrated the classic grade-recovery relationship, where pushing for higher cumulative recovery (up to 75.59%) often leads to a dilution of the concentrate grade. Mineralogical analysis of the process revealed significant enrichment of Pyroxene in the concentrate, increasing from 15.9% in the feed to 73.4%, while Chromite was effectively rejected from the concentrate, dropping from 74.4% in the feed to 19.3%. Additionally, Amphibole was noted to also float, contributing to the gangue material.

REFERENCES

Bicak,O.,Ekmekci,Z.,Bradshaw,D.J.,Harris,P.J.,2007.Adsorption of guar gum and CMC on pyrite. Miner.Eng.. 20,996–1002.https://doi.org/10.1016/j. mineng.2007.03.002.

Chipfunhu,D.,Bournival,G.,Dickie,S.,Ata,S.,2019.Performancecharacterisationof newfrothersforsulphidemineralflotation.Miner.Eng.131,272–279.https://doi. org/10.1016/j.mineng.2018.11.014.

Corin, K.C.; McFadzean, B.J.; Shackleton, N.J.; O'Connor, C.T. Challenges related to the processing of fines in the recovery of platinum group minerals (PGMs). Minerals 2021, 11, 533. [CrossRef]

Feng, D., Aldrich, C., 1999. Effect of particle size on flotation performance of complex sulphide ores. Miner. Eng. 12, 721–731. https://doi.org/10.1016/S0892-6875(99) 00059-X.

Finkelstein, N.P., Allison. S.A. 1976 The Chemistry Of Activation, Deactivation And Depression In The Flotation Of Zinc Sulfide: A Review. ed. M. C. Fuerstenau, ed., Vol. I, AIME, New York, pp. 414-457.

Ghorbani, Y.; Zhang, S.E.; Nwaila, G.T.; Bourdeau, J.E.; Safari, M.; Hoseinie, S.H.; Nwaila, P.; Ruuska, J. Dry laboratories— Mapping the required instrumentation and infrastructure for online monitoring, analysis, and characterization in the mineral industry. Miner. Eng. 2023, 191, 107971. [CrossRef]

Junge, M.; Oberthur, T.; Osbahr, I.; Gutter, P. Platinum-group elements and minerals in the lower and middle group chromitites ofthe western Bushveld Complex, South Africa. Miner. Depos. 2016, 51, 841–852. [CrossRef]

Lai, H., Deng, J., Fan, G., Xu, H., Chen, W., Li, S., Huang, L., 2019. Mechanism Study of Xanthate Adsorption on Sphalerite/Marmatite Surfaces by ToF-SIMS Analysis and Flotation. Minerals 9, 205. https://doi.org/10.3390/min9040205.

Langa, M.M.; Jugo, P.J.; Leybourne, M.I.; Grobler, D.F.; Adetunji, J.; Skogby, H. Chromite chemistry of a massive chromitite seam in the northern limb of the Bushveld Igneous Complex, South Africa: Correlation with the UG-2 in the eastern and western limbs and evidence of variable assimilation of footwall rocks. Miner. Depos. 2021, 56, 31–44. [CrossRef]

Liu, J., Hao, J., Dong, W., Zeng, Y., 2021. Depression mechanism of environment-friendly depressant dithiocarbamate chitosan in flotation separation of Cu-Zn sulfide. Colloids Surf A Physicochem Eng Asp 615, 126290. https://doi.org/10.1016/j. colsurfa.2021.126290.

Maree, W., Kloppers, L., Hangone, G., Oyekola, O., 2017. The effects of mixtures of potassium amyl xanthate (PAX) and isopropyl ethyl thionocarbamate (IPETC) collectors on grade and recovery in the froth flotation of a nickel sulfide ore. S. Afr. J. Chem. Eng. 24, 116–121. https://doi.org/10.1016/j.sajce.2017.07.001.

Murthy, Y.R.; Tripathy, S.K.; Kumar, C.R. Chrome ore beneficiation challenges & opportunities—A review. Miner. Eng. 2011, 24, 375–380. [CrossRef]

Norori-McCormac, A., Brito-Parada, P.R., Hadler, K., Cole, K., Cilliers, J.J., 2017. The effect of particle size distribution on froth stability in flotation. Sep. Purif. Technol. 184, 240–247. https://doi.org/10.1016/j.seppur.2017.04.022.

Oberthur, T.; Junge, M.; Rudashevsky, N.; de Meyer, E.; Gutter, P. Platinum-group minerals in the LG and MG chromitites of the eastern Bushveld Complex, South Africa. Miner. Depos. 2016, 51, 71–87. [CrossRef]

Pearse, M.J., 2005. An overview of the use of chemical reagents in mineral processing. Miner. Eng. 18, 139–149. https://doi.org/10.1016/j.mineng.2004.09.015.

Rahman, R.M., Ata, S., Jameson, G.J., 2012. The effect of flotation variables on the recovery of different particle size fractions in the froth and the pulp. Int. J. Miner. Process. 106–109, 70–77. https://doi.org/10.1016/j.minpro.2012.03.001.

Sefako, R.; Sekgarametso, K.; Sibanda, V. Potential Processing Routes for Recovery of Platinum Group Metals from Southern African Oxidized PGM Ores: A Review. J. Sustain. Metall. 2017, 3, 797–807. [CrossRef].

Wang, C., Liu, R., Zhai, Q., Wu, M., Jing, N., Xie, F., Sun, W., 2022. Influence of calcium and ferric ions on the depression of chalcopyrite by CMC: Flotation performance and adsorption mechanism study. Miner. Eng. 184, 107667 https://doi.org/10.1016/j. mineng.2022.107667.

Wills, B.A., Finch, J.A., 2015. Wills' mineral processing technology: an introduction to the practical aspects of ore treatment and mineral recovery, 8th ed. ed. Elsevier/BH, Amsterdam; Boston, MA.

Xuemin, Q., Hongying, Y., Guobao, C., Shuiping, Z., Chuangkai, C., Bibo, L., 2020. Inhibited mechanism of carboxymethyl cellulose as a galena depressant in chalcopyrite and galena separation flotation. Miner. Eng. 150, 106273 https://doi. org/10.1016/j.mineng.2020.106273.

Yudovskaya, M.A.; Kinnaird, J.A. Chromite in the Platreef (Bushveld Complex, South Africa): Occurrence and evolution of itschemical composition. Miner. Depos. 2010, 45, 369–391. [CrossRef]



Phumlani Siwela

Process Superintendent
Minopex

I am a seasoned metallurgical environmental professional with 16 years of experience in the mining industry. Starting as a student, I demonstrated unwavering dedication and perseverance, rising through the ranks to attain the esteemed position of Superintendent.

Throughout my illustrious career, I have gained extensive expertise in various commodities, including Platinum Group Metals (PGM), chrome, and coal. This diverse experience has equipped me with a unique understanding of the complexities and challenges associated with different mining operations.

A holder of two master's degrees, I have earned an Mtech in Metallurgical Engineering and an MBA. This exceptional academic background has provided me with a strong foundation in both the technical and business aspects of the industry.

As a respected leader, I continue to drive innovation and excellence in metallurgical environmental management, leveraging my expertise to optimize processes, ensure sustainability, and foster growth in the mining sector.

Automated statistical anomaly detection in an integrity monitoring application for a furnace

T. Moodley[1], W. Smith[2], J. Yelland[3]

[1]Hatch, South Africa
[2]Hatch, Australia
[3]Hatch, Canada

Furnace integrity is a critical concern in high-temperature metallurgical operations, directly impacting safety, campaign life, and business continuity. As such, there is a need for early detection and prevention of failures. Due to the high number of data sources, drawing connections between signal behaviour and failure events is challenging. In one such operation, integrity engineers were manually reporting on data from over 500 instruments — a process that was time-consuming, subjective, and prone to human error. The aim of this study was to develop a simple algorithmic solution to streamline the manual integrity monitoring process by automating the detection of specific anomalous timeseries behaviours that integrity engineers were manually identifying. Secondly, the aim was to integrate these algorithms into a prototype reporting tool, allowing an integrity engineer to review detected anomalies and prepare material for peer review. An analysis of a sample of the manual reports revealed six timeseries behaviours – five univariate and one multivariate - for which six statistical anomaly detection rules were specifically designed. Four univariate, parametric rules were designed, and two non-parametric, multivariate rules were designed. The parametric rules are designed to quantify statistical significance with respect to a historical reference period – two years in this study. All six rules have tuneable parameters to enable adjustment per sensor. The rules were tested across a series of temperature, flow and displacement sensors. With specific comparison to the manual reports, 76% of human-detected anomalies over a four-month period were automatically detected, with five of the six undetected anomalies confirmed to be insignificant on further review by the integrity engineer. These algorithms were implemented into a proof-of-concept system that extracts live data from site systems to perform cloud-based computation. Anomalies were automatically detected and presented to the engineer through a user interface designed around asset hierarchy and risk areas. By automating routine analysis, the system frees up capacity to focus on risk mitigation.

Keywords: furnace integrity, anomaly detection, machine learning, operations technology

INTRODUCTION

Furnace Integrity Management

Furnaces are key assets in metallurgical value chains. Failure events significantly impact production and pose critical safety risks to operators. Moreover, meeting or extending campaign life is of paramount concern to a business' capital investment regime. Furnace integrity management is a discipline aimed at maintaining reliable and safe operation of the asset and avoiding critical failures.

For example, one element of integrity management is refractory monitoring. Insufficient care can result in dangerous molten metal run-outs, from minor leaks to severe breach of containment (Sadri *et al.*, 2023). This can occur from various causes:

1. **Binding/refractory movement.** Refractory bricks are held together through compression by the furnace binding system. A compromised binding system could result in leaks and run-outs by allowing extreme expansion or excessive refractory movement due to thermal cycling.
2. **Refractory wear.** Refractory wear starts with the operation of the furnace. Extreme thermomechanical and thermochemical furnace activities result in mechanical failure, chemical attacks and dissolution of refractories. Improper cooling can cause accelerated wear of the refractory lining, leading to compromised chemical and structural properties. Weakened refractory lining can lead to high heat transfer to and subsequent damage of the furnace structure.
3. **Water ingress.** Sudden cooling water ingress into the furnace can result in instant vaporisation and a subsequent steam explosion, damaging the furnace lining. Gradual release of water can cause rapid expansion of the lining due to a hydration reaction, weakening the lining. There is often a high risk of water ingress around tapholes due to uncontrolled tapping or poor lancing practice degrading the tapblock.

Management of such risks requires inspection and monitoring of furnace components. The binding systems, cooling systems, and the refractory lining must be continuously inspected and monitored, both via instrumentation and manually. Constant and careful examination of process and integrity data is required, to identify potential integrity risks. Furthermore, the integrity of the instruments themselves must also be verified.

Manual Detection of Anomalies in Timeseries Data

In this paper we examine the anomaly detection process at a nickel smelting furnace, as a part of the overall furnace integrity management program. This furnace utilises over 500 instruments collecting high-frequency data for integrity monitoring, including:

- Cooling water temperatures and flow rates
- Refractory temperatures
- Tapblock temperatures
- Binding system movement
- Feed and fuel rates
- Electrode powers

The incumbent approach for managing integrity at this furnace involved a bi-weekly manual review of such instrument data. Similar instruments were plotted together, with time periods ranging from weeks to months, depending on the instrument. engineers scanned through each plot, looking to identify any anomalous conditions such as sustained trends, step changes or abnormal spikes in the timeseries data. Table I lists examples of the types of anomalies often identified by engineers, along with their implications for furnace integrity.

Anomalies can be categorised as either univariate or multivariate. Univariate anomalies are identifiable from a single instrument. By contrast, multivariate anomalies are only identifiable through multiple instruments, due to information provided by their relationship to one another. While univariate anomalies can provide important signals for possible integrity risks, most risks must be understood through multiple sensors; excessive expansion of the binding system for example must be observable over an array of movement sensors, as a change in one sensor alone could be an indication of a calibration fault.

Table I. Examples of commonly detected anomalous behaviours

Timeseries behaviour	Type	Possible implications
1. Large step change	Univariate	Instrument failure or calibration event
2. Small step change	Univariate	Instantaneous change in furnace conditions
3. Short-term gradient (hourly trend)	Univariate	Rapid change in furnace conditions
4. Long-term gradient (daily – monthly trend)	Univariate	Slow change in furnace conditions or instrument drift
5. Spike	Univariate	Short event or instrument malfunction
6. Change in relationship to proximate instruments	Multivariate	Complex furnace condition change or instrument issue

Figure 1 shows an extract from a manual report, highlighting a step change anomaly detected in a temperature signal, indicating an instrument failure. Such types of anomalies may also indicate a change in integrity conditions, such as the example shown in the extract in Figure 2. It is worth noting that in both cases, while the large number of signals on each plot provides context over a group of similar instruments, it often hides regions of any specific signal.

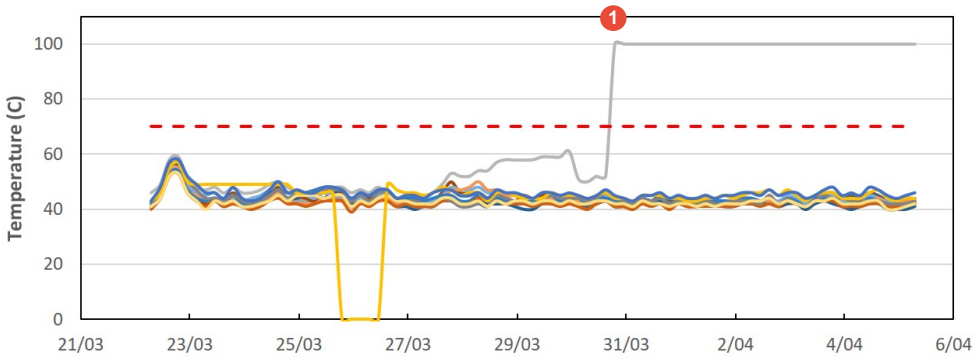


Figure 1. An extract from a manual report showing a human-detected large step change anomaly in temperature data (at point 1), indicating instrument failure.

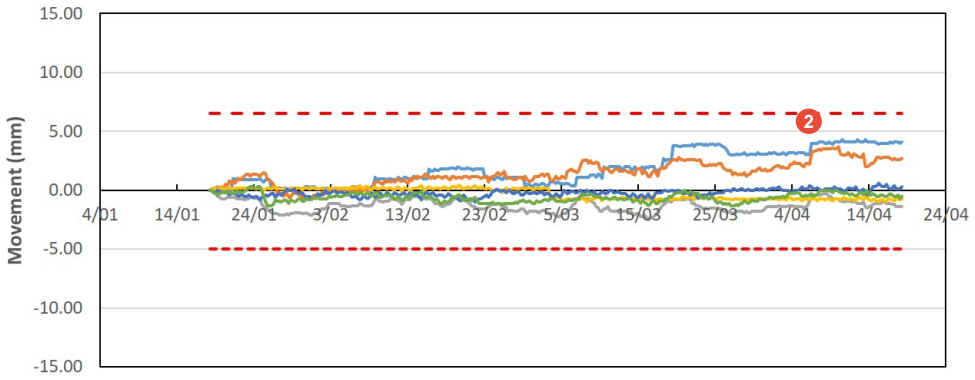


Figure 2. An extract from a manual report showing a human-detected small step change anomaly in movement data (at point 2), indicating sudden expansion of the binding system.

This manual process involves the review of several tens of graphs, typically taking multiple days. The resulting report, produced bi-weekly, does not contain prior anomalies for context. Human judgement varies between engineers, creating a reliance on prior experience to correctly discern integrity anomalies

from normal operational variations. We aim to propose a more efficient method for detecting these specific types of integrity anomalies (from Table) using statistical and machine learning techniques.

Statistical and Machine Learning Approaches to Anomaly Detection in Timeseries Data
In the context of furnace integrity management, the goal of anomaly detection algorithms is to correctly identify anomalous conditions that could signal an integrity risk, without over-identifying false positives. Missed anomalies can be catastrophic, whilst false positives create more work for the engineer. It is also important to indicate to the engineer, where possible, why a certain rule detected an anomaly and classify the severity, as this information assists in diagnosing the underlying cause and identifying required actions.

Nelson rules
The Nelson rules (Nelson, 1984) are simple and explainable methods of detecting statistical anomalies. There are eight Nelson rules, listed in Table II. However, their effectiveness is necessarily dependent on the frequency of sampling, given that they rely on distinct numbers of points to determine an out-of-control condition. Therefore, these rules are more likely to be useful for a discrete process rather than measurement of a continuous variable and were not utilised in this study.

Table II. The eight Nelson rules for determining if a variable is out of control (Nelson, 1984)

Rule	Description
1	One point more than three standard deviations from the mean
2	Nine consecutive points on the same side of the mean, within one standard deviation of the mean
3	Six consecutive points trending in the same direction
4	Fourteen consecutive points alternating between increasing and decreasing
5	Two of three consecutive points on the same side of the mean, more than two standard deviations from the mean
6	Four of five consecutive points on the same side of the mean, more than one standard deviation from the mean
7	Fifteen consecutive points are within one standard deviation of the mean
8	Eight consecutive points are all outside one standard deviation from the mean, on both sides of the mean

Spatial distance algorithms for multivariate anomalies
Anomalous conditions across an array of related variables can be identified using algorithms that partition spatial data by density, for example DBSCAN (Ester *et al.*, 1996) or OPTICS (Ankerst *et al.*, 1999). Clusters of points can be identified that are sufficiently close together (defined by some minimum distance parameter). Outliers can be identified as clusters that have too few points (or a single point). Another similar approach to testing whether a point is anomalous is to find its kth nearest neighbour and determine if it is sufficiently far away to be considered an outlier.

Advanced machine learning methods
Recent advances in machine learning have produced unsupervised (not requiring the manual labelling of anomalies) methods for anomaly detection, such as Auto-encoders (Neloy and Turgeon, 2024). Such methods can use deep learning architectures to understand underlying distributions in multivariate data and provide a mechanism to encode and decode these data points. Data points that are not well re-constructed by the decoder do not fit the underlying distribution and are thus considered anomalous. These methods were not considered for use in this study in favour of simpler, more explainable methods that could explicitly identify the behaviours in Table . However, further exploration of these methods would be warranted in the domain of furnace integrity.

APPROACH

Statistical Univariate Anomaly Detection Methods

While complex machine learning methods exist for timeseries anomaly detection, the aim of this study is to specifically identify a series of discrete behaviours, as opposed to generic timeseries anomaly detection. As such, a series of simple parametric rules were designed to specifically detect the types of univariate anomalies listed in Table I. The basis of design of these rules was to allow them to be:

- Calibrated to a period of historical data for each sensor
- Tuned-in sensitivity, by the engineer, according to the nature of each sensor
- Specific to each kind of behaviour to provide a deeper level of insight
- Able to quantify the statistical severity of each anomaly with respect to the historical dataset.

Each of the following four rules works with respect to a historical reference data set, to derive statistical quantities to determine whether a behaviour is anomalous or not. The following notation will be used throughout the subsequent rule definitions.

The entire set of n data points, including the historical reference set, is denoted as X, as in equation [1]. The historical reference set of the first m points is denoted as R in equation [2], and the set of points on which to detect anomalies can be denoted as Z in equation [3].

$$X = \{x_1, x_2, \cdots, x_n\} \quad [1]$$

$$R = \{x_i : 1 \leq i \leq m\} \quad [2]$$

$$Z = \{x_i : m < i \leq n\} \quad [3]$$

Absolute step change – timeseries behaviour 1

This rule is designed to detect step changes that are large in magnitude with respect to the historical data set. An anomaly is detected when the absolute magnitude of the difference between two adjacent points is greater than some multiple α of the standard deviation of the historical data set. The set of anomalous points is thus defined as:

$$A = \{z_i \in Z : |z_i - z_{i-1}| \geq \alpha\sigma_R\} \quad [4]$$

Where σ_R is the sample standard deviation of the reference set R. The statistical significance of an anomaly can be quantified by its percentile in the distribution of differences across the entire data set.

This rule can be tuned to only identify significantly large step changes. An example of differentiating between step changes of different magnitudes is shown in Figure 4. In this example, the α parameter has been tuned to detect the step change at point 2 but ignore the step change at point 1.

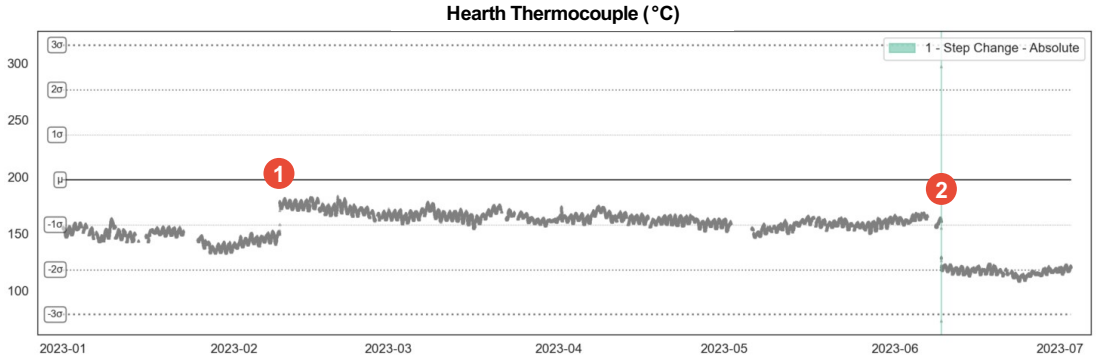


Figure 3. The absolute step change rule can be tuned to only detect significantly large step changes; the point-to-point difference at point 1 is below the threshold while the difference at point 2 is above the threshold. $\alpha = 0.5$.

Relative step change – timeseries behaviour 2

For step changes that are more subtle when compared to the historical variance of the sensor, anomalies can instead be detected by comparing the magnitude of the difference over several points to some multiple α of the average short-interval data range (with some window size a) over the recent past (some larger window size b).

The set of short-interval ranges can be defined as follows:

$$S = \{s_i = \max(x_{i-a}, x_{i-(a-1)}, \cdots, x_i) - \min(x_{i-a}, x_{i-(a-1)}, \cdots, x_i) : 1 \leq i \leq n\} \quad [5]$$

Anomalous points are then defined as follows:

$$A = \{z_i \in Z : |z_{i+3} - z_{i-3}| \geq \alpha \frac{1}{n} \sum_{j=i-b}^{i} s_j\} \quad [6]$$

In this case, the difference was chosen to be calculated over 3 points before and 3 points after the point being analysed, to best suit the nature of the data – step changes often happened over multiple points. This number could be adjusted as required. The statistical significance of an anomaly is given by the percentile in the distribution of short-interval ranges S.

The rationale behind this rule is to identify sudden jumps in data that are outside the normal variation, as measured by the average short-interval range. These may not be detectable using the absolute step change rule however, as such step changes might be small when compared to the standard deviation of the entire data set, especially if the variable exhibits significant drift over time. An example of this kind of step change being detected is shown in Figure 4.

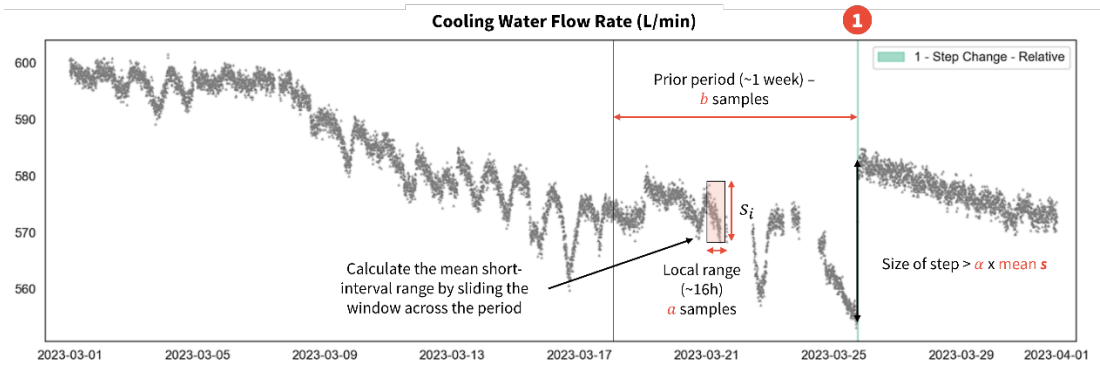


Figure 4. The relative step change rule can identify step changes, such as at point 1, that are within reason given the standard deviation of the entire data set, but large with respect to recent variation. α = 2.5, a = 16 hours, b = 168 hours.

Gradient – timeseries behaviours 3 and 4

This rule was designed to be versatile such that it can detect gradients over any period, by defining a window size parameter a. For each point being tested, a linear regression is applied across all data points that fall within one window size prior. The gradient of this regression line is then compared to a historical distribution of gradients (as calculated using the same method on the historical set). Any points with a gradient more than some multiple standard deviations α away from the mean of this gradient distribution are considered anomalous (and necessarily so is the whole window prior).

A set of gradients G can be computed at each point in the data set, using a least-squares regression function over the data in the window, denoted by f:

$$G = \{g_i = f(x_{i-a}, x_{i-(a-1)}, \cdots, x_i) : 1 \leq i \leq n\} \quad [7]$$

The mean and standard deviations of the historical set can be computed:

$$\mu = \frac{1}{m}\sum_{i=1}^{m} g_i \quad [8]$$

$$\sigma = \sqrt{\frac{1}{m-1}\sum_{i=1}^{m}(g_i - \mu)^2} \quad [9]$$

Giving the set of anomalous points as:

$$A = \{z_i \in Z : |g_i - \mu| \geq \alpha\sigma\} \quad [10]$$

The statistical significance of an anomaly can be given by the percentile in the distribution of gradients over the entire data set. An example of the gradient rule detecting significant rates of change in a thermocouple is given in Figure 5.

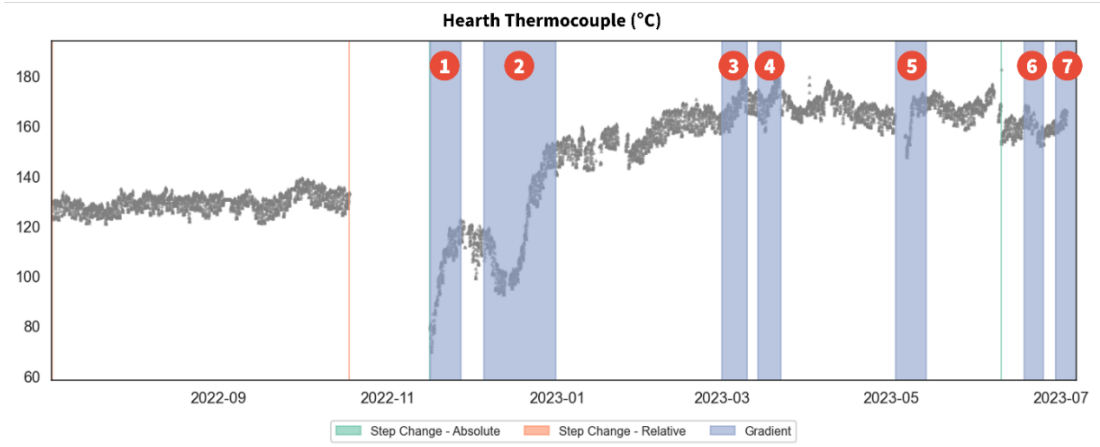


Figure 5. The gradient rule can detect both short and sustained trends. Anomaly 5 exhibits a short but high rate of change, in comparison to point 2 which shows a sustained period of downward and then upward temperature change. α = 1.5, a = 168 hours.

Spike – timeseries behaviour 5

Many signals undergo regular daily variation around their longer-term trend. For example, furnace temperature has a component that fluctuates with the daily rise and fall of the ambient temperature. An anomaly may be present when the magnitude of these fluctuations exceeds the usual distribution, for example due to excessive furnace temperature during the day.

In general, this rule is designed to detect abnormally large peaks or troughs in a signal and has parameters that can be adjusted to calibrate the sensitivity to peaks of various frequencies. It works by generating a distribution of the historical set of differences between two moving averages: one at some higher frequency and another at a lower frequency – for example several-hourly and weekly. The lower frequency moving average represents the longer-term trend, and the higher frequency moving average represents short-term fluctuations, either due to daily external causes or furnace dynamics. Anomalous points are defined as those differences more than α multiple standard deviations away from the mean of this difference distribution.

The set of differences can be defined as follows, with a window size a for the lower frequency and b for the higher frequency:

$$D = \{d_i = \left(\frac{1}{a}\sum_{j=i-\frac{a}{2}}^{i+\frac{a}{2}} x_i\right) - \left(\frac{1}{b}\sum_{j=i-\frac{b}{2}}^{i+\frac{b}{2}} x_i\right) : 1 \leq i \leq n\} \quad [11]$$

The mean and standard deviations of the historical set can be computed:

$$\mu = \frac{1}{m}\sum_{i=1}^{m} d_i \quad [12]$$

$$\sigma = \sqrt{\frac{1}{m-1}\sum_{i=1}^{m}(d_i - \mu)^2} \quad [13]$$

Giving the set of anomalous points as:

$$A = \{z_i \in Z : |d_i - \mu| \geq \alpha\sigma\} \quad [14]$$

The statistical significance of an anomaly can be quantified by the percentile in the distributions of differences over the entire data set. An example of the spike rule detecting transient conditions is shown in Figure 6.

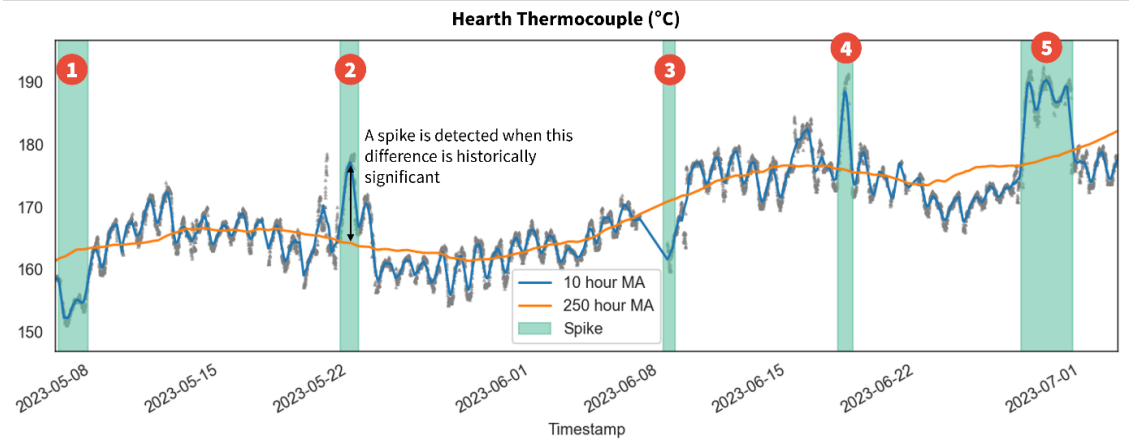


Figure 6. The 5 anomalies detected in this hearth thermocouple are examples of deviations away from the longer-term trend. The daily rise and fall in temperature driven by ambient temperature change is visible in the 10-hour moving average, and the longer-term trend visible in the 250-hour moving average. α = 2, a = 250 hours, b = 10 hours.

Multivariate anomaly detection methods

The following methods were employed to detect complex multivariate anomalies that are difficult to identify by manual inspection of the data. While these two rules are unable to specifically identify exact behaviours or the statistical severity of each anomaly, they are still trained on a historical reference set and can be calibrated in sensitivity by the engineer. The same notation applies as in equations [1], [2], and [3], however each point instead represents a vector of points at the same time index, across multiple sensors.

DBSCAN – timeseries behaviour 6

The clustering algorithm DBSCAN was tested as a method for identifying anomalies across sets of sensors, primarily arrays of thermocouples found on tapblocks, or hearth or refractory areas. DBSCAN aims to identify points as core, border or outlier points (Ester *et al.*, 1996). Core points have at least some minimum number of neighbouring points within a specified radius. Border points are within the minimum radius of a core point, but don't themselves have enough nearby neighbours. All other points are considered outlier points. An illustration of this algorithm is shown in Figure 7.

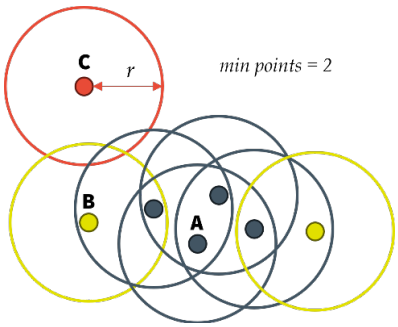


Figure 7. DBSCAN classifies points according to the number of neighbours within a given radius r. In this example, a point must have at least two neighbours to be considered a core point (e.g., A). Point B is a border point as it has one neighbour. Point C has no neighbours and is considered an outlier point.

In this case, DBSCAN is applied to the entire data set X, and any outlier points in the set Z are marked as anomalous. It has two parameters: r for the minimum radius and p for the minimum number of points. An example of this algorithm detecting a subtle outlier is shown in Figure 8. DBSCAN can detect subtle changes in an array of sensors by identifying a combination of conditions that has not been seen previously. While this may assist engineers in identifying a condition that is relatively undetectable otherwise, it may also result in false positive signals without detailed explanation as to what exactly has changed, simply due to that exact combination of normal conditions not having been seen prior.

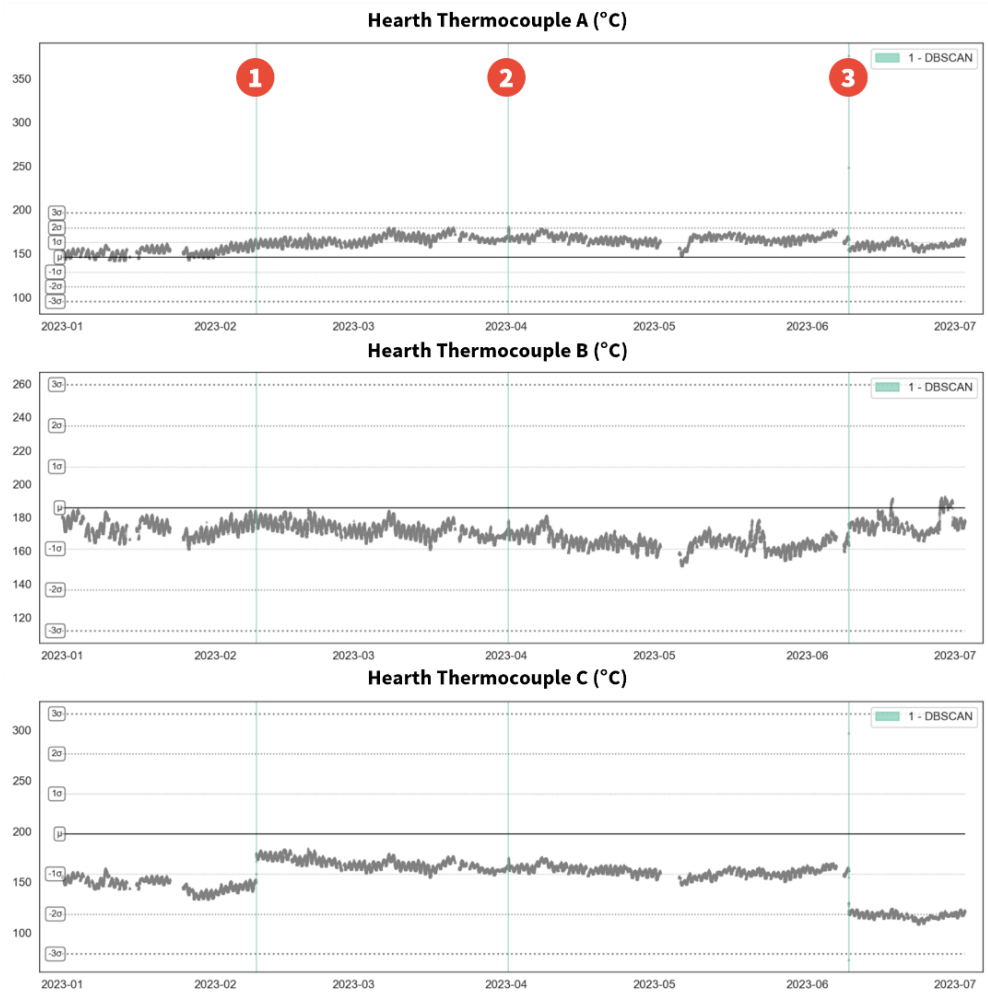


Figure 8. DBSCAN can detect the two step changes in thermocouple C (points 1 and 3) but importantly can also identify a small spike in temperature (point 2) that happens simultaneously across all three sensors.

Cosine similarity – timeseries behaviour 6

For certain conditions involving an array of sensors, the relationship between the values of each sensor is more important than the magnitude of each. In a multivariate sense, this means examining the direction of the vector representing the sensors, while ignoring the magnitude. Cosine similarity is a good measure of the similarity of two vectors that quantifies the cosine of the angle between them. A cosine value of 1 indicates the vectors have an identical direction, a value of zero represents orthogonal vectors, and a value of -1 indicates vectors in opposite directions. This method was applied to detecting anomalies by taking each vector of points in the set Z and calculating the cosine similarity between each point and all the vectors in the reference set R. Any vector for which the highest similarity value is below a minimum threshold α is considered an anomaly.

This rule was tested on an array of tapblock thermocouples, specifically aiming to identify a case of mismatched wiring across six thermocouples, in which A and D had been connected the wrong way. During a tapping event, the temperature of all six thermocouples rises synchronously, with the magnitude of each being dependent on the proximity to the molten metal. Without this rule, the switched wiring is difficult to detect manually as all six still rise as expected. The incorrect wiring being detected is shown in Figure 9.

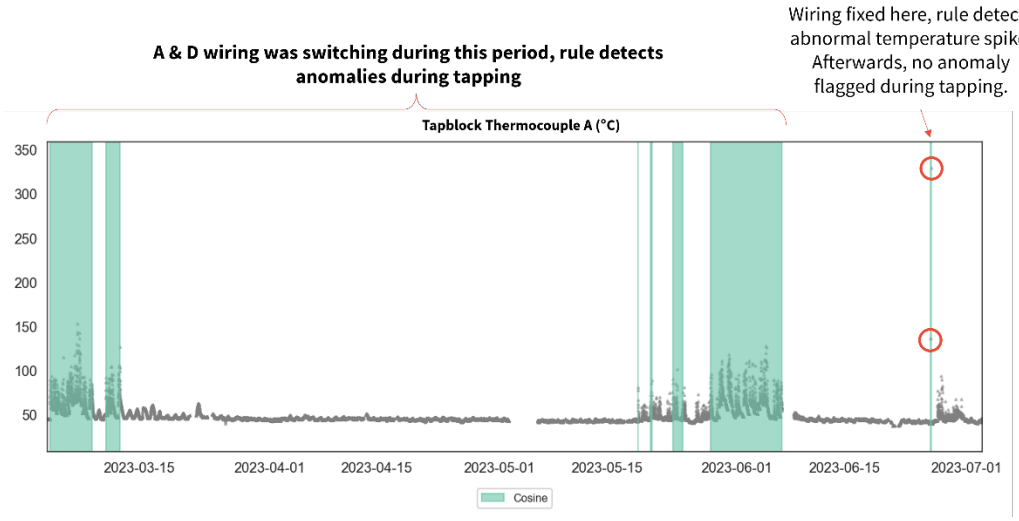


Figure 9. Cosine similarity can identify, during tapping events, that the relationship between the six thermocouples has changed due to the wiring of A & D being switched. After this is fixed, the rule no longer flags during tapping events.

RESULTS

Automatic Detection of Anomalies from Manual Reports

These rules were applied to a selection of 17 integrity monitoring sensors, over a four-month period. The historical reference period was set as two years of data prior. The aim was to automatically detect all manually-detected anomalies during this period. Parameters were selected individually per sensor group to maximally detect all manual anomalies. The results are shown in Table III. DBSCAN was not necessary to detect any of the manual anomalies during this period.

Table III. Results of using the anomaly detection rules in a four-month period of integrity data. 76% of manual anomalies were detected automatically using this method.

Sensor Group	Rules Used	Manual Anomalies	Manual Anomalies Detected Automatically	Anomalies not Detected Manually
Hearth temperature	Absolute step change, relative step change, gradient, spike	10	4	6
Binding movement	Absolute step change, relative step change, gradient	6	6	9
Cooling water flow rate	Absolute step change, relative step change, gradient, spike	1	1	5
Cooling water temperature	Spike	0	-	6
Sidewall temperature	Absolute step change, relative step change, gradient	2	2	10
Tapblock temperature	Cosine similarity	6	6	1
Total	-	*25*	*19 (76%)*	*37*

If one assumes the manual report is 100% accurate, this yields a precision score of 0.39, a recall score of 0.76, and an F1 score of 0.47.

Reporting Tool Prototype
To enable more efficient integrity management, the above algorithms were built into a prototype cloud-based application to automatically ingest site data, run anomaly detection daily, and assist the engineer in compiling a bi-weekly report for peer review. The following are some of the features of this prototype.

Operations technology integration
To enable regular integrity management and reporting, it was necessary to ingest data into the system daily. This gave the engineer the ability to review fewer anomalies daily, rather than reviewing two weeks of anomalies at once (a process that would typically take days). To enable the automatic daily detection, software was deployed on-site to integrate directly with the process historian and extract data to a cloud platform. This was done no more than once per day to avoid unnecessary overload on the historian.

Furnace hierarchy and sensor health
It is helpful to classify the furnace in a hierarchical structure, ranging from furnace area (e.g., hearth) to functions such as cooling systems, down to individual instruments. Anomalies detected on an instrument level could be aggregated into risk scenarios at the function or area level. Furthermore, sensor health could be quantified by identifying flatlining, excessive noise or out-of-range conditions, and health metrics could be cascaded up the hierarchy. This hierarchy was used to organise sensors within the application.

Contextualisation with related process conditions
To provide further context when reviewing anomalies and timeseries data, the application allowed the engineer to overlay related conditions such as feed rate or fuel rate. For example, excessive reaction shaft temperature could be compared to feed or fuel rate to provide a possible correlation. The application would also automatically exclude feed-off periods to avoid flagging unnecessary anomalies during these periods, as these periods would necessarily cause large drops in temperatures, for example.

Anomaly review, commentary and summary for reporting purposes
The application was based around a timeseries chart for each sensor, overlaid with any algorithmically detected anomalies. Each anomaly could be reviewed and either rejected or accepted with a category and commentary. This metadata was included alongside the timeseries data and flagged anomalies in an automatically-generated, comprehensive PDF document report for archiving and peer review with the wider site team. The commentary also allowed for previous anomalies to be surfaced in the application for use as context.

Manual anomaly addition
As these algorithms are unable to detect every integrity anomaly, the application also allowed the engineer to manually select and flag portions of the timeseries data as an anomaly, along with any categorisation or commentary, to be added to the report.

DISCUSSION

Algorithmic Accuracy
When compared to the manual reports, there were six anomalies present in the reports that the algorithms did not detect. On further investigation, five of these six gradient anomalies appeared to be significant when viewed on a two-week timescale but did not surpass the threshold of being 1.5σ away from the mean of the prior two years of week-long gradients. This result was verified by the integrity engineer. Taking into consideration these five anomalies improve the detection rate (recall score) to 95%.

There were also an additional 37 anomalies detected using the algorithms that were not detected in the manual reports. Whilst a notional precision score was noted at a relatively low value of 0.34, it was outside the scope of this paper to investigate the validity of these additional anomalies from an integrity

perspective, and therefore there is limited ability to draw a conclusion from this number. When these algorithms are used within the reporting tool, the integrity engineer is presented with the option to accept or reject any detected anomalies. It is preferential then for these algorithms to have a higher false alarm rate than to miss anomalies, as the engineer can simply reject any false positives. Comparatively, it is far more time consuming to manually identify any missed anomalies.

Parameter Tuning
These algorithms were designed to be manually tuneable in sensitivity within the reporting tool, both by enabling or disabling specific rules per sensor, and by adjusting the rule parameters per sensor. This was done to enable the integrity engineer to adjust and improve the detection performance over time using specific domain expertise. For this reason, at this stage there is no analysis of the sensitivity of the algorithms to their parameter selection, or of any tuning processes.

Limitations
Whilst the manual parameter tuning process enables fine control of the system, it adds a new dimension of time input required for furnace integrity management. However, at this stage this system is simply intended to lay the foundation for more streamlined anomaly detection and integrity management, and in future the learnings from such tuning would be incorporated into the algorithm design. It would also be worth investigating methods for automatically tuning the sensitivity of the rules based on the feedback from the accepted and rejected anomalies.

Choosing rules specifically to match human-detected behaviour overlooks the possibility of more nuanced anomalies being detected. The two non-parametric rules, DBSCAN and Cosine ssimilarity, aim to make progress in identifying more complex behaviours. However, it would be worth investigating the applicability of more advanced machine learning methods that can identify any kind of anomalous condition based on prior patterns, to supplement these simple rules.

CONCLUSION

The developed rules, in conjunction with the reporting tool prototype, were shown to successfully function as a replacement for manual anomaly detection over this specific four-month period. This is on the basis that, notionally, 95% of significant anomalies could be detected automatically. With the understanding that the manual reports themselves contain human error, a more detailed analysis must be done to effectively evaluate the precision and F1 score of these algorithms. At this stage, these algorithms do not function as a direct replacement for the expertise of an integrity engineer, but rather as a tool to streamline the integrity management process. The ability to automatically detect, classify and quantify the statistical significance of anomalies in several hundred sensors lays the foundation for an improved and more efficient integrity management regime, reducing the time required for integrity risk management. Future work should focus on comparing the algorithms to other kinds of statistical process control and advanced machine learning methods for timeseries anomaly detection.

REFERENCES

Ankerst, M., Breunig, M.M., Kriegel, H.-P. and Sander, J. (1999) 'OPTICS: ordering points to identify the clustering structure.' *Proceedings of the 1999 ACM SIGMOD International Conference on Management of Data*. New York, NY, USA Association for Computing Machinery, pp.49–60.

Ester, M., Kriegel, H.-P., Sander, J. and Xu, X. (1996) 'A density-based algorithm for discovering clusters in large spatial databases with noise.' *Proceedings of the Second International Conference on Knowledge Discovery and Data Mining*. Portland AAAI Press, pp.226–31.

Neloy, A.A. and Turgeon, M. (2024) 'A comprehensive study of auto-encoders for anomaly detection: Efficiency and trade-offs', *Machine Learning with Applications*, 17, p.100572. Available at: https://www.sciencedirect.com/science/article/pii/S2666827024000483.

Nelson, L.S. (1984) 'The Shewhart Control Chart—Tests for Special Causes', *Journal of Quality Technology*, 16, pp.237–39. Available at: https://doi.org/10.1080/00224065.1984.11978921 .

Sadri, A., Cramer, M. and Ying, W.L.W. (2023) 'Predictive Furnace Refractory Maintenance Procedures to Extend Campaign Life and Reduce Waste.' *Proceedings of the 61st Conference of Metallurgists, COM 2022*. Cham Springer International Publishing, pp.175–92.



Thessy Moodley
Regional Director - Digital
Hatch

Thessy Moodley brings 18 years of post-qualification experience as a digital transformation consultant, control and instrumentation engineer in various industries such as pulp and paper, bulk materials handling, oil and gas, and smelting industries through all asset phases including early engineering, execution, commissioning, start up and optimisation. His working experience has spanned projects and leadership roles in South Africa, Norway, Guatemala, Australia and the United Arab Emirates.

Under his leadership, as Regional Director for Digital in Africa, Europe and the Middle East, Hatch's Digital team in the region has grown from inception to execute Industry 4.0 based projects in optimisation, advanced planning and scheduling, digital value chains, integrated operations, artificial intelligence and digital twins for the metals, energy and infrastructure sectors. Thessy holds a Master's Degree in Control Engineering.

Comparison of technical operating flexibility and operating cost performance at selected underground platinum mines for long-term operational viability

B.M. Grobbelaar[1], C. Musingwini[2], L.J. Mohloki[2], B. Mutandwa[2]

[1]Anglo-American Platinum Joint Venture Operations (now Valterra Platinum), South Africa
[2]University of the Witwatersrand, South Africa

Technical operating flexibility is a performance metric that is measured using a Flexibility Index (FI). Its analysis is undertaken in support of long-term operational viability through consideration of practices aimed at improving operating cost performance. This metric is important particularly in an ever-changing business operating environment. For example, the business operating environment for platinum mining has experienced relatively depressed platinum prices post-2008, leading to some platinum group metal (PGM) mines being downsized or placed on *'care-and-maintenance'*. Anglo-American Platinum (now Valterra Platinum) uses 'Immediately Mineable Stopes (IMS)' as a proxy for FI. IMS is extended to Immediately Available or $FI_{_extended}$. This paper uses selected underground PGM mines to demonstrate that technical operating flexibility affects operating cost performance. The influence of type of mining method on technical operating flexibility is also evaluated. The paper recommends some practices for improving levels of technical operating flexibility to improve operating cost performance for long-term operational viability of PGM mines.

INTRODUCTION

Technical operating flexibility, which is measured using a Flexibility Index (FI), is an important mine planning metric because it indicates the ability of a mining operation to adjust, adapt or respond to changes in the business operating environment (Musingwini *et al.*, 2007). Changes must be made when operating conditions change, to ensure long-term operational viability. For example, when geological features such as unexpected potholes, faults, sills and dykes are encountered in production panels to be mined, mining plans must change so that these geological features can be negotiated for safety reasons or to minimise dilution. Changes must also be made to respond to changes in the business operating environment such as when prolonged commodity price movements are experienced or restructuring of company ownership occurs. A recent example of change of ownership is that of Anglo-American Platinum (Amplats), which is a South African platinum mining company that demerged from Anglo-American on the 28th of May 2025 and began trading as Valterra Platinum on the Johannesburg Stock Exchange. Such a change can affect the business operating environment for the company because changes in ownership can also bring concomitant changes in work culture. These changes reflect inherent geological, economic, market and operational uncertainty associated with mining operations. Therefore, flexible mine plans are desirable because they can easily adapt to changes in the business operating environment. Accordingly, it is important to analyse mine plans, so that the long-term operational viability of the mining operations can be achieved. Such analysis includes analysing how technical operating flexibility affects the ability of a mining operation to meet its production targets and expected cost performance.

The operating cost performance of a mining operation as indicated by its position on its respective industry cost curve, is a proxy for profitability and long-term operational viability. This is because when commodity prices fall, mining operations within the 1st quartile (Q1) of the industry cost curve are more likely to remain profitable compared to mines positioned in the 4th quartile (Q4) of the industry cost curve, which may become unprofitable. If commodity prices remain relatively depressed, then unprofitable mines in Q4 of the industry cost curve sometimes end up being downsized or placed on '*care-and-maintenance*' if the downsizing fails to curtail costs. However, profitability can also be affected by other factors such as the product mix of polymetallic mines as is the case with platinum group metal (PGM) mines, and black swan events like fatal accidents that force mines to halt production while remedying causes of the accident, until the mining inspectorate is satisfied that it is safe to resume production operations.

TECHNICAL OPERATING FLEXIBILITY IN A PGM MINING CONTEXT

An operating mining company generally has two types of flexibility; namely strategic flexibility and technical operating flexibility (Musingwini *et al.*, 2007). At a strategic mine planning level, strategic mine planning options are evaluated so that the best option which aligns with the most probable long-term planning scenario from among several different scenarios is selected. Strategic or corporate-level flexibility ensures that the required return on investment for shareholders can be achieved at an acceptable level of risk. Strategic flexibility has synonymously been referred to as 'managerial flexibility' within the discipline of real options analysis (Kajner and Sparks, 1992; Samis and Poulin, 1998; Davis, 1998; Dapena and Fidalgo, 2003; Kazakidis and Scoble, 2003). Accordingly, Kazakidis and Scoble (2003) introduced a flexibility index, F, as a metric to measure managerial flexibility as indicated in Equation 1.

$$F = \frac{OV}{NPV\ passive\ (base\ case)}\ x\ 100 \qquad \text{Equation 1}$$

where option value (OV), which must be greater than zero, is the option value or the additional net present value (NPV) over the passive (or base case) NPV for the mining project. The OV would be the value that is derived when one of the alternatives created by introducing flexibility is exercised to reduce risk associated with the project. However, additional costs will be incurred upfront to create the options (or alternatives) and these costs must be borne by the project, hence it is imperative that one of the flexible options must be exercised to benefit from investing in creating options.

At an operational level, choice decisions must be made to minimise deviations from planned targets such as planned grades, tonnages, and equipment allocations. Technical operating flexibility is required to swiftly relocate mining operations to different production faces or stopes when technical issues such as grade control or unforeseen geological structures are encountered during mining operations. Accordingly, Musingwini *et al.*, (2007) proposed that technical operating flexibility in a mining context should be measured using an FI as indicated in Equation 2.

$$FI = \frac{Available\ fully\ equipped\ alternative\ stopes\ +\ Stopes\ already\ in\ production}{Stopes\ required\ to\ meet\ planned\ production}\ x\ 100$$

Equation 2

This definition assumes that fully equipped stopes have already been developed, ledged, and equipped and are close to the working stopes so that no production shift is lost when relocating production crews to the available alternative stopes. The interpretation of FI as defined in Equation 2 implies the following for a mining operation:

- If $FI > 100\%$, operating flexibility is adequate, and the mining operation is operationally flexible.

- If *FI* =100%, the operation has break-even operating flexibility because any loss of production stopes or production panels due to unforeseen conditions causes the operation to slip into a situation of inadequate or no flexibility at all.
- If *FI* < 100%, the operation has inadequate operating flexibility since fewer stopes are available than are required to meet the planned production rate. Under this condition, the net cash flows of the project are often negative, forcing management to temporarily close the mining operation (i.e., put it under *'care-and-maintenance'*) and only resume operations when operating and/or economic conditions have improved.

Some examples of studies that have considered flexibility as articulated by Kazakidis and Scoble (2003) and/or Musingwini *et al.,* (2007) include Elkington (2012), Botin *et al.,* (2013), Chibaya (2013), del Castillo (2014), Haque *et al.,* (2014), Savolainen (2016), Ali and Quasir Rafique (2024) and Jetmore and Roos (2025). These studies amplify the importance of analysing strategic (or managerial) flexibility and technical operating flexibility for mining projects and operations.

Whatever adaptation is made, whether on strategic or operating flexibility, the operating cost performance is affected, further impacting the profitability of the mining operation. Therefore, it is necessary to measure technical operating flexibility. This paper focuses on technical operating flexibility with a focus on selected underground PGM mines as case study examples. The term 'Immediately Mineable Stopes (IMS)' is used in the underground PGM narrow reef mining environment as a proxy for FI. IMS is an indicator of the portion of Ore Reserves that has been completely developed and equipped and is ready for mining and is called Developed Ore Reserves (DOR). IMS has been extended into $FI_{extended}$ as another measure of technical operating flexibility called 'Immediately Available (IMA)' stopes. For example, Andersen (2010) indicated that in Anglo-American Platinum (now Valterra Platinum), IMS is classified as the portion of Proved Ore Reserve that can be mined at full production without requiring further development and equipping work to be undertaken such as ledging, equipping, ventilation, and other essential services. IMS is calculated as shown in Equation 3.

$$IMS = \frac{Equipped\ Panels\ Ready\ to\ Mine\ +\ Current\ Equipped\ Panels\ Being\ Mined}{Equipped\ Panels\ Planned\ to\ be\ Mined}$$

Equation 3

Between 2010 to about 2019, the norm for most underground PGM narrow reef mining operations has been to set a target IMS ratio of about 1.5. In the post-2019 period, the IMS framework was extended to the IMA framework, which is a form of an $FI_{extended}$ that includes DOR. DOR is assumed to be achieved when a ledged production panel has associated raise lines that have holed but have not yet been equipped. IMA (or $FI_{extended}$) is calculated using Equation 4.

$$IMA = \frac{[DOR\ (Raise\ Line\ Holed\ and\ Ledged)\ +\ IMS\ (Equipped\ Panels\ Ready\ to\ Mine\ +\ Current\ Equipped\ Panels\ Being\ Mined)]}{Equipped\ Panels\ Planned\ to\ be\ Mined}$$

Equation 4

Post-2020, the norm for most underground PGM narrow reef mining operations has been to set a target IMA (or $FI_{extended}$) ratio of about 2; IMA is regarded to be a good indicator of how well a PGM mining operation is achieving its primary development, with IMA equal to or greater than 2 indicating good progress on primary development.

Underground platinum mining was selected to illustrate the concept of technical operating flexibility for two main reasons. Firstly, the platinum mining industry has experienced operational turmoil post-2008 due to declining platinum prices (Figure 1), which caused financial pressure squeezes on platinum mining operations.

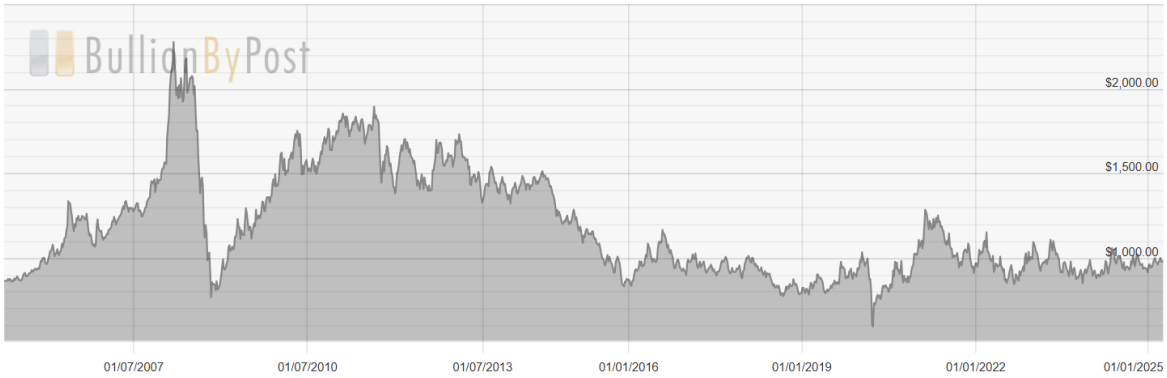


Figure 1: A 20-year platinum price trend (Source: BullionByPost, 2025).

Prior to 2008, platinum price had increased over a 10-year period from about US$380/oz in 1997 to about US$2,200/oz in 2008. In response to the growth in platinum prices, most mines embarked on expansion projects which then led to oversupply, thus, causing the platinum price to decline. As Figure 1 indicates, platinum price had reached a peak of about US$2,200/oz in 2008 but dropped sharply thereafter to below US$1,000/oz despite experiencing a temporary recovery around 2012 and has since remained relatively depressed to date. This challenge requires in-depth analysis of the financial performance of mining operations to be undertaken, such as the study undertaken by Moodley (2013) to estimate the position of Modikwa platinum mine on the industry cost curve of Southern African platinum mines (Figure 2). Figure 2 shows that the Modikwa Joint Venture (JV) (one of the selected platinum mines in this paper) was in Q4 of the industry cost curve in 2012 (i.e., it was within 75% to 100% of all the mines). Figure 2 also shows that Bafokeng Rasimone Platinum Mine (BRPM) JV and Mototolo JV (the other two selected platinum mines in this paper) were in Q1 (i.e., within 25% of all the mines).

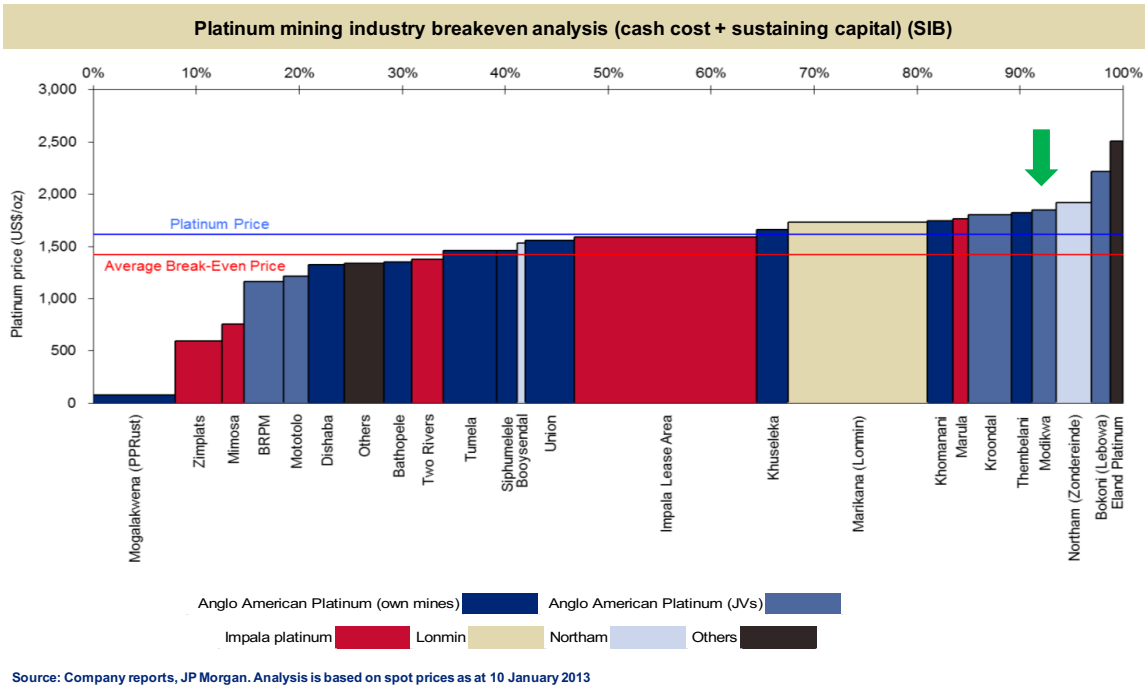


Figure 2: Industry cost curve analysis of PGM mines in Southern Africa in 2012 (Source: Moodley, 2013).

Moodley (2013) pointed out that the platinum mining industry in Southern Africa had, during post-2008, witnessed a reduction in the mining project pipeline. This was due to mining companies preferring to reapportion resources away from platinum mining operations with cash costs falling within the 3rd quartile (Q3) and Q4 of the industry cost curve to more profitable operations with cash costs sitting below the average break-even price.

The second reason for selecting underground platinum mining operations to illustrate the concept of technical operating flexibility is that the first author of this paper works for a platinum mining company and has direct access to operational data. This author was also able to provide company internal reasoning behind some of the decisions taken to improve technical operating flexibility.

This paper defines technical operating flexibility, its measurement and importance. Logically, a relationship should exist between technical operating flexibility and a mining operation's cost performance, hence this paper compares technical operating flexibility and cost performance at selected underground platinum mines in South Africa. Conclusions were then made based on the comparisons and recommendations made on how such analysis can assist mining operations in ensuring long-term profitability and viability.

PLATINUM MINES SELECTED FOR ANALYSIS

The classification system of narrow reef tabular underground platinum mines by mining method in Valterra Platinum managed and JV operations, is generally in any of the following three broad categories:

- Trackless mobile mining method (TMM or TM^3) with bord-and-pillar (B&P) configuration.
- Conventional track-bound mining.
- Hybrid mining.

The category of mining method has an impact on how well the mining operation can generate adequate operating flexibility to support high production efficiencies. However, the operating flexibility can also be affected as ground conditions change. FI can improve when mining operations are going through good ground conditions or can drop if mining operations are going through bad ground conditions. In the case of Mototolo JV which has intentionally and consistently maintained high levels of technical operating flexibility, FI has been relatively high despite the mine occasionally mining through geotechnically challenging ground conditions. Three mines namely, BRPM JV (conventional), Mototolo JV (B&P) and Modikwa JV (hybrid) were selected for comparison as they cover all three mining method categories, and all had readily available FI data for comparison and appeared in the industry cost curves obtained. Since the mines are characteristically narrow reef tabular underground platinum mines, the production is typically measured in square metres (m^2) or centares of stope or panel production face advanced during the period of measurement, typically monthly.

COMPARATIVE ANALYSIS OF TECHNICAL OPERATING FLEXIBILITY AND COST PERFORMANCE FOR THE SELECTED MINES

The selected mines were compared by category of mining method based on FI or FI calculated using Equation 2 and their relative positions on industry cost curves. The target business plan (BP) FI is 1.50. Table I presents a comparison of 3-year (2010-2012) average FIs. The next sub-sections discuss observations and inferences that could be drawn from Figure 2 and Table I.

Table I: Comparison of 3-year average Flexibility Index values for the three selected mines (2010-2012)

Mine	Mototolo JV (TM^3)	BRPM JV (Conventional)	Modikwa JV (Hybrid)
Flexibility Index (FI)	1.39	1.32	1.11
FI Status	FI>1	FI>1	FI~1

TM^3 Category

The mine in the TM^3 category had the highest technical operating flexibility compared to conventional and hybrid mining methods. This is attributable to the fact that it is often easier to build flexibility in mechanised bord-and-pillar operations compared to the other mining methods. Building flexibility is easier because multiple mining faces are created since the TM^3 method involves driving parallel roadways (bords) and leaving support pillars between bords, hence creating multiple extraction faces along the roadways. The flexibility is enhanced because the multiple extraction faces can be mined simultaneously, thus creating options for production faces. This higher flexibility translates into meeting the required key performance indicators of the BP such as volumes blasted and tonnes hoisted. Achieving higher volumes further translates into better production efficiencies and delivery of bottom-line results, thus, placing Mototolo JV in Q1 of the cost curve (Figure 2).

Conventional Mining Category

The conventional (track-bound) mining method has slightly lower flexibility than TM^3 due to its technical limitations. The limitations are due factors such as logistical challenges associated with constrained equipment movement which limits the number of production faces that can be cleaned at any time. Another example of a technical limitation factor is the inherent potential inefficiencies arising from the traditional layouts associated with the type of mining and challenges associated with ensuring safety by balancing production face advance rate with hanging wall stability. These limitations result in a lower flexibility index, often leading to fewer volumes being blasted and fewer tonnes hoisted, thus translating to lower bottom-line results. Despite these technical limitations, BRPM JV was within Q1, due to the concerted effort made at BRPM JV from the board level down to the operating level in early 2012 to improve technical operating flexibility (or IMS). Actions that were initiated and carried out at BRPM JV to increase its technical operating flexibility include the following:

- IMS governance structures and monitoring processes such as IMS audits, monthly IMS reports, and monthly IMS meetings were established.
- Pre-development was given greater focus in areas with geologically challenging ground conditions.
- Additional ledging and equipping resources were made available to increase the panel conversion rate to IMS.
- The board reviewed the IMS status quarterly.
- Senior executives were held accountable for the IMS status of the organisation.

Table II illustrates the progressive impact of the cocktail of actions listed above, on the flexibility index or IMS. The month-to-month progession for 2012 indicates that the impact was positive as IMS generally improved from about 1.00 in January 2012 to about 1.48 in December 2012. The December 2012 IMS was very close to the BP target of 1.50 for IMS.

Table II: March 2013 presentation on BRPM Ore Reserves and IMS status (Source: BRPM, 2013)

Description	Unit	Target	2012											
			Jan	Feb	Mar	Apr	May	Jun	Jul	Aug	Sep	Oct	Nov	Dec
IMA Life in Months	Months	28	23.9	23.9	23.3	24.6	24.8	23.6	24.8	26.2	26.0	26.8	25.6	25.6
IMS Life in Months	Months	7	4.9	5.5	5.1	6.0	6.3	5.8	6.3	6.8	7.5	7.8	8.2	8.5
Panel Teams	no.	120	112	112	114	109	112	112	117	118	115	113	114	115
IMS Panel Ratio	ratio	1.5	1.00	1.08	1.02	1.08	1.20	1.12	1.16	1.22	1.36	1.45	1.44	1.48
IMS panels available	no.	180	112	121	116	118	134	125	136	144	156	164	164	170
IMS Face Length available	m	5962	3669	4048	3865	3937	4490	4163	4528	4786	5249	5549	5524	5712

Hybrid Mining Category

Modikwa JV, which is at the tail-end of the cost curve (i.e., within Q4), had all-in sustaining costs (AISC) per platinum ounce (oz) produced that exceeded the basket price, thus rendering the operation financially unsustainable. Its operating flexibility was close to break-even FI, and the implication of this level of operating flexibility is that when unexpected challenging geological conditions are encountered during mining, it becomes difficult to easily relocate production teams from affected areas resulting in lower production volumes. Hybrid mining is meant to overcome the shortcomings of conventional and B&P mining, while capitalising on their strengths. However, in practice having two different mining methods to work in unison can also create challenges related to inadequate synergy. This is seen in the case of Modikwa JV.

MORE RECENT COMPARATIVE ANALYSIS OF THE THREE SELECTED MINES

From the preceding comparison, it was necessary to further compare how the mines have performed given that some changes have happened post-2012 and some recent data for the 5-year period (2020-2024), has become available. This period includes the period 2020-2022 when the world suffered from the impacts of the global COVID-19 pandemic which peaked in 2021 and started to show signs of tailing off in 2022. In 2018, Anglo-American Platinum (now Valterra Platinum) increased its ownership of the Mototolo JV from 50% to 100% (Mining Technology, 2018). The BRPM JV was run by Anglo-American Platinum (now Valterra Platinum) and Royal Bafokeng Platinum (RBPlat) until 2018 when RBPlat became the sole owner of the BRPM JV (Impala Bafokeng, 2024). Later in 2023, RBPlat was acquired by Impala Platinum and became Impala Bafokeng, a wholly owned subsidiary of Impala Platinum (Impala Bafokeng, 2024). Such changes in the ownership structure of operations can impact work culture as operations must adjust to the new corporate culture of the controlling entity. Changes in work culture can impact the overall cost performance of an operation resulting in a change of its position on the industry cost curve. For example, this can be seen in with Mototolo JV which maintained its Q1 position from 2012 (Figure 1) to 2021 (Figure 3) but dropped slightly to the 2nd quartile (Q2) in 2024 (Figure 4). Over the same period, BRPM JV moved down from Q1 (Figure 1) in 2012 to Q3 (Figure 3) in 2021 but rolled back to Q1 in 2024 (Figure 4). Over the same period Modikwa JV remained among the high-cost producers as it moved from Q4 in 2012 (Figure 1), to Q2 in 2021 (Figure 3) and Q3 in 2024 (Figure 4).

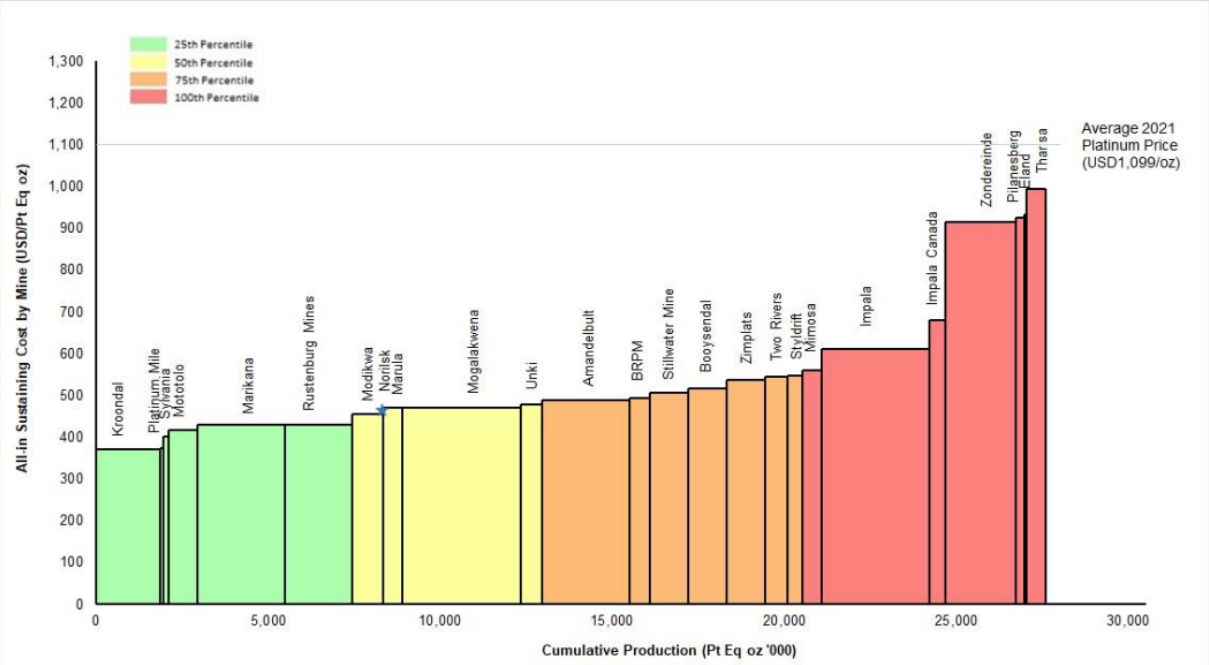


Figure 3: Industry AISC cost curve analysis of PGM mines in 2021 (Source: Minxcon (2023).

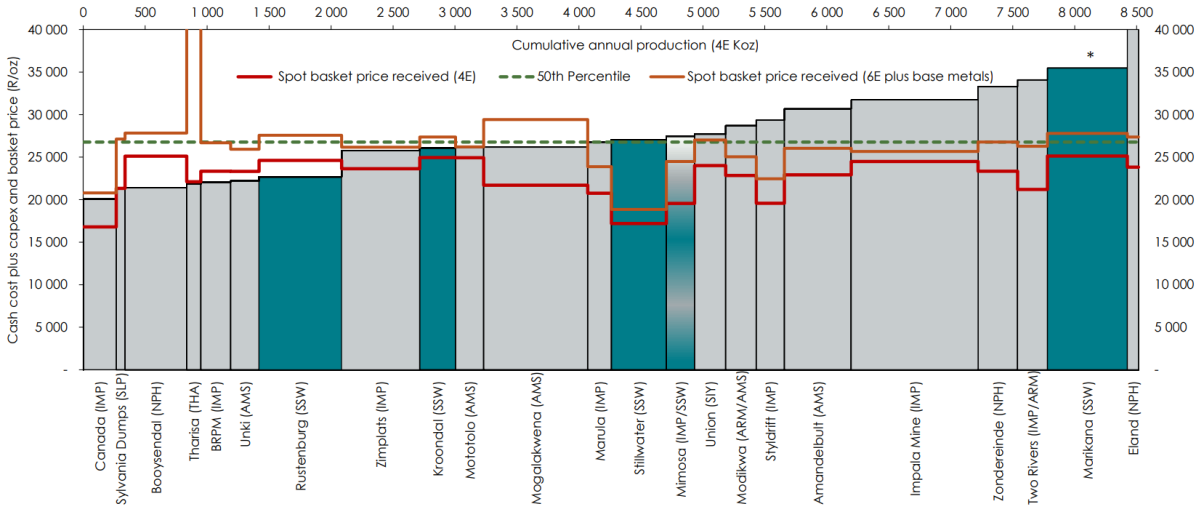


Figure 4: Industry AISC cost curve analysis of PGM mines in 2024 (Source: Sibanye-Stillwater (2024).

Table III shows the IMS and IMA data for the three selected mines for the 5-year period (2020-2024). The data for BRPM JV could not be obtained as the operation became a wholly owned subsidiary of Impala Platinum post 2018 as explained earlier.

Table III: Comparison of Flexibility Index values for the three selected mines for 2020-2024

Year		2020	2021	2022	2023	2024
Mototolo JV (B&P)	**IMS**	2.57	0.27	0.26	0.81	1.71
	IMA	1.59	0.96	1.24	1.70	1.99
BRPM JV (Conventional)		N/A	N/A	N/A	N/A	N/A
Modikwa JV (Hybrid)	**IMS**	0.48	0.32	0.28	0.30	0.20
	IMA	2.57	2.05	1.69	1.34	1.09

Mototolo JV is accessed by two decline shafts which are the Lebowa shaft on the northern side of the mining area and Borwa shaft on the southern side. By 2020, mining in the Lebowa shaft had come to the end of its life as it approached the St. George's fault. An agreement for a ground swap with Two Rivers Platinum was concluded to extend the life of Lebowa shaft. Secondly, Borwa shaft was extended. Combined with additional Ore Reserves, there was a subsequent drive to improve efficiencies using dashboards to track Overall Equipment Effectiveness for the TM³ fleets as part of driving improvement in IMA. These actions increased the operating flexibility as observed in Table III; hence, the improvement in IMA from 2021 to 2024. The change for Mototolo JV from being a joint venture with limited overhead costs to become a fully managed operation under Anglo-American Platinum (now Valterra Platinum) in 2020 came with the addition of group overhead costs, hence, Mototolo JV changed from Q1 to Q2 of the industry cost curve as indicated by Figures 3 and 4. The recent demerger of Anglo-American Platinum from Anglo-American to become Valterra Platinum, is likely to have a positive impact in reducing operating costs due to lowered overhead costs from a new company structure.

During COVID-19, most mines were placed on 50% operating capacity to try and mitigate the effects of the pandemic. During that period, Modikwa JV implemented a form of modified cycle mining, with some crews remaining as normal crews per single panel. This approach enabled Modikwa JV to realise some increases in crew efficiency during that period, hence it improved its position on the industry cost curve as shown in Figure 4. Looking at Table III, it can be observed that Modikwa JV experienced a steady decline in both IMS and IMA from 2020 to 2024. Consequently, some interventions were made to correct this trend, and these included the introduction of a contractor to accelerate development. Modikwa JV has now developed a new strategy to increase its operating flexibility by maintaining production teams at current levels for the next three years, while accelerating TM³ development through infrastructure upgrades and new fleets to replace ageing TM³ fleets and accelerate development.

CONCLUSIONS AND RECOMMENDATIONS

The following conclusions can be drawn from the comparative analysis of the selected underground platinum mines:

- Technical operating flexibility is tacitly implied in the IMS definition.
- Technical operating flexibility affects a mining operation's position on the industry cost curve.
- Technical operating flexibility is affected by the mining method in use at a mining operation. In the case of underground PGM mining, TM³ tends to have the highest technical operating flexibility, followed by conventional (track-bound) mining and lastly, the hybrid mining method.
- Operations that set technical operating flexibility targets and implement governance structures and processes to achieve it (e.g., BRPM JV and Mototolo JV), tend to achieve better operating cost performance.

Based on this paper's findings, the following recommendations can be made to ensure that the levels of technical operating flexibility can be achieved, and operating cost performance can be improved to maintain long-term operational viability:

- Understand and recognise the significance of technical operating flexibility.
- Continually audit or monitor levels of IMS and IMA and keep track of corresponding positions of the mining operation on the industry cost curve relative to the IMS and/or IMA.
- Establish governance structures at executive and operational levels to drive the implementation of actions to achieve desired levels of operating flexibility.
- Achieving and maintaining operating flexibility targets must be non-negotiable and carry a higher weighting within the performance contracts for managers and executives.

ACKNOWLEDGEMENTS

The authors are grateful to Anglo-American Platinum (now Valterra Platinum) for providing access to their historical data which was used for analysis in the work reported in this paper. The financial support provided by the School of Mining Engineering, University of the Witwatersrand, to enable the authors to present this paper at the SAIMM *9th International PGM Conference*, is also gratefully acknowledged.

REFERENCES

Ali, M. A. and Quasir Rafique, Q., 2024. Strategic Integration of Real Options for Enhanced Valuation and Optimization in Mining Project Planning under Uncertainty: A Comprehensive Review, *International Journal of Project Management*, Vol. 6, No. 2, pp. 26–50.

Andersen, D., 2010. Mining Operational and Reporting Standard Definition, Anglo-American Platinum Group Standard, Anglo-American Platinum Company Internal Document Ver. 3, Aug. 2010.

Bafokeng Rasimone Platinum Mine (BRPM) Joint Venture (JV), 2013. IMS Presentation 2012, Boschkoppie, Mar. 20, 2013, Anglo-American Platinum Company Internal Document.

Botin, J., del Castillo, M. F. and Guzman, R., 2013. A real options application to manage risk related to intrinsic variables of a mine plan: a case study on Chuquicamata Underground Mine Project, *The Journal of the Southern African Institute of Mining and Metallurgy*, Vol. 113, No. 7, pp. 583–592.

BullionByPost, 2025. 20 Year Platinum Price History in US Dollars per Ounce. [Online]. Available from: https://www.bullionbypost.co.uk/platinum-price/20-year-platinum-price-history-dollars-ounce/. [Accessed: 10-Jul-2025].

Chibaya, A., 2013. Geometallurgical Analysis - Implications on Operating Flexibility (A Case for Geometallurgy for Orapa A/K1 deposit), *MSc Research Report*, University of the Witwatersrand, Johannesburg, South Africa, 2013.

Dapena, J. P. and Fidalgo, S., 2003. A real options approach to tender offers and acquisitions processes, [Online]. Available from: http://www.realoptions.org/papers2003/DapenaDoctrabapproach.pdf. [Accessed: 31-Mar-2006].

Davis, G. A., 1998. One project, two discount rates, *Mining Engineering*, Apr. 1998, pp. 70–74.

del Castillo, M. F., 2014. Effects of Price and Geological Uncertainty over the Life of Mine and Ultimate Pit Limit, *MEng Thesis*, McGill University, Canada, 2014.

Elkington, T., 2012. Real Option Value Optimisation, in *Project Evaluation Conference, Melbourne*: The Australasian Institute of Mining and Metallurgy, 2012, pp. 35–40.

Haque, Md. A., Topal, E. and Lilford, E., 2014. A numerical study for a mining project using real options valuation under commodity price uncertainty, *Resources Policy*, Vol. 39, pp. 115–123, Mar. 2014, DOI: 10.1016/j.resourpol.2013.12.004.

Impala Bafokeng, 2024. Fact Sheet Jan. 2024. [Online]. Available: https://www.implats.co.za/pdf/fact-sheets/2024/fact-sheet-impala-bafokeng.pdf. [Accessed: 10-Jul-2025].

Jetmore, K. and Roos, C., 2025. Strategic Underground Mine Planning Through Nested Stopes And Constraint-based Scheduling, in *SME Annual Meeting, 2022*. [Online]. Available from: https://onetunnel.org/documents/strategic-underground-mine-planning-through-nested-stopes-and-constraint-based-scheduling-sme-annual-meeting. [Accessed: 09-Jul-2025].

Kajner, L. and Sparks, G., 1992. Quantifying the value of flexibility when conducting stochastic mine investment analysis, *CIM Bulletin*, Vol. 85, No. 964, pp. 68–71, 1992.

Kazakidis, V. N. and Scoble, M., 2003. Planning for flexibility in underground mine production systems, *Mining Engineering*, Vol. 55, No. 8, pp. 33–39, Aug. 2003.

Mining Technology, 2018. Anglo-American Platinum increases stake in Mototolo JV to 100%, Nov. 5, 2018. [Online]. Aavilable from: https://www.mining-technology.com/news/anglo-american-platinum-mototolo-jv/?cf-view&cf-closed. [Accessed: 10-Jul-2025].

Minxcon, 2023. Platinum cost curves Apr. 2023. [Online]. Available: https://www.minxcon.co.za/wp-content/uploads/2023/04/Platinum-cost-curves-April-2023-4.pdf. [Accessed: 08-Jul-2025].

Moodley, A., 2013. Modikwa Performance Letter, Jan. 2013. Anglo-American Platinum Company Internal Document.

Musingwini, C., Minnitt, R. C. A. and Woodhall, M., 2007. Technical operating flexibility in the analysis of mine layouts and schedules, *The Journal of the Southern African Institute of Mining and Metallurgy*, Vol. 107, No. 2, Feb. 2007, pp. 129–136.

Samis, M. and Poulin, R., 1998. Valuing management flexibility: a basis to compare the standard DCF and MAP valuation frameworks, *CIM Bulletin*, Vol. 91, No. 1019, pp. 69–74, Apr. 1998.

Savolainen, J., 2016. Real options in metal mining project valuation: Review of literature, *Resources Policy*, Vol. 50, pp. 49–65, Dec. 2016, DOI: 10.1016/j.resourpol.2016.08.007.

Sibanye Stillwater, 2024. Strategic differentiation and value creation: Operating and financial results for H2 and 2024. [Online]. Available: https://thevault.exchange/?get_group_doc=245/1740108720-ssw-presentation-h2-YE2024-31december2024.pdf. [Accessed: 08-Jul-2025].



Lefu J. Mohloki

Lecturer
School of Mining Engineering, University of the Witwatersrand

Lefu Mohloki is an experienced mining engineer who holds BSc (Mining Engineering) and MSc (Mining Engineering) degree both obtained from the University of the Witwatersrand, Johannesburg, South Africa. He also holds an LLB degree obtained from the University of South Africa (UNISA). He also holds a Mine Managers Certificate of Competency (MMC) and is a member of the Southern African Institute of Mining and Metallurgy (SAIMM). He has over 30 years of multi-commodity mining industry experience in EPCM Project Management, Supply Chain Management, Contract Management, Mine Design and Planning, Mining Consulting, Mining Project Execution, Production Management and more recently in academia as a lecturer. He previously presented a technical paper at the SAIMM *4th International Platinum Conference* in 2010.

Optimisation of proportional influence of mining and processing costs on the production of an open pit mine

R.G. Thage, F.K. Mulenga

University of South Africa, South Africa

It is well-established that mining and processing costs are critical to the actual production planning in both open pit and underground mining. Yet, little attention is being given to ensuring a sensible overlap between the two costs and the production plan. The proposed study presents a sensitivity analysis of mining and processing costs on mine production planning. To this end, the *NewMan1* block model was utilised concurrently with the SimSched Direct Block Scheduling computer code to achieve the objectives of the study. The results indicate strong potential for improving net present value (NPV) through cut-off grade optimisation. The break-even cut-off grade supports a longer mine life and sustained metal output, particularly during the early years of production. However, increases in processing costs were shown to raise the cut-off grade and reduce metal output, while higher mining costs had a comparatively smaller impact on NPV. The analysis further revealed that when the orebody contains high-grade or high-value by-products, production planning must account for their influence on overall plant performance to prevent excessive dilution. Therefore, conducting sensitivity analyses on both mining and processing costs is essential to ensure that low-grade, uneconomic zones of the orebody are not mined.

Keywords: net present value (NPV), comminution costs, cut-off grade, pit optimisation, mining costs, processing costs

INTRODUCTION

Comminution refers to the reduction in size of rock by crushing and grinding into smaller or finer particles. In both underground and surface mining operations, and for almost all mineral ores, a reduction in size is necessary. According to Khumalo (2007), comminution operations can account for up to 50% of the total energy consumed in a processing plant. When considered as part of the whole mine production chain, it accounts for 30 – 70% of the total operational costs (Nadolski *et al.*, 2014). In this paper, the mine production chain is considered to entail mining, comminution, and concentration.

Concordant studies have shown that comminution alone represents 50 – 70% of the processing costs (Musingwini, 2016). As such, an opportunity exists to systematically investigate the effects of comminution costs on a typical surface mining operation. This is to identify avenues for cost savings and improved comminution practices. The decision to send the blasted rock from the pit to the plant is dictated by the economic value of the material. The economic value, in turn, is dependent on the operational costs incurred along the mine production chain. These costs then guide the production plan as it seeks to optimise the sequence of extraction of waste and ore from the pit. The production plan is therefore defined over a term in such a way as to make the most out of the net value of the ore body.

This paper uses the computer-based block model of an ore body selected from MineLib, a database of publicly available block models. The amount of ore contained in each discretised block of the ore body is characterised in terms of waste and total mineable tonnage. Mining and processing costs are accounted for in the estimation of the expected profit of individual blocks. The key contribution of the proposed work is that the relative proportion of processing costs is varied to mimic the contribution of comminution to the profitability of the open pit mining project.

The paper is organised into four sections: The foundation for the theoretical framework underpinning the work presented in this paper; simulation tools and data collection programmes; results and discussion, and relevant conclusions are drawn.

Theoretical background

The economics of open-pit mining operations are primarily governed by factors such as mineral or metal prices, mining costs, process recovery, and processing costs. The uncertainty attached to commodity prices, for instance, affects the sustainability of the mining project as well as the confidence with which optimal operating conditions can be reached. Moreover, the intensity of the problem is exacerbated by the fact that it is the market that fixes the price of minerals and metals. As such, several studies (Asad and Topal, 2011; Ramazan and Dimitrakopoulos, 2013) are of the view that operations should control their mining operational costs and processing costs.

This section presents a concise review of key principles and existing research on pit optimisation. It presents the impact that comminution has on the overall costs of the mine. It further looks at the Lerch-Grossman algorithm used and the optimisation of the net present value (NPV) of an open pit.

Comminution economics

Researchers argue that processing costs are an important economic factor of a mining operation (Abouzeid and Fuerstenau, 2009). Some other facts are self-evident; for example, commodity prices fluctuate erratically and are driven by the market. Secondly, large high-grade and easy-to-process ore deposits are uncommon. Lastly, energy conservation is a matter of civil and often national strategic interest. Consequently, mineral processors adapt to the changing economic environment by specifically adjusting operating conditions at the comminution stage. The challenge is that in current low-grade mining operations, the magnitude of consumables and energy used is extraordinary, especially around the comminution section (Charles and Gallagher, 1982).

Optimisation of the Net Present Value of an open pit

Pit optimisation is used to define the most profitable pit shells (or nested pit shells) for a given set of economic parameters. What is economically mineable from a given deposit is determined by the final pit limit that in turn differentiates between blocks to be mined and blocks to be left unmined. This starts from the definition of the economic block model of the ore deposit. Each block is then tested by using its economic value to decide whether its value will compensate for the overburden removal. The estimation is based on the breakeven calculation that tests whether the undiscounted income earned from a given ore block will pay for the undiscounted cost of waste block mining. Once the ore deposit is modelled visually and numerically, following the workflow in Figure 1, the design and production schedule of the mine can be developed. At this point, engineering economics and optimisation principles are contemplated. Here, optimisation and simulation techniques such as graph theory, linear and integer programming, dynamic programming, mixed integer programming, moving (or floating) cones, genetic algorithm, and network analysis are considered (Erarslan and Çelebi, 2001).

The attainment of pit limits that maximise NPV requires that, in defining which blocks should be mined and which should be left behind during the life of the mine, the time value of money should be considered. As such, a cut-off grade, or grade used during scheduling to distinguish between ore and waste, should be determined from breakeven economic analysis. This then allows for planning and scheduling (Dagdelen, 1992). Note that an algorithm for computing cut-off grades that optimise the NPV of a project subject to mine, mill, and refinery capability limitations was proposed by Lane (1964). This has been implemented in various computer packages (Lane, 1988; Erarslan and Çelebi, 2001;

Whittle, 1999). Computer-based implementations of the Lane method for the optimal cut-off grade strategy have since led to improved estimations of the NPV in mining projects.

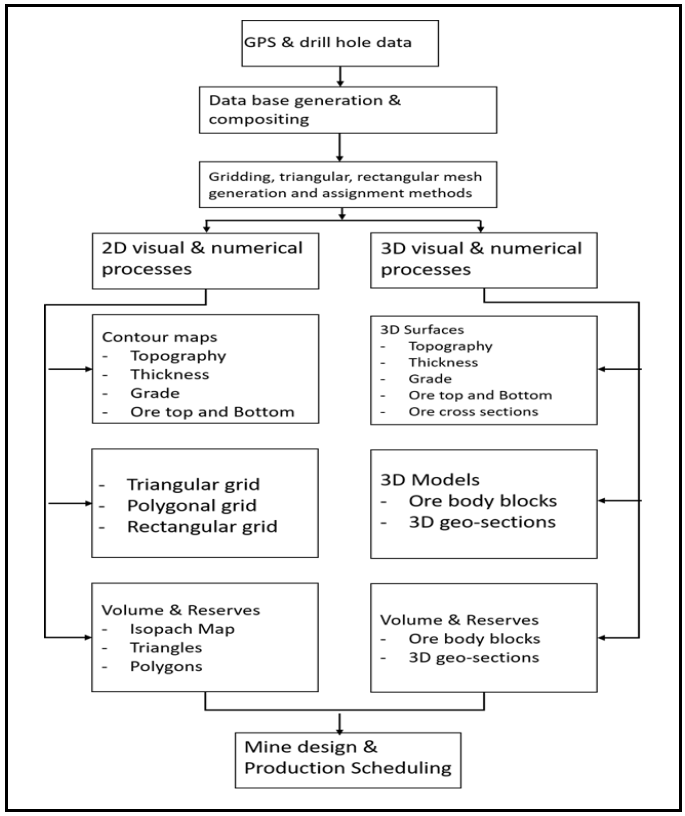


Figure 1: Computer-aided orebody modelling work flowchart (Erarslan, 2012).

Lerch-Grossman algorithm

Successful open pit design and output scheduling (OPOPS) is crucial in surface mining projects. Modern OPOPS is based on the well-known Lerch-Grossman (LG) algorithm (Lerchs and Grossman, 1965) implemented as the Nested Lerch-Grossman (Whittle, 1988 & 1997; Whittle and Rozman, 1991). The associated sequence for pit wall design is illustrated in Figure 2 using the floating cone method (i.e., LG method) applied in two dimensions (Lerchs and Grossman, 1965).

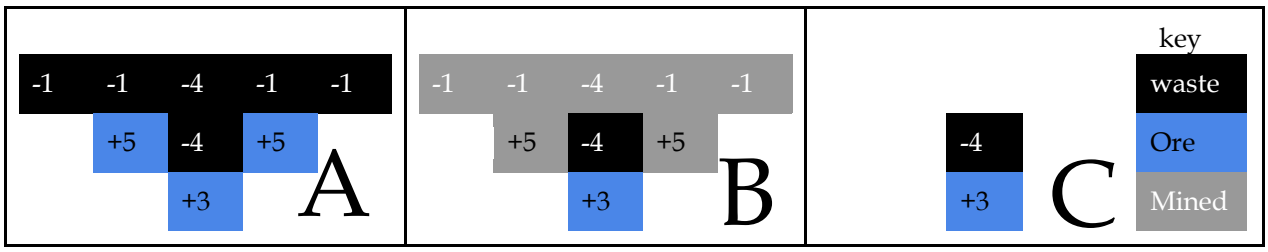


Figure 2: Sequence for pit wall design.

As shown in Figure 2a, the cone is floated from left to right along the top row of blocks in the segment. Where there is a positive square, it is eliminated or mined. Seeing that the top row has no positive block, the negative blocks are then removed to get access to the second row, as shown in Figure 2b, which shows the mined blocks from the first row to the second. To get the positive block, one starts from the left and searches for the positive block. If the total number of blocks falling inside the cone is positive, the blocks are mined. Note that the floating cone has a slope of 45°, which implies that access to a block in the second row requires the removal of three blocks in the first row. In a three-dimensional system,

the concepts can be extended to the removal of five blocks above the targeted block below. These geotechnical constraints are handled by SimSched Direct Block Scheduling (DBS) with ease. From Figure 2b, the floating cone process is followed until the bottom row, and no more blocks can be removed, as shown in Figure 2c. At this point, the last positive block cannot be mined, which leads to the final pit design. The profitability of the mined area can be found by adding the values of the blocks that have been removed. The values of the blocks are determined as follows:

Block value for both the Ore: $BV = (P - s) * g_B * y - c - m$ (1)

Block value for both waste: $BV = -m$ (2)

Where P = Price; s = Sales cost; c = Processing cost; y = Recovery; m = Mining cost; g_B = Block grade; and BV = Block value.

From the final pit design, the overall stripping ratio can also be determined as the number ratio of positive blocks to negative blocks.

Finally, the value of a systematic approach to the planning and design of pits using sound geotechnical engineering methods cannot be over-emphasised. Indeed, open pit mines need to be operated in an integrated manner, safely and economically. Pit construction should be done at a minimum unit cost and under acceptable social and legal constraints (de Bruyn *et al.*, 2019). This is to ensure that the operation is maintained for the longest time at a profit. Known as the life of mine, the time duration of the operation is mostly influenced by the mining rates, the production processes, the production dump, as well as the size, shape, and orientation of the excavation.

Simulation setup

This section covers the techniques employed to collect the data for analysis in line with the objectives set out for this work. The methodology revolves around computer simulation. This was used to investigate the effects of variable comminution costs on mine planning.

SimSched, the Direct Block Scheduler

SimSched DBS is a commercial software (plugin of SGeMS) from MiningMath (Chaves *et al.*, 2020). By means of an underlying mathematical optimisation problem covered earlier in the paper, it has the potential to assign extraction periods and destinations to the blocks. The SimSched DBS approach provides a holistic view of the mine scheduling problem by performing NPV maximisation. The software has the flexibility to import different block models of one or multiple projects at the same time.

The characteristics of the Newman1 block model downloaded from the MineLib database are summarised in terms of the minimum and maximum values recorded, including X, Y, Z indices; copper and gold grades; ore density (t/m³); and economic values for both process and waste. Each field is linked to a financial value. Each block value should be accounted for by the linked field as a function of its terminus, grades, recovery, mining costs, transport, treatment, and sale price. After importing the CSV file, the additional data relating to the dimensions and grade units of the imported blocks can be defined. Grade units are imported from the same initial CSV file with the grades in copper and gold of individual blocks. Copper grade is expressed in % while gold grade is in ppm (equivalent to g/t).

Optimisation and planning of open pit mines in SimSched DBS

For any mining enterprise or operation, open pit mine output preparation for long-term planning is an essential activity. Mining blocks must be prepared for extraction over several years, and each of them must be allocated a destination. Optimisation has been carried out in open pit mines with the guidance of nested pits developed by the LG algorithm. Predefined block destinations and DBS are considered by the LG algorithm, in which individual blocks are selected for extraction and destinations are allocated for certain periods.

The operational parameters of the mine scheduling problem are non-linear. This non-linearity results in cumbersome computations and, therefore, the time to produce the outcome is increased (Osanloo *et*

al., 2008). However, the SimSched DBS deploys linear programming mechanisms to accelerate the computational time using the objective function below:

$$\sum_{b \in B} \sum_{t \in T} \sum_{d \in D} \vartheta_{btd} y_{bt} \tag{3}$$

Where $b \in B$: a setting of all blocks b

$t \in T$: a set of periods inside the horizon

$d \in D$: a set of all destinations d

ϑ : discounted value linked with the final destination of a block b in period t

y: 1 if block b is mined in period t, 0 otherwise.

The objective function is subjected to several constraints, such as slope, process recoveries, time, etc. These constraints vary per application; however, they can be mathematically represented as follows:

$$\sum_{b \in B} c_b y_{bt} \leq \underline{C} \tag{4}$$

Where c and $\underline{C}$ represents the consumption of resources associated with the extraction of block and minimum (maximum) resource bound in any period (tons), respectively. Figure 3 shows the process taken by SimSched DBS to solve the optimisation problem.

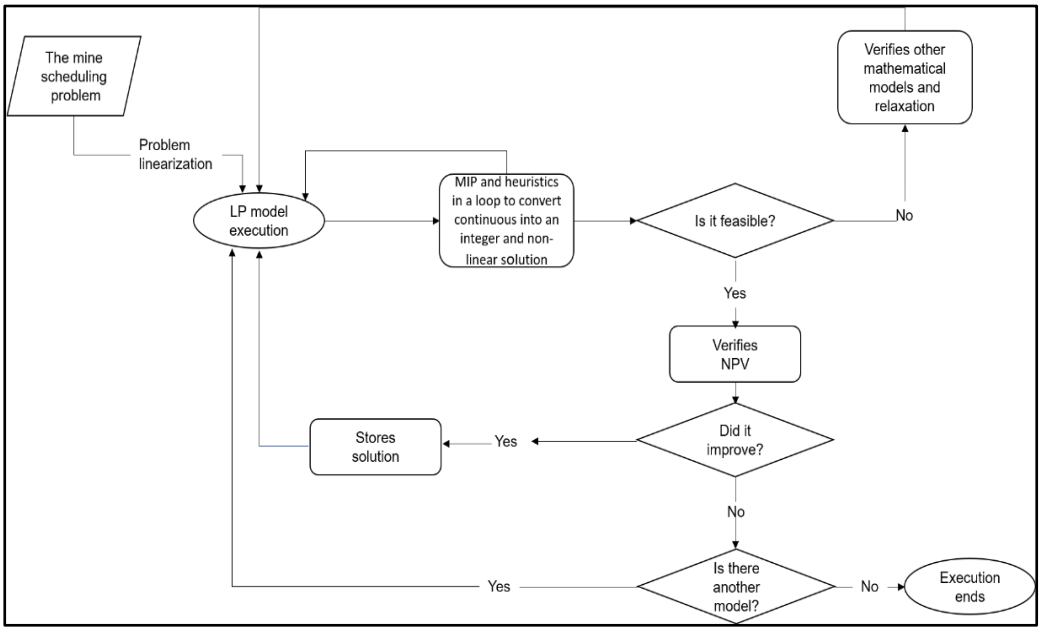


Figure 3: Mine scheduling problem.

As shown in the mine scheduling problem in Figure 3, problem linearisation is the first phase in the process. It is a phase that is undertaken to transform the operational parameters into linear constraints. At this point, SimSched DBS executes the model and checks its feasibility. Should the solution not be feasible, the mathematical equation and its relation must be checked. On the other hand, should the solution be feasible, SimSched will run the optimisation procedure until the NPV is maximised, then the solution is stored.

Modelling and simulation work

One key objective of the simulation work is to determine the optimal capacity of the Newman1 orebody model, in which the NPV of the mining project is maximised. As such, the value of a systematic

approach to the planning and design of mines using soundly based geotechnical engineering methods cannot be over-emphasised. Open pit mines need to operate in an integrated manner for the mine to operate safely and economically. Mine preparation and construction have an integrated mine system design in which the mineral is extracted and prepared to the required industry specification. Life of mine (LOM) is mostly influenced by mining rate, production process, production dump, as well as the size, shape, and orientation of the excavation. It is a geotechnical parameter that is explained with results on how it affected the life of the block model considered for this paper in the last section.

Assumptions for pit optimisation

Open-pit mining can be argued to be superior to underground mining in terms of ore recovery, production power, grade control, and dilution losses. With that in mind, the following heuristic assumptions were made: (i) dimensions of the blocks are 30 x 30 m with a bench slope of 45°, (ii) density is 2.75 t/m^3 which is fairly used in this field, (iii) discount rate of 10%, (iv) recovery for Cu and Au process are 0.88 and 0.60 respectively, (v) process 1 is 30 000 000 tons and Dump 1 is 50 000 000 tons with a total of 80 000 000 tons each period and (vi) all other limitations and constraints are inherently taken into account when executing the algorithm for pit limit optimisation.

Mining and processing costs

In order to explore the influence of processing costs and specifically comminution costs on the anticipated net profit value of the ore body, the following scenarios were considered based on existing literature (Božić, 1998; Gokhal, 2010):

- Mining costs can fluctuate from 70% to 140% of the baseline mining costs, so that the NPV is evaluated.
- Similarly, processing costs vary from 70% to 140% while the strategy on cut-off grade is appraised.

SimSched DBS is used to simulate the proportional influence of mining costs as well as processing costs on the production plan of the typical open pit mine built around the Newman1 deposit. The simulation scenarios are optimised in terms of the NPV of the mining projects generated.

Simulation scenarios considered

The Newman1 block model is selected for the purpose of this study and has 1060 blocks, 3922 rules of precedence, and 6 time periods. Login parameters that SimSched DBS requires as input data are a valued block model that considers at least two economic destinations for process and disassembly, using Equations (5) and (9). The subsequent formulas demonstrate exactly how the value of a block is determined:

$$BT = BV \times BD \tag{5}$$

$$TCu = BT \times G_{Cu} \tag{6}$$

$$TAu = BT \times G_{Au} \tag{7}$$

$$Economic\ Value\ Waste = [TCu \times RCu \times (PCu - sCu)] \ldots + [TAu \times RAu \times (PAu - sAu)] - [BT \times (c + m)] \tag{8}$$

$$Economic\ Value\ Waste = -BT \times m \tag{9}$$

Where BT = block tonnes, m = mining costs, BV = block volume; BD = block density; TCu = tonnes copper; G_{Cu} = grade copper; TAu = tonnes gold; G_{Au} = grade gold; RCu = recovery copper; PCu = selling price copper; sCu = selling cost copper; TAu = tonnes gold; RAu = recovery gold; PAu = selling price gold; sAu = selling cost gold; BT = block tonnes; c = processing cost; and m = mining cost.

Calculations are performed for each block considering assumptions on input data as well as on mining and processing costs presented earlier in the paper. In addition to this, the economic and geometric parameters that remain fixed are listed below. Simulation model inputs included: mining fixed cost (1.5

USD/t), rehandling cost (0.8 USD/t), annual discount rate (10%), minimum mined width (50 m), bottom width (100 m), and maximum vertical advance rate (150 m). Block data encoded slope angles, metallurgical recovery, and Au grades (ppm).

Optimisation based on SimSched DBS – Parameters and assumptions

Using initial input parameters and supporting assumptions previously covered together with fixed mining and rehandling costs set at 1.5 USD and 0.8 USD, respectively, SimSched DBS was used to develop production plans of various scenarios for later analysis. For this research paper, a matrix was made with different periods to get the optimal production rate. Mining and processing costs were systematically varied from 70% to 140% while the NPV associated with each case was estimated.

Determination of the break-even cut-off grade

A break-even cut-off grade (COG) is the grade whose income covers all cash-dependent expenses, including fixed and variable expenses, corporate and mining assessments, and other allocated capital uses. According to Dagdelen and Kawahata (2007), the monetary break-even COG is the grade that can be used to distinguish the metal from the waste. It is managed by comparing the incentive at the plant to the incentive at the dump. This break-even COG is generally used to determine the last pit limits. Polymetallic deposits are mineral deposits that contain more than one metal of financial worth (Rendu, 2008). Estimating the COG in this case should account for the contribution of every metal to the income.

The COG of a multi-mineral ore deposit can be determined using parametric COGSs. This intrinsically means that for a deposit like Newman1, with copper being the fundamental mineral and gold (Au) the by-product, the grade can be stated in terms of copper equivalent as follows:

$$Cu\ Equivalent\ Grade = G_{Cu} + \frac{G_{Au} \times [RAu \times (PAu - sAu) - cAu]}{G_{Cu} \times (PCu - sCu) - cCu} \quad (10)$$

Where G_{Au} = grade gold; RAu = recovery gold; PAu = selling price gold; sAu = selling cost gold; cAu = element processing cost gold; and cCu = element processing cost copper.

From Equation (10), a single parametric COG can now be applied to copper and gold simultaneously. The COG is used both to assess the final pit and to decide whether to process or discard a certain tonnage of material.

Based on the supporting Equation (10), it is possible to obtain an estimate of the break-even COG applicable to the Newman1 block model. However, it is imperative to clarify the costs used in the calculations of the break-even cut-off (Mugwagwa, 2017). This is summarised in Table 1.

Table 1: Assumptions on prices and costs used in estimating the break-even cut-off grade

Description	Symbol	Units	Value
Dilution	*D*	%	
Processing cost	*H*	USD/t milled	43.87
Unit time costs	*F*	USD/t milled	37.53
Copper recovery	*Y*	%	95
Cu metal exchange	*PCu*	USD/t metal	9 000
Selling cost per tonne	*KCu*	USD/t metal sold	495.88
Element processing cost – copper	*HCu*	USD/t copper contained in feed	671.35

The break-even *COG*, applicable to both copper and gold present in the Newman1 deposit, can be expressed as follows:

$$COG = \frac{D \times (H + F)}{Y \times (PCu - KCu) - HCu} \quad (11)$$

Therefore, $COG = \frac{43.87 + 37.53}{95 \times (9000 - 495.88) - 671.35} = 1\ \%$

The break-even COG in this production process is 1% which includes the contribution of gold to the revenue. Anything beneath the COG is regarded as waste. Based on the data generated with the SimSched DBS software, it was estimated that 24 494 758 tons of the material is of grade below 1.0%. This represents 41% of the mineralised material going to the dump site.

This research work is limited to the simulation of the Newman1 model. The DBS engine of SimSched was used for the purpose. The engine relied on the Linear Programming engine, which works only on linearised versions of all mining and processing parameters of the optimisation model. This slightly erodes the value of the final solution of the pit optimisation problem.

RESULTS

In this section, output data collected from the simulation work covered earlier were analysed. The key objective was to evaluate the influence of mining and processing costs on the production plan of a typical open-pit mine. The motivation for the scenario analysis is to evaluate whether there is a benefit in implementing cost savings on comminution operations from the point of view of strategic mine planning. Subsequent to this, the implications of cost savings on the COG are also explored. All the above is tested on the Newman1 block model, a copper-gold deposit hosted on the MineLib electronic database.

Sensitivity analysis of comminution costs on mine planning

A baseline was established for the Newman1 block model in terms of achievable NPV and throughput. A mine plan arising from the effort was generated for a predefined break-even COG. This made it possible to estimate the tonnages to be mined and associated grades of copper and gold over the LOM. In this subsection, the idea is to test scenarios whereby the proportion of processing costs relative to mining costs is varied. In doing so, insights into the contribution of comminution costs to mine planning are gained. A detailed description of the varied comparison scenarios is outlined.

Comparison of cut-off grade policy

Figure 4 presents a detailed trend comparison of the average and input grade of Au and Cu. It is clear from the graph that there is a general decline in both gold (Au) and copper (Cu) grades over the observed 21-year period, with noticeable fluctuations across different time points. While the input grades for both Cu and Au show intermittent increases, the findings show that they do not consistently translate into higher average output grades. These results suggest existing variability in process efficiency or ore quality inconsistencies which may be due to the fact that the distributions are mostly controlled by the added stockpiles. The input grades for Cu and Au are below the break-even COG of 1% determined by Equation 3.9. Metals with a grade below the COG go to the production dump. The average grade shows that copper and gold are above the COG. The results suggest that the current COG policy may be too low, allowing lower-grade material into processing and thereby reducing overall metal recovery efficiency.

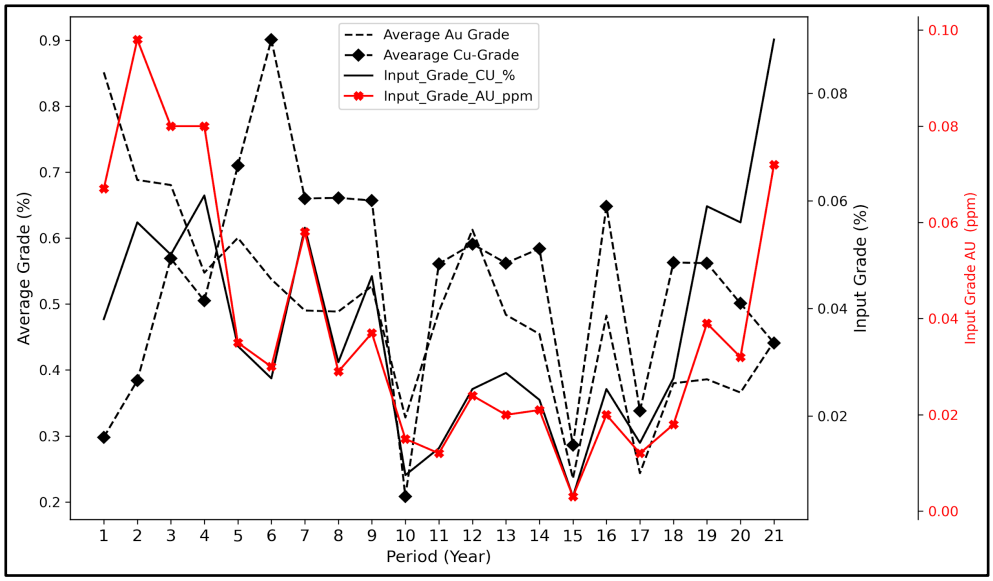


Figure 4: Cut-off grade policy.

Comparison of mined tonnages

Figure 5 presents a comparison of NPV, Production, and SimSched Production levels over the mine's life. As shown, NPV values are highest during the initial years, consistent with the objectives of COG optimisation, and decline significantly from around year ten onwards. The production tonnage closely follows the SimSched production trend, although SimSched outputs are generally higher due to optimisation effects. During the first five years, the treatment of higher-grade ore results in elevated metal yields and stronger economic returns. While SimSched DBS reflects optimistic production forecasts, a noticeable decline in metal output is observed between years ten and fifteen. Overall, production capacity appears to be fully utilised through a blend of high- and low-grade ores throughout the mine life.

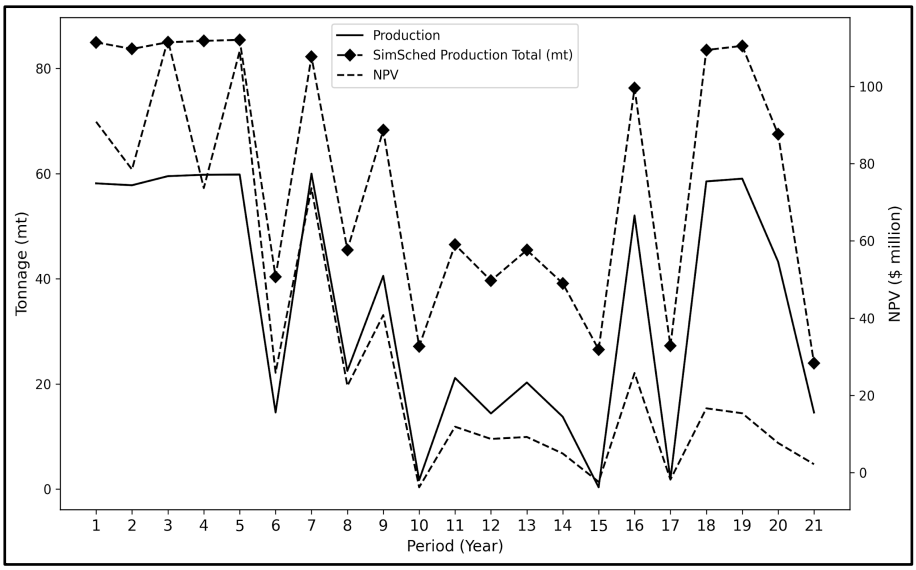


Figure 5: Comparison of mined tonnages.

The stripping backlog is evident during the first five years of the mine's life, corresponding with higher production and NPV values. While SimSched production remains consistently higher, NPV shows fluctuations, declining sharply around the midpoint of the mine life before modest recovery in later

periods. Both the existing mine plan and the break-even COG policy effectively sustain productive operations within the initial five-year window.

Effect of processing costs on the cut-off grade

Figure 6 illustrates the relationship between processing costs, total copper grade (%TCu), and metal output, with processing costs varied between 70% and 140% of the baseline. As shown in Figure 6, a slight increase in COG occurs between 70% and 75% cost levels, but the overall trend indicates that rising processing costs lead to progressively higher COGs. Conversely, metal output declines sharply as processing costs increase, reflecting reduced economic viability at higher cost levels.

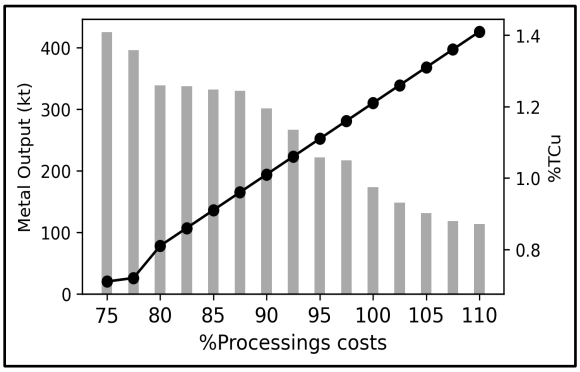


Figure 6: Relationship between processing costs and key production metrics.

Figure 6 further demonstrates that increasing the COG leads to a reduction in metal output from the orebody. A gradual decline in metal output is observed as processing costs rise, with minimal changes between 80% and 95% of the baseline cost. However, from 100% to 140% the decline becomes pronounced, indicating a substantial reduction in ore reserves available for processing. This trend confirms that higher processing costs, coupled with increased COGs, significantly limit the volume of economically treatable ore.

Effect of mining and processing costs on the NPV

Figure 7 depicts variations of NPV with percentage changes in mining and processing costs ranging from 70% to 140% of the baseline costs.

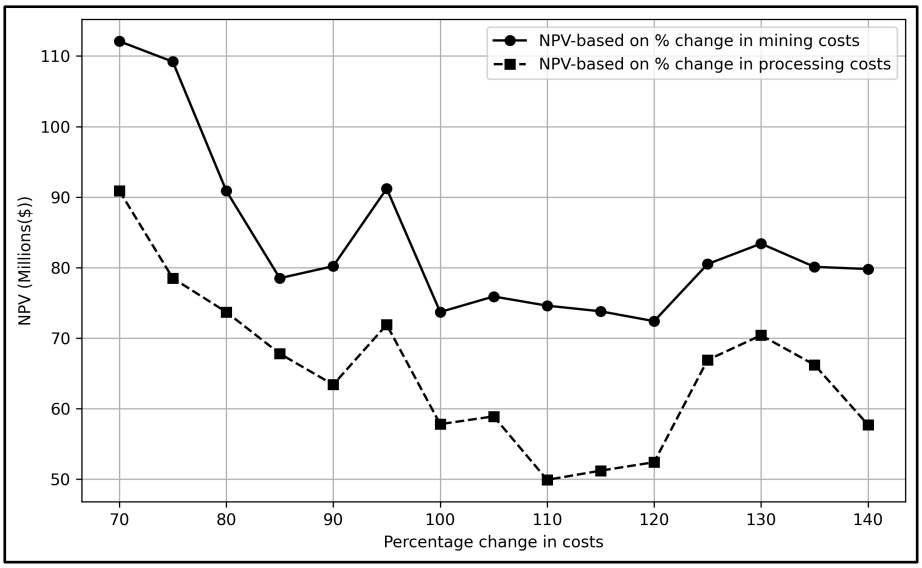


Figure 7: Variations of NPV with mining and processing costs.

Figure 7 shows that NPV values range between approximately USD 50 million and USD 112.1 million. Most NPV values cluster around 79%-80%, likely influenced by cut-off grade optimisation. Mining cost variations appear to have a limited impact on NPV, as relatively high values are maintained across most cost levels. Between 70% and 85% of mining costs, NPV declines gradually followed by a slight recovery around 90%. Overall, the findings reveal the existence of an inverse relationship between NPV and mining costs is observed within the 70%-85% range, with NPV stabilising between 100% and 140%. Further, Figure 7 illustrates the sensitivity of NPV to incremental changes in processing costs, showing that NPV generally remains lower as processing costs increase. The findings generally depict an inverse relationship between NPV and processing costs, with significant inverse relationships observed within the 70%-90%. It can be clearly seen that processing costs exert a stronger influence on NPV than mining costs.

Effect of the discount rate on the NPV

The discount rate is commonly used in capital budgeting to determine the rate at which the NPV of all cash flows from a project equals zero. Consequently, it was essential for this study to examine the sensitivity of the NPV to changes in the discount rate. Figure 8 presents all graphs for various scenarios, showing that discount rate values above the baseline of 10% yield lower NPV values than those produced at the baseline rate, as generated in SimSched. This analysis shows that trying to recover capital by increasing the discount rate does not work for the Newman1 block model. The total NPV additionally diminishes when the discount rate is increased. High discount rates negatively affect the estimation of the block model.

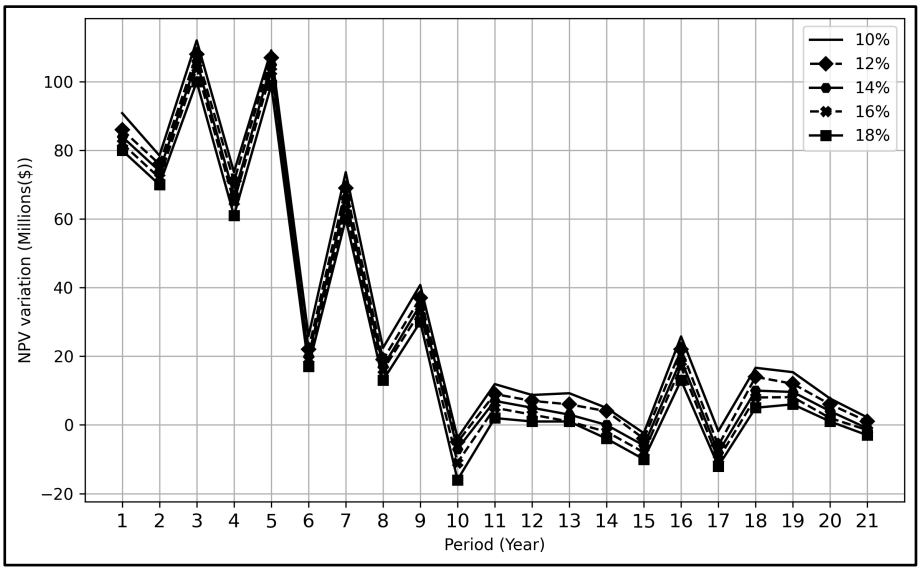


Figure 8: Effects of the discount rate on the NPV over the mine life.

Indeed, the distribution of NPV variation with several discount rates has shown that the distribution is not neutral throughout; there is an increase and a decrease in the distribution observed along the curves (see Figure 8). All the curves follow the same pattern as that of the 10% discount rate (baseline curve). The higher the discount rate, the lower the NPV.

CONCLUSION

This paper explored the effects of processing and mining costs on open pit mine planning. Simulations were carried out to generate production schedules from the block model of a copper-gold deposit. Mine planning was done using SimSched DBS, a freely downloadable software for pit optimisation. Various scenarios were considered as part of the simulation work. The findings revealed that there is a great opportunity to boost the NPV of the block model by properly aligning processing and mining costs. This exploratory paper opens possibilities for further improvements on the NPV in mining projects. The

pressing issue is to determine the interrelation between processing and mining costs, which in this paper was assumed non-existent.

ACKNOWLEDGEMENT

We would like to express our gratitude to the University of South Africa for supporting this work. A word of thanks to the MiningMath Associates who provided us with the opportunity to freely use SimSched and supported us.

REFERENCES

Abouzeid, A.Z.M., Fuerstenau, D.W., 2009. Grinding of mineral mixtures in high-pressure grinding rolls. International Journal of Mineral Processing, vol. 93, no. 1, pp. 59 – 65.

Asad, M.W.A., Topal, E., 2011. Net present value maximization model for optimum cut-off grade policy of open pit mining operations. Journal of the Southern African Institute of Mining and Metallurgy, vol. 111, no. 11, pp. 741 – 750.

Božić, B., 1998. Control of fragmentation by blasting. Rudarsko-Geološko-Naftni Zbornik, vol. 10, no. 1, pp. 49 – 57.

Charles, W.D., Gallagher, A.E.J., 1982. Comminution energy usage and material wear. Design and Installation of Comminution Circuits, pp. 248 – 274.

Chaves, L.S., Carvalho, L.A., Souza, F.R., Nader, B., Ortiz, C.E.A., Torres, V.F.N., Câmara, T.R., Napa-García, G.F., Valadão, G.E.S., 2020. Analysis of the impacts of slope angle variation on slope stability and NPV via two different final pit definition techniques. REM – International Engineering Journal, vol. 73, no. 1, pp. 119 – 126.

Dagdelen, K., 1992. Cutoff grade optimization. Proceedings of 23rd Application of Computers and Operations Research in the Mineral Industry (APCOM), University of Arizona, Tucson, Arizona, pp. 157 – 165.

Dagdelen, K., Kawahata, K., 2007. Cut-off grade optimization for large scale multi-mine, multi-process mining operations. Proceedings of International Symposium on Mine Planning and Equipment Selection (MPES).

Erarslan, K., Çelebi, N., 2001. A simulative model for optimum open pit design.

Erarslan, K., 2012. Computer aided ore body modelling and mine valuation. Earth Sciences, vol. 16, pp. 345 – 372.

Gokhal, V.B., 2010. Cost analysis of rotary blasthole drilling. CRC Press, ISBN 9781138496255.

Khumalo, N., 2007. The application of the attainable region analysis in comminution. PhD thesis, University of the Witwatersrand, Johannesburg.

Lane, K.F., 1964. Choosing the optimum cutoff Grade. Colorado School of Mines Quarterly, vol. 59, pp. 811 – 829.

Lane, K.F., 1988. The economic definition of ore: Cut-off grades in theory and practice. Mining Journal Books Limited, London.

Lerchs, H., Grossman, L., 1965. Optimum design of open-pit mines, vol 68, pp. 17 – 24.

Mugwagwa, D., 2017. Cut-off grade optimisation for a bimetallic deposit: A case study of the Ruashi Mine Copper-Cobalt deposit. Master of Science dissertation, University of the Witwatersrand, Johannesburg.

Musingwini, C., 2016. Optimization in underground mine planning-developments and opportunities. Journal of the Southern African Institute of Mining and Metallurgy, vol. 116, no. 9, pp. 809 – 820.

Nadolski, S., Klein, B., Kumar, A., Davaanyam, Z., 2014. An energy benchmarking model for mineral comminution. Minerals Engineering, vol. 65, pp. 178 – 186.

Osanloo, M., Gholamnejad, J., Karimi, B., 2008. Long-term open pit mine production planning: a review of models and algorithms. International Journal of Mining Reclamation Environment, vol. 22, no. 1, pp. 3 – 35.

Ramazan, S., Dimitrakopoulos, R., 2013. Production scheduling with uncertain supply: a new solution to the open pit mining problem. Optimization and Engineering, vol. 14, no. 2, pp. 361 – 380.

Rendu, J.-M., 2008. An introduction to cut-off grade estimation. Society for Mining, Metallurgy and Exploration, Littleton, Colorado, USA.

Whittle, J., 1988. Beyond optimisation in open pit design. Canadian Conference on Computer Applications in the Mineral Industries, pp. 331 – 337, Balkema, Rotterdam.

Whittle, J., 1997. Optimization in mine design. WH Bryan Mining Geology Research Centre, Brisbane, Australia.

Whittle, J., 1999. A decade of open pit mine planning and optimization – The craft of turning algorithms into packages. 28th Proceedings of the Application of Computers and Operations Research in the Mineral Industry (APCOM), pp. 15 – 23, Colorado School of Mines, Golden, Colorado, USA.

Whittle, J., Rozman, L., 1991. Open pit design in 90s. Proceedings of the Mining Industry Optimisation Conference, pp. 13 – 19, Sydney.

The impact of data quality on budget development and reporting in mining operations

Z. Mqoqi[1], H.P.R. Joubert[1,2], J.H. Marais[2]

[1]ETA Operations (Pty) Ltd, South Africa
[2]North-West University, South Africa

The mining sector uses budgets for operational effectiveness and strategic planning of financial and material resources. Additionally, budgets support informed decision-making by anticipating growth, cost reduction opportunities, and tracking efficiency programs. The integrity of these budgets relies on the quality of input data. Poor data quality undermines budget development, compromising the integrity of financial reporting, and may result in misguided decision-making. This, in turn, can result in inefficient resource allocation and significant financial losses.

This paper examined the influence of data quality on budget development and reporting accuracy within the platinum group metals mining sector. Using the International Standardization Organization (ISO) 25012 framework, seven key dimensions of data quality, accuracy, completeness, consistency, credibility, traceability, and availability, were assessed through a structured case study of ten mining operations.

The case study highlighted accuracy, completeness, and currentness as the most critical data quality challenges affecting budgeting outcomes. Inaccurate or incomplete data, alongside outdated information, led to significant budget deviations, inaccurate reporting, and poor cost control. The proposed 'Data Quality Toolbox', comprising subsystem-level analysis, growth and reduction reviews, and real-time reporting, offered a practical pathway to strengthen budgeting processes. The paper underscores the need for robust data governance, subsystem-level analysis, and real-time reporting to enhance data quality and improve budget reliability, supporting better decision-making and operational alignment in mining.

Keywords. Data quality, budget development, Platinum Group Metals (PGM), Reporting integrity, mining, reporting

INTRODUCTION

The mining industry plays a critical role in the global economy by supplying raw materials essential to industries such as construction, energy, and manufacturing (Firmansyah. *et al*., 2025). In addition to supporting economic growth, it generates employment and drives infrastructure development. As global demand for natural resources increases, the mining sector must adapt to challenges such as fluctuating commodity prices, stricter environmental regulations, and the need for improved operational efficiency (Firmansyah. *et al*., 2025). These pressures are mirrored in South Africa amplifying the need for effective resource management (Matthee *et al*., 2024).

In this context, effective budget management and reporting becomes vital for ensuring operational sustainability and maintaining competitiveness in a demanding global market (Vöth *et al.,* 2020). Budgets serve not only to forecast revenue and expenses but also as key tools for evaluating a mine's performance. For these reasons, it is essential that mine budgets are comprehensive, accurate, and transparent (van Aarde *et al*., 2020).

Despite advances in budgeting methodologies, including Incremental, Activity-Based, Zero-Based, and Value Proposition budgeting, the accuracy of outputs is compromised when input data is flawed (AL-Zubaidi, 2023, Malambo and Sikombe, 2022, Ouassini, 2018). In practice, poor data quality and availability are the most significant challenges across mining operations. Issues such as meter faults, missing or outdated readings, and delayed data submissions undermine baseline figures (Matthee *et al*., 2024, van Aarde *et al*., 2020).

This study shows that the primary challenge is not the choice of budgeting, but rather the quality of the operational data feeding the method. The focus is shifted from budgeting methods to the quality of operational data, proposing a practical framework to diagnose and address data issues. To structure the study's findings and practical solutions, a Data Quality Toolbox is proposed, designed to assist mining operations in diagnosing and addressing the specific data issues that compromise budget reliability.

Budget development and its limits in practice

Various budgeting methods are used, depending on operational preference and strategic objectives. The most common budgeting method is incremental budgeting, where historical or actual data is used with an estimated increment or decrement adjustment to create a new budget; however it comes with its disadvantages (Ouassini, 2018). While the method is easy, it does not accurately reflect the current operational changes by assuming the mines will be operating similarly to the base year of the budget (Ouassini, 2018, van Aarde *et al*., 2020).

A survey of 63 mining shafts in South Africa done by van Aarde *et al.,* (2020) found that their budgeting practices typically involve the following steps:

1. Setting a measurement boundary
2. Selecting a measurement period and budget intervals
3. Assessing data availability within the defined boundary and intervals
4. Applying routine adjustments for production and related energy changes
5. Incorporating utility costings

In an effort to improve the accuracy of these budgets and avoiding early obsoletion, studies have incorporated a certain level of measurement and verification principles to their development such as accuracy checks, consistency reviews, and reliability assessments (Fourie, 2016, Tsolas and Cruz, 2019, van As, 2017). However, these practices are not widespread and often lack formal structure or auditing. These practices were used to guide the development of the proposed framework.

Understanding Data Quality in Industrial Operations

There are many benefits to accurate budgeting and reporting. In energy savings reporting, accurate reporting enhances financing for other projects and realisation of other similar projects as their proven track record is often associated with fewer risks (van As, 2017). The ISO 25012 standard provides a comprehensive framework of 15 data quality dimensions that guide the management and enhancement of data quality. This study focuses on seven of these dimensions, defined in Table I, using their ISO descriptions. These data quality dimensions are the different attributes that determine the overall standard of data quality (Buddiga, 2020).

Table I: Data quality dimensions with their ISO 25012 description (Miller et al., 2024)

Dimension	Description
Accuracy	The degree to which data have attributes that correctly represent the true value of the intended attribute of a concept or event in a specific context of use.
Completeness	The degree to which subject data associated with an entity have values for all expected attributes and related entity instances in a specific context of use.
Consistency	The degree to which data have attributes that are free from contradiction and are coherent with other data in a specific context of use. It can be either or both among data regarding one entity and across similar data for comparable entities.
Credibility	The degree to which data have attributes that are regarded as true and believable by users in a specific context of use. Credibility includes the concept of authenticity (the truthfulness of origins, attributions, commitments, etc.).
Currentness	The degree to which data have attributes that are of the right age in a specific context of use.
Traceability	The degree to which data have attributes that provide an audit trail of access to the data and of any changes made to the data in a specific context of use.
Availability	The degree to which data have attributes that enable them to be retrieved by authorised users and/or applications in a specific context of use.

METHODOLOGY

This study uses a case study approach to determine how data quality influences budget performance across ten platinum group metal (PGM) mining operations, with particular attention to its effect on energy budget variance and forecasting accuracy. Seven months of operational data (January–July 2025) were collected from ten PGM shafts named Shaft A-J. These included planned and actual energy consumption, production data, budget reports, production logs, and utility metering information. Data was supplemented with questionnaires completed by on-site engineers responsible for budgeting inputs, providing operational context for anomalies.

Budget construction

The budgeting approach followed common industry practices identified in a survey of 63 South African mining shafts (van Aarde *et al.*, 2020). For each shaft, the total energy consumption for the 2023 financial year and corresponding production data were used as baseline inputs. A simple linear regression model was applied to establish the relationship between total energy consumption and production output. Data from July 2023 to June 2024 was used to project growth, reductions, or operational changes, with manual adjustments incorporated to reflect planned deviations. Historical tariff data was then applied to forecast energy costs for 2025.

Variance normalisation

Due to production variability across operations, expected energy use was recalculated using actual production values in the regression model. This normalised variance isolated deviations unrelated to production changes, enabling more accurate comparisons between budgeted and actual performance.

Data quality assessment and audit

A standardised checklist adapted from the ISO 25012 standard was developed to assess seven data quality dimensions: accuracy, completeness, consistency, credibility, currentness, traceability, and availability. Each dimension included targeted key questions, with responses gathered from engineers familiar with data sources such as supervisory control and data acquisition (SCADA) systems, meters, and logbooks, shown in Table II.

A detailed audit of each shaft's budget inputs was conducted, during which subsystems such as ventilation, refrigeration, mining, and pumping were analysed separately. This audit process, which was not part of the original budgeting method, enabled the identification of missing inputs, metering

faults, and unaccounted operational changes that would have remained hidden in total shaft-level consumption figures.

Table II: Data quality questionnaire using dimensions adopted from ISO 25012

Dimension	Assessment Criteria	Key Questions
1. Accuracy	Data correctly reflects actual values from operations, free from errors, mistakes, or misinformation.	Are data values free from entry/calculation errors?
		Do numbers match physical records?
2. Completeness	All required data points and fields are present.	Are all necessary inputs (production, historical energy, anticipated growth & reductions, cost ratio) recorded?
		Any missing periods or gaps?
3. Consistency	Data is presented uniformly across systems	Are units of measurement standardised?
		Any contradictory figures?
4. Credibility	Data is sourced from trusted, verifiable systems or personnel.	Are sources clearly defined and trusted?
		Is there a known level of manual adjustment?
		Is the data viewed as reliable by operations?
5. Currentness	Is the data up-to-date and reflect the current situation, not outdated?	Does it reflect current operations?
		Any use of outdated inputs in budget?
6. Traceability	Data lineage is clear; all changes and sources are trackable.	Can the origin and transformation of the data be traced?
		Who entered or modified the data?
7. Availability	Data is accessible when and where it is needed.	Are there delays in accessing data?
		Are reports or databases available to relevant teams without friction?
		Are there system access issues?

RESULTS

The analysis was structured to move from raw variance and data quality results towards a targeted set of interventions. The seven ISO 25012 data quality dimensions assessed in the study were first scored for each operation using the standardised checklist (Table II). A frequency count of how many operations experienced significant challenges in each dimension were produced, as shown in Figure 1.

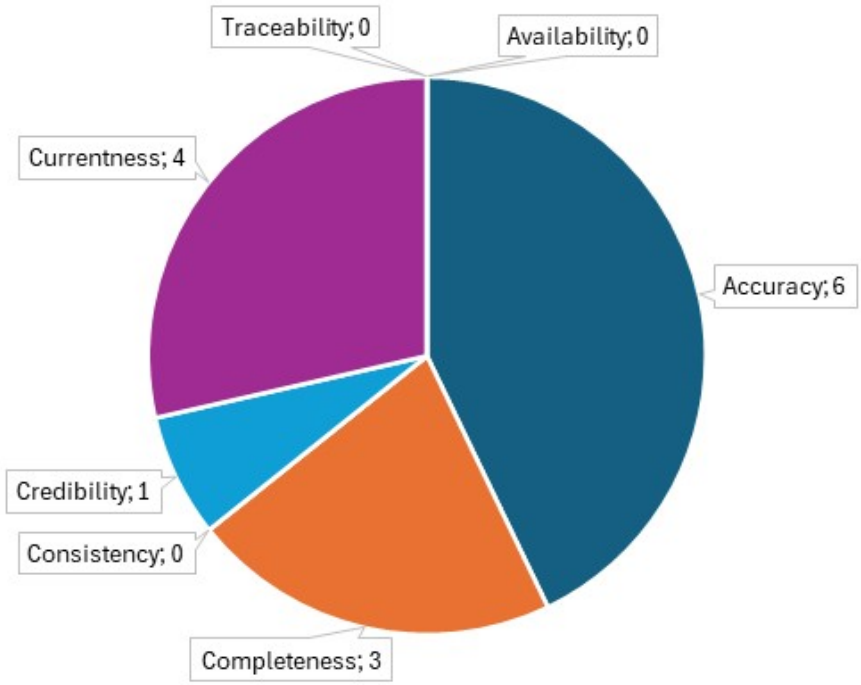


Figure 1. Number of operations per data quality dimension.

Accuracy issues were present in 60% of operations, currentness in 40%, and completeness in 30%. Consistency, traceability, credibility, and availability were not identified as significant issues in the reviewed period. These results indicate that accuracy, completeness, and currentness are the most critical weaknesses in budgeting data for the sampled operations. Had this study relied solely on numerical data and existing reports, many of the underlying data quality issues would have remained hidden. Instead, a more robust methodology, combining qualitative questionnaires with technical audits, revealed several systemic weaknesses in how budget data is generated, tracked, and reported.

The findings pointed to a key insight: Data issues were not isolated errors but systemic failures in how information was collected, segmented, and updated across operations. In several cases, unbudgeted savings masked poor performance in other areas, while offsetting mistakes created the appearance of accurate budgeting, effectively a result of chance rather than sound planning. Furthermore, operational changes, such as delayed equipment shutdowns or section consolidations, were not consistently communicated to reporting teams, creating discrepancies between planned and actual budgets. This combination of findings underlines the importance of interpreting budget performance not solely through variance figures but also through a data quality lens, forming the basis for the toolbox of practical interventions discussed in the following section.

DISCUSSIONS

Rather than addressing each dimension separately, the analysis applied a toolbox approach with three intervention methods, each designed to improve all three dimensions simultaneously but from different operational entry points, namely 1) Subsystem level analysis, 2) Growth and reduction review, and 3) Real-time reporting. The findings formed the basis of a proposed data quality toolbox (Figure 2), consisting of the above-mentioned interventions designed to address the critical data quality dimensions simultaneously. This framework formed part of the existing budgeting practices in some mining shafts in South Africa.

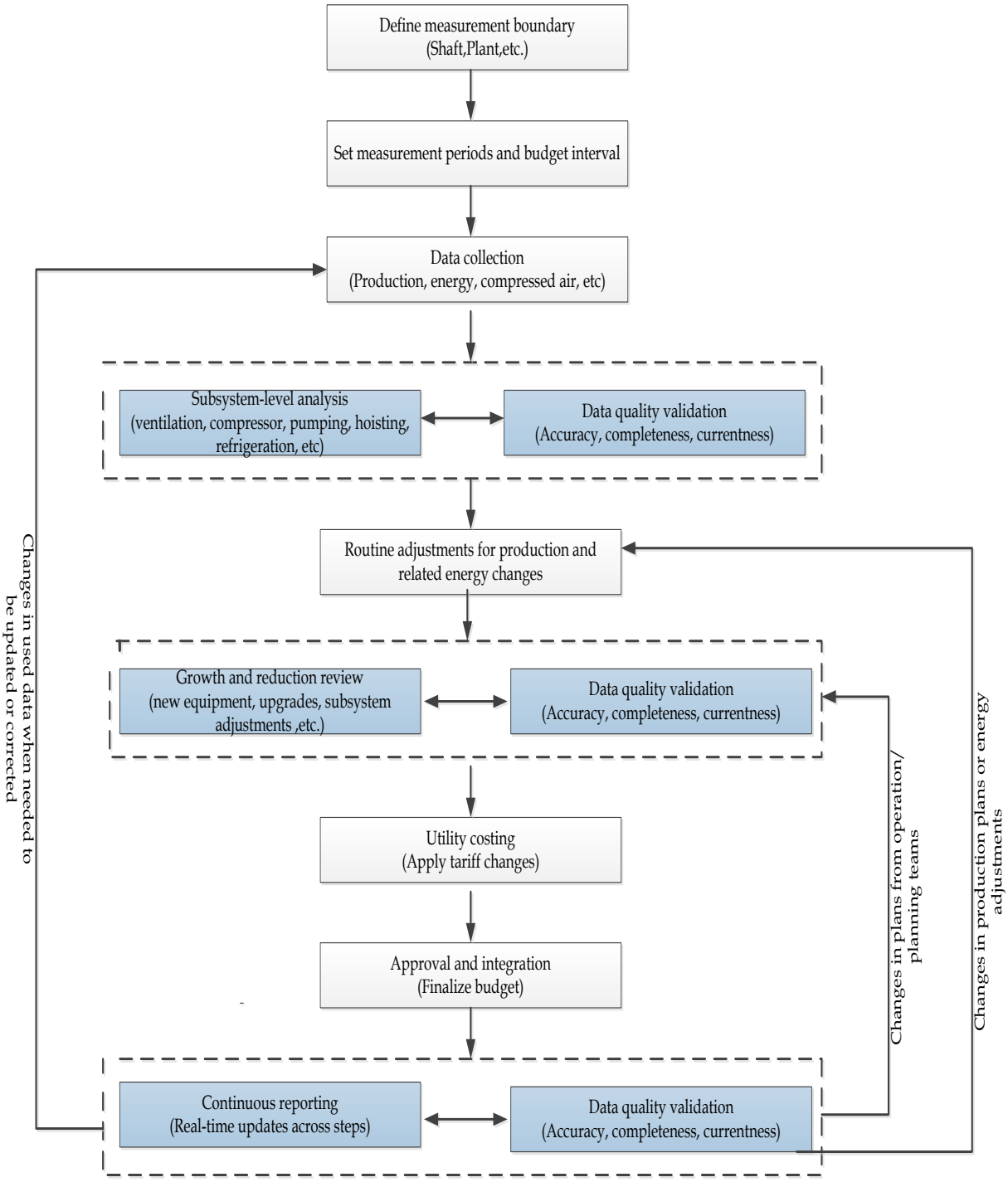


Figure 2: Proposed data quality toolbox for improved budgeting and reporting.

The proposed framework was applied to the ten mining shafts chosen for this study. The costs associated with the data quality improvements, compared to initial costs are shown in Table III, illustrating how the identified data quality issues resulted in over or under-budgeting, directly impacting cost control and reporting reliability. These costs are only for the seven months reporting period chosen for the study.

Table III. Comparison of initial and validated budget costs across ten PGM shafts, highlighting discrepancies and their underlying data quality issues (accuracy, completeness, and currentness)

Shaft	Initial cost	Validated cost	Difference	Impact
Shaft A	R45 402 581,14	R23 931 507,72	R21 471 073,42	Overbudget – ventilation adjustment not accounted for
	R112 790 981,82	R113 807 490,49	-R1 016 508,68	Underbudget – accuracy issue
Shaft B	R78 539 633,33	R78 924 449,89	-R384 816,56	Underbudget – accuracy issue
Shaft C	R112 949 129,73	R112 945 008,09	R4 121,64	Overbudget – minor accuracy issue
Shaft D	R4 113 330,81	R0,00	R4 113 330,81	Overbudget – outdated incomer included
	R61 240 323,35	R62 385 953,81	-R1 145 630,46	Underbudget – incomplete consolidation
Shaft E	R125 066 391,31	R128 011 922,24	-R2 945 530,93	Underreported – meter calibration issue
Shaft F	R59 544 195,84	R77 717 993,46	-R18 173 797,62	Underbudget – operational changes not included
Shaft G	R10 870 925,25	R19 188 106,33	-R8 317 181,08	Underbudget – unreported plan changes
Shaft H	R22 939 714,48	R22 939 714,48	R0,00	No issue
Shaft I	R77 156 900,48	R77 156 900,48	R0,00	No issue
Shaft J	R73 681 465,05	R73 681 465,05	R0,00	No issue

Subsystem level analysis

Typical budget data gathered by South African mines includes monthly total energy consumption for each shaft, plant, and business unit (van Aarde *et al.*, 2020). For shafts, total energy consumption is composed of subsystems such as pumping, compressors, ventilation, refrigeration (where applicable), winders, and remainder (e.g., change house). However, since budgets are often built from total shaft consumption without examining subsystem contributions, this aggregation masks important operational changes that directly affect accuracy, completeness, and currentness. Breaking down energy data into subsystem-level analysis improves accuracy by pinpointing exactly where mismatches between forecasted and actual consumption occur; completeness by ensuring all subsystems are included in the budget scope and currentness by making it easier to identify when operational changes in a specific subsystem are not yet reflected in the budget.

The subsystem audit in this study revealed several such cases. For example, Shaft A with three fans, reduced ventilation consumption and costs by 50%, by operating one fan at a time instead of two, a change not reflected in budget assumptions. In the 2023 baseline year, all three fans were in operation with two running at a time; by 2025, only one was running. A simple comparison of SCADA data, meter logs, or direct input from operations could have prevented both currentness and accuracy issues. Ventilation accounts for a significant portion of the energy consumed in mining networks, reported to be 25 to 50% (Nel *et al.*, 2019). An estimated R21 million was allocated towards fans not in use, which further emphasises the need for optimising resource allocation (Rakos and Man, 2016).

Other findings included misalignments in metering data and source document consolidation, spanning up to five months for three operations (Shaft A-C), resulting in discrepancies between the sum of subsystem usage and reported total consumption. Additional issues included budget allocations for a substation's incomer that had not been in use for over a year, and incomplete meter data consolidation, both of which compromised baseline accuracy. The associated cost implications can be seen in Table III, Shaft D.

Growth and reduction review
Budgets often incorporate planned operational changes such as equipment shutdowns, ventilation reductions, or system consolidations. If these changes are incomplete or not updated, the budget quickly loses relevance.

In 2024, electrical lines from a non-producing shaft were switched to Shaft F to reduce energy demand in the inactive shaft. While operationally efficient, the change increased feeder demand for Shaft F by an average of 33% per month. Neither the reduction in one shaft nor the corresponding increase in Shaft F was reflected in the budget. This rendered the budget obsolete from the first month of the reporting year. Similarly, the ventilation reduction described in the subsystem analysis was planned but not accounted for in budget inputs. This resulted in overbudgeting for the shaft, reducing the potential cost allocation for other projects.

Another contributing factor was equipment calibration. For example, meters at Shaft E had not been calibrated for an extended period, resulting in incorrect readings. While baseline data was correct, the 2025 actuals were inaccurate, leading to misleading variance comparisons. This resulted in an estimated R2.9 million, underreported for the shaft. Accurate and regularly calibrated energy meters are crucial for fair billing, consumer protection, and efficient grid management, as even small measurement errors can cause significant financial losses and operational challenges (Hakrama and Petro, 2025). These findings underscore the need for calibration records and operational changes to be reviewed regularly and factored into the budgeting process.

Real-time reporting
Operational plans often change mid-year due to production pressures, maintenance delays, or safety considerations. If these changes are not promptly communicated to budgeting and reporting teams, the integrity of performance tracking is compromised. Effective budgetary control depends on operations managing the significant time and resource investment in budget preparation while establishing credibility and trust in both the budget and the control processes (Halwiindi and Mwanza, 2022).

Studies show that the most successful mining projects intervene early with a clear focus on rigorous feasibility, strong early economics, delivery excellence, and execution productivity (McKinsey and Company, 2024). Early-stage clarity allows operational and financial plans to be adjusted before decisions are locked in, making timely and accurate reporting essential. In contrast, during the case study, Shaft G planned to operate one fan at a time starting in January 2025, a change incorporated into the budget. However, operations postponed the change until April without updating the budget. This delay meant that the financial reporting failed to reflect actual conditions, obscuring the variance analysis and limiting the ability to take corrective action early. It also meant the shaft was under-budgeted by R8.3 million. Without real-time updates, opportunities to influence outcomes are lost, and budgets risk becoming reactive rather than strategic.

Such reporting gaps can lead to incorrect conclusions about performance against budget targets and undermine decision-making. Furthermore, they can lead to frequent plan deviations, reactive work, and missed interdepartmental requirements instead of well-informed, collaborative plans that align with production and financial targets, incorporate broad departmental input, address potential issues, and minimise deviations (KPMG, 2023).

CONCLUSION

While the study focused on energy- and cost budgeting, the proposed solution can be tailored to other utilities and the needs of each operation. This paper underscores the critical role of data quality in the accuracy and reliability of energy budgeting within mining operations. The findings revealed challenges in accuracy, completeness, and currentness. These are not isolated issues but rather systemic failures stemming from insufficient data segmentation, outdated operational inputs, and inadequate communication between operational and budgeting teams.

The conventional reliance on aggregated shaft-level data obscures important subsystem-level variances, leading to misleading budget forecasts and masking significant inefficiencies. By implementing a granular subsystem-level analysis, mining operations can pinpoint the exact sources of variance. This improves budget precision and enable targeted operational interventions.

The need to incorporate planned operational changes such as equipment shutdowns, ventilation adjustments, and energy redistribution is also highlighted. This prevents obsoletion of budgets shortly after their creation, undermining their usefulness as planning and control tools. The issue is further exacerbated by lapses in meter calibration and data reporting delays, which introduce additional inaccuracies with direct financial and operational consequences.

Lastly, real-time reporting allows timely adjustments and fostering greater trust and credibility between operations and financial teams. Without it, budgets risk becoming reactive documents, that do not support strategic decision-making. Ultimately, the combination of subsystem audits, growth and reduction reviews, and real-time data integration forms a robust toolbox. This toolbox can transform budgeting from a static, retrospective exercise into a dynamic, collaborative process aligned with production realities and financial goals.

This comprehensive approach offers mining companies an improved pathway to mitigate financial risk, enhance operational efficiency, and strengthen organisational alignment. Future research and industry practice should prioritise embedding data quality frameworks into budgeting processes, emphasising continuous calibration, cross-functional communication, and real-time data flows. This approach will ensure energy budgets become not just targets, but powerful tools for driving sustainable performance improvements in the mining sector.

ACKNOWLEDGEMENTS

The authors would like to thank the engineers of the chosen mining operations for their valuable inputs and data provided.

REFERENCES

AL-Zubaidi, A.G.M. 2023. Using The Activity-Based Budget (Abb) In Implementing: The Cost Leadership Strategy And Improving Profitability: Applied Study In Al Diwaniyah Tire Factory. *World Economics & Finance Bulletin (WEFB),* 19**,** 39-46.

Buddiga, S.K.P. 2020. From Data to Decisions: The Impact of Data Quality on Business Performance. *Journal of Technological Innovation,* 1.

Firmansyah., Juanda, A. & Leniwati, D. 2025. Optimizing Budget Accuracy in the Mining Industry Through Zero-Based Budgeting. *Indonesian Interdisciplinary Journal of Sharia Economics (IIJSE),* 8**,** 5698-5711.

Fourie, H. 2016. Improvement in the overall efficiency of mining equipment: A case study. *Journal of the Southern African Institute of Mining and Metallurgy,* 116.

Hakrama, K. & Petro, J. 2025. High-Accuracy Calibration of Electrical Energy Meters. *Ingenious,* 5**,** 65-85.

Halwiindi, H. & Mwanza, B.G. 2022. The Effect of Budgetary Control on Financial Performance A Case Study of a Mining Company. *European Modern Studies Journal* 6**,** 502-512.

KPMG 2023. Mining in Focus: Mining Operations Report 2023. *Mining operations.* KPMG Australia.

Malambo, O. & Sikombe, S. 2022. Analysis of annual budgeting method at Barrick Lumwana Mine. *International Journal of Recent Research in Thesis and dissertation (IJRRTD),* 3**,** 144-153.

Matthee, F.J.L., Marais, J.H. & van Laar, J.H. 2024. Enhanced Measurement and Verification Practices in Deep-Level Mines: The Current State. *Mining,* 4**,** 401-416.

McKinsey & Company. 2024. The capex crystal ball: Beating the odds in mining project delivery. *Metals & Mining and Operations Practices* [Online]. Available: https://www.mckinsey.com/industries/metals-and-mining/our-insights/the-capex-crystal-ball-beating-the-odds-in-mining-project-delivery [Accessed 06 August 2025].

Miller, R., Whelan, H., Chrubasik, M., Whittaker, D., Duncan, P. & Gregório, J. 2024. A Framework for Current and New Data Quality Dimensions: An Overview. *Data,* 9.

Nel, A.J.H., Arndt, D.C., Vosloo, J.C. & Mathews, M.J. 2019. Achieving energy efficiency with medium voltage variable speed drives for ventilation-on-demand in South African mines. *Journal of Cleaner Production,* 232**,** 379-390.

Ouassini, I. 2018. An introduction to the concept of Incremental Budgeting and Beyond Budgeting. Available: https://ssrn.com/abstract=3140059 [Accessed 25 July 2025].

Rakos, I.-S. & Man, M. 2016. Cost Budgeting — A Relevant Instrument for Improving the Performances of a Coal Mine Case Study: Jiului Valley, Romania. *Journal of Accounting and Auditing: Research & Practice***,** 1-22.

Tsolas, I.E. & Cruz, F. 2019. Mine Performance Assessment by Means of Stochastic Frontier Analysis. *Mathematical Problems in Engineering,* 2019.

van Aarde, C., Gous, A. & Kleingeld, M. 2020. Improved Energy Budgeting Process Using Measurement and Verification Principles. *South African Journal of Industrial Engineering,* 31**,** 58-68

van As, R. 2017. *An improved baseline model for a mine* Master of Engineering in Mechanical Engineering, North-West University, Potchefstroom, South Africa.

Vöth, S., Rebrowa, N., Kovalev, A., Frik, O., Sargsyan, G., Cehlár, M., Janocko, J., Straka, M., Nuray, D., Szurgacz, D., Petrova, M., Tan, Y. & Abay, A. 2020. Budgeting as an Instrument of Increasing Competitiveness and Sustainability of Mining Enterprise. *V International Innovative Mining Symposium*. T.F. Gorbachev Kuzbass State Technical University, Kemerovo, Russian Federation: E3S Web of Conferences.



Zilungile Mqoqi

Engineer
ETA Operations

Zilungile holds a master's degree in chemical engineering from the Cape Peninsula University of Technology, where her research focused on the treatment of municipal wastewater. Since joining ETA Operations in January 2023, she has held roles in both water management and utility management, supporting operational performance and regulatory compliance across a range of client sites. In her role in water management, she was responsible for conducting on-site audits, compiling water balances and layouts, monitoring consumption for compliance with water use licenses, and investigating surface water issues. Her work involved close collaboration with engineers, environmental officers, and foremen to develop practical, data-driven solutions to water-related challenges.

She later joined the utility management team, where her responsibilities included compiling digital utility reports, and managing a proprietary meter reading application. She oversaw the application's configuration, supported client integration, conducted user training, developed reporting processes, and coordinated with developers to improve functionality.

In her current position as Measurement and Verification Engineer, she is responsible for compiling key performance reports, including intensity reports, energy and cost savings, compiling budgets, and performing ad-hoc reporting to inform strategic decisions.

Improving compressed air system efficiency using Life of Mine planning

Q.A. Bekeur[1], J.H. Marais[2], P. Burger[1]

[1]ETA Operations, South Africa
[2]North-West University, South Africa

The South African mining industry faces increased pressure to reduce energy consumption due to national energy supply constraints and rising electricity costs. Platinum mining relies extensively on compressed air for operations such as drilling, cleaning, material transport, and refuge bays. Up to 70% of compressed air generated in deep-level mines is wasted, significantly contributing to energy inefficiency. Previous research has highlighted aspects of these inefficiencies but has rarely integrated strategic mine planning with compressed air management. Many deep mines maintain compressed air supply infrastructure in inactive areas, unnecessarily consuming energy. This study proposes using Life of Mine (LoM) planning data to systematically identify inactive mining sections, facilitating targeted audits and infrastructure adjustments. The approach bridges operational data and long-term planning, creating an innovative strategy responsive to changes in active mining locations. The method involves comparing LoM plans with updated compressed air reticulation layouts to locate inactive areas. Targeted audits and coordinated infrastructure blanking during scheduled air shutdowns mitigate air losses, verified through follow-up audits. Two case studies from South African platinum mines demonstrate this method's effectiveness. The first case achieved an 18% reduction in air consumption by blanking off seven inactive half-levels, saving R 32 million annually without affecting production. In the second case, blanking off compressed air in 12 inactive half-levels boosted compressed air pressure at active stoping faces, increasing hoisted tonnes by 13%. Integrating LoM planning data with operational audits and infrastructure changes significantly enhances energy efficiency, improves system pressure, and reduces operational costs.

INTRODUCTION

Background

South Africa's platinum mining industry is a vital sector of the economy, as the country supplies roughly 73% of the world's known platinum-group metals (Hughes *et al.*, 2021). The increasing costs of electricity in South Africa risks mining production and profit margins (Mmutle, Daw and Khobai, 2022). High energy costs, declining ore grade, and increased carbon taxes are putting pressure on platinum mines to improve energy efficiency (Igogo *et al.*, 2021; Lumadi and Nyasha, 2024).

The government's commitment to reduce greenhouse gas emissions and the implementation of a carbon tax on large emitters further increases pressure on mines to curb electricity waste. Improving energy efficiency in key systems has therefore become imperative for South African platinum mines to remain both economically viable and compliant with sustainability objectives (National Treasury, 2023; Tang & Qin, 2024).

A highly energy-intensive utility used on platinum group metals (PGM) mines in South Africa is compressed air. This can account for 18 - 38% of a mine's total energy usage (Zietsman, Marais and Schoeman, 2019; De Jager, 2021). The use of this is typically inefficient, as a large part of compressed air can be lost to leaks and restrictions before reaching equipment. This means that there is large scope to reduce compressed air wastage and improve network efficiency, which will in turn save compressor electricity consumption (Burger, Vosloo and van Laar, 2024).

Compressed air is used in mine production areas, which is typically planned out for the entire Life of Mine (LoM) and updated annually. Mine planning mainly prioritises production areas and ventilation, while the layouts and expansion of compressed air pipelines are often left undocumented (Burger, Vosloo and van Laar, 2024). The improper planning of compressed air pipelines leaves these networks vulnerable for open ends that feed inactive areas, which creates large scope to improve energy efficiency of these compressed air systems (Zietsman, Marais and Schoeman, 2019).

Compressed air systems in deep-level mining

Compressed air systems are essential in deep-level underground mining, particularly in South African platinum operations where they power a variety of production activities. Pneumatic drills and loading equipment in narrow-reef platinum stopes rely on compressed air for rock drilling and ore handling, and air supply is also used for tasks such as clearing blast debris and pressurising refuge bays (van der Merwe, Gous and Schutte, 2022). The appeal of compressed air lies in its versatility and inherent safety. Air-powered tools produce no sparks or dangerous heat, making them suitable for methane-prone mines, and compressed air can be distributed over long distances through piping to reach remote sections of the mine (Ray *et al.*, 2022). These qualities have made compressed air a backbone of deep-level mining operations.

Unfortunately, compressed air systems are inefficient and costly to run. Large compressors at the surface force air through extensive reticulation networks, spanning several kilometres of shafts and tunnels, to supply working levels (van der Merwe, Gous and Schutte, 2022). Along the way, substantial energy is lost to friction and heat, and any leaks or improper uses in the network directly waste compressed air. In practice, a large fraction of the input electrical energy never translates into useful work underground. Leaks, open pipe ends, and other losses can consume more than half of the compressed air in the system, and studies have found that in some cases over 70% of generated compressed air is ultimately wasted before it ever reaches pneumatic equipment (Burger, Vosloo and van Laar, 2024). This inefficiency makes compressed air one of the most expensive utilities on a mine, often accounting for around one-fifth of a typical mine's total electricity usage (Zietsman, Marais and Schoeman, 2019). The high cost and energy loss associated with compressed air present a significant opportunity for improvement. Both industrial and commercial users, along with entities like Eskom, recognise this, with Eskom providing services to help optimise energy use. Generally, 30% of the total electrical energy used to compress air is wasted due to factors such as air leaks, poor maintenance, misapplication, and poor control (Eskom, 2021). Efforts such as leak detection and repair, better control of air flow to match demand, and modernising old air networks can yield cost savings and productivity benefits by reducing the energy wastage in current systems.

Mine layouts and planning

Because compressed air drives production-critical processes like drilling and blasting, its performance has a direct impact on mine output. Adequate air pressure and flow at the stopes are needed to achieve the drilling rates required for daily advance. If the delivered pressure is too low or variable, drilling penetration slows and fewer holes can be drilled, which in turn delays blasting and reduces the ore tonnage broken per shift. In other words, shortfalls in compressed air supply translate to lost production time (Rahimdel and Zafarzadeh, 2024). Overlooking the capacity or health of the compressed air system can lead to unforeseen bottlenecks underground, such as pneumatic drills stopping due to low pressure, resulting in costly production losses (Rahimdel and Zafarzadeh, 2024). Conversely, an oversupply of compressed air incurs unnecessary energy costs without improving production. Efficient production thus depends on providing the right amount of compressed air, at the right locations and times, which requires careful management and planning of the air network (Mare, Bredenkamp and Marais, 2017).

Traditionally, however, mine planning has focused overwhelmingly on ore extraction and development scheduling, often neglecting the detailed planning of service infrastructure like compressed air networks (van Tonder, Bolt and van Rensburg, 2012) (Fouché, 2017). LoM plans typically address the sequencing of shaft sinking, level development, and stoping to optimally extract the orebody, assuming that services like compressed air will be scaled up as needed. This siloed approach means that compressed air systems are frequently expanded or adjusted in a reactive manner rather than being proactively designed in tandem with production needs. The result is that many mines suffer from over-capacity and inefficiency, where compressors and piping remain configured for past requirements and waste energy delivering air to areas no longer in use.

There is a clear need to integrate compressed air considerations into the mine planning and management processes. Recent research emphasises the importance of proactive planning for compressed air systems to support continuous production and efficiency (Burger, Vosloo and van Laar, 2024). Integrating energy considerations into mine planning creates opportunities to optimise system efficiency. In particular, aligning mine planning with shaft layouts provides a systematic basis for identifying and closing inactive areas, thereby enhancing compressed air system efficiency. This presents the opportunity to develop a methodology that can be applied to various shafts which can reduce compressed air wastage by isolating compressed air pipes feeding inactive areas.

DEVELOPMENT OF METHODOLOGY

This section will summarise the developed methodology which can be followed on typical PGM shafts to achieve energy savings. The methodology includes identifying inactive areas by cross-referencing production planning with shaft layouts, auditing these areas to identify possible open ends, and isolating these areas.

Step 1: Identifying inactive areas

The strategy that was followed in this study overlays the LoM plan onto the mine layout to pinpoint areas with no planned tonnages in the current or upcoming periods. If a particular level, half-level, cross-cut, or raise has zero ore tonnage scheduled in the plan (meaning the reserves there have been exhausted or deemed uneconomical), that section can be flagged as a candidate for being inactive. This approach is supported by strategic mine planning principles – the multi-year mine plan delineates the active mining sections (Otto and Musingwini, 2019), so any area omitted from the plan can be considered mined-out or idle.

Once such areas are identified on paper, they can be validated through discussions with shaft personnel such as mine managers, engineers, and shift overseers. The purpose is to confirm the status of each flagged section. There may be cases where an area has no tons in the official plan but is kept available as contingency or is undergoing reclamation. Therefore, input from on-site personnel is crucial (Swart, 2003). If the plan review and personnel feedback concur that a section has no further production planned, it can be labelled as an inactive area. It should be noted that mine personnel may not always have full knowledge of the compressed air layouts (Gruting *et al.*, 2022). By using the LoM schedule in this way, the method ensures that only non-productive parts of the mine are targeted. This systematic identification of active or inactive sections is a proactive step also noted in recent studies. For instance, integrating the mine's three-year plan with its compressed air model allowed researchers to determine exactly which mining areas would be active (Burger, Vosloo and van Laar, 2024).

Step 2: Audits

After mapping out inactive zones via planning, the next step is to conduct physical audits underground to verify conditions and identify opportunities to shut off services to those zones. These audits involve comprehensive on-site inspections of the compressed air network leading into each inactive section. A team walks from the shaft barrel to the inactive area (half-level or cross-cut), examining the compressed air piping infrastructure. The team looks for compressed air lines feeding into areas where production has ceased.

Although walkthrough audits are time-consuming and labour-intensive, the required input is reduced by only auditing pipelines leading to identified inactive areas in Step 1. Special attention is paid to the configuration of the piping, the locations of isolation valves, and whether those valves are shut or still open. When such situations are encountered, such as in Figure 1, the specific location should be recorded. The audit results therefore confirm the state of the air supply to inactive areas. This information feeds directly into isolating those inactive sections from the compressed air network.



Figure 1. Photo taken by author of a compressed air pipeline leading into the ventilation wall of an inactive half-level.

Step 3: Isolating Inactive Areas

Once an inactive area has been identified and its air supply status documented, the final step is to isolate that section to eliminate compressed air wastage. Isolation is achieved by physically closing off the compressed air line feeding the area. In practice, this is done by installing blank plates, also known as blank flanges, or other shut-off devices in the pipeline. The blanking plate is inserted at a convenient point, which is usually at a flange upstream of the branch that leads into the inactive area. This effectively seals the pipe so that no air can flow beyond that point into the abandoned working. Removing a pipe section downstream from the blank plate allows observation of the seal quality without need for instrumentation. Where there is a chance that an area might be re-opened in future, an isolation valve can be installed at the entry instead. This allows the section to be easily reopened when needed. In either case, the aim is to ensure that inactive sections are not left inadvertently connected to the live air network.

The installation of blank plates and closure of valves to inactive areas must be carried out in a safe manner that does not disrupt mining operations. Upon installation of the blanking device, the compressed air system must be partially or fully depressurised to ensure safety. By doing the work on non-production days, the risk of interrupting compressed air supply needed during the work week was eliminated (Pelders, Magweregwede and Rupprecht, 2021). The procedure typically involves coordinating with the ventilation/compressed air engineer to shut off or bypass the relevant air supply, verifying that the line is vented and safe, installing the blank plate on the flange, and then gradually re-pressurising the main system. After isolation, the previously supplied area is effectively removed from the air network until such time as re-connection is required (if ever). This approach has an immediate benefit: it stops the persistent waste of compressed air into that area. Moreover, it can improve air delivery to active faces (by raising available pressure, since less air is being lost elsewhere), and it reduces the load on compressors (Rahimdel and Zafarzadeh, 2024; van der Merwe, Gous and Schutte, 2022). By systematically blanking off all verified inactive sections, the mine can avoid supplying air into ‘closed-off’ areas where valves were left open, a scenario identified as a major avoidable wastage in studies of deep-level mine air systems. Thus, the combination of careful planning, thorough audits, and well-timed isolation work (using blank plates on days with no production) ensures that inactive parts

of the mine are effectively sealed from the compressed air distribution, as shown in Figure 2. This methodology not only saves energy costs but also contributes to more stable air pressures in the active workings, aligning with industry best practices for demand-side compressed air management. It is important to verify that blank-offs were done correctly by looking at flow and pressure differences (Fojtášek, Dvořák and Krabica, 2019), or auditing in person.



Figure 2. Photo taken by author of a blanking plate installed on a compressed air pipe isolating an inactive section.

RESULTS

The proposed method was implemented on two separate platinum mine shafts, denoted as Shaft A and Shaft B. In each case, LoM planning data was used to identify sections of the compressed air network that no longer supported active mining, and targeted interventions were carried out to eliminate unnecessary compressed air supply to those areas. The outcomes at both shafts demonstrated significant improvements in compressed air system performance and mining metrics. The results for each shaft, including quantitative changes in compressed air consumption, system pressure, and production output are discussed in the following section.

Shaft A: Decreased Air Consumption with Sustained Production

At Shaft A, LoM planning analysis revealed multiple inactive areas still being supplied with compressed air. A detailed audit identified seven inactive half-levels with legacy compressed air lines that were no longer needed for production. These sections were isolated from the compressed air network over the span of two months, on non-production days. This ensured safe operations while not risking production.

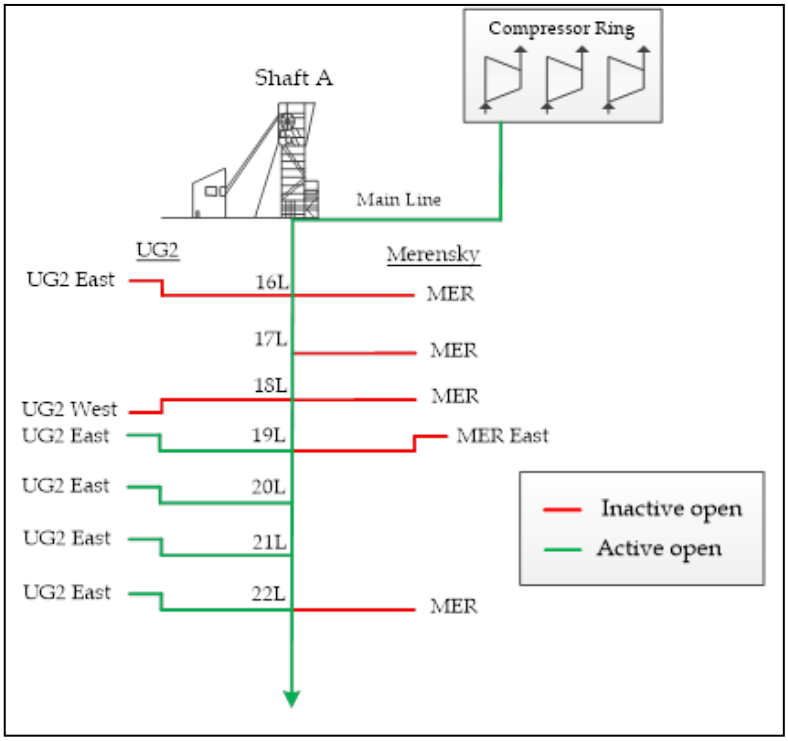


Figure 3. Shaft A compressed air reticulation.

Figure 3 provides a schematic overview of the Shaft A network before and after the intervention, highlighting the segments that were removed from service in red. The elimination of supply to the inactive half-levels produced a marked reduction in compressed air consumption for Shaft A. Post-implementation measurements indicate that the total air demand on the shaft during peak periods dropped by approximately 18% relative to the baseline. This decrease in airflow demand reflects the amount of air that was previously being wasted in areas. Notably, this reduction aligns with observations in prior studies that a large fraction of generated compressed air in deep mines is often consumed by leaks, open pipe ends, and other wastages rather than useful work (van der Merwe, Gous and Schutte, 2022; Burger, Vosloo and van Laar, 2024). Figure 4 shows the compressor energy consumption before and after isolating inactive areas on Shaft A.

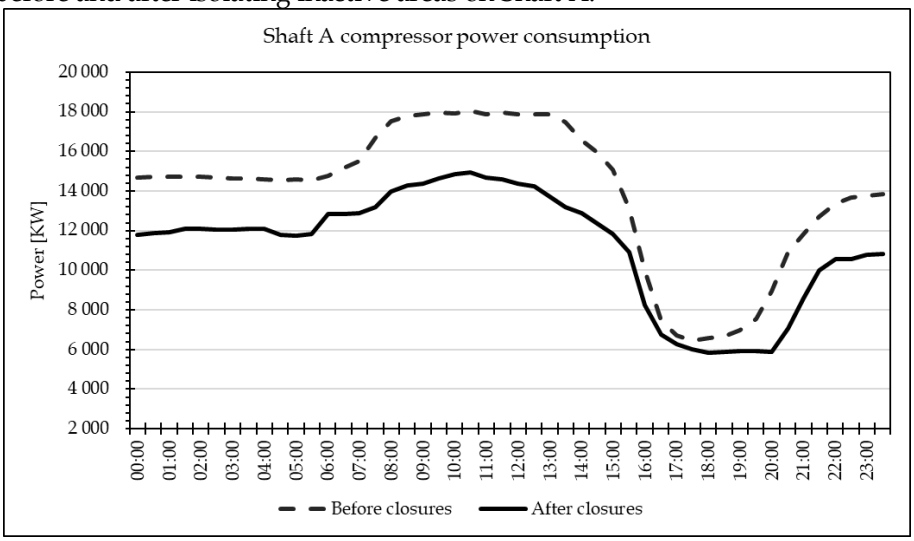


Figure 4. Shaft A average compressor power consumption profile before and after closures.

Crucially, the reduction in air consumption did not negatively affect production outputs at Shaft A. Mining production performance before and after the intervention showed no significant change, remaining at the baseline level within normal variation. All active working areas continued to receive sufficient air supply and maintained their output. In prior research, inadequate air pressure in deep mines has been linked to reduced drilling rates and lost production (Burger, Vosloo and van Laar, 2024). The Shaft A intervention avoided such losses by improving pressure stability at the faces without adding new equipment.

The drop in compressed air consumption at Shaft A translated into substantial energy savings. With less airflow required to maintain operational pressures, the compressors supplying Shaft A could be run at lower load for the same production output. Analysis of the compressor power data showed a reduction in energy consumption. The energy saved by the 18% airflow reduction is estimated at roughly R32-million in electricity costs annually. This figure was obtained using the mine's electrical tariff and the measured reduction in compressor motor power. In summary, Shaft A's case study demonstrates that leveraging LoM planning to cut off compressed air supply to inactive areas can yield a reduction in energy consumption with no compromise to production.

Shaft B: Increased Production with Sustained Air Consumption

Shaft B presented a different result from Shaft A. Instead of achieving a reduction in power consumption, the primary outcome was boosting production output which was previously limited by excessive compressed air wastage. Using the LoM plan, the team identified 12 areas that had ceased production activities but were still connected to the compressed air network. The Shaft B schematic overview is provided in Figure 5. These inactive sections were continuously consuming air and thereby reducing the available airflow and pressure for the active mining faces.

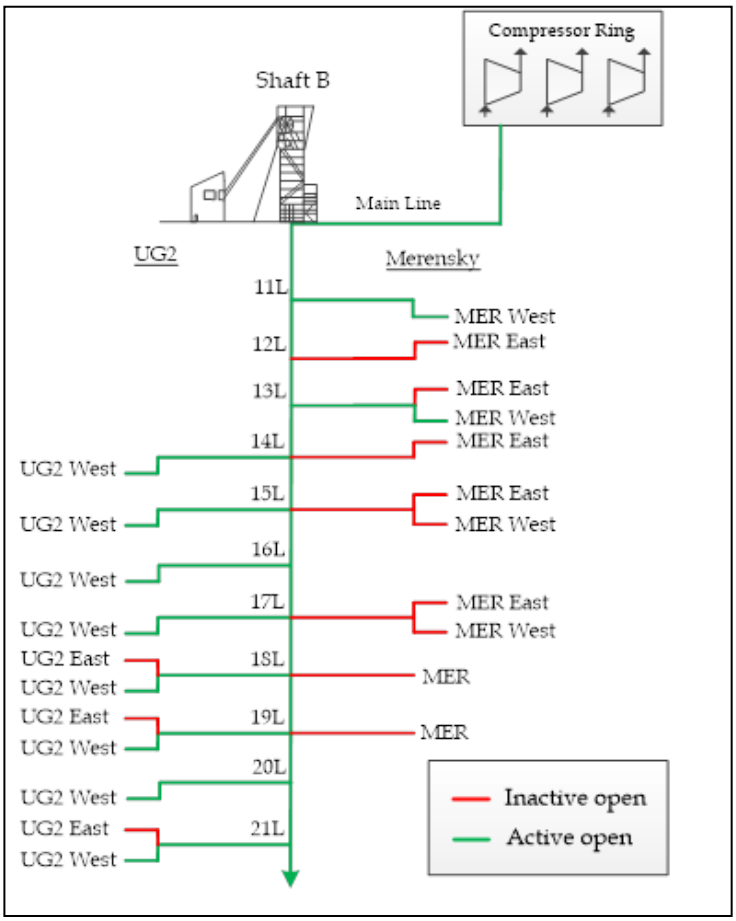


Figure 5. Shaft B compressed air reticulation.

Once again, a series of audits and consultations with mine personnel were conducted, and the 12 identified inactive segments were isolated from the network by blanking off pipes and closing valves. Mining production increased significantly after the intervention, without any upgrades to compressors or addition of new air supply. In the months following the changes, Shaft B recorded roughly a 13% increase in ore hoisting tonnage from the baseline level. It is important to note that the 13% production gain was achieved with no increase in compressed air supply capacity. The same compressors and infrastructure were simply being used more effectively. The intervention led to previously wasted compressed air being repurposed for productive use. This efficiency gain is attributable to better system management.

This rise in production output is linked to the improved compressed air delivery to the active sections. By cutting off the 'dead-end' branches that previously wasted compressed air, the system could maintain higher pressures during the drilling shift that occurs from about 08:00 to 15:00. The improvement in the pressure profile can be observed in Figure 6. With adequate air pressure for drills and pneumatic equipment the drilling penetration rates and loading efficiencies improved, enabling crews to mine more ore within the same shift time. This mechanism is supported by prior research: ensuring proper air pressure at drill sites is critical for production, as drill performance and advance rates drop off when pressure is insufficient (Van Jaarsveld, Ebben and Ashanti, 2008; Burger, Vosloo and van Laar, 2024). For example, in a study by Diaan Nel, a 45kPa improvement in rock drill pressures resulted in a 25% increase in rock penetration rate (Nell, 2017). Shaft B's outcome validates these findings. Once the pressure constraints were removed, production immediately improved.

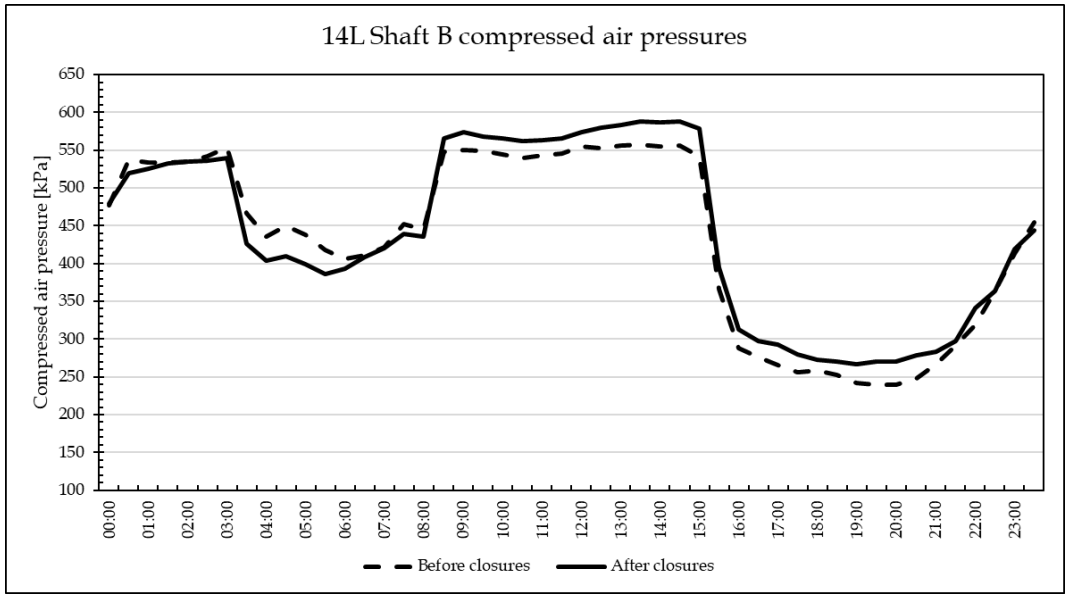


Figure 6. 14L Shaft B average compressed air pressure profile before and after closures.

Before the intervention, Shaft B struggled with pressure drops along the haulages feeding its deepest working areas, especially during peak drilling shifts. After isolating the 12 inactive areas, pressure logs showed that the compressed air pressure during peak drilling hours increased by between 18 and 36 kPa. Although this pressure increase was measured near the shaft bank, it should also be reflected at deeper working areas. After the closures, mine personnel reported that pneumatic drills operated with fewer interruptions, and no air-related delays were noted during the shift reports post-implementation.

In summary, Shaft B's case study demonstrates that strategic elimination of unnecessary air supply can improve production. In this case yielding a 13% boost in output with no additional energy consumption.

CONCLUSION

This paper set out to bridge the gap between mine production planning and day-to-day energy management of compressed air systems. The results from Shaft A and Shaft B confirm that integrating LoM planning data with compressed air network optimisations can yield substantial benefits for both energy efficiency and production performance. In Shaft A, isolating inactive sections of the air network led to an 18% reduction in compressed air consumption without any loss of production output. In Shaft B, a similar intervention enabled a 13% increase in ore production with no additional air power input.

The success of these case studies demonstrates that many deep-level mines are running with significant inefficiencies in their compressed air usage, largely due to legacy infrastructure and a lack of adaptive planning. Studies have shown that typically only 10–30% of generated compressed air is actually used productively underground (van der Merwe, Gous and Schutte, 2022; Rahimdel and Zafarzadeh, 2024; Burger, Vosloo and van Laar, 2024). The findings from this study reinforce this. By eliminating air supply to non-productive areas, the mines were able to recover wasted capacity – either to save energy (Shaft A) or to reinvest that capacity into productive work (Shaft B). The net effect is improved pressure delivery to active workings and the avoidance of the production losses that occur when pressure is inadequate. Such a high-level approach can sometimes be overlooked when implementing energy management initiatives.

A key innovation of this approach is the use of LoM planning as a tool for energy management. Mine plans are usually focused on ore extraction scheduling and reserve management, while services like compressed air are seldom planned with the same detail (Burger, Vosloo and van Laar, 2024). This work shows that LoM planning data is an underutilised resource for identifying efficiency opportunities.

Overall, the implementation of LoM planning-integrated compressed air management at Shaft A and Shaft B has validated a scalable methodology for deep-level mines. By routinely comparing the mine plan to the compressed air layouts, operations can identify misalignments and quickly correct them with minimal capital expenditure. This continuous maintenance loop creates a more sustainable mining operation that adjusts its energy usage to the production profile. The study's findings encourage broader adoption of this methodology across the mining industry, especially in energy-intensive sectors like platinum and gold mining where electricity constraints and cost pressures are acute.

In conclusion, bridging mine planning and compressed air system management presents a powerful lever for optimisation in deep-level mining. The case studies of Shaft A and Shaft B illustrate that mines can simultaneously reduce energy waste and enhance production by managing their compressed air networks using planning insights. It is recommended that mining operations incorporate this approach into their standard practices. For instance, a policy could be implemented to review compressed air reticulation whenever mine plans are updated, and to conduct periodic audits focusing on planned closures. Future work can build on these results by exploring the use of automated sensors and digital twin models to further refine the identification of inefficiencies in real-time, as well as extending the approach to other utilities. Adopting such strategies will be crucial for mines aiming to improve their energy sustainability and maintain productivity in an era of rising energy costs and evolving operational challenges (Tang and Qin, 2024). The success of the presented methodology at Shaft A and B serves as a compelling proof-of-concept for the mining industry's journey toward more intelligent and sustainable resource utilisation.

REFERENCES

Burger, P., Vosloo, J.C. and van Laar, J.H. (2024) 'Future mines' compressed air planning using digital twin simulations', *South African Journal of Industrial Engineering*, 35(3), pp. 96–112. Available at: https://doi.org/10.7166/35-3-3094.

Eskom (2021) *Compressed air: Industrial sector Fact Sheet*. Available at: https://www.eskom.co.za/eas/wp-content/uploads/2021/05/COMPRESSED-AIR-FACTSHEET-Final-.pdf (Accessed: 17 August 2025).

Fojtášek, K., Dvořák, L. and Krabica, L. (2019) 'Comparison and Mathematical Modelling of Leakage Tests', *EPJ Web of Conferences*, 213, p. 02019. Available at: https://doi.org/10.1051/epjconf/201921302019.

Fouché, S.J. (2017) Improving efficiency of a mine compressed air system. *Master's Dissertation*. North-West University, South Africa.

Gruting, U, Schutte, C.S.L., Pelser, W.A. and van Laar, J.H.(2022) 'Investigating the link between compressed air wastage and ventilation shortfalls in deep-level mines', *South African Journal of Industrial Engineering*, 33(3), pp. 109–123. Available at: https://doi.org/10.7166/33-3-2786.

Hughes, A.E., Haque, N., Northey, S.A. and Giddey, S.. (2021) 'Platinum group metals: A review of resources, production and usage with a focus on catalysts', *Resources*. MDPI. Available at: https://doi.org/10.3390/resources10090093.

Igogo, T., *Awuah-Offei, K., Newman, A., Lowder, T. and Engel-Cox, J.*. (2021) 'Integrating renewable energy into mining operations: Opportunities, challenges, and enabling approaches', *Applied Energy*, 300, p. 117375. Available at: https://doi.org/10.1016/J.APENERGY.2021.117375.

Van Jaarsveld, A., Ebben, S. and Ashanti, A. (2008) 'Development and implementation of an electrically-powered stope rockdrill for Tautona mine', *The Southern African Institute of Mining and Metallurgy* [Preprint], (Narrow Vein and Reef 2008).

De Jager, M. (2021). Using simulation to prioritise implementation of platinum mine compressed air efficiency solutions. *Master's Dissertation*. North-West University, South Africa.

Lumadi, V.W. and Nyasha, S. (2024) 'Technology and growth in the South African mining industry: An assessment of critical success factors and challenges', *Journal of the Southern African Institute of Mining and Metallurgy*, 124(4), pp. 163–172. Available at: https://doi.org/10.17159/2411.

Mare, P., Bredenkamp, J.I.G. and Marais, J.H. (2017) 'Evaluating compressed air operational improvements on a deep-level mine through simulations', *Proceedings of the Conference on the Industrial and Commercial Use of Energy, ICUE* [Preprint]. Available at: https://doi.org/10.23919/ICUE.2017.8068011.

van der Merwe, A., Gous, A.G.S. and Schutte, C.S.L. (2022) 'USING ZERO-WASTE BASELINES TO IDENTIFY COMPRESSED AIR SYSTEM INEFFICIENCIES IN DEEP-LEVEL MINES', *South African Journal of Industrial Engineering*, 33(3), pp. 55–68. Available at: https://doi.org/10.7166/33-3-2803.

Mmutle, T., Daw, O.D. and Khobai, H. (2022) 'Effects of Energy Pricing on the Mining Sector Performance in South Africa: An Econometric Approach', *International Journal of Energy Economics and Policy*, 12(6), pp. 283–292. Available at: https://doi.org/10.32479/ijeep.13678.

National Treasury (2023) *Carbon tax discussion paper: Phase two of the carbon tax*. Available at: https://www.treasury.gov.za/public%20comments/TaxationOfAlcoholicBeverages/Phase%20two%20of%20the%20carbon%20tax.pdf (Accessed: 16 August 2025).

Nell, D. (2017) Optimising production through improving the efficiency of mine compressed air networks with limited infrastructure. *Master's Dissertation*. North-West University, South Africa.

Otto, T.J. and Musingwini, C. (2019) 'A spatial mine-to-plan compliance approach to improve alignment of short-and long-term mine planning at open pit mines', *Journal of the Southern African Institute of Mining and Metallurgy*, 119(3), pp. 253–259. Available at: https://doi.org/10.17159/2411-9717/2019/V119N3A4.

Pelders, J., Magweregwede, F. and Rupprecht, S.M. (2021) 'Optimization of shift cycles in the South African mining sector', *The Journal of the Southern African Institute of Mining and Metallurgy*, 121. Available at: https://doi.org/10.17159/2411.

Rahimdel, M.J. and Zafarzadeh, F. (2024) 'Assessing and Improving Compressed Air Systems in Underground Mines (A Case Study in Iran)', *Rudarsko-geološko-naftni zbornik*, 39(4), pp. 13–21. Available at: https://doi.org/10.17794/RGN.2024.4.2.

Ray, S.K. *et al.* (2022) 'Review of preventive and constructive measures for coal mine explosions: An Indian perspective', *International Journal of Mining Science and Technology*, 32(3), pp. 471–485. Available at: https://doi.org/10.1016/J.IJMST.2022.02.001.

Swart, E. (2003) 'The South African legislative framework for mine closure', *The South African Institute of Mining and Metallurgy*, pp. 489–492.

Tang, Z. and Qin, D. (2024) 'Sustainable mining and the role of environmental regulations and incentive policies in BRICS', *Resources Policy*, 90. Available at: https://doi.org/10.1016/j.resourpol.2024.104718.

van Tonder, A.J.M., Bolt, G. and van Rensburg, J.F. (2012) 'Compressed air alternative solutions: Challenges encountered in deep level mining', in *2012 Proceedings of the 9th Industrial and Commercial Use of Energy Conference*. Cape Town, South Africa, p. 1. Available at: https://ieeexplore.ieee.org/abstract/document/6330156 (Accessed: 17 August 2025).

Zietsman, L.N., Marais, J.H. and Schoeman, W. (2019) 'A Practical Method for Compressed Air Leak Localisation in Deep-Level Mines', *SSRN Electronic Journal* [Preprint]. Available at: https://doi.org/10.2139/SSRN.3650457.



Quinton Aidan Bekeur

Engineer and Master's candidate
ETA Operations and North-West University

Quinton Bekeur graduated with a bachelor's degree in mechanical engineering from the University of Pretoria in 2024. He is currently pursuing a master's degree in mechanical engineering at North-West University. During his undergraduate studies, he worked part-time as a Makerspace technician at the University of Pretoria, assisting with 3D printing, scanning, and IoT projects. Quinton gained experience in design consultation and hands-on experience in 3D printer maintenance. He completed engineering vacation work at AFMS International, where he supported the construction of BSL-3 laboratories, developed HVAC component drawings, and created airflow calculation templates. Since January 2024, Quinton has been employed by ETA Operations as an Engineer, focusing on energy efficiency in mining. Quinton's role focuses on energy management, with an emphasis on reducing compressed air wastage on mining shafts, where he analyses shaft consumption and implements initiatives to reduce energy use.

A method to reduce compressed air usage through half-level control and usage scheduling

W. Bekker[1,2], J.H. Marais[2], W.H. Sterrenberg[1,2]

[1]ETA Operations (Pty) Ltd, South Africa
[2]North-West University, South Africa

In underground platinum mining, compressed air is used for powering equipment and supporting operational processes. Due to uncontrolled usage, however, compressed air systems often result in significant energy costs and inefficiencies. This paper presents a method to reduce compressed air usage through the installation of automatic actuating valves. Valves are configured with a tailored set-point according to the compressed air demand of each operational half-level. This method involves calculating and applying specific air pressure set-points based on multiple parameters. Using these parameters enables accurate set-point development, resulting in reduced compressed air usage by eliminating oversupply. A case study involved a single half level, equipped with an automatic actuating valve, a pressure meter, and a flow meter. These instruments enabled real-time monitoring and precise regulation of compressed air. The effectiveness of this approach was assessed through continuous monitoring of air flow- and pressure data over time. Results showed an average of 10 000 m^3/h reduction during travel times, cleaning shift, and blasting shift. This translates to an average 4.7 GWh reduction per annum. This not only resulted in significant cost- and energy savings but also helped create a more stable and controlled air distribution system underground. This project demonstrated that compressed air management, achieved through data analysis and automation, is an effective method for enhancing cost-effectiveness and sustainability in the platinum group metal mining industry. The results support expanding this approach across more sections of the mine and potentially to other mining sites using similar systems.

INTRODUCTION

Compressed air is a vital utility in platinum mining. It is also the largest energy consumer of mining operations, adding significantly to electricity costs. Inefficient or uncontrolled usage of compressed air can lead to substantial energy wastage. Proper control strategies help mitigate the wastages and improves efficiency (Emerson, 2022).

Background

Compressed air is one of the most widely used utilities in underground mining operations, particularly in platinum group metal (PGM) mines (Emerson, 2022). Compressed air powers drilling, cleaning, material handling, and other operational tools and equipment. Despite its broad application, compressed air systems are inherently energy-intensive and often inefficient, primarily due to poor control practices, oversupply, wastage and leaks. Compressed air systems are responsible for a substantial portion of energy costs in deep-level mining operations (van Gruting, 2022).

Traditional compressed air supply strategies often rely on set-point pressure settings and generalised control, without accounting for the fluctuating demands of individual levels or shifts. This results in substantial energy wastage, especially during periods of reduced activity such as travel times and non-operational shifts (Liebenberg, Velleman and Booysen, 2012). Consequently, there is a growing need to implement smarter, more targeted control strategies that match compressed air supply with demand.

Minimising compressed air wastage is a simple, yet effective, way of reducing energy usage on the mine and saving cost on electricity (Mathews *et al*., 2019). This paper proposes a solution centred on half-level control using automatic actuating valves configured with set-points tailored to specific operational needs. The approach not only improves compressed air delivery but also introduces a data-driven foundation for continuous improvement and scalability.

Shift pressure requirements and time schedule

There are three main shifts during mining operations: drilling, blasting and cleaning. Each of these operational shifts has their own pressure requirements (Nell, 2017). Figure 1 shows the pressure profile throughout a normal operational day.

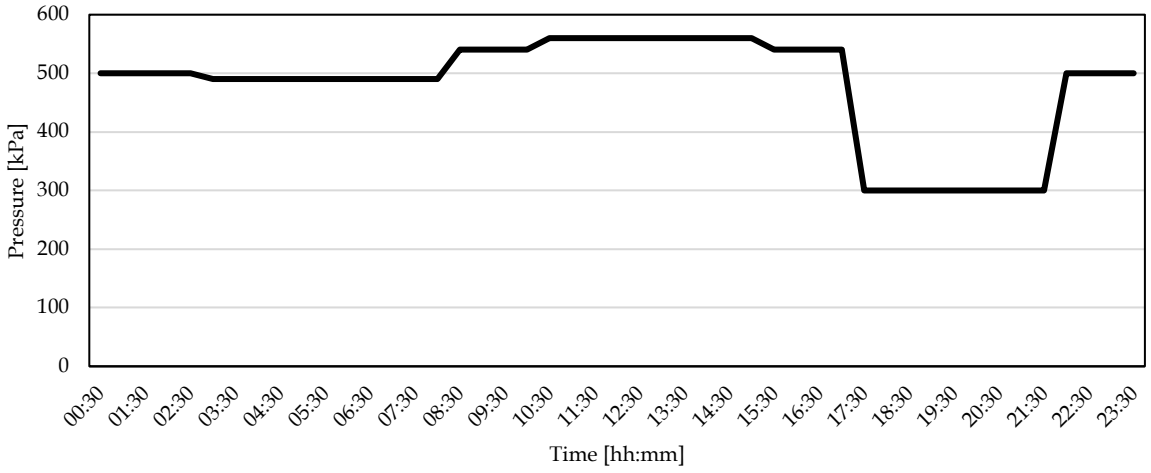


Figure 1. Compressed air pressure profile according to mining shifts on Mine A.

The pressure demand for drilling shift usually requires higher pressure than cleaning shift, as noted in Figure 1. During blasting shift the pressure demand is at its lowest due to compressed air that is only fed to refuge bays to ensure a positive pressure for safety requirements.

Compressed air is generated by surface compressors and distributed through a network of pipelines to the demand areas underground. To manage the supply, open/close valves are typically installed at each level. These valves allow operators to isolate sections of the system when closing air during blasting shifts or when maintenance and repairs are required on the compressed air pipelines but does not give any control over the amount of compressed air fed to each level or half-level (Fouché, 2017).

METHOD

This section explains and illustrates a method to identify inefficiencies in compressed air usage underground, gathering data, analysing data and the development of a solution. The steps taken to find the usage inefficiencies and regular half-level pressure set-point updates lays the foundation of a more active approach to minimise compressed air consumption. The proposed methodology is illustrated in Figure 2.



Figure 2: Proposed method for reducing compressed air usage and reducing pressure set-points.

The flowchart, illustrated in Figure 2, is a continuous feedback loop in which data is regularly reviewed to actively monitor wastage and sustain efficiency. This process operates on both a scheduled basis and in response to operational changes. The flowchart is continually applied to individual half-levels set-points, and then again on shaft pressure set-points when optimal half-level pressure set-points are achieved. The energy and cost saving will be noted when shaft pressure set-points are reduced, and compressor combinations are changed throughout the day.

CASE STUDY RESULTS

This method was applied and implemented at a conventional platinum mine in North-West province of South Africa, which will be referred to as 'Mine A'.

Gather available resources and information

Mine A forms part of an existing compressed air ring supplied by multiple surface compressors feeding several shafts (Sullair, 2021). Units can operate on individual set-points or be coordinated via supervisory control and data acquisition (SCADA), which switches compressors on or off according to demand. Efficient operation requires consideration of compressor number and capacity; the ring feeding Mine A consists of 10 compressors with an installed capacity of 51 MW, and daily shaft set-points are shown in Figure 1.

Accurate data is essential to ensure continuity and avoid production losses. Pipe sizes, distances, and leakage rates were obtained from audits and planning drawings, while calibrated pressure and flow meters provided by SCADA data for analysing under- or oversupply and enabling informed adjustments (U.S. Department of Energy & Compressed Air Challenge, 2003).

Analyse current data and operations

By measuring pressure and flow, current compressed air usage was analysed in relation to operations and shift schedules. While many inefficiencies arise from broader practices, optimising air usage is more

practical—for example, reducing consumption during changeovers or blasting rather than altering the mining schedule (Shaw, 2019).

An effective way to detect over- or under-supply of compressed air is by analysing the inverse relationship between flow and pressure. As illustrated in Figure 3 from Mine A, flow increases while pressure drops during drilling, and the opposite occurs before blasting. Figure 3 reflects data from a half-level where an automatic pressure-controlled valve was installed but left fully open for the entire day. This approach aligns with established diagnostic methods using time-series analysis of flow and pressure to pinpoint supply inefficiencies (Titova & Kosturkov, 2025).

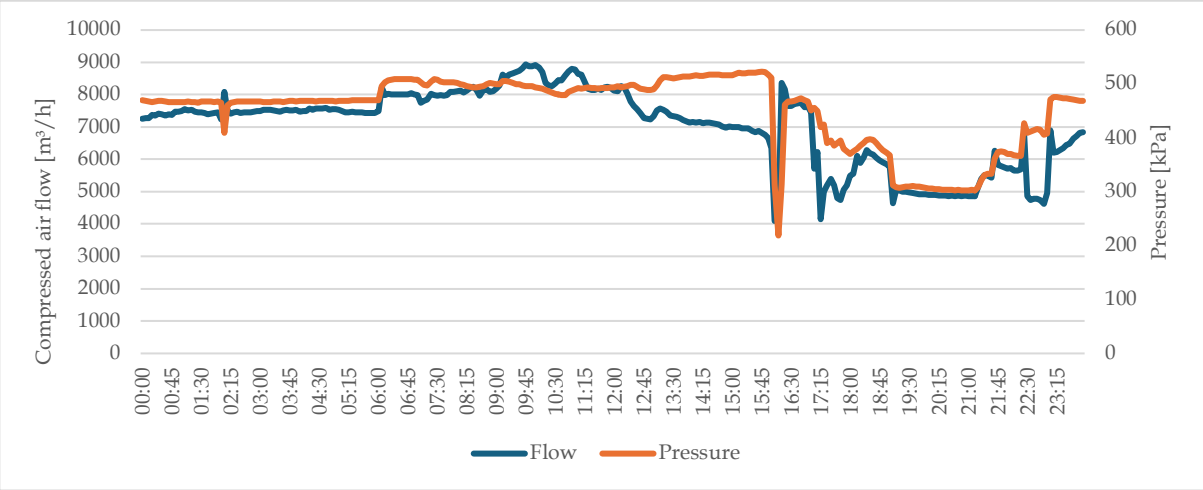


Figure 3: Compressed air flow compared with pressure.

As additional equipment consumes additional compressed air, system pressure decreases, requiring greater power input at the compressors to maintain supply, as shown in Figure 2. Mine A's compressor ring operates according to fixed pressure set-points, and the compressors will continue to maintain or attempt to maintain the designated pressure regardless of demand. Consequently, when fewer equipment uses compressed air than accounted for, the system will oversupply, resulting in unnecessary power consumption and increased operational costs (Compressed Air Challenge, 2003).

Pressure requirement simulations

Compressed air demand at each half-level is first established through a baseline based on crew numbers, equipment, pressure needs, and shift schedules. This creates a zero-waste baseline—an ideal performance target while also highlighting opportunities for improvement in the reticulation network (van der Merwe, Gous & Schutte, 2022).

The zero-waste baseline was refined through audit findings such as leaks, idle cross-cuts, or faulty valves, ensuring supply better matched actual demand. Additional factors—including ring feeds, piping distance, and system capacity—also affect pressure and flow (Prompt, 2025). Considering these variables produced a more reliable pressure baseline, forming the first step in set-point creation.

As mining operations continually evolve, it is essential to review this step regularly to ensure that the pressure set-points for each half-level remain aligned with current mine planning and operational requirements.

Identify inefficiencies

As previously discussed, the graphs in Figure 3 highlight notable inefficiencies, by investigating the inverse correlation of pressure and flow data. Data received form Mine A illustrated how a concise decision can be made on where certain areas were optimisable. Refer to the highlighted sections in Figure 4, which shows certain time periods throughout the day where small to large inefficient uses of

compressed air are pointed out. These areas are marked due to the pressure that either stays constant with flow or shows a strong inverse correlation.

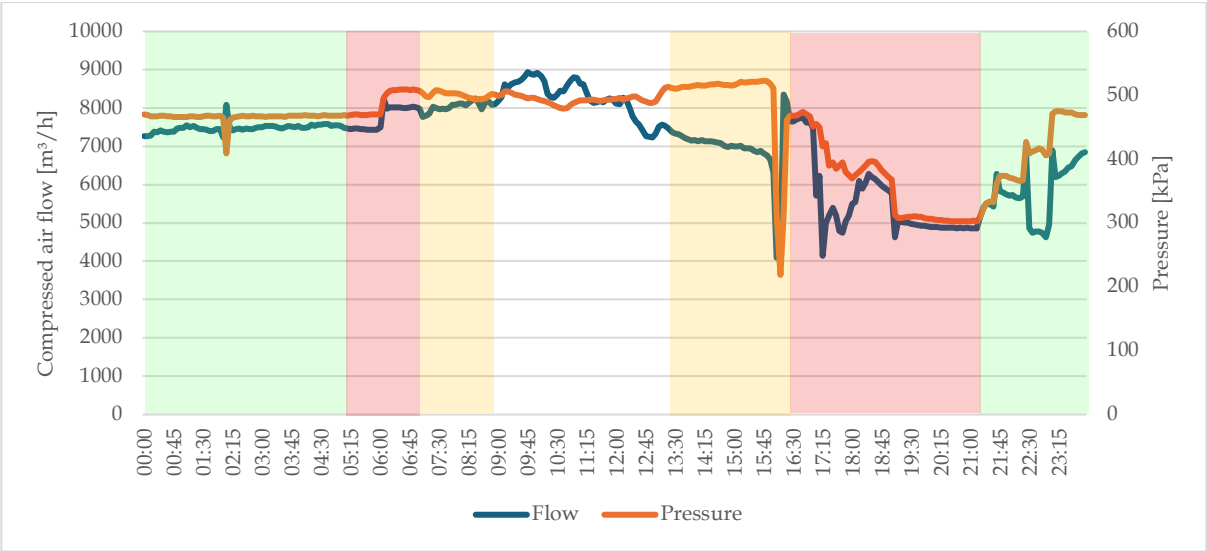


Figure 4: Inefficiency identifications.

The highlighted sections seen from Figure 4 can be explained as follow:

- **Green:** Cleaning shift, where compressed air is mainly used for hoisting and loaders. Pressure set-points can be reduced to match equipment and crew requirements.
- **Orange:** Travel, planning, or start-up periods. Demand rises as crews enter working areas and reduces before blasting as they leave.
- **Red:** Changeovers (05:00–07:00; 16:30–17:30) and blasting. Air is only needed for refuge bays, so pressure can be lowered while maintaining positive pressure.
- **White:** Indicates the drilling shift, which is crucial for production. Therefore, changing drilling shift pressure needs to be well evaluated before being changed.

Forecast new set-points

The forecasting of set-points consolidates all preceding steps and the information gathered to develop an updated and optimised set-point for each half-level. This process ensured that the set-points were aligned with operational requirements, while simultaneously accounting for wastages and reducing inefficiencies throughout the day (Burger, 2024). By comparing the pressure data shown in Figure with the forecasted set-points illustrated in Figure , it became evident where compressed air flow could be optimised, thereby reducing wastage.

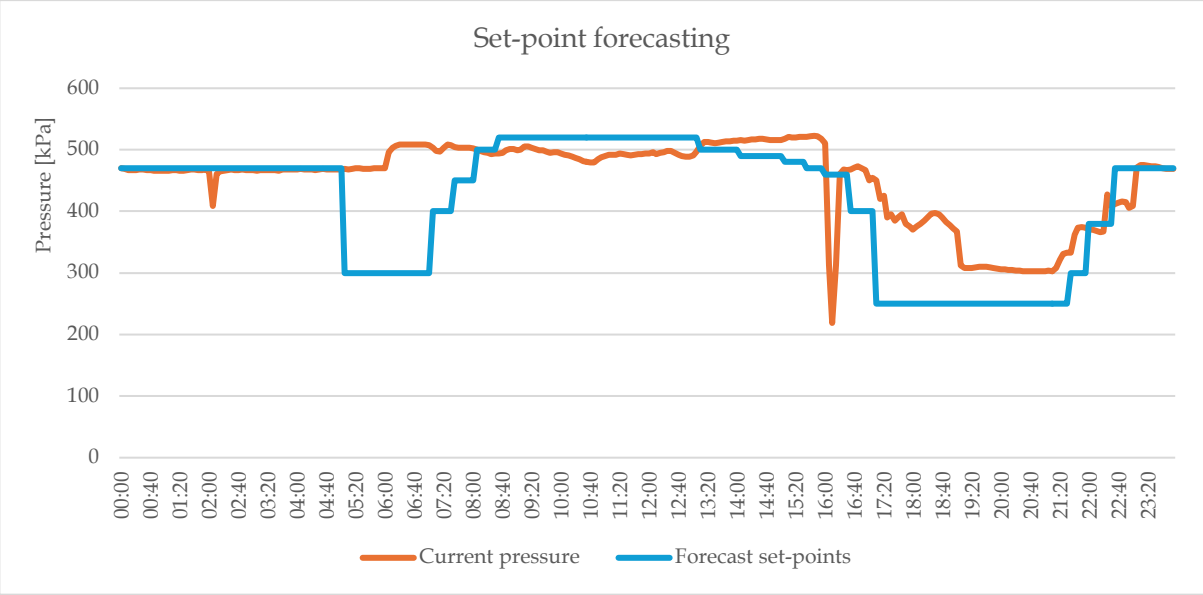


Figure 5: Pressure set-point forecasting.

Significant adjustments were implemented during travel times and the blasting shift, as these periods present key opportunities for cost savings without affecting production activities.

Propose new set-points
The implementation of new set-points was documented, approved, and clearly communicated to all stakeholders, ensuring production and maintenance remain unaffected. Forecasted set-points were justified with calculations and aligned with mine planning.

Implement new set-points
After sign-off was received and communication sent out, the set-points was implemented on the SCADA for the controlling valves. Date and time of implementation were taken to be able to compare changes to previous set-points.

If it happens that multiple valve set-points need to be changed at once, then it would be good practice to apply the same method to each individual half-level, to ensure validity and reliability.

Analyse Results
Analysing new set-points is essential for cost savings and to confirm whether compressor combinations are optimal. Reviewing half-level set-points also requires assessing shaft pressures, since changes underground affect surface conditions. The same method used for half-level optimisation can be applied to surface set-points to prevent unnecessary compressor starts and enable efficient power use aligned with actual demand.

Analysis of the adjusted half-level compressed air set-points at Mine A demonstrated clear opportunities for improved air usage. Figure 6 illustrates the improvements on compressed air flow for one half-level after the new set-points were implemented. Most improvements are noted during the change-overs, start-ups and blasting shift. It is assumed that no repairs were made to the compressed air leakages during the time of baseline creation and after implementation. Therefore, a baseline of ± 4000 m^3/h can be assumed to be wasted due to open cross-cuts valves, leakages and refuge bays during

the blasting shift when it was confirmed that no equipment was using compressed air from 18:00 until 21:00 as seen in Figure 6.

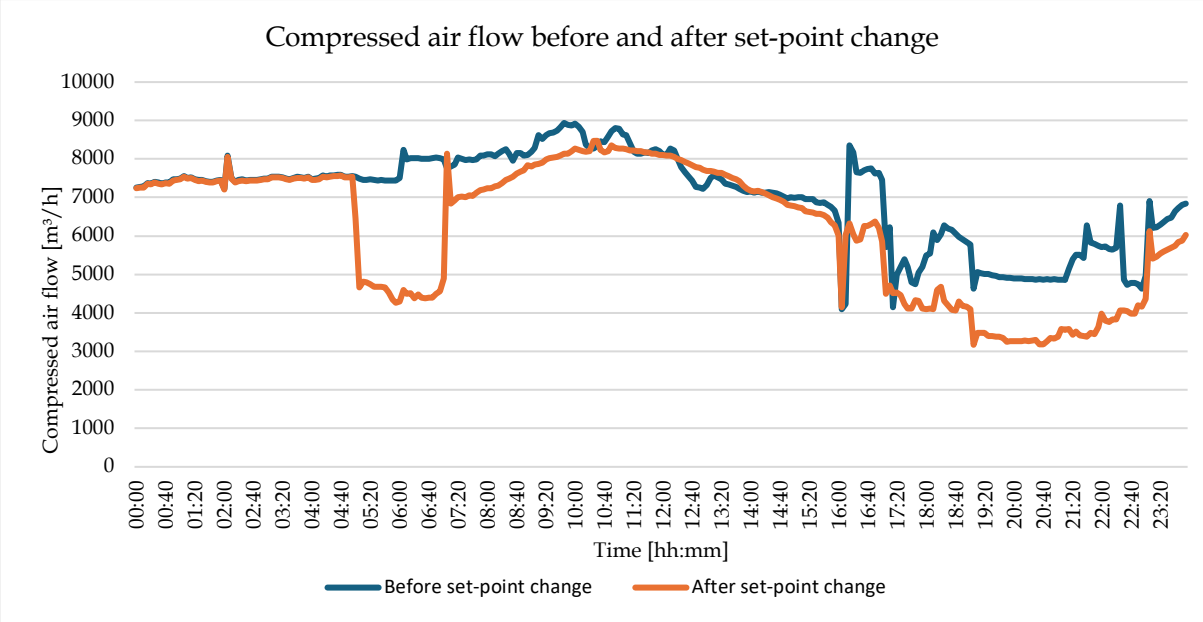


Figure 6: Compressed air flow before and after set-point change.

Follow-ups on compressed air complaints and data analysis on hoisted tonnes were done frequently to ensure that the changes that were made, as seen in Figure 6 did not disrupt production. The application of the proposed methodology at Mine A demonstrated measurable improvements in compressed air efficiency. An average of 10 000 m³/h reduction was noted by reducing the pressure set-points according to the methodology.

Analysis of pressure and flow data revealed that significant inefficiencies occurred during changeovers, start-up periods, and blasting shifts, where demand was minimal, yet compressors continued to maintain higher pressures. Implementation of the new set-points through the SCADA system resulted in noticeable reductions in unnecessary compressor operations. Figure 6 highlights the improvement, showing lower compressed air wastage particularly during blasting shifts and crew travel times.

Assuming that 10 000 m³/h is equal to an average electricity demand reduction of 8 MW by taking into account the number of installed compressors, average power usage and compressed air generation, it totals to an average of 4.7 GWh reduction per annum. This accounts for an average cost saving of R 11.35 million per annum. The cost saved is in accordance with the individual compressor capacities, optimisation of compressor combinations running to maintain pressure set-point and the electricity cost, with consideration taken of winter and summer tariffs per kWh. This data made it possible to determine the rough estimate of cost per cube, which is R 0.19/m³. Importantly, production remained unaffected, as confirmed through regular monitoring of hoisted tons and operations feedback.

CONCLUSION

This research confirmed that optimising only one half-level's pressure set-points can bring substantial cost savings to deep-level platinum mining operations. By means of the introduction of automatic actuating valves, accurate flow- and pressure measurements, and a formal data analysis and prediction process, inefficiencies were identified and remedied.

The results of Mine A demonstrate that one half-level can, on average, reduce air consumption by approximately 10 000 m³/h. Focusing on non-productive times, such as changeovers and blasting shifts, yields the greatest return while maintaining safe and effective operations. This amounts to an energy reduction of 4.7 GWh per annum. Furthermore, extending the methodology to half-level and shaft pressure set-points enables more effective compressor operation by preventing unwanted starts and oversupply.

In conclusion, the paper illustrates the value of data-driven compressed air management as a scalable energy optimisation solution for platinum mining. Regular review and revision of set-points, incorporated into mine planning, ensures sustained efficiency improvements and cost savings in the long term.

REFERENCES

Burger, P., 2024. Future mines' compressed air planning using digital twin simulations. *South African Journal of Industrial Engineering (SAJIE)*, 35(3), pp.1–12. Available at: https://scielo.org.za/pdf/sajie/v35n3/10.pdf

Compressed Air Challenge (CAC), 2003. *Improving Compressed Air System Performance: A Sourcebook for Industry*. 2nd ed. Washington, D.C.: U.S. Department of Energy. Available at: https://www.airbestpractices.com/system-assessments/piping/storage/system-assessments/piping/storage-0

Emerson, 2022. *Compressed Air in a Mine: Case Study of an Underground Platinum Mine near Rustenburg*. Available at: https://www.emerson.com/documents/automation/case-study-compressed-air-in-a-mine-en-10214228.pdf

Fouché, S., 2017. *Improving efficiency of a mine compressed air system*. Master's thesis. North-West University, South Africa.

Liebenberg, L., Velleman, D. & Booysen, W., 2012. A simple demand side management solution for a typical compressed air system at a South African gold mine. *Journal of Energy in Southern Africa*, 23(2), pp.20–29.

Mathews, G.E., Taljaard, J., van Laar, J.H., Vosloo, J.C. & Mathews, E.H., 2019. Practical low-cost method to sustain mine compressed air savings. *Proceedings of the 17th Industrial and Commercial Use of Energy (ICUE) Conference*, Cape Town, South Africa, 2019. IEEE, pp. 1–6.

Nell, D., 2017. *Optimising production through improving the efficiency of mine compressed air networks with limited infrastructure*. Doctoral dissertation. North-West University, South Africa.

Prompt, 2025. *Compressed Air Piping Design Handbook*. [pdf] Available at: https://www.prompt.tennessee.edu/uploaded-files/2P8014/fetch.php/CompressedAirPipingDesignHandbook.pdf

Shaw, W., 2019. Using specific energy as a metric to characterise compressed air system performance. *Energy Efficiency*, [online] Available at: https://www.sciencedirect.com/science/article/abs/pii/S2213138818301656

Sullair, 2021. *Using Compressed Air in the Mining Industry*. [pdf] Available at: https://europe.sullair.com/sites/default/files/2021-01/Sullair%20Blog%20-%20Using%20Compressed%20Air%20in%20the%20Mining%20Industry.pdf

Titova, T. & Kosturkov, R., 2025. Analysis of the time series of compressed air flow and pressure and determining criteria for diagnosing causes of pressure drop in pneumatic systems. *Applied Sciences*, 15(17), article 9536. doi:10.3390/app15179536

van Gruting, U., 2022. Investigating the link between compressed air wastage and ventilation shortfalls in deep-level mines. *South African Journal of Industrial Engineering*, 33(3), pp. 49–59. Available at: https://www.scielo.org.za/scielo.php?pid=S2224-78902022000300010&script=sci_arttext

van der Merwe, A., Gous, A.G.S. & Schutte, C.S.L., 2022. Using zero-waste baselines to identify compressed air system inefficiencies in deep-level mines. *Proceedings of the 33rd Annual Conference of the Southern African Institute for Industrial Engineering (SAIIE33)*, 3–5 October 2022, Zimbali, South Africa. Johannesburg: Southern African Institute for Industrial Engineering, pp.1–12.



Werner Bekker
Project Engineer and Master's candidate
ETA Operations (Pty) Ltd and North-West University

Werner is a qualified Mechanical Engineer with a strong foundation in engineering design, energy management, and business development, particularly within the mining and industrial pumping sectors. With a bachelor's degree in mechanical engineering from North-West University, he has cultivated a diverse skill set through hands-on experience across project engineering, consulting, and international client relations.

Currently working as a Project Engineer at ETA Operations where he leads and supports initiatives aimed at improving operational efficiency and reducing energy costs. Werner's role involves daily data analysis on compressed air, ventilation, and refrigeration systems, conducting feasibility studies, and collaborating closely with mining personnel to implement cost-saving strategies.

Other aspects of his role at ETA Operations includes conducting power failure simulations, underground audits, and drop tests, as well as identifying inefficiencies and compressed air leakages in mining systems. Demonstrating a strong ability to communicate and build trust with stakeholders at various levels, including mine engineering managers and engineers, ensuring smooth execution and alignment on project goals.

Prior to his work in the mining sector, he served as a business development and engineering consultant at Vesconite Bearings. In this role, he provided technical and designing consulting services to clients across Europe and the United States, creating tailored solutions for bushing and bearing applications. His experience also included conducting GAP analyses and delivering client-focused presentations.
Werner thrives in high-pressure environments and enjoys solving complex problems. With a personal motto of, "Every problem has a solution," which reflects a determined mindset. Being a team-oriented professional who embrace challenges and adapts quickly to different fields, always seeking opportunities to drive improvement and innovation.

Energy savings achieved through compressed air control valve control

W. Biermann[1], J. van Rensburg[2], T. Deysel[3], I. Rudolph[3], L. Mukengeshayi[3]

[1]ETA Operations (Pty) Ltd, South Africa
[2]North-West University, South Africa
[3]Valterra Platinum (Pty) Ltd, South Africa

South Africa's energy landscape is characterised by rising electricity tariffs, with Eskom's rates increasing by over 60% in the past five years. These growing energy costs threaten profitability and long-term sustainability, making energy efficiency and innovative management essential priorities. Valterra Platinum, formerly known as Anglo American Platinum, is working to improve operational efficiency, cut its carbon footprint, and ensure the long-term viability of its operations amid an increasingly complex energy environment.

One of the projects identified at the Amandelbult mining complex focuses on the compressed air system. Compressed air systems are crucial in mining operations, not only powering various tools and machinery but also providing vital support for life-sustaining refuge chambers. Consequently, compressors are among the most energy-intensive systems, representing a significant portion of a mine's energy use. Inefficient operations, such as leaks, high-pressure supply, and malfunctioning components such as valves and actuators, inevitably result in energy wastage.

Significant energy savings were achieved through the implementation and monitoring of control valves on the compressed air system. These valves play a crucial role in regulating the pressure of the compressed air supplied to the various operations. By regulating the pressure, the system requires less airflow, which directly lowers the energy demand from the compressor system.

After gaining control over the valves, the pressure supply to various operations was dynamically adjusted to meet demand. This change reduced the flow of compressed air while still meeting operational needs. The pressure supply was further optimised throughout the day by leveraging the Eskom time-of-use tariff structure. Due to the altered compressed air demand profile caused by the control valves, the compressor schedule was also modified to maximise savings potential. This approach resulted in a cost saving of R56 million for 2024.

The control valves are monitored daily and require regular maintenance to sustain the savings. Daily reports have been created to monitor the status of each valve, enabling quick response if a valve fails.
Further optimisation is still possible; however, this initiative has not only improved the efficiency of the compressed air system but also contributed to a reduction in operational costs. The energy savings achieved through this initiative highlight the significance of operational efficiency and continuous energy management.

INTRODUCTION

Background

South Africa's energy landscape has become increasingly unstable due to persistent challenges faced by the national utility, Eskom. Over the past five years, Eskom has implemented cumulative tariff increases exceeding 60%, placing considerable financial pressure on energy-intensive sectors such as the mining and heavy industry (Eskom, 2024), (NERSA, 2024). Given that the mining sector is among the most electricity-dependent industries in the country, these rising costs pose a substantial threat to its operational sustainability and long-term viability (Arnoldi, 2023; Botha, 2022).

To further manage national electricity demand, Eskom has historically employed time-of-use (TOU) tariff structures, particularly under its Megaflex tariff, which targets large industrial consumers such as mines. These structures incentivise users to reduce or shift electricity consumption away from peak periods, thereby alleviating pressure on the grid (Lunika, Mtakati and Silwal, 2023), (Eskom Holdings SOC Ltd., 2024). While such mechanisms may promote system stability, they also increase the complexity of energy management for large-scale operations and reinforce the need for improved energy efficiency and demand-side interventions.

In response to these challenges, Valterra Platinum has committed to a long-term energy efficiency strategy aimed at improving both energy intensity and reducing its associated carbon footprint. Anglo-American Platinum (now Valterra Platinum) has set a target to reduce its energy intensity by 30% by 2030 as part of its broader sustainability objectives (Valterra Mining Ltd., 2024). Achieving this target will require the identification, evaluation, and implementation of targeted energy efficiency projects and operational improvements across all operations.

One of these projects is on the compressors running at the Amandelbult complex. These compressors have an installed capacity of 55 MW and make up an estimated 32% of the electrical energy consumption of Amandelbult. At present, there are 11 compressors with a potential 12th compressor being considered for installation, which would increase the installed capacity. These compressors service the entire Amandelbult which consists of a concentrator, two main shafts (Tumela 1# and Dishaba 2#), and various smaller mining sections classified either as footwalls (FW) or raise bores (RB). Figure 1 shows the energy distribution at the mining complex and highlights the portion of energy used by the compressors.

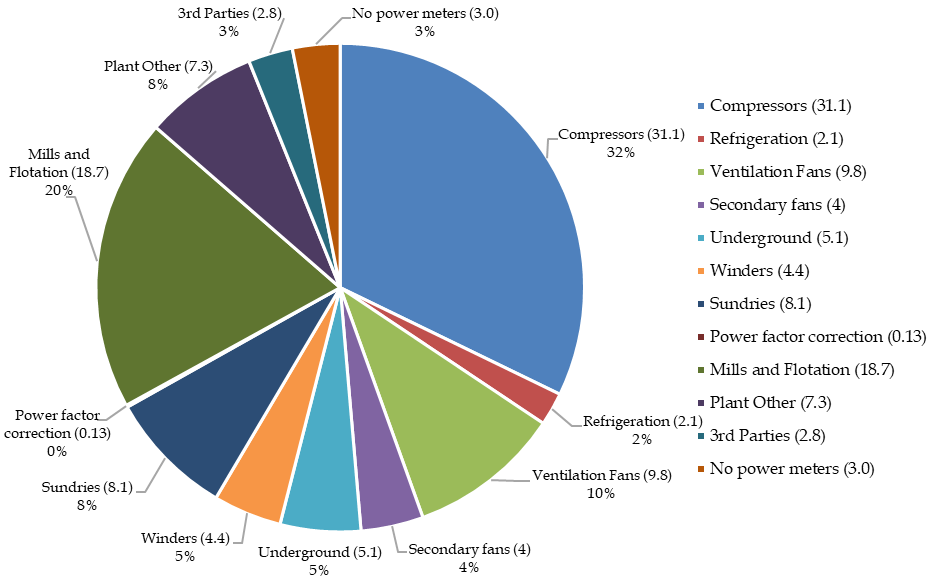


Figure 1 - Amandelbult's power distribution.

Problem statement
Compressed air systems are inherently inefficient. Studies show that in many industrial environments, up to 50% (Matthee, 2021) of the energy used for compressed air is wasted due to poor design, leaks, over-pressurisation, and suboptimal scheduling. At the Amandelbult mining complex, compressed air is the largest energy consumer, representing over 32% of the total electrical energy bill.

Objective
The primary objective of this project was to reduce energy consumption and operational costs within the compressed air network by:

- Reviving and optimising pressure control valves across the system
- Optimising compressor scheduling in response to improved control
- Implementing continuous monitoring and reporting to sustain performance gains
- Reducing energy usage during Eskom's peak demand periods
- Lowering overall energy costs and energy intensity across the mining complex.

METHODOLOGY

System description
Amandelbult operates 11 compressors feeding into a surface compressed air network spanning over 25 km. The four primary compressor stations are situated far apart and need to maintain an average system pressure of 500 kPa and supply a peak demand of 170,000 CFM. Figure 2 indicates the average pressure and flow supply as well as the locations of the compressors.

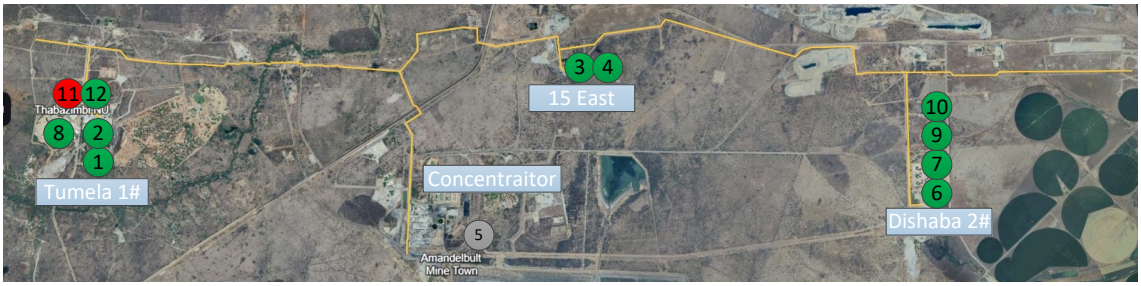


Figure 1 - Compressor locations.

To meet the required pressure and flow demands, a combination of the 11 operational compressors is utilised. Specifications for each compressor are provided in Table I.

Table II. Amandelbult compressor list

Operation	Nr.	Description	Control	Rated power (kW)	Rated flow (CFM)
Tumela	1	Brown Boveri - Sulzer	Trim	4.8	30 000
	2	Brown Boveri - Sulzer	Trim	4.8	30 000
	8	VK125	Baseload	15	65 000
	11	Siemens	Trim	2.85	21 000
	12	Siemens	Trim	2.85	21 000
15 East	3	Centac	Baseload	4.8	30 000
	4	Centac	Baseload	4.8	30 000
Concentrator	5	Ingersoll Rand (Decommissioned)	Baseload	2.8	15 680
Dishaba	6	GHH	Baseload	4.8	30 000
	7	Brown Boveri - Sulzer	Trim	4.8	30 000
	9	Siemens	Trim	2.85	21 000
	10	Siemens	Trim	2.85	21 000
Totals	**12**	**-**	**-**	**55.2**	344 680

Given the integrated compressor network, continuous monitoring of critical equipment is essential. Key operational data—including compressor power consumption, guide vane and blow-off valve positions—is recorded and stored on the historian (a central repository for all operational data). Additionally, flow and pressure measurements are captured at compressor stations, underground distribution points, and individual mining levels, enabling comprehensive performance assessment and system control.

Reinstatement of old control valves

To improve pressure supply within the compressed air network, control valves at multiple locations were reinstated and commissioned. On the surface, valves at key sites, including 28W FW, 15E FW, 15E RB, the concentrator (Conc), 44E FW, 50E FW, and 62E FW, have been restored. Underground, control valves have been revived at Tumela across levels 8L to 16L, and at Dishaba from levels 10L to 19L.

The restoration of these valves facilitates dynamic control of compressed air pressure in response to varying demand and operational requirements. By adjusting valve positions, the system can maintain optimal pressure levels, reduce unnecessary air leaks through reduced pressure supply, and improve overall energy efficiency across both surface and underground networks (Liebenberg, Velleman and Booysen, 2012). This targeted pressure control is essential for sustaining stable operations and minimising energy consumption within the mining complex.

The control valves are pneumatically operated and adjusted based on a pressure setpoint. A pressure profile is used to open or close the valve to match the downstream pressure to the setpoint by restricting the supply. However, if the supply pressure is already below the setpoint, the valve remains open, and no control or reduction is possible. Figure 3 illustrates this control process, with a valve position of 0% indicating when the valve is completely open, and 100% indicating it is fully closed.

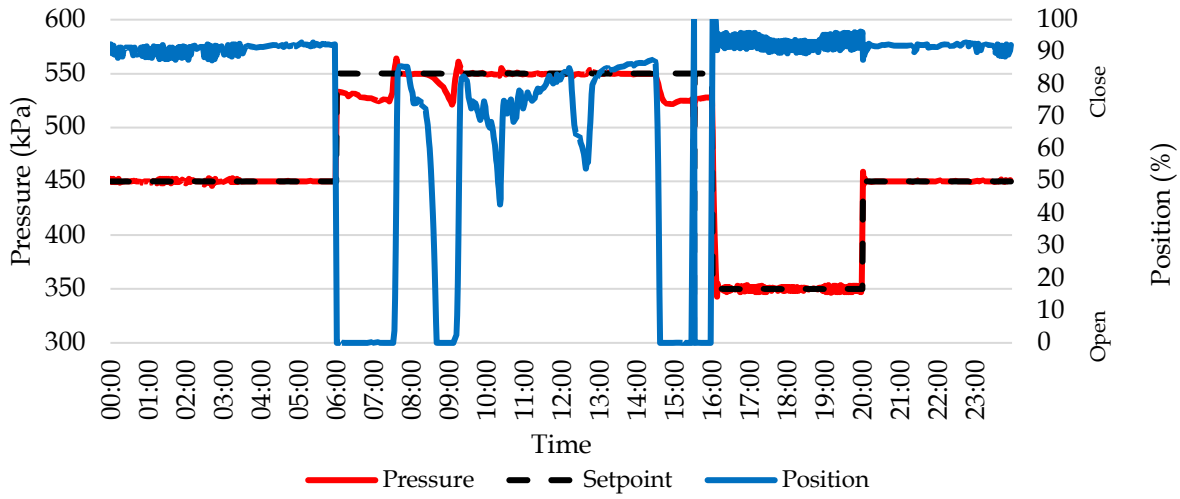


Figure 3 - Valve control.

Pressure supply and demand matching

Compressed air was supplied to the main ring at an average pressure of 550 kPa throughout the day. With the reinstatement of control valves, pressure delivery to specific areas can now be regulated more effectively. By supplying only the required pressure, based on operational demand, the load on the compressors is reduced, leading to lower energy consumption and improved overall efficiency.

Compressed air is mainly used for drilling, refuge chambers and pneumatic equipment such as loaders. To reduce the pressure of the system, the end users' pressure requirements must be taken into consideration. The operational area of the equipment is also important, as the pipe network underground is extensive and can lead to large pressure drops, especially if there are air leaks in the system.

Drilling: The bulk of the compressed air is used for drilling. As a result of the distance and inefficiencies of the underground air network, high pressure must be maintained during the drilling shift to avoid any production losses. The drilling shift is usually between 07:00 and 15:00.

Refuge chambers: Compressed air must be supplied at all times to the refuge chamber as per the Mine Health and Safety Act. This is to ensure that the refuge chambers are pressurised, and no harmful gases enter the chamber. Refuge chambers have a relatively low-pressure requirement, and small changes to the system will have little to no effect. Refuge chambers are mostly located in the main haulage, and the pressure drop at the delivery point is relatively low.

Pneumatic equipment: This includes loaders, air pumps, agitation etc., which require low volumes of air at high pressures (450 kPa and above) to operate effectively. The pneumatic equipment is operated sporadically throughout the day. Most of the pneumatic equipment is located near the main shaft, therefore drops in pressure because of network inefficiencies will not have as great an influence as with drills. However, loaders are mainly used at night during the cleaning shift and are located at the far ends of the shaft, in areas where active development and mining operations are concentrated. Subsequently, loaders are the limiting factor to consider during evening pressure reduction.

A summary of the pressure requirements for the different equipment is indicated below in Figure 4. The current supply pressure is also indicated. From the figure one can deduct that only during the drilling shift does the supply pressure match the required pressure. During the remaining periods, the compressed air pressure supply is higher than needed, especially during the blasting shift. This additional pressure is not being utilised and is wasted through inefficiencies such as leaks.

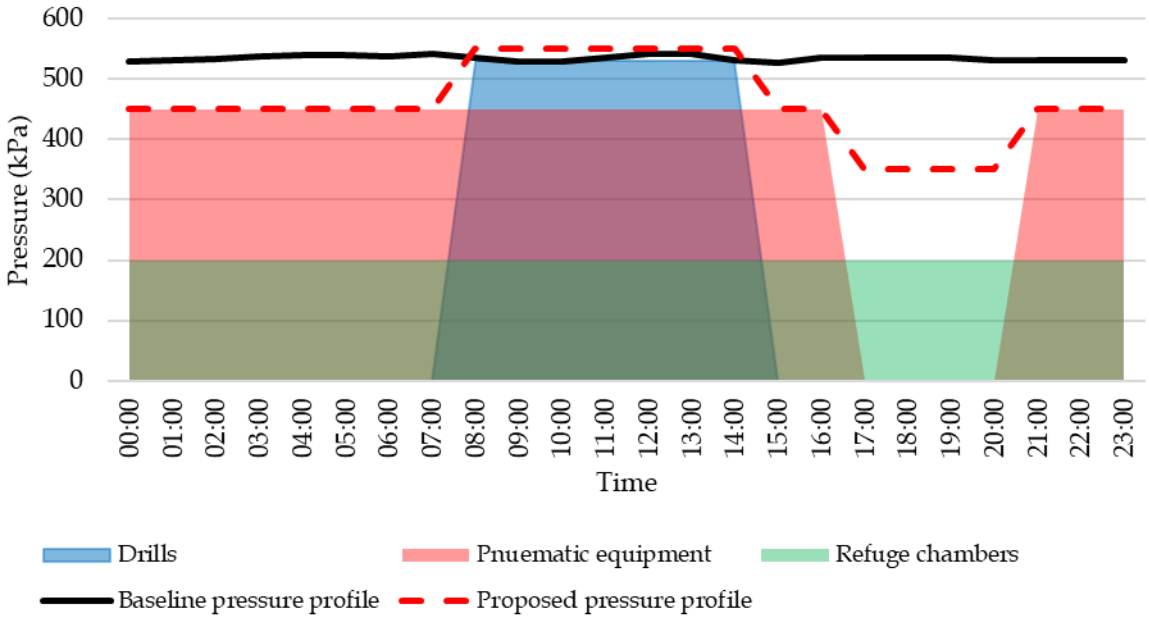


Figure 4 – Compressed air ring supply pressure vs required pressure.

Scheduling

The operation of the compressors is controlled by each of the different sites based on the guidelines as shown in Table II. Additionally, the operators also ensure that a pressure of 500 kPa is maintained and will start additional compressors if needed to maintain this pressure.

Table II. Amandelbult complex compressor start and stop guidelines

Shaft	Compressor	Start time	Stop time	Run time
Tumela	1	09:15	12:30	03:15
	2	Off	Off	(Alternating 1 and 2)
	8	Baseload		-
15 East	3	Baseload		-
	4	Baseload		-
Dishaba	5	Baseload		-
	6	Baseload		-
	7	07:30	13:45	06:15
	9	08:30	11:30	03:00
	10	Off	Off	(Alternating 9 and 10)

Due to the interconnected nature of the compressed air ring, the actions of individual operations directly impact the entire network. For instance, if pressure drops below 500 kPa at one site, the resulting system-wide pressure drop can trigger multiple operations to start additional compressors. This can lead to oversupply, increased energy consumption, and unnecessary cycling of compressors.

Additionally, the reintroduction of control valves significantly alters system dynamics, making effective control of compressors essential. While reduced air demand creates potential for energy savings, these benefits can only be realised if compressor output is adjusted accordingly. To ensure this, compressor usage must be closely aligned with actual system requirements. Due to the dynamic nature of mining operations, a static compressor schedule is inadequate. Therefore, the compressor scheduling strategy must be continuously reviewed and updated to reflect these changes and maintain overall system efficiency.

Operational patterns do not only fluctuate daily but also weekly, monthly, and annually. To ensure optimal efficiency, the valve schedule must be dynamically adjusted to align with periods of reduced compressed air demand. These periods typically include off-Saturdays, Sundays, public holidays, pay weekends—when production activities often slow down—and extended shutdowns such as the December holiday break. By proactively adapting the valve schedule to these low-demand times, unnecessary energy consumption can be minimised, contributing to overall cost savings and improved system efficiency.

Tariff strategy (Time of use)
Building on the improved control enabled by the reinstated air valves and adaptive compressor scheduling, Eskom's TOU tariff was also leveraged to further optimise energy costs. By reducing compressed air supply and limiting compressor operation during high-tariff periods, the system avoided unnecessary energy usage and reduced peak demand charges. This integration of pressure control and TOU alignment ensured that energy reductions translated into direct cost savings across the compressed air network.

Simulation Software
Simulation software enables detailed modelling of compressed air networks, replicating real conditions to test control strategies and identify inefficiencies without disrupting production. Integrating scenario analysis with historical data supports accurate predictive modelling and reduces implementation risks. In-house simulation software (Process Toolbox) was used to develop a digital twin of the compressed air system. The simulation was used to evaluate scenario and to identify potential future energy savings requiring capital investment.

Baseline Data Collection and Audit
A means to measure the impact of the initiative is required after the improvements on the system have been completed. A baseline of the compressor network was created before any changes were made to the system. Energy profiles have been created for weekdays, Saturdays and Sundays. During the baseline period, compressors 9,10, 11 and 12 were not yet installed, while compressor 5 was operational

at the time. Compressors 9 to 12 were later installed to provide additional compressed air supply capacity.

Historical data, from the beginning of 2023/01/03, up until 2023/9/11, was used to create the baselines. Days where significant data loss occurred were excluded from the baselines. The resulting baseline power profiles are shown in 5.

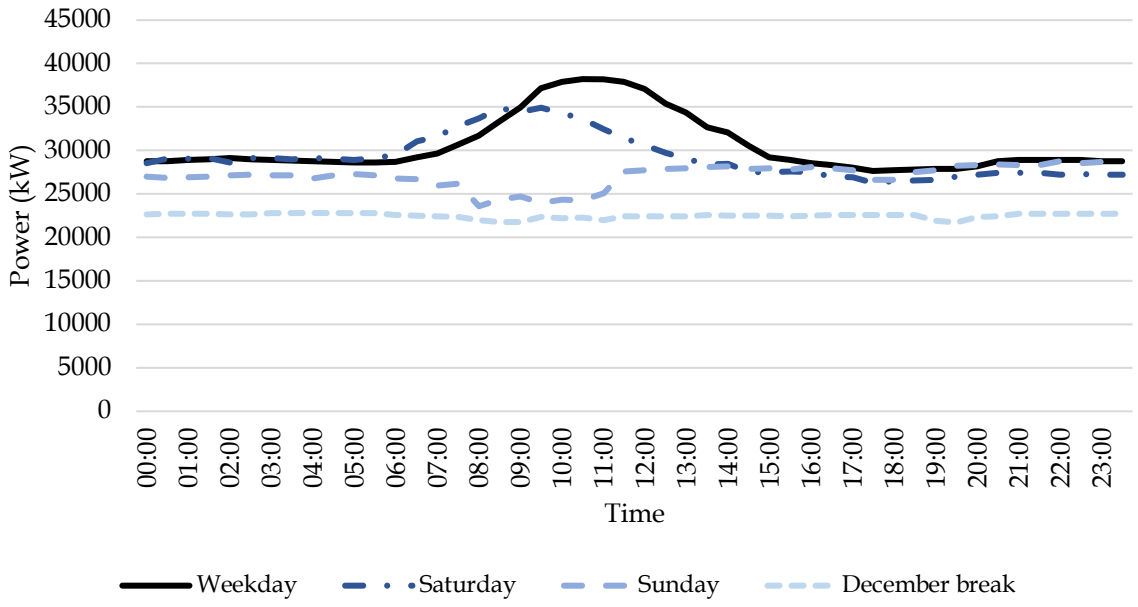


Figure 5 - Baseline profiles.

For public holidays, a Sunday average power profile is recommended. Each public holiday will be evaluated, and an appropriate baseline will be used. The baseline is currently not scaled. Scaling of the baseline can be done to adjust for future changes in production, technology used, etc.

RESULTS

Control valve commissioning

The commissioning of control valves was carried out in a phased approach, prioritising areas with the highest compressed air usage. Dishaba was selected as the starting point for implementation due to a combination of its availability and high usage profile. Once the system was successfully deployed and tested at Dishaba, the project advanced to Tumela shaft. Both Dishaba and Tumela consist of multiple working levels that each require individual valve control to effectively manage compressed air demand.

Following the successful commissioning at the main shafts, the control system was expanded to include surface installations, particularly at the raise bores and footwall mining areas. These areas also contribute significantly to air usage and benefit from the same demand-driven control strategy. Figure 6 illustrates the progress made during the commissioning process, reflecting the systematic efforts and the scale of implementation across both underground and surface infrastructure.

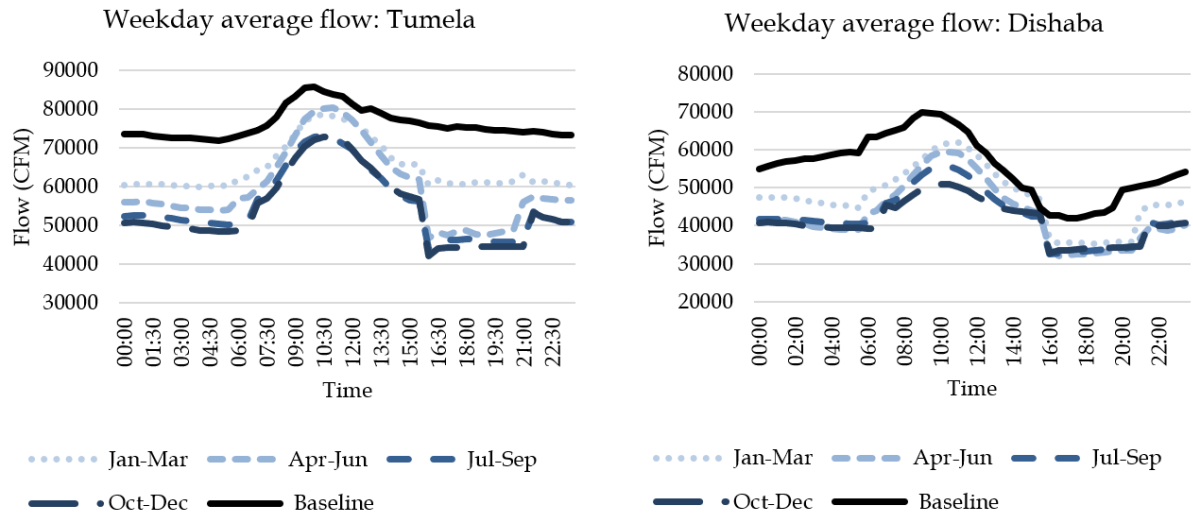


Figure 6 – Valve control progression (Tumela left, Dishaba right).

Control valve pressure setpoint reduction
Pressure supply was reduced based on mining demand, as outlined in the pressure supply and demand matching strategy. Equipment such as drills, refuge chambers, and pneumatic tools were considered when setting each valve's pressure setpoints.

During peak production, the setpoint was limited to 550 kPa to ensure optimal drilling performance, as higher pressure improves drilling speed. Once drilling is complete and blasting occurs—when most personnel are out from underground—air demand drops significantly. Only minimal usage remains at loading boxes near the shaft or on the surface.

Pressure regulations during this period are limited by the valve design. These valves are fail-to-open and require a minimum pressure to function. Below this threshold, the valves fully open and lose control capability. Additionally, due to valve and pipe sizing, pressure cannot be reduced below 300 kPa, as the valve is nearly shut at this point. To avoid instability, the minimum setpoint was kept at 350 kPa.

After blasting, the cleaning phase begins. Compressed air is needed for refuge chambers, loading boxes, and other low-demand equipment. The main constraint is the loading boxes, which need relatively high pressure to operate under the weight of broken rock. As a result, the setpoint during this phase was limited to 450 kPa.

The time periods were refined and optimised after the initial implementation and the learnings thereof.

The surface valves were optimised similarly; however, they were greatly limited because of their location. These valves supply the whole mining section, meaning that the surface loading boxes are also affected. This was partially overcome by supplying a dedicated line to the loading box. As a result, the pressure supply was limited by 450 kPa at a minimum and increased to 550 kPa when the drilling shift was in effect.

Compressor schedule adjustments
The implementation of control valves led to a significant reduction in compressed air demand, particularly during low-demand periods. To align with the reduced demand, the compressor running schedule was revised, improving overall system efficiency. These adjustments were made dynamically in response to real-time demand patterns, allowing for continued optimisation of both energy use and system performance.

Alongside the demand reduction, several key system changes impacted the supply strategy.

Compressor 5 at the concentrator was decommissioned, and four new compressors were added – Compressors 9 and 10 at Dishaba, followed by Compressors 11 and 12 at Tumela. These additions required a reassessment of the compressor schedule to ensure reliable and efficient air delivery across the network. Ongoing adjustments to the compressor schedule were essential to maintain a balanced supply-demand relationship. This ensured that only the necessary compressors were running at any given time, avoiding excess generation and unnecessary energy costs.

Further savings were achieved by aggressively cutting back valve setpoints during known low-demand periods, such as pay weekends, Sundays, off-Saturdays, and the December break. By leveraging these predictable downtimes, the system was able to operate at a minimal compressed air supply without affecting production, unlocking additional energy and cost savings.

Monitoring
As part of the control and optimisation strategy, daily reports were generated and distributed to relevant stakeholders. These reports provided a clear overview of valve compliance for each working level across the shafts.

Valve compliance referred to how closely the actual downstream pressure aligned with the set points for each level. Monitoring this allowed the team to quickly identify any deviations or malfunctioning valves that could compromise efficiency or system stability. For instance, if a valve remained open during a scheduled low-demand period, it would be flagged in the report for immediate investigation and corrective action.

By tracking compliance daily, the team was able to maintain tight control over the compressed air network, ensure operational discipline, and support continuous improvement. These reports also helped drive accountability at the shaft level, as recurring non-compliance could be traced to specific areas or shifts. Ultimately, the daily reporting process played a crucial role in sustaining the energy savings and performance improvements achieved through the implementation of the control valves.

Cost savings
The baseline established in the methodology served as the reference point for evaluating project performance. The actual energy consumption data was collected and compared to this baseline to assess the impact of the implemented interventions. This includes all compressors that were added to the system after the baseline period. The resulting differences were used to quantify energy and cost savings, incorporating Eskom's TOU tariff structure for accurate financial assessment.

Figure 7 presents a summary of the 2024 monthly actual consumption values alongside the baseline figures, clearly illustrating the reductions achieved through improved control valve implementation and compressor scheduling. A total energy saving of 27,323 MWh was achieved, resulting in a cost saving of R51.9 million.

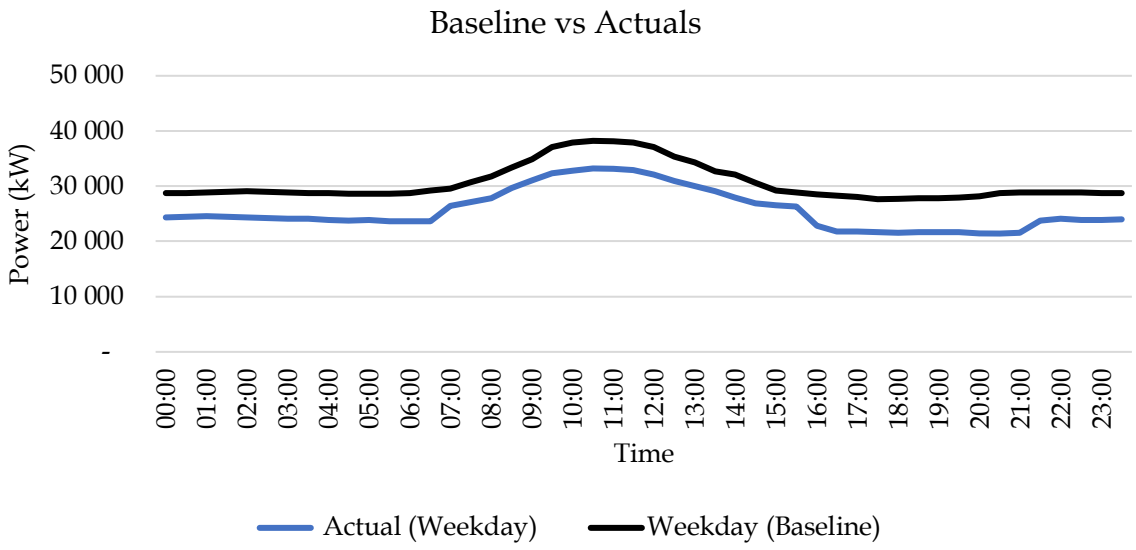


Figure 7- Actual compressor performance (2024).

DISCUSSION

Technical insights

The use of control valves introduced flexibility previously unavailable in a rigid compressed air setup. It allowed operations to transition from a 'supply-dominant' to a 'demand-driven' system.

Challenges encountered

Ageing valve infrastructure – Many of the older valves are prone to mechanical failure and require frequent repairs. This not only increased maintenance workload but also affected the project performance when valves could not maintain their setpoints. In a few cases, the valves were completely replaced.

Change management – Shifting operational practices from long-standing methods proved challenging. Overcoming the "that's how we used to do it" mindset required consistent communication, on-site training, and demonstrating the measurable benefits of the new control strategy.

Surface pressure requirements – Certain pneumatic equipment located on the surface required higher operating pressures than the optimised setpoints allowed. This created a conflict between energy-saving targets and operational needs. The issue was resolved by installing a dedicated supply line to this equipment, ensuring it received the required pressure without affecting the rest of the network or compromising overall system efficiency.

Lessons learned

- Involving operational staff in planning improved acceptance of the system.
- Daily monitoring dashboards were essential in detecting and addressing faults.
- Pressure control, when paired with demand analysis, yields significant gains.

Future work

Planned next steps include:

- Further optimisation of the control valves
  - Reduced impact on compressors with control valve schedules
  - Reduce the limitations of the valve's control abilities
- Reduction of demand pressure requirements during low-demand periods
- Implementation of a centralised control system on the compressors.

CONCLUSION

This initiative demonstrates the value of combining engineering control, digital monitoring, and tariff-based scheduling to significantly reduce energy usage and costs in compressed air systems. An energy saving of 27,323 MWh and cost saving of R51.9 million was achieved. This result from the mining complex validates the benefits of demand-matched compressed air supply, enhanced system monitoring, and continuous performance tracking.

The project not only yielded financial savings but also built technical and organisational momentum toward broader energy efficiency practices.

REFERENCES

Arnoldi, M., 2023. Electricity tariff increase will push mining costs up 33% by end-2024. *Engineering News*, 13 January. [online] Available at: https://www.engineeringnews.co.za/article/electricity-tariff-increase-will-push-mining-costs-up-33-by-end-2024-2023-01-23 [Accessed 11 August 2025].

Botha, Z., 2022. The mining industry and the energy crisis – What is the role we are to play? *Journal of the Southern African Institute of Mining and Metallurgy*, 122(11), November. [online] Available at: https://www.scielo.org.za/scielo.php?script=sci_arttext&pid=S2225-62532013001100012 [Accessed 11 August 2025].

Eskom, 2024. *Tariff history*. [online] Available at: https://www.eskom.co.za/distribution/tariffs-and-charges/tariff-history/ [Accessed 4 August 2025].

Eskom Holdings SOC Ltd., 2024. *Megaflex tariff structure*. Johannesburg, South Africa. [online] Available at: https://www.eskom.co.za/tariffs/megaflex [Accessed 11 August 2025].

Liebenberg, I., Velleman, D. and Booysen, W., 2012. *Expanding compressed air demand side management through selective level control*. M.Eng. dissertation, North-West University, Potchefstroom, South Africa. [online] Available at: <insert link here if available>.

Lunika, J., Mtakati, S. and Silwal, K., 2023. A load management solution for peak periods in South Africa. In: *Proc. Int. Conf. on the Domestic Use of Energy (DUE)*. Cape Town, South Africa, April 2023. IEEE, pp. 1–6. doi:10.1109/DUE57842.2023.10129368.

Matthee, F., 2021. *Evaluating the feasibility of integrating mine compressed air systems for energy savings*. Master's thesis, North-West University (South Africa).

National Energy Regulator of South Africa (NERSA), 2024. *Eskom tariff increase decision 2024/25*. Pretoria, South Africa. [online] Available at: https://www.nersa.org.za [Accessed 11 August 2025].

Valterra Mining Ltd., 2024. *Sustainability and energy efficiency targets report*. Johannesburg, South Africa.



Waldo Biermann

Project Engineer
ETA Operations

I consider myself to be a dedicated and innovative engineer with nearly a decade of experience at ETA Operations, a leading engineering and technology consultancy based in Pretoria. During my tenure, I have played a key role in projects aimed at improving energy efficiency, systems optimisation, and sustainable engineering solutions within the mining sector.

While working full-time, I pursued and successfully completed my master's degree in engineering, further strengthening my technical and analytical

capabilities. This achievement complemented my practical experience in implementing advanced simulation tools, data-driven process optimisation strategies, and real-time control systems.

I have a practical, solutions-oriented approach, and have contributed to several high-impact initiatives that aligned with energy-saving goals. I am committed to innovation, continuous learning, and operational excellence. I believe I have made a lasting impact on both the projects I was a part of and the teams I have supported.

Evaluating water performance on platinum mine shafts using a benchmarking technique

J. Korkie[1,2], J.H. van Laar[2], A.G.S. Gous[2], C.S.L. Schutte[2]

[1]ETA Operations (Pty) Ltd, South Africa
[2]Stellenbosch University, South Africa

South Africa's intensifying water scarcity poses a significant risk to the platinum mining sector, where a reliable water supply is essential for productivity, economic performance, and long-term operational sustainability. Effective water management is therefore critical, requiring the identification of inefficiencies and a focus on continuous improvement. While benchmarking is widely used to improve operational performance, its application to water systems in platinum mining remains limited due to a lack of industry-specific guidance. This paper addresses that gap by applying a structured benchmarking approach to assess water usage across platinum mining shafts through a case study methodology.

The evaluation followed three steps: assessing the performance of individual shafts, comparing performance across shafts, and identifying improvement opportunities based on internal comparisons and external industry benchmarks. The analysis of potable- and service water usage relative to production revealed a substantial variation—up to 51% in potable water and 34% in service water usage.

These disparities highlight clear opportunities for optimisation. Potential reductions in potable water use range from 1 – 51%, and in service water 9 – 34%. Key areas for improvement include leak detection and repair, reducing misuse of chilled and cooling water, enhancing dust suppression practices, improving water supply control during non-peak operational periods, and closing supply to inactive areas.

This paper demonstrates the value of structured benchmarking in identifying water performance gaps. By offering a practical framework for monitoring and improving water efficiency, it supports enhanced water stewardship and the long-term sustainability of platinum mining operations in a water-stressed South Africa.

INTRODUCTION

Background

South Africa faces a critical water security crisis, characterised by limited water availability, deteriorating quality, and increasing threats to long-term sustainability. Classified as a water-scarce country, South Africa is projected to face a national water deficit by 2030, driven by climate variability, population growth, and competing demands across sectors (Department of water and sanitation communication services 2016; Ahmadi *et al.*, 2020; Water Research Commission 2023). Effective water management—through optimised allocation, reduced losses, and enhanced productivity—is essential to mitigate this crisis (Kohler 2016). Water, a critical resource, underpins South Africa`s economic stability and environmental resilience, making water security a national priority (Department of water and sanitation communication services 2016).

The mining sector, a cornerstone of South Africa's economy, is particularly vulnerable to water scarcity. It contributes approximately R425.6 billion to GDP and employs over 477,000 people (Minerals Council South Africa 2024). In 2023, the sector faced pressures from declining commodity prices, rising capital costs, and economic constraints, amplifying the need for efficient resource management, particularly water (Statistics SA 2006). Although mining accounts for only 5% of South Africa's total water consumption (Statistics SA 2006), its localised impact is significant, especially in water-stressed regions where mines are often the largest single water users (Northey *et al*., 2016).

South Africa leads as the world`s top platinum supplier, producing 69% of the global platinum group metals (PGMs) in 2013. Therefore, this water-intensive industry requires in-depth attention to ensure sustainable operations (Geological Survey 2024). PGMs are critical for industrial applications, including catalytic converters and renewable energy technologies, underscoring the strategic importance of sustaining platinum operations. In deep-level platinum mines, water is used for mineral processing, underground cooling, hydropower, and dust suppression, with operations divided into potable water (safe for human consumption, used in refuge bays and surface facilities) and service water (used for industrial processes like chilled systems and stope-level dust control). Service water constitutes approximately 73% of total water usage, with potable water accounting for 27%, managed through separate reticulation networks (Haggard, Sheridan & Harding 2015). These systems are critical to operational efficiency and occupational health but are prone to inefficiencies such as leaks and overuse (Botha 2010).

Despite the urgency of water management, the South African mining sector often lacks robust practices for measuring, managing, and reporting water-related risks. Research indicates that companies with proactive water stewardship—through transparent reporting and stakeholder engagement—achieve better water efficiency (Askham & Van der Poll 2017). However, many mines fail to quantify their water footprints or implement systematic conservation strategies, limiting their ability to address water risks effectively (Latiff & Marimuthu 2021). This gap is particularly evident in platinum mining, where site-specific water management is crucial due to varying water demands across the mine lifecycle and regional differences in water availability (Northey *et al*., 2016).

Previous approaches to water management in platinum mining have primarily relied on qualitative assessments, water balance frameworks, or site-wide sustainability metrics, which often lack the granularity needed for shaft-specific optimisation (Danoucaras et al., 2014; Northey & Mudd, 2023). For example, water balance frameworks, such as the Water Accounting Framework, provide transparency in site-wide water flows but do not enable detailed comparisons of shaft-level performance (Danoucaras et al., 2014). Similarly, qualitative assessments focus on broad water stewardship goals without quantifying inefficiencies at the operational level. Benchmarking offers a superior and complementary approach by providing a quantitative, data-driven framework to compare water usage across shafts, identify high-consumption areas, and prioritise targeted interventions. Unlike previous methods, benchmarking leverages standardised metrics like water intensity (kL/tonne ore processed) to enable precise, cross-shaft comparisons, fostering accountability and supporting continuous improvement in water efficiency (Department of Water and Sanitation, 2016).

Raising awareness of water usage is a key driver for improving efficiency, and benchmarking offers a proven method to achieve this (Northey & Mudd 2023). By comparing performance against industry standards or peers, benchmarking highlights inefficiencies, fosters accountability, and guides targeted interventions (Department of Water and Sanitation 2016). Studies demonstrate its effectiveness in enhancing resource use, yet its application in mining water systems remains limited (Department of Water and Sanitation 2016). The problem lies in the scarcity of cross-industry comparisons of water performance and the lack of quantitative methods to evaluate water usage across platinum mining shafts (le Roux, van Laar & Schutte 2024). Existing research often focuses on qualitative assessments or broad sustainability metrics, overlooking detailed, data-driven approaches to compare shaft-level water performance (Northey & Mudd 2023). This gap hinders the ability to identify high-consumption areas, optimise reticulation systems, and implement site-specific improvements.

This study aims to address these challenges by applying structured benchmarking to assess water usage across platinum mining shafts. By quantifying potable- and service water performance,

comparing shafts, and identifying inefficiencies, it aims to provide a robust framework for enhancing water efficiency. This approach not only raises awareness of water usage but also supports sustainable water stewardship, ensuring the long-term viability of South Africa's platinum mining sector amid intensifying water security challenges.

Literature review

Water management in mining

Effective water management is vital for sustainable platinum mining operations. A study by Askham and Van der Poll (2017) found that mining companies recognise water risks in annual reports but often overlook supply chain water management, limiting holistic strategies (Askham & Van der Poll 2017). Research by Askham (2016) indicated that while 90% of water-intensive companies report water usage, only 60% set reduction targets, highlighting inconsistent water stewardship (Askham 2016). A Water Accounting Framework developed by Danoucaras *et al.*, (2014) enhances reporting transparency by reconciling water data across sites, though incomplete water networks undermine benchmarking reliability (Danoucaras, Woodley & Moran 2014). Work by Osman applied Water Accounting Framework to a base metals' refinery, stressing water balance validation for trustworthy data, but did not focus on mining shafts (Osman 2016). A simulation-based approach by Monteiro predicted service water needs for gold mine planning, excluding potable water and current usage evaluations, revealing a gap in real-time water management for platinum mining (Monteiro, van Laar & Schutte 2022).

Benchmarking in water usage

Benchmarking effectively identifies utilities' inefficiencies in mining. Research by Kunneke adopted a benchmarking method for potable and service water in platinum mines, correlating consumption with production and employee numbers, though constant variables like shaft depth limited generalisability (Kunneke 2022). A study by Ngwaku showed that benchmarking potable water intensity in gold mines supports conservation through monthly reporting, but omitted change house water usage, leaving gaps for platinum mining applications (Ngwaku 2020). A framework by Alghamdi for academic buildings emphasised standardised data for reliable comparisons, a principle applicable to mining shafts (Saeed *et al.*, 2021). A study by Cilliers benchmarked electricity use in deep-level mines by analysing five high-electricity usage systems correlations with different mining variations. The study demonstrated cross-site comparison benefits, but lacked water-specific applications, underscoring the need for tailored water benchmarking in platinum mining (Cilliers 2015).

Shaft-level variability and water usage

Shaft-specific factors, such as production, drive water usage variability, necessitating targeted analysis. Investigations by Kunneke and Le Roux *et al.*, highlighted variability in water consumption due to operational differences (Kunneke 2022; le Roux *et al.*, 2024). A comparative study by Le Roux *et al.* evaluated four techniques for identifying water wastage in chilled water systems, proposing a three-step method (identification, quantification, reduction) using zero-waste baselining, though it focused on underground systems (le Roux *et al.*, 2024). Research by Jordaan *et al.* developed a zero-waste baseline accountability framework for gold mines, reducing wastage through reporting and pressure valve optimisation, but did not address platinum mines (Jordaan, van Rensburg & du Preez 2024). Studies by Botha and Du Plooy targeted energy savings in water reticulation systems, not water usage reduction, indicating a gap in shaft-level water performance evaluations (Botha 2010; Du Plooy 2022).

South Africa's platinum mining industry, vital to the economy, faces significant water management challenges in a water-scarce environment. Despite the recognised importance of benchmarking and transparent reporting for improving water efficiency, there is a critical lack of quantitative, shaft-specific frameworks to evaluate potable and service water usage in platinum mining shafts.

The absence of standardised methods for cross-shaft comparisons limits the ability to identify inefficiencies and adopt sustainable water management practices. Current research predominantly focuses on gold mining or site-wide water management, with minimal attention to platinum mining shafts, and lacks robust reporting strategies to promote water-saving awareness. This gap hinders the industry's capacity to optimise water use and ensure responsible water stewardship.

This study aims to apply an existing benchmarking technique to assess potable and service water usage across ten deep-level platinum mining shafts in South Africa, evaluating performance to identify water-saving opportunities for both potable and service water, thereby enhancing real-time data-driven water management for sustainable operations.

This study focuses exclusively on deep-level platinum mining shafts in South Africa, utilising a case study methodology involving ten operational production shafts. The focus is on the application of a benchmarking method to evaluate water usage within these shafts.

The benchmarking was conducted in the context of external comparison, where shafts were evaluated relative to each other using cluster allocations. This approach was used to assess the applicability of the method in identifying differences in water consumption, production, intensities and highlighting potential shafts for improvement. The paper is confined to shaft-level analysis of potable- and service water usage and does not extend to other mining sectors or broader site-wide systems.

Method

The method developed in this paper was informed by attributes of existing benchmarking approaches previously applied in the mining industry. While it initially drew from four main sections, the final method was refined and expanded into seven distinct steps in Figure 1**.**

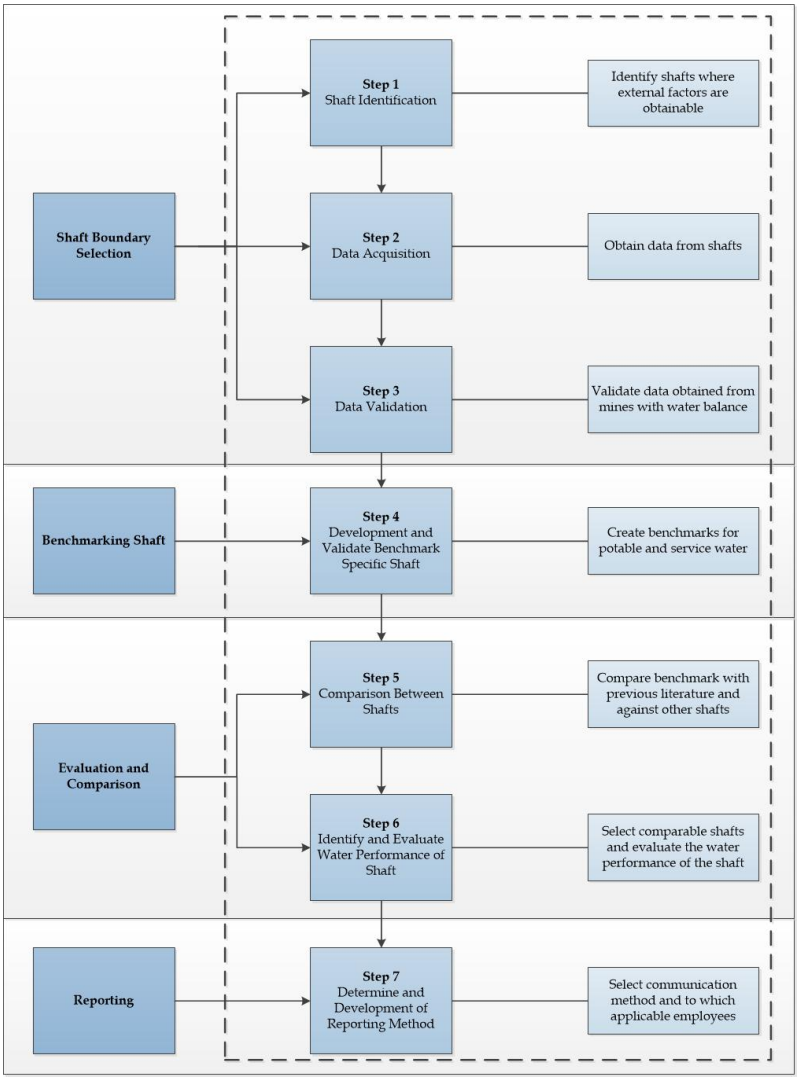


Figure 1: Proposed water benchmarking method for PGM mines.

Shaft identification
Shaft identification was conducted using specific criteria to ensure suitability for benchmarking potable and service water usage in deep-level platinum mining, guided by established practices (Kunneke 2022). The process involved verifying active operational status, assessing monthly potable and service water consumption, mapping potable and service water networks including consumer details and flow meter locations, and evaluating the quantity of hoisted tons to confirm operational significance (Jordaan *et al.,* 2024). A case study approach defined clear boundaries for each shaft's water systems, facilitating targeted data collection and analysis of water usage metrics to identify water-saving opportunities in South Africa's water-scarce context (Ngwaku 2020).

Data acquisition
Water usage data, including potable- and service water volumes, are collected from the supervisory control and data acquisition (SCADA) database for each of the 10 shafts, providing accurate real-time metrics (Osman 2016). Operational reports, shaft locations and process flow diagrams are obtained through site visits and collaboration with mine engineers, adapting Ngwaku's data collection strategy for gold mines to platinum contexts (Ngwaku 2020). Secondary data from industry reports contextualise water usage benchmarks (Theresa Askham 2016).

Data validation
Data confirmation ensures the accuracy, consistency, and reliability of water usage metrics for effective benchmarking of potable and service water systems (Xiao & Watson 2019). SCADA and Zednet data alone are often insufficient for identifying water leaks and infrastructural inefficiencies due to incomplete sensor placement across water networks, potential calibration errors in flow meters, and their inability to detect physical infrastructure issues, such as faulty pipe joints or unmetered water loss, in complex underground systems (Du Plooy 2022). To ensure data quality and consistency, water audits and physical inspections were conducted, involving direct measurements and on-site observations to validate automated data sources. Flow meters were cross-checked using ultrasonic flowmeters to confirm accuracy, and calibration checks were performed to detect and correct discrepancies. Missing or incomplete data were addressed through interpolation based on historical trends or exclusion from analysis if unreliable, ensuring robust benchmarking (Osman *et al*., 2017).

Two methods are employed: **Water balance analysis**, adapted from Osman *et al*. and Potgieter, systematically compares water supply, usage, and distribution to identify discrepancies such as physical losses (leaks), apparent losses (metering inaccuracies), and unauthorised consumption, quantifying non-revenue water and supporting regulatory compliance (Osman *et al*. 2017; Potgieter 2022). This enhances data validation and informs sustainable water management across sectors, including mining (Ngwaku 2020; Kirstein *et al*., 2021). **Statistical box-plot technique for outlier detection**, as described by Kirstein *et al*., identifies anomalies in water usage data, ensuring robust analysis (Kirstein *et al*., 2021). These methods reduce misinformation risks and support transparent reporting and decision-making (Potgieter 2022).

Development and validate benchmark specific shaft
A shaft-specific benchmarking framework is developed, based on the utility cost-saving methodology for platinum mines (Kunneke 2022). Key performance indicators (KPIs), such as water intensity (kL/tonne ore processed), are defined in several previous studies (Cilliers 2015; Ngwaku 2020; Kunneke 2022; Caromba, Schutte & van Laar 2023). The benchmark is validated by comparing shaft-specific data against industry standards, ensuring relevance to platinum mining (Saeed *et al.,* 2021).

Comparison between shafts
Monthly water intensities (kL/ton ore processed) are calculated for potable- and service water across the 10 shafts to enable external comparison, adapting Cilliers, Kunneke`s and Coromba`s benchmarking approach (Cilliers 2015; Kunneke 2022; Caromba *et al*., 2023). Due to variations in shaft operations, not all shafts can be evaluated individually, necessitating a clustering method based on water intensity, consumption, and production (Xiao & Watson 2019). **K**-means clustering was chosen over other methods, such as hierarchical clustering , due to its computational efficiency, suitability for moderate-sized datasets like the 10 shafts studied, and ability to produce interpretable clusters based on water

usage and production metrics. K-means minimises within-cluster variance, ensuring compact and well-separated clusters, which is critical for identifying comparable shafts in this context (Ahmed *et al*., 2020). Statistical analysis of monthly intensity data highlights variations, ensuring robust comparisons for benchmarking (Osman 2016). K-means clustering technique is an unsupervised machine learning technique used to partition data into K distinct, non-overlapping clusters based on feature similarity, in this case water, production and intensity. It iteratively assigns data points to the nearest cluster centroid, then updates the centroids by calculating the mean of assigned points, minimising the within-cluster variance (Ahmed *et al*., 2020). This technique is used to determine which shafts are comparable to each other.

Identify and evaluate water performance of shaft
Monthly water intensities (kL/ton ore processed) are calculated for potable- and service water across the 10 shafts to enable external comparison, adapting Cilliers benchmarking approach (Cilliers 2015). Due to variations in shaft operations, not all shafts can be evaluated individually, necessitating a clustering method based on water intensity, consumption, and production (Caromba *et al*., 2023). Statistical analysis of monthly intensity data highlights variations, ensuring robust comparisons for benchmarking (Osman 2016).

Determine and development of reporting method
A shaft-level reporting method is developed, adapting Bredenkamp's seven-step guideline for Integrated Energy Management Systems to water management for platinum mines (Bredenkamp 2016). The framework focuses on potable- and service water independently, as their water management teams may differ, providing daily, weekly, or monthly performance indicators (e.g., water intensity) to relevant water management teams members (Ugwu & Haupt 2007; Bredenkamp 2016). The reporting framework ensures accuracy, consistency, and timeliness. Report actionability and usability, as emphasised by Botes *et al*., enhance impact by enabling water management teams members to optimise water usage and address nonconformities (Botes *et al*., 2020). Visualisations, such as bar plots of water intensity, support data interpretation and decision-making for sustainable water management.

RESULTS

Case study: Application on a platinum mine shaft

Shaft identification
The shaft identification process, as detailed in the Methods section, confirmed the suitability of deep-level platinum mine shafts for benchmarking potable- and service water usage based on criteria including active operational status, daily water consumption, network mapping, and hoisted tons (Ngwaku 2020; Kunneke 2022; Jordaan *et al*., 2024). This ensured the selected shafts were appropriate for evaluating water-saving opportunities in South Africa's water-scarce context.

Data acquisition
Potable water consumption data were collected from environmental officers for each shaft, covering monthly records from January 2022 to May 2025. Daily potable water data were retrieved from SCADA and Zednet systems. Total production data were obtained monthly for the same period. Locations of potable water flowmeters were documented during on-site audits at each shaft.

Service water data, including flowmeter readings, were retrieved from the SCADA database, covering September 2024 to April 2025. Service water flowmeter locations were identified using SCADA layouts and consultations with shaft personnel. For benchmarking and evaluation, monthly data provided the primary basis, while daily data supported the identification of opportunities and data validation.

Data validation
The box-plot method, a standard statistical approach for identifying outliers (Xiao & Watson 2019), was used to detect and remove anomalous water usage data, enhancing reliability for benchmarking potable- and service water systems. Following outlier removal, a water balance was conducted, integrating flowmeter locations and site audits, as described in the Methods section, to complete detailed flow diagrams for potable- and service water networks (Osman 2016). Selected flowmeters

were cross-checked on-site using an ultrasonic flowmeter to verify accuracy. Figure 2 illustrates consumption point readings with a stacked graph of individual meter data and a dotted line representing the shaft intake check meter, which monitors total water inflow. These validations confirmed a consistent water balance, except for an imbalance between October 2022 and January 2023, indicated by a black dashed line in Figure 2. Investigation revealed a faulty meter, leading to the exclusion of this period's data from analysis. A new meter, installed and calibrated in January 2023, restored a reliable water balance, ensuring accurate data for subsequent benchmarking.

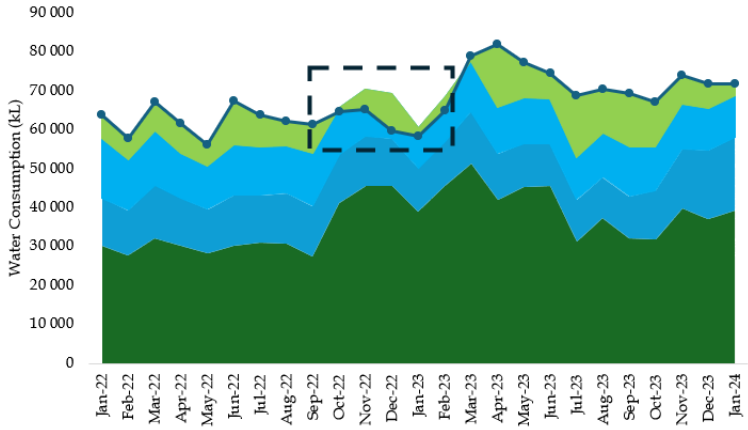


Figure 2: Case study shaft potable water balance.

Development and validation of water performance

It was found in the literature review that using water consumption intensities is the most common, effective and efficient method for benchmarking potable- and service water usage (Cilliers 2015; Department of Water and Sanitation 2016; Ngwaku 2020; Kunneke 2022; le Roux *et al*., 2024). Figure 3 shows strong linear correlation between water consumption (kL) and production (tons) with correlation factor, $R^2 = 0.798$. Across the 10 shafts, the coefficient of determination (R^2) between average water consumption (kL) and average production (t) varied from 0.024 to 0.188, with a standard deviation of 0.057, indicating moderate variability in the strength of this correlation across shafts.

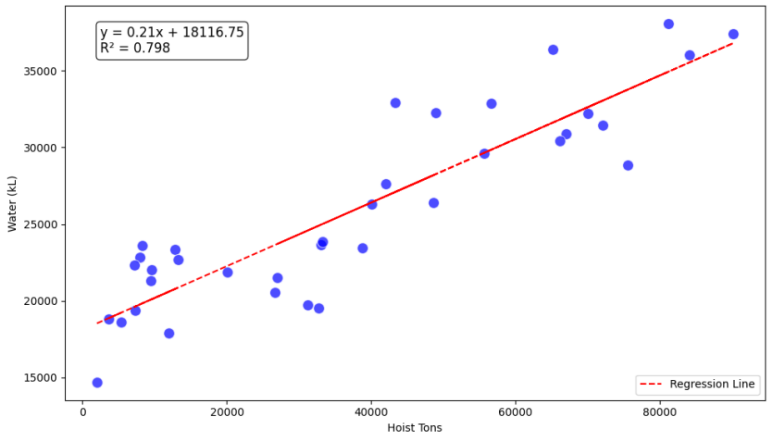


Figure 3: Correlation between water and production at the case study shaft.

The intensity benchmarking method was used to develop the benchmark for each shaft using Equation 1. Figure 4 and Figure 5 show the monthly intensity of a shaft's potable water and service water, respectively. This shows that the potable water intensity is much lower than the service water intensity.

Intensity Benchmark = Water Consumption (kL)/Production of shaft (tons) [1]

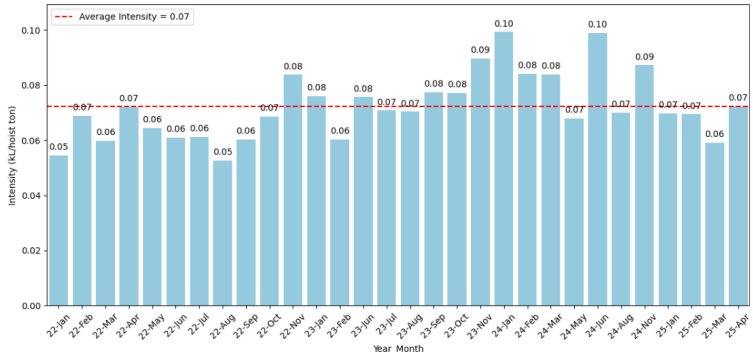


Figure 4: Monthly intensity per shaft (potable water).

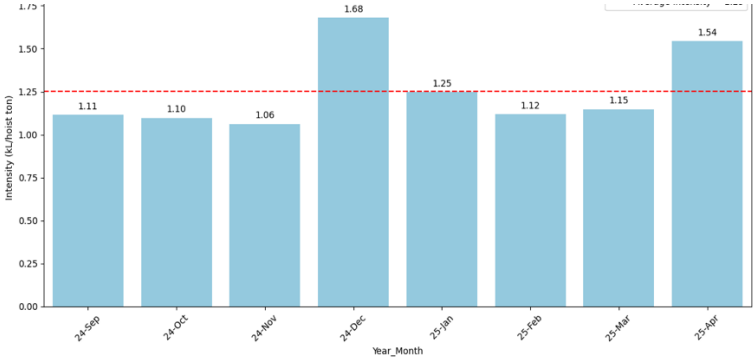


Figure 5: Monthly intensity per shaft (service water).

Comparison between shafts

Figure 6 and Figure 7 show the monthly intensity benchmarks for all individual shafts. Shaft 5 and shaft 7 show the worst potable intensity of all shafts. Shaft 4 is the worst performing shaft on the service intensity graph. However, based on these intensity graphs, it is not possible to determine which shafts should be compared, nor can any water-saving opportunities be identified to improve the overall efficiency of the shafts.

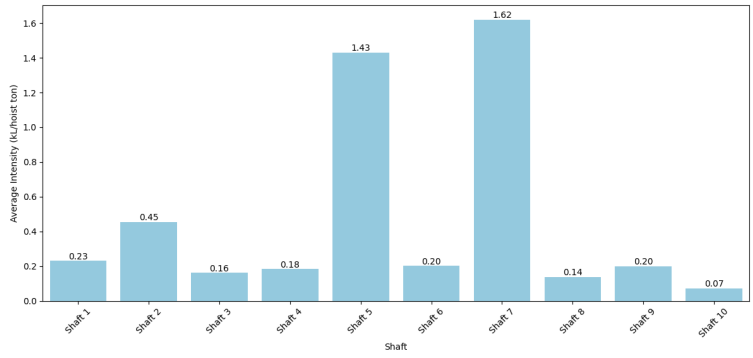


Figure 6: Average intensity per shaft (potable water).

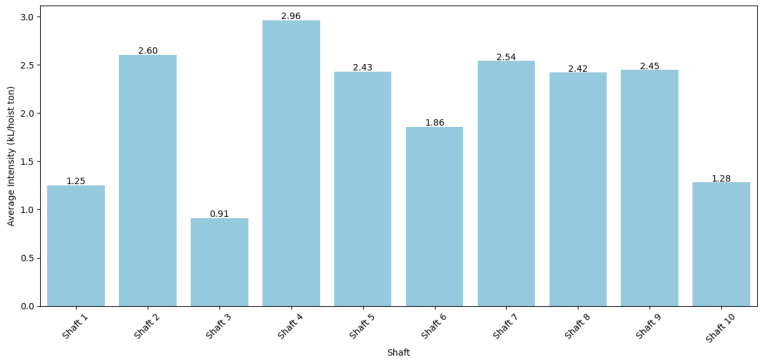


Figure 7: Average intensity per shaft (service water).

Identify and evaluate water performance of shafts

A K-means clustering algorithm was previously tested on water consumption and showed great success to identify energy usage saving initiatives (Caromba *et al.*, 2023). The optimal number of clusters (K) in K-means clustering was determined using within-cluster sum of squares and the Silhouette Score for their complementary strengths. Within-cluster sum of squares identifies an optimal K through an 'elbow' in its plot, balancing cluster compactness and complexity. The Silhouette Score measures cluster cohesion and separation, with higher scores indicating well-defined clusters. Together, these methods ensure a robust K, yielding compact, well-separated clusters for improved data segmentation and pattern recognition(Ahmed *et al.*, 2020). The K-means clustering technique was implemented on both potable- and service water data sets to discover two dominant clusters. These clusters Figure 8 and Figure 9 were used to select shafts for evaluation against each other.

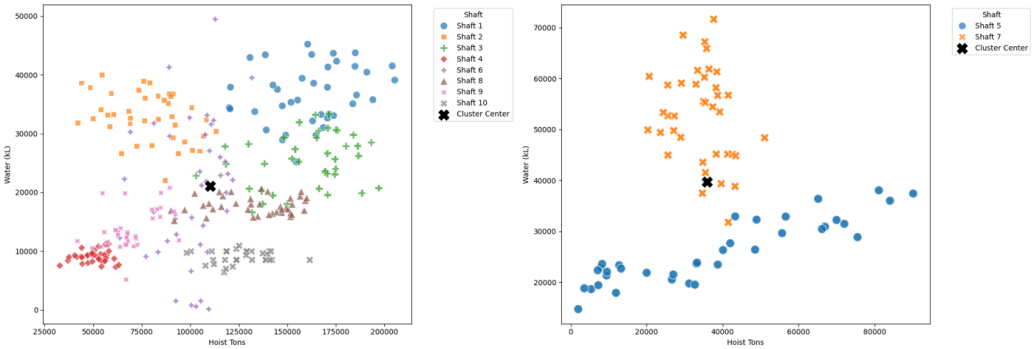


Figure 8: Water shaft clusters (potable).

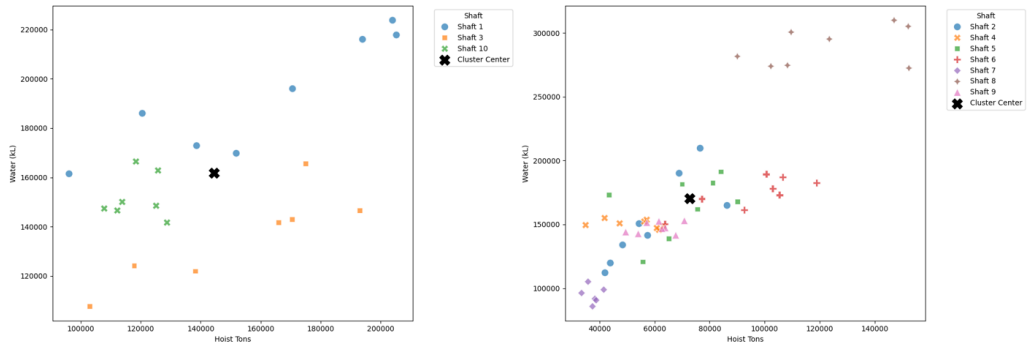


Figure 9: Water shaft clusters (service).

To evaluate potential water savings, a tailored Intra-Cluster Intensity Ranking and Percentage Savings Analysis method was employed, ranking shafts within each K-means cluster from highest to lowest

water intensity. The potential saving for each shaft was calculated as the percentage reduction in intensity needed to match the next lower-ranked shaft, with the lowest-intensity shaft highlighting improvement opportunities. This approach, inspired by clustering evaluation techniques ensures robust, cluster-specific insights, enhancing water efficiency in applications like data segmentation and resource management. Analysis of water intensity data revealed a standard deviation of 0.532 kL/tonne for potable water and 0.641 kL/tonne for service water across the 10 shafts. Optionally, 95% confidence intervals for the mean intensities are 0.138 to 0.798 kL/tonne for potable water and 1.673 to 2.467 kL/tonne for service water, confirming substantial differences in shaft performance.

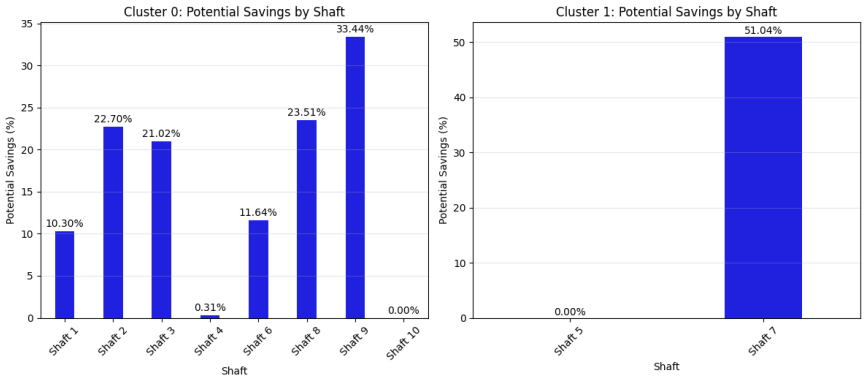


Figure 10: Potential water savings (%) by shaft per cluster (potable water).

Figure 10 shows in Cluster 0, Shaft 9 demonstrated the highest potable water saving opportunity at 33.44%, while in Cluster 1, Shaft 7 showed the greatest potential at 51.04%. Overall, the identified potable water saving opportunities range from 0.31% to 51.04%.

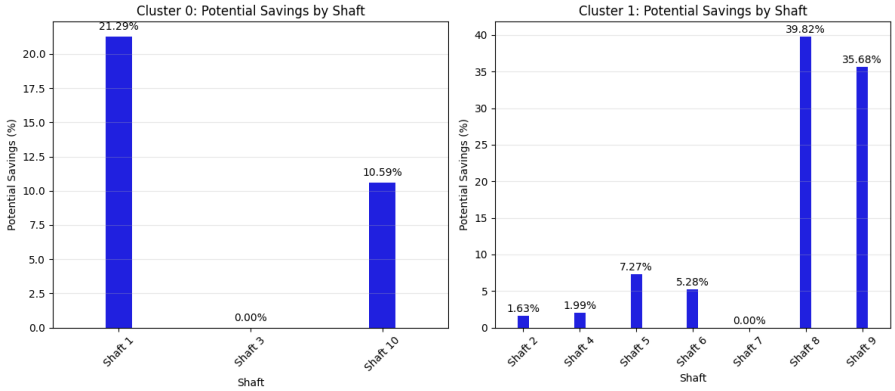


Figure 11: Potential water savings (%) by shaft per cluster (service water).

Figure 11 shows in Cluster 0, Shaft 1 demonstrated the highest service water saving opportunity at 21.29%, while in Cluster 1, Shaft 8 showed the greatest potential at 39.82%. Overall, the identified service water saving opportunities range from 1.63% to 39.82%.

Determine and development of reporting method

Shaft-level Reporting

Shaft-level reporting implemented to provide shaft engineers, environmental officers, and section engineers with actionable insights into water usage, following adapted guidelines from Bredenkamp's thesis (Bredenkamp 2016). Monthly reports detailed potable- and service water consumption for each shaft, focusing on site-specific KPIs such as water intensity (litres per ton of production). These reports highlighted individual shaft performance, enabling targeted interventions to address nonconformities and optimise water usage. For example, a shaft engineer at Shaft 7, identified with a 51.04% potable water saving opportunity, could prioritise leak detection and implement automated control valves

during non-peak periods to reduce water intensity. Similarly, section engineers at Shaft 4 could adjust service water flow for dust suppression to align with Cluster 1's lower-intensity shafts, achieving up to 39.82% savings. These reports flagged shafts with elevated water intensities for immediate review, achieving potential reductions in water usage through operational adjustments, aligning with industry benchmarks for actionable reporting (Ugwu & Haupt 2007; Botes *et al.*, 2020).

Cluster-Level Reporting

For top management and engineering managers, cluster-level reporting utilised K-means clustering to group shafts based on water intensity, water usage, and production data, with optimal clusters determined using within-cluster sum of squares and Silhouette Score (Ahmed *et al.*, 2020). The Intra-Cluster Intensity Ranking and Percentage Savings Analysis method ranked shafts within each cluster from highest to lowest water intensity, calculating potential savings as the percentage reduction needed to match the next lower-ranked shaft's intensity. For instance, engineering managers could use cluster-level reports to allocate resources toward high-intensity shafts like Shaft 9 in Cluster 0, implementing water-efficient technologies such as low-flow nozzles for dust suppression and sweeping or upgrading reticulation systems to reduce leaks. Top management could use these insights to develop company-wide water conservation policies, targeting reduction in potable water usage across Cluster 1 shafts. This approach identified high-impact opportunities, with some shafts showing potential potable water savings of up to 51% and service water savings up to 39%, enabling strategic resource allocation and policy decisions to enhance water efficiency across the mining group (Ugwu & Haupt 2007; Botes *et al.*, 2020).

CONCLUSION

This study developed and applied a structured benchmarking approach to assess potable- and service water usage in deep-level platinum mining shafts in South Africa, identifying significant water-saving opportunities in a water-scarce context. The analysis revealed considerable variation in water usage, with potential savings ranging from 0.31% to 51.04% for potable water and 1.63% to 39.82% for service water, achieved through validated data and shaft-specific metrics like water intensity (kL/tonne ore processed). This approach provides a practical framework for pinpointing inefficiencies and guiding sustainable water management at the shaft level.

Shaft-level and cluster-level reporting tools were developed to equip engineers and decision-makers with actionable data, enhancing transparency and supporting continuous improvement in water efficiency. For example, managers can use shaft-level reports to prioritise leak repairs in high-intensity shafts or adjust water supply schedules, while cluster-level reports enable strategic investments in water-efficient technologies across similar shafts. While successfully demonstrated in platinum mining, the framework's broader applicability requires further testing.

The benchmarking framework can be adapted to other mining sectors, such as gold or coal, due to its flexible components. Data validation methods, including water balance analysis and outlier detection, are applicable across mining contexts to ensure reliable metrics. The water intensity KPI (kL/tonne) can be tailored to different commodities, and K-means clustering can group similar operational units in any mining sector.

Implementing this framework may face challenges, including high costs for upgrading flow meters and SCADA systems in older platinum mines and ensuring reliable data collection from complex service and underground networks. These challenges can be addressed through phased implementation, prioritising high-impact shafts, and engaging stakeholders to build support. Future research should explore the framework's use in other mining operations, such as gold mines, to advance sustainable water management across the mining industry.

ACKNOWLEDGEMENTS:

This work was supported by ETA Operations (Pty) Ltd., South Africa (ETA). The first author is enrolled for a Masters in Industrial Engineering at Stellenbosch University.

Data availability statement: Third-party data: restrictions apply to the availability of these data. Data were obtained from ETA and are available from the corresponding author with the permission of ETA.

Conflicts of interest: The authors declare no conflict of interest.

Nomenclature

PGM	Platinum Group Metals
GDP	Gross domestic product
SCADA	Supervisory control and data acquisition
PLC	Programmable logic controller
KPI	Key performance indicator
IEMS	Integrated Energy Management Systems

REFERENCES

Ahmadi, M. S., Sušnik, J., Veerbeek, W. & Zevenbergen, C., 2020, 'Towards a global day zero? Assessment of current and future water supply and demand in 12 rapidly developing megacities', Sustainable Cities and Society, 61, 102295.

Ahmed, M., Seraj, R. & Islam, S. M. S., 2020, 'The k-means algorithm: A comprehensive survey and performance evaluation', Electronics, 9 (8), 1295.

Askham, T. M. & Van der Poll, H. M., 2017, 'Water sustainability of selected mining companies in South Africa', Sustainability, 9 (6), 957.

Botes, L. A., Hamer, W., Nell, D., Goosen, P. & Brand, H. G., 2020, 'Evaluating the impact of operational reports', South African Journal of Industrial Engineering, 31 (3), 156–169.

Botha, A., 2010. Optimising the demand of a mine water reticulation system to reduce electricity consumption (Doctoral dissertation, North-West University).

Bredenkamp, J.I., Mathews, M.J. and Vosloo, J.C., 2016, August. An integrated energy management strategy for the deep-level gold mining industry. In 2016 International Conference on the Industrial and Commercial Use of Energy (ICUE) (pp. 133-139).

Caromba, C., Schutte, C. & Van Laar, J., 2023, 'Application of clustering techniques for improved energy benchmarking on deep-level mines', Energies, 16 (19), 6870.

Cilliers, C., 2016. Benchmarking electricity use of deep-level mines (Doctoral dissertation, North-West University (South Africa), Potchefstroom Campus).

Danoucaras, A. N., Woodley, A. P. & Moran, C. J., 2014, 'The robustness of mine water accounting over a range of operating contexts and commodities', Journal of Cleaner Production, 84, 727–735.

Department of Water and Sanitation, 2016, Benchmarks for water conservation and water demand management (WC/WDM) in the mining sector, Department of Water and Sanitation, Pretoria, South Africa.

Department of Water and Sanitation Communication Services, 2016, South Africa is a water scarce country: Clean up and protect water resources, Clean Rivers Campaign, Department of Water and Sanitation, Pretoria, South Africa.

U.S. Geological Survey, 2024, Mineral commodity summaries 2024, U.S. Geological Survey, Reston, VA.

Haggard, E.L., Sheridan, C.M. and Harding, K.G., 2015. Quantification of water usage at a South African platinum processing plant. Water SA, 41(2), pp.279-286.

Jordaan, E. G., Van Rensburg, J. & Du Preez, J., 2024, 'New accountability approach: Utilising dynamic zero-waste baselines to mitigate water wastage in gold mines', Mining, 4 (4), 943–965.

Kirstein, J. K., Høgh, K., Rygaard, M. & Borup, M., 2021, 'A case study on the effect of smart meter sampling intervals and gap-filling approaches on water distribution network simulations', Journal of Hydroinformatics, 23 (1), 66–75.

Kohler, M., 2016, 'Confronting South Africa's water challenge: A decomposition analysis of water intensity', South African Journal of Economic and Management Sciences, 19 (5), 831–847.

Kunneke, J., 2022. Applying a benchmark method to identify utility cost-saving opportunities on a platinum mine (Doctoral dissertation, North-West University (South Africa).).

Latiff, N. & Marimuthu, F., 2021, 'Water-related sustainability reporting practices amongst South African mining and non-mining corporations', Environmental Economics, 12 (1), 112–123.

Minerals Council South Africa, 2024, The Minerals Council facts and figures pocketbook 2023, Minerals Council South Africa, Johannesburg, South Africa.

Monteiro, C.A., van Laar, J.H. and Schutte, C.S.L., 2022. A simulation-based water management strategy for life-of-mine water planning. South African Journal of Industrial Engineering, 33(3), pp.248-261.

Ngwaku, S. R., 2020, A strategy for potable water conservation in gold mines, Master's thesis, North-West University, South Africa.

Northey, S. A. & Mudd, G. M., 2023, 'Approaches for benchmarking mine site water management and contexts', Journal of Cleaner Production, 418, 138147.

Northey, S. A., Mudd, G. M., Saarivuori, E., Wessman-Jääskeläinen, H. & Haque, N., 2016, 'Water footprinting and mining: Where are the limitations and opportunities?', Journal of Cleaner Production, 135, 1098–1116.

Osman, A., 2016, Water management at a base metals refinery, MSc dissertation, University of the Witwatersrand, Johannesburg, South Africa.

Osman, A., Crundwell, F., Harding, K. G. & Sheridan, C. M., 2017, 'Application of the water footprinting method and water accounting framework to a base metal refining process', Water SA, 43 (4), 722–729.

Du Plooy, H. W., 2022, Reducing energy consumption of a deep-level platinum mine dewatering system through infrastructure reconfiguration, PhD thesis, North-West University, South Africa.

Potgieter, Y., 2022, Water balance development for legal compliance of gold mines in South Africa, Master's thesis, North-West University, South Africa.

Le Roux, M., Van Laar, J. H. & Schutte, C. S. L., 2024, 'A comparative analysis of magnetite-based nanoparticles in water treatment for enhanced efficiency', Mining, Metallurgy and Exploration, 41 (1), 111–122.

Saeed, A., Alghamdi, M., Eng, M. & Eng, B. S., 2021, Performance assessment and benchmarking of higher education institutions and academic buildings in Canada: A sustainability perspective, PhD thesis, University of British Columbia, Canada.

Statistics South Africa, 2006, Natural resource accounts: Updated water accounts for South Africa: 2000, Report No. D0405, Statistics South Africa, Pretoria, South Africa, 1–64.

Askham, T., 2016, Water sustainability: Measurement, management, engagement, and disclosure of selected water-intensive companies, PhD thesis, University of Pretoria, South Africa.

Ugwu, O. O. & Haupt, T. C., 2007, 'Key performance indicators and assessment methods for infrastructure sustainability: A South African construction industry perspective', Building and Environment, 42 (2), 665–680.

Water Research Commission, 2023, 'Water resources: Water scenarios for the future: A glimpse of what is to come', Water Wheel, 22 (5), 4–9.

Xiao, Y. & Watson, M., 2019, 'Guidance on conducting a systematic literature review', Journal of Planning Education and Research, 39 (1), 93–112.



Jane-Pierre Korkie

Senior Project Engineer and Master's candidate
ETA Operations (Pty) Ltd and Stellenbosch University

Jane-Pierre Korkie holds a bachelor`s degree in Industrial Engineering from North-West University (Potchefstroom), earned in 2019, and is currently pursuing a master`s degree in Industrial Engineering at Stellenbosch University.

He serves as a Senior Project Engineer at ETA Operations, where he drives continuous improvement through operational efficiency projects. His work integrates advanced simulation, project management, and business improvement to support life-of-mine extension initiatives.

Instope water handling strategies to achieve a dry mine

L.N. Senda[1,2], J.F. van Rensburg[2], J.C. Vosloo[2], S.M. Sithole[1], K.P. Petja[1], D.N Morare[3], N. Bandi[3]

[1]ETA Operations (Pty) Ltd, South Africa
[2]North West University, South Africa
[3]Impala Platinum Holdings Limited, South Africa

Water in underground mines is used for dust suppression, lubrication, cooling, and for cleaning the mining stopes. In the past, water usage was in the order of 1 to 2 tonnes of water per tonne of ore mined. With the reduction of mineral reserves, mining entities are opting to go deeper. As such, water consumption has increased to as high as 10 tonnes per tonne of ore mined. The substantial increase in consumption has resulted in inadequate handling of instope water. This leads to localised haulage flooding which damages ore-moving equipment (belts or locomotives) and is a threat to the productivity and profit of a mine. The purpose of this paper was to understand the current strategies for controlling instope water and propose an improved strategy. The improved strategy was developed through a case study methodology, in which underground audits of the instope water handling system at a case-study mine were performed. Data on the water handling strategies were obtained and analysed. From the analysis of the system's challenges, an improved method for instope water handling was developed with the use of simulation modelling. This improved method was then implemented in the case study mine. Results show an average decrease of 34% in flooding reports and a decrease of 27% in lost blasts due to flooding. With the aid of this improved strategy approximately R2.8 million of production revenue loss was avoided. With adequate maintenance, this figure can be improved upon and the goal of a dry mine achieved.

Keywords: Water Control, Lost Blast, Instope water, Mine Dewatering, Pumping, Simulation

INTRODUCTION

The typical mine value chain is shown in Figure 1. During underground mining, the ore body is broken up through a series of controlled explosions known as a blast. This is achieved through the drilling of the ore body and priming it with explosives (Perry, 2024). If for any reason a planned blast was to not take place or break the ore body to generate the planned tonnes, it is then categorised as a 'lost blast' (Sebutsoe and Musingwini, 2017). Fragmented rocks from successful blasts are transported to a refinery plant in which the ore is processed to reveal the precious minerals. These are then taken to the open market to aid in manufacturing of electronics, cosmetic items and a list of valuable consumer goods.

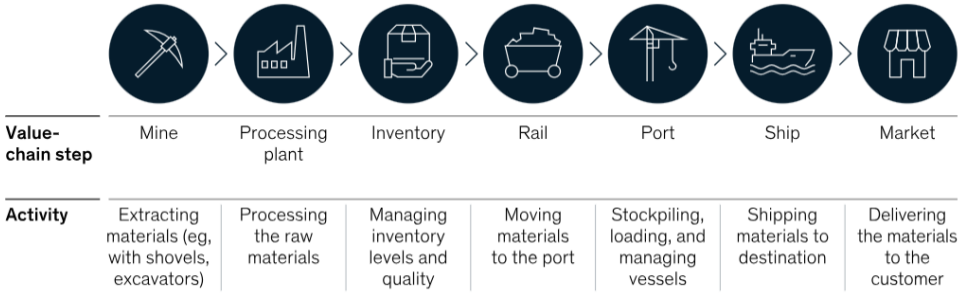


Figure 1. Overview of mining value chain (Gorner at el.*, 2020).*

Current Factors Affecting Profitability of Underground Mines

In 2023, approximately R444.2 billion was contributed to South Africa's Gross Domestic Product (GDP) through mining. However, as large a contribution this may be, this is in fact a reduction of 8.1% compared to 2022 (Minerals Council, 2023). The decline in GDP contributions is owed to reasons within the micro and macro-environment of mining operations. Figure 2 shows items that belong to each environment.

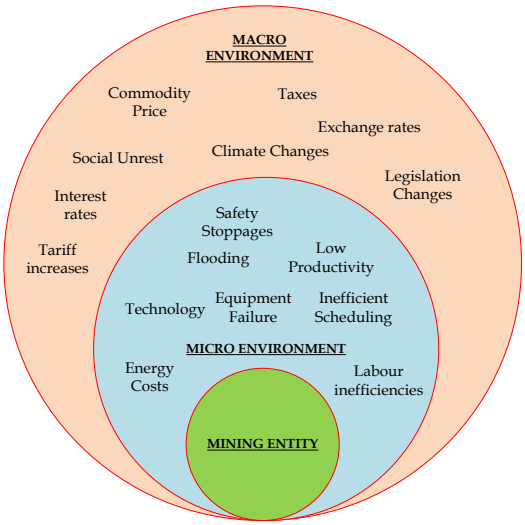


Figure 2. Micro and macro-environment of a typical mining entity (Misha and Mohanty, 2020).

Since the micro-environment is a region that the mining entity has full control over, factors in this space can be further explored. These factors typically increase the operating costs of the mine and put it at risk of profit losses. Equipment failure refers to production equipment that aid in generation or extraction of ore such as conveyor belts, compressors, locomotives or trackless mobile machinery (TMM). Energy costs refer to costs dedicated to mine ventilation, pumping and hoisting of ore (Misha and Mohanty, 2020). Inefficient scheduling leads to bottlenecks in the system thus hampering the flow of ore (Mishra *at el.*, 2023). These are three significant contributors to mining profitability; however, the fourth most important would be flooding. Underground flooding can halt production through damage of ore-moving equipment, increase pumping costs and raise humidity levels underground, thus increasing ventilation costs (Rupperecht, 2016). These effects can lend themselves to increasing labour inefficiencies and compromising the safety of employees.

Need for Study and Objective

With such a wide range of effects, flooding and instope water handling should be considered a very critical point in the profitability of mines. Due to increase in water consumption as mines go deeper and

the potential profit loss due to flooding, there is a need for instope water handling strategies that minimise flooding and its effects.

The objective of the study is to develop an improved instope water handling strategy. This will be through the case study methodology. This methodology was selected as it allows for real world contextualisation of the problem, implementation and review of the solution in a mine setting.

LITERATURE STUDY

Underground Water Reticulation

Underground mine water can be classified into two categories, 'clean water' and 'dirty water' (Rubio *et al.*, 2012). Clean water, used for drilling, is fed into the working areas through a series of pipes highlighted blue in Figure 3. Once used, it is classified as dirty water. This dirty water is removed from the working areas, through means of an instope water handling strategy indicated by the red box in Figure 3. The dirty water is sent to a settling facility. This facility removes suspended solids from the water through flocculation making it clean (Vutukuri and Singh, 1993). This clean water is sent back to surface through an interconnected system of pumps and dams which form part of the dewatering network shown by the green box in Figure 3.

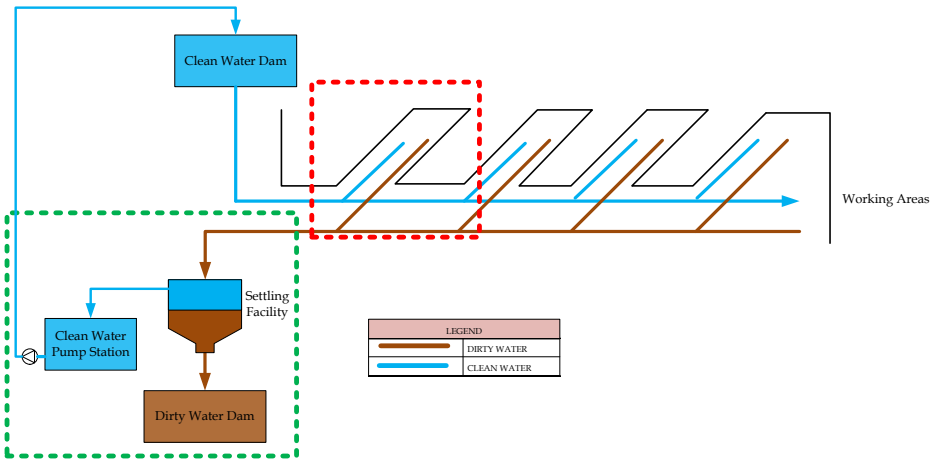


Figure 3. Typical underground mine water reticulation.

Factors Affecting Instope Water Handling System

From Figure 3, the instope water handling strategy is the first stage of water control before the shaft dewatering system. As such, it is important that this portion of the system be executed perfectly. From literature, four factors have been identified that affect current instope water handling systems.

The first factor was the lack of redundancy. Rubio *at el.*, (2012) provided knowledge on keeping redundancy within a pumping system. Their approach was redundancy through standby pumps. These pumps must be capable of dealing with scenarios such as main pump failure and sudden increases in mine water inflow. Not covered by Rubio *at el.*, is the design of the auxiliary system informed by simulation, nor the handling of silt within the instope water control.

The second factor identified was the lack of system design and sizing. Rasul and Vermeulen (2007) discussed improvement strategies for mine water handling systems. Their methodology included mapping out problematic areas, analysing pumping infrastructure and optimising the infrastructure through mathematical modelling using Bernoulli's equation. This allowed for correct sizing of pipes and pumps based on the expected water consumed in the area. Rasul and Vermeulen's research was geared more towards large scale dewatering systems and not instope water handling systems; however the principles used are also applicable to small-scale systems.

The third factor was water impurity. Rubio *at el.*, (2012) and Rasul and Vermeulen (2007) agreed that dewatering systems are faced with handling water of high impurity. They highlighted the need to have methods to separate the harmful impurities from the water. The impurities (usually in the form of stones) would damage valves and pump seals. Trommel screens were suggested, however it was seen that these are not effective for large particles (6 mm in diameter). The suggested method was using silting ponds. The outcome was that through gravity large particles would settle at the base of the pond while clearer water is pumped out. This allowed for the extension of life on the pumping system. During trialling it was noted that frequent maintenance of the ponds was needed. Once again, this research was geared more towards large scale dewatering systems.

The last factor is handling inrush of water, stagnant water or emergency water from the stoping section. In this case, Rupprecht (2016) highlights that low level catchment points must be installed to remove water in areas where inadequate water control is observed or where water is stagnant. It was noted that such structures tend to be maintenance-intensive. Not covered by Rupprecht (2016) is the approach to the design of the structures, the handling of silt nor was an integrated system for water handling outlined.

From these studies, there is a present gap in literature whereby an integrated design on component level informed by simulation and focusing on instope water handling is needed. This design must account for the water control auxiliaries, stagnating water, silt handling and have effective redundancy if needed.

METHODS AND MATERIALS

Rasul and Vermeulen (2007), outline a case study methodology in which problematic areas are identified, analysis based on mathematical modelling of existing infrastructure is performed, and solutions are proposed. Morton (1993) supplies the same methodology but integrated with model construction, simulation and calibration of the model, and live implementation. An adapted case study methodology based on both authors will be used to propose an instope water handling strategy. The case study methodology is preferred as it allows for real world contextualisation of the problem, data collection from a case study mine, implementation and validation of the proposed solution in a live setting. Figure 4 shows the step-by-step method used to approach the development of the solution.

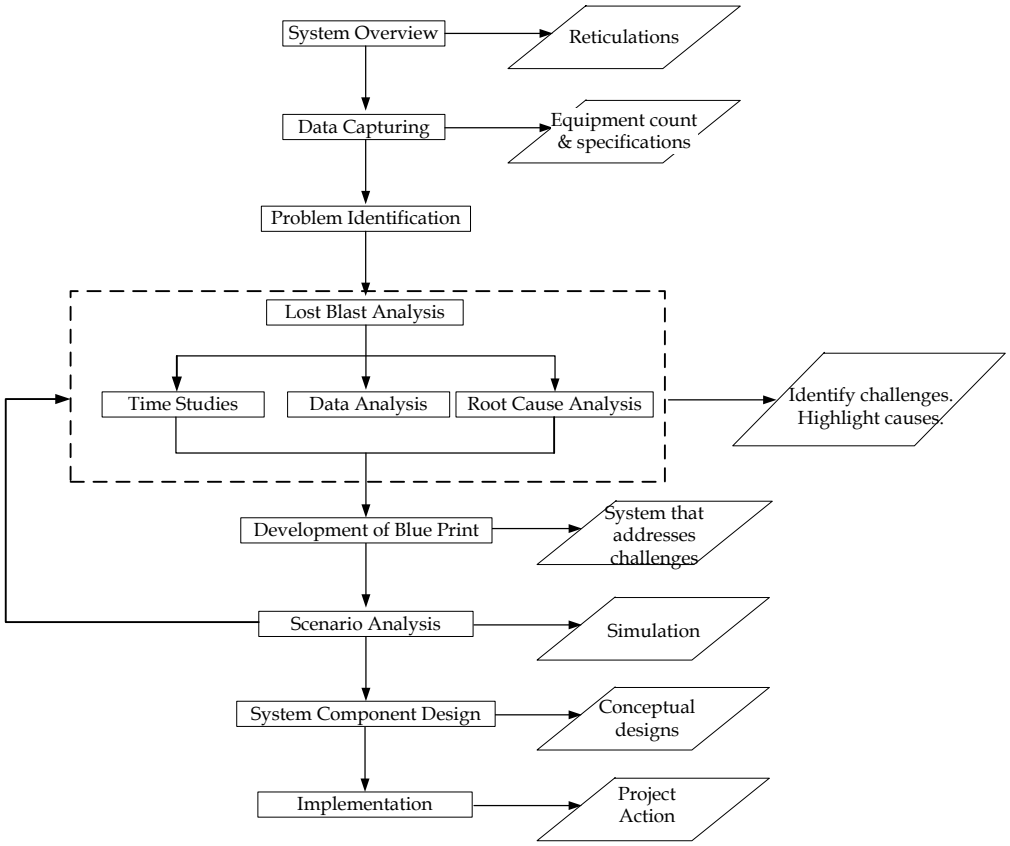


Figure 4. Step-by-step case study methodology (Adapted from Rasul and Vermeulen, 2007; Morton, 1993).

The development of the improved instope water handling solution will involve primary data collection. This collection of data will be through surface and underground audits whereby an overview of the system will be highlighted. Data on the system specifications will be captured. This includes size and number of water handling equipment, working areas and number of water generating equipment. As part of problem identification, a lost blast analysis to quantify the severity of the flooding from a business standpoint will be conducted. This lost blast will involve data analysis of lost blast frequency due to flooding and reports of underground floodings.
Time-in-motion studies to observe the underground challenges and effects of inadequate instope water handling will be performed. Additionally, these underground visits will allow for a root cause analysis (RCA) that will layout the key causes of haulage flooding and inadequate water handling.

Based on the RCA, a blueprint for the perfect instope water handling system will be created. This blueprint will be informed by various scenarios to ensure that each failure mode is covered. The components will be designed and sized through simulation to align with the current challenges and layout of the case study mine. The simulation will highlight the expected results of implementing the design. This design will then be actioned in the case study mine using the mines resources.

RESULTS AND DISCUSSION OF METHODOLOGY

System Overview

The case study mine is a decline shaft platinum mine (referred to as mine A). Mine A has an approximate depth of 500 m below surface. The mine's general underground water reticulation can be seen in Figure 5.

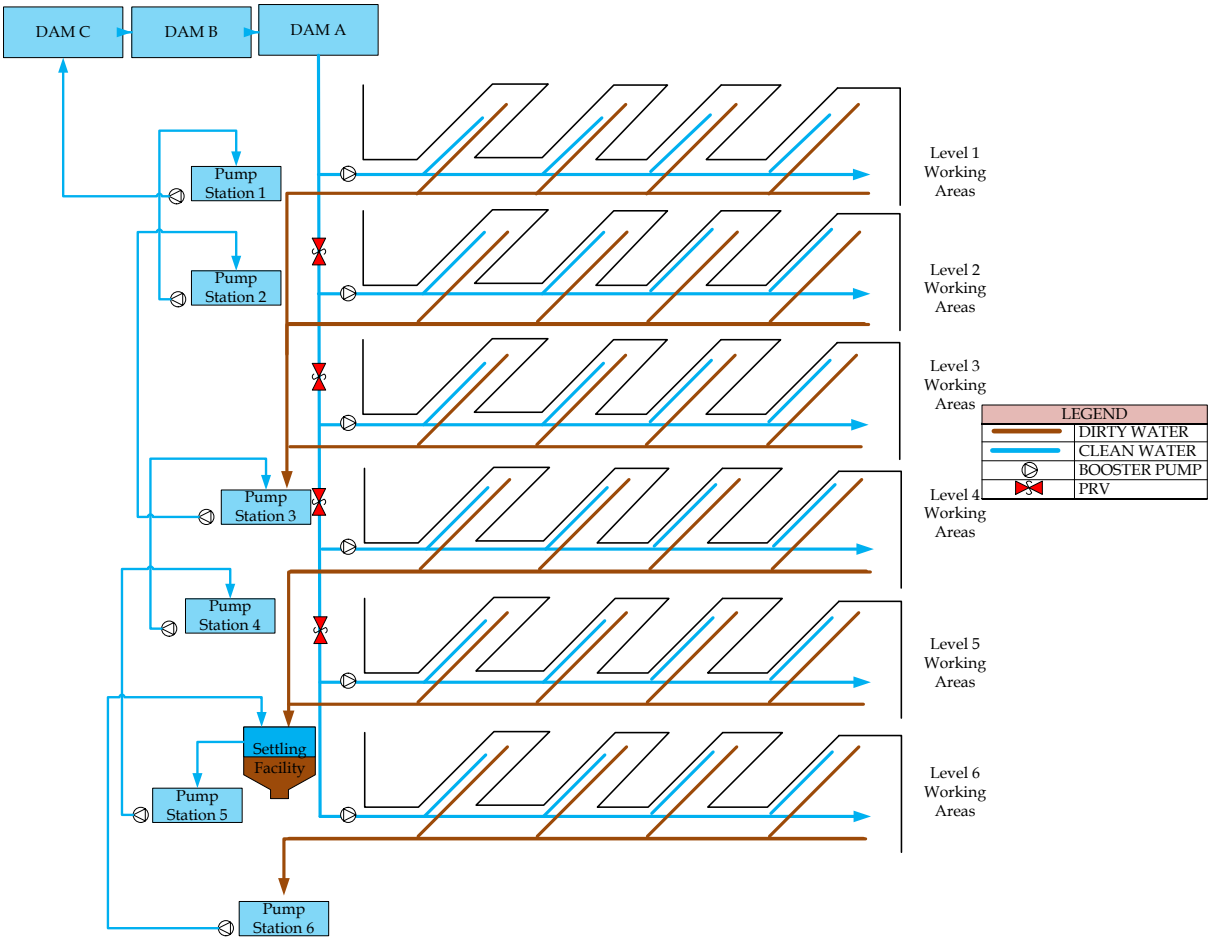


Figure 5. General layout of water reticulation of Mine A.

The clean water system is comprised of three surface dams (Dam A, B & C), underground pressure reducing valves (PRVs) and booster pumps. Clean water for drilling is gravity-fed from surface Dam A to underground. PRVs assist in controlling the pressure buildup in the pipeline along the decline. Booster pumps placed at the entry of each level increase water pressure to ensure sufficient supply to the working areas further downstream of the level.

Once used, clean water (now dirty water) is pumped from the working areas through pneumatic pumps. Multiple pumps deliver water either onto the level haulage or a single steel tank. Figure 6 shows the typical arrangement of instope water handling of Mine A.

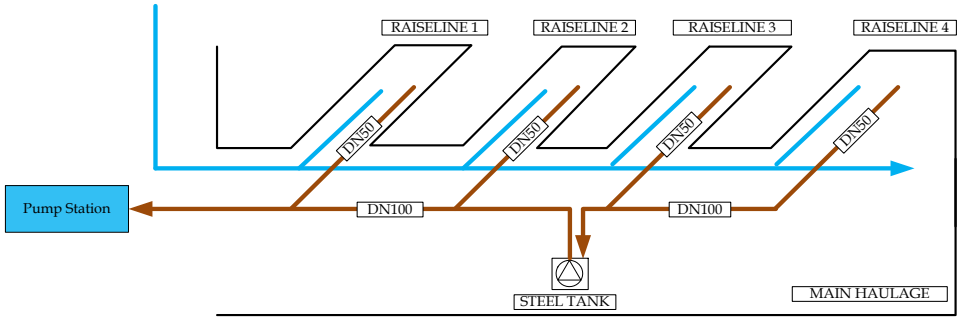


Figure 6. View of a typical working area.

Depending on location, the dirty water makes its way either to a pump station or to passive settlers located at the lower depths of Mine A. The settlers separate the sediments, thus creating clean water. This clean water is continually pumped from the bottom of the mine through the five pump stations till surface is reached. Once on surface, additional passive settling takes place on Dam B and C with the water overflowing from Dam C to Dam A and being gravity-fed once more to the underground working areas.

This system is monitored through various instruments such as dam level sensors and surface flow meters on Mine A's supervisory control and data acquisition (SCADA). The SCADA is in the Control Room where reports on the operation and failure of the system in each working area are generated.

Data Capturing

From underground audits, Mine A makes use of a combination of 50 mm, 100 mm and 150 mm piping along the haulage. Along the raiseline, it was common practice to use 50 mm pipes for dewatering with 47% of working areas having 50 mm pipes. Two categories of dams were identified, catchments and steel tanks. Each structure was equipped with a single submersible pump (power ranging from 11 kW to 37 kW) and a single outlet valve at the base of the structure.

Handheld drill numbers were obtained from analysis of crew structures. Level 6, shown in Figure 5, contains the highest number of rock drills with a number of 83. During the audit no flow meters were discovered underground, however, on the surface there are two flow meters. One flowmeter measuring water sent underground and the other measuring the water pumped from underground.

Problem Identification: Lost Blast Analysis

A lost blast analysis was conducted using data recorded on Mine A's organisational software. Figure 7 shows the top ranging lost blast reasons and kilo-tonnes lost.

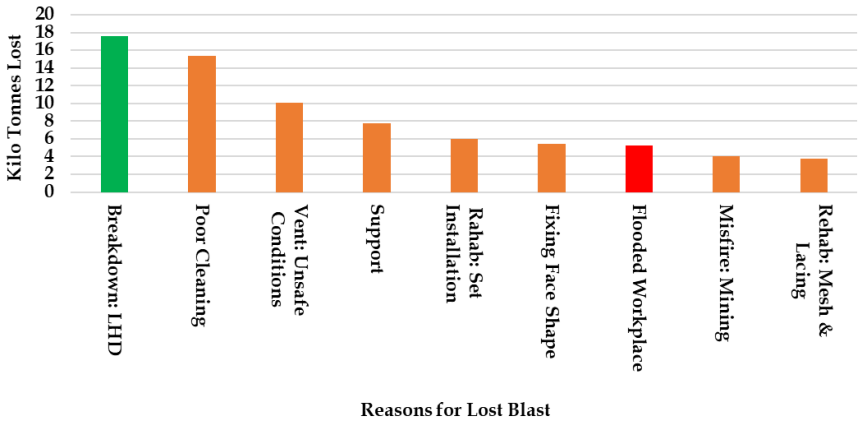


Figure 7. Kilo-tonnes lost due to various lost blast in 2023.

From this data, approximately 5.26 kilo-tonnes of ore was not extracted due to flooding (red bar in Figure). This roughly translates to R15 million of lost revenue. Figure 7 also lists 'Breakdowns: LHD (Load Haul Dump)' vehicles as an additional reason for lost blasts (green bar in Figure 7). In 2023, approximately 29 water-related breakdowns due to flooding were logged. This signals the far-reaching effects flooding has on Mine A's production and revenue generation.

Problem Identification: Data Analysis

Due to limitations of the organisational software, additional data was required to understand areas affected and the root causes. From reports generated by the Control Room, data on flooding was obtained. Figure 8 highlights levels where frequent flooding takes place. Conversely these are also areas of high mining activity as highlighted in the data capturing section. From the figure, the problematic areas are levels 5 and 6.

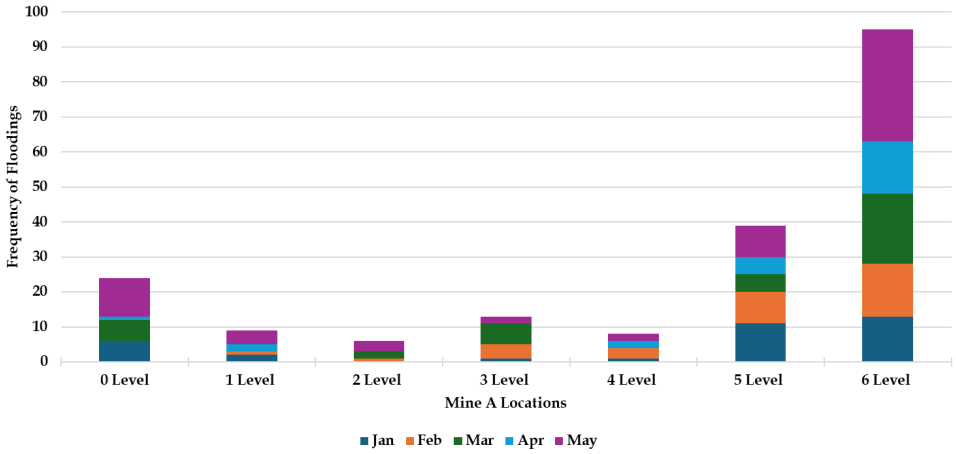


Figure 8. Frequency of flooding in various location of Mine A.

Problem Identification: Time-in-Motion Study

Using data from Figure 8, additional underground visits during time-in-motion studies were performed. During these visits, several water handling equipment were silted with no feasible cleaning method observed. Dewatering pipes choked with mud were discovered. Pools of stagnant water in low lying areas of the travel and belt ways were common. Multiple water pumps had failed with no redundancy and no visible strategy on water control. The flooding typically increased the underground travel time there by reducing the available time for drilling and ultimately affecting the entire mining cycle.



Figure 9. Left: Mud choked Dewatering pipe. Right: Flooded travel way.

Problem Identification: Root Cause Analysis

The observations made from the audits allowed for the development of a fishbone root cause to the flooding. The fishbone was split into five categories which are Equipment, Methods, People, the Environment and Material. Under each category a root cause is defined. Figure 10 showcases the fishbone and all root causes. In this case, an instope water handling system must be designed to address all factors found in the fishbone diagram.

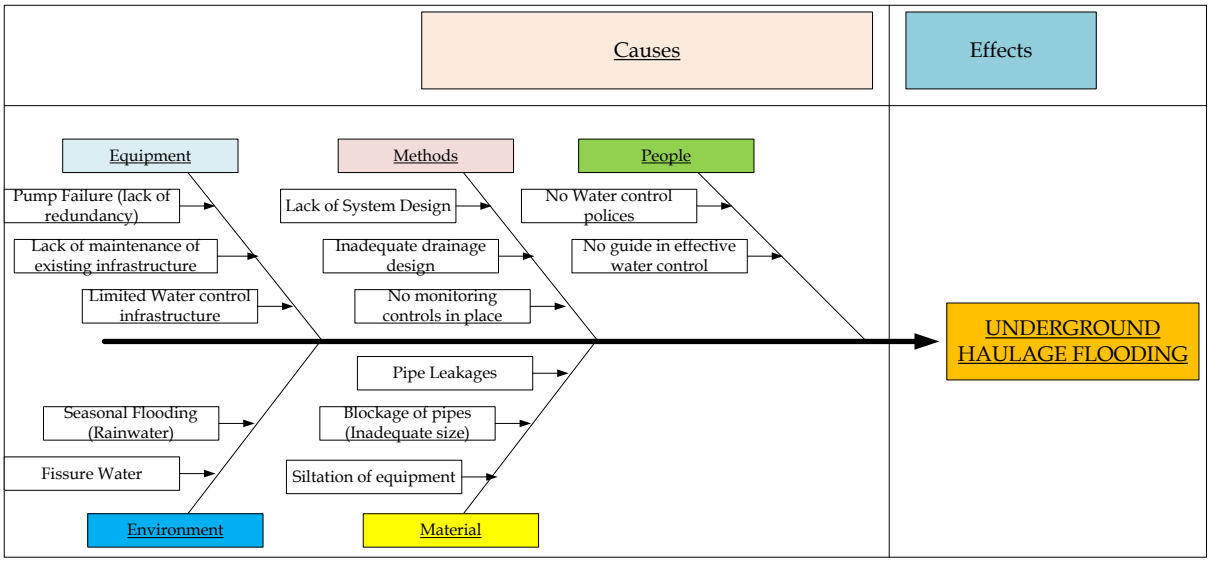


Figure 10. Fishbone diagram showing root causes to the flooding.

Development of Blueprint

Figure 11 shows the constructed model of Mine A's level 6. This model was based on information gathered during system overview and the data capturing. Level 6 was chosen due to the high frequency of floodings (Figure 8). The base model contains two half levels, North and South. The North side contains three working areas, each dewatering into one steel tank fitted with an 11 kW submersible pump, pumping into a 100 mm dewatering line. The South side contains three working areas dewatering directly into the half level pump station through 100 mm and 150 mm dewatering lines using only pneumatic pumps. The model was simulated to highlight the current flaws within the system. Additional models with varying layout configurations were simulated to remedy the current model's flaws and the root causes highlighted in the fishbone RCA.

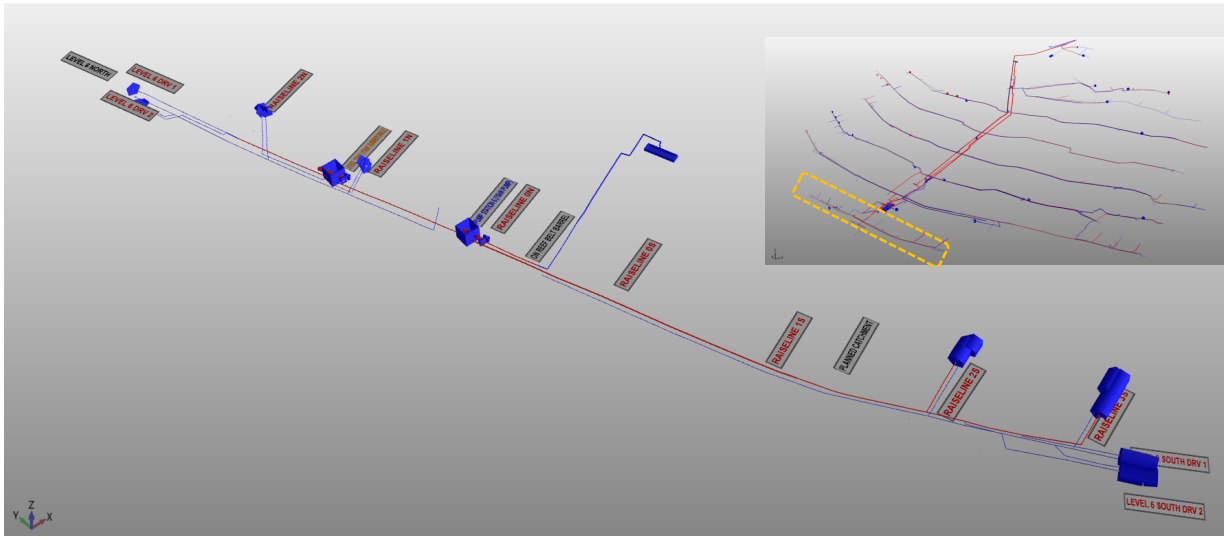


Figure 11. Model of level 6 with current layout. Full scale model on top right corner.

Scenario Analysis

From simulation, the one steel tank that caters to three northern working areas is constantly at risk of overflowing. To minimise this risk, each working area was equipped with its own steel tank and simulated. Figure 12 shows the steel tank levels when one steel caters for three working areas compared

to a steel tank per working area. In the figure, two of the three steel tanks do not reach the 100% limit. With this set up, less pressure is placed on the singular steel tank and redundancy has been introduced into the system.

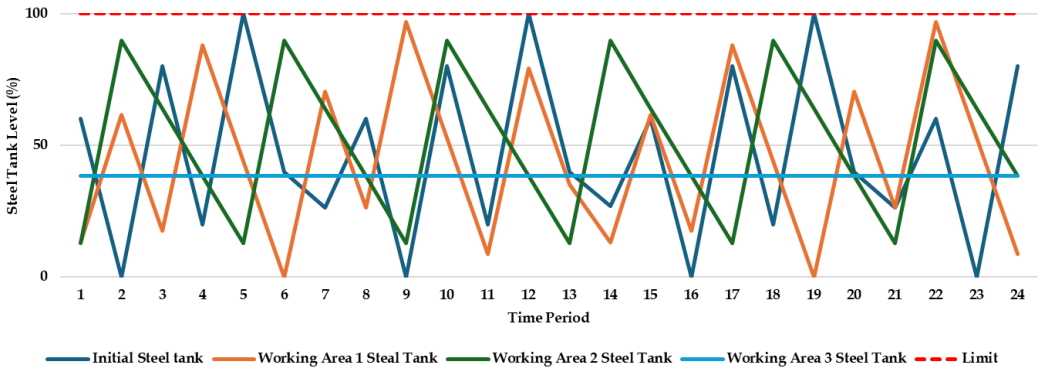


Figure 12: Steel tank level of initial set up and with each working area having a dedicated steel tank.

An additional scenario investigated was the failure of the steel tank pump. Observations from the underground audits showed that this water would report to the low lying areas of the haulage. As such, roadway sumps in low areas were added to the model. The sumps work to remove water due to steel tank failure; pipe leaks or additional water into the system such as fissure water.

The last scenario considered is the integrity of the piping infrastructure if all steel tanks operated at the same time. From simulation, the existing 100 mm dewatering pipe exceeds the recommended 3 m/s by 1.02 m/s. As such, it can be expected to have high pumping pressure loss for these high flows. Therefore, an increase to 150 mm pipes is needed. This increase resulted in a pipe velocity of 3.14 m/s, allowing for lower pressure drop. Additionally, the increased pipe size allows for additional dewatering capacity in the level compared to the 100 mm pipe.

Based on simulation and scenario analysis, the proposed system blue-print for instope water handling can be seen in Figure 13 and will operate in the following manner: Water from each working area will report to its own respective steel tank through piping installed in the working area. This water will be pumped from the steel tank to a 150 mm dewatering column in the haulage. In the event of an emergency, a roadway sump will be constructed as per working in a low lying position. This sump will collect water if the steel tank were to fail or an in rush of uncontrolled water took place (such as a pipe burst). The sump will pump the water into the same main dewatering column.

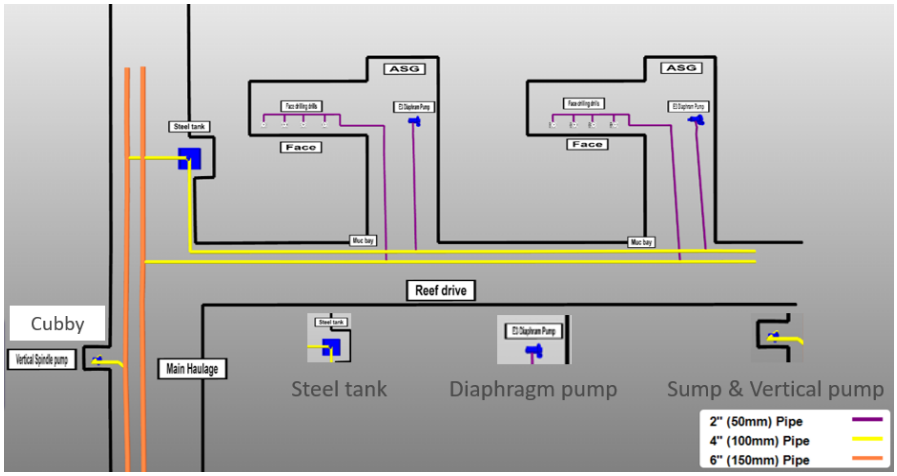
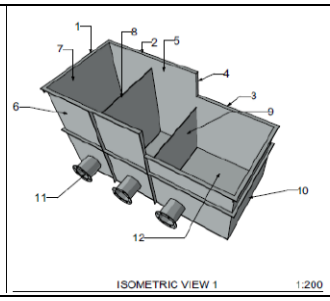
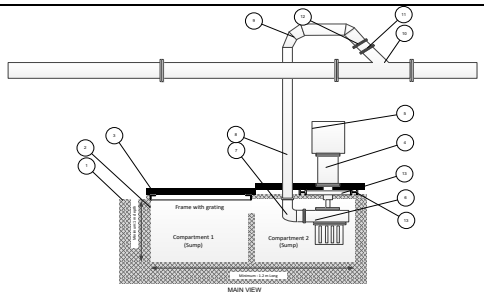


Figure 13: Proposed instope water handling system to be installed in each working area (raiseline).

System Component Design
Steel tanks, sumps and 6-inch piping make up the new instope water control system. Table I showcases each component; the design and the root causes that will be addressed.

Table I. Improve instope water handling components, their design, function and root causes addressed

Component	Design	Function and addressed flooding root cause
Steel Tank		Additional water control infrastructure. Main collection point of water pumped from the working area. Three bottom mud valves allow ease of maintenance. Three compartments desilt water. Root cause addressed: siltation of components and limited water control infrastructure.
150mm pipes	Standard Schedule 40 Galvanised 150mm pipe	All for larger volumes of water. Size will prevent blockage of piping. Root cause addressed: Blockage of pipes
Sump		To be used in emergency cases (steel tank pump failure and pipe leaks). Two compartments to allow for desilting of water. Root cause addressed: pump failure (redundancy), inadequate drainage design and pipe leakages

IMPLEMENTATION
With the value-add shown from the simulations. The system outlined was then implemented. Table II shows the required and installed equipment for the critical levels. Level 3, 4, 5, and 6 were selected for implementation due to their high mining activity, high flooding frequency and being the future of Mine A.

Table II. Components installed for the improved instope water handling system

Level	Steel Tanks (Installed/ Required)	Sumps (Installed/ Required)	150mm pipes (Installed/ Required)
Level 3	3/4	10/10	0/522
Level 4	0/3	10/10	0/332
Level 5	0/4	5/5	33/516
Level 6	0/3	4/4	64/158

From Table II, much of the components set to be installed in Mine A were incomplete. During implementation it was highlighted that for the control of instope water, dedicated mining personnel are needed for the oversight of the system. This includes identifying additional locations for equipment, educating mining personnel on the system, maintenance and implementation of the system.

This lack of oversight presented itself as an additional root cause not initially identified under the 'People' branch in the fishbone diagram. Despite the challenges, the installed equipment shown in Figure 14 provided promising results. Implementation began in May 2024 with the installation progressing till December 2024.



Figure 14: Left: Image of silted constructed sump. Right: Image of installed steel tank.

From the 'Lost Blast Analysis' section, a correlation between flooding and lost blasts is displayed. This correlation was present during the implementation period as with the decrease or increase of flooding frequency; the lost blast frequency follows the same trend. From Figure 15 (left), a visible decline in flooding frequency is given with the overall flooding frequency decreasing by as much as 34% due to the installed instope water handling components. Figure 15 (right), compares the lost blast frequency due to flooding of 2023 and 2024 during the implementation period. Using 2023 as a baseline during this period, a total of 39 lost blasts were recorded in 2024, a decrease of 27% (or 15 less lost blast) compared to the 54 lost blasts recorded in 2023.

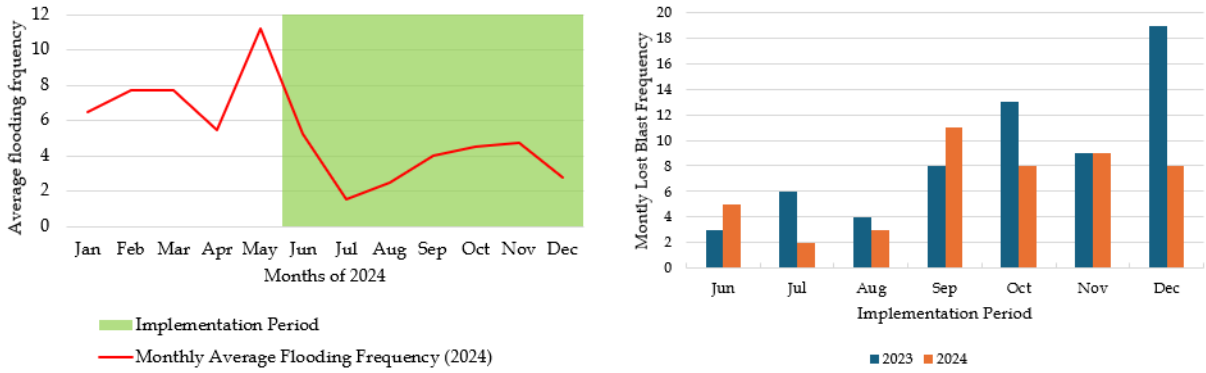


Figure 15: 2024 Flooding frequency 2024 (left), Lost Blast frequency due to flooding for 2023 and 2024 (right).

The variations in flooding frequency in Figure 15 (left) are owed to the lack of scheduled maintenance of the installed instope water handling components. Without effective cleaning, components would silt, as shown in Figure 14 (left) which compromises the dewatering capacity and damages the equipment thus rendering it ineffective. The end result can be seen in Figure 15 (left) whereby a steady increase in flooding frequency from July to October is observed.

The increase in lost blast frequency numbers from September to December is owed to two factors. One is the lack of maintenance of the installed instope water handling components. Two, an increase in water input due to rain as these months fall within the rainy season (Ramsey, 2025). This additional intake of rainwater (or in some cases fissure water) is assumed to contribute to the underground flooding. In 2024, this increase was better controlled and better managed leading to fewer lost blasts compared to 2023.

Management of these lost blasts due to flooding allows for a reduction in revenue lost. Based on Mine A's production data, one blast is equivalent to 72.9 tonnes. Each tonne has approximately 2.83 grams of platinum. With a pricing of $47 per gram this places the expected revenue of a blast at $10 761 (equivalent to R189 342). As such Mine A avoided a revenue loss of approximately R2.8 million due to flooding with the instope water handling strategy assisting in this achievement.

CONCLUSIONS AND RECOMMENDATIONS

As mines go deeper, water consumption increases. Part of this increase is owed to inadequate water handling which can potentially affect production by damaging ore-moving equipment, increase pumping costs and raise underground humidity. In literature, various water control improvement methods were presented, such as low point catchments equipped with pumps for water removal, effective redundancy, and methods for silt removal. However, the identified gap was that there was no integrated design on a component level for instope water handling based on simulation.

The paper presents a method for the development of an instope water handling strategy. This method involved underground audits, root cause identification, simulation to develop an instope water handling blueprint, component and system designed informed by the root causes and implementation. Based on components implemented, an average reduction of 34% in flooding was achieved. Furthermore, a 27% reduction in lost blasts due to flooding was observed when comparing 2024 to 2023. This reduction allowed for an avoided revenue loss of approximately R2.8 million due to flooding

These results are an indication of the effectiveness of the method and the possibility of achieving a dry mine, but they are not without challenges. During implementation it was noted that to increase effectiveness, additional supervision is needed to ensure maintenance of components.

To further analyse the holistic impact of the instope water handling strategy, the following recommendations are made: An analysis of the additional power consumption and energy cost added into the system. The value-add of re-using the captured silt in the components towards production and lastly, the effect reduced flooding has on TMM machinery.

ACKNOWLEDGEMENTS

The author would like to take this opportunity to express sincere gratitude to the mine's leadership which provided invaluable guidance during the study and implementation of the improved system. Special thanks are also extended to the teams that showed hard work and commitment to the construction and commissioning of the instope water handling components.

REFERENCES

Gorner, S., Mori, L., & Reiter, S. (2020, October 5). *The mine-to-market value chain: A hidden gem*. Retrieved from Mckinsey & Company: https://www.mckinsey.com/industries/metals-and-mining/our-insights/the-mine-to-market-value-chain-a-hidden-gem#/

Minerals Council. (2023). *Minerals Council Comprehensize Facts and Figures.* Retrieved from Minerals Council : https://www.mineralscouncil.org.za/all-categories?task=download.send&id=2310:comprehensive-facts-and-figures-2024&catid=18#:~:text=Page%2012-,Overview%3A%20the%20state%20of%20mining%202023%20continued,%2Don%2Dyear%20in%202023.

Misha, P. C., & Mohanty, M. K. (2020). A review of factors affecting mining operation. *World Journal of Engineering*, 457-459.

Mishra, P. C., Panigrahi, R. R., & Shrivastava, A. (2023). Geo-environmental factors' influence on mining operation: an indirect effect of managerial factors. *Environment, Development, Sustainability* , 1-7.

Morton, K. (1993). A Phase Approach to Mine Dewatering. *Mine Water and The Environment*, 27-34.

Rasul, M. G., & Vermeulen, P. J. (2007). Improvement Strategies for Mine Dewatering Process. *WSEAS International Conference on Fluid Mechanics* (pp. 137-142). Queensland: Gold Coast.

Rubio, R. F., Fabregas, A. L., & Fernadez, D. L. (2012). Underground Mining Drainage. Stae of the Art. *International Mine Water Association* , 102-107.

Rupperecht, S. M. (2016, October 15). Innovation in managing water usage in the stope environment. pp. 1-13.

Sebutsoe, T. C., & Musingwini, C. (2017). Characterizing a mining production system for decision making purposes. *The Journal of the Southern African Institute of Mining and Metallurgy*, 201-202.

Vutukuri, V. S., & Singh, R. N. (1993). Recent developments in pumping systems in underground metalliferous mining. *Mine Water and The Environment*, 71-94.



Lance Nkosana Senda

Optimization Engineer and Masters Candidate
ETA Operations (Pty) Ltd and North-West University

Lance Senda is currently part of a dynamic, young and energetic engineering team at ETA Operations a company aimed at optimizing industries. He is the holder of a bachelor's degree in mechanical engineering from the University of Pretoria and uses the gained skills in optimizing processes, conceptual design of solutions and execution of projects relating to water, energy and compressed air systems.

Currently Lance is in pursuit of his Masters in Engineering through NWU with a research topic focused on water as it is his keen interest and passion. Outside of work, he enjoys exploring the outdoors through the hiking trails of Gauteng, a lover of football with Premier League club Manchester United and a fan of film.

Time, water and energy to clean a stope panel using water jetting

P.D. Fraser

Hydropower Equipment (Pty) Ltd, South Africa

Water jets have been used successfully to clean blasted rock in stope panels in the narrow, slightly-dipping, tabular ore bodies of South African PGM and gold mines for since the early 1980s.

This paper describes a calculation model that estimates the jetting time and calculates the water and energy required for typical dip inclinations, reef types, panel dimensions and jet nozzle diameters. A straightforward methodology quantifies the cleaning TASK from the panel dimensions and estimates the cleaning RATE. This allows the cleaning TIME to be calculated and adjusted for a particular dip angle. The heart of the model is a power law correlation between the effective jet impact FORCE at 5 metres from the nozzle and the cleaning RATE at a standard DIP. The methodology includes an allowance for the drop-off of the impact force with distance from the nozzle, rock that is throw-blasted directly into the gully, and a THRESHOLD force below which jet cleaning is ineffective. The power law parameters are determined by curve fitting measured cleaning RATE data with the effective jet impact FORCE.

The Jet Cleaning Model allows panel lengths to be optimized for cleaning and the most suitable jet cleaning tool and power pack to be selected. The model also allows an estimated reduction in cleaning cycle time to be converted into a probable improvement in average production using a simple statistical approach.

In addition, key practical issues are discussed including safety, mud-rush risk, dirty water management, effects on stope environmental conditions, and the matching of power pack capacity for both water hydraulic drilling, and cleaning.

Keywords: Water jet stope panel cleaning, cleaning time calculation, water usage, energy usage

INTRODUCTION

The old adage: "the ART of mining lies in the cleaning" explains why water jet cleaning of blasted rock in the shallow-dipping stope panels of PGM and gold mines has been be so successful, often replacing face scrapers. Jet cleaning tools are light, quick to setup, and move rock down shallow slopes (typically 10 to 30°), in narrow stopes, sometimes less than 1 m high. They work in confines further restricted by support props, and where wheeled or tracked vehicles either do not fit, or grip, and also where face scrapers add risk. Because jet cleaning delivers production, mines have tolerated the obvious disadvantage of jetting that results from poor handling of significant volumes of dirty water, settled fines, and mud.

Stope cleaning using jetting is essentially a practical endeavour, and with the exception of pioneering papers by the Chamber of Mines research Organization (COMRO) and some early adopters, little has been researched or written. This paper endeavours to close this gap by presenting a Jet Cleaning Model which estimates the time, water and energy required to jet clean a panel.

Importantly, the Model allows the calculation of cleaning times and optimization of panel face length for cleaning. Shorter activity times enable more drill-blast-support-clean cycles to be completed per month. This translates into improved production, lower unit costs and more profitable operations.

In particular, this paper addresses the following questions:

1. How long will it take to clean a panel?
2. What is the optimum panel length?
3. How much water will be used?
4. How much energy will be used?
5. What production increases are possible?
6. How safe are jet cleaning tools?
7. What are the effects on the working environment?
8. How can the dirty water be managed?
9. What other issues need to be considered?
10. What is the most suitable jet cleaning tool?

Additionally, integration of water hydraulic drilling with water jet cleaning allows conventional compressed air mines to be weaned off compressed air one panel or raise line at a time; ie in manageable transitional steps.

The Cleaning Model Methodology

The Jet Cleaning Model methodology is made up of the following 8 steps:

STEP 1: Quantify the Cleaning TASK

This depends on: panel length, stope width, advance, in-situ rock specific gravity (SG), gully size and mass of rock throw-blasted into the gully. The Cleaning TASK concept is illustrated in Figure 1 and defined as:

Cleaning TASK = (TONS not blasted into gully) x (Average METRES to be moved) [t.m]

It assumes the centre of mass of the rock pile to be moved lies approximately midway between the top the pile and the top of the gully.

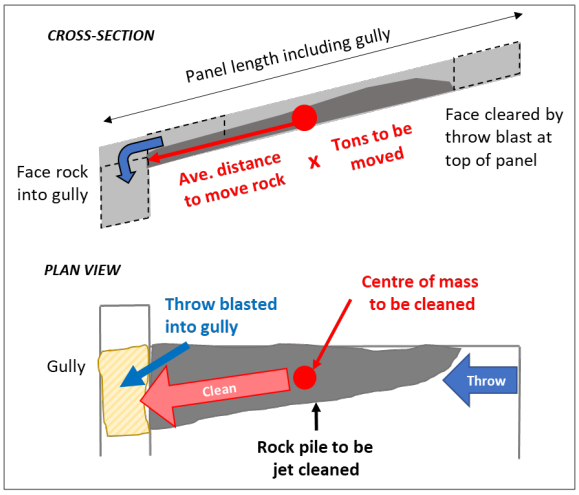


Figure 1. Cleaning TASK diagram.

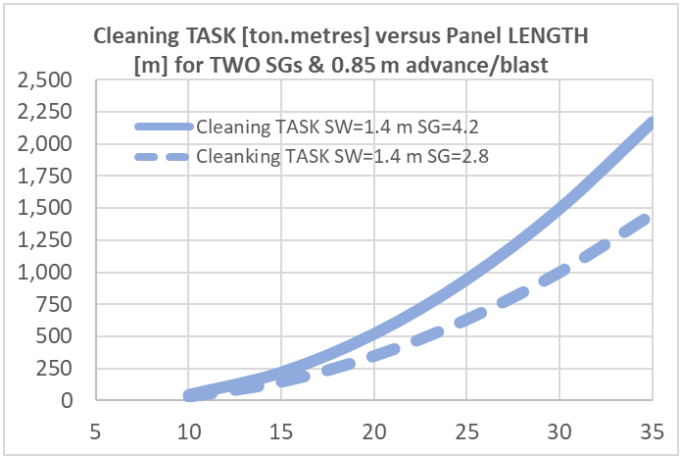


Figure 2. Cleaning TASK versus Panel LENGTH.

STEP 2: Select Nozzle DIAMETER and supply PRESSURE into hose Combination Fuse/Isolation (Combi) Valve and calculate the Effective Jet Impact FORCE at 5 m from the nozzle

This involves a standard hydraulic calculation of the pressure losses in the reticulation from the power pack or station to the nozzle to determine the nozzle pressure and hence flow rate, jet velocity and jet force at the nozzle. The nozzle jet force is derated for the fall-off in impact force with increasing distance from the nozzle due to increasing jet de-coherence. This depends on the nozzle diameter and impact distance. See details in the Appendix.

STEP 3: Calculate the Standard Cleaning RATE at 22.5° Dip using the Effective Jet Impact FORCE at 5 m to and the empirically-based power law correlation formula

Measured cleaning RATES from various mines were plotted against effective jet impact FORCE at 5 m (see Appendix). This resulted in the following power law formula:

$$\text{Standard cleaning RATE} = 57.6 \times (F_{5m})^{0.353} \text{ [t.m/h]}$$

where F_{5m} = effective jet FORCE [kgf] at 5 m less the TRESHOLD force [kgf].

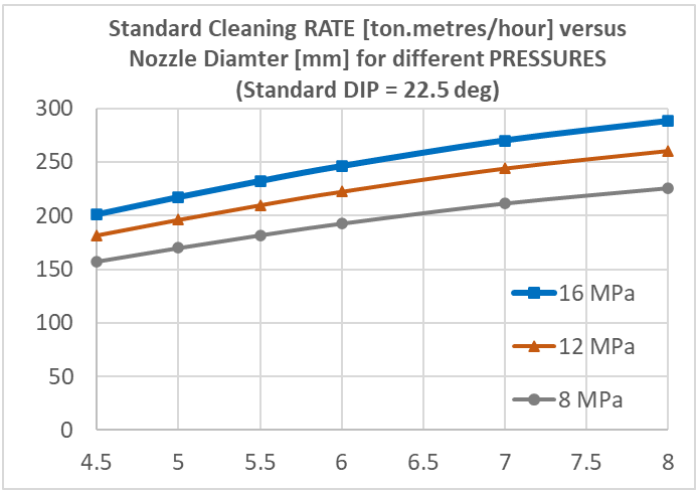


Figure 3. Standard Cleaning RATE at 22.5° dip versus Nozzle DIAMETER for three PRESSURES based on the power law correlation.

(By comparison to jet cleaning **without** face scrapers, Tarr, 1994 and Pickering, 2013 both mention cleaning RATE of face scraper cleaning rates assisted by water jets of ~550 t.m/h.)

STEP 4: Calculate DIP Factor for dips that differ from the standard 22.5°

Gravity aids cleaning at steeper dips shortening the Cleaning TIME, while shallower dips increase the cleaning TIME. Figure 4 shows this. Reducing the dip from at 22.5° to 15° increase the cleaning TIME by a DIP factor of 1.22.

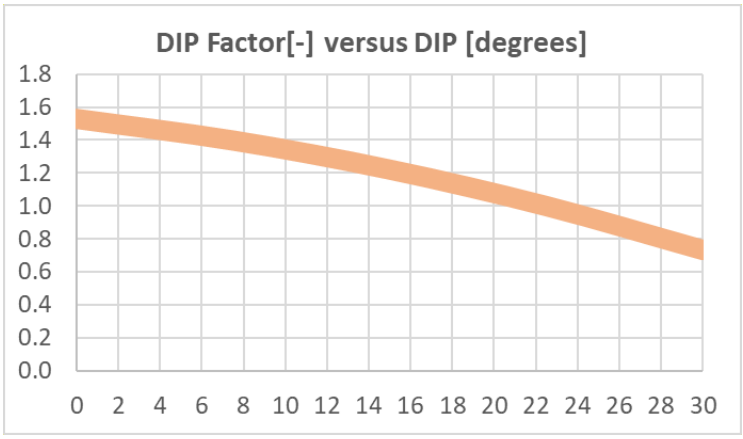


Figure 4. DIP Factor versus DIP angle of inclination.

STEP 5: Calculate the Dip-Adjusted Cleaning TIME

Dip adjusted cleaning TIME = (Cleaning TASK) x (DIP Factor) / (Cleaning RATE at Std Dip) [h]

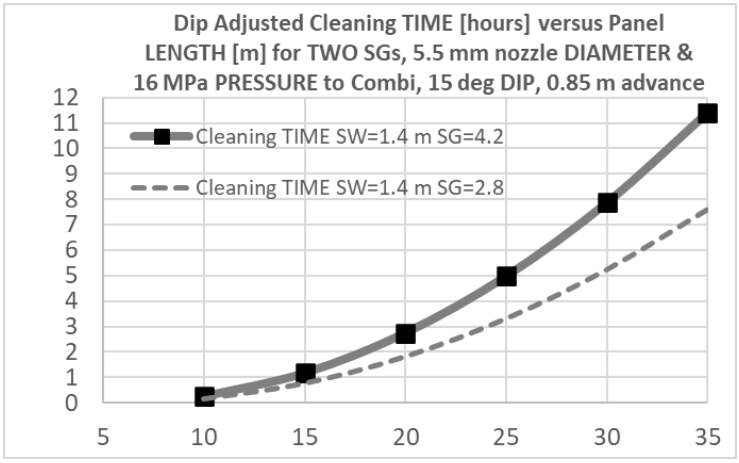


Figure 5. Dip Adjusted Cleaning TIME versus Panel LENGTH of two specific gravities (SGs).

This dip-adjusted cleaning TIME in Figure 5 is for **average** fragmentation, footwall smoothness, throw and operator skill. It is the typical time from the start to end of jet cleaning including cleaning tool move time etc.

It excludes other operations (making safe, support installation, etc) and delays due to excessive footwall unevenness, rolls, steps, over-size rocks and poor gully or raise scraper performance.

Actual panel cleaning can be much longer or shorter depending on whether cleaning is affected by these other factors. Recurring delays, new bottlenecks, and persistent sub-optimal factors, will need to be dealt with as part of normal mining management improvement processes.

NOTE: Figure 5 shows the dramatic effect of increasing the panel LENGTH. A 20% increase in LENGTH from 25 to 30 m increases the dip adjusted cleaning TIME from 5 to 8 hours, a 60% jump. Conversely, a 20 m panel will take about 2.7 hours, ie one third of that of a 30 m panel. This is not well understood, but the quadratic relationship makes sense, as an increase in the panel LENGTH increases both the TONS and the average METRES that the rock has to be moved. This understanding is a key result of the Model.

STEP 6: Calculate the WATER Usage

Jet cleaning tool with automatic shut-off trigger valves, only use water when the trigger s depressed. Water flow stops on release of the trigger. The instantaneous flow will vary with the nozzle DIAMETER and supply PRESSURE to the hose Combi Valve. This is shown in Table 1 for a particular prop-mounted Panel Cleaning Tool (PCT).

Table 1: Instantaneous FLOW rate [litre/s] versus nozzle DIAMETER at various supply PRESSURES [MPa] into the hose Combi Valve for an HPE prop-mounted Panel Cleaning Tool (PCT).

FLOW l/s	**Nozzle DIAMETER [mm]**					
		4.5	**5**	**5.5**	**6**	**6.5**
MPa	**16**	2.65	3.24	3.86	4.52	5.19
	14	2.48	3.03	3.61	4.23	4.85
	12	2.29	2.80	3.35	3.91	4.49

The total volumetric water USAGE depends on the cleaning TIME, the instantaneous FLOW rate, and the flow DIVERSITY. The flow DIVERSITY takes into account that during a cleaning cycle cleaning tools fitted with automatic shut-off valves will not be using water while jetting stops, eg to relocate to a new jetting position, to move a temporary prop, etc. For example, an assumed typical flow DIVERSITY of 75%, means that for 25% of the time, water is not being used. (NOTE: For so-called "dump guns", the flow DIVERSITY is 100% because the water is dumped to the footwall at low pressure even when not jetting, thereby increasing water and energy USAGE by ~30%).

Water USAGE per PANEL
= Cleaning TIME [h/panel] x Flow DIVERSITY x FLOW Rate [l/s] x (3.6 m^3/h per l/s)
= (5,0 hours from Figure 5) x 75% x (3,86 from Flow RATE Table 2) x 3.6 = 52.1 m^3/panel

Water USED per TON reef
= Water USED per PANEL [m^3/panel] / TONS per [t/blast]
= (52.1) / 125 = 0,42 m^3/t

(Note: The cleaning TIME depends on the cleaning TASK which includes for the effect of the in-situ rock specific gravity.)

STEP 7: Calculate the Energy USAGE

Power pack energy USAGE: This depends on power pack run hours to deliver the volume of water used for cleaning (both fully and part loaded), delivery pressure, cleaning tool flow rate and efficiencies of the pump and motor under full and part-load – See Appendix for details.

De-watering pump energy USAGE: This depends on de-watering pump lift, column friction losses, run hours (both fully and part loaded), delivery pressure, cleaning tool flow rate, and efficiencies of the pump and motor under full load – See Appendix for details.

STEP 8: Estimate the Possible IMPROVEMENT in Production

This depends on the current strike rate (ie percentage of blasts achieved per month), the current average cycle activity time, possible reduction in the activity time, and assumes a normal distribution of activity times about a mean with standard deviation typically about 20% of the mean.

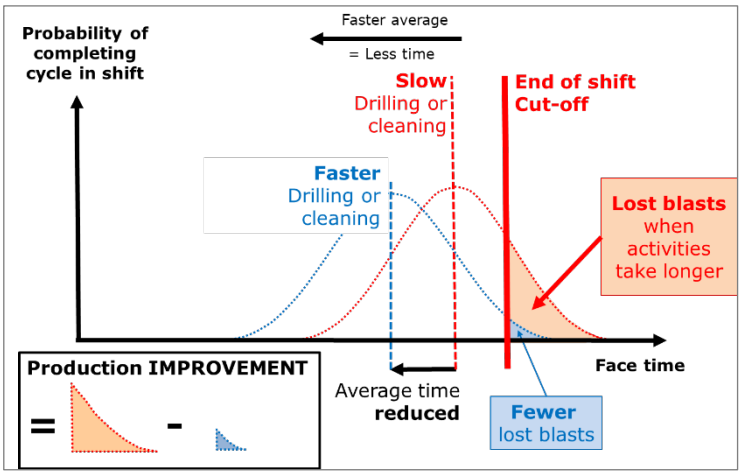


Figure 6. Diagram illustrating how reducing the mean time of the activity reduces the probability of completing the activity in the time available.

Table 2. Possible production improvements given a current strike rate and average activity time before implementation of jetting and average reduction in cleaning time achieved after implementing jet cleaning.

Example

- mine currently achieves **14 of 23 possible blasts** (ie 60% strike rate)
- faster drill & clean **reduces activity time by 1 hr**
- results in **28% higher production**

Ave. reduction in time [hours]	Current strike rate 40%	50%	60%	70%	80%
0.5	21%	19%	16%	11%	6%
0.75	31%	27%	23%	17%	11%
1.0	38%	34%	**28%**	22%	14%
1.25	45%	39%	33%	25%	17%
1.50	50%	43%	35%	27%	18%

Improvements of 20 to 35% are possible

Actual results will depend on current performance, drilling & cleaning time reductions, & the ability to remove other bottle necks & delays

Final jet cleaning tool and power pack selection will involve repeating the steps above until an acceptable cleaning TIME is achieved that also addresses the following:

- Panel lengths that fit the mine layout,
- Adequate Mine Service Water (MSW) flow capacity and pressure,
- Adequate Dirty Water Management (DWM) and de-watering capacity, and
- Other power pack sizing needs eg face and support drilling with water hydraulic drills.

Typical Model results

Table 3. Typical Jet Cleaning Model results.

For 5.5 mm nozzle DIAMETER, 16 MPa PRESSURE, 15° DIP, 0.85 m advance, UG2 SG=4.2, and assuming 75% Flow DIVERSITY	
Tons for 25 m x 1.4 m panel x 0,85 m adv x 4.2 SG= 25 x 1.4 x 0,85 x 4.2	125 t/blast
Question	**Answer**
What is the **optimum panel length?**	< 25 m (Merensky longer)
How long will it take to clean a panel?	~5 hrs (Merensky less)
How much water will be used per panel?	52 m^3 /panel (Merensky less)
How much water will be used per ton reef?	0.42 m^3 /t (Merensky same)
How much energy will be used by the power pack?	2.7 kWh/t
How much energy will be used by the de-watering pumps?	2.9 kWh/t
What **production increase** is possible?	20 to 35%
What other factors need to be considered?	Panel jet pump, centre raise drainpipe + dirty water pumping on level, improve blast throw, drilling accuracy

Opportunities (and a concern) arising from Jet Cleaning

1. **Changing panel length:** Shorter versus longer panels as discussed above.
2. **Throw blasting:** Throw blasting rock into the gully and further down the panel reduces the Cleaning TASK, and hence Cleaning TIME. With suitable drilling and face angles relative to the gully, more or less clear space can be made for rock to be thrown before it chokes the face. For example, a face at 90° to the gully, but drilled at 70 degrees can angle the blast throw backwards away from the face.
3. **Optimizing gully size:** If the gully is too small to hold the thrown blasted rock it will increase the Cleaning TASK and TIME.
4. **Accurate drilling:** Good drilling practice, with parallel holes ending in the same plane, and uniform burdens and spacings, will improve the fragmentation and throw thus shortening the Cleaning TIME.
5. **Twin Gully Split Panel (TGSP) layout:** In this layout an extra scraper equipped gully is added halfway up the panel. This effectively halves the panel length and maximizes the throw effect dramatically reducing Cleaning TIME. This also adds cycle flexibility, increases rock storage volume, and adds another access. However, the extra gully increases reef dilution and requires another scraper.
6. **Removal of a face scraper:** Jet cleaning of the panel face allows face scrapers to be removed with obvious safety and time benefits.
7. C**leaner panels and fewer sweepings**: Scrapers do not clean the last ~100 mm or so of rock and cannot clean or sweep rock blasted into the back area. This affects temporary prop installation and often means that a shift is devoted to sweeping before month end measuring. In a mine not equipped with jets, Mine Service Water in 25NB hoses is inefficiently used to sweep fly rock, thereby wasting water.
8. **Carbon Leader Reef concern**: It is possible that jetting in gold mines where gold particles are loosely attached can result in reduced Mine Call Factor as fine gold particles are lost to cracks. R.G.B. Pickering, in private discussion with the author, said the COMRO had investigated going as far as lifting the footwall and did not find significant gold in the cracks etc. However, this is contrary to the results reported by Anglo Gold (Tarr, 1994). A plausible explanation is that some small loose gold particles are washed out by the jet and are not recovered due to poor sweeping practices. Follow up vacuum sweeping and vamping suggests that significant precious metal is left behind due to poor sweeping in both face scraper and jet cleaning.

Safety Record and Ergonomics
Sadly, hand-held jet cleaning tools have been responsible for several fatalities since their introduction in the mid-1980s.

The Chamber of Mines Research Organization who pioneered jet cleaning of stope panels, recommended a maximum reaction force of about 35 kgf, but soon some suppliers reportedly increased the force up to 43 kgf (Tarr, 1994) to reduce Cleaning TIMES. Foot stirrups and breast plates were added to reduce operator fatigue, but at the same time the role of cleaning tools changed from assisting face scrapers to replacing them, thus reducing the risk of face scraper related accidents.

To address these safety and operator fatigue issues and to dramatically reduce Cleaning TIMES, a prop-mounted cleaning tools with jet reaction of 80 to 120 kgf were developed. They were introduced at the request of a mine who, because they used a centralized high-pressure gravity hydropower system, were able to supply the water needed by a more powerful cleaning tool. Within 3-months of introduction, production increased by 30% to levels unattainable with hand-held jet cleaning tools.

Importantly, the design of this tool included an automatic shut-off mechanism that activates immediately if the prop comes loose. It was also designed such that the hose leak does not pose a risk to the operator. In 25-years of use, the 18 MPa x 8 mm prop-mounted Panel Cleaning Tool (PCT) has had an excellent safety record.

To protect stope personnel from uncontrolled energy release associated with a pipe or hose failure all high-pressure water hydraulic mining tools are protected with combined isolation/hydraulic fuse valves or Combi valves. These close automatically, and immediately, if the flow rate exceeds about 37% of the maximum rated flow (like tan electrical circuit breaker).

Furthermore, these tools are designed to comply with international pressure equipment, piping and valve codes, and equipment is pressure and functionally tested.

Operator Personal Protection Equipment (PPE) should include gloves, mesh ~~googles~~ goggles or visor, and a dust mask. The dust mask is especially important in gold mines where unhealthy quartzite dust can be liberated in the early stages of cleaning if the rock pile has not been effectively watered down.

Mud-rush Risk
Where water can enter an ore-pass it is possible for blasted rock, fines and mud to accumulate and then, under certain conditions, be suddenly released in a "mud rush" with damaging and possibly fatal consequences. This risk is common to all mining areas here water is introduced and where ore-pass box front systems cannot handle mud, fines and blasted rock or which are inadequately designed or installed.

It is recommended that a slotted chute door be used to drain the inevitable water entering an ore-pass. Additionally, an actuator with positive control, such as a water hydraulic cylinder and a design that incorporates a second safety door further reduces risk. In all cases, the ore-pass box front unit must comply with the SANS 10208-4:2011 prescribed loading and be correctly installed.

Effects on Workplace Environment
Water jet cleaning tools, if supplied with chilled water, provide significant "positional cooling" in the working area. Additionally, the water jet entrains air creating a comfortable "breeze" over the operator.

In deep and/or hot mines, the jetting water helps cool the freshly blasted warm rock, and in turn, the water warms up. If this water is removed without significant contact with the stope air, the heat in the rock can be removed to the de-watering pumps and removed from the mine, thus reduce stope heat load.

However, if spent water ponds in the cross-cut and/or haulage, then both heat and moisture can be transferred into the air, warming and humidifying the working environment. This is undesirable, but can be substantially prevented if the dirty water is optimally managed as described below.

Dirty Water Management
This involves: (1) pumping dirty water off the footwall into a hose and (2) running it out of the stope through a gravity drainpipe down the centre raise and travelling way. This is shown and explained in Figure 7.

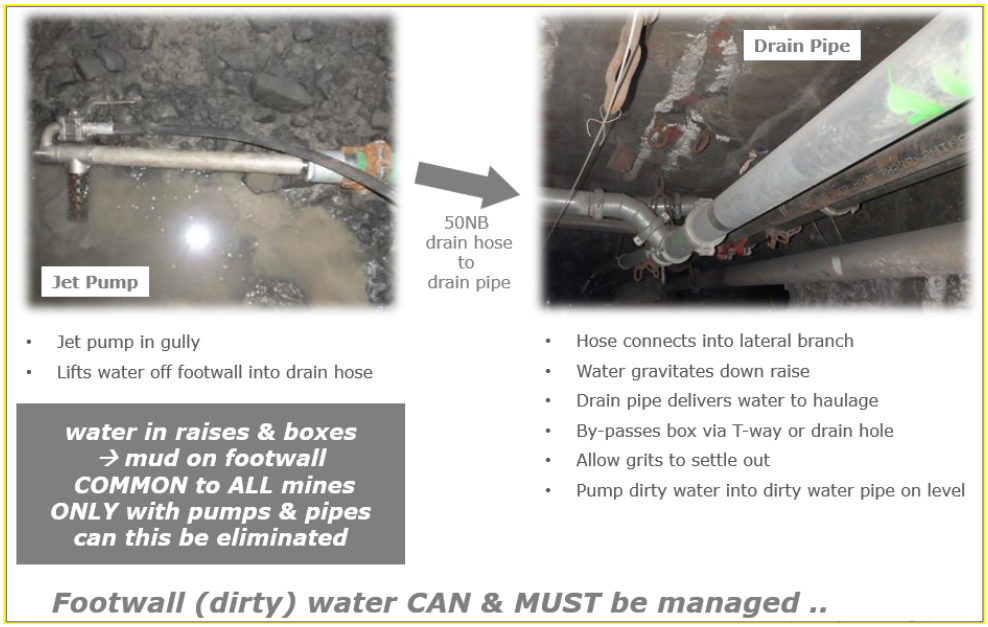


Figure 7. Dirty Water Management if water can be pumped into a centre raise gravity drain pipe and pumped out on the level.

Once in the crosscut or haulage, the warm dirty water should be de-gritted (ie fines allowed to settle out and then removed by a loader) and the grit-free dirty water pumped away in a pipe to the de-watering drain hole.

A half-round 300 mm wide channel drain, falling at a slope of 1:200, is unlikely to handle more than a few panels being simultaneously jetted, and will probably silt up for a considerable distance resulting in unwanted ponding.

Other Issues to be Considered

1. **Mine Service Water (MSW) supply and pipe size**: A 100NB pipeline serving a half level is too small to supply the water needed for jet cleaning in a full half level. Hence installing a 150NB MSW pipeline, which can supply the volume with acceptably small pressure losses, is recommended. The existing 100NB MSW can be repurposed to remove dirty water to the de-watering drain hole. The smaller diameter dirty water line is possible as average outgoing flow rates are lower than the incoming supply peak flow rate demand. Additionally, a significant fraction of the water used goes out with the rock.
2. **Possible new bottlenecks**: Improved cleaning rates demand higher gully and centre raise scraping rates and corresponding improved ore-pass clearing/increased tramming rates.
3. **Operator skill and cleaning sequences**: There are many sequences and ways in which rock can be moved with jets. There is benefit in working with jet tool operators to determine the best sequences and most effective jetting range before finalizing the mine standard. Engaging with the users will result in the most effective jet cleaning practices.

4. **Prop setting:** Temporary support props must be set properly to resist up to 120 kgf reaction forces for an 8 mm nozzle with an 18 MPa connected to the supply

Most Suitable Cleaning Tool
Various types of cleaning tool are compared in Table 4.

Table 4. Types of Jet Cleaning Tool.

Operating pressure	**Low-pressure (6 to 8 MPa)**		**High-pressure (12 to 18 MPa)**	
Type of control valve	**"Dump"**	**Auto shut-off**		
Support cleaning tool	**Hand-held**			**Prop-mounted**
Reaction force	**35 to 43 kgf with Nozzle DIAMETER matched to PRESSURE**			**40 to 120 kgf**
Fatigue & safety	**Tiring to operate & least safe**			**Easy & most safe**
Water & Energy USAGE per ton	**Dumping adds 30%**	**Comparable**		
Cleaning rate	**Comparable**			**Highest. Prop takes higher forces**
Instantaneous flow rate	**High**		**Low**	**Modest to very high (Note 1)**

Note 1: The 18 MPa x 8 mm cleaning tools are best supplied by centralized gravity hydropower systems. A 16 MPa x 5.5 mm prop-mounted tool requires a modest 3.9 l/s which can be supplied by a power pack.

CONCLUSIONS

1. A fit-for-purpose Jet Cleaning Model based on fundamental principles and calibrated with measured data has been presented and explained.
2. The Model estimates the time water and energy required for water jet cleaning of stope panels. It also quantifies the water and energy usage and possible production improvements.
3. The paper offers insight into the effects of changing panel length on cleaning time and identifies some emergent opportunities.
4. It also discusses safety, mud-rush risk, effects on the working environment, dirty water management and other factors to be considered.

RECOMMENDATIONS

1. Where possible, panel length and resulting cleaning times should be optimized to ensure more drill-blast-support-clean cycles are completed per month.
2. Combine water jet cleaning with water hydraulic drilling, using a single common power pack and reticulation system, to reduce mining cycle times compared with conventional compressed air systems. This offers both fast drilling and cleaning, higher production, and hence lower costs per ton.
3. Include a Dirty Water Management (DWM) system including jet pumps, a centre raise gravity drainpipe, grit removal, and dirty water on the level be installed. This will reduce ponding and transport warm, dirty water to the de-watering system without adding heat to the stope environment.

4. Use prop-mounted panel cleaning tools (PCTs) with medium size nozzle diameter (~5.5mm) supplied with ~16 MPa. These are safer and less tiring to operate than hand-held cleaning tools. They require the support of temporary props, which helps ensure that support in installed early in the shift, and offers higher jet impact forces, and hence shorter cleaning times.
5. Install 150NB Mine Service Water pipes from the station if more than two or three panels are to be cleaned. Repurpose the legacy 100NB MSW pipes to remove de-gritted dirty water and heat.

Appendix: Theory, Assumptions and Accuracy

Jet reaction force at nozzle: This requires a knowledge of the pressure behind the nozzle and the Coefficient of Discharge (typically 0.95 to 0.97). The pressure behind the nozzle can be determined by measurement of the Flow Coefficient, Cv = (Flow RATE)/sqrt(Pressure drop) in the tool valve and barrel, the hose, the combined fuse isolation valve, and the reticulation from the power pack. Jet Velocity = Cd x sqrt(2 x P/Ro), where P = nozzle static pressure and Ro = density of water, all in S.I. units The Nozzle reaction force = Rate of change of momentum of water = (Mass flow rate) x (Velocity change through the nozzle).

Jet Impact FORCE 5m from the nozzle: The effective impact force is assumed to be that measured by the impacting the jet on a 200 mm disc at a typical average safe distance from the rock pile. It reflects the decrease of force with distance due to jet de-coherence. A COMRO "rule of thumb" states that jets remained coherent over distance of about (1 000 to 1 500) x (Nozzle DIAMETER) (Perlwitz, July 1982). In this Cleaning Model an experimental relationship was used: (Impact FORCE at 5 m) / (Nozzle reaction force) = 0.575 + 0.044 x (Nozzle DIAMETER in mm) which give ~82% for a 5.5 mm nozzle.

THRESHOLD Force: Below a certain minimum jet impact FORCE or THRESHOLD force, jetting cannot move rock effectively. The Model allows for a THRESHOLD to be used to reflect this minimum, but assumed it to be zero in this paper. A typical THRESHOLD is estimated be in the range of 10 to 15 kgf.

Power law correlation approach: At a high-level, the kinetic energy of the jet supplies energy to move rock against friction. Relating the Cleaning RATE to the Effective Jet Impact FORCE therefore makes physical sense. The power law relationship: (Cleaning RATE) = K x (Effective Impact FORCE)^n, where the constant, K and exponent, n are determined experimentally. This function increases smoothly and monotonically from zero.

Measured cleaning RATES from various mines were plotted against Effective Jet Impact FORCE at 5 m as shown in Figure 8 and fitted to a power law curve with an acceptable Coefficient of Correlation (R^2 = 0.7). (In each case the measured cleaning RATES were adjusted back to a RATE for a standard dip of 22.5°).

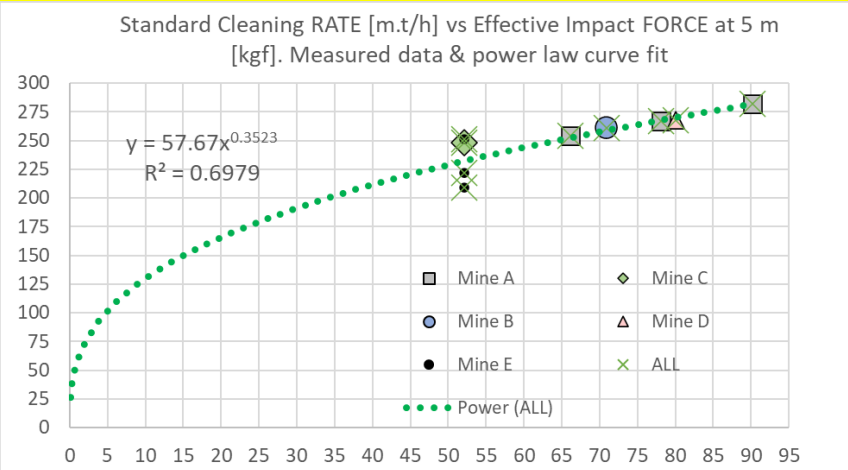


Figure 8. Cleaning RATE versus Effective Jet Cleaning FORCE correlation power law curve fit.

DIP Factor: This factor takes into account the dip. It allows for the component of weight acting down dip assisting rock movement down dip and the coefficients of friction rock providing frictional drag and preventing the rock from freely sliding down the dip. The relationship in Figure 4 is calculated assuming a friction angle or angle repose of 37.5°.

Mining Layout: In this paper it is assumed that the panels are breast mined ie the rock is moving down the steepest dip.

Accuracy: This Jet Cleaning Model is a fit-for-purpose mining tool to aid in the selection and sizing of a jet cleaning tool and to estimate cleaning TIME. It is most accurate for comparing similar systems or relative changes. Errors between model predictions and practice will vary most at extremes of dip (eg **.5° and 30°**) and very long and/or wide high panels. Only about 20 data points were used in the correlation and not all of these were accurate. Of the 10 data points for the same panel the measured averaging 2.9 hours, the standard deviation was 16%. Hence, variations of half an hour either way are expected in either a measured or predicted cleaning TIMES. The assumptions and methodology of this Model are conservative resulting in cleaning TIMES that are realistic rather than optimistic, however shorter times may be possible. Ultimately, measured average cleaning times of multiple panels are better than theoretical estimation, but in the absence of multiple data sets this model allows many alternatives to be compared.

Power Pack Energy USAGE:
PP Power [kW] = (Delivery pressure [MPa]) x (Flow Rate [l/s]) / ((Pump efficiency) x (Motor efficiency))
PP plunger pump efficiency ~85% and Equivalent FULL LOAD run hours = (Cleaning TIME [h]) x ((Flow DIVERSITY + (1- Flow DIVERSITY) x (UNLOADED Power / FULL LOAD Power)).
Energy USAGE [kWh] = (Power [kW]) x (Equivalent FULL LOAD run hours [h]).

De-watering Pump Energy USAGE:
Pump Power [kW] = (Delivery pressure [MPa]) x (Flow rate [l/s]) / ((Pump efficiency) x (Motor efficiency))
Delivery pressure [MPa] = 1.03 x (Total vertical lift from pumpstation to surface [m]) /102 which assumes column and valve friction losses of 3%.
Typical overall multistage centrifugal pump-set efficiencies are ~70%.
Pump run hours = (Cleaning TIME [h]) x (Flow DIVERSITY)
Energy USAGE [kWh] = (Power [kW]) x (Pump run hours [h]).

REFERENCES

CAMPBELL, D., PICKERING, R.G.B. Determination of parameters and development of equipment for water jet stope cleaning. COMRO Stoping Technology Laboratory Research Report No. 45/82, October 1982.

TUMPHOLME, E.R., WYMER, D.G. and PICKERING, R.G.B. Optimising the design of high-pressure water-jet stope cleaning equipment, Association of Mine Managers of South Africa, Papers and Discussions, 1982-1983.

PERLWITZ, P.J. Hand-held Double barrel Water Jetting Gun, COMRO Stoping Technology Laboratory report TN/02/88/PE Task No. GS1F02, February 1988. (Useful data measured date on drop off of impact force with distance).

PERLWITZ, P.J. Fundamentals of Water Jetting, COMRO Stoping Technology Laboratory report TN/05/88/PE Task No. GS1F02, July 1988. (Useful data measured date on drop off of impact force with distance).

TARR, R.G., FOUCHE, J. Water jets: A Review of the Usage of High-pressure Water jets on Some of Anglo Gold Division Mines, Productivity for Present Profitability and Posterity's Prosperity, SAIMM Colloquium, Randburg, 29 March 1994.

FRASER, P.D. The Energy Required to Drill a Hole. Platinum in Transition Conference. The South African Institute of Mining and Metallurgy, Sun City, 2010.

DU PLESSIS, A., PICKERING, R.G.B. Review of Hard-rock Mining Technology Research and Development in South Africa Pre-1990. The Centre for Mechanised Mining Solutions (CMMS), University of Witwatersrand, 2013.



P.D.Fraser

Hydropower Equipment (Pty) Ltd

Peter Fraser is a Professional Engineer and holds master's degrees in both mechanical engineering and business administration. He started his career with the Chamber of Mines Research Organisation (COMRO) and has recently retired from Hydro Power Equipment (HPE) where he was involved with innovation and growing market awareness of the water hydraulic mining solutions for nearly 28 years. Peter has contributed many papers to the Southern African Institute of Mining and Metallurgy mainly focusing on the performance, water usage and energy consumption of water hydraulic mining equipment.

Automating energy baseline development for energy-intensive mining systems in South Africa

N.T. Tshitenge[1], J.A. Swanepoel[2], J.H. Marais[3], H.P.R. Joubert[3]

[1]Tshwane University of Technology (TUT) & ETA Operations (Pty) Ltd, South Africa
[2]Tshwane University of Technology (TUT), South Africa
[3]North-West University & ETA Operations (Pty) Ltd, South Africa

The mining industry in South Africa is under pressure to reduce energy use due to national electricity constraints. This pressure makes timely energy efficiency intervention critical. Mining systems, such as compressed air, ventilation, and refrigeration, use energy to support operations. Energy data is one of the primary parameters utilised by mines to assess the performance of these systems and develop baseline profiles. These profiles are essential for measuring improvements and identifying inefficiencies. Energy consumption datasets are inherently large due to frequent sampling, multiple points of measurement, and extended retention periods. These large datasets, along with the effort required to develop baseline profiles, present a significant challenge. Traditional methods are often unable to process the datasets within a reasonable time frame. As a result, there are delays in performance assessment. Automating the process is therefore advantageous for obtaining baseline profiles with reduced time and effort. To solve this problem, an automated script, based on a combination of existing methods from literature and industry good practices, was developed and compared against a traditional method, through a comparative case study of an energy-intensive mining system. This script generated accurate daily energy consumption baseline profiles while reducing processing time by 99%, as well as minimising human intervention. The success of this automated baseline development in an energy-intensive mining system has prompted us to consider rolling it out to other energy-intensive mining systems and relevant non-mining operations.

Keywords: Automation, energy consumption baseline profiles, energy-intensive mining systems, large datasets, time and effort reduction

INTRODUCTION

The mining industry is one of the major energy-intensive industries in South Africa (Eskom, 2024). Its operations mainly rely on energy sourced from electricity (Majola and Langerman, 2023). As shown in Figure 1, electricity accounts for approximately 75% of the total energy sources used in underground mining operations.

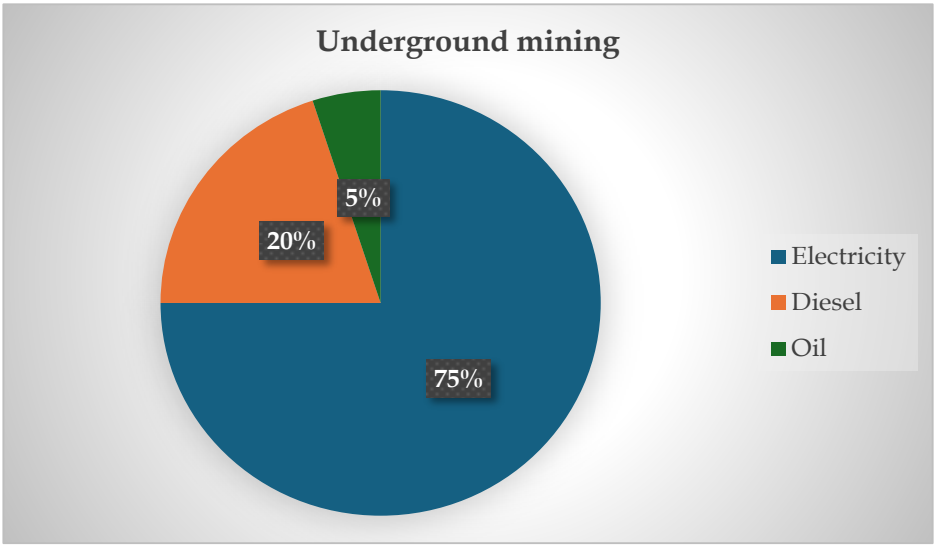


Figure 1. Proportion of energy carriers used in underground mining operations (Majola and Langerman, 2023).

The mining industry is compelled to curtail energy use during specified prescribed times due to national electricity constraints (Ateba et al., 2019). This requirement, in turn, makes the need for timely energy efficiency intervention critical. Furthermore, as depicted in Figure 2, the average electricity prices in the mining industry have shown a significant year-on-year increase, further intensifying the need for the efficiency intervention.

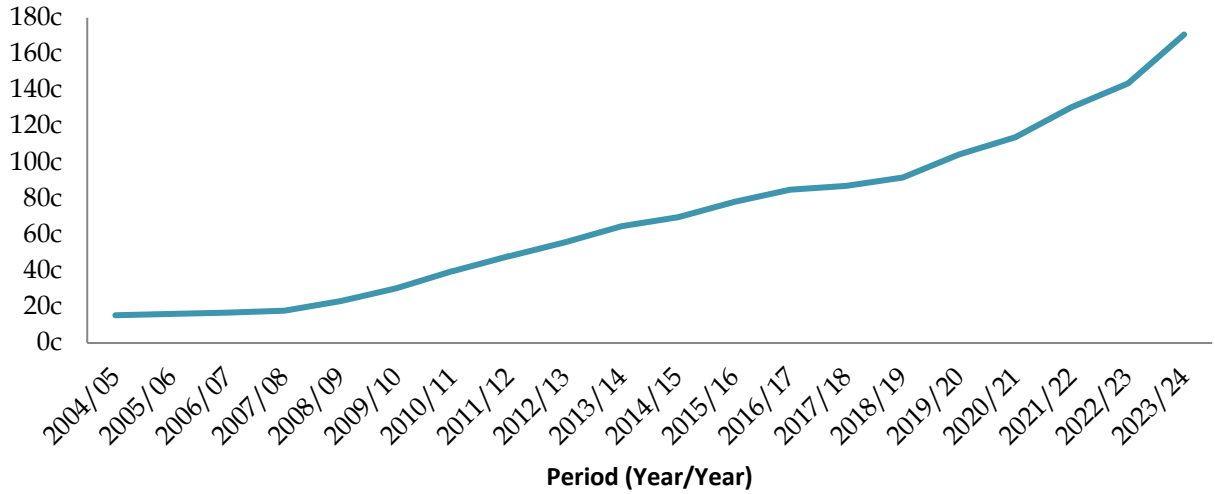


Figure 2. Average electricity prices for mining in South Africa (Eskom, 2025).

Mining systems such as compressed air, ventilation and refrigeration use energy to support operations (Majola and Langerman, 2023, Marais, 2024). Energy data is one of the primary parameters utilised by mines to assess the performance of these systems (Majola and Langerman, 2023, Marais, 2024) and to develop baseline profiles. A baseline profile provides a quantitative reference against which energy performance can be compared (Batlle et al., 2020). This baseline profile is a critical component in evaluating any energy efficiency intervention, as it enables the measurement of improvements and the identification of inefficiencies (Barnard and Grobler, 2012). Energy consumption datasets are inherently large due to frequent sampling (e.g., every 30 minutes), multiple points of measurement and the

extended retention periods (Benítez and Díez, 2022, Majola and Langerman, 2023). These large datasets, along with the effort involved in developing the consumption baseline profiles, present a significant challenge. The datasets are often too large to process using traditional methods in a timely manner. As a result, there are delays in performance assessment.

As mentioned in the preceding paragraph, a critical component in evaluating any energy efficiency intervention is to develop a baseline for the system being analysed (Barnard and Grobler, 2012); however, with traditional methods, the process is time consuming.

While *reduced time* refers to the decrease in the duration needed to execute the baseline development method, *reduced effort* refers to the minimisation of human intervention during the execution of the baseline development process (Tamir et al., 2008). In this context, *automation* refers to the execution of a script to perform a process without direct human intervention (Groover, 2016).

According to Groover (2016), automation in process industries operates across five hierarchical levels:

1. Device level, where sensors and actuators form the basic control loops for individual operations.
2. Regulatory level, which manages unit operations.
3. Supervisory control level, which coordinates multiple interconnected processes.
4. Plant level, which focuses on production scheduling, material flow tracking, and monitoring equipment performance.
5. The enterprise level, which deals with strategic planning, information management, and overall enterprise oversight.

Automation capability is shown in enabling large-scale energy consumption analysis with minimal effort, as demonstrated by Labbus et al. (2019) in the automotive industry.
Additionally, the research by Matthee et al. (2024) has mentioned that in the evaluation of 26 projects, the Measurement and Verification (M&V) process initially required a total of 156 hours, using the traditional method. However, by implementing automated methods, the time required for M&V was significantly reduced to 6 hours, reflecting a remarkable 96% improvement in efficiency. To end, Cornaro et al. (2019) conducted a study comparing a manual calibration process with an automatic calibration method by applying both to a dynamic simulation model of a real office building in Rome city. The automatic calibration resulted in a higher processing speed and reduced calibration time.

In this paper, we present an automated baseline development method that uses energy consumption data to generate daily baseline profiles for each month of the year (month-to-month baselines), using a programming language. This approach aligns each reporting month with its corresponding baseline month, accounting for seasonal and operational variations. This method is compared to a traditional method to evaluate differences in time and effort. Both methods are applied to a case study involving an energy-intensive system in the mining sector.

PROBLEM STATEMENT

Traditional baseline profiling is time-consuming and leads to delays in performance assessment. These delays hinder timely identification of inefficiencies in energy-intensive mining systems, resulting in poor energy performance.

AIM AND OBJECTIVES

Automating baseline development is advantageous because it produces baseline profiles in reduced time and with minimised effort. This study aligns with the supervisory-control level of automation, focusing on energy-intensive systems.

To successfully achieve this aim, the objectives of this paper are as follows:

- Review existing literature on automated methods for baseline profile development.
- Identify industry good practices in automated baseline profile development.
- Develop an automated baseline development process.
- Apply the process and validate the solution that addresses the research problem.

SUMMARY OF LITERATURE/ SIGNIFICANCE OF THE STUDY

In this section, we present an overview of the investigated studies, summarise the critical outcomes and shortcomings from each study in connection with automating energy baseline profile development.

Labbus et al. (2019) proposed statistical methods and clustering algorithms for the automated evaluation of large-scale energy datasets in automotive production. These methods are rooted in the engineering principles of data mining and statistical pattern recognition. They were prototypically realised in a Python framework. These methods resulted in high detection accuracy for anomalies in baseline energy profiles with reduced time and minimal effort, however, they are not applied in the context of energy-intensive mining systems.

Chen et al. (2020) introduced a method of automated verification of a security baseline in Information Technology (IT) systems. The method was based on Security Content Automation Protocol (SCAP) standards and cloud scanning technology. It was implemented using a custom system architecture framework. This approach utilised standards-based compliance checking and automation steps. Although this method achieved high accuracy in baseline verification with reduced time and minimal effort, it has not been contextualised to energy-intensive mining systems.

Sarmas et al. (2024) proposed an ensemble model for precisely estimating baseline energy consumption, applied using a Python-based Artificial Intelligence (AI)-empowered autonomous software systems. This approach is based on machine learning and ensemble modelling theory. The results revealed efficient energy consumption predictions with less effort, yet the study is not evaluated in energy-intensive mining systems.

Cornaro et al. (2019) developed an automatic calibration method and compare it to a manual process, both applied to a dynamic simulation model of an office building in Rome. The automatic approach relied on mathematical and statistical methods which use optimisation algorithms with GenOpt, an optimisation program. While the manual method relied on expert adjustments, the automatic method achieved better calibration metrics with less time and effort; however, the study focused only on office buildings and was not extended to energy-intensive mining systems.

Granderson et al. (2017) suggested the use of automation to streamline the M&V process. Although the automated methods achieved a reduction in time and effort needed to process large datasets, the study is limited to whole-building data evaluation and is not tested in energy-intensive mining systems.

Van As (2017) developed a baseline model intended for post-project reassessment, using a regression model in Microsoft Excel. This study utilised time-series analysis to model energy baselines for a mine cooling system, incorporated local and international standards to ensure that industry good practices can be used to solve a problem at Mine A. However, the study did not make use of automation to generate the baseline, an aspect that could further improve the baseline model.

The good practices identified in this study include:

- Application of time-series analysis to reflect operational realities and seasonal trends in the baseline.
- Consideration of weekdays and weekend electricity rate structures during baseline development to reflect varying operational and tariff conditions.

These practices are supported by guidance from the International Performance Measurement and Verification Protocol (IPMVP). This protocol underlines the need for baseline periods to represent all typical operating modes of the system (Efficiency Valuation Organisation, 2018). In addition, the South African National Standard (SANS) 50001:2024 emphasises the importance of evaluating past and present energy use and consumption for energy review (South African Bureau of Standards, 2025).

Table I below shows the evaluation criteria based on the published work. Findings from this literature indicates that no single method satisfies all four evaluation criteria simultaneously: application to the mining industry, relevance to energy-intensive systems, use of automation, and the ability to achieve time and effort reduction. This gap in present research highlights the need for future work to focus on developing an automated method to generate baseline profiles for energy-intensive mining systems, with reduced time and effort.

In Table I, "✓" indicates the reference's relevance to the respective evaluation criteria, while "**X**" indicates that the criteria were not addressed in the reference study.

Table I. State-of-the-art matrix indicating evaluation criteria based on published work

Author/Ref	**Year**	**Evaluation criteria**				**Findings/ Method used**
		Existing automated method	**Mining industry**	**Energy-intensive systems**	**Time & effort reduction**	
(Labbus et al.)	2019	✓	X	X	✓	Uses statistical methods and clustering algorithms, implemented using a Python framework.
(Chen et al.)	2020	✓	X	X	✓	Utilises standards-based compliance checking and automation steps, within a custom system architecture.
(Sarmas et al.)	2024	✓	X	X	✓	Applies machine learning and ensemble modelling theory, through a Python-based AI-empowered autonomous software systems.
(Cornaro et al.)	2019	✓	X	X	✓	Suggests mathematical and statistical methods which use optimisation algorithms with GenOpt, an optimisation program.
(Granderson et al.)	2017	✓	X	X	✓	Uses an automated M&V 2.0 tool to streamline the M&V process.
(Van As)	2017	X	✓	✓	X	Uses a regression model for the baseline development, realised in Excel.

Based on the findings, automation has been implemented in most of the reviewed studies, primarily within general or non–energy-intensive applications. However, it has not yet been applied to energy-intensive mining systems. The single study addressing an energy-intensive mining context (Van As, 2017) relied on traditional baseline development method. This observation indicates that while automation frameworks are emerging, their integration into mining and energy-intensive mining systems is limited. Developing an automated method for baseline generation in such environments therefore requires specialised expertise in data management, automation design, and energy-intensive mining operations.

METHODOLOGY AND MODEL

In this section, we propose a case study research design methodology for the research design, as the research is characterised by intensive data generation (Verschuren et al., 2010). We also present an overview of the research design methodology for a single case study. The research begins by establishing the need for the study, which outlines the present limitations of using traditional methods to develop energy baseline profiles for energy-intensive mining systems. Following this step, a literature review is conducted to explore existing knowledge on baseline automation methods. The next step covers energy performance guidelines drawn from industry standards, which define good practices for baseline development. The subsequent steps involve developing an automated method using Python and constructing a traditional manual method in Microsoft Excel. Python is proposed because of its scalability, and the availability of a wide range of data and libraries it encapsulates (López-Fernández et al., 2024). Microsoft Excel is utilised for its accessibility and user familiarity in both academic literature and industrial environments, particularly for manual data processing and baseline construction (Van As, 2017). These two methods are then applied to a single case study involving energy-intensive mining systems. The results from these two methods are then analysed and compared. This comparison of automated and traditional methods is expected to highlight performance improvements brought by automation. The final step provides recommendations for the study. The entire research design methodology steps are depicted in Figure 3.

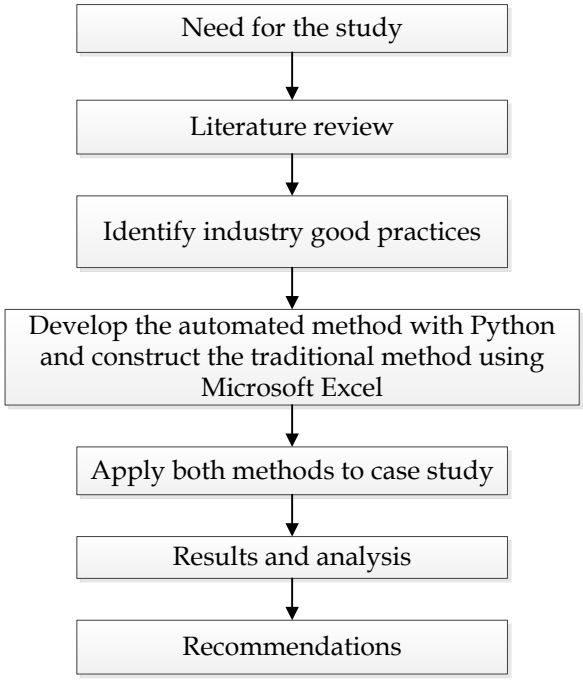


Figure 3. Research design methodology for the case study (Teegavarapu et al., 2008).

So far, in this paper, we have covered the need for the study, the literature review, and the identification of industry good practices. In the upcoming sections, the remaining steps will be carried out in accordance with Figure 3.

Automated Method Development Steps

Figure 4 depicts the proposed procedure for the developed automated method (Furumele, 2024, Labbus et al., 2019).

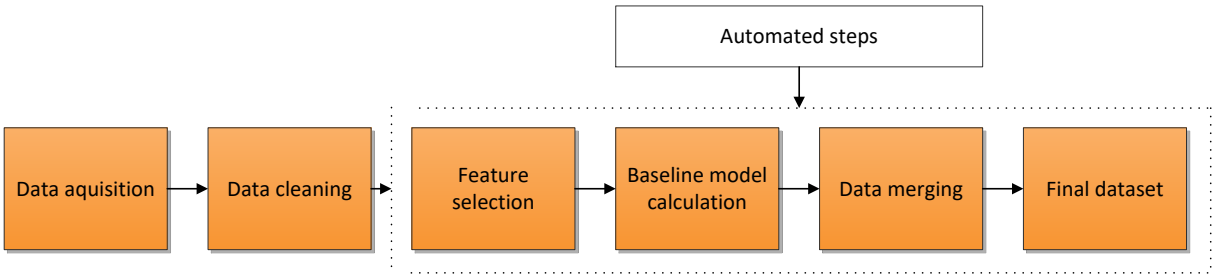


Figure 4. Proposed automated baseline model development steps.

Data acquisition
The energy data for the baseline period is obtained from the mine's Supervisory Control and Data Acquisition (SCADA) historian system, extracted with a data resolution of 30-minutes. Its user interface provides options to select three key fields "Tag Name", "Begin Date & Time" and "End date & Time". A *tag* is a unique identifier containing a name which is used to store data that is measured from a specific component (De Meyer, 2022). This is a convenient method for storing all data associated with a component from a specific location. An example of a tag name is as follows, "SiteX_ComponentY_Energy", where:

- Site X: the component's location,
- ComponentY: the component type, and
- Energy: the parameter being measured.

Data is exported in CSV format according to the selected tag names, date and time range to ensure relevance.

In this step, we selected compressor tags to export data for an entire region in the Rustenburg area with a baseline period from 01/01/2023 at 00:00 to 31/12/2023 at 23:30, to account for seasonality, operational variability, and day-type classification: Weekdays [Monday to Friday], Saturday, and Sunday (Oosthuizen, 2018, Van As, 2017).

Data cleaning
The exported dataset was checked for outliers by examining whether values fell within the expected operating range of each parameter; no outliers were detected. Missing data was identified using a data filtering option, which revealed that two 30-minute time intervals in the dataset were missing. Since the baseline profile is calculated by averaging values at each 30-minute interval across the same day-type classification within the monthly baseline period, the impact of these missing intervals was considered negligible. This negligible impact is due to the averaging process, as defined in the automated steps formula, which automatically excludes intervals without data and uses only available intervals, thereby maintaining the integrity of the baseline profile.

Automated steps
Through the 'Feature selection' step, the developed automated script converts the 'Date' and 'Time' fields into a structured format called "datetime" objects. This format makes it easier to extract meaningful time-based components. From these datetime objects, the following new features were generated: Month, day of the week and day-type classification. This feature enabled the model to distinguish operational patterns and adapt the baseline accordingly.

As part of the 'Baseline model calculation' step, a multi-index pivot table script was created to compute the average energy consumption per tag name, grouped by: Month, day-type classification, and each 30-minute time interval within a 24-hour day.
This baseline calculation is referred to as:

$$\bar{E}_{m,w,t}^{(tag)} = \frac{1}{n_{m,w,t}^{(tag)}} \sum_{i=1}^{n_{m,w,t}^{(tag)}} x_i^{(tag)} \quad [1]$$

Where:

$\bar{E}_{m,w,t}^{(tag)}$: Average energy consumption for a given tag, calculated for each 30-minute interval "t", in a 24-hour period, separately for each weekday classification "w", within a given month "m".

m: Month (1–12) in which the measurement is taken.

w: Weekday classification.

t: 30-minute time interval in the 24-hour profile (e.g., 00:00, 00:30, …, 23:30).

$n_{m,w,t}^{(tag)}$: The number of valid (non-missing) observations available for the tag in month 'm', weekday classification 'w' and interval 't'.

$x_i^{(tag)}$: i-th observed energy value for the tag, month 'm', weekday classification 'w', and interval 't'.

i: Index of each observation in the group, where $i = 1, 2, \ldots, n_{m,w,t}^{(tag)}$.

Through "Data merging" step, a date-time table covering the reporting year (e.g., 2025) is generated with 30-minute intervals. This ensures alignment between the reporting dataset and the baseline model.

In the "Data merging" step, a date-time table is created as a calendar for the full reporting year (e.g., 2025). It lists every 30-minute interval (00:00, 00:30, 01:00 … 23:30) for each day, ensuring a complete and continuous timeline. This continuous timeline aligns the reporting dataset with the baseline model, so that every measurement is mapped to the correct interval.

Final dataset
The dataset is exported automatically as a clean CSV file for further usage.

Construction of the Traditional Method Development Steps
Figure 5 depicts the proposed procedure for the traditional method (Labbus et al., 2019, Furumele, 2024).

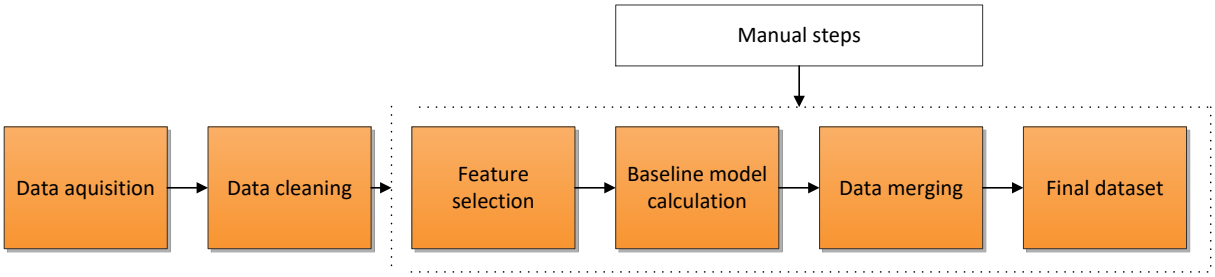


Figure 5. Proposed traditional method baseline model development steps.

Data acquisition and data cleaning steps are identical to those used in the automated method and will therefore not be discussed here.

Manual steps
In the manual approach, initial baseline calculations were attempted using AVERAGEIFS formulas in a single Microsoft Excel spreadsheet, referencing multiple cells across multiple tags. However, the spreadsheet soon became increasingly slow and prone to crashing. Consequently, the method was revised and executed in three steps, with the baseline process completed sequentially for each tag.

In the Feature selection step, the data was manually filtered in an Excel spreadsheet using Pivot Table tools. Filters for Date, Month, and Weekday were applied to the day-type classification.

During the Baseline model calculation step, pivot tables were created with 'Time' as the row field, 'Tag Name' as the column, and "Average of Tag Value" as the values field. This setting allowed the calculation of average energy consumption per time interval for each day-type classification and month.

In the Data merging step, each day-type classification was saved in a separate sheet tab. This setting was set to form a complete baseline reference, ensuring that day-type classification patterns were preserved for the reporting period.

Final dataset
The baseline profiles for day-type classification were manually combined into a single structured dataset aligned with the reporting period's 30-minute time intervals, ready for further analysis.

IMPLEMENTATION

In a case study involving an energy-intensive mining system within a platinum mining group near Rustenburg, the presented automated method steps were implemented using the Python platform.
In contrast, the traditional method was implemented using Microsoft Excel.

RESULTS AND ANALYSIS

Both methods, automated and traditional, were applied in the case study to generate a month-to-month baseline profile, using 2023 as the baseline year and 2025 as the reporting year.

The two methods output identical baseline values, however, the automated method processed 13 tags from the energy-intensive system in approximately 5 seconds with a single "run" command in Python, compared to the Excel-based approach, which required 39 minutes for the same 13 tags (3 minutes per tag) and needed multiple manual actions to complete the baseline process. This comparison shows the improvement achieved through automation, particularly when handling large datasets involving multiple tags.

Figures 6 and 7 show the two identical baseline and actual energy profiles, respectively, for the energy-intensive system, using July 2023 as the baseline period and July 2025 as the reporting period.

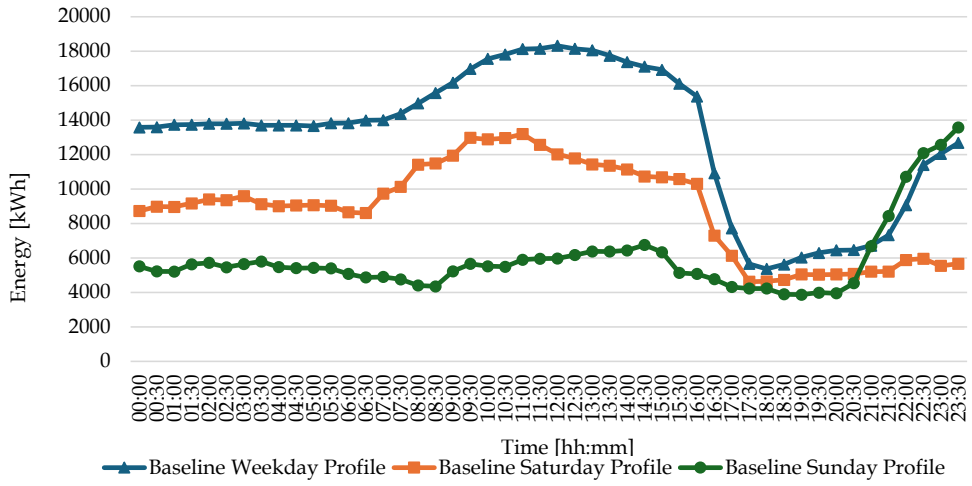


Figure 6. Baseline energy profiles for compressors.

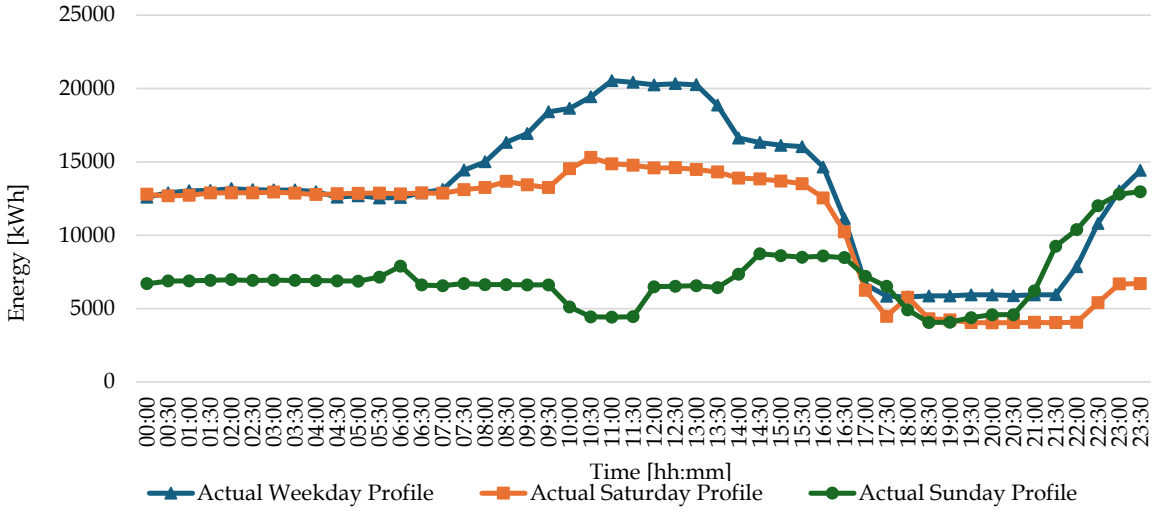


Figure 7. Measured energy profiles for compressors.

Further evaluation of the baseline profiles' accuracy was unnecessary as the two baseline methods produced identical values.

CONCLUSION, RECOMMENDATIONS AND ROLLOUT PLAN

This study developed and evaluated an automated method for generating daily energy consumption baseline profiles using an energy-intensive mining system case study. The method was compared against a traditional approach to assess differences in time and effort. The baseline profile was generated by averaging each time interval across the same day-type classification within a month.

By implementing the presented automated method, based on an established approach from literature and industry good practice, the time required for the baseline development process was reduced significantly. In the traditional method, generating baselines for 13 tags took 39 minutes (about 3 minutes per tag). With the automated method, the same task was completed in just 5 seconds. These results reflect a remarkable 99% improvement in reduction as well as minimised human intervention, as the automated method only required pressing a single 'run' command in Python.

It is advantageous to utilise an automated method in energy-intensive mining systems, where datasets are inherently large, it can save 24h 56 min of work for 500 tags. This time saving makes the method approximately 468 times faster than the traditional approach.

The adoption of this automated method can reduce delays in performance assessment by more than 90%. This reduction in delays promotes the timely identification of inefficiencies in energy-intensive mining systems. Such timely identification subsequently supports improvements in overall energy performance.

However, while isolated missing data in the baseline period had negligible impact due to the averaging process, gaps can occur when data for a time interval is absent across all instances of a given day-type classification in a month. To address this limitation, future research should consider applying imputation techniques, which can estimate missing values using neighbouring data points, and could improve the automated method in such cases.

The success of the automated baseline development in an energy-intensive mining system has prompted us to consider extending it to other energy-intensive systems such as ventilation and

refrigeration, as well as relevant non-mining operations, particularly manufacturing sectors (e.g., automotive plants) where electrical energy is a primary cost driver.
The rollout plan involves assessing data availability, granularity, and system integration requirements for each target process prior to automating baseline development. This assessment includes validating measurement boundaries, data completeness, and control-system compatibility. By successfully implementing automated steps, the innovation will support broader industrial applications beyond mining.

ACKNOWLEDGEMENTS

The authors express their gratitude to the Lord for the gift of life and gratefully acknowledge the support of Tshwane University of Technology (TUT) and ETA Operations (Pty) Ltd for this conference paper. The authors also extend their gratitude to Dr. Jean van Laar, Dr. Frans Matthee, Mr. Kabir Prema, and Mr. Emmanuel Ndumbi for their valuable inputs to this work.

REFERENCES

Ateba, B.B., Prinsloo, J.J. & Gawlik, R. 2019. The significance of electricity supply sustainability to industrial growth in South Africa. *Energy Reports,* 5**,** 1324-1338.

Barnard, F.C. & Grobler, L.J. Baseline service level adjustment methodologies for energy efficiency projects on compressed air systems in the mining industry. 2012 Proceedings of the 9th Industrial and Commercial Use of Energy Conference, 2012. IEEE, 1-8.

Batlle, E.A.O., Palacio, J.C.E., Lora, E.E.S., Reyes, A.M.M., Moreno, M.M. & Morejón, M.B. 2020. A methodology to estimate baseline energy use and quantify savings in electrical energy consumption in higher education institution buildings: Case study, Federal University of Itajubá (UNIFEI). *Journal of Cleaner Production,* 244.

Benítez, I. & Díez, J.L. 2022. Automated Detection of Electric Energy Consumption Load Profile Patterns. *Energies,* 15.

Chen, Y., Wang, Q., Sun, M., Chen, P., Qiao, Z. & Chen, Z. 2020. Automatic Security Baseline Verification Method Based on SCAP and Cloud Scanning. *The 8th International Conference on Computer Engineering and Networks (CENet2018).*

Cornaro, C., Bosco, F., Lauria, M., Puggioni, V.A. & De Santoli, L. 2019. Effectiveness of Automatic and Manual Calibration of an Office Building Energy Model. *Applied Sciences,* 9.

De Meyer, J.N. 2022. *Determining the integrity of single-source condition-based maintenance data.* D.Eng. thesis, Potchefstroom, North-West University.

Efficiency Valuation Organisation 2018. International Performance Measurement and Verification Protocol: Generally accepted principles. Washington: Efficiency Valuation Organisation.

Eskom. 2024. *Eskom Integrated Report 2024* [Online]. Available: https://www.eskom.co.za/wp-content/uploads/2024/12/Eskom-integrated-report-2024.pdf [Accessed 23/03/2025].

Eskom. 2025. *Historical Average Price increase* [Online]. Available: https://www.eskom.co.za/distribution/tariffs-and-charges/tariff-history/ [Accessed 15/06/2025].

Furumele, M.C. 2024. *Dynamic control of deep-level mine cooling systems using artificial intelligence.* M.Eng. dissertation, Potchefstroom, North-West University.

Granderson, J., Touzani, S., Fernandes, S. & Taylor, C. 2017. Application of automated measurement and verification to utility energy efficiency program data. *Energy and Buildings,* 142**,** 191-199.

Groover, M.P. 2016. *Automation, production systems, and computer-integrated manufacturing*, Pearson Education India.

Labbus, I., Teiwes, H., Filz, M.A., Herrmann, C., Gonter, M., Rössinger, M. & Thiede, S. 2019. Automated statistical evaluation of energy data in the automotive production. *Procedia CIRP,* 81**,** 1154-1159.

López-Fernández, A., Gómez-Vela, F.A., del Saz-Navarro, M., Delgado-Chaves, F.M. & Rodríguez-Baena, D.S. 2024. Optimized Python library for reconstruction of ensemble-based gene co-expression networks using multi-GPU. *The Journal of Supercomputing,* 80**,** 18142-18176.

Majola, C.M.D. & Langerman, K.E. 2023. Energy efficiency in the South African mining sector: A case study at a coal mine in Mpumalanga. *Journal of the Southern African Institute of Mining and Metallurgy,* 123**,** 451-462.

Marais, R.F. 2024. *A zero-wastage approach to benchmark energy efficiency on platinum mines.* D.Eng. thesis, Potchefstroom, North-West University.

Matthee, F.J.L., Marais, J.H. & van Laar, J.H. 2024. Enhanced Measurement and Verification Practices in Deep-Level Mines: The Current State. *Mining,* 4**,** 401-416.

Oosthuizen, C.J. 2018. *A compressed air cost savings identification model for deep-level mines.* M.Eng. dissertation, Potchefstroom, North-West University.

Sarmas, E., Forouli, A., Marinakis, V. & Doukas, H. 2024. Baseline energy modeling for improved measurement and verification through the use of ensemble artificial intelligence models. *Information Sciences,* 654.

South African Bureau of Standards. 2025. Energy management systems - Requirements with guidance for use. Pretoria: South African Bureau of Standards.

Tamir, D., Komogortsev, O.V. & Mueller, C.J. 2008. An Effort and Time Based Measure of Usability. *In Proceedings of the 6th international workshop on Software quality.*

Teegavarapu, S., Summers, J.D. & Mocko, G.M. Case study method for design research: A justification. International design engineering technical conferences and computers and information in engineering conference, 2008. 495-503.

Van As, R.S. 2017. *An improved baseline model for a mine surface cooling plant DSM project.* M.Eng. dissertation, Potchefstroom, North-West University.

Verschuren, P., Doorewaard, H. & Mellion, M.J. 2010. *Designing a research project*, The Hague: Eleven international publishing.



Ndumbi Tite Tshitenge

Engineer and Master's candidate
Tshwane University of Technology (TUT) & ETA Operations Pty (Ltd)

Ndumbi is an optimist and dedicated engineer in the energy management field.

He completed his Bachelor of Technology in Industrial Engineering at the Tshwane University of Technology in 2019.

From June 2021 to May 2023, he worked as a Control Room Engineer, where he was actively involved in live system operations. His responsibilities included optimising compressed air systems, monitoring energy initiative projects and assisting with power control execution. Operating across rotating shifts, including morning, afternoon and night helped him to develop solid situational awareness and quick decision-making skills.

Since June 2023, he has held the role of Engineer in Utility Management, where he specialises in building and maintaining daily utilities reports within a digital infrastructure. To date, he has developed over 15 detailed daily utilities reports used to track energy consumption trends, evaluate energy performance and identify improvement opportunities. These reports support data-driven decision-making across engineering departments and contribute to measurable energy and cost savings.

In this role, he also assists as the first point of contact for system and data support requests within the energy and utility management team. He assists with troubleshooting, dashboard support and ensuring continuous access to accurate and reliable data across platforms.

A significant focus of his present work involves developing energy baseline profiles for performance reporting. He applies statistical and engineering methods to ensure these baseline profiles are accurate, reliable and aligned with efficiency initiative projects.

While working, he is also pursuing his master's degree in industrial engineering at the Tshwane University of Technology.

